



HAL
open science

Preliminary design and sizing of actuation systems

Marc Budinger

► **To cite this version:**

| Marc Budinger. Preliminary design and sizing of actuation systems. Mechanical engineering [physics.class-ph]. UPS Toulouse, 2014. tel-01112448

HAL Id: tel-01112448

<https://hal.science/tel-01112448>

Submitted on 3 Feb 2015

HAL is a multi-disciplinary open access archive for the deposit and dissemination of scientific research documents, whether they are published or not. The documents may come from teaching and research institutions in France or abroad, or from public or private research centers.

L'archive ouverte pluridisciplinaire **HAL**, est destinée au dépôt et à la diffusion de documents scientifiques de niveau recherche, publiés ou non, émanant des établissements d'enseignement et de recherche français ou étrangers, des laboratoires publics ou privés.



Université
de Toulouse

Habilitation à Diriger des Recherches

Délivrée par : **Université Toulouse 3 – Paul Sabatier**

Discipline : **Génie Mécanique**

Présentée par :

Marc BUDINGER

Docteur en Génie Electrique

Agrégé de Physique Appliquée

Titre :

Preliminary design and sizing of actuation systems

Soutenue le 22 septembre 2014 devant le jury composé de :

Willy CHARON	Professeur à l'UT de Belfort-Montbéliard	Rapporteur
Laurent GERBAUD	Professeur à l'INP de Grenoble	Rapporteur
Giovanni JACAZIO	Professeur au POLITECNICO de Turin	Rapporteur
Alain BERLIOZ	Professeur à l'UPS Toulouse	Examineur
Eric BIDEAUX	Professeur à l'INSA de Lyon	Examineur
Jean-Charles MARE	Professeur à l'INSA de Toulouse	Examineur

Ecole Doctorale : **MEGEP**

Unité de Recherche : **Institut Clément Ader (EA 814)**

Établissement de rattachement : **Institut National des Sciences Appliquées de Toulouse,
Université de Toulouse**

Remerciements

Les travaux présentés dans ce mémoire ont été réalisés au sein de l'Institut Clément Ader de Toulouse dirigé par M. Marc SARTOR et M. Philippe OLIVIER. Je tiens à les remercier pour leur dévouement pour le bien commun et pour les discussions et échanges scientifiques que j'ai pu avoir avec eux.

J'exprime ma profonde reconnaissance à M. Jean-Charles MARE qui m'a accueilli dans son équipe et ouvert les portes de la conception préliminaire des actionneurs dans le monde aéronautique.

J'adresse ma reconnaissance à M. Willy CHARON, M. Laurent GERBAUD et M. Giovanni JACAZIO et M. Eric BIDEAUX qui m'ont fait l'honneur d'être rapporteurs ou examinateur et pour le temps, les remarques judicieuses et le retour qu'ils ont pu me faire dans leur rapport, leurs questions ou nos discussions.

Mes plus chaleureux remerciements vont à M. Alain BERLIOZ qui m'a fait l'honneur de présider mon jury.

Je remercie M. Xavier ROBOAM et M. Bernard MULTON pour les travaux et réflexions que nous avons pu mener ensemble ainsi que M. Frank THIELECKE et l'ensemble des membres de l'institut FST à TUHH pour l'accueil et leur disponibilité pendant les quelques mois passés en Allemagne.

Je tiens également à remercier l'ensemble du personnel du département de Génie Mécanique de l'INSA et des autres départements de l'INSA auprès duquel j'ai pu travailler et pour l'ambiance générale positive et constructive qui y règne.

Je tiens à remercier également les doctorants que j'ai eu la chance d'encadrer, Jonathan LISCOUET, Toufic El HALABI, Fabien HOSPITAL, Amine FRAJ, Xavier GIRAUD et Aurélien REYSSET et à l'ensemble des chercheurs, ingénieurs et stagiaires que j'ai pu côtoyer ces dernières années.

Enfin, je réserve une place toute particulière à mes enfants et à ma femme, qui ont su m'apporter amour et complicité pendant toutes ces années.

Table of contents

Preface

Introduction to preliminary design and sizing

Chapters and papers

Chapter 1 - Estimation models with scaling laws

Paper 1 - Estimation models for the preliminary design of electromechanical actuators

Chapter 2 - Simulation models for preliminary design

Paper 2 - Modelling approach for the Simulation-Based Preliminary Design of Power Transmissions

Chapter 3 - Evaluation models and sizing for lifetime and reliability

Paper 3 - An integrated methodology for the preliminary design of highly reliable electromechanical actuators: Search for architecture solutions

Chapter 4 - Metamodels for model-based-design of mechatronic systems

Paper 4 - Scaling-law-based metamodels for the sizing of mechatronic systems

Chapter 5 - Design graphs for sizing procedures and optimization problems definition

Paper 5 - Optimal preliminary design of electromechanical actuators

Postface and perspectives

Annexes

Annex 1 - Curriculum Vitae, version détaillée (French)

Annex 2 - Curriculum Vitae, short version (English)

Annex 3 - Publications

The synthesis report is written so that included publications can be read as a continuation or a deepening of each chapter. It is recommended that the reader read each paper numbered from 1 to 5 after the chapter bearing the corresponding number.

Preface

Since my recruitment at INSA in September 2006, I have worked at research level in the Clément Ader Institute (ICA), mainly with J-Ch Maré on the preliminary design of power systems with electromechanical actuators in the aerospace field. This theme of research has been developed around three areas:

- Technologies: mechatronic systems and their actuation systems include power transmission elements from different fields, which are usually treated independently. The goal of my research is to synthesize them in a coupled manner;
- Models: the models to set up in order to design a system are of different natures. Simulation models are used to calculate all quantities that influence the choice of the components. Evaluation models enable lifetime or reliability to be calculated. Estimation models give rapid access to component characteristics, generally obtained after detailed design.
- Methods: to optimize a design, it is advantageous to develop meta-models to replace time consuming simulations, to analyse the uncertainty of results, and to help the implementation of the design procedures.

Figure 1 synthesizes these research areas and how the PhD students, whom I co-supervised, were able to participate.

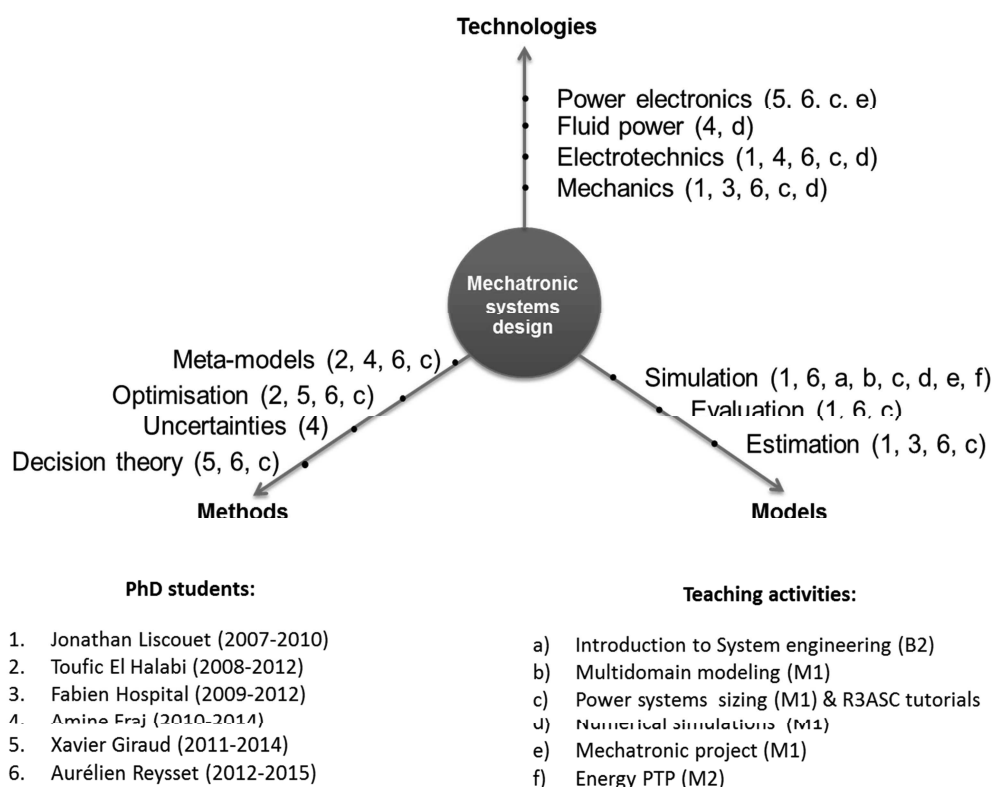
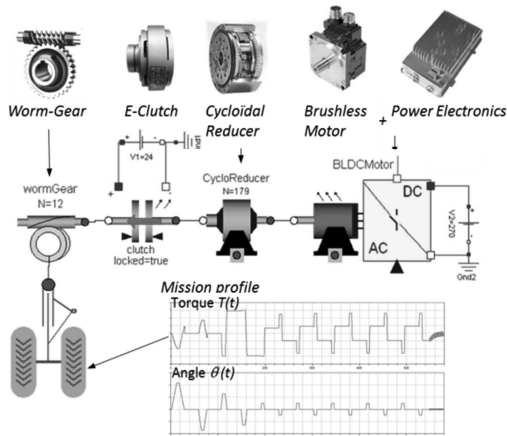


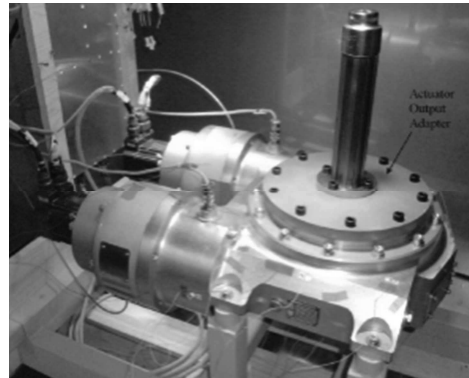
Figure 1 – Research areas, PhD students and teaching activities

The PhD thesis of Jonathan Liscouet (2007-2010), funded by and structured around the European project DRESS and the French ANR project SIMPA2 C6E2, laid the foundations methodologies, such as inverse simulation, scaling laws, and equivalent sizing variables, to reduce the complexity and the size of design loops. The simulation models suitable for preliminary design (e.g. considering the dimensioning thermal effects for an electric motor) have been developed and implemented in the Modelica (Figure 2a) language. To facilitate design exploration, the parameters needed for the simulation are based on scaling laws models. The designer thus handles a reduced set of parameters: the technological reality is considered with reference to an industrial component, both of which contribute to the deriving of parameters (such as mass, inertia, the thermal time constant) from a reduced number of design parameters (such as the equivalent thermal torque). These research activities were carried out in collaboration with the LAPLACE laboratory (C6E2) and the

LMS-Imagine (C6E2) and Messier Bugatti Dowty (DRESS) companies. They led to the creation of the steering actuator prototype for a nose landing gear shown in Figure 2b.



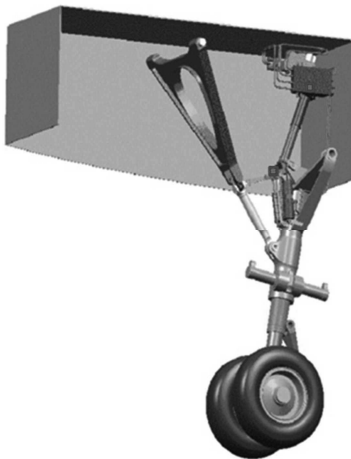
a) Modelica predesign library



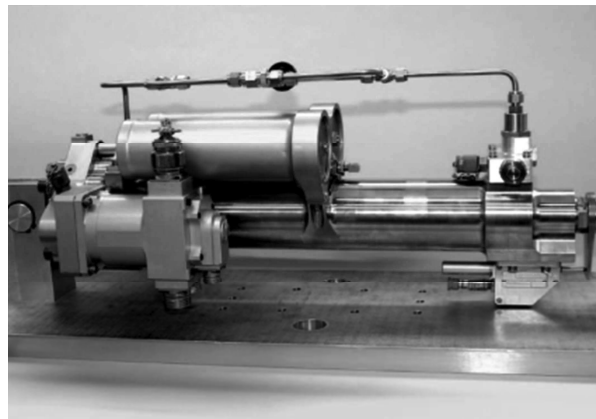
b) Distributed and Redundant Electrical nose gear Steering System (DRESS) actuator

Figure 2 – Jonathan Liscouet PhD - French ANR project SIMPA2-C6E2 and European project DRESS

The PhD thesis of Toufic El Halabi (2008-2012), funded by the FUI project CISACS of the ASTECH cluster, applied these models to the optimization of the design of landing gear actuation systems. To reduce the calculation time associated with the simulation of transient mission profiles, response surfaces were used to optimize of the geometrical and kinematic integration of the actuators (Figure 3a). These research activities were conducted in collaboration with Messier-Bugatti-Dowty and Sagem companies. The project led to the realization a prototype for a landing gear extension/retraction actuator as shown in Figure 3b.



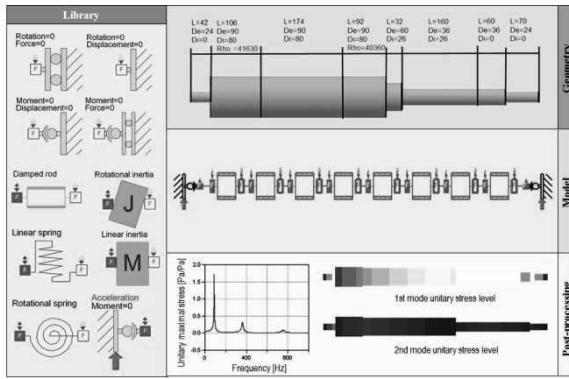
a) Geometrical integration



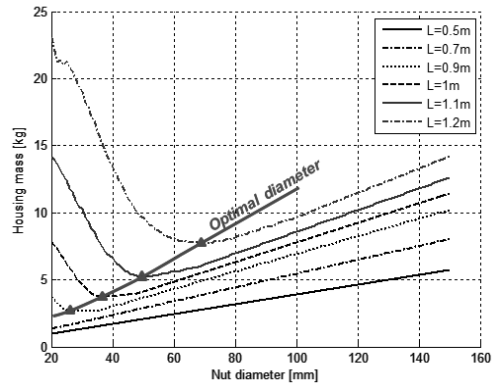
b) Extension/retraction nose landing gear actuator

Figure 3 – Toufic El Halabi PhD - French FUI project CISACS (Concept Innovant de Système d'Actionnement de Commandes de vol secondaires et de Servitudes)

The PhD thesis of Fabien Hospital (2009-2012), funded by an AMN ministerial scholarship, mainly treated the mechanical aspect of component selection and control synthesis. The Figure 4 illustrates the work performed on the sizing of housings of long actuators, e.g. of a slanding actuator, in severe vibratory environment. The models studied showed that vibrations were a key sizing criterion for long EMA (Electro Mechanical Actuator) housing but not for SHA (Servo Hydraulic Actuator) housing (mostly sized by the internal pressure strength). Some exploratory studies were performed on the housing geometry to highlight the compromise between diameter, thickness and extended length in vibration design.



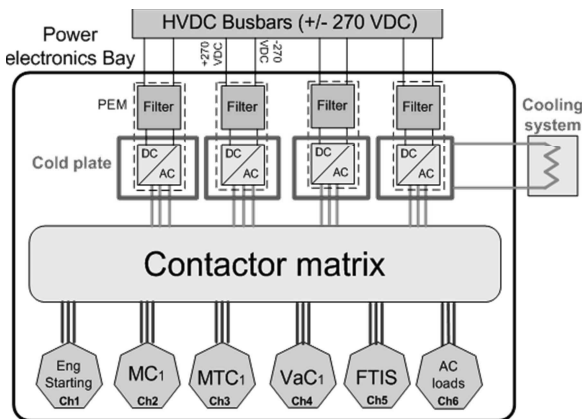
a) Modal and stress analysis of long actuator



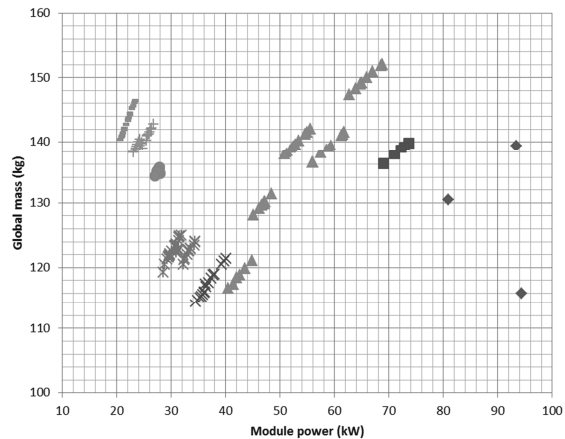
a) Optimal diameter of linear actuator

Figure 4 – Fabien Hospital PhD - AMN funding

The PhD thesis of Xavier Giraud (2011-2014), funded by Airbus, deals with the preliminary design of the embedded electrical network and associated modular power electronics bay (Figure 5a). The work addressed the optimization (Figure 5b) of multi-physics problem (power electronics) with large combinatorial aspects (allocation of loads, operational scenarios). The thesis was prepared in collaboration with Marc Sartor of the ICA laboratory and Xavier Roboam and Hubert Piquet of the LAPLACE laboratory.



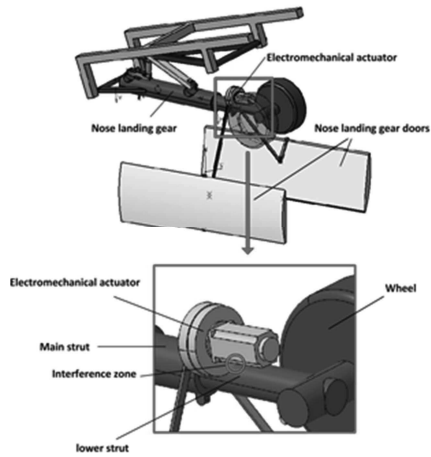
a) Modular power electronic bay



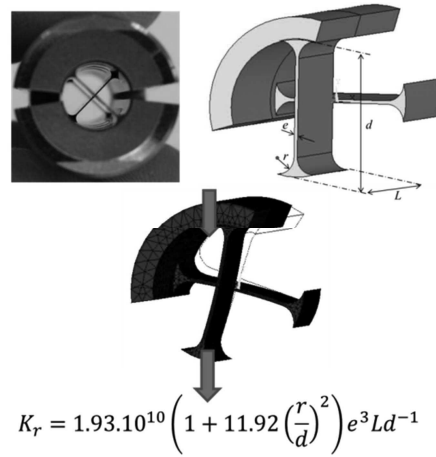
b) Mass optimization : complexity/sizing compromise

Figure 5 – Xavier Giraud PhD - Airbus Cifre

The PhD thesis of Amine Fraj (2010-2014), funded by the FUI project SYRENA, has the aim of quantifying the effects of uncertainties in mission profiles and the estimation models and of building bridges between 1D and 3D design using scaling laws as shown in Figure 6. Further projects are underway including the European project Actuation 2015 which began in late 2011 and deals with the standardization of electromechanical actuators for aerospace. I am responsible for the Model Based Design Tools work package. In this context, PhD student Aurélien Reyset is working on mission profiles analysis, automatic generation of sizing procedures and analysis of the effects of standardization.



a) 3D CAD link with scaling laws



b) Scaling laws based meta models (SLAWMM)

Figure 6 – Amine Fraj PhD - French FUI project SYRENA

The following synthesis of this research period is written so that included publications can be read as a continuation or a deepening of each chapter. This research work had also many interactions with my teachings made primarily on System Engineering aspects of the Mechanical Engineering Department in INSA Toulouse. Students are between bachelor 2 and master 2 levels. Table 1 describes briefly these courses and Figure 1 illustrates the links between my research and teaching activities. Over the past two last R3ASC conferences (2012 & 2014), I also made a tutorial of one day on the preliminary design of electromechanical actuators. The public of thirty participant was predominantly industrial and from varied geographical and institutional origins as illustrated in Figure 7.

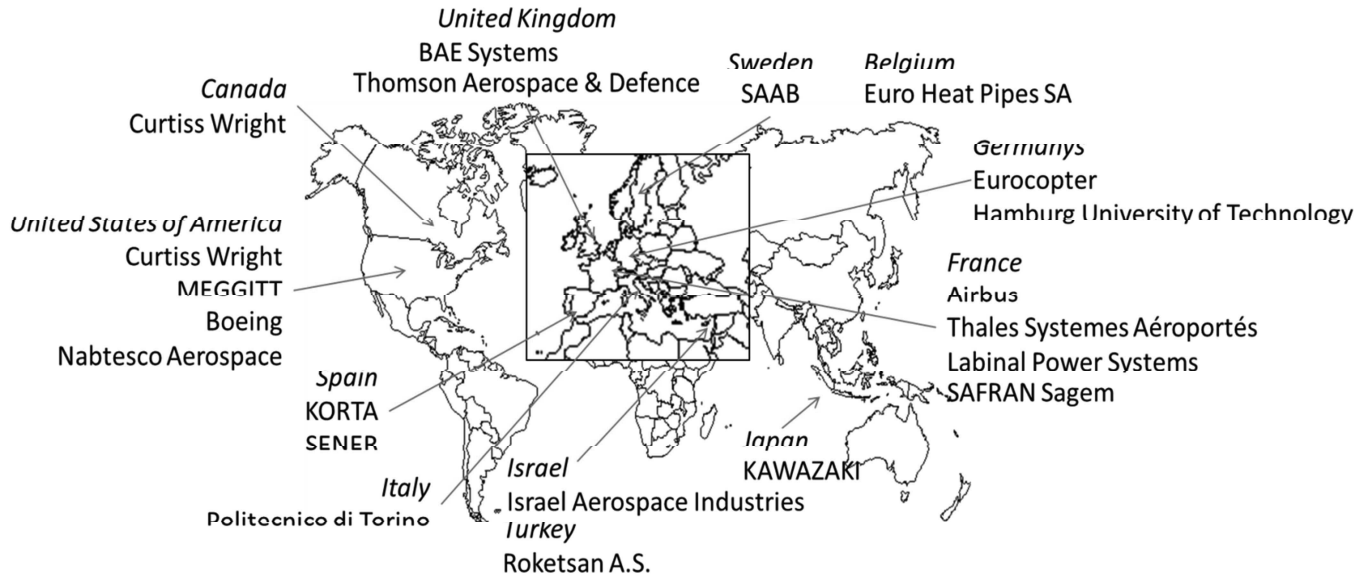
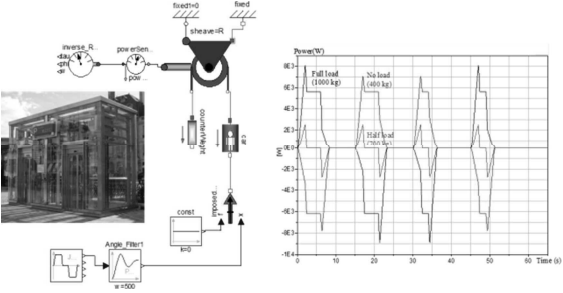
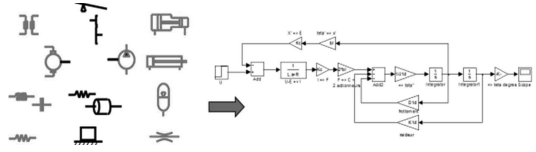
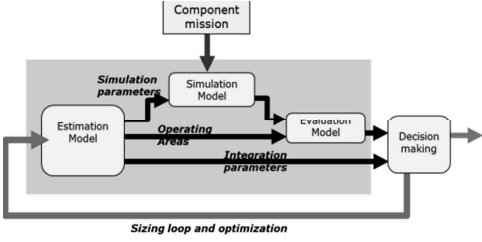
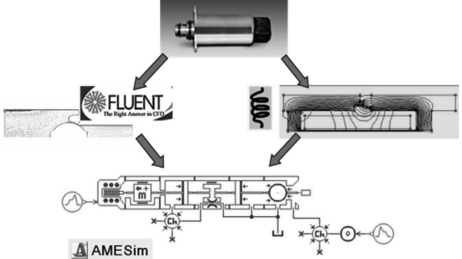
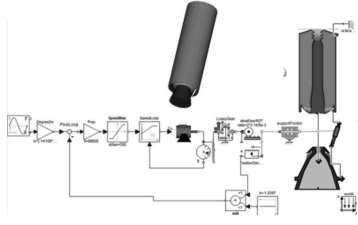



Figure 7 – R3ASC tutorial

Table 1 - Marc Budinger, teaching activities (INSA Toulouse)

Title / Level	Teaching description	Teaching illustration
<p>Introduction to system engineering</p> <p>Bachelor 2</p>	<p>This module is an introduction to systems engineering: functional analysis, specifications, modeling and design of multi-domain (meca / elec / hydro / control) system. A subject of study chosen by the students (steering, lift, flight control) is used to illustrate and apply these concepts.</p>	
<p>Multidomain modeling</p> <p>Master 1</p>	<p>This module lays the foundation for the modeling of mechatronic systems with lumped parameter models: networks approach for elec / mecha / thermal / hydro systems, bond graph, DOE/ADE solvers, causal / acausal modeling. Simulation tools: Modelica, Simulink, AMESim</p>	
<p>Power systems</p> <p>Master 1</p>	<p>This module deals with the design of multi domain power transmissions under architectural and sizing aspects. The sizing part use the same template as this document: estimation models, simulation models, evaluation models, meta-models and design graphs.</p>	
<p>Numerical simulations</p> <p>Master 1</p>	<p>This module deals with numerical simulations applied to electromagnetic actuator, fluid power and structural mechanics. Local aspects (FEM, CFD) and global aspects (multibody, OD/ID) and their relationships are discussed and illustrated through two examples (common rail pressure regulator, fast steering mirror).</p>	
<p>Mechatronics project</p> <p>Master 1</p>	<p>The students are brought to design a mechatronic system from the establishment of specifications with a real customer (industrial), the proposal of architectures to the design and simulation of a virtual prototype. Examples of subjects: thrust vector control actuator, brake landing gear actuator.</p>	
<p>Energy PTP</p> <p>Master 2</p>	<p>Students are brought to modelize a mild hybrid vehicle in Modelica and propose a simple command to optimize the consumption. Some of them may participate in the establishment of a small electric vehicle and its test bench.</p>	

Introduction to preliminary design and sizing

ABSTRACT

This introduction defines the specificities of mechatronic products and their actuation systems. Some examples of products and components are given. The main types of requirements and the design choices to be made are then introduced. The complexity of these choices requires the adoption of a design process that distinguishes preliminary design, corresponding to the specification of components or modules of the system, from detail design, corresponding to the geometrical and physical definition of the components. This preliminary design requires the implementation of different types of models (estimation, simulation and evaluation models) and their combination into a dedicated process for design and optimization. The following chapters and papers provide details of the implementation of each of the models.

Keywords: mechatronics products and components, actuation system, V design cycle, model based design.

TABLE OF CONTENTS

1.	Mechatronic and actuation systems	3
1.1.	Definitions	3
1.2.	Examples of actuation systems and components	3
1.3.	Characteristics of actuation systems.....	6
2.	Preliminary design in the overall design process	7
2.1.	System engineering of mechatronic systems.....	7
2.1.	Model levels in V cycle	9
3.	Description of chapters and papers	10
4.	Bibliography.....	13

NOTATION

Acronyms

AC	Alternating Current	MDO	Multi-Disciplinary Optimization
DC	Direct Current	PMAC	Permanent Magnet Alternating Current
DoE	Design of Experiments	TVC	Thrust Vector Control
EHA	Electro-Hydrostatic Actuator	0D/1D	Lumped parameter model
EMA	Electro-Mechanical Actuator	2D/3D	Distributed parameter model

1. MECHATRONIC AND ACTUATION SYSTEMS

1.1. Definitions

Mechatronics, as defined by standard NF E 01-010 [1], is an approach aiming at the synergistic integration of mechanics, electronics, control theory, and computer science within product design and manufacturing, in order to improve and/or optimize its functionality. As illustrated in Figure 1, a mechatronic system expands the capabilities of conventional mechanical systems through the integration of various technological areas around:

- a power transmission part, which is a combination of components from mechanical, electrical, power electronics or fluid power technologies;
- an information processing part, which is a combination of electronics, instrumentation, automatic, signal processing, and information technologies.

A mechatronic system can also be called a mechatronic product or a mechatronic component according to its degree of complexity and integration [2]. This document focuses mainly on the power transmission part of mechatronic systems and the examples developed are mainly actuation systems. The approaches presented could however be applied to any other technological system (electrical, hydraulic, mechanical, thermal, etc.) used as an operating part of a mechatronic system.

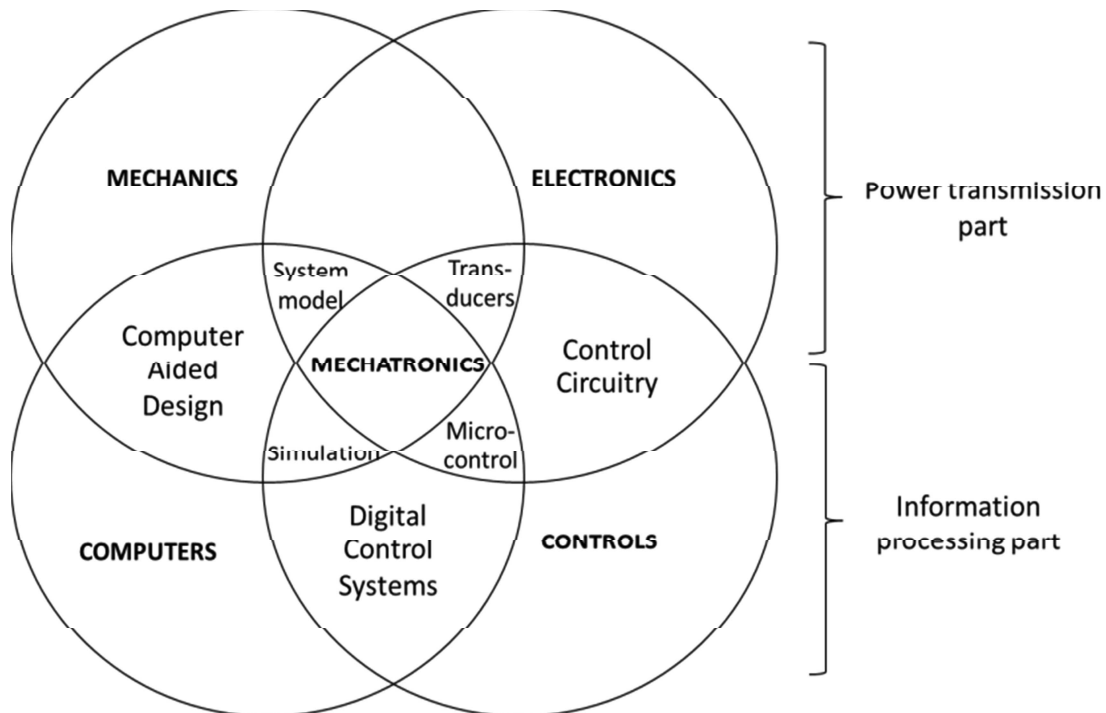


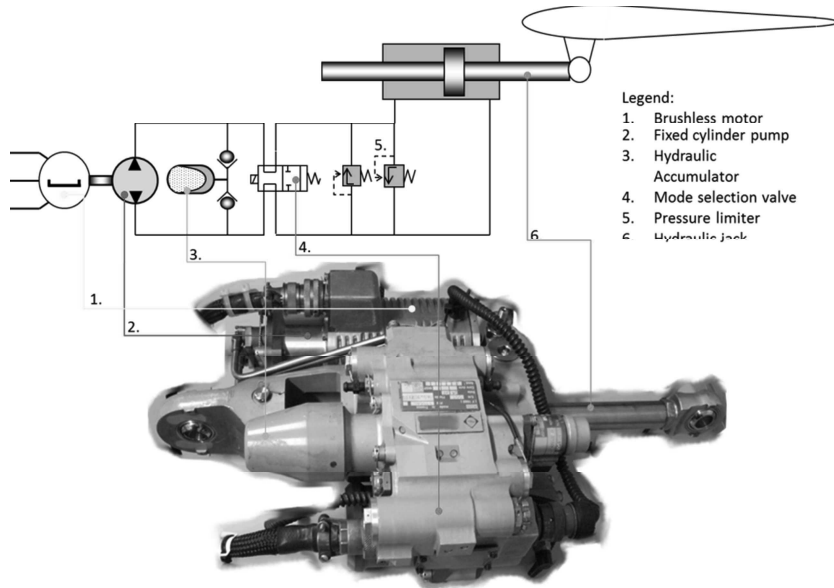
Figure 1 – Mechatronics

1.2. Examples of actuation systems and components

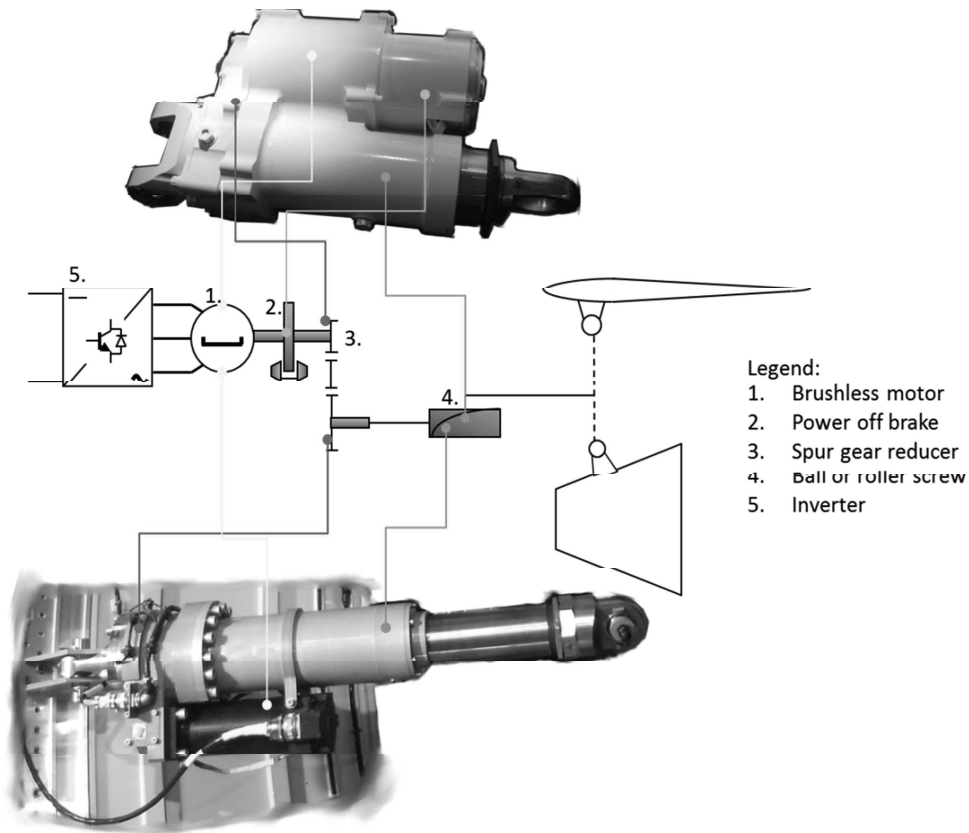
Figure 2 gives some examples of the architecture or combination of components for various mechatronic applications. These actuation systems typically should achieve various functions:

- **Feed and modulate** the power from a source of primary energy (hydraulic or electric) depending on orders from the information processing part;
- **Convert** this energy into mechanical energy;
- **Transform or adapt** the mechanical power to the load characteristics;
- **Transmit** this power to the load.

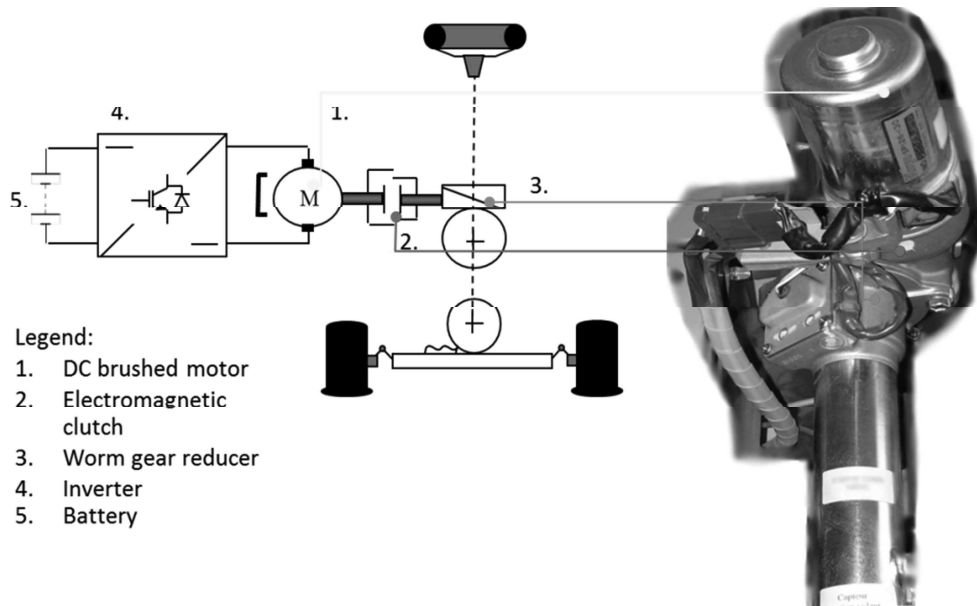
Table 1 summarizes the components conventionally used for these different functions for different technologies.



a) EHA (Electro Hydrostatic Actuator) flight control actuator



b) EMA (ElectroMechanical Actuator) actuator of spoiler and TVC (Thrust Vector Control)



c) Electrical power steering of car

Figure 2 – Examples of actuation systems of mechatronic products

Function / Technology	Feed	Modulate	Convert	Adapt	Transmit
Electromechanic	AC network, DC network, battery, wire, filter, capacitor	Chopper, inverter, contactor, clutch, brake	DC motor, PMAC motor, induction motor, etc.	Spur gear, epicycloid gear, worm gear, ball/roller screw, rack & pinion	Rod end, thrust bearing, connecting rod
Fluid power	Pump, regulator, filter, hydraulic line, accumulator	Orifice, control valve, servovalve	Pump, hydraulic motor, linear jack	-	Rod end, thrust bearing, connecting rod

Table 1 - Example of typical components and function within mechatronic products

In addition to the features already mentioned, an actuation system may have to manage other functions stemming from reliability requirements (e.g. fail safe) or corresponding to specific operational modes (such as damping of an aileron actuator). This functional integration linked to physical integration gives systems that are complex to design especially if the environmental constraints (vibration, temperature, etc.) are harsh. This physical and functional integration can be provided by technological solutions where several functions are performed by a single mechatronic component. Figure 3 shows how autofocus functions classically specific to a power off brake, a DC motor, a reducer and a clutch can be performed with one ultrasonic motor [3].

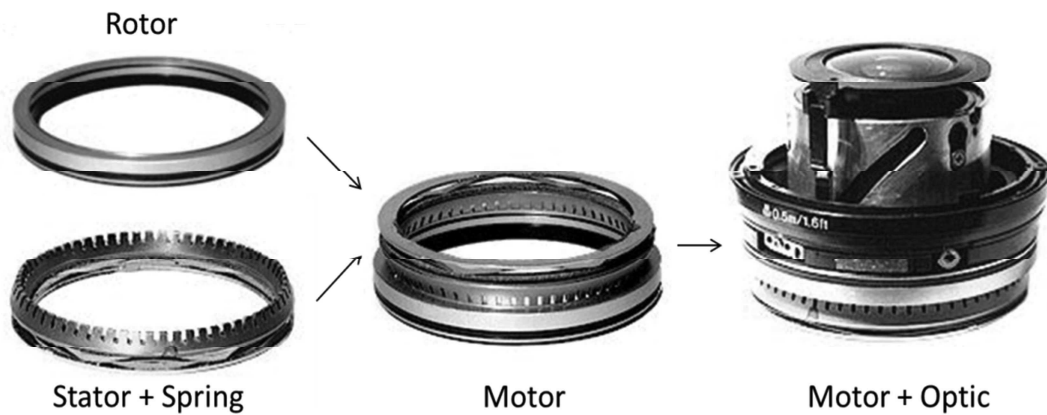


Figure 3 – Ultrasonic motor (Canon USM)

1.3. Characteristics of actuation systems

This work focuses on the synthesis of the operative part of the actuation systems. Such systems must meet a variety of requirements:

- At functional level, multiple operational modes may be requested. In addition to the primary function of positioning in active mode, specific modes can be added for each application: no load standby or passive damping for an aileron control surface, active damping for a TVC, free casting for steering, etc. These functions will require additional specific components or control loops (max speed limitation function of position or flight condition, load limitation, etc.).
- At performance level, the requirements may relate to transient or continuous forces, maximum speeds, damping coefficients, accuracy levels, bandwidths, stability coefficients, stiffness or disturbance rejection, etc. These different levels of performance and endurance can also be expressed by typical or critical mission profiles.
- At integration level, the requirements may constrain the geometrical envelope or the mass, or define the attachment points. The environmental constraints are also numerous for embedded systems : thermal stress, shocks and vibrations, electromagnetic pollution, humidity levels ... The first two points, heat and vibration can have a dramatic effect on electrical components or slender mechanical housings.
- At reliability level, a critical system like an aileron must present a fail-safe operation associated with a high rate of reliability for each mode. These requirements may have a significant impact on the complexity of the architecture for power transmission, monitoring or control.

Figure 4 is a graphic illustration of how classical types of requirements and the key design drivers are associated. The designer has a panel of degrees of freedom to respond to. The choice of the components, their combination and their technology, i.e. the architecture, provides a first set. The size chosen for the components, the parameters of the kinematic transmission, the shapes of displacement curves, i.e. the sizing, give a second set. The overlaps between these degrees of freedom and requirements are numerous and interconnected.

The design of the operating part of a mechatronic system therefore involves a relatively large number of components of different technologies. Each component has specific design drivers to satisfy multiple requirements. The following section presents the design process [4] generally used for the synthesis and integration of such products.

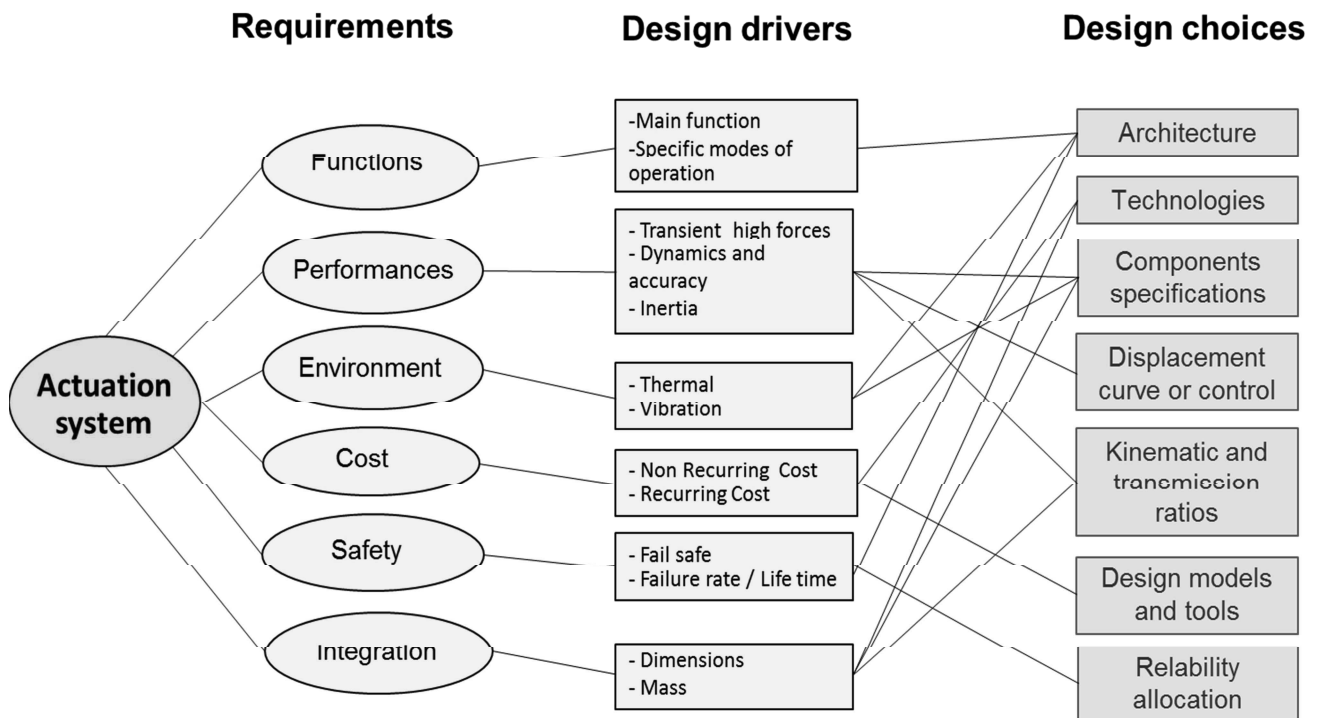


Figure 4 – Requirement and design choices

2. PRELIMINARY DESIGN IN THE OVERALL DESIGN PROCESS

2.1. System engineering of mechatronic systems

A mechatronic system is part of a set of complex technological systems to which different standards derived from system engineering [5] [6] [7] or technical engineering [8] [9] [10] may apply. These standards differ primarily by the product types or processes they describe. Figure 5 illustrates the various fields covered by these standards and their different levels of detail.

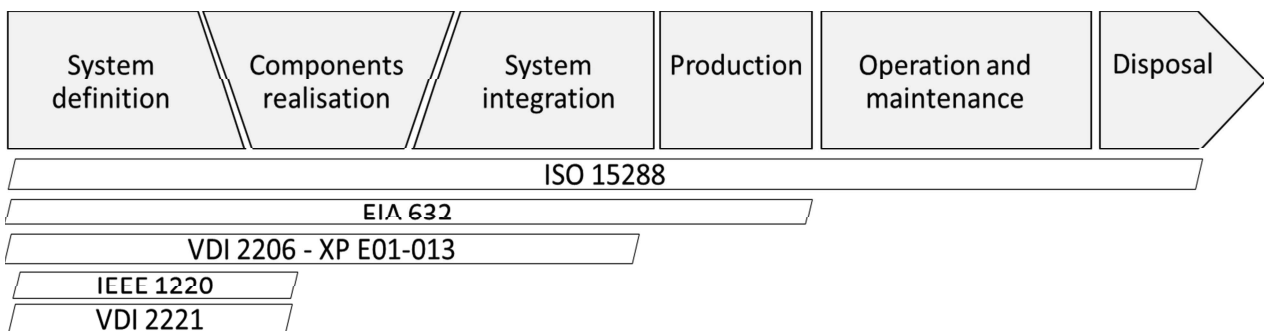


Figure 5 – Areas covered by the main standards of system engineering

The design process that interests us here is more precisely defined by IEEE 1200 [6] and VDI 2221 [8] for general technical systems and by VDI 2206 [9] and AFNOR XP E01-03 [10] for mechatronic systems. These standards define the interdisciplinary tasks required to transform needs, requirements and constraints encountered throughout the life cycle of the system into a system solution. Figure 6 illustrates the system design process of IEEE 1220 [6] and VDI 2221 [8].

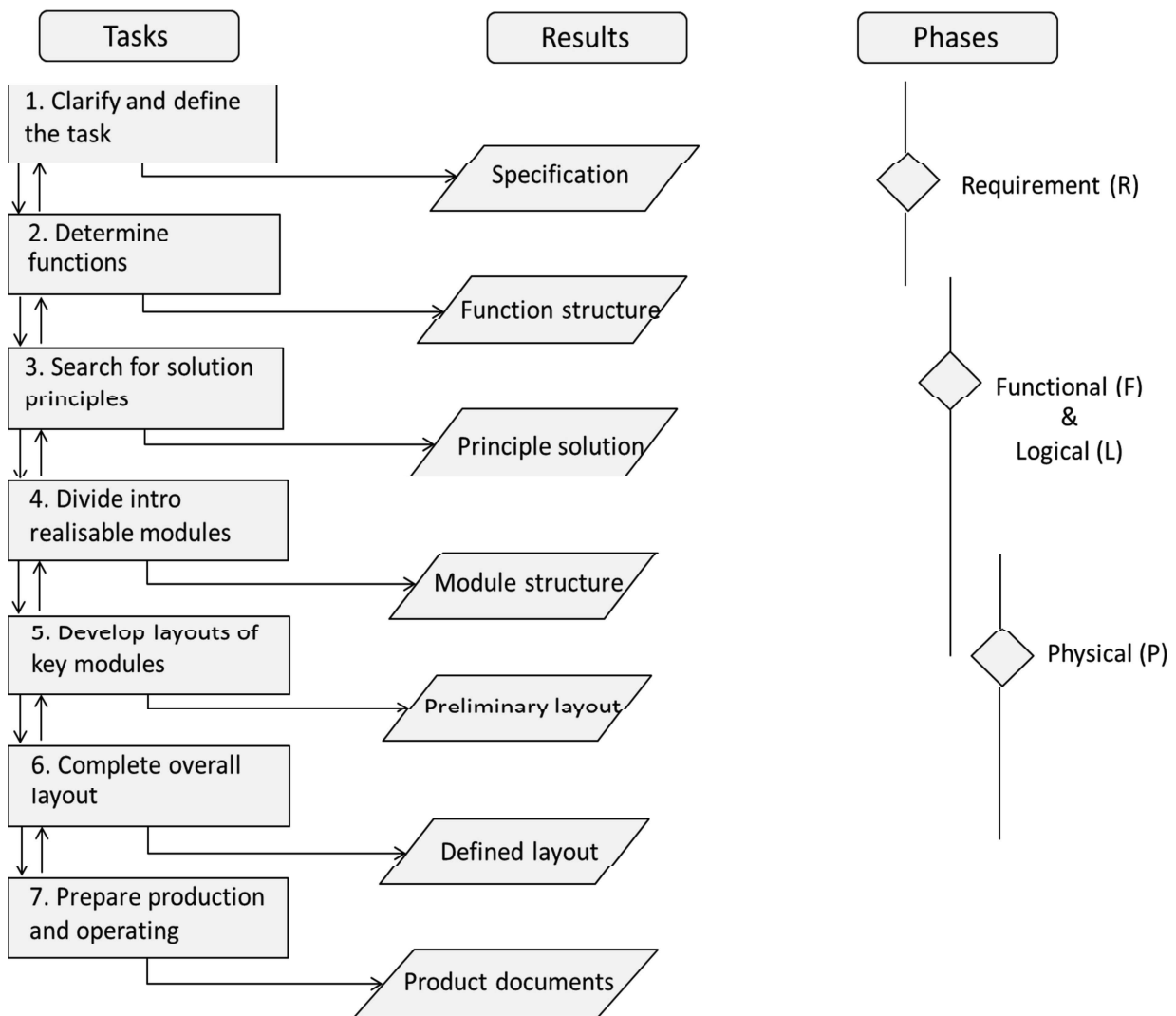


Figure 6 – Processus of VDI 2221

For these two standards, three sub-processes associated within the design of the system are present:

- Statement of needs: this process starts from the needs and constraints of the project participants to reach the technical specifications that the solution must meet ;
- Functional and logical design process: this process includes functional analysis with the allocation of requirements to functions and the design of a logical architecture that meets the requirements;
- Physical design process: this process leads to a physical architecture with the specifications allocated to the components to be developed or procured.

These three processes can be found in the descending branch of the V-cycle defined in the standard 2206 [9] which is dedicated to mechatronic products. The preliminary design which covers the logical and physical design process must start from the overall requirements to synthesize and evaluate different architectures or associations of components and compare them before the detailed design of each component is undertaken. The designer or integrator of mechatronic systems thus has to handle a wide range of components and model them in order to meet the expectations of the global products.

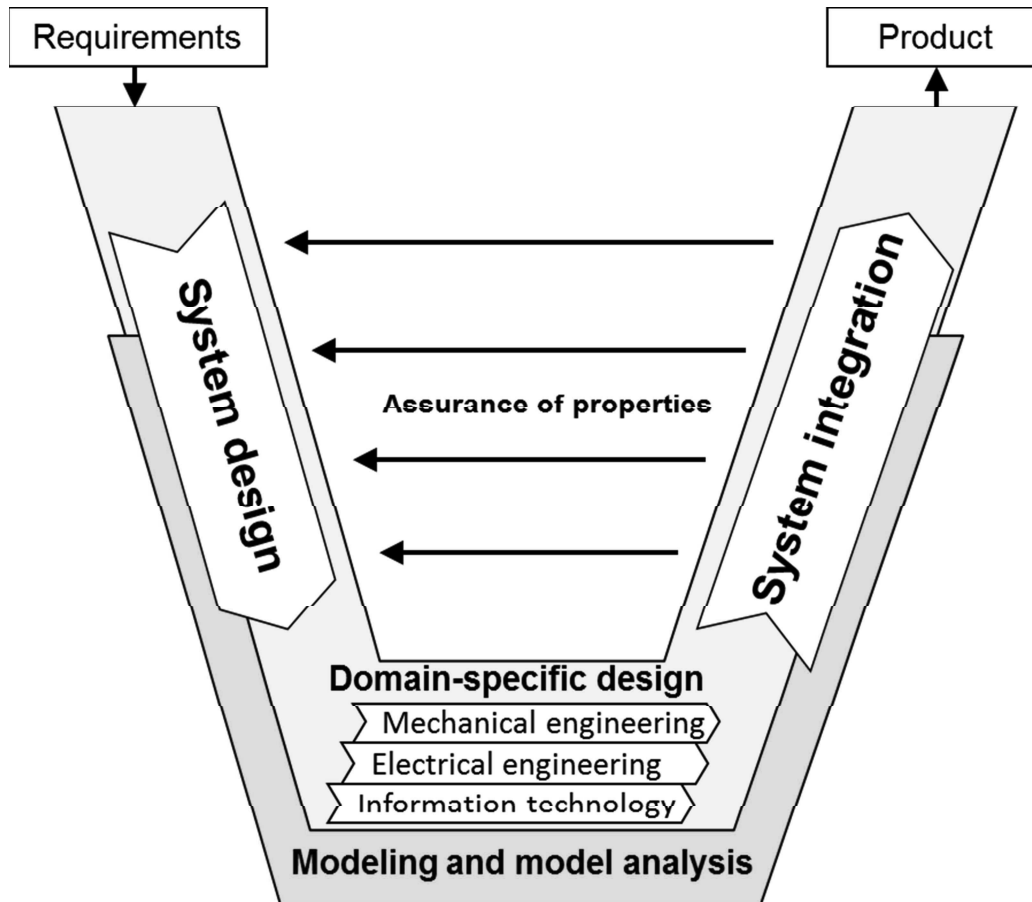


Figure 7 – V design cycle [9]

2.1. Model levels in V cycle

As shown in Figure 8, different types of models are used during the process of developing of a mechatronic system. In the descending phase of the V cycle, the system is gradually defined and the complexity of the models increases accordingly. During the first phase, modeling and simulation are typically used to validate the correctness of the design choices. First, a functional description of the system to be developed is made using functional simulation models (software tools: UML, SysML, etc.). In a second step, the "solution concepts" are identified and corresponding physical or behavioural simulation models are developed. These physical models can be static (software tools: Matlab, Mathcad, spreadsheet, etc.) or dynamic (software tools: Matlab / Simulink, Dymola, AMESim, etc.). During the specific design phase, the various components of the solution concepts are defined in more detail. It is then possible to produce 3D models of these components (software tools: Catia, Abaqus, Flux3D, etc.). These 3D models can perform local computations (finite element) and can thus verify the properties of the developed components more accurately. Finally, during the system integration phase, the various components are assembled to form the solution concepts and validate their performance. To do this, the highly detailed 3D simulation models, are transformed into less detailed 0D-1D macro-models in order to perform physical simulations.

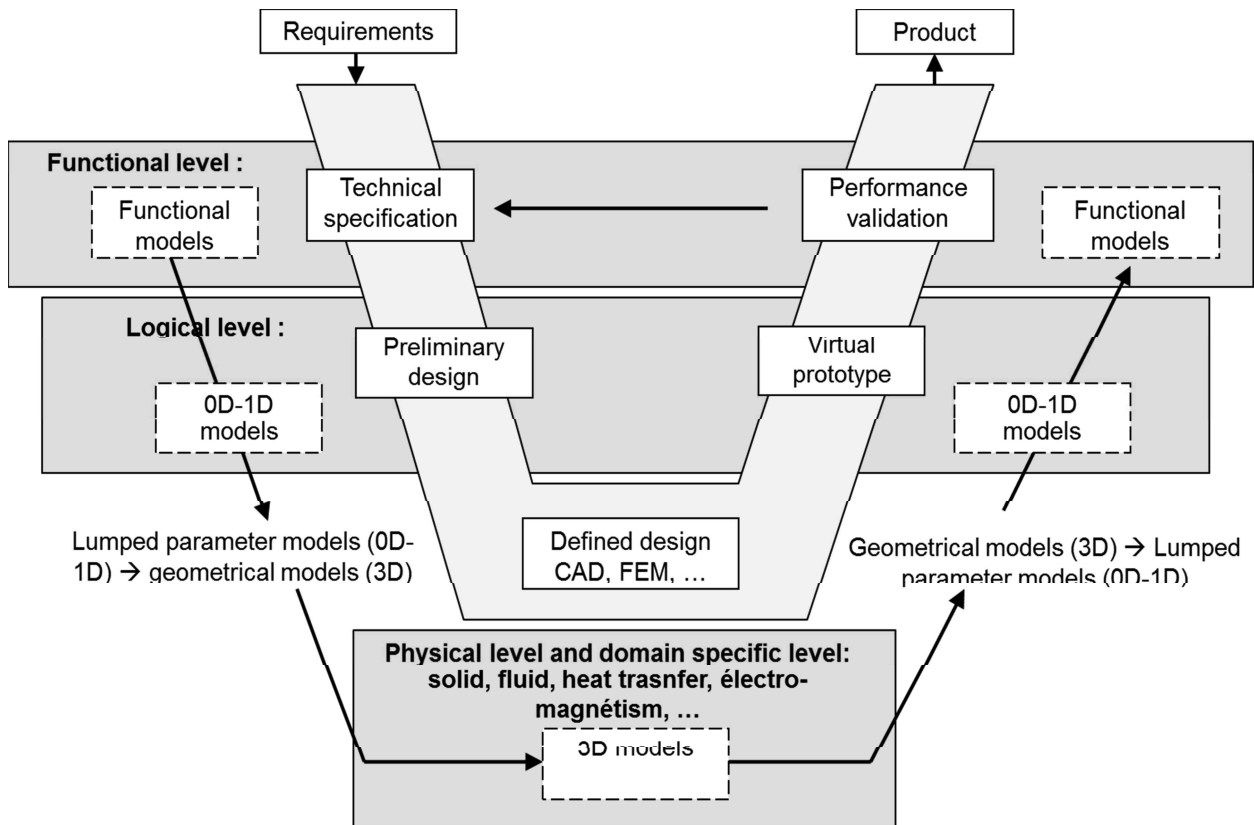


Figure 8 – V design cycle of a mechatronic system and associated modeling levels

3. DESCRIPTION OF CHAPTERS AND PAPERS

This document deals with the preliminary or conceptual design of mechatronic actuation systems. The work to be performed is at an intermediate level of design between the requirements of the overall system and the requirements of each component making up the solution architecture. This level of design focuses on the interactions between components and not on the detailed design of each component. It requires specific models and processes. Figure 9 describes the information exchanges between those different models and defines the structure suitable for model-based design of mechatronic systems.

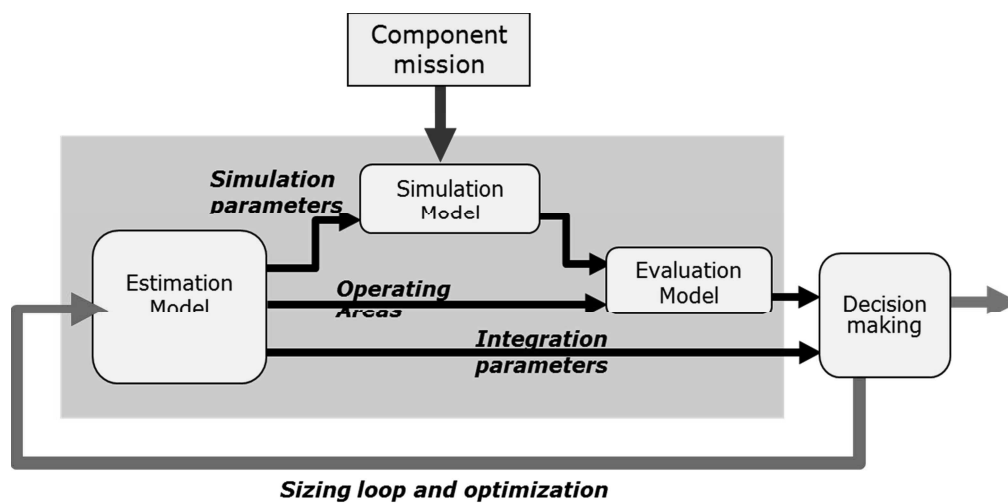


Figure 9 – Component models structure for model-based preliminary design

Chapter 1 describes the role of estimation models and how they are established. The goal of these models is to estimate the characteristics of components useful in system design, without going into their detailed

design. The approach adopted here to develop these estimation models is based on scaling laws. Buckingham's theorem is used to show that power laws of this form have, under given assumptions, a physical basis. These assumptions, such as geometric similarity, greatly simplify the implementation of such models. The use of these models is illustrated with some examples and the limits of scaling laws are also highlighted. The end of the chapter shows how to model the uncertainties in the models and how to use these uncertainties to assist in the specification of the components. The paper entitled "Estimation models for the preliminary design of electromechanical actuators" and published in the Journal of Aerospace Engineering of the Institution of Mechanical Engineers illustrates this type of modeling [11]. Models that are developed in this paper enable all the parameters required by a multi-objective design to be generated from a limited number of input parameters. The proposed approach is illustrated with the major components involved in aerospace electromechanical actuator design. The scaling laws established provide the designer with parameters needed for integration into the airframe, power sizing, thermal balance, dynamics and reliability. The resulting estimation models are validated with industrial data.

Chapter 2 is devoted to simulation models. The goal of these models is to establish relationships between the different components of a system and to access the variables influencing the selection of these components. The term simulation as used here differs from the finite element simulation of a component performed during the specific domain design. Here, simulations are mainly static or transient resolutions of lumped parameter models. The objectives of these models are different from those of models used for the synthesis of control or during virtual prototyping of the system. In contrast to the integration phase (ascending part of the V cycle), during the synthesis steps (descending part of the V cycle) little information is available on components, which have not yet been selected. The level of modeling should thus be as simple as possible so as to minimize the number of parameters to be provided, and as fast as possible so as to allow optimization while providing access precisely to the design variables. How such models are obtained by deduction or reduction techniques is illustrated using two examples of electromechanical drives. Paper 2, entitled "Modelling approach for the simulation-based preliminary design of power transmissions" and published in the journal Mechanism and Machine Theory [12], illustrates how scaling laws and acausal modelling can be used as a design tool, exploiting inverse simulation capabilities to evaluate technological alternatives quantitatively from limited design detail information.

Chapter 3 deals with the evaluation model, the goal of which is to check the ability of a component to operate in its safe operating area for the required lifetime and with the required reliability. After reviewing the state of the art on the main degradation phenomena that limit the performances and endurance of mechatronic components, this chapter describes the possible models and ways of implementing them in system simulation environments by focusing on lifetime evaluation and sizing of components. The associated paper 4, entitled "An integrated methodology for the preliminary design of highly reliable electromechanical actuators: Search for architecture solutions" and published in the journal Aerospace Science and Technology [13], describes the reliability aspect with an integrated hybrid (top-down/bottom-up) methodology for generating, selecting and assessing architectures for electromechanical actuators, paying special attention to safety and reliability.

Chapter 4 illustrates how metamodeling techniques can be applied to models used in the preliminary design of mechatronic systems. After a review of the different families of metamodels, standard regression techniques are applied to obtain estimation models from catalogue data and to represent transient simulations. Emphasis is placed on the possibility of using dimensional analysis and transformations to extend the scope of these expressions and these methods. Paper 5, entitled "Scaling-law-based metamodels for the sizing of mechatronic systems" and accepted by the journal Mechatronics [14], illustrates how these approaches can be adapted to the generalization and synthesis of scaling laws from finite element simulations.

The last chapter focuses on the combination of these different models to develop sizing and optimization procedures. This chapter begins with a state of the art on the tools and methods available for design and optimization. A first category used for Multi-Disciplinary Optimization (MDO) employs Design of Experiments (DoE), Metamodels and Optimization algorithms on numerical models. A second category uses constraint networks and graph theory to represent the constraints and links between models. The chapter exemplifies how these methods can be used with graphical tools. These design graphs can be used pedagogically to introduce students to design. They can also be implemented by algorithms to help the designer in the case of more complex devices. Paper 5, associated with this chapter, is entitled "Optimal preliminary design of electromechanical actuators" and was published in the journal of Aerospace Engineering of the Institution of Mechanical Engineers [15]. The paper presents a methodology for the

optimal preliminary design of electro-mechanical actuators. The main design drivers, design parameters and degrees of freedom that can be used for preliminary design and optimization of EMA are described. The different types of models used for model based design (estimation, simulation, evaluation and meta-model) are presented together with their associations. The process preferred for its effectiveness in terms of flexibility and computational time is then described and illustrated with the example of an electromechanical actuator of a spoiler. The proposed approach, based on meta-models obtained using the surface response methods and scaling law models, is used to explore the influence of anchorage points and transmission ratio on the different design constraints and the overall mass of the actuator.

4. BIBLIOGRAPHY

- [1] UNM, NF E 01-010 11-08 : Mécatronique. Vocabulaire, AFNOR, Éd., 2008.
- [2] P. Devalan, «Introduction à la mécatronique,» *Techniques de l'Ingénieur*, vol. BM 8000, 2010.
- [3] T. Sashida, *An Introduction to Ultrasonic Motors*, Oxford Science Publications, 1993.
- [4] O. Penas, R. Plateaux, C. J-Y., H. Kadima, T. Soriano, C. Combas et A. Riviere, «Conception mécatronique - Vers un processus continu de conception mécatronique intégrée,» *Techniques de l'Ingénieur*, vol. BM 8020, 2011.
- [5] EIA, «EIA/ANSI 632: Processes for Engineering a System,» EIA, 1998.
- [6] IEEE, IEEE standard 1220 - Systems engineering - Application and Management of the Systems Engineering Process, IEEE, Éd., 2005.
- [7] ISO, ISO 15288 Systems engineering—System life cycle processes, International Standards Organisation, 2002.
- [8] C. f. S. D. VDI, VDI 2221 - Systematic Approach to the Design of Technical Systems and Products, V. D. Ingenieure, Éd., 1987.
- [9] VDI-EKV, VDI 2206 - Design methodology for mechatronic systems, V. D. Ingenieure, Éd., Düsseldorf: VDI, 2004.
- [10] UNM, XP E01-013 - Mechatronics - Lifecycle and design of products, AFNOR, Éd., 2009.
- [11] M. Budinger, J. Liscouet, J. Mare et others, «Estimation models for the preliminary design of electromechanical actuators,» *Proceedings of the Institution of Mechanical Engineers, Part G: Journal of Aerospace Engineering*, vol. 226, n° 13, pp. 243-259, 2012.
- [12] J. Liscouet, M. Budinger, J.-C. Mare et S. Orioux, «Modelling approach for the simulation-based preliminary design of power transmissions,» *Mechanism and Machine Theory*, vol. 46, n° 13, pp. 276-289, 2011.
- [13] J. Liscouet, J.-C. Mare et M. Budinger, «An integrated methodology for the preliminary design of highly reliable electromechanical actuators: Search for architecture solutions,» *Aerospace Science and Technology*, vol. 22, n° 11, pp. 9-18, january 2012.
- [14] M. Budinger, J.-C. Passieux, C. Gogu et A. Fraj, «Scaling-law-based metamodels for the sizing of mechatronic systems,» *Mechatronics, Elsevier*, accepted, 2014.
- [15] M. Budinger, A. Reysset, T. El Halabi, C. Vasiliu et J.-C. Mare, «Optimal preliminary design of electromechanical actuators,» *Proceedings of the Institution of Mechanical Engineers, Part G: Journal of Aerospace Engineering*, Published online before print August 6, 2013.

Chapter 1 – Estimation models with scaling laws

ABSTRACT

This chapter presents the estimation models that calculate the component characteristics requested for their selection without requiring a detailed design. Scaling laws are particularly suitable for this purpose. After introducing the assumptions necessary for the implementation of these laws, various examples of use are given. The chapter ends with the modeling errors and uncertainties inherent in this type of model. The associated paper, entitled "Estimation models for the preliminary design of electromechanical actuators" and published in the Journal of Aerospace Engineering, illustrates how to obtain scaling laws for the typical components of electromechanical actuators.

Keywords: estimation models, scaling laws, geometric similarity, dimensional analysis, uncertainty.

TABLE OF CONTENTS

1.	Estimation models for Preliminary Design	17
1.1.	Design model vs estimation model of mechatronic components	17
1.2.	Main assumptions to simplify design model into estimation models	17
2.	Estimation models with Scaling laws.....	20
2.1.	Scaling laws and Buckingham theorem	20
2.2.	Examples of scaling laws	21
3.	Example of use of scaling laws	23
3.1.	Application presentation and main requirements	23
3.2.	Architectures and reference components	25
3.3.	Preliminary analyses using graphical nomograms.....	28
3.4.	Components selection and specification	30
3.5.	Geometrical integration	32
3.6.	Estimation of simulation parameters	32
3.7.	Design space exploration	33
4.	Uncertainty and scaling laws.....	33
4.1.	Limitations of scaling laws.....	33
4.1.	Form of statistical laws	34
4.1.	Correlation between errors.....	35
4.2.	Influence of choice of reference on the mean error	36
4.3.	Standard deviation	36
4.4.	Examples of effects of uncertainties of estimation models during preliminary design.....	37
5.	Conclusion.....	39
6.	Bibliography.....	40

NOTATION

Acronyms

e.m.f	electromotive force	RMC	Root Mean Cube
MDO	Multi-Disciplinary Optimization	RMS	Root Mean Square
PMAC	Permanent Magnet Alternative Current	RSM	Response Surface Modeling

Nomenclature

a	Power constant parameter	π_i	Dimensionless number
C	Load	Ω	Speed
d_i	Geometrical dimensions	ε	Relative error
k	Multiplication constant parameter	μ	Esperance
J	Inertia	σ	Standard deviation
L	Main geometrical dimension		
M	Mass		
P	Power		
p_i	Materials properties		
T	Torque		
t	Time		
y	Secondary characteristic		

Indices and exponents

X_{ref}	Reference parameter	x^*	Jufer scaling law notation
em	Electromagnetic		

1. ESTIMATION MODELS FOR PRELIMINARY DESIGN

A mechatronic system is an assembly of components from different technologies and different areas. The purpose of preliminary design is to specify these components before the detailed design of each of them is undertaken. To take the different design constraints into account, it is necessary to have models, called estimation models here [1], to represent the characteristics of the components without defining them completely.

1.1. Design model vs estimation model of mechatronic components

The system-level design steps require models (Figure 1a) directly linking primary characteristics, which define the component functionally, to secondary characteristics, which can be seen as the features of imperfections [1]. Generally, at component level, the models (Figure 1b) link the physical dimensions and characteristics of materials used to the primary and secondary characteristics. Design at component level is an inverse problem that requires the primary characteristics as inputs. This inversion may be done through design codes from design mechanical standards [2], by algebraic solvers or by optimization algorithms [3]. However at system level, the approach requires very significant expertise and time for each component.

Another first approach consists of using databases as is done in some design software packages [4]. The main disadvantage is that it is cumbersome or even impossible to implement them in the absence of a product range as is the case in the aerospace field. Although interesting for optimization, data mining combined with response surface modelling (RSM) [5] may be inappropriate here for the same reason. The use of scaling laws, also called similarity laws or allometric models, has the advantage of requiring only one reference component for a complete estimation of a product range. Such a modelling approach has already been successfully used for component design or comparison of technologies [6] [7] [8] [9] [10] [11]. This approach is developed here for system level design here since it appears to be one of the most appropriate means of speeding up the preliminary design of mechatronic systems.

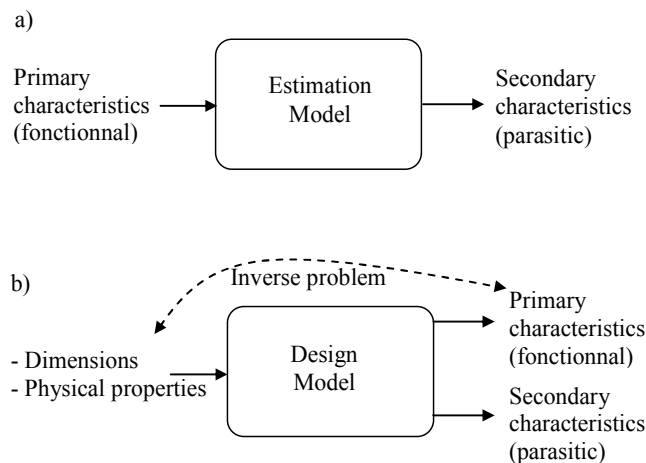


Figure 1 - Component models a) for system level design b) for component level design.

1.2. Main assumptions to simplify design model into estimation models

We use the example of permanent magnet (PMAC) motors, here, to highlight:

- the difference between the detailed design model and an estimation model for the predesign of a mechatronic power transmission.
- assumptions that can reasonably be taken into account to reduce the complexity of obtaining the estimation models.

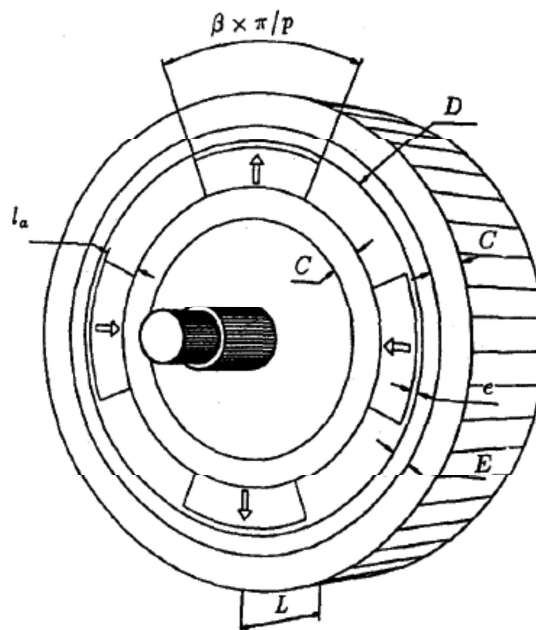
At system and preliminary level, the design is driven by the following main aspects to meet the various requirements: integration (mass, geometrical envelope) with embedded structure and actuated load, resistance to environment (thermal and vibration), power and energy, dynamic performance, service life, reliability, tolerance for failures, etc. When dealing with these various topics in a model-based way, the designer often fails to obtain the relevant parameters of the component models rapidly. In order to generate the estimation model from a reduced number of key data, we propose to categorize these parameters as follows:

- Integration parameters: to evaluate the masses and major dimensions (e.g. diameter, length) of the components;
- Simulation parameters: to perform a static or a transient simulation of a sizing scenario (e.g. inertia, resistance and heat capacity, electrical resistance and inductance, ...);
- Operating domain parameters: required to verify the component use with respect to endurance (e.g. mean winding temperature) or maximal performance (e.g. maximal torque or speed).

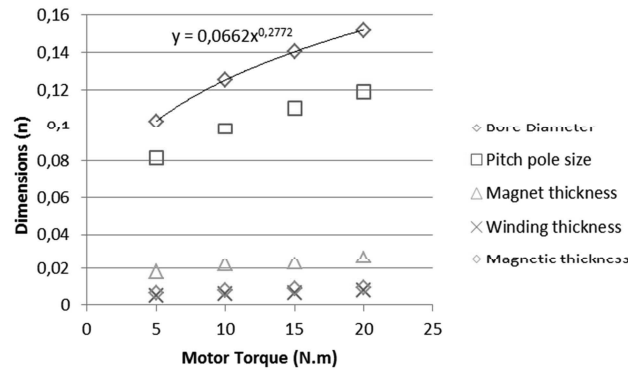
At component and detailed design level, the objective is to define the set of parameters required to industrialize the component. For the example of PMAC motors, these parameters are numerous and of various types:

- Structural parameters: at the stator with the number of phases, the presence or absence of teeth, the number and the shape of slots; at the rotor with the number of poles and the positions of magnets in the rotor (buried or surface technology);
- Material parameters: the choice of amagnetic (insulating) and soft magnetic (iron sheet) materials, the type of permanent magnet and all relevant physical properties (electrical and thermal conductivity, permeability, remanent and saturation magnetic fields, etc.);
- Geometrical parameters: the choice of dozens of parameters in the form of dimensions, angles and ratios.

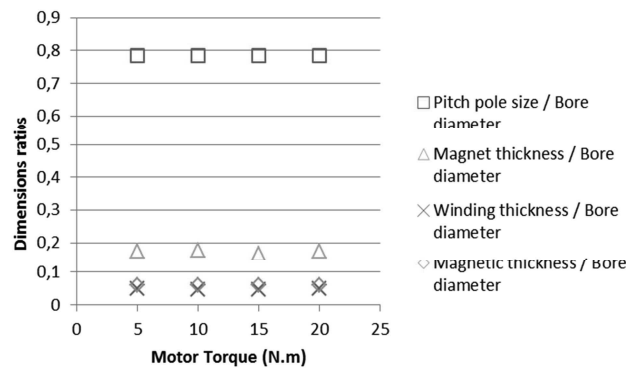
The parameters handled during detailed design and preliminary design overlap only partially. During predesign, the internal and exact definition of a component is less important than the relative change in global parameters. The component designer often defines a range of components of the same type by imposing the same constraints. To obtain optimum performance or optimal cost, the designer of PMAC motors will for example set the type of materials such as iron sheets and permanent magnets. The physical parameters are thus generally fixed. To obtain a motor with small torque pulsations, he selects a given number of teeth and poles [12], e.g. the 10 poles / 12 slots in Figure 3. He also determines the shape of the poles and slots to eliminate harmonics on e.m.f [13]. To avoid vibration or thermal problems, he fixes or limits the value of some form factors as the ratio length/diameter of the rotor or stator. He can finally optimize the free geometric parameters according to given criteria. Figure 2 shows the evolution of dimensions according to the torque for the machine model described in [3]. The goal here is to have the torque required while minimizing Joule losses. One can observe that the different dimensions evolve homothetically.



a) PMAC motor geometry (source [3])



b) Evolution of dimensions for different torques



c) Evolution of dimensions ratio for different torques

Figure 2 – PMAC motor optimization: evolution of dimensions for different torques

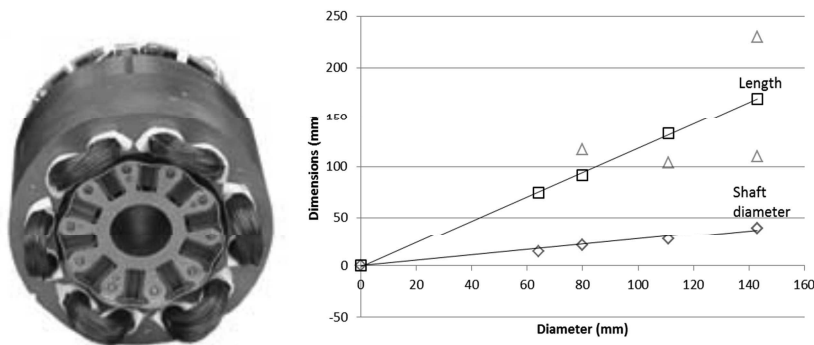


Figure 3 – Parvex NK range of frameless PMAC motors: evolution of dimensions function of external diameter

This geometric similarity is also found in industrial ranges as shown by the dimensions of NK Parvex frameless motors (Figure 3). One can assume that, although the detailed design of a component requires the definition of a significant number of parameters, the estimation of changes for these parameters compared to an existing component can take a simplified form. The concept of scaling laws reduces the complexity of the inversion problem of Figure 1b by using the modelling assumptions introduced on the input parameters:

- all material properties are assumed to be identical to those of the component used as the reference;
- the ratio of the lengths of the component considered to the lengths of the reference component is constant.

It is then easy to express, Figure 4a before inversion and Figure 4b after inversion, all the useful relations according to a few key design parameters that are associated with the component to be selected. We propose

to call them the definition parameters, according to the layout of the proposed estimation model (Figure 4b). The next section describes the mathematical form of scaling laws.

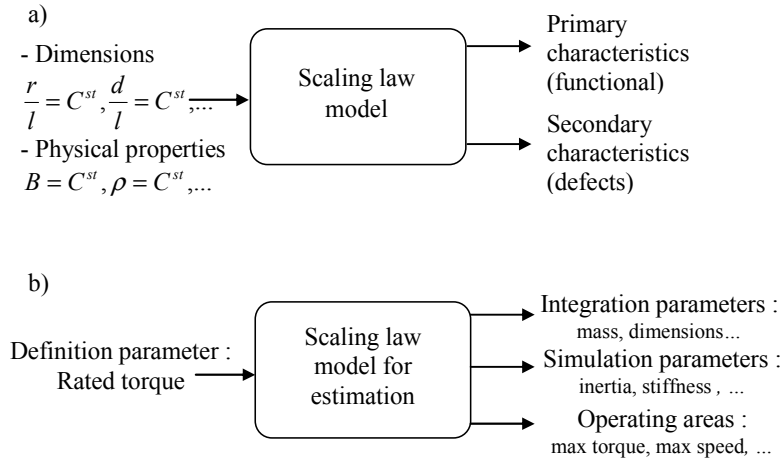


Figure 4 - Scaling laws models a) according to dimension variation b) according to definition parameter.

2. ESTIMATION MODELS WITH SCALING LAWS

2.1. Scaling laws and Buckingham theorem

The mathematical form of scaling laws is a power law:

$$y = kL^a \tag{1}$$

with y the secondary characteristic to be estimated, L the main dimension of the component, and k and a constants. For simplicity of notation, k means a constant coefficient which may have different numerical values in the different equations.

This mathematical form is obtained if, from two previous assumptions:

- a. Material similarity: all material and physical properties are assumed to be identical to those of the reference component;
- b. Geometric similarity: the ratio of all the lengths of the component under consideration to all the lengths of the reference component is constant;

, a third one can be added:

- c. Uniqueness of design driver: only one main dominant physical phenomenon drives the evolution of the secondary characteristic y .

The Buckingham theorem [14] [15] can be used to demonstrate these 3 assumptions. Indeed, an estimation model seeks to identify a relationship between $2+n+m$ parameters:

$$f\left(\underbrace{y}_1, \underbrace{L, d_1, d_2, \dots, d_n}_{1+n}, \underbrace{p_1, \dots, p_m}_m\right) = 0 \tag{2}$$

with:

- 1 parameter corresponding to the secondary characteristic y to be estimated;
- $1+n$ parameters characterizing the geometrical dimensions L and d_i ;
- m parameters characterizing the physical and material properties p_i ;

Depending on the number of physical units u (e.g. m, kg, s, etc.) involved in the problem, this relationship can be rewritten using dimensionless parameters π_i :

$$f'\left(\pi_y, \underbrace{\pi_1, \pi_2, \dots, \pi_n}_n, \underbrace{\pi_{p1}, \dots, \pi_{pm'}}_{m'}\right) = 0 \tag{3}$$

where:

$$\pi_y = yL^{a_L} \prod p_i^{a_i} \quad (4)$$

$$\pi_i = \frac{d_i}{L} \quad (5)$$

$$\pi_{p_i} = L^{a_{Lp_i}} \prod p_j^{a_j} \quad (6)$$

The number m' , usually smaller than m , depends on the number of physical units u as expressed by the Buckingham theorem:

$$m' = 1 + m - u \quad (7)$$

If only one main simple physical phenomenon drives the evolution of the secondary characteristic y , the number m' is often equal to zero. If m' is not equal to zero, the remaining dimensionless numbers can generally be expressed through ratios of material properties with similar units. Thus these m' dimensionless numbers often do not depend on L . With this condition and the first two assumptions a. and b., the π_i and π_{p_i} dimensionless numbers are constant and it follows that:

$$\pi_y = yL^{a_L} \prod p_i^{a_i} = \text{constant} \quad (8)$$

which gives relation (1) if we assume the material or physical properties p_i to be constant during the sizing.

2.2. Examples of scaling laws

To illustrate the construction and use of such laws, two examples will be given here. These examples address conventional components of mechatronic systems: brushless motors and bearings. We assume here that the main design criterion for the motor is the winding temperature. The dominant thermal phenomenon is taken to be convective. The bearings are designed to withstand a maximum mechanical stress.

For the brushless motors, equations (2), (3) and (1) become the following:

- For thermal aspects: the current density J can be linked to the dimensions through

$$f\left(\underbrace{J, L, d_1, d_2, \dots, d_n}_{1+n}, \underbrace{\rho, \theta, h}_m\right) = 0 \quad (9)$$

which, according to the Buckingham theorem, leads to (10)

$$f'\left(\frac{\rho J^2 L}{h\theta}, \underbrace{\frac{d_1}{L}, \frac{d_2}{L}, \dots, \frac{d_n}{L}}_n\right) = 0 \text{ where } m'=0$$

and (11)

$$J = kL^{-0,5}$$

- For magnetic aspects : the torque T can be linked to dimensions and current density through

$$f\left(\underbrace{T, L, d_1, d_2, \dots, d_n}_{1+n}, \underbrace{J, B_r}_m\right) = 0 \quad (12)$$

which, according to the Buckingham theorem, leads to (13)

$$f'\left(\frac{T}{JB_r L^4}, \underbrace{\frac{d_1}{L}, \frac{d_2}{L}, \dots, \frac{d_n}{L}}_n\right) = 0 \text{ where } m'=0$$

and (14)

$$T = kJL^4$$

with : J the current density, L the length of the motor, d_i other geometrical dimensions, ρ the resistivity of the copper, θ the maximal temperature rise for the winding insulation, h the convection coefficient, B_r the remanent induction of the permanent magnet, and T the electromagnetic torque.

Combining these two aspects provides an estimate of torque depending on motor size:

$$T = kL^{3,5} \quad (15)$$

The assumptions a. and b. allow the motor weight to be estimated:

$$M = kL^3 \rightarrow M = kT^{3/3,5} \quad (16)$$

With the same approach, the weight of the bearing can be estimated from their load-bearing capacity C :

$$C = kL^2 \text{ and } M = kL^3 \rightarrow M = kC^{3/2} \quad (17)$$

Figure 5 and Figure 6 compare these relationships to data from industrial catalogues, and show that scaling laws can provide good fits for the quantities of interest of such components.

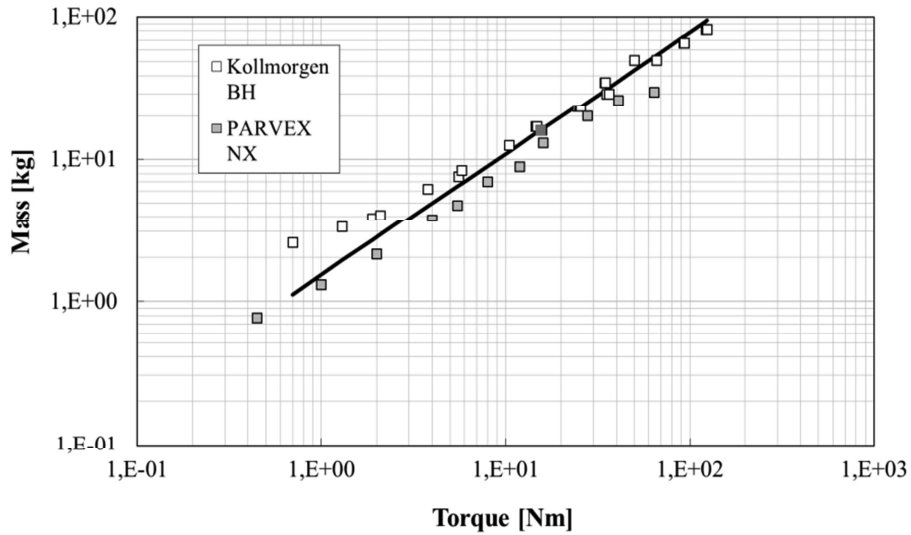


Figure 5 - Brushless motor masses according to the nominal torque.

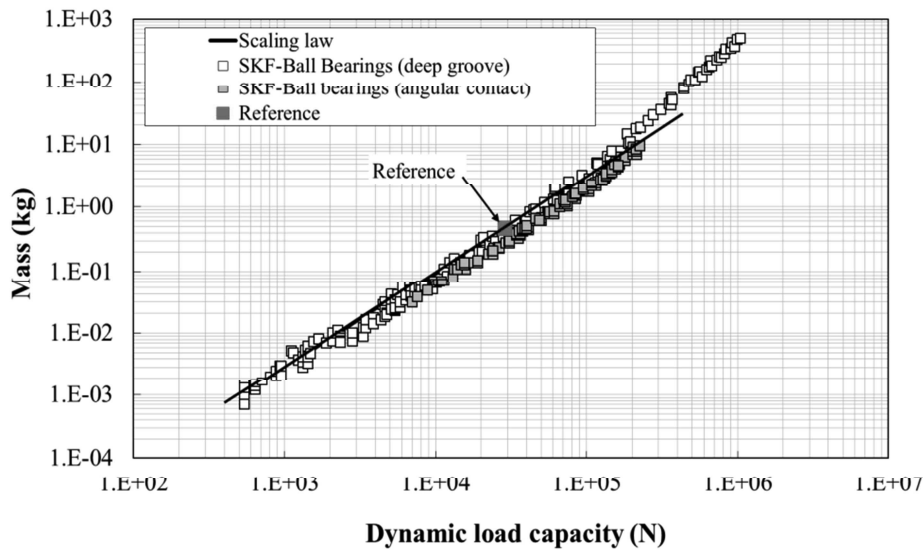


Figure 6 – Bearing masses according to the load capacity.

Figure 5 and Figure 6 validate the scaling laws by comparison with industrial ranges of components. However scaling laws can be used even if only one reference is available for a component. For example, if a motor of torque T_{ref} and mass M_{ref} is known, a possible mass M for a motor of torque T of similar technology is:

$$M = M_{ref} \left(\frac{T}{T_{ref}} \right)^{3/3,5} \text{ or } M = kT^{3/3,5} \text{ with } k = \frac{M_{ref}}{T_{ref}^{3/3,5}} \quad (18)$$

Scaling laws can also be written with the following notation (*) proposed by M. Jufer in [31]. The x^* scaling ratio of a given parameter is calculated as:

$$x^* = x/x_{ref} \quad (19)$$

where x_{ref} is the parameter taken as the reference and x is the parameter under study. With this notation relation (15) is written:

$$M^* = T^{*3/3.5} \quad (20)$$

It should also be noted that the scaling laws may be obtained without dimensional analysis by direct manipulation of the equations. More details and examples of the development of such laws for mechanical and electromechanical components are given in Paper 1 [16].

3. EXAMPLE OF USE OF SCALING LAWS

Various uses of estimation models are illustrated here with the simple example of a lift drive. As part of a preliminary design, the scaling laws can be used to:

- analyze trends and compare technologies, in particular by the early establishment of graphical templates or synthesis. In the example used here, the objective is to estimate the influence of the inertia of the electric motors on the torque requirement and to help with the selection of a gear ratio;
- support integration studies and weight estimation. In the present example, the envelope of the actuator and its size relative to the pulley will be evaluated.
- conduct simulations by estimating the needed parameters. The example illustrates the possibility of estimating the thermal and loss parameters in order to assess the evolution of the temperature of the motor or the electrical power consumption.
- explore the design space by experimental design or optimization algorithms. The effect of the radius of the pulley on the size of the motor are evaluated here.

3.1. Application presentation and main requirements

The objective of the preliminary design, here, is to evaluate the feasibility of a compact drive, with brushless motor technology, to avoid the construction of a machine room on the roof. Table 1 summarizes the main performance required at the elevator car. Specifications in acceleration and jerk, are imposed by the comfort and physiological limits of the user. These dynamic specifications can be translated into a mission profile (Figure 7) typical of the use of the elevator. The cycle of ascents and descents is assumed to be repeated for 8 hours of operation per day and for a lifetime of 20,000 hours of use. The ambient operating temperature is 40 ° C.

Max. acceleration	1 m/sec ²
Max. speed	2 m/sec
Max Jerk (acceleration derivation)	2,5 m/sec ³
Max. load	600 kg

Table 1 – Dynamic performances of the elevator

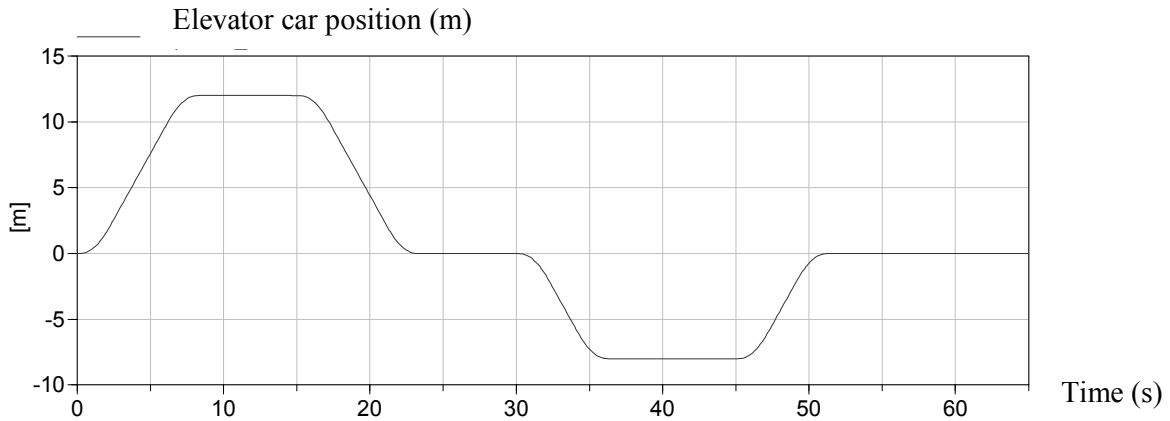


Figure 7 – Mission profile

The force or torque to be supplied by the drive to the pulley can be obtained by means of a simplified mechanical model. Figure 8 shows the main modeling assumptions.

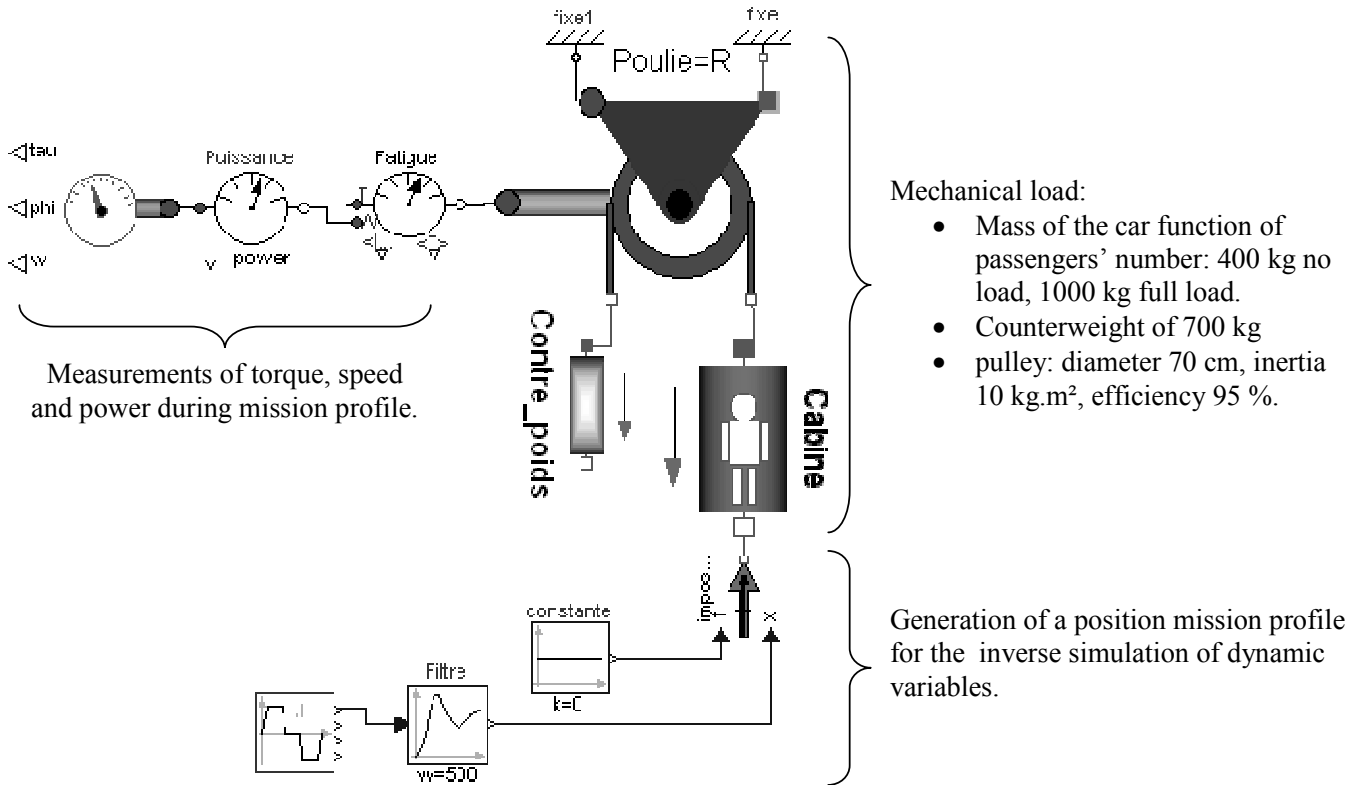


Figure 8 – Load model

Figure 9 and Figure 10 give the evolution of power and torque for three load configurations: empty elevator (cabin 400 kg), half load (cabin 700 kg), full load (cabin 1000 kg). The graphs were obtained using inverse simulations in Modelica [17] [16] [19] but more conventional tools such as Excel or Matlab, can be used. More details on inverse simulation are given in Chapter 2 and Paper 2.

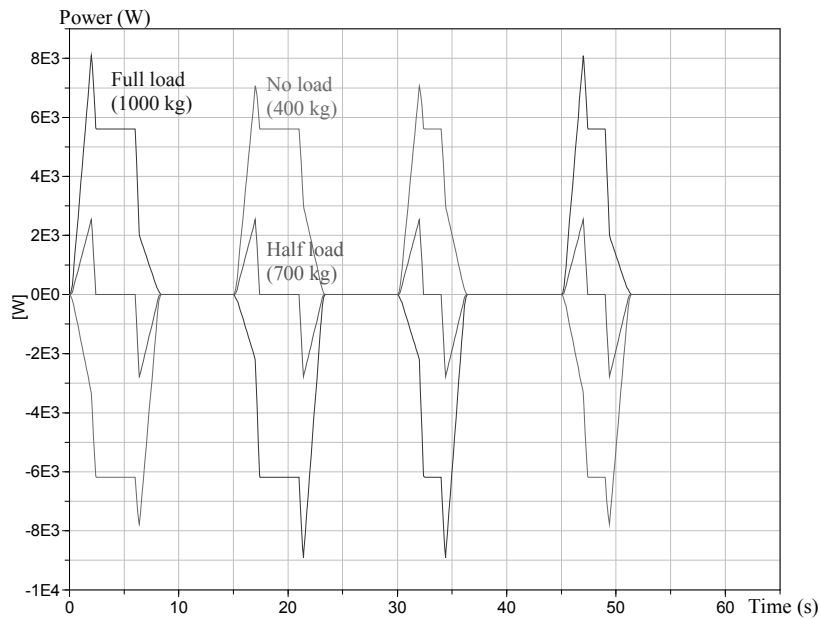


Figure 9 – Power for different loads

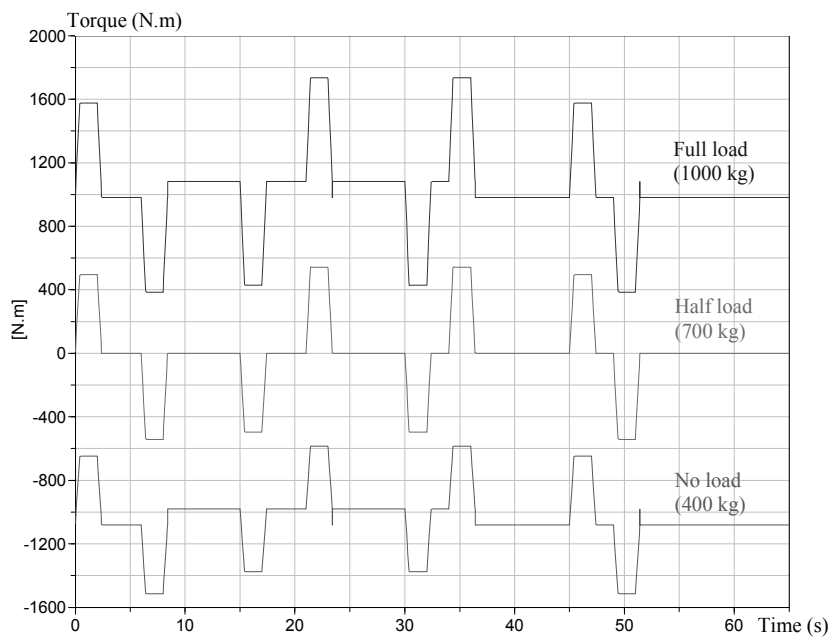


Figure 10 – Torque for different loads

3.2. Architectures and reference components

Following these initial results, we can already observe that:

- The application requires positive and negative force and speed : the drive must be able to manage four quadrants of the torque-speed plane;
- The electrical power can be positive and negative : power electronics should be able to manage the reverse power (by reversibility or braking resistors);
- The most restrictive case for power and force is the fully loaded elevator: we will use this case for sizing the lift drive;
- The highest rotational speeds are of the order of 55 rpm for this cycle with a pulley diameter of 70 cm: the electric motor may be combined with a reduction gear or be direct drive and then have high torque / low speed characteristics.

Two configurations will be evaluated:

- a combination of cylindrical brushless motor and planetary gearbox;
- a gearless torque motor .

In both cases, a power off brake is added to hold the car when its speed is zero.

Scaling laws and the references used for these components are summarized in Tables 2, 3 and 4. More information about how the laws were established and validated are given in Paper 1 [17]. The reference components may be specific designed components. In this example, we use industrial components in order to compare the results of the estimation models with constructors' data.

Parameters	Units	Cylindrical motor	DANAHER BH626E480
<i>Definition parameters</i>			
Nominal electromagnetic torque	Nm	$T_{em,nom}^* = l^{*3.5}$	25,6 N.m
Supply voltage	V	$U^* = n^* l^*$	480 V AC
<i>Integration parameters</i>			
Length and diameter	m	$l^* = T_{em,nom}^{*/3.5}$	367,8 mm (length) 142 mm (diameter)
Mass	kg	$M^* = T_{em,nom}^{*/3.5}$	23,1 kg
<i>Simulation parameters</i>			
Inertia	$kg.m^2$	$J^* = l^{*5} = T_{em,nom}^{*/3.5}$	$3,04.10^{-3} kg.m^2$
Thermal resistance	K/W	$R_{th}^* = l^{*2} = T_{em,nom}^{*-2/3.5}$	0,36 K/W
Thermal capacitance	J/K	$C_{th}^* = l^{*3} = T_{em,nom}^{*/3.5}$	5518 J/K
Thermal time constant	min	$\tau_{th}^* = l^{*1} = T_{em,nom}^{*/3.5}$	33 min
Copper losses coefficient	$W/(Nm)^2$	$\alpha_{th}^* = l^{*-5} = T_{em,nom}^{*-5/3.5}$	$1,53 W/(N.m)^2$
Iron losses coefficient	$W/(rd/s)^b$	$\beta_{th}^* = l^{*3} = T_{em,nom}^{*/3.5}$	$12,62.10^{-3} W/(rd/s)^b$
<i>Operating area</i>			
Max. torque	Nm	$T_{em,max}^* = T_{em,nom}^*$	87,1 N.m
Max. transient speed (mechanical limit)	rpm	$\Omega_{abs,max}^* = l^{*-1} = T_{em,nom}^{*-1/3.5}$	3850 rpm
Max. continuous speed (iron losses)	rpm	$\Omega_{cont,max}^* = l^{*-1/b} = T_{em,nom}^{*\frac{-1}{3,5b}}$	6500 rpm

Table 2 – Cylindrical brushless motor: scaling laws and reference

Parameters	Units	Annular motor	ETEL TMB0291-050
<i>Definition parameters</i>			
Nominal electromagnetic torque	Nm	$T_{em,nom}^* = l^{*3}$	101 N.m
Supply voltage	V	$U^* = n^* l^{*3} \omega_{elec,max}^*$	600 V DC
<i>Integration parameters</i>			
Length and diameter	mm	$l^* = T_{em,nom}^{*1/3}$	100 mm (length) 310 mm (diameter)
Mass	kg	$M^* = T_{em,nom}^{*2/3}$	20 kg
<i>Simulation parameters</i>			
Number of poles pairs	-	$p^* = l^* = T_{em,nom}^{*1/3}$	22
Inertia	$kg.m^2$	$J^* = T_{em,nom}^{*4/3}$	$39.10^{-2} kg.m^2$
Thermal resistance	K/W	$R_{th}^* = T_{em,nom}^{*-2/3}$	0,27 K/W
Thermal capacitance	J/K	$C_{th}^* = T_{em,nom}^{*2/3}$	$10,2.10^3 J/K$
Thermal time constant	s	$\tau_{th}^* = 1$	45 min
Copper losses coef.	$W/(Nm)^2$	$\alpha_{th}^* = l^{*-4} = C_{em,nom}^{*-4/3}$	$3,65.10^{-2} W/(N.m)^2$
Iron losses coef.	$W/(rad/s)^b$	$\beta_{th}^* = l^{*2+b} = T_{em,nom}^{*2+b/3}$	$0,487 W/(rad/s)^b$
		$P_{pertes} = \underbrace{\alpha}_{P_l} T_{em}^2 + \underbrace{\beta}_{P_{fer}} \omega^b$	
<i>Operating area</i>			
Max. torque	Nm	$T_{em,crête}^* = T_{em,max}^*$	416 N.m
Max. continuous speed (iron losses)		$\Omega_{cont,max}^* = T_{em,nom}^{*-1/3}$	800 rpm
Max. transient speed (mechanical limit)	rpm	$\Omega_{abs,max}^* = T_{em,nom}^{*-1/3}$	-
Max. voltage speed (voltage supply limit)		$\Omega_{elec,max}^* = U^* n^{*-1} l^{*-3}$	950 rpm

Table 3 – Annular brushless motors: scaling laws and reference

Parameters	Unit	Planetary gear reducer (n_s stages)	Redex Andantex SRP1 (1 stage)
<i>Definition parameters</i>			
Nominal torque	$N.m$	Nominal torque of stage i $T_{i,nom}^* = \frac{T_{n_s,nom}^*}{k \left(1 - \frac{1}{p}\right) \left(1 - \frac{i}{n_s}\right) \eta^{n_s-i}}$, $i < n_s$ With a global reduction ratio k	370 N.m
Reduction ratio			Reduction ratio 7
<i>Integration parameters</i>			
Length (l) and diameter (d)	m	$d_i^* = T_{i,nom}^{*/3}$	170 mm (length) 179 mm (diameter)
Mass	Kg	$l_i^* = T_{i,nom}^{*/3}$, $l_i \geq l_{i,min}$ $M_i^* = l_i^{*3} = T_{i,nom}^*$	13,8 kg
<i>Simulation parameters</i>			
Inertia	$kg \cdot m^2$	$J_i^* = l_i^{*3} = T_{i,nom}^{*5/3}$	$6,5 \cdot 10^{-4} kg \cdot m^2$
Torsional stiffness	$N.m/rad$	$K_i^* = l_i^{*3} = T_{i,nom}^*$	515 kN.m/rad
<i>Operating area</i>			
Max. Torque	Nm	$T_{max}^* = T_{n_s,nom}^*$	650 N.m
Max. transient speed (mechanical limit) and max. continuous speed (fatigue)	rad/s	$\Omega_{max}^* = l_i^{*-1} = T_{1,nom}^{-1/3}$	5000 rpm (mechanical limit) and 1600 rpm (fatigue)

Table 4 – Planetary gear reducers: scaling laws and reference

3.3. Preliminary analyses using graphical nomograms

In the case under study, the accelerations of the mission profile can induce motor rotor inertia torque and significantly influence the total electromagnetic torque. A graphical analysis of the mission profile can assess the importance of this effect even before the application is sized. Scaling laws enable the analysis nomograms to be built. Figure 11 shows the characteristic point of the lift drive system with:

- x-axis : corner power product of the maximum speed by the maximum torque (generally not achieved simultaneously);
- y-axis : the power rate product of the maximum torque by the maximum acceleration.

These two quantities are preserved through the transmission ratio (neglecting losses of reducer gear) and enable the technological capabilities of the motors to be compared directly, without presupposing a reduction ratio.

The corner power and the power rate can be evaluated using scaling laws:

$$P_{max}^* = T_{max}^* \Omega_{max}^* = l^{*3,5} l^{*-1} = l^{*2,5} \text{ and } T_{max}^* \left(\frac{d\Omega}{dt} \right)_{max}^* = \frac{T_{max}^{*2}}{J_{max}} = \frac{l^{*7}}{l^{*5}} = l^{*2} \quad (21)$$

These two quantities are related, for cylindrical brushless motors, by the equation:

$$T_{max}^* \left(\frac{d\Omega}{dt} \right)_{max}^x = P_{max}^{*2/2,5} \quad (22)$$

and, for annular brushless motors, by the equation:

$$T_{\max}^* \left(\frac{d\Omega}{dt} \right)_{\max}^* = l^{*3} l^{*-1} = l^{*2} = P_{\max}^* \quad (23)$$

The last two relationships (22) and (23) are represented in Figure 11 with logarithmic coordinates, through networks of straight lines. Such networks represent the proportion of the maximum torque of the motor used to provide the acceleration required by the application depending on the corner power. From this nomogram, we can deduce that the elevator is not constrained from the dynamic point of view, because the load is very dominant in terms of kinetic energy. Specific inertia of the motor contributes far less than 1% to the total electromagnetic torque.

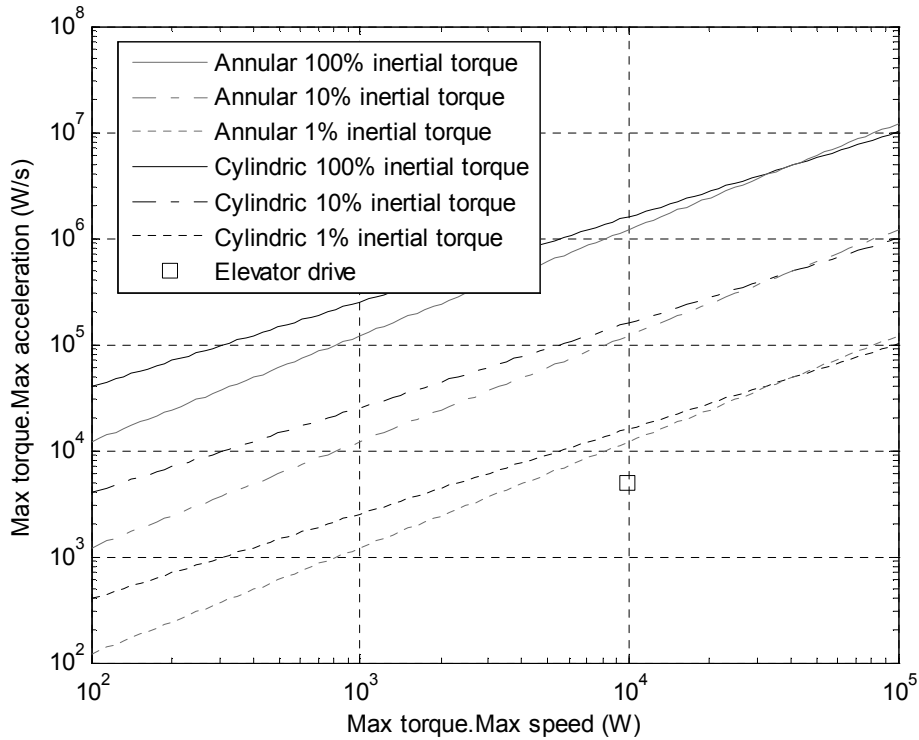


Figure 11 – Evaluation of effect of inertia on electromagnetic torque

For the architecture with a reducer, the gear ratio is therefore not based on inertia and will be chosen so as to use the electric motor just below its maximum operating speed. The latter is a function of the torque and may also be linked to the corner power:

$$\Omega_{\max}^* = l^{*-1} = \left(T_{RMS}^* \Omega_{\max}^* \right)^{-1/2,5} \quad (24)$$

Figure 12 depicts this relationship graphically. Neglecting the losses of the gear reducer, the point corresponding to the RMS torque (see paragraph 3.4) and the maximum speed of the load can be found on the nomogram without presupposing the reduction ratio. The maximum motor speed can thus be estimated at 4150 rpm. Knowing the maximum speed of the load and the maximum speed of the motor, we can deduce a reduction ratio and start selecting components. The following calculations will be made with a reduction ratio of 75.

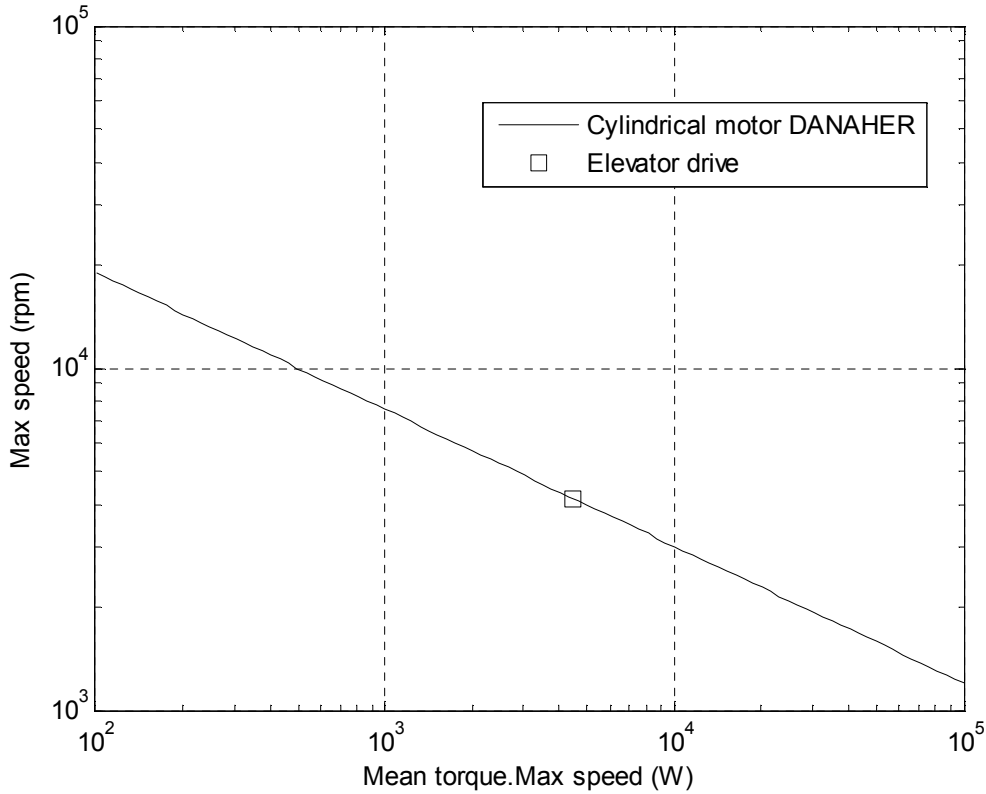


Figure 12 – Maximal speed and reduction ratio estimation

3.4. Components selection and specification

The selection of components of the architecture requires the main sizing quantities to be computed, such as the maximum torque and speed or the representative quantities for thermal or mechanical stress. More details about these quantities are given in Chapter 3. These values required by the application can then be compared to manufacturers’ data. Scaling laws allow an evaluation of these components parameters to be obtained and accelerate the design process by avoiding roundtrips between the calculations and the search for components’ characteristics, especially when there is no data catalogue. An estimate of these characteristics from a known component can also help to specify the design of a specific component.

For gearless architecture, it is important to check the thermal behavior of the motor. The Joule losses are proportional to the square of the electromagnetic torque and can be evaluated through the Root Mean Square (RMS) torque when the thermal inertia of the motor is sufficient to smooth the temperature variations during the operating cycle. The thermal time constants of motors are several tens of minutes which are high compared to the 65 seconds of the mission profile. For the elevator application, a parking brake relieves the motor during stops and, in these conditions, the RMS torque at the pulley is:

$$T_{RMS} = \sqrt{\frac{1}{t_{profile}} \int T^2(t).dt} = 760 \text{ N.m} \tag{25}$$

From this torque value it is possible to estimate the main characteristic of the motor based on data of Table 3. Here we choose a nominal torque of 806 Nm in order to compare the results with an industrial component (Table 5).


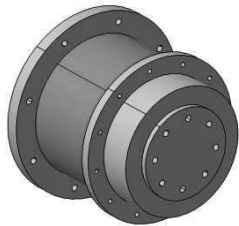
	Scaling laws results	Similar industrial component: Annular brushless motor ETEL TMB0530
Definition torque	806 N.m	806 N.m
Max. torque	3320 N.m	3320 N.m
Max. speed (thermal limit)	400 rpm	350 rpm
Thermal time constant	45 min	58 min
Mass	80,5 kg	94 kg
Inertia	0.62 kg.cm ²	0.92 kg.m ²
Diameter	620 mm	565 mm
Length	200 mm	160 mm

Table 5 – Annular brushless motor of the gearless lift drive

The gear reducer must be selected to withstand the maximum and average torques. The mean torque corresponding to mechanical fatigue is calculated as for the bearings using the following formula:

$$T_{RMC} = \sqrt{\frac{1}{\Omega_{mean} t_{profile}} \int |C^3(t) \cdot \Omega(t)| dt} = 1175 \text{ N.m} \quad (26)$$

Depending on the desired reliability and on the average speed, torque may be weighted. Here we choose a nominal torque of 1370 Nm in order to compare the estimates of scaling laws with catalogue data (Table 6). The RMS torque of the motor is 10.7 Nm. We then choose a motor of 11.1 Nm in order to also compare the results with the catalogue data (Table 6).

	Scaling laws results	Similar industrial component: Planetary gear reducer Redex Andantex SRP3
Low speed shaft torque	1370 N.m	1370 N.m
Reduction ratio	75	65
Stage number	2	2
Max. speed	5130 rpm	5000 rpm
Mass	64 kg	76 kg
Diameter	277 mm	300 mm
Length	328 mm	319 mm

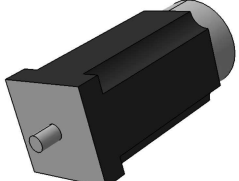
	Scaling laws results	Similar industrial component: Cylindrical brushless motor DANAHER BH-424-D
Definition torque	11,1 N.m	11,1 N.m
Max. torque	37,7 N.m	37,5 N.m
Max. speed (mechanical limits)	4060 rpm	3700 rpm
Thermal time constant	26 min	25 min
Mass	11.3 kg	12.5 kg
Inertia	9.2 kg.cm ²	6.6 kg.cm ²
Diameter	112 mm	130 mm
Length	290 mm	369 mm

Table 6 – Gear reducer and brushless motor of the geared lift drive

The main simplifying assumptions made for these models are material similarity and geometric similarity. Components in catalogues do not always strictly follow the latter assumption, often for reasons of economic rationalization. It follows that the estimate made by the scaling law is a possible component but not exactly the component present in the catalogue.

3.5. Geometrical integration

Scaling laws can be used to assess integration parameters such as mass or volume and can therefore contribute in an interesting way to preliminary studies of geometric integration. In the case of the elevator, attention is paid to the dimensions of the unit to avoid the use of a machine room on the roof. Figure 13 shows the relative dimensions of the solutions, based on data obtained from simulations, compared to the dimensions of the pulley. This CAD draft may serve as a starting point for stronger integration between bearings, actuator and pulley. We can see that the gearless solution seems the most promising in terms of integration as its a smaller lateral dimension facilitates direct integration into the sheath.

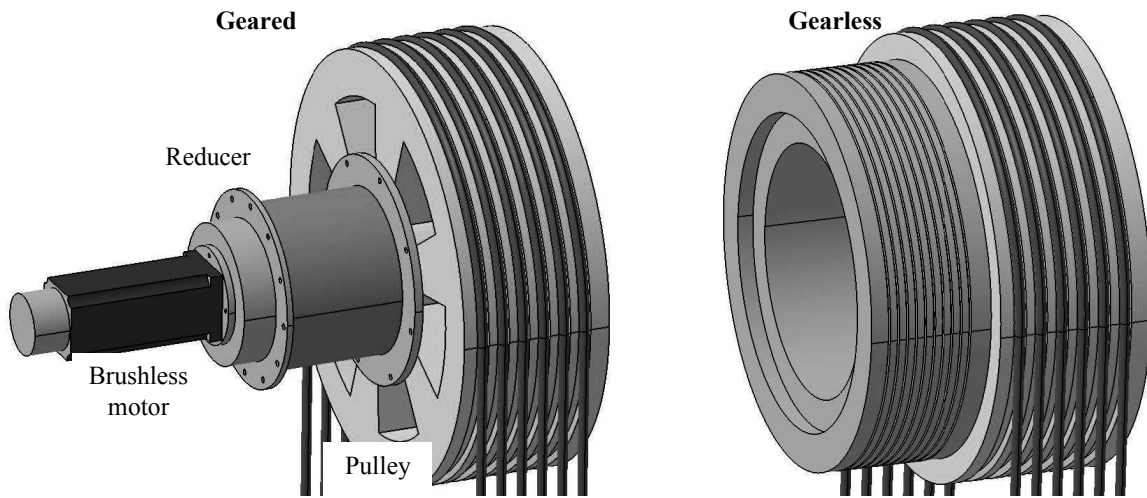


Figure 13 – Geometrical integration: architectures comparison

3.6. Estimation of simulation parameters

It may be helpful to complete the preliminary design studies with 0D/1D simulations using lumped parameter dynamic models. The parameters useful for the simulation can be estimated using the scaling laws. For the example studied, the concept of RMS torque (equation (25)) takes only into account the copper losses for a given external temperature. Thus a thermal study may be interesting in order to evaluate the effects of copper losses, iron losses and the external temperature. Figure 14 shows the a simple thermal model for which the scaling laws of Table 2 and 3 are used to estimate the heat capacity C_{th} , the thermal resistance R_{th} . The losses are estimated with the equation:

$$P_{losses} = \overbrace{\alpha_{th} \cdot T_{em}^2}^{P_{copper}} + \overbrace{\beta_{th} \cdot \Omega^b}^{P_{iron}} \tag{27}$$

where the copper losses (P_{copper}) are proportional to the square of the electromagnetic torque, while the iron losses (P_{iron}) are a function of the electrical frequency, i.e. the angular velocity:

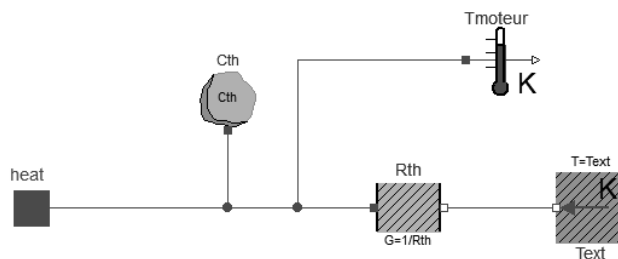


Figure 14 – One-body thermal model

The simulations performed on the mission profile, depending on the torque and speed of the motor, show that:

- for the solution with an annular motor, the iron losses are small relative to copper losses as the motor is used in a low speed range (55 rpm) compared to its maximum potential (400 rpm). An ambient temperature of 40°C, above the rated ambient temperature of 20°C, induces a higher temperature than the 130°C allowed by the technology. It is necessary to select a motor of 840 Nm, and not 760 Nm.
- for the geared solution, the motor is used over its entire speed range and iron losses then play a more important role. These additional losses induce a temperature of 200 ° C with a motor of 10.7 Nm. Selecting a 11.5 Nm motor decreases to 180°C, an admissible value for this technology.

3.7. Design space exploration

The estimation models can also be used to explore the design space and the influence of different design choices, such as gear ratios, or given requirement specifications. In the example, the radius of the pulley can have a significant effect on the size of the actuator. The radius of the pulley is limited by the curvature that is possible for the steel cables, but new technologies, such as flat belts, allow these radii to be greatly reduced. Figure 15 provides a graphical summary of the sizing when the diameter of the pulley varies from 70 to 10 cm. The CAD drawing presents a simplified view of what could be the gearless solution for the smallest pulley diameter.

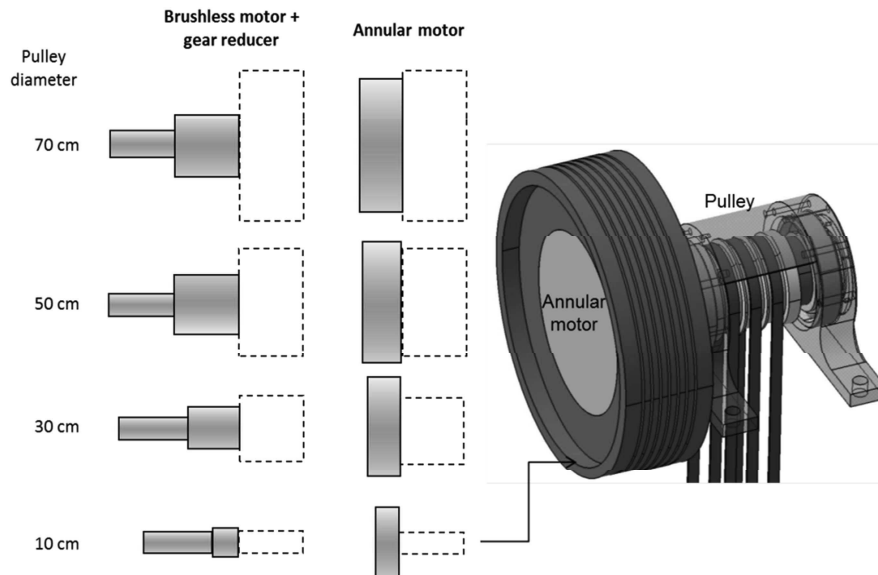


Figure 15 – Geometrical integration for different pulley radii

4. UNCERTAINTY AND SCALING LAWS

4.1. Limitations of scaling laws

Scaling laws have characteristics that make them attractive for the design of mechatronic systems [18] [19] [20]. Their simple form makes them easy to manipulate and customize as they require only one reference to determine the multiplier coefficient k , the power coefficient a being determined by the physical phenomena. They have a monotonous progression valid over a wide range of sizes (several orders of magnitude) which avoids the risk of possible mathematical aberrations of metamodels used outside their construction bounds.

However they have some limitations. Although the similarity of the materials can be easily verified for a given technology, the geometric similarity is not necessarily verified or sought. For motors (Figure 5), this point mainly explains the estimation errors of scaling laws in Figure 5. Manufacturers may tend to use the same motor diameter (i.e. the same iron sheet) for different lengths and torques (as illustrated by the Δ points of Figure 3) for economic reasons. Obtaining a scaling law also requires a dominant physical phenomenon.

For example, in the case of the electric motor, if the conductive heat transfer phenomenon cannot be neglected, relations (9) and (10) should take the form:

$$f\left(\underbrace{J, L, d_1, d_2, \dots, d_n}_{1+n}, \underbrace{\rho, \theta, h, \lambda_1, \lambda_2, \dots}_m\right) = 0 \quad (28)$$

which gives

$$f'\left(\frac{\rho J^2 L}{h\theta}, \underbrace{\frac{d_1}{L}, \frac{d_2}{L}, \dots, \frac{d_n}{L}}_n, \underbrace{\frac{\lambda_1}{hL}, \frac{\lambda_2}{hL}, \dots}_m\right) = 0 \quad (29)$$

with λ_i the thermal conductivities of the various materials of the motor.

If this had been the case, either it would have been impossible to establish a global scaling law or its domain of validity would have been smaller.

A first way to overcome these limitations is to obtain more accurate scaling laws taking more parameters into account, such as form factors and more physical phenomena. Paper 4 shows how to obtain them from finite element simulations. A second way is to model the uncertainty in order to quantify the possible errors when using scaling laws. The purpose of this section is to determine the laws that can be used to model these uncertainties. To do this, we will rely on the analysis of the relative errors compared to data from industrial catalogues.

4.1. Form of statistical laws

We focus, here, on the form of laws that can be used to represent the uncertainties within scaling laws. A scaling law is a relationship of the form:

$$y_{est} = kx^a \quad (30)$$

where x is the variable definition and y_{est} is the estimated parameter of the component considered.

This relationship predicts the characteristic y of a component with an error ε :

$$y = y_{est}(1 + \varepsilon) \quad (31)$$

The quantity ε is modeled here as a random variable. Sources of error are multiple: not following the geometric similarity assumption (for a potentially large number of dimensions), not taking design constraints into account, changing material properties and physical properties, etc. The distribution commonly used to model phenomena representing multiple random events is the normal law. The corresponding probability density is the Gaussian distribution and is expressed by the relationship:

$$f(\varepsilon) = \frac{1}{\sigma\sqrt{2\pi}} e^{-\frac{1}{2}\left(\frac{\varepsilon-\mu}{\sigma}\right)^2} \quad (32)$$

with μ the mean and σ the standard deviation.

Figure 16 shows the distribution of the relative error for the estimated bearing mass according to the static load. The scaling law has the form of equation (17) where k is calculated for a reference component taken in mid-range. The definition of the middle of a range will be given more precisely in the section 4.2. The distributions of errors calculated for 150 SKF bearings (radial ball bearings) are shown in Figure 16. These errors correspond to the data shown in Figure 6.

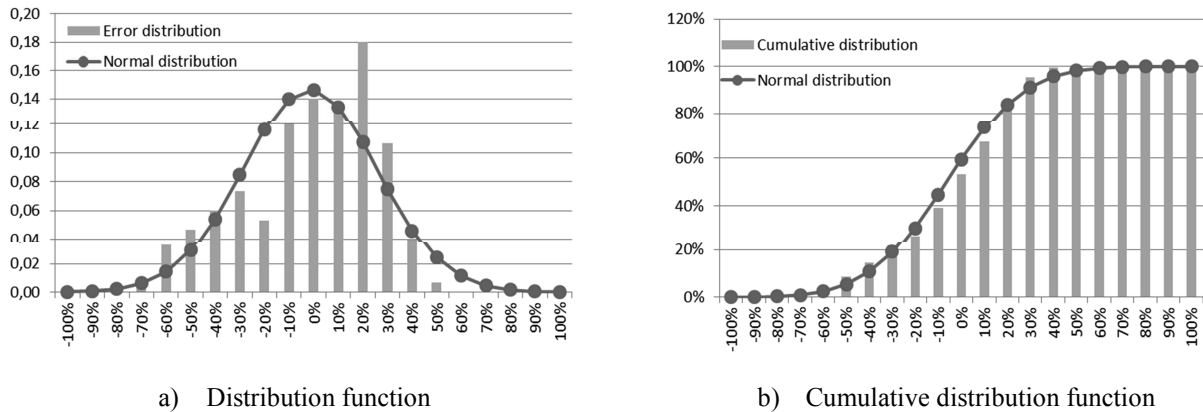


Figure 16 – Comparison of error distribution to a normal law

To assess the adequacy of the observed distribution to a Gaussian distribution, a Henry diagram can be used. This graphical method adjusts a series of observations to a Gaussian distribution along a straight line and the mean and standard deviation of such a distribution can be read quickly. Figure 17 confirms that the distribution of the previous error can be modelled by a normal distribution with a mean of -3% and a standard deviation of 14%.

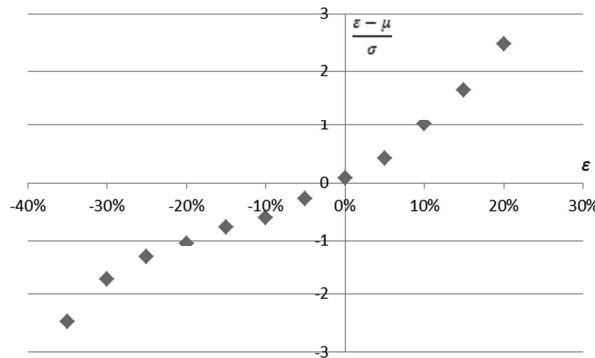


Figure 17 – Henry diagram

Several questions could now be asked:

- Can the different errors be considered as independent or linked?
- Can the esperance be always assumed to be zero or low?
- What variance should be adopted? Does the value depend on the characteristics handled?

The following sections will answer these questions by a study of industrial data ranges and finally give simple examples of the use of these distributions in the sizing process.

4.1. Correlation between errors

The implementation and effect of the uncertainty estimation models depends on whether the different random variables representing estimation errors are independent or not. If all the variables are highly correlated, their uncertainty can be represented by a single random variable. Otherwise, the error of each parameter should be represented by its own random variable. This dependency can be studied using a correlation analysis on the estimation errors. The Figure 18 corresponds to correlations between the diameter, mass and inertia for three ranges of brushless motors.

a) Etel motors (TMB range)

	diameter	mass	inertia
diameter	1		
mass	-0.439	1	
inertia	0.647	-0.683	1

b) Parvex motors (NX range)

	diameter	mass	inertia
diameter	1		
mass	0.711	1	
inertia	0.832	0.653	1

c) Kollmorgen motors (BH range)

	diameter	mass	inertia
diameter	1		
mass	0.457	1	
inertia	-0.260	-0.827	1

Figure 18 – Correlation between errors

It may be noted that, although the variables can be correlated, the correlation value is never the same. It is therefore difficult to draw a general conclusion. Without information, it seems best to assume that the errors are independent.

4.2. Influence of choice of reference on the mean error

The mean estimation error is mainly influenced by the choice of the reference. It is therefore interesting to analyse the variation of the mean error based on the choice of the reference. Figure 19 shows the variation of the mean error of the mass estimation according to the torque of the reference motor (for Kollmorgen PMAC motors, BH range). We clearly see that the error tends to be smaller when the reference is located on the geometric mean of the extremes of the range:

$$X_m = \sqrt{\max(x_i) \min(x_i)} \tag{33}$$

with X_m the geometrical mean of the reference, x_i the value of the definition parameters.

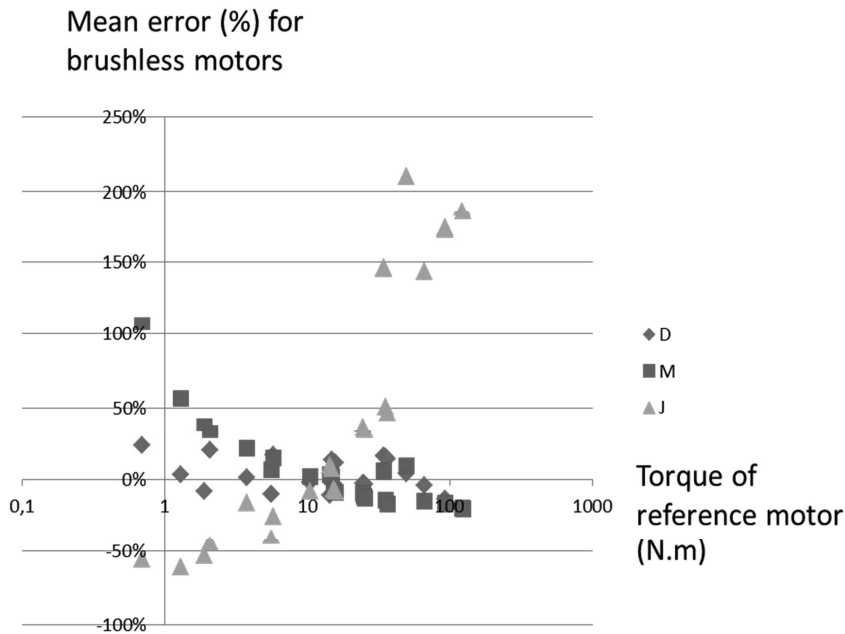


Figure 19 – Mean errors according to reference chosen (Kollmorgen, BH range)

For this choice of reference, the average errors are small enough to be treated as zero. This conclusion remains true for other ranges of components. It is therefore possible to assume that, for components not too far (a decade around the reference) from the reference, the mean of the distribution of error is zero:

$$\mu = 0 \tag{34}$$

4.3. Standard deviation

The error variance takes different values depending on the quantities estimated. As scaling laws take the form of a power law of a geometric dimension, uncertainty on a dimension may be amplified if the power is greater than 1. It thus seems interesting to evaluate the standard deviations of the errors according to the power of the scaling laws. Figure 20 shows the variation of the standard deviation for all references of the range NX from Parvex, a manufacturer of PMAC motors.

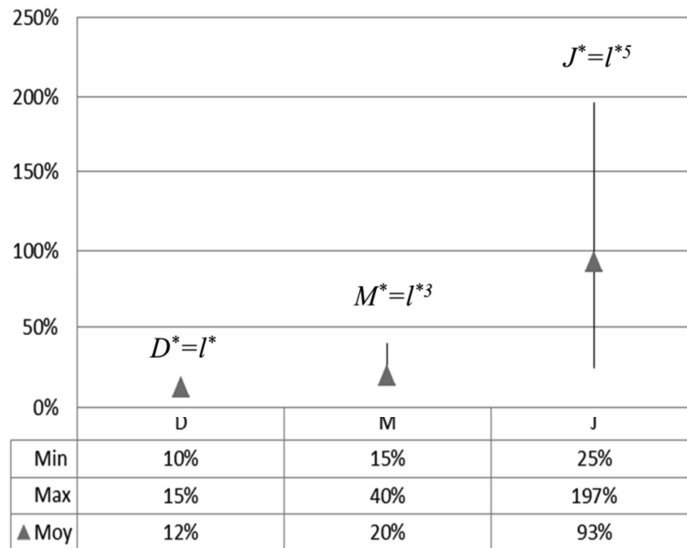


Figure 20 – Standard deviation according to parameter type

Figure 20 confirms that the potential error is greater if the power of the scaling law is higher. For quantities linked directly to geometrical parameters, if no more information it is available, robustness studies or sensitivity analyses can assume that uncertainties follow the power of the scaling laws: such as 10% for diameter, 30% for mass, 50% for inertia, etc. For quantities linked to geometrical parameters but also related to several technology limitations or design choices, the risk of uncertainty is greater. For example, the maximum motor speed can vary considerably as shown in Figure 21. The maximum speed can be selected on the criterion of mechanical strength or for electrical matching with an inverter. Before analysing the data, it may be interesting to apply a filter such as a Pareto front in order to keep only the best components.

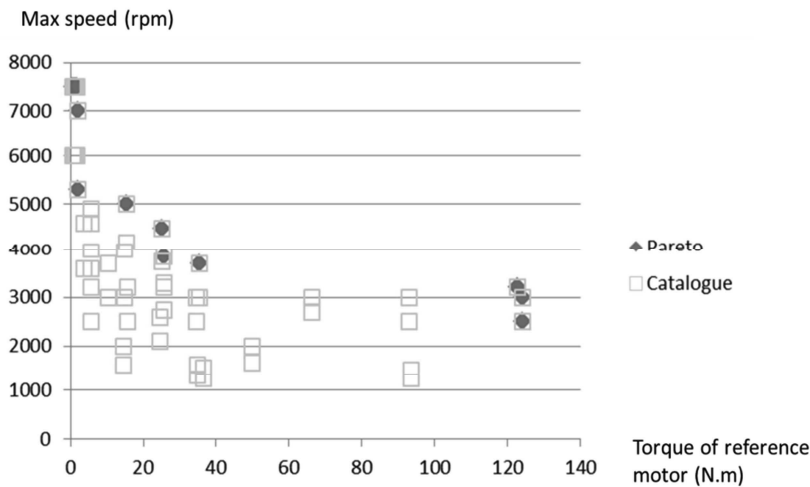


Figure 21 – Maximum speed versus torque for BH Kollmorgen brushless motors

4.4. Examples of effects of uncertainties of estimation models during preliminary design

The preliminary design aims to specify the components of an architecture from the requirements of the complete system. The estimation models enable the characteristics of a possible component to be obtained in order to perform sizing or optimization. The associated calculations are deterministic in nature. The proposed component, which can be used for the specifications, may not correspond to the one that will actually be made. It may be interesting to add studies to assess firstly the risk of that changes in characteristics of the components imply for the performance of the entire system. The models proposed in this section can be used to establish the magnitude of uncertainty associated with each parameter. If performances is highly sensitive to certain characteristics of components, it may be interesting to determine an acceptable range for these characteristics and enrich the components specifications in order to mitigate the development risks.

To illustrate this process, Table 7 shows the specifications and sizing results for a linear actuator. The calculations carried out here are very simple and are used primarily to illustrate trends or concepts. For example, the performance of the mechanical transmission chain is assumed to be 100%. During the sizing, the use of scaling laws can address the issue of selecting the gear ratio to minimize the mass of the motor. Depending on the circumstances, the choice may be made:

- If the inertial effects of the rotor are negligible, as in case a) of the aileron, use the motor within its maximum speed range to minimize the torque. In this case, the reduction ratio is given by:

$$N = k_{\Omega}^{7/5} F_{max}^{-2/5} v_{max}^{-7/5} \quad (35)$$

with k_{Ω} enabling the maximal speed of the motor to be estimated:

$$\Omega_{max} = k_{\Omega} T_{max}^{-1/3.5} \quad (36)$$

- If the inertial effects are important, as in case b) of thrust vector control, adapt load and motor inertias by means of a good choice of reduction ratio. In this case, the reduction ratio is given by:

$$N_{opti} = k_J^{-7/4} F_{max}^{-3/4} a_{max}^{-7/4} \quad (37)$$

with k_J enabling the rotor inertia of the motor to be estimated:

$$J_{mot} = k_J T_{max}^{5/3.5} \quad (38)$$

The corresponding values and components parameters are given in Table 7.

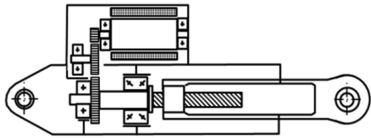
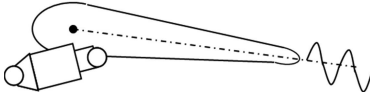
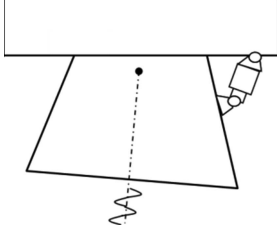
Linear EMA	a) Aileron actuator	b) TVC actuator
		
Specifications		
Static force	20 kN	40 kN
Inertia	200 kg	800 kg
Displacement magnitude	3 mm	10 mm
Frequency	0.5 Hz	5 Hz
No load max speed	20 mm/s	200 mm/s
Max sinusoidal speed (v_{max})	20 mm/s	314 mm/s
Max acceleration (a_{max})	29.6 mm/s ²	9870 mm/s ²
Maximum force (F_{max})	20 kN	47.9 kN
Sizing		
Reduction ratio (N)	76750 rad/m	1015 rad/m
Motor torque	0.26 N.m (mean)	95 N.m (max)
Rotor inertia	8.28 10 ⁻⁶ kg.m ²	4.73 10 ⁻³ kg.m ²

Table 7 – Linear actuator specifications and sizing

If the mean characteristics of the components are now fixed on the result of this design, it is possible to look at the effect of estimation error on system performance. The orientation of the calculations is no longer

in the same direction and can provide the achievable acceleration with the corresponding uncertainty: a 50% uncertainty on the motor inertia induced uncertainty of 0.2% in the case of the aileron and 39% for the case of TVC actuator. These two examples illustrate that a high uncertainty on the characteristics of a component can have negligible or significant effects depending on the type of application. In the case of TVC, it seems important to specify the motor more precisely by adding to the torque an inertia requirement with a tolerance. If an uncertainty of 5% is acceptable in terms of acceleration, it is possible to deduce a tolerance of about 6.5% over the inertia.

The previous example illustrated the effect and possible treatment of a single uncertainty. In the general case, the standard deviation of performance may be due to a combination of multiple uncertainties. If we take the example of a design criterion aimed at verifying the increase of temperature (θ_{rise}) over a short time (t) and limited by the thermal capacity of the windings (C_{th1}) for a given torque (T):

$$\theta_{rise} = C_{th1}^{-1} P_{th} t = C_{th1}^{-1} \alpha T^2 t \quad (39)$$

The uncertainty for the temperature rise depends on the uncertainty of the thermal capacity (C_{th1}) and the thermal loss coefficient (α):

$$\sigma_{\varepsilon T_{rise}} = \sqrt{\sigma_{\varepsilon C_{th1}}^2 + \sigma_{\varepsilon \alpha}^2} \quad (40)$$

If this uncertainty is too large, two approaches are possible:

- If we assume that the variables are independent: specify tolerances for both C_{th} and α assuming, for example, that these tolerances are proportional to the uncertainties initially assumed:

$$\sigma_{TC_{th1}} = k \cdot \sigma_{\varepsilon C_{th1}} \text{ and } \sigma_{T\alpha} = k \cdot \sigma_{\varepsilon \alpha} \text{ with } k = \frac{\sigma_{T\theta_{rise}}}{\sqrt{\sigma_{\varepsilon C_{th1}}^2 + \sigma_{\varepsilon \alpha}^2}} \quad (41)$$

This approach allows the tolerances to be adjusted depending on the type characteristics but gives narrow tolerances on component characteristics if the acceptable uncertainty ($\sigma_{T\theta_{rise}}$) for the temperature is low.

- If more magnitude is necessary on these characteristics: request a design that correlates these variables, assuming, for example, that

$$\varepsilon_{C_{th1}} = \varepsilon_{\alpha} \quad (42)$$

In this case, whatever the variations of the parameters, the temperature remains constant.

5. CONCLUSION

The estimation models presented in this chapter help in the preliminary system design of mechatronic power transmissions. These models, based on scaling laws, are used to estimate the main characteristics of mechatronic components. They do not replace the detailed design models specific to each technology, as they rely on simplifying assumptions such as geometric similarity, but they can quickly extrapolate the characteristics of a known component to the desired component that uses the same technology. This modeling methodology can be applied to various physical domains and different design constraints. The same reasoning can therefore be applied in the study of a complete mechatronic system. The associated article, Paper 1, illustrates how to obtain scaling laws for the typical components of electromechanical actuators. The parameters from these models can be used for different types of analyses during preliminary design. This chapter has also presented how to model and handle uncertainty associated with these low complexity models.

6. BIBLIOGRAPHY

- [1] P. Krus, «Performance Estimation Using Similarity Models and Design Information Entropy,» chez *Workshop on Performance Prediction in System-Level Design, International Design Engineering Technical Conference and Computers and Information in Engineering Conference (IDETC/CIE)*, 2008.
- [2] F. Roos, H. Johansson et J. Wikander, «Optimal selection of motor and gearhead in mechatronic applications,» *Mechatronics*, vol. 16, n° 11, pp. 63-72, 2006.
- [3] F. Messine, B. Nogarede et J.-L. Lagouanelle, «Optimal Design of Electromechanical Actuators: A New Method Based on Global Optimization,» *IEEE transactions on magnetics*, Vols. %1 sur %2vol. 34, no. 1, 1998.
- [4] *ControlEng, ServoSoft software, www.controleng.ca.*
- [5] T. Simpson, J. Peplinski, P. Koch et J. Allen, «Metamodels for Computer-Based Engineering Design: Survey and Recommendations,» *Engineering with Computers*, vol. Vol. 17, pp. pp. 129-150, 2001.
- [6] G. Pahl et W. Beitz, *Engineering Design: A Systematic Approach*, Springer, Éd., 2007.
- [7] M. Jufer, «Design and Losses - Scaling Law Approach,» chez *Nordic Research Symposium Energy Efficient Electric Motors and Drives, Skagen, Denmark.*, 1996.
- [8] G. Ricci, «Mass and rated characteristics of planetary gear reduction units,» *Meccanica*, vol. vol. 27, pp. pp. 35-45, 1992.
- [9] G. Ricci, «Weight and rated characteristics of machines: positive displacement pumps, motors and gear sets,» *Mechanism and Machine Theory*, vol. vol. 18, pp. pp. 1-6, 1983.
- [10] B. Multon, H. Ben Ahmed, M. Ruellan et G. Robin, «Comparaison du couple massique de diverses architectures de machines tournantes synchrones à aimants,» chez *Société de l'Electricité, de l'Electronique et des Technologies de l'Information et de la Communication (SEE)*, pp. 85-93, 2006., 2006.
- [11] K. J. Waldron et C. Hubert, «Scaling of robotic mechanisms,» chez *IEEE International Conference on Robotics & Automation, San Francisco, CA.*, 2000.
- [12] J. Cros et P. Viarouge, «Synthesis of High Performance PM Motors With Concentrated Windings,» *IEEE TRANSACTIONS ON ENERGY CONVERSION*, Vols. %1 sur %2Vol. 17, n°. 2, 2002.
- [13] T. Jahns et W. Soong, «Pulsating Torque Minimization Techniques for Permanent Magnet AC Motor Drives-A Review,» *IEEE TRANSACTIONS ON INDUSTRIAL ELECTRONICS*, Vols. %1 sur %2Vol. 43, n° 2, 1996.
- [14] G. Murphy, *Similitude in engineering*, The Ronald press company. New York, 1950.
- [15] E. S. Taylor, *Dimensional Analysis for Engineers*, Oxford University Press, 1974.
- [16] M. Budinger, J. Liscouët, F. Hospital et J.-C. Maré, «Estimation models for the preliminary design of electromechanical actuators,» *Proceedings of the Institution of Mechanical Engineers, Part G: Journal of Aerospace Engineering*, vol. 226, n° %13, pp. 243-259, 2012.
- [17] M. Budinger, J. Liscouët, J. Maré et others, «Estimation models for the preliminary design of electromechanical actuators,» *Proceedings of the Institution of Mechanical Engineers, Part G: Journal of Aerospace Engineering*, vol. 226, n° %13, pp. 243-259, 2012.
- [18] M. Pfenning, F. Thielecke et U. Carl, «Recent Advances Towards an Integrated and Optimized Design of High-lift Actuation Systems,» chez *SAE Int. J. Aerosp.* 3(1):55-64, 2010, doi:10.4271/2009-01-3217., 2010.

- [19] M. Petersheim et S. Brennan, «Scaling of hybrid-electric vehicle powertrain components for Hardware-in-the-loop simulation,» *Mechatronics*, vol. 19, p. pp 1078–1090, 2009.
- [20] J. Liscouet, M. Budinger, J.-C. Maré et S. Orioux, «Modelling approach for the simulation-based preliminary design of power transmissions,» *Mechanism and Machine Theory*, vol. 46, n° 13, pp. 276-289, 2011.

Paper 1 - Estimation models for the preliminary design of electro-mechanical actuators

ABSTRACT

This paper presents estimation models for the model-based preliminary design of electro-mechanical actuators. Models are developed to generate all the parameters required by a multi-objective design, from a limited number of input parameters. This is achieved by using scaling laws in order to take advantage of their capability to reflect the physical constraints driving the actuator's component sizing. The proposed approach is illustrated with the major components that are involved in aerospace electromechanical actuator design. The established scaling laws provide the designer with parameters needed for integration into the airframe, power sizing, thermal balance, dynamics and reliability. The resulting estimation models are validated with industrial data.

Keywords: electro-mechanical actuator, estimation model, more electric aircraft, model-based design, preliminary design, scaling laws, power-by-wire.

Referencing: M Budinger, J Liscouët, F Hospital, and J-C Maré, *Estimation models for the preliminary design of electromechanical actuators*, Proceedings of the Institution of Mechanical Engineers, Part G: Journal of Aerospace Engineering, March 2012.

Estimation models for the preliminary design of electromechanical actuators

M Budinger^{1*}, J Liscouët^{1,2}, F Hospital¹, and J-C Maré¹

¹Institut Clément Ader, Université de Toulouse, Toulouse, France

²Fly By Wire, Bombardier Aerospace, Montréal, Quebec, Canada

The manuscript was received on 16 December 2010 and was accepted after revision for publication on 11 April 2011.

DOI: 10.1177/0954410011408941

Abstract: This article presents estimation models for the model-based preliminary design of electromechanical actuators. Models are developed to generate all the parameters required by a multi-objective design, from a limited number of input parameters. This is achieved using scaling laws in order to take advantage of their capability to reflect the physical constraints driving the actuator's component sizing. The proposed approach is illustrated with the major components that are involved in aerospace electromechanical actuator design. The established scaling laws provide the designer with parameters needed for integration into the airframe, power sizing, thermal balance, dynamics, and reliability. The resulting estimation models are validated with industrial data.

Keywords: electromechanical actuator, estimation model, more electric aircraft, model-based design, preliminary design, scaling laws, power-by-wire

1 CONTEXT

The current technical developments in aviation aim to make aircraft more competitive, greener, and safer. The more electric aircraft offers interesting perspectives in terms of performance, maintenance, integration, reconfiguration, ease of operation, and management of power [1]. Using electricity as the prime source of energy for non-propulsive embedded power systems is considered by aircraft makers as one of the most promising means to achieve the above-mentioned goals. Actuation for landing gears and flight controls is particularly concerned as it is one of the main energy consumers. This explains why, during recent years, a great effort has been put into the development of Power-by-Wire (PbW) actuators at research level (e.g. POA, MOET, and DRESS European projects). This recently enabled PbW actuators to be introduced in the new generation of commercial aircraft [2, 3], in replacement of

conventional servohydraulic ones (e.g. Boeing B787 EMA brake or spoiler, Airbus EHA, and EBHA). On their side, space launchers are following the same trend for thrust vector control (TVC), as illustrated by the European VEGA project [4] and NASA projects [5]. However, these technological step changes induce new challenges, especially for the preliminary design process for actuation systems and components, which cannot simply duplicate former practices. Moreover, up to now, optimizing the aerospace actuators has not been consistent with the systematic use of generic and standard (off-the-shelf) components as is the case for industrial applications. Therefore, specific actuator components are specified for each new project. In consequence, the actuator design loop requires significant time, particularly for the architectural trade-off of numerous candidate solutions. To accelerate the design process [6, 7], a general trend is to extend the role of modelling in design and specification [8, 9]. In the frame of this evolution, this study aims to propose efficient, simple prediction models as enabling tools for quick and easy preliminary design of electromechanical actuators.

*Corresponding author: Université de Toulouse, INSA/UPS, Institut Clément Ader, Toulouse 31077, France.
email: marc.budinger@insa-toulouse.fr

Section 2 sums up the state of the art to make a need assessment of models to predict both the nature of technological components and the parameters to be calculated. The beginning of section 3 describes the various methodologies for implementing estimation models and the modelling assumptions of the methodology proposed in this article. Section 4 addresses the main design drivers of the components of electromechanical actuator (EMA). The laws derived from these constraints are then used in section 5 to establish models for the components and parameters defined in section 2. Section 5.3 validates these models on constructors' data. Section 6 gives examples of possible applications of these estimation models.

2 NEEDS FOR PREDICTION MODELS

From the overall requirements, the preliminary design task should allow candidate solutions to be synthesized, assessed, and compared before decisions are taken and detailed design starts. These overall requirements include, in particular, the following.

1. Functional requirements for the different operation modes, as inputs to the architecture design task that must define which types of component are involved and how they are organized. This topic is addressed in section 2.1.
2. Performance requirements and design constraints, as inputs to the multi-objective sizing of the components. Section 2.2 lists the relevant parameters or characteristics of components required for these different design steps.

2.1 What components for aerospace electromechanical actuators?

As contributors to the safety of embedded critical functions, aerospace actuators are subject to specific design requirements. In electromechanical PbW solutions, high-reduction ratios between the motor and the load cannot be avoided in response to the low torque density of electric motors. Reliability requirements are usually met at the expense of multiple redundancies. Depending on the application, as the ultimate safety mode of operation, the load may have to be held in position (no motion), or its free motion may have to be damped. Based on recent examples [4, 5, 10–16], Table 1 summarizes the main components that are involved in PbW aerospace actuators in response to these constraints. The last line of Table 1 points out the components that have been considered as sufficiently generic to make the development of dedicated estimation

models worthwhile. The objective of these models is to provide tools that enable a quick evaluation of different actuators architectures during the preliminary design.

2.2 What parameters for the preliminary design?

The actuator design is driven by the following main aspects to meet the various requirements: integration (mass, geometrical envelope) between airframe and actuated load, resistance to environment (thermal and vibration) [17], instant power and energy saving, dynamic performance, service life, reliability, and resistance to or tolerance of failures. When dealing with these various topics in a model-based way, the designer often fails to obtain the relevant parameters of the component models rapidly. In order to generate the estimation model from a reduced number of key data, these parameters are proposed to categorize as follows.

1. Integration parameters, required to evaluate the masses and major dimensions of the components.
2. Simulation parameters, required for sizing from a dynamic simulation of the mission profile (e.g. inertia or moving mass, heat capacity, and reducer compliance).
3. Operating domain parameters, required to verify the component use with respect to, e.g. service life or safe operating areas.

Table 2 is used to help the categorize component characteristics (columns) according to the multiple design tasks (lines), which are generally considered individually, as illustrated by the bibliographical references. In the following sections, all the parameters listed in this table will be derived from key design parameters, called definition parameters here, to make the estimation model as versatile as possible.

3 ESTIMATION MODELS FOR SYSTEM-LEVEL DESIGN

3.1 Estimation models

As described in section 2.2, the system-level design steps require models (Fig. 1(a)) directly linking primary characteristics, which define the component functionally, to secondary characteristics, which can be seen as the features of imperfections [27]. Generally, at component level, the models (Fig. 1(b)) link the physical dimensions and characteristics of materials used to the primary and secondary characteristics. The design at component level is an inverse problem which requires the primary

Table 1 Part count of aerospace electromechanical actuator major components

Application, project and references	Main function: move mechanical load			Management of reliability requirements (only effects on power transmission)	Management of specific modes of operation
	Convert electrical power into mechanical power	Adapt power output to load kinematics	Transmit power to the load		
US X38 Crew Return Vehicle project: Flap actuator [10]	Three high speed brushless motors	One bull gear One cycloidal reducer	One arc shape segment of a wheel Three rollers	Dual-fault tolerance (two electrical failures) → Duplex active-active architecture	Stand thermal environment while exposed to re-entry conditions → No spherical bearing on the flap
US NASA research program: TVC actuator [5, 11]	Two or four cylindrical brushless motor	One or two stages spur gear reducer	One roller screw Two spherical bearings	Idem	Prevent vibrations and resonance effects at engine start → Active damping through electrical force feedback
European Vega Launcher: P80 TVC actuator [4]	One cylindrical brushless motor	Three-stage spur gears	One roller screw Two spherical bearings	Short mission (2 min) → Simplex architecture	Idem → load sensor integrated in tailstock
German 'InHus' project (Helicopter CH-53G): Individual Blade Control Actuator [12]	One cylindrical brushless motor	One cycloidal reducer	Information not available	Dual-fault tolerance (two electrical failures) → Brushless motor with three redundant electrical sections	Bandwidth, energy recovery between actuators → No information available
US EPAD project (F18 aircraft): Aileron actuator [13, 14]	Two brushless motors	Two spur gears One single stage speed summing	One ball screw Two spherical bearings	Fault tolerance → Duplex architecture, velocity-summing differential Structural impact protection → Skewed roller clutch into differential	Prevent flutter with a trail damped mode → Permanent magnetic damping of the brushless motors
European DRESS project: Nose-Landing Gear Steering Actuator [15, 16]	Two brushless motors	Two cycloidal reducers	One worm gear	Jamming tolerance → Duplex active-active architecture with torque summing and clutch	Free castoring → Clutch throwout
French MELANY project: nose landing gear extension/retraction actuator [16]	One torque brushless motor One power off brake	Direct transmission	Roller screw Spherical bearing	Jamming tolerance → Duplex architecture, if jamming, a brake releases the emergency mechanical path	Emergency mode, free fall → Damping achieved by a magnetic device
Components	Brushless motors (cylindrical or annular)	Spur gear reducer Cycloidal reducer Gearbox reducer Pinions for speed or torque summing	Roller and ball screw Spherical bearing Axial and radial load bearings	Pinions Clutch Brake	Clutch Brake

Table 2 Component parameters used for the different preliminary design views

Parameters or characteristics of components	Integration				Simulation				Operating domain			
	Corresponding design or sizing viewpoints	Mass	Length/diameter	Stroke	Ratio/Pitch	Inertia	Stiffness/backlash	Fricition/Efficiency	Electrical parameters	Thermal parameters	Max torque or speed	Rated torque or speed
Integration	Mass [18] Geometrical envelope [18, 19] Transient stress [12]	⊗	⊗	⊗ ⊗						⊗		
Mechanical resistance	Fatigue/thermal/wear stress [20] Vibration [14, 21]			⊗			⊗			⊗		⊗
Reliability	Lifetime/MTBF/failure rate [20] Failure/critical cases: winding short circuit, jamming, and shock [5, 14]	⊗	⊗	⊗		⊗	⊗			⊗	⊗	⊗
Dynamic/control	Natural modes [22]				⊗	⊗	⊗					
Power/energy	Bandwidth [4] Precision [23] Transient input power [24] Energy consumption [25, 26]				⊗	⊗	⊗		⊗		⊗	⊗

Note: MTBF, mean time between failures.

characteristics as inputs. This inversion may be done through design codes from design mechanical standards [23], by algebraic solvers or by optimization algorithms [28]. At system level, this approach requires very significant expertise for each component. It is therefore cumbersome to implement and it shrinks the component range to a reduced number of candidate technologies.

A first direct approach consists of using databases as is done in some design software packages [29]. Its main disadvantage is that it is cumbersome or even impossible to implement in the absence of a product range as is the case in the aerospace field. Although it is interesting for optimization, data mining combined with response surface modelling [30] seems inappropriate here for the same reason. The use of scaling laws, also called similarity laws or allometric models, has the advantage of requiring only one reference component for a complete estimation of a product range. Such a modelling approach has already been used with success for component design or comparison of technologies [31–35]. This approach is developed here for system-level design with the components defined in section 2.1, since it appears to be the most appropriate means of speeding up the preliminary design of aerospace actuators.

3.2 Main assumptions

Scaling laws study the effect of varying representative parameters of a component compared with a known reference. This article uses the notation proposed by Jufer [31]. The x^* scaling ratio of a given parameter is calculated as

$$x^* = x/x_{ref} \tag{1}$$

where x_{ref} is the parameter taken as the reference and x the parameter under study.

The scaling laws reduce the complexity of the inversion problem of Fig. 1(b) using two key modelling assumptions on the input parameters.

1. All material properties are assumed to be identical to those of the component used for reference. All corresponding scaling ratios are thus equal to 1. For example, $E^* = \rho^* = 1$ with E^* and ρ^* being, respectively, the variation of the Young's modulus and density of the material.
2. The ratio of all the lengths of the considered component to all the lengths of the reference component is constant. Used in range definition [36], this geometric similarity assumption leads to dimension scaling ratios that are all identical and equal to a dimension variation, noted l^* here.

Using scaling laws reduces the number of inputs, as shown in Fig. 2(a). It is then easy to express all the useful relations (section 2.2) as a function of a key design parameter that is associated with the component under design. We propose to call it the definition parameter, according to the layout of the proposed estimation model, Fig. 2(b). The remainder of this article will describe how to obtain these parameters by pointing out the main assumptions and the physical or design drivers that are at the origin of the relevant scaling law. The scaling laws supporting parameter estimation will be given as tables in section 5.

3.3 Direct effect of geometrical similarity on parameters

The parameters representing geometric quantities can be directly derived from the assumption of geometric similarity. For example, the variation of the volume V of a shaft (cylinder) of length l and radius r , in the case of identical variation for all geometrical dimensions ($r^* = l^*$) is

$$V^* = \frac{V}{V_{ref}} = \frac{\pi r^2 l}{\pi r_{ref}^2 l_{ref}} = r^{*2} l^* = l^{*3} \quad (2)$$

This result remains valid for any other geometry. In the same way, it is possible to calculate the variation of the mass, M , and rotational moment of inertia, J , of the shaft

$$\begin{cases} M = \int \rho_m dV \Rightarrow M^* = l^{*3} \\ J = \int r^2 dM \Rightarrow J^* = l^{*5} \end{cases} \quad (3)$$

where ρ_m is the mass density of the shaft.

3.4 Different ways of finding the scaling laws

The scaling laws can be obtained in different ways. Three of them will be illustrated using the example of the thermal time constant of an electric motor. It is assumed here that the motor temperature rise is uniform and is mainly due to convection between the stator and the air (this assumption can be refined, cf. section 5.2.1).

3.4.1 Direct approach

The first approach [31] directly uses the analytical expression for the quantity under study. The thermal time constant τ_{th} can thus be expressed by

$$\tau_{th} = R_{th} \cdot C_{th} \quad (4)$$

with R_{th} the thermal resistance and C_{th} the thermal capacity. As

$$R_{th} = 1/hS \Rightarrow R_{th}^* = l^{*-2} \quad (5)$$

with h the convection coefficient and S the thermal exchange surface and

$$C_{th} = c_v \cdot \rho \cdot M \Rightarrow C_{th}^* = l^{*3} \quad (6)$$

with c_v the thermal capacity density, ρ the density, and M the motor mass the corresponding scaling law for the thermal time constant becomes

$$\tau_{th}^* = l^* \quad (7)$$

3.4.2 Dimensionless number approach

A second approach uses the dimensionless number obtained from the ratio of power or energy [36, 37].

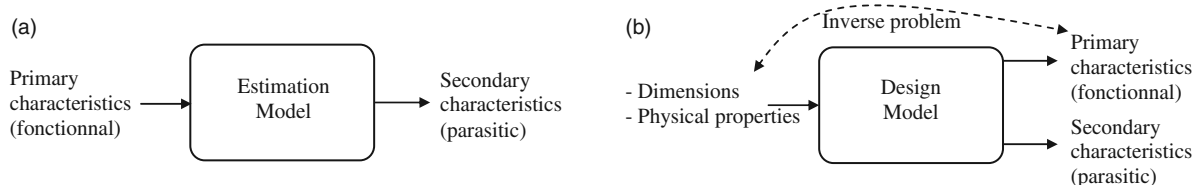


Fig. 1 Component models for (a) system-level and (b) component-level designs

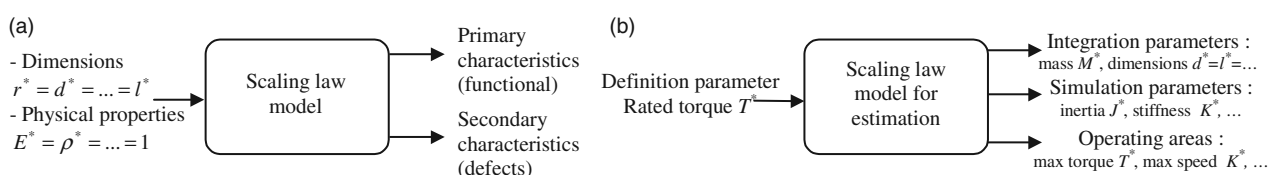


Fig. 2 Scaling laws models according to (a) dimension variation and (b) definition parameter

The dimensionless number corresponding to the present example, close to the Fourier number, is obtained as the ratio of the energy stored in a solid to the convective heat flux

$$\frac{\text{Energy rate of storage in solids}}{\text{Energy rate of convection}} = \frac{c_m \cdot l}{h \cdot t} \quad (8)$$

with t a characteristic time for the phenomena. This number is constant for

$$t = \frac{c_m \cdot l}{h} \quad (9)$$

Thus

$$\tau_{th}^* = l^* \quad (10)$$

3.4.3 Buckingham theorem approach

A third approach uses the Buckingham π theorem [38, 39] to obtain dimensionless π numbers. For our example, there is a relationship

$$f(\tau_{th}, d, l, h, c_v, \rho) = 0 \quad (11)$$

with d and l the diameter and the length of the motor, respectively.

Using the Buckingham π theorem, this relationship becomes

$$F\left(\frac{c_v \rho l}{h \tau_{th}}, \frac{l}{d}\right) = 0 \quad (12)$$

The assumption of geometric similarity reduces the π numbers to be considered. We thus find the relation

$$F\left(\frac{c_v \rho l}{h \tau_{th}}\right) = 0 \quad (13)$$

Thus

$$\frac{c_v \rho l}{h \tau_{th}} = C^{te} \quad (14)$$

and finally

$$\tau_{th}^* = l^* \quad (15)$$

4 MAIN DESIGN DRIVERS FOR ELECTROMECHANICAL COMPONENTS

Product ranges are usually defined using the same material stresses and the same design drivers. The induced relations link the dimensions with the different parameters (definition, integration, simulation, and operation area) associated with the components. This section summarizes these design drivers for electromechanical components and prepares the writing of estimation models of section 5.

4.1 Mechanical design drivers

4.1.1 Mechanical stress

For mechanical components, the mechanical stresses in the materials must be kept below elastic, fatigue, or contact pressure (Hertz) limits [40]. Taking the same stress limit σ [36] for a full product range yields

$$\sigma^* = 1 \Rightarrow F^* = l^{*2} \quad (16)$$

The dimensional analysis enables the transmitted force F , or the transmitted torque T to be linked with geometrical dimension for a rotational component

$$F^* = l^{*2} \Leftrightarrow T^* = l^{*3} \quad (17)$$

From the previous expression, the evolutions of the diameter, length, mass, inertia, and all other parameters can be expressed as a function of the transmitted nominal force F^* or torque evolution T^* .

The ratio between fatigue stress and maximum stress is fixed for a given material. In the case of a reducer, the absolute torque that the reducer can transmit corresponds to the maximum stress it can withstand. Therefore, the change in maximum peak torque T_{\max} is proportional to the change in nominal torque T_{nom}

$$T_{\max}^* = T_{\text{nom}}^* = T^* \quad (18)$$

4.1.2 Stress–strain relationship effects

For components with a maximal constant stress, the stress–strain relationship gives

$$\sigma = E \cdot \varepsilon \Rightarrow \Delta l^* / l^* = 1 \quad (19)$$

with E the Young's modulus.

This suggests that, for a given technology, a range of rotary components (e.g. gear reducers) has a constant backlash

$$\Delta \theta^* = \Delta l^* / l^* = 1 \quad (20)$$

and a stiffness that is proportional to the transmitted torque

$$K^* = T^* / \Delta \theta^* = T^* \quad (21)$$

4.1.3 Maximal speed of rotation

The maximal rotational speed ω_{\max} of a mechanical component can be limited by mechanical constraints induced by centrifugal forces or by axial or transverse vibrations. At high speeds, rotating components, e.g. permanent magnets of brushless motors, run a risk of

detachment due to centrifugal forces. Assuming all dimensions vary with the same ratio gives

$$\sigma_{centr}^* = \omega^{*2} \cdot l^{*2} \quad (22)$$

The resonance frequency f can be linked to density ρ , Young's modulus E , and dimension l using a dimensional analysis

$$f^* = \frac{1}{l^*} \sqrt{\frac{E^*}{\rho^*}} \quad (23)$$

With the assumptions $\sigma^* = E^* = \rho^* = 1$, these two equations provide the same scaling law for maximal speed

$$\omega_{max}^* = l^{*-1} \quad (24)$$

4.2 Electromagnetic design drivers

The main design driver of electromagnetic devices concerns their magnetic and electrical circuits.

4.2.1 Magnetic circuit with permanent magnets

For a magnetic circuit including permanent magnets, such as those encountered in brushless motors, the magnetic field can be high even with a significant air gap. The flux density in the common iron sheet must not exceed given values in order to avoid saturation and corresponding associated losses. A range of electromagnetic components must be sized with a constant maximal flux density. Hence

$$B^* = 1 \quad (25)$$

For a magnetic circuit involving a magnet characterized by a remanent magnetization B_r , a length L_m and an airgap of width e , the flux density can be expressed by the following relation [41]

$$B = B_r \frac{1}{1 + (e/L_m)} \Rightarrow B^* = 1 \quad (26)$$

The assumption of geometric similarity induces a constant magnetic field for an entire range of

products. The electromagnetic torque can therefore be deduced from the Laplace forces [31, 35]

$$T = \int JBr \, dv \Rightarrow T^* = J^* l^{*4} B^* = J^* l^{*4} \quad (27)$$

4.2.2 Magnetic circuits without permanent magnets

For magnetic circuits without permanent magnets, such as those encountered in clutches and brakes, air gaps must be small in order to get large magnetic fields. The mechanical constraints described in the preceding paragraph must also be taken into account. Assuming homothetic variation and using the notations of Fig. 3(b), the flux density can be expressed by the following relation [41]

$$B = JA_{co} \frac{1}{(e/\mu_0)(1 + (A_{iron}/\mu_r e))} \Rightarrow B^* = J^* l^* \quad (28)$$

The magnetic fields increase with machine size, which could lead to iron saturation. For small size magnetic circuits, the electromagnetic force is expressed by

$$F^* = J^* l^{*3} B^* = J^* l^{*4} \quad (29)$$

4.2.3 Electrical circuits

Electrical circuits including windings should be designed to make their operating voltage compatible with the power source or the power electronics. This voltage is related to the number of coil turns n . An analysis of the back emf constant K enables to find n as a function of the operating voltage U

$$K^* = \frac{U^*}{\Omega^*} = n^* l^{*2} B^* \Rightarrow n^* = \frac{U^*}{l^{*2} B^* \Omega^*} \quad (30)$$

The number of turns is also involved in the expressions for winding resistance and inductance

$$R^* = n^{*2} l^{*-1} \quad (31)$$

$$L^* = n^{*2} l^* \quad (32)$$

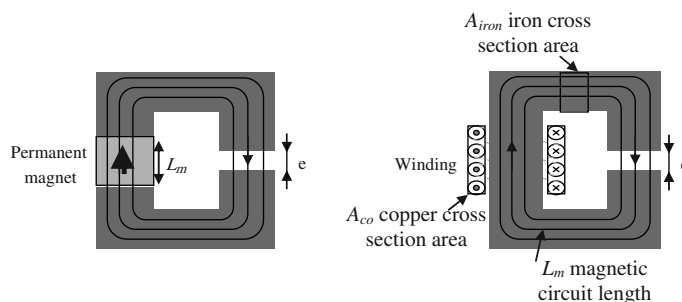


Fig. 3 Induction in magnetic circuit with (a) permanent magnet and (b) coil

4.3 Thermal design drivers

4.3.1 Temperature rise limits

Thermal stress is an important design driver for electromechanical components. The temperature rise of the winding insulation and of the lubricant of mechanical components must not exceed given temperatures if they are to operate correctly. The maximum temperature θ should be constant throughout a range of products, giving

$$\theta^* = 1 \quad (33)$$

For electromechanical components, the relationships between energy loss and temperature are established assuming a geometric similarity. Heat dissipation is essentially proportional to the convective surface area because the materials involved, mainly metals, are good thermal conductors. The temperature gradients are essentially localized at the outer surfaces for convection with the surroundings or at the insulation of the coils for conduction (the insulation thickness is constant for a given voltage range). Therefore

$$P_{\text{loss}}^* = l^{*2} \cdot \Delta\theta^* \Rightarrow P_{\text{loss}}^* = l^{*2} \quad (34)$$

The design constraints induced depend on the nature of the losses encountered.

4.3.2 Electromagnetic losses

For brushless motors or electromagnetic devices, the Joule effect is the main source of losses at low speed

$$P_{\text{loss, Joules}}^* = J_{el}^{*2} l^{*3} \quad (35)$$

with J_{el} the surface current density.

With a fixed maximum admissible temperature, the nominal current density in the conductors is thus expressed by [31]

$$J_{el}^* = l^{*-1/2} \quad (36)$$

The iron losses can become significant for higher speeds, especially in the brushless motors used in aerospace applications, with high speed or high torque and a large number of poles. Some brushless motors are thus not limited in speed by the centrifugal forces on the magnets but rather by the thermal constraints and iron losses. The losses of a motor are given mainly by the sum of the Joule losses P_J (copper) and iron losses, P_{iron}

$$P_{\text{loss, motor}} = P_J + P_{\text{iron}} \quad (37)$$

According to the Steinmetz-like formula provided in reference [42], the variation of the iron losses can be expressed as

$$P_{\text{iron}}^* = f^{*b} \cdot M_{\text{iron}}^* \quad (38)$$

where f is the electrical frequency and M_{iron} the iron mass.

Based on the study of Grellet [42], an average value of 1.5 can be considered for b . According to the thermal limit of the motor, the maximum iron losses $P_{\text{iron}, \omega_{\text{max}}}$ that occur at the maximum speed (when not limited by the centrifugal constraint) are equal to the maximum admissible power losses since no electromagnetic torque causes Joule losses (Fig. 8). Thus, the evolution of the f_{max} maximum electrical frequency with respect to the thermal limit is

$$f_{\text{max}}^* = l^{*-1/b} \quad (39)$$

Taking into account of the number of pairs of poles, the maximum admissible speed of a motor with respect to its thermal limit can be expressed easily.

4.3.2 Mechanical losses

Other sources of loss are the frictional losses in mechanical parts. These losses increase with speed, causing the temperature to rise. Consequently, the lubricant becomes more fluid, with degraded bearing properties that increase the friction coefficient. Beyond a critical temperature, i.e. at maximum speed ω_{max} , this phenomenon causes unacceptable wear damage. This speed limit is common to many mechanical components, e.g. rolling bearings, which are also present in screws or reducers

$$P_{th}^* = v^* \cdot F_{nom}^* = \omega^* \cdot l^* \cdot F_{nom}^* \Rightarrow \omega_{\text{max}}^* = l^* F_{nom}^{*-1} \quad (40)$$

5 EMA COMPONENT MODELS

This section describes estimation models for the electromechanical components of Table 1. The models are oriented to minimize entry definition parameters as proposed in Fig. 2(b). The bulk of the contribution of this section is contained in Tables 3 to 7.

5.1 Mechanical components

5.1.1 Bearings and ball/roller screws

Bearings and ball/roller screws, Fig. 4, are mainly modelled here assuming a constant admissible stress, as explained in section 4.1. Resulting scaling laws are given in Table 3.

Table 3 Established scaling laws for bearings and ball and roller screws

Parameter	Unit	Rolling bearings (incl. end-bearings)	Spherical bearing	Ball and roller screws (nut and screw)	Equation
<i>Definition parameter(s)</i>		Dynamic load capacity C_{nom} (N)	Nominal static load C_0 (N)	Nominal output force F_{nom} (N)	
<i>Integration parameters</i>					
Length, diameter, width and depth	M	$l^* = C_{nom}^{1/2}$	$l^* = C_0^{1/2}$	$l^* = F_{nom}^{1/2}$ (diameter)	(41)
Inner diameter	M	$d_{in} = d_{ext} - (F^*)^{1/2} \Delta d_{ref}$	$d_{in} = d_{ext} - (F^*)^{1/2} \Delta d_{ref}$	-	(42)
Mass	kg	$M^* = C_{nom}^{3/2}$	$M^* = C_0^{3/2}$	$M^* = F_{nom}^{3/2}$ (nut)	(43)
Mass per unit length	kg/m	-	-	$M_l^* = F_{nom}^*$ (screw)	
<i>Simulation parameters</i>					
Moment of inertia	kg.m ²	-	-	$J_n^* = F_{nom}^{5/2}$ (nut)	(44)
Moment of inertia per unit length	kg.m	-	-	$J_l^* = F_{nom}^2$ (screw)	(45)
<i>Operational limit parameters</i>					
Maximum force	N	$C_{max}^* = C_{nom}^*$	$C_{max}^* = C_0^*$	$F_{max}^* = F_{nom}^*$	(46)
Maximum speed	rad/s	$\omega_{max}^* = C_{nom}^{*-1/2}$	-	$\omega_{max,vib}^* = F_{nom}^{*1/2} \cdot I_s^{*-2}$ $\omega_{max,nut}^* = F_{nom}^{*-1/2}$	(47)

Table 4 Established scaling laws for gear assembly and worm gear reducers

Parameter	Unit	Pinion or wheel	Equation	Worm gear	Equation
<i>Definition parameter(s)</i>		Nominal torque T_{nom} (Nm) Number of teeth Z		Nominal output (wheel) torque T_{wh} (Nm) Internal wheel diameter $d_{wh,in}$ (m)	
<i>Integration parameters</i>					
Tooth module	M	$m^* = T_{nom}^{1/3} \cdot Z^{*-1/3}$	(48)		
Diameter	M	$d^* = m^* \cdot Z^* = T_{nom}^{1/3} \cdot Z^{*2/3}$	(49)	$d_{wh,ext}^* \Delta d_{wh}^* = T_{wh}^* 2/3$	(50)
Width	M	$b^* = m^* = T_{nom}^{1/3} \cdot Z^{*-1/3}$	(51)	$l_{wh}^* = d_{sc}^* = T_{wh}^* 1/3$ $l_{sc}^* = d_{wh,ext}^*$	(52)
Mass	kg	$M^* = d^{*2} b^* = T_{nom}^* \cdot Z^*$	(53)	$M_{ug}^* = T_{wh}^*$	(54)
<i>Simulation parameters</i>					
Moment of inertia	kg.m ²	$J^* = d^{*4} b^* = T_{nom}^{5/3} \cdot Z^{*7/3}$	(55)	$J_{ug}^* = T_{wh}^{5/3}$	(56)
<i>Operational limit parameters</i>					
Maximum torque	N.m	$T_{max}^* = T_{nom}^*$	(57)	$T_{wh,max}^* = T_{wh,nom}^*$	(58)
Maximum speed	rad/s	$\omega_{max}^* = \omega_{max,bearing}^*$	(59)	$\omega_{max}^* = \omega_{max,sc}^*$	(60)

Table 5 Established scaling laws for the speed reducers

Parameter	Units	Speed reducer - 1 stage Cycloidal, harmonic drive	Speed reducer - n stages Planetary gearboxes	Equation
<i>Definition parameter</i>		Nominal output torque T_{nom} (Nm) Transmission ratio k	Nominal output torque (Nm), stage number i $T_{i,nom}^* = \frac{T_{n_s,nom}^*}{k^{(1-\frac{1}{i})} (1-\frac{1}{n_s}) \eta^{n_s-i}}$, $i < n_s$ Total reduction ratio k	(66)
<i>Integration parameters</i>				
Length (l) and diameter (d)	M	$d^* = T_{nom}^{1/3}$ $l^* = T_{nom}^{1/3}$	$d_i^* = T_{i,nom}^{1/3}$ $l_i^* = T_{i,nom}^{1/3}$, $l_i \geq l_{i,min}$	(67) (68)
Mass	kg	$M^* = T_{nom}^*$	$M_i^* = T_{i,nom}^*$ or $M_i^* = T_{n_s,nom}^{2/3} \cdot l_i^*$	(69) (70)
<i>Simulation parameters</i>				
Moment of inertia	kg.m ²	$J^* = T_{nom}^{5/3}$	$J_i^* = T_{i,nom}^{5/3}$ or $J_i^* = T_{n_s,nom}^{4/3} \cdot l_i^*$	(71) (72)
Torsional stiffness	Nm/rad	$K^* = T_{nom}^*$	$K_i^* = T_{nom,i}^*$ or $K_i^* = T_{n_s,nom}^{4/3} \cdot l_i^{*-1}$	(73) (74)
<i>Operational limit parameters</i>				
Maximum torque	Nm	$T_{max}^* = T_{nom}^*$	$T_{max}^* = T_{n_s,nom}^*$	(75)
Maximum speed	rad/s	$\omega_{max}^* = T_{nom}^{-1/3}$	$\omega_{max}^* = T_{1,nom}^{-1/3}$	(76)

Table 6 Established scaling laws for brushless motors

Parameter	Units	Cylindrical motor	Annular motor	Equation
<i>Definition parameter</i>				
Nominal continuous torque	Nm	$T_{em,nom}^* = l^{*3.5}$	$T_{em,nom}^* = l^{*3}$	(78)
Operating voltage	V	$U^* = n^* l^*$	$U^* = n^* l^{*3} \omega_{elec,max}^*$	(79)
<i>Integration parameters</i>				
Length and diameter	m	$l^* = T_{em,nom}^{*1/3.5}$	$l^* = T_{em,nom}^{*1/3}$	(80)
Mass	kg	$M^* = T_{em,nom}^{*3/3.5}$	$M^* = T_{em,nom}^{*2/3}$	(81)
<i>Simulation parameters</i>				
Moment of inertia	kg·m ²	$J^* = T_{em,nom}^{*5/3.5}$	$J^* = T_{em,nom}^{*4/3}$	(82)
Joule loss coefficient	W/(Nm) ²	$\alpha^* = T_{em,nom}^{*-5/3.5}$	$\alpha^* = T_{em,nom}^{*-4/3}$	(83)
Iron loss coefficient	W/(rad/s) ^b	$\beta^* = T_{em,nom}^{*3/3.5}$	$\beta^* = T_{em,nom}^{*2+3/b}$	(84)
Thermal resistance(s)	K/W	$R_{th}^* = T_{em,nom}^{*-2/3.5}$	$R_{th}^* = T_{em,nom}^{*-2/3}$	(85)
Thermal capacitance(s)	J/K	$C_{th}^* = T_{em,nom}^{*3/3.5}$	$C_{th}^* = T_{em,nom}^{*2/3}$	(86)
Thermal time constant(s)	S	$\tau_{th}^* = T_{em,nom}^{*1/3.5}$	$\tau_{th}^* = 1$	(87)
Torque or emf constant	N/A or V/(rad/s)	$K^* = U^* T_{em,nom}^{*1/3.5}$	$K^* = n^* l^{*3} = T_{em,nom}^*$	(88)
Electrical resistances	⊗	$R^* = U^{*2} T_{em,nom}^{*-3/3.5}$	$R^* = n^{*2} l^{*2} = T_{em,nom}^{*2/3}$	(89)
Electrical inductances	H	$L^* = U^{*2} T_{em,nom}^{*-1/3.5}$	$L^* = n^{*2} l^{*2} = T_{em,nom}^{*2/3}$ if $n^* = 1$	(90)
<i>Operational limit parameters</i>				
Absolute maximum torque	Nm	$T_{em,peak}^* = T_{em,nom}^*$	$T_{em,peak}^* = T_{em,max}^*$	(91)
Absolute maximum speed (mechanical limit) Maximum speed (electrical limit)	rad/s	$\omega_{abs,max}^* = T_{em,nom}^{*-1/3.5}$	$\omega_{abs,max}^* = T_{em,nom}^{*-1/3}$ $\omega_{elec,max}^* = U^* n^{*-1} l^{*-3}$ $= U^* T_{em,nom}^{*-1}$ if $n^* = 1$	(92)
Continuous maximum speed (thermal limit)	rad/s	$\omega_{cont,max}^* = T_{em,nom}^{*-1/3.5}$	$\omega_{cont,max}^* = T_{em,nom}^{*-1/3}$	(93)

Table 7 Established scaling laws for electromagnetic clutches and brakes

Parameter	Units	Clutch and brake	Equation
<i>Definition parameter</i>			
Torque	Nm	$T^* = l^{*4}$	(94)
Operating voltage	V	$U^* = n^* l^{*1/2}$	(95)
<i>Integration parameters</i>			
Length and diameter	m	$l^* = T^{*1/4}$	(96)
Mass	kg	$M^* = T^{*3/4}$	(97)
<i>Simulation parameters</i>			
Moment of inertia	kg·m ²	$J^* = T^{*5/4}$	(98)
Loss	W	$P_{th}^* = T^{*1/2}$	(99)
Thermal resistance	K/W	$R_{th}^* = T_{em,nom}^{*-1/2}$	(100)
Thermal capacitance	J/K	$C_{th}^* = T_{em,nom}^{*3/4}$	(101)
Thermal time constant	S	$\tau_{th}^* = T_{em,nom}^{*1/4}$	(102)
Electrical resistance	⊗	$R^* = U^{*2} T^{*-1/2}$	(103)
Electrical inductance	H	$L^* = U^{*2}$	(104)
<i>Operational limit parameters</i>			
Absolute maximum torque	Nm	$T_{em,peak}^* = T_{em,nom}^*$	(105)
Absolute maximum speed	rad/s	$\omega_{abs,max}^* = T_{em,nom}^{*-1/4}$	(106)

5.1.2 Gear assembly and worm reducer

Gear assemblies and worm gearings, Fig. 5, are used to adapt the motor to the load impedance and also for

power summation or power split. Force summation allows duplex power paths or geometric adaptation to the load (distance between centres, interface with load, countershaft, etc.). Their description, even at preliminary level, may therefore require geometric

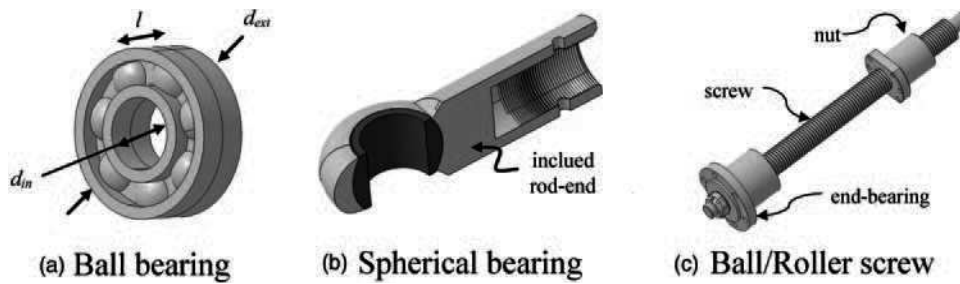


Fig. 4 Bearings and ball/roller screws: (a) ball bearing, (b) spherical bearing, and (c) ball/roller screw

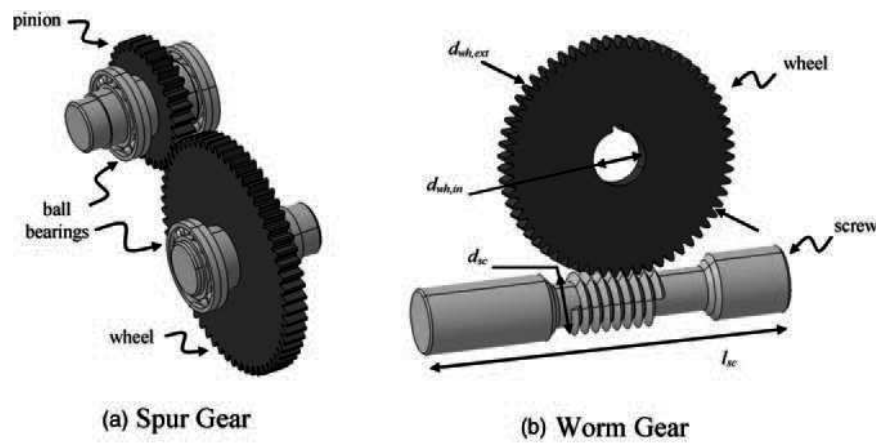


Fig. 5 Gear assembly and worm gear reducers: (a) spur gear and (b) worm gear



Fig. 6 Reducers and gear boxes [43–45]: (a) cycloidal drive, (b) harmonic drive, and (c) epicycloidal reducer

parameters to be used with increased attention. The assumption of geometric similarity is made here on the tooth or the screw thread which bears the mechanical stress.

By associating scaling law models, in particular for pinions and wheels as described in Table 4, a spur gear model can be built in agreement with the reduction ratio, the minimal number of pinion teeth and use of the same tooth module for pinion and wheel. In the same way, a worm gear scaling law can be defined. The ball bearing model of the previous section can also be used to complete this reducer definition.

5.1.3 Reducers and gearboxes

The estimation models can be used for planetary gear, harmonic drive [43], or cycloid drive reducers [44] (Fig. 6). Unlike harmonic and cycloid drives, planetary gearboxes involve multiple gear stages to provide high reduction ratios. Therefore, Table 5 distinguishes single-stage (or first stage) and multiple-stage reducers. Once again, the main modelling assumptions are the geometric similarity (section 3.3) and the range sizing at constant admissible stress (section 4.1).

For planetary (epicycloidal) gearboxes, the manufacturers' data show that each stage can reach a fixed maximum reduction ratio, $k_{i,\max}$ (e.g. 10 for the planetary gearings in reference [45]) due to geometrical interference. The overall reduction ratio k is assumed to be shared equally between the n_s stages here ($k_i = k^{1/n_s}$). On the one hand, the last stage ($i = n_s$, low speed shaft) is sized with respect to the torque to be transmitted. The scaling laws developed previously respect this requirement and therefore are applied to the last stage without changes. On the other hand, the torque values transmitted by the supplemental stages are significantly reduced. Their sizing is not only driven by the transmitted torque but also by fatigue phenomena. Therefore, these stages are sized to match the lifetime of the last stage with respect to fatigue. The lifetime and the associated cumulated damages Q_h , of a gearing with respect to fatigue is a function of its nominal torque and nominal speed, ω_{nom} [46]

$$Q_h = T_{nom}^p \cdot \omega_{nom} \quad (61)$$

where p is an experimental constant that is equal to 10/3 or 3 depending on the bearing technology.

Equalizing the cumulated damages of the i th stage of reduction (for $i < n_s$) with that of the last stage by considering the transmission ratio and mechanical efficiency of each stage gives

$$T_{i,nom}^* = \frac{T_{n_s,nom}^*}{k^{(1-\frac{1}{p})(1-\frac{1}{n_s})} \eta^{n_s-i}} \quad (62)$$

where $T_{i,nom}$ is the nominal torque of the i th stage. It should be noted that the fatigue constraint in the supplemental stages may be superseded by manufacturing or thermal constraints. There results a minimum length, l_{\min} , for a reduction stage. The total length of the planetary gear train is the sum of the stage lengths

$$l_{tot} = \sum_{i=1}^{n_s} l_i \quad (63)$$

A detailed analysis of manufacturers' catalogues shows two tendencies: the first one (69) where geometrical similarity is used for each stage, the second one (70) where, to rationalize production, outer diameters of the supplemental stages are imposed, identical to the last one in general. The total mass of the reducer is the sum of the stages masses.

In the same way, the inertia, J_i , of the i th supplemental stage is given by equation (71) or (72). The total equivalent inertia, J_{eq} , at the high speed shaft is

the sum of the stage equivalent inertias, with a reduction equally shared among the stages

$$J_{eq} = \sum_{i=1}^{n_s} \frac{J_i}{k^{2(i-1)/n_s}} \quad (64)$$

The torsional stiffness, K_i , of the i th supplemental stage is given by equation (73) or (74). The total equivalent stiffness K_{eq} at the low-speed shaft is the combination of the different stage equivalent stiffnesses $K_{i,eq}$

$$K_{eq} = \left(\sum_{i=1}^{n_s} K_{i,eq}^{-1} \right)^{-1}, \text{ where } K_{i,eq} = K_i \cdot k^{2(n_s-i)/n_s} \quad (65)$$

The mechanical limit to the maximum torque is given by the last stage of reduction, where this constraint is maximized. On the other hand, the limit to the maximum speed of the assembly is given by the first stage that has the smallest conductive surface area and the highest rotational velocity. Therefore, the expressions for the maximum peak torque (75) of the maximum admissible speed (76) are applied to the last and first stages, respectively.

5.2 Electromechanical components

5.2.1 Brushless motors

The permanent magnet brushless motor can have two different geometrical configurations:

- cylindrical (Fig. 7(a)) with a constant number of poles and homothetic variation of all the dimensions;
- annular (Fig. 7(b)) with an increasing number of poles and a constant ring thickness e , for an increasing radial dimension.

For both types of motors, the estimation models can be obtained under the same main assumption of a constant magnetic field, as described in section 4.2. However, the assumptions of geometric similarity differ and generate two different sets of relations, as presented in Table 6. Depending on the type of motor, the typical operational areas can also be different. As shown in Fig. 8, it can be interesting to distinguish the speed limit from original mechanical constraints (section 4.1) $\omega_{\text{abs,max}}$ from those of thermal origin (section 4.3) $\omega_{\text{cont,max}}$. In the latter case, it is important to take into account the general trend of losses. As explained in section 4.3, the Joule (or copper) losses are proportional to the square of the electromagnetic torque, while the iron losses, as

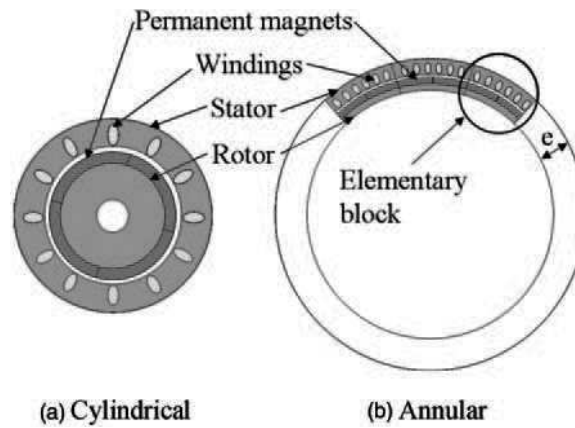


Fig. 7 Brushless motors (based on reference [35]): (a) cylindrical and (b) annular

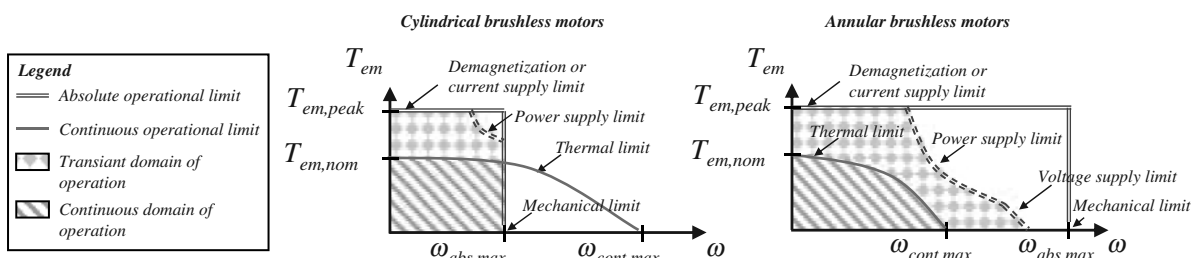


Fig. 8 Typical operational boundaries of cylindrical (left) and annular (right) brushless DC motors

given in reference [42], are a function of the electrical frequency, i.e. the angular velocity

$$P_{\text{loss, motor}} = \underbrace{\alpha \cdot T_{em}^2}_{P_j} + \underbrace{\beta \cdot \omega_{\text{rotor}}^b}_{P_{\text{iron}}} \quad (77)$$

where the coefficients α and β are the Joule and iron loss coefficients, respectively.

The estimated iron losses are also of importance when their damping effect (negative slope in torque/speed characteristic) is used to avoid flutter [14]. This loss model can be connected to one- or two-body thermal models (distinguishing the copper temperature from the iron temperature or not) [47], where the thermal resistances are proportional to the surface area and the thermal capacitances are proportional to the mass.

5.2.2 Electromagnetic clutches and brakes

The dimensions of electromagnetic clutches and brakes are mainly related to those of their electromagnet. The design criteria are therefore those described in section 4.2.3.

5.3 Validation of estimation models

Unlike the similarity laws obtained statistically [27], the form and the exponents of the relations

established in section 5 were justified by the physical considerations of section 4. These scaling laws have been compared with manufacturing company data [43–45, 48, 49] for validation. The proposed equations remain valid for extrapolating the performance of a single component. Figure 9(a) to (c) illustrates the interest of the estimation models for motors and reducers. The good agreement is also confirmed for other components. Log–log graphs have the advantage of covering a large definition range by giving straight lines as a result of the analytical form of the scaling laws. The slope of the log/log graph is given by the exponent of the power law while the selected reference product fixes a particular point of this curve

$$\begin{aligned} y^* = x^{*b} &\Rightarrow y = \frac{y_{\text{ref}}}{x_{\text{ref}}^b} x^b \Rightarrow \log(y) \\ &= \log\left(\frac{y_{\text{ref}}}{x_{\text{ref}}^b}\right) + b \cdot \log(x) \end{aligned} \quad (107)$$

Figure 9(a) to (c) validates the scaling laws established for mass, inertia, and maximal speed estimations. In the context of technology selection, it can be seen in Fig. 9(a) that all the three types of reducers studied have comparable torque/mass ratios, although the harmonic drives show the best characteristics, followed closely by the cycloid reducer. Motor data are plotted for framed cylindrical motors as well as frameless annular motors. The

latter, therefore, have an advantage with respect to mass considerations, partly for their hollow rotor shaft and absence of rotational bearings.

Figure 9(a) shows that the scaling laws established for the motors' thermal simulation parameters provide an efficient estimation of the effective values given by the manufacturer. The dispersion observed for annular motors comes from the non-homothetic scaling of the whole product range as designed by the manufacturer according to his catalogue. Different lengths of motors are proposed for a given diameter, allowing easy derivation of a given design to obtain an extended range. This is one limitation of the

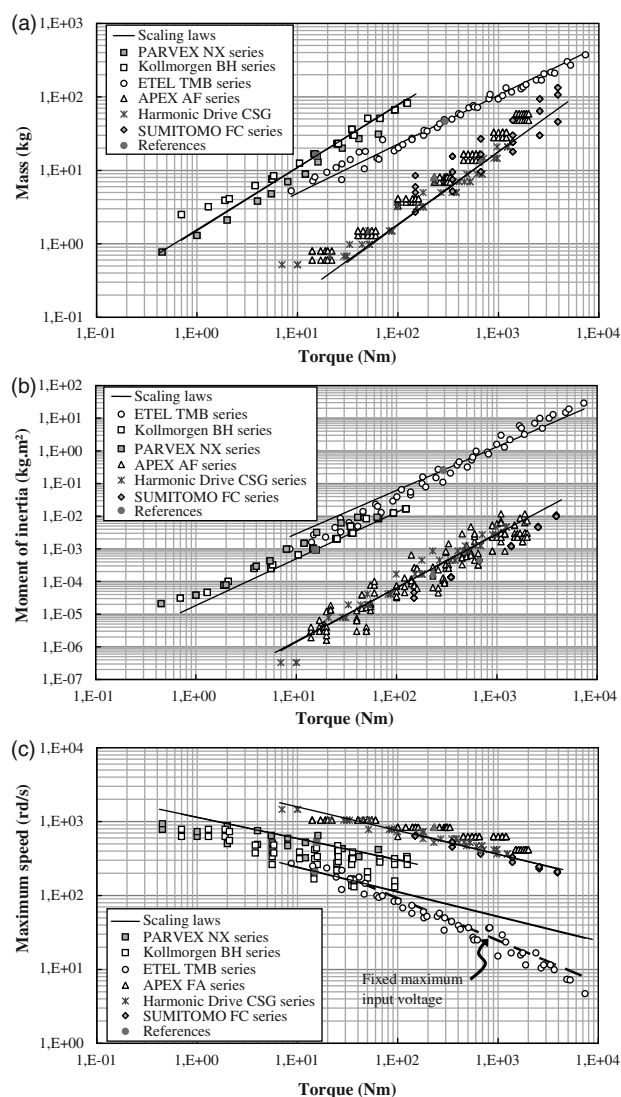


Fig. 9 Mass, inertia, and speed as a function of the nominal torque for brushless motors and reducers: (a) brushless motor and speed reducer masses as a function of the nominal torque, (b) brushless motor and speed reducer moments of inertia as a function of the nominal torque, and (c) maximum speed as a function of the nominal torque

estimation models developed on the basis of the geometrical similarity principle.

Figure 9(c) globally confirms the capability of scaling laws to estimate the maximal admissible speed. However, the maximum losses of annular torque motors do not differ significantly from the estimated value for definition torques below 40 Nm. Analysing the manufacturers' data shows that these motors become limited by the maximal input voltage. The design driver used to establish the scaling laws is no longer applicable. The speed limit evolution for a fixed maximum input voltage (here 600 VDC) has been represented by a dashed line in Figure 9(c). This input voltage constraint can be explained by the rationalization of the power electronics product range associated with the motors. In this sense, the established scaling law provides the maximum speeds that the motors could reach without restriction on power electronics.

The predictive significance of the scaling laws of Table 4 can be observed in Fig. 10, which plots the manufacturing company's data [50–53] versus what is predicted from the estimation model. Figure 10 shows that points representative of mass and inertia of gear and worm pinions fall closely around a straight line of slope one with a standard deviation

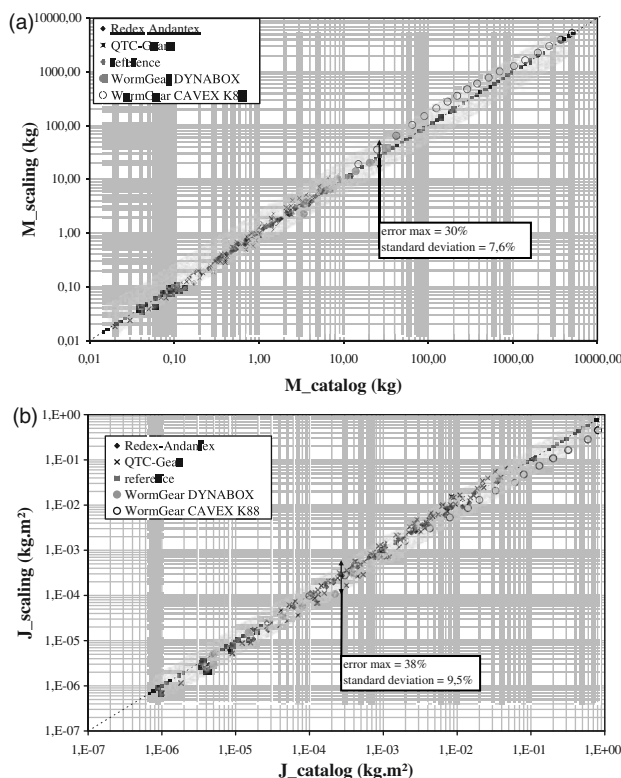


Fig. 10 Mass and inertia of pinions and wheel in gear and worm reducers: (a) pinion masses for spur and worm gears and (b) pinion inertia for spur and worm gears

for the error of these models of less than 10 per cent. Estimation models for other components such as ball bearings and roller screws are validated in reference [54].

6 FURTHER APPLICATIONS OF THE ESTIMATION MODELS

The objective of this article is to provide enabling tools for the pre-design, simulation or optimization tasks. The proposed estimation models associated with other system simulations, CAD, reliability, and optimization models support the preliminary design efficiently, where only a few design parameters are available but major technical decisions are to be taken.

1. Their use with system simulation models and inverse simulation enable quick sizing and architecture evaluation even with complex mission cycles. References [18, 54–56] give examples of the implementation of such CAE tools in the Modelica language [57] dealing with examples of an aileron, a spoiler or nose landing gear steering actuators.
2. Their connection with CAD software can improve and accelerate the integration study. Reference [19] gives an example of a geometrical integration study in the CATIA framework for a nose-landing gear door actuator.
3. Their uses with degradation models enable life-time and reliability to be assessed. Thus, reference [58] deals with the design for reliability of electro-mechanical actuators.
4. Their use in the design of experiments and optimization algorithms enables optimal design of electromechanical actuators. Reference [59] is an example of optimal geometrical integration of a linear actuator with a minimal mass objective.

7 CONCLUSION

A technology shift towards more electric solutions is emerging in aerospace actuation. New technology brings new challenges, especially for the preliminary design process of actuation systems and components that cannot simply be a duplicate of former practices. In this way, it is no longer meaningful to proceed to sizing by points (as for hydraulic actuators). Instead, it is necessary to take into account mission profiles covering all possible sizing drivers (e.g. maximum speed and torque, fatigue, thermal behaviour, vibrations, and shocks) and addressing various design criteria (e.g. geometrical envelope, weight and reliability). For this purpose, appropriate top level

evaluation tools should be developed to support an efficient preliminary design. In this article, such tools have been proposed in the form of models for the major generic EMA components, which are first identified by a state-of-the-art of the actuation systems in aerospace and aeronautics. This state-of-the-art also highlights the different stages or design points of view encountered in early preliminary studies. Then, a classification of the design parameters associated with these stages has been proposed to fit into a model-based design approach. Obtaining these parameters quickly and easily is a critical issue for sizing calculations and early simulations in the framework of risk mitigation. The scaling law approach presented in this article responds to this issue by allowing the development of component models from a limited number of input parameters. Moreover, the scaling laws developed are representative of the state-of-the-art of technology and require a single component reference instead of a large amount of data that are cumbersome to set-up and maintain. These laws have been compared with manufacturers' catalogue data to validate their relevance. Finally, the usefulness of these estimation models has been illustrated with potential applications for EMA model-based designs.

FUNDING

This work was partly funded by the following projects: the FP6 European DRESS project (Distributed and Redundant Electro-mechanical nose gear Steering System, 2006/2009) and the French FUI CISACS project (Concept Innovant de Systèmes d'Actionnement de Commandes de vol secondaires et de Servitudes).

© INSA TOULOUSE – ICE 2011

REFERENCES

- 1 Rosero, J.A., Ortega, J.A., Aldabas, E., and Romeral, L. Moving towards a more electrical aircraft. *Aerosp. Electron. Syst. Magn., IEEE*, 2007, **22**(3), 3–9.
- 2 Van den Bossche, D. A380 primary flight control actuation system. In International Conference on *Recent advances in aerospace actuation systems and components*, Toulouse, 13–15 June 2001, pp. 1–4.
- 3 Todeschi, M. Airbus – EMAs for flight actuation systems – perspectives. In International Conference on *Recent advances in aerospace actuation systems and components*, Toulouse, 13–15 June 2010, pp. 1–8.
- 4 Dée, G., Vanthuyne, T., and Alexandre, P. An electrical thrust vector control system with dynamic force feedback. In International Conference on *Recent advances in aerospace actuation systems and components*, Toulouse, 13–15 June 2010, pp. 75–79.

- 5 **Cowan, J. R. and Weir, R. A.** Design and test of electromechanical actuators for thrust vector control. In *The 27th Aerospace Mechanisms Symposium*, NASA Ames Research Center, 1992, pp. 349–366.
- 6 Technical Division Product Development and Mechatronics. *Design methodology for mechatronic systems*, VDI-Richtlinien, 2004 (VDI, Düsseldorf).
- 7 **Haskins C., Forsberg K., Krueger M., Walden D., Hamelin R. D.,** INCOSE Systems Engineering Handbook, USA INCOSE, International Council on Systems Engineering 2010.
- 8 **Estefan, J. A.** *Survey of model-based systems engineering (MBSE)*, INCOSE MBSE Focus Group, 25 May 2007.
- 9 **Han, L., Paredis, C. J. J., and Khosla, P. K.** Object-oriented libraries of physical components in simulation and design. In *2001 Summer Computer Simulation Conference*, Orlando, Florida, 15–19 July 2001, pp. 1–8.
- 10 **Hagen, J., Moore, L., Estes, J., and Layer, C. H.** The X-38 V-201 flap actuator mechanism. In *Proceedings of the 37th Aerospace Mechanisms Symposium*, Johnson Space Center, Houston, 19–21 May 2004.
- 11 **Schinstock, D. E. and Scott, D. A.** Controller design for EMA in TVC incorporating force feedback, NASA/MSFC Technical Report, University of Alabama, Mechanical Engineering Department, 1998.
- 12 **Fuerst, D. and Neuheuser, T.** Development, prototype production and testing of an electromechanical actuator for a swashplateless primary and individual helicopter blade control system. In *1st International Workshop on Aircraft System Technologies (AST 2007)*, Hamburg, Germany, 29–30 March 2007, pp. 7–19.
- 13 **Jensen, S. C., Jenney, G. D., and Dawson, D.** Flight test experience with an electromechanical actuator on the f-18 systems research aircraft. In *The 19th Digital Avionics Systems Conferences*. Philadelphia, Pennsylvania, USA, 7–13 October 2000, 7–13.
- 14 **Kopala, D. J. and Doel, Ch.** High performance electromechanical actuation for primary flight surfaces (EPAD Program Results). In *International Conference on Recent advances in aerospace actuation systems and components*, Toulouse, France, 13–15 June 2001.
- 15 **Liscouët, J., Orioux, S., and Maré, J. C.** An innovative top-down approach for the preliminary design of electromechanical actuators. In *Proceedings of the 26th International Conference on Aerospace sciences*, Anchorage, 14–19 September 2008.
- 16 **Chevalier, P-Y., Grac, S., and Liegois, P-Y.** More electrical landing gear actuation systems. In *International Conference on Recent advances in aerospace actuation systems and components*, Toulouse, France, 5–7 May 2010.
- 17 DOE 160, *Environmental conditions and test procedures for airborne equipment*, Standard for environmental test of avionics hardware, 2005 (RTCA Incorporated, Washington, DC).
- 18 **Hospital, F., Budinger, M., Liscouët, J., and Maré, J-Ch.** Model based methodologies for the assessment of more electric flight control actuators. In *13th AIAA/ATIO Aviation technology, Integration, and Operation Conference*, Fort Worth, Texas, 13–15 September 2010.
- 19 **Budinger, M., Fraj, A., El Halabi, T., and Maré, J-Ch.** Coupling CAD and system simulation framework for the preliminary design of electromechanical actuators. IDMME virtual concept, Bordeaux, France, 20–22 October 2010.
- 20 **Liscouët, J, Budinger, M., and Maré, J.-Ch.** Design for reliability of electromechanical actuators. In *International Conference on Recent advances in aerospace actuation systems and components*, Toulouse, France, 5–7 May 2010.
- 21 **Grand, S. and Valembos, J-M.** Electromechanical actuators design for thrust vector control. In *International Conference on Recent advances in aerospace actuation systems and components*, Toulouse, France, 24–26 November 2004.
- 22 **Cochoy, O., Hankea, S., and Carla, U. B.** Concepts for position and load control for hybrid actuation in primary flight controls. *Aerosp. Sci. Technol.*, 2007, **11**(2–3), 194–201.
- 23 **Roos, F.** *Towards a methodology for integrated design of mechatronic servo systems*, 2007, pp. viii–203 (KTH, Machine Design, Sweden).
- 24 **Girion, S., Baumann, C., Piquet, H., and Roux, N.** Analytical modeling of the input admittance of an electric drive for stability analysis purposes. *Eur. Phys. J. Appl. Phys.*, 2009, **47**, 11101.
- 25 **Maré, J. Ch and Budinger, M.** Comparative analysis of energy losses in servo-hydraulic, electro-hydrostatic and electro-mechanical actuators. In *The 11th Scandinavian International Conference on Fluid power*, SICFP'09, Linköping, Sweden, 2009, 2–4 June 2009.
- 26 **Liscouët-Hanke, S, Pufe, S., and Maré, J-Ch.** A simulation framework for aircraft power management. *Proc. IMechE, Part G: J. Aerospace Engineering*, 2008, **222**(6), 749–756.
- 27 **Krus, P.** Performance estimation using similarity models and design information entropy *Workshop on Performance prediction in system-level design, international design engineering technical conference and computers and information in engineering conference (IDETC/CIE)*, 3 August 2008.
- 28 **Messine, F., Nogarede, B., and Lagouanelle, J-L.** Optimal design of electromechanical actuators: a new method based on global optimization. *IEEE Trans. Magn.*, 1998, **34**(1), 25–34.
- 29 ControlEng, ServoSoft software, available from www.controleng.ca.
- 30 **Simpson, T., Peplinski, J., Koch, P., and Allen, J.** Metamodels for computer-based engineering design: survey and recommendations. *Eng. Comp.*, 2001, **17**, 129–150.
- 31 **Jufer, M.** Design and losses - scaling law approach. In *Nordic research symposium energy efficient electric motors and drives*, 1996, pp. 21–25 (Skagen, Denmark).
- 32 **Ricci, G.** Mass and rated characteristics of planetary gear reduction units. *Meccanica*, 1992, **27**, 35–45.

- 33 Ricci, G. Weight and rated characteristics of machines: positive displacement pumps, motors and gear sets. *Mech. Mach. Theory*, 1983, **18**, 1–6.
- 34 Waldron, K. J. and Hubert, Ch. Scaling of robotic mechanisms. In IEEE International Conference on Robotics & Automation San Francisco, California, April 2010.
- 35 Multon, B., Ben Ahmed, H., Ruellan, M., and Robin, G. Comparaison du couple massique de diverses architectures de machines tournantes synchrones à aimants. *Société de l'Electricité, de l'Electronique et des Technologies de l'Information et de la Communication* (SEE), 2006, pp. 85–93.
- 36 Pahl, G., Beitz, W., Blessing, L., Feldhusen, J., Grote, K.-H., and Wallace, K. *Engineering design: a systematic approach*, 2007 (Springer-Verlag London Limited, London).
- 37 Kline, S. J. *Similitude and approximation theory*, 1965 (McGraw-Hill Book Company, New York).
- 38 Taylor, E. S. *Dimensional analysis for engineers*, 1974 (Oxford University Press, UK).
- 39 Glenn Murphy. *Similitude in engineering*, 1950 (The Ronald Press Company, New York).
- 40 Budynas, R. and Nisbett, J. K. *Shigley's mechanical engineering design, SI version*, 2007 (McGraw-Hill, New York).
- 41 Fitzgerald, A. E., Kingsley, Ch., and Umans, S. D. *Electric machinery*, fifth edition, 1992 (McGraw-Hill Book Company, New York).
- 42 Grellet, G. Pertes dans les machines tournantes. *Techniques de l'Ingénieur*, .
- 43 Units CSG-2UH Digital Catalogue, Harmonic Drive, 2005, available from <http://www.harmonicdrive.net/>
- 44 Fine Cyclo Catalogue, Sumitomo Drive Technologies, 2005, available from <http://www.sumitomo-driveeurope.com/>
- 45 AF Series Catalogue, APEX Dynamics Inc., 2009, available from <http://www.apexdyna.com/>
- 46 Budynas, R., Nisbett, and Shigley's, J. K. *Mechanical engineering design, SI version*, eighth edition, 2007, p. 1088 (McGraw-Hill, New York).
- 47 Iles-Klumpner, D., Serban, I., Risticvic, M., and Boldea, I. Comprehensive experimental analysis of the IPMSM for automotive applications. In Power Electronics and Motion Control Conference, EPE-PEMC 2006, 12th International, Portoroz, 30 August to 1 September 2006, pp. 1776–1783.
- 48 Synchronous Servomotors Series GOLDLINE™ BH, Technical description, Installation, Commissioning, Kollmorgen, 2000, available from <http://www.kollmorgen.com/>
- 49 Torque Motors Data Sheets, TMB Series, ETEL Motion technology, 2007, available from <http://www.etel.ch/>
- 50 Modular rack & pinion system, available from www.andantex.com.
- 51 Quality Transmission Components, available from www.qtcgears.com.
- 52 CAVEX - Worm Gear Units, F. D. a. Automation, 2005, available from <http://flender.com>.
- 53 Dynabox - Right angle servo gearheads, G. T.-P. gearheads, 2008, available from www.girard-transmissions.com.
- 54 Liscouët, J., Budinger, M., Maré, J-Ch., and Orioux, S. Modelling approach for the simulation-based preliminary design of power transmissions. *Mech. Mach. Theory*, 2011, **46**(3), 276–289.
- 55 Allain, L., Budinger, M., Liscouët, J., Lefevre, Y., Fontchastagner, J., and Abdenour, A. Preliminary design of electromechanical actuators with modelica, Modelica 2009. In Proceedings of the 7th Modelica Conference, Como, Italy, 20–22 September 2009.
- 56 Budinger, M., Liscouët, J., Cong, Y., and Mare, J-Ch. Simulation based design of electromechanical actuators with modelica. IDETC 09, San Diego, 30 August–2 September 2009.
- 57 Mattsson, S. E., Elmqvist, H., and Otter, M. Physical system modeling with Modelica. *Control Eng. Pract.*, 1998, **6**, 501–510.
- 58 Liscouët, J., Budinger, M., and Maré, J.-C. Design for reliability of electromechanical actuators. In International Conference on *Recent advances in aerospace actuation systems and components*, Toulouse, France, 2010, 5–7 May.
- 59 El Halabi, T., Budinger, M., and Maré, J.-C. Optimal geometrical integration of electromechanical actuators. In International Conference on *Recent advances in aerospace actuation systems and components*, Toulouse, France, 5–7 May 2010.

Chapter 2 – Simulation models for preliminary design

ABSTRACT

The objective of simulation models is to establish the relationships between the different components of a system and to access the variables influencing the selection of these components. The sizing scenarios at system-level can often be represented by lumped parameter models simulated with static, transient or harmonic solvers. The level of modeling should be as simple as possible to minimize the number of parameters to be provided, and as fast as possible to allow optimization while giving access precisely to the design variables. Such models can be obtained by deduction or reduction methods. The associated paper, entitled "Modelling approach for the Simulation-Based Preliminary Design of Power Transmissions" and published in the journal Mechanism and Machine Theory, illustrates how transient inverse simulation and estimation models with scaling laws can be used to size actuation systems.

Keywords: simulation models, sizing scenarios, mission profiles, forward and inverse simulation, model deduction, model reduction.

TABLE OF CONTENTS

1.	Simulation models.....	45
1.1.	Objectives of simulation models.....	45
1.2.	Modelling formalisms and modelling levels.....	46
1.3.	Orientation and use of simulation models during sizing activities.....	48
2.	Representation of design scenarios	51
2.1.	Design scenarios and design drivers	51
2.2.	Sizing scenario types	52
2.3.	Mission profile analysis and simplification.....	54
3.	Choice of modeling levels.....	57
3.1.	Deduction approach	58
3.2.	Reduction approach	61
4.	Conclusion.....	64
5.	Bibliography.....	65

NOTATION

Acronyms

DAE	Differential-Algebraic Equations	RMS	Root Mean Square
DC	Direct Current	SOA	Safe Operating Area
EMA	Electro-Mechanical Actuator	PDE	Partial Differential Equations
ODE	Ordinary Differential Equations	0D-1D	Lumped parameters models
PMAC	Permanent Magnet Alternative Current	2D-3D	Distributed parameters models
PDE	Power Drive Electronic		

Nomenclature

e	Effort (bond-graph)	V	Speed
f	Viscous friction coefficient or flux (bond-graph)	α	Fatigue coefficient
F	Force		
M	Mass		
x	Position		
\dot{x}	Speed		
\ddot{x}	Acceleration		

Indices and exponents

th	Thermal	RMC	Root Mean Cube
RF	Rolling fatigue	RMS	Root Mean Square

1. SIMULATION MODELS

1.1. Objectives of simulation models

This chapter is devoted to simulation models at system level. The simulations used here differ from the geometrically based simulations of a component during its detailed design. References [1] and [2] stress that the design of multi-domain mechatronic systems requires different modelling layers as represented in Figure 1:

- A mechatronic layer, to account for the functional and physical coupling between components. This level of modeling is usually achieved using 0D-1D models [1], also called lumped parameter models, represented by algebraic equations, ordinary differential equations (ODE) or differential algebraic equations (DAE) [3].
- A specific domain layer, to describe the performance limits and parameters necessary in the previous layer, based on a geometric representation. The specific domain phenomena are generally represented through partial differential equations (PDE). This level of modeling can be achieved, for simplified geometries, by using analytical models or, for complex 2D and 3D geometries, by using numerical approximations, like the finite element method (FEM) for instance.

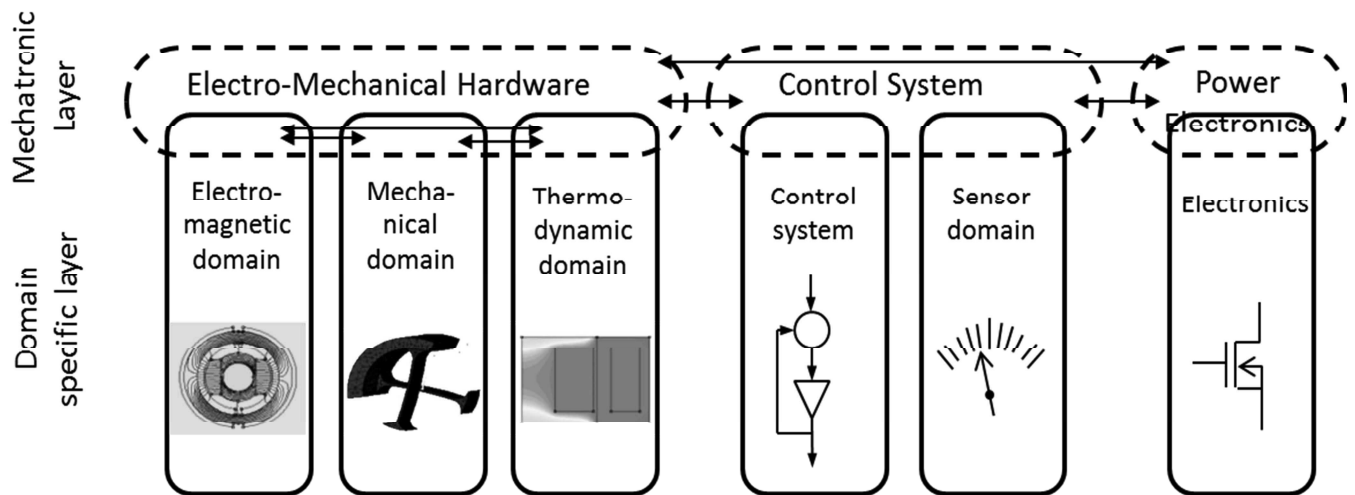


Figure 1 – Hierarchical design models (based on reference [2])

This chapter will focus on the models to be developed in the mechatronic layer for the synthesis of the operative part of a physical system and more particularly of an actuator. The goal of these models is to establish relationships between different components of a system and access the variables influencing the selection of components. These variables can concern power and energy (e.g. force, speed) or other physical variables (e.g. temperature) which can cause a component to deteriorate rapidly or gradually. In the example of section 1, the design of a spoiler required the representation of different configurations of use called sizing scenarios. These scenarios may take the form of:

- operating points with power, speed or force constants for applications with steady states.
- a transient mission profile, such as a temporal mechanical profile giving access to the maximum speed, forces and fatigue of mechanical components or a transient thermal profile providing access to the thermal stress of a brushless motor;
- critical events, such as jamming of the control surface, which can create violent internal efforts by the sudden deceleration of the motor inertia, or a violent gust of wind requiring a rapid decline of the control surface.

Several questions can then arise:

- How can the simulation be performed? What tool and what kind of resolution should be adopted? The end of this section deals with the type of models usually chosen in mechatronic design.

- How can the sizing scenarios which can be operating points, mission profiles or critical events, be defined? Section 2 will focus on the main design drivers of EMA components and will describe how to take them into account through simulations.
- Which model level should be adopted for the simulation? How can the adequacy of the simulation model and the sizing scenario be ensured? Section 3 illustrates the concepts of model deduction or model reduction to define the level best suited to the design phases under consideration.

1.2. Modelling formalisms and modelling levels

To represent the main design variables and the interaction between components, the modelling of mechatronic systems mainly uses lumped parameter models. A lumped element model simplifies the description of the behaviour of spatially distributed physical systems into a topology consisting of discrete entities. Table 1 summarizes the main representation formalisms and simulation tools available with the example of a DC motor.

The balance between the needs of the application and the simulation model will depend on the response times and the bandwidths to be represented:

- For phenomena that vary relatively slowly, steady state or quasistatic analyses can be used. The resolution is done through a set of algebraic equations manipulating constants or harmonic amplitudes.
- When the mission profiles show faster changes it may be necessary to take into account one dynamic effect, as the inertia of the rotor. This type of simulation can be represented with one state.
- With rapid transients, resonance modes can be excited and add significant oscillations. This type of simulation requires several states to represent inertial and capacitive effects.

The representation of the components will depend on the phenomena to be simulated. For preliminary design, a hydraulic cylinder can often be initially modelled without considering inertial and capacitive effects, which have little effect on the power demand. An electromechanical actuator, on the other hand, may require the representation of transient effects of thermal capacity or mechanical inertia. Table 2 develops different modeling levels for some typical components of actuators as an illustration.

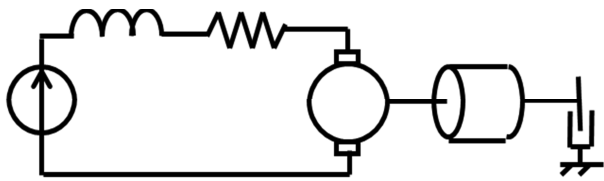
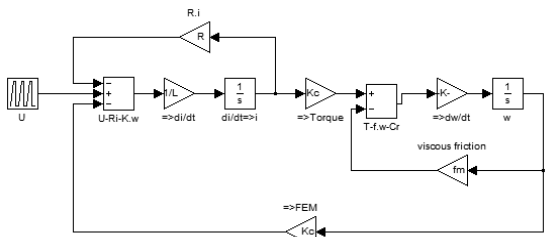
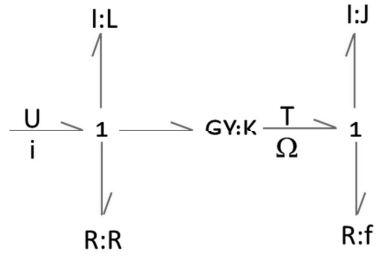
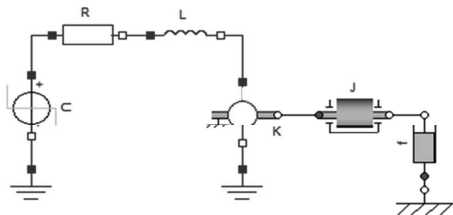
<p>Lumped parameter model to be represented</p> 	<p>The DC motor can be modelled by a set of differential-algebraic equations (DAE):</p> $\begin{cases} \dot{x} = f(x, y, u(t)) \\ 0 = h(x, y, u(t)) \end{cases}$ <p>where Kirchoff's laws provide algebraic equations and characteristic equations of elements give the state variables.</p>
<p>Block diagram and state space representation</p>  <p>Typical software packages: Matlab/Simulink [4], Scilab/Xcos [5]</p>	<p>A link transmits a signal representing a variable. The solver is able to solve ordinary differential equations (ODE):</p> $\dot{x} = f(x, u(t))$ <p>The equations of the DC motor need to be rearranged in order to be rewritten as:</p> $\frac{di}{dt} = \frac{U - Ri - K\omega}{L} \text{ and } \frac{d\omega}{dt} = \frac{Ki - f\omega}{J}$ <p>, before block diagram is drawn up or state space is modelled.</p>
<p>Bond-graph and causal models representation</p>  <p>Typical software: 20-sim [6], AMESim [7]</p>	<p>A link transmits a set of two power variables (effort / flow variables). The resulting representation is much more physical and enables knowledge to be built up and stored in dedicated libraries.</p> <p>The analysis of causality generates model structures leading directly to ordinary differential equations. This analysis can be done graphically by prohibiting certain non-causal associations [8].</p>
<p>Nodal representation and declarative or non-causal models :</p>  <p>Typical software: Modelica [9], VHDL-AMS, Matlab/Simscape</p>	<p>A link transmits the necessary quantities to Kirchoff's laws (across / through variables).</p> <p>The models are declaratives with no preferred orientation. A symbolic treatment enables the equations resulting from the combination of basic models to be oriented [10].</p>

Table 1 - Representation formalisms and examples of available simulation tools for lumped parameter models

Components	Functional model (transformers)	Main imperfections	
		Quasistatic (losses)	Transient (capacity and inertia)
Hydraulic jack	$\frac{P}{Q} \rightarrow TF \rightarrow \frac{F}{V}$	$\frac{P}{Q} \rightarrow 0 \rightarrow TF \rightarrow 1 \rightarrow \frac{F}{V}$ R leakage R friction	Compressibility C Mobile mass I $\frac{P}{Q} \rightarrow 0 \rightarrow TF \rightarrow 1 \rightarrow \frac{F}{V}$ R R
Ball screw	$\frac{T}{\Omega} \rightarrow TF \rightarrow \frac{F}{V}$	$\frac{T}{\Omega} \rightarrow TF \rightarrow 1 \rightarrow \frac{F}{V}$ R friction	Inertia I Stiffness K $\frac{T}{\Omega} \rightarrow 1 \rightarrow TF \rightarrow 1 \rightarrow \frac{F}{V}$ R
Reducer	$\frac{T_1}{\Omega_1} \rightarrow TF \rightarrow \frac{T_2}{\Omega_2}$	$\frac{T_1}{\Omega_1} \rightarrow TF \rightarrow 1 \rightarrow \frac{T_2}{\Omega_2}$ R friction	Inertia I Stiffness K $\frac{T_1}{\Omega_1} \rightarrow 1 \rightarrow TF \rightarrow 1 \rightarrow \frac{T_2}{\Omega_2}$ R
DC motor	$\frac{U}{i} \rightarrow GY:K \rightarrow \frac{T}{\Omega}$	$\frac{U}{i} \rightarrow 1 \rightarrow GY:K \rightarrow \frac{T}{\Omega} \rightarrow 1$ R:R R:f	$\frac{U}{i} \rightarrow 1 \rightarrow GY:K \rightarrow \frac{T}{\Omega} \rightarrow 1$ I:L I:J R:R R:f

Table 2 – Different level of modelling represented with bond graph formalism

1.3. Orientation and use of simulation models during sizing activities

The advantage of a non-causal model is its ability to carry out both direct (or forward) and inverse simulations [11] [12]. Inverse simulation eliminates control loops and corresponding blocks by calculating the inputs to be applied to the components (current, voltage to the motor, for example) for a given load mission profile [13]. Figure 2 illustrates how the effort required to obtain an imposed displacement on a sliding mass with viscous friction can be found through direct simulation or inverse simulation. Modelica enables these two simulation modes thanks to its acausal modelling capability [14].

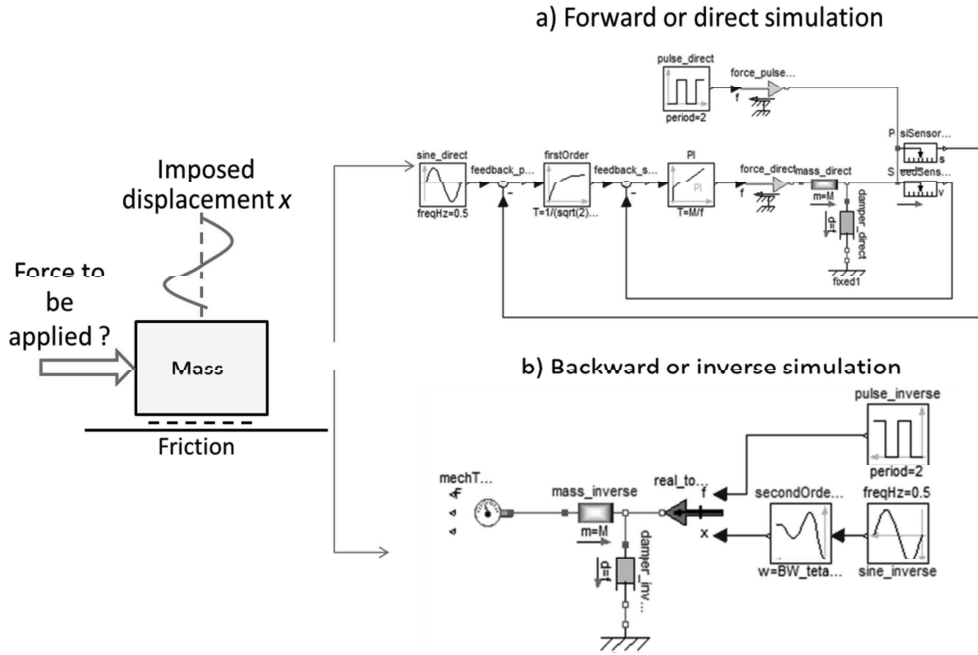


Figure 2 – Direct vs inverse simulation

To perform an inverse simulation, the roles of u and y in the following system of equations have to be reversed [12]:

$$\begin{cases} \dot{x} = f(x, u) \\ y = g(x, u) \end{cases} \text{ which becomes, after linearization, } \begin{cases} \dot{x} = Ax + Bu \\ y = Cx + Du \end{cases} \quad (1)$$

If $D \neq 0$, inverse system state equations are deduced straightforwardly. If $D = 0$, the inverse of the system is obtained from α successive time derivation of the output y until the input u appears [15]:

$$\begin{cases} \dot{x} = \tilde{A}x + \tilde{B}y^{(\alpha)} \\ u = x + y^{(\alpha)} \end{cases} \quad (2)$$

with $\tilde{A} = A - B(CA^{\alpha-1}B)^{-1}CA^{\alpha}$, $\tilde{B} = B(CA^{\alpha-1}B)^{-1}$, $\tilde{C} = -(CA^{\alpha-1}B)^{-1}CA^{\alpha}$ and $\tilde{D} = (CA^{\alpha-1}B)^{-1}$

For the example of Figure 2, two successive derivations have to be applied to inverse the system.

$$\begin{cases} \begin{pmatrix} \dot{x} \\ \ddot{x} \end{pmatrix} = \begin{pmatrix} 0 & 1 \\ 0 & -\frac{f}{M} \end{pmatrix} \begin{pmatrix} x \\ \dot{x} \end{pmatrix} + \begin{pmatrix} 0 \\ 1/M \end{pmatrix} F \\ y = x = (0 \ 1) \begin{pmatrix} x \\ \dot{x} \end{pmatrix} \end{cases} \text{ becomes } \begin{cases} \begin{pmatrix} \dot{x} \\ \ddot{x} \end{pmatrix} = \begin{pmatrix} 0 & 1 \\ 0 & 0 \end{pmatrix} \begin{pmatrix} x \\ \dot{x} \end{pmatrix} + \begin{pmatrix} 0 \\ 1 \end{pmatrix} \ddot{y} \\ u = F = (0 \ f) \begin{pmatrix} x \\ \dot{x} \end{pmatrix} + (M) \dot{y} \end{cases} \quad (3)$$

Within Modelica these derivations are achieved by manipulating equations [16] and using the second order filter which is added to the imposed displacement. The inverse simulation is not always possible, however. For example, in the case of a Coulomb friction, for efforts located in the cone of friction, matrix B is null and the state inversion is impossible.

To illustrate the precautions to be taken when using inverse simulation through a numerical case, simplified simulation conditions, nevertheless respecting the order of magnitude of the conditions of an aileron in cruise flight, are used:

- The displacement requested is a sinusoidal movement with an amplitude of 3 mm and a frequency of 0.5 Hz;
- The mass, which accounts of the inertia of a brushless motor, is $20 \cdot 10^3$ kg, the viscous friction, which represents few percent (5%) of the maximum load at maximum speed, is equal to 30 kN/m.s^{-1} ;
- The required bandwidth for the position loop is 2 Hz at -3 dB gain;

- A disturbing force, acting as a driving load with steps between 10 kN and 20 kN, simulates the effect of aerodynamic efforts and also the change of quadrant and efficiency in a screw/nut system.

Without disturbing efforts, if the dynamics of the correctors (direct simulation) and filter (inverse simulation) are set to obtain the required bandwidth, then the effort, speed and position variables are exactly the same. The “inverse simulation” filter not only allows inverse simulation but can also simulate the dynamic response required of the actuator on a mission profile. The inverse simulation then avoids having to calculate the controller parameters and accelerates model design and shortens simulation time [17].

With a disturbing force, direct and inverse simulation may present greater differences when the bandwidth of the speed loop is low and the disturbance rejection is poor. Figure 3, however, shows that for the case studied here, the differences are small. In the case of an electromechanical actuator, the bandwidths of different control loops are indeed well separated effects: typically 1-10 Hz for the position loop, 50-100 Hz for the velocity loop, 500-1000 Hz for the torque or current loop.

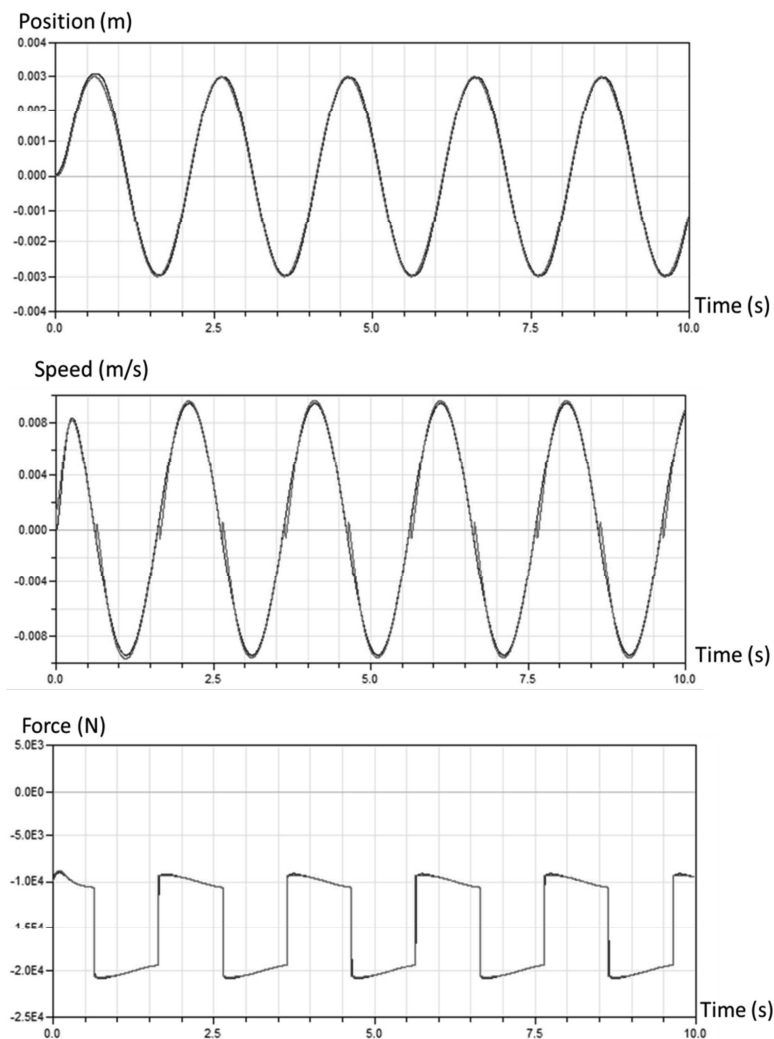


Figure 3 – Simulation results (direct and inverse) with disturbance force

The activities of sizing and design at system level may need to use the models according to two resolution modes:

- Inverse simulation, which allows backward propagation of power variables can be used during power sizing for a quasi-static operational point or a transient mission profile, for life time calculation, etc.
- Direct or forward simulation can be used for critical case simulation (short-circuit, jamming), resonance mode calculation, transient thermal simulation, closed loop performance estimation (bandwidth, response time), etc.

2. REPRESENTATION OF DESIGN SCENARIOS

2.1. Design scenarios and design drivers

Design scenarios are shaped to describe situations that the mechatronic system can encounter during its service life. These situations result from operating and environmental conditions, and also from performance indicators and duty cycle requirements. In addition to this system integrator knowledge, the system suppliers' knowledge is required to complete the definition and validation of design scenarios as illustrated in Figure 4 for flight control actuation systems. The airframe manufacturer possesses information that does not relate to specific components or technology, whereas the system supplier has detailed information on component functions and characteristics. At the first stage most of the information is strictly qualitative except for environmental conditions, mission profiles and operating points. Figure 5 shows the information breakdown pertaining to both the airframe manufacturer and the system supplier during the requirements and design scenarios definition process. In Figure 5 design drivers refer to component performance limitations. The limitations can be of two different types, due to rapid or gradual degradation. Typically, a rapid degradation design driver is linked to maximum values that must not be exceeded, while a gradual degradation driver refers to fatigue effects over a repeated number of cycles. Not all the rapid and gradual degradation drivers of a component may be reached during sizing; they must, nevertheless, be addressed and validated. A description of the main design drivers of the main mechatronic components is given in chapter 4. In addition to these drivers, components have some parasitic characteristics like mechanical friction, stiffness inertia etc. which can have an impact on the whole actuator sizing. For this reason, they will be considered as new (parasitic) drivers. Examples of parasitic effects are given Table 2. Integration can also impact part design, adding new geometrical design drivers.

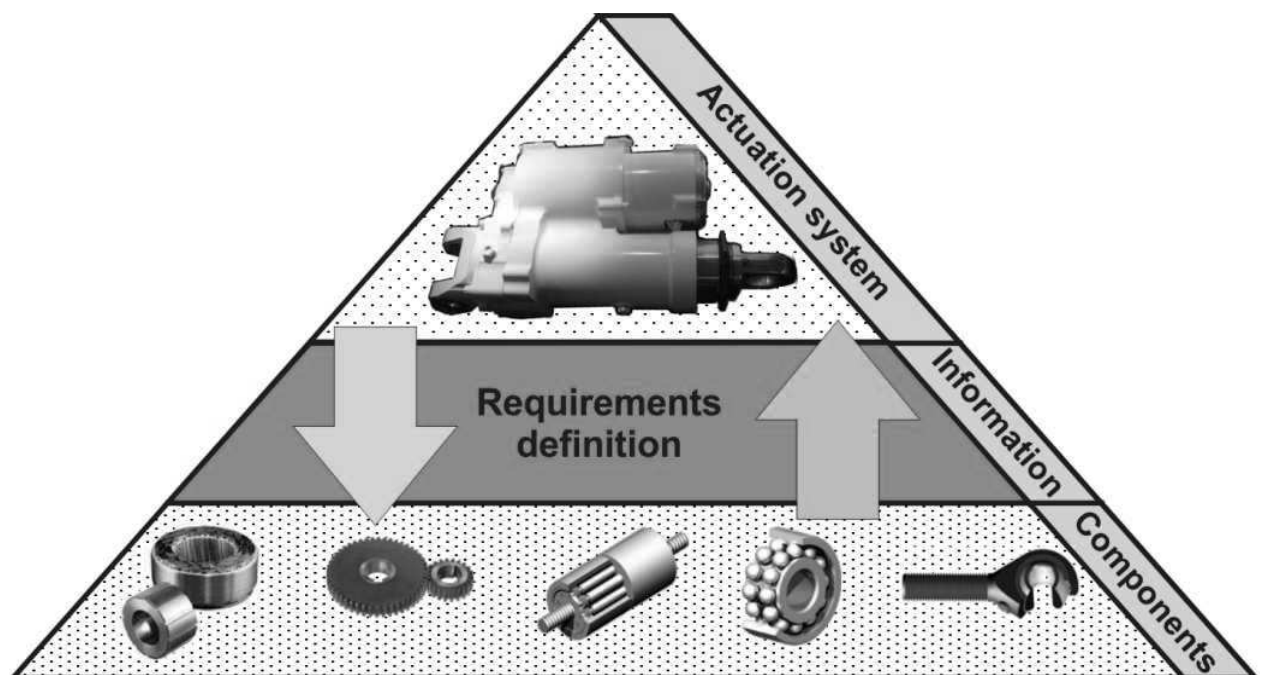


Figure 4 - Informations exchanges between system supplier and airframe manufacturer during definition of design scenarios [18]

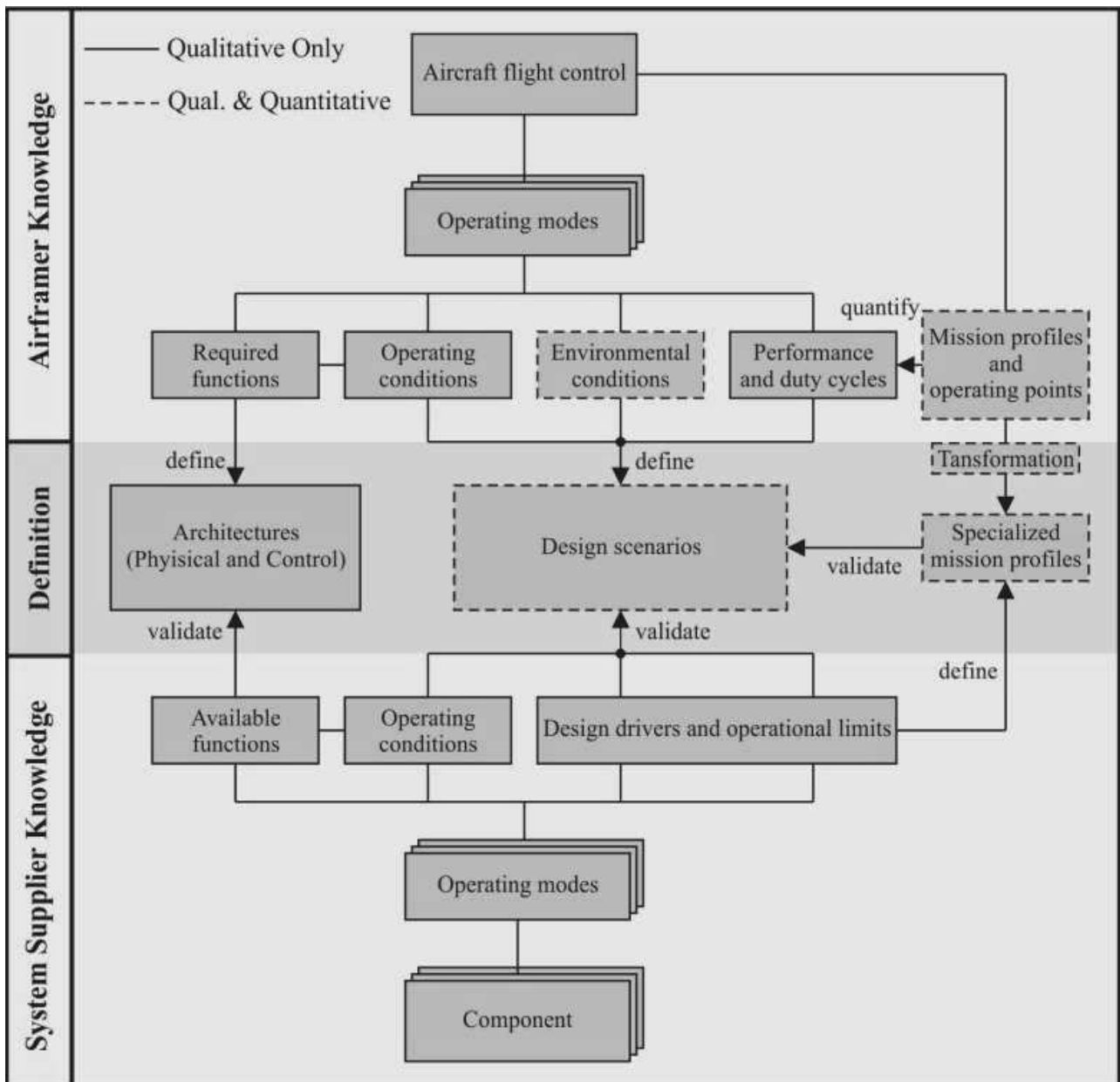


Figure 5 - Design scenario definition process [18]

2.2. Sizing scenario types

The design scenarios can take different forms: steady state operational points, transitory mission profiles or critical cases. Operational points and mission profiles express the power demand of the load. Critical cases express abnormal or extreme uses of the system. Figure 6 illustrates a mission profile expressing the variation in needs for force, position, and speed with time, expressed at the level of the load, and which have to be driven by the nose landing gear steering actuator. This power requirement is often represented in a force/speed plane in order to superimpose the capacities of the actuator and the requirements of the load in the same plane. Figure 7 illustrates this approach with the example of a hydraulic actuator and an electric actuator.

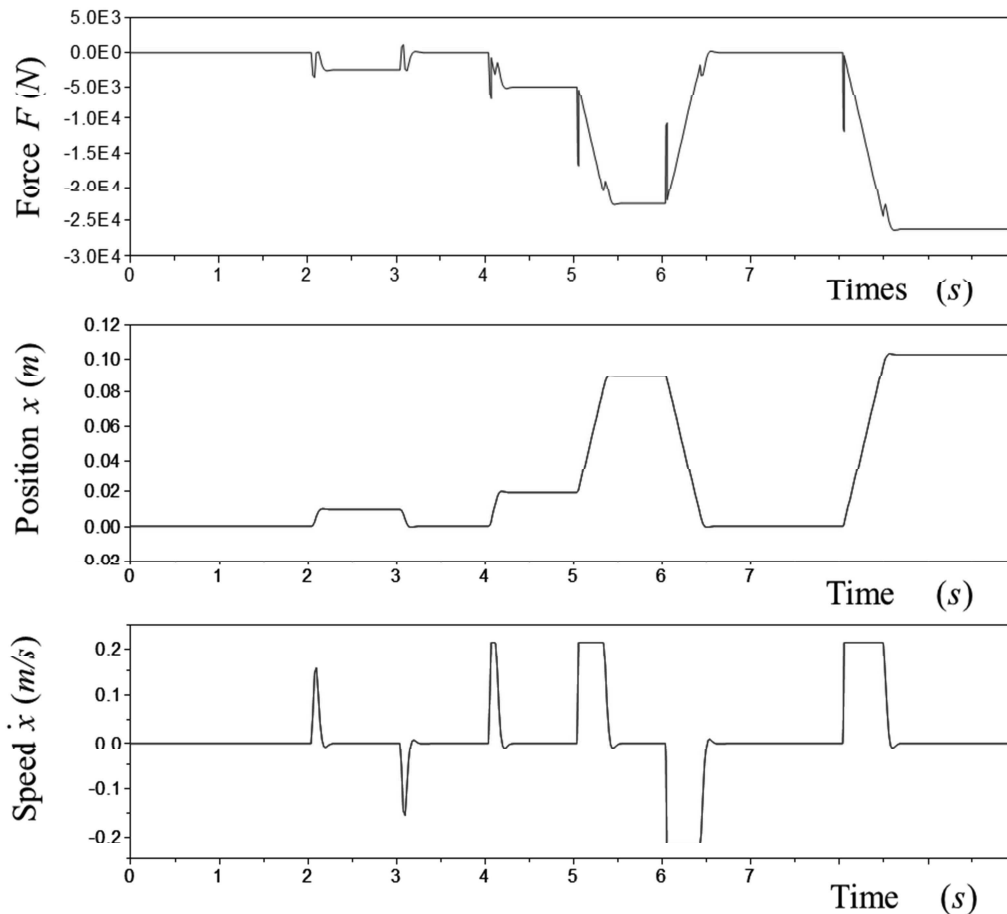


Figure 6 - Example of mission profile for a nose landing gear steering actuator

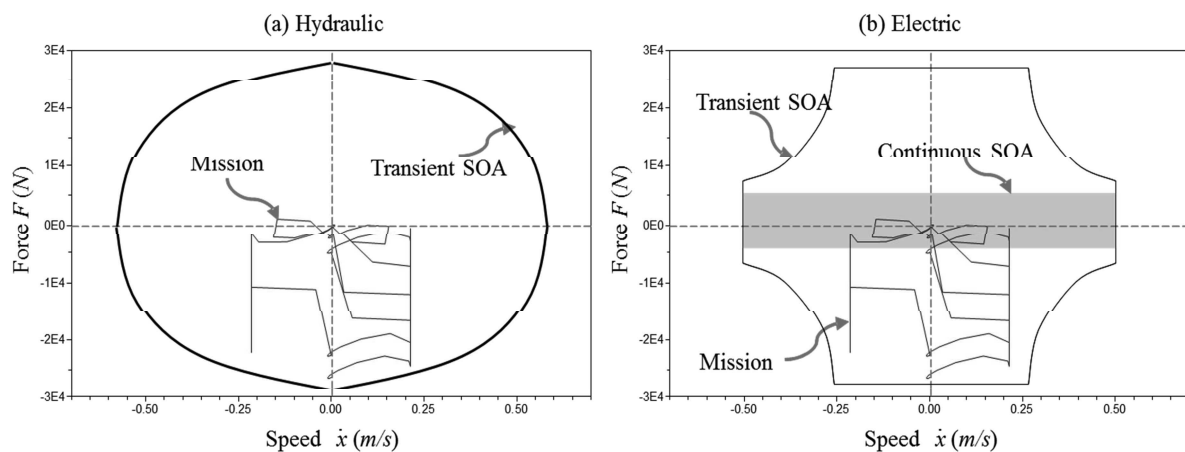


Figure 7 - Example of mission profile compared to a) hydraulic and b) electric actuator safe operating areas

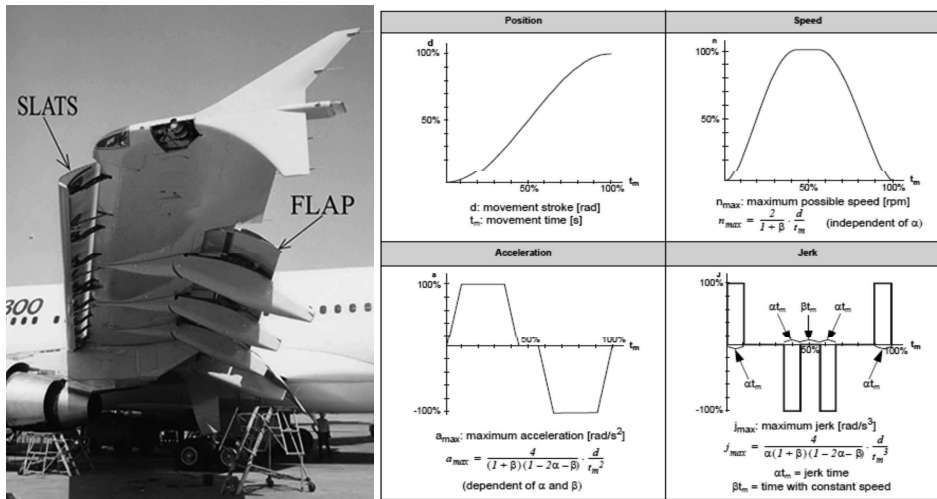
Figure 7a shows that the need for power which is expressed in the force/speed plane is included in the safe operating area of the hydraulic actuator. This envelope is representative of the continuous and transitory capacity of the actuator. Therefore, the actuator is able to meet the need. The mission profile may thus be extremely simplified and represented by effort/speed operational points. On the other hand, as shown in Figure 7b, the electric technology is characterized by a transitory operational area different from the thermal continuous limits. It is then necessary to evaluate the entire mission profile and not just operational points.

The synthesis of a mission profiles depends on the application as illustrated in Figure 8 :

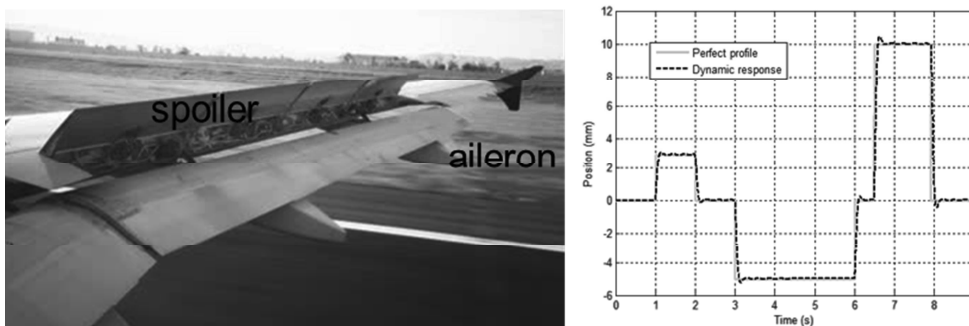
- **Predefined mission profiles:** the displacement curve/ profile can be fixed once and for all by a point-to-point displacement curve. For aircraft actuation systems, typical applications are

landing gear, doors and some secondary flight controls (flaps and slats). Some shape parameters can be used to optimize the actuator on the criterion of velocity, acceleration or maximum power.

- **Mission profiles extracted from simulator or measurements:** Effort/movement profiles are generated by a global system simulator or directly acquired by measurements on previous applications. For aircraft actuation systems, typical applications are primary flight control as ailerons or rudder. This mission profiles can present non-physical discontinuities & higher dynamics than that required (sampling, various flight stages put together). A filter implemented as a state model can be used to adapt a profile with dynamics compatible with the main saturations or main power limits of actuators.



a) Predefined mission profile



b) Mission profiles from simulator or measurements

Figure 8 – Different types of transient mission profiles

2.3. Mission profile analysis and simplification

Design scenarios represent stresses involving slow or rapid degradation. Gradual degradation scenarios are those that cause failure of the actuator after an expected lifetime. While rapid degradation is produced by maximum performance, transient power demand or failure conditions. For permanent flight control actuators like ailerons and elevators, airframe manufacturer mission profiles contain the required actuator speed and applied loads for a long period of time. Such profiles, containing multiple phases as illustrated in Figure 9, are usually complex. It can be convenient to simplify them in order to validate specific duty cycle requirements and shorten the preliminary optimal sizing process and further tests. The process for doing this consists of finding the simplest equivalent test profiles that can stress the components equally. For that purpose graphical maps and numerical indicators can be used in order to compare complete and simplify mission profiles.

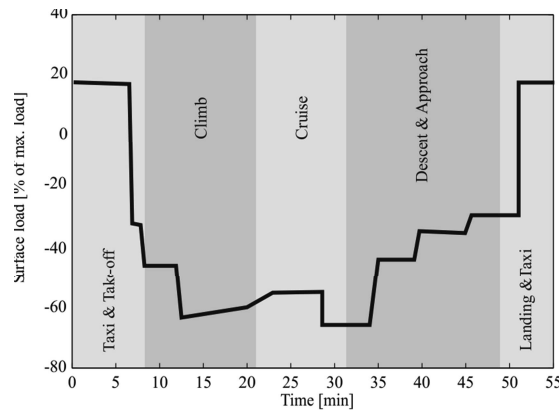


Figure 9 – Different phases of an airframe manufacturer's mission profile for an aileron [18]

Generally, the highest speeds and loads must be kept in the profile in order to verify the behaviour of mechanical and electrical components against required actuator performance levels. If the mission profile actuator dynamics do not match the specification, as illustrated in Figure 10, a state space filter can be added in order to adapt the mission profile. An implementation of such a filter is shown in Figure 11, and includes:

- An acceleration limitation: linked to maximum motor torque/ power electronics maximum intensity and global inertia.
- A speed limitation: linked to the Power Drive Electronics (PDE) voltage limit, rotor mechanical limit or electronic switching.

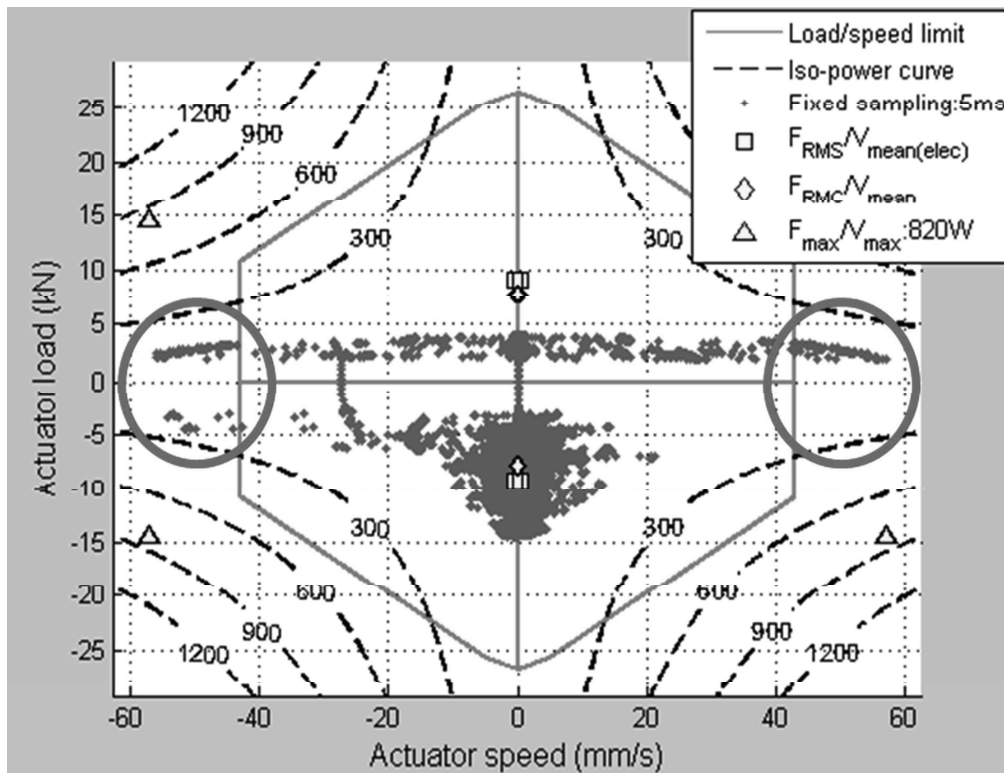


Figure 10 – Actuator mission profile

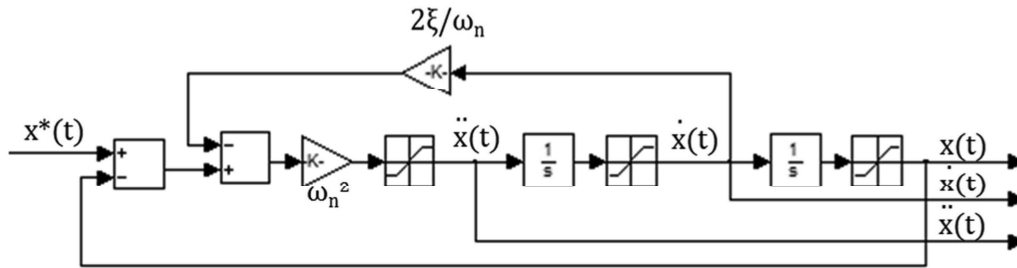


Figure 11 – State model filter

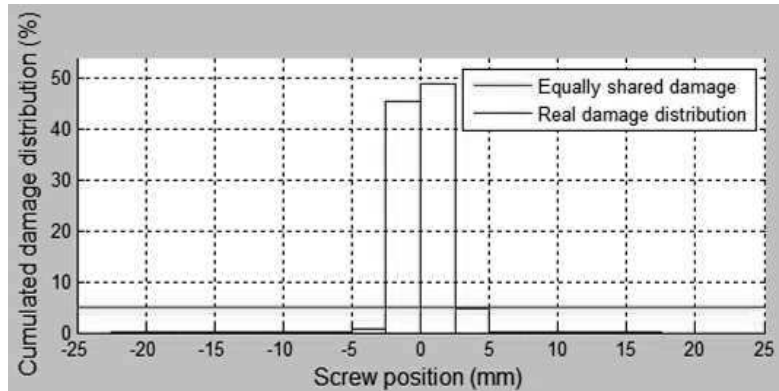
Concerning mechanical fatigue and cyclic phenomena, rolling-fatigue can be characterized by the indicator:

$$Q_{RF} = \int |F^\alpha V| dt \quad (4)$$

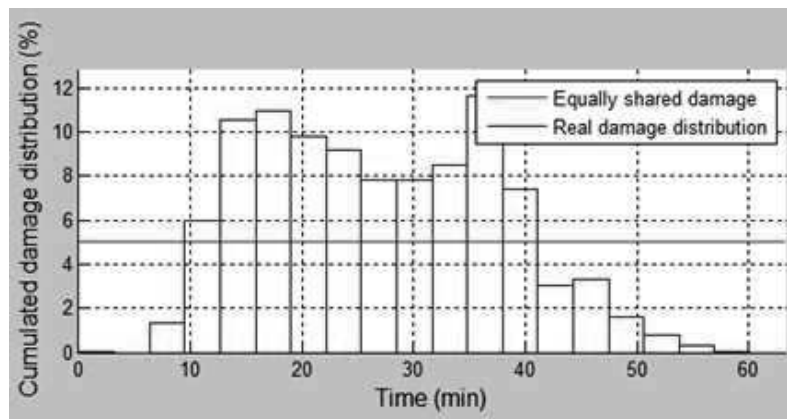
where α depends on the rolling contact geometry (3 for circular contact and 10/3 for linear), while F and V are respectively the force and speed developed. Figure 12a and b give 2 examples of the rolling fatigue distribution (% of total mission fatigue) calculated:

- on position intervals to see if fatigue is shared equally over the whole screw thread.
- on time intervals to see if fatigue is shared equally over the flight.

For this example, most of the damage occurs during the cruise phase and is concentrated on few screw threads as suggested by the rolling fatigue distributions. It is then possible to define a simplified sinusoidal motion profile with constant load during a reduced time. This leads to the same maximal degradation as the original airframe manufacturer's profile with the advantage of easier design calculations and validation tests.



a) Position



b) Time

Figure 12 – Rolling fatigue distribution in time and space [18]

Representing motor overheating is more complex because the behavior of a thermal model has to be considered to compare transient winding overheat to average overheat. The latter can be represented mechanically with the Root-Mean-Square (RMS) of the mechanical load F as,

$$F_{RMS} = \left(\frac{1}{t} \int |F^2| dt \right)^{\frac{1}{2}} \leftrightarrow \left(\frac{1}{t} \cdot \int |i^2| dt \right)^{\frac{1}{2}} \quad (5)$$

This is proportional to the copper losses, which depends on the square of the current i of the motor. To characterize the electric motor's transitory thermal behaviour, the square load can be filtered by using a function with the same time response as a typical brushless motor. The thermal model shown schematically in Figure 14 can be used for this purpose.

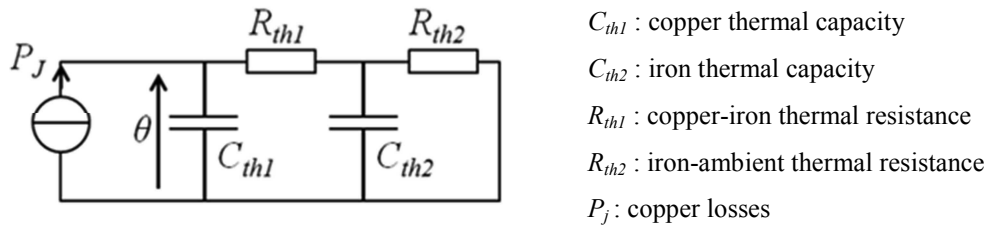


Figure 13 – 2-body electric motor thermal model [18]

A simplified equivalent profile must lead to the same motor thermal behaviour as the original profile. For this purpose, the evolution of the RMS filtered load can be analysed as shown in Figure 14 for an aileron application. Since an exact thermal time constant is not known, the motor's thermal model can be varied between possible extreme values in order to observe critical behaviour. For this analysis it has been assumed that the actuator has no time to cool down during the aircraft preparation phase on the ground. The complete mission profile can be replaced by a constant load with a small sinusoidal movement for a reduced time. Figure 14 shows that the maximum temperature is the same for the complete mission profile and for the simplified one.

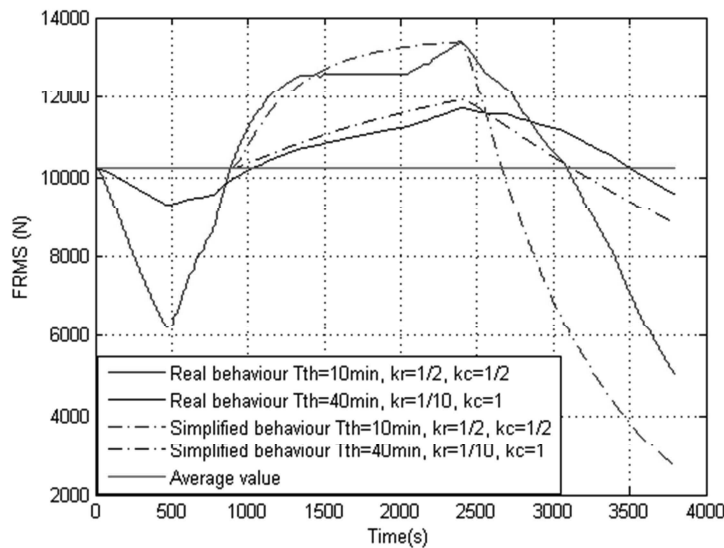


Figure 14 – Filtered RMS load given by two different 2-body thermal models [18]

Dimensionless indices can also be used to compare degradation phenomena of the different components and determine the most important ones e.g. root-mean-cubic load which is related to rolling-fatigue can be compared to maximum load.

3. CHOICE OF MODELING LEVELS

During the downward-sloping branch of the V cycle, the information available on components, which have not yet been selected, is limited. The modelling level should be as simple as possible to minimize the number of parameters to be provided, should be as fast as possible to allow optimization, while providing

access to the useful design variables. Way of obtaining such models by deduction or reduction [19] are illustrated here with two examples of electromechanical drives.

3.1. Deduction approach

The model deduction approach gradually refines the model until the appropriate level of modelling is obtained: the components are first represented by their ideal functional behaviour and the imperfections are added to represent phenomena with smaller and smaller time constants (Table 2). To illustrate this approach, we will look at the modelling of a fan motor assembly present in a cooling tower of a power plant where the heated water is cooled by a stream of upward cool air. These induced draft cooling towers are tending to replace conventional natural draft cooling towers for reasons of visual impact and flexibility of adjustment. The fan motor, Figure 15, shown on top of the tower, comprises an induction motor, a shaft, a gear reducer and the propeller fan. The motor is directly connected to the electrical network via switches and protective elements. No variable speed controller is used and therefore the motor operates in a steady state at a fixed speed except when starting up.

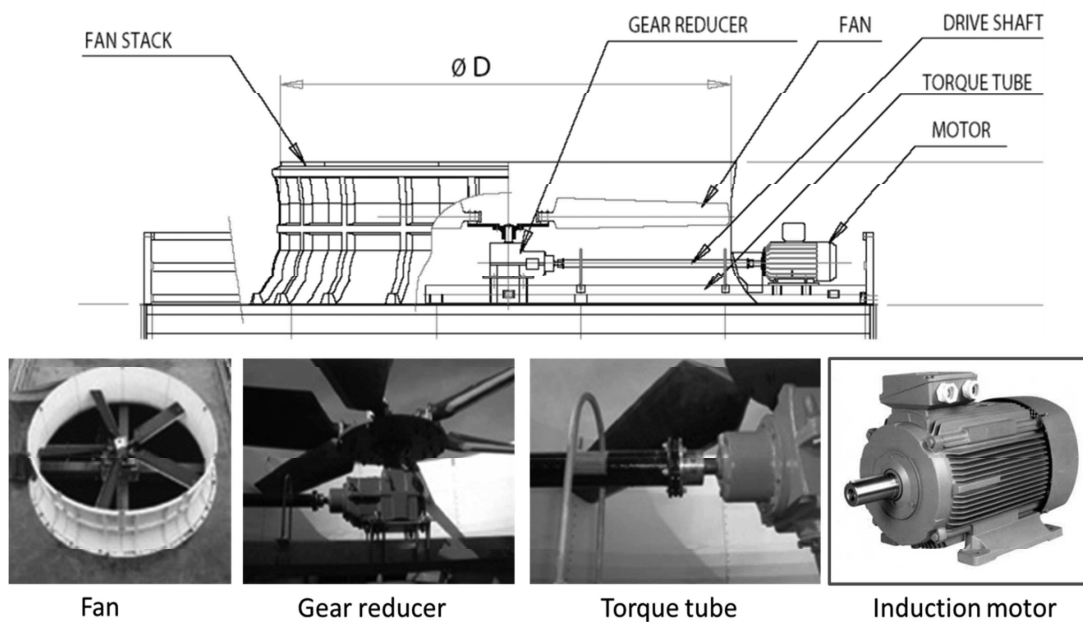
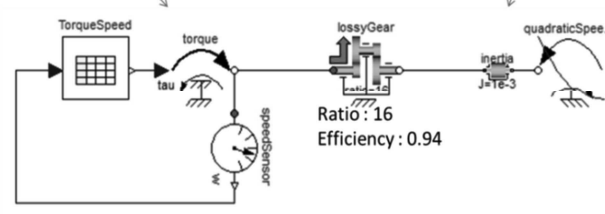
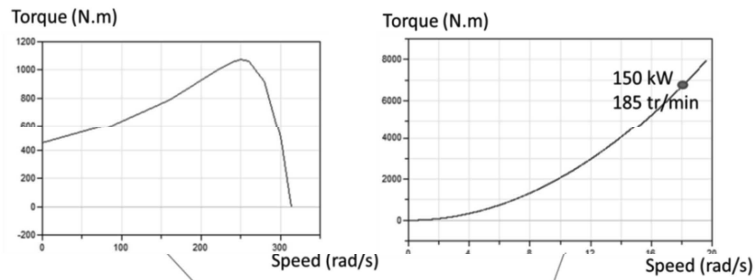


Figure 15 - Diagram and components of the fan motor (source [20])

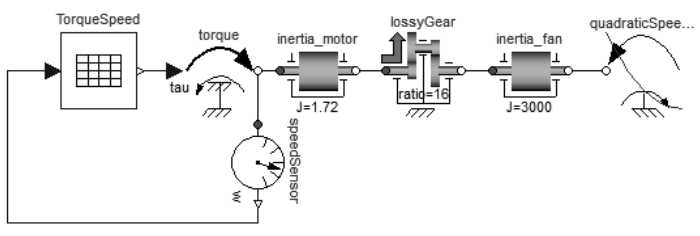
The Figure 16 presents the different levels of modeling with gradually increasing complexity:

- The first level model, quasi-static, represents only the torque / speed characteristics of the motor and load, and the reducer with its transformation and loss aspects. This model represents torque and speed in the steady state after startup.
- The second level represents the inertia of the engine and the propeller, and can take the acceleration and the maximum torque of the induction motor during start-up into account.
- The third level takes the flexibility of the shaft into account, which can generate oscillations in conjunction with the inertias.
- The last level takes the electrical time constants of the stator and rotor into account.

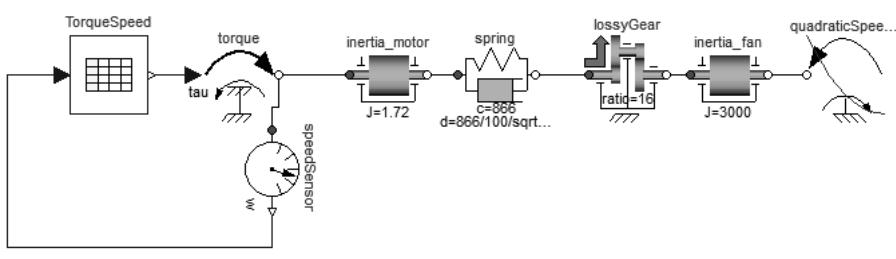
Figure 17 gives simulation results at the high speed shaft of the gear reducer for each modelling level. The objective of these simulations is to evaluate the maximum torque applied on this component. Steady state results are similar for all modelling levels. However, during start-up, the maximum torque is highly sensitive to the model chosen. For this application, the stiffness of the shaft and the mechanical resonance mode thus seem to be of primary importance. This mode is excited by the torque step due to direct-on-line connection and also by the negative damping characteristic of the first part of the torque / speed curve of an induction motor. The last level d) does not provide any additional information for this maximum torque. The proper model here is the level c).



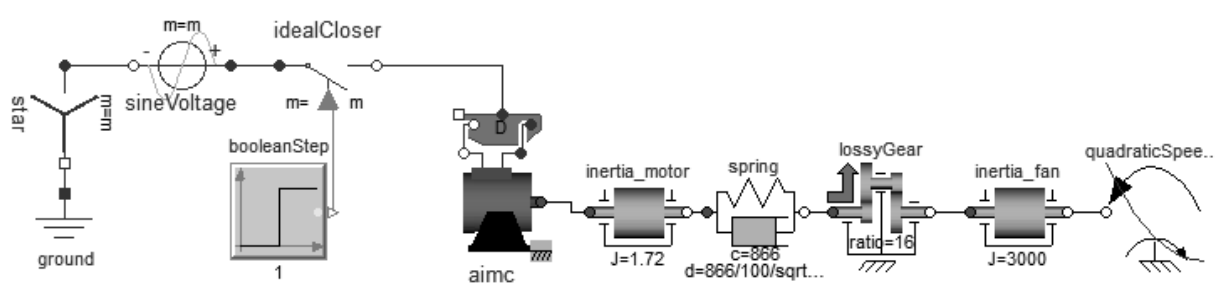
a)



b)

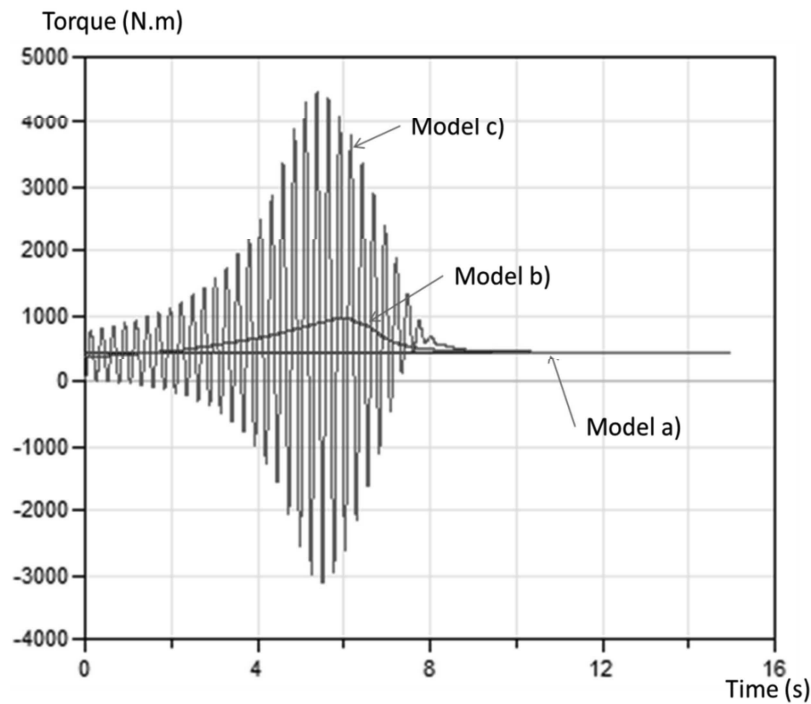


c)

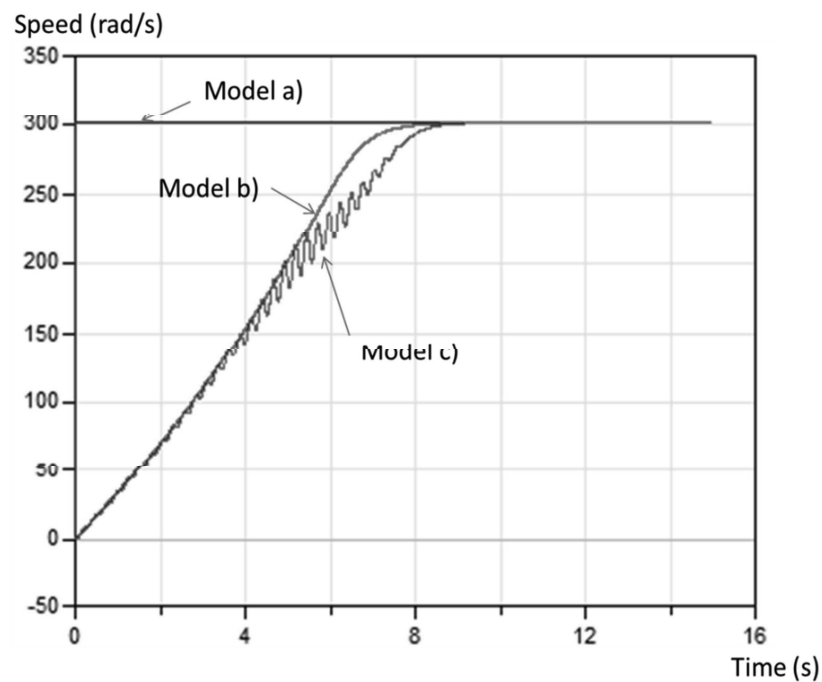


d)

Figure 16 - Different modelling levels for the motor fan



a) High speed shaft reducer torque



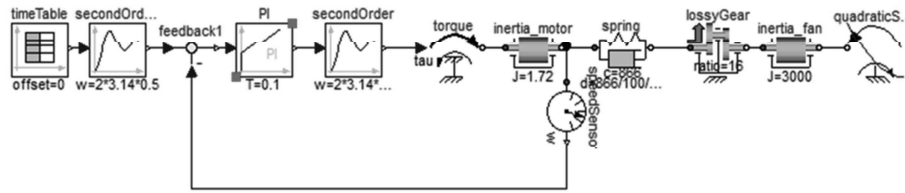
b) High speed shaft reducer speed

Figure 17 - Simulations of the different modelling levels (high speed shaft)

The high start-up torque of an induction motor can be reduced if a smooth speed profile is applied thanks to a speed controller. Figure 18 shows the corresponding model where the speed controller can be represented by a PI controller or by an inverse simulation. The inverse simulation avoids having to design the controller with the desired performance by imposing a zero error directly between the reference speed and the movement obtained. Both models provide the same results. It may be noted, Figure 19, that the maximum torque applied to the gear reducer has a much lower value in this case compared to previous

architecture and the torque oscillations are significantly reduced. Level b) of modeling could even be used in this case with small error.

Forward simulation with speed controller :



Inverse simulation :

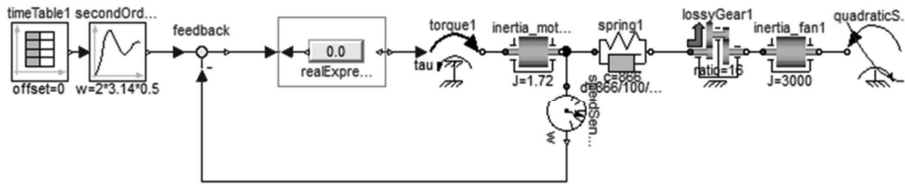


Figure 18 – Motor fan with speed controller

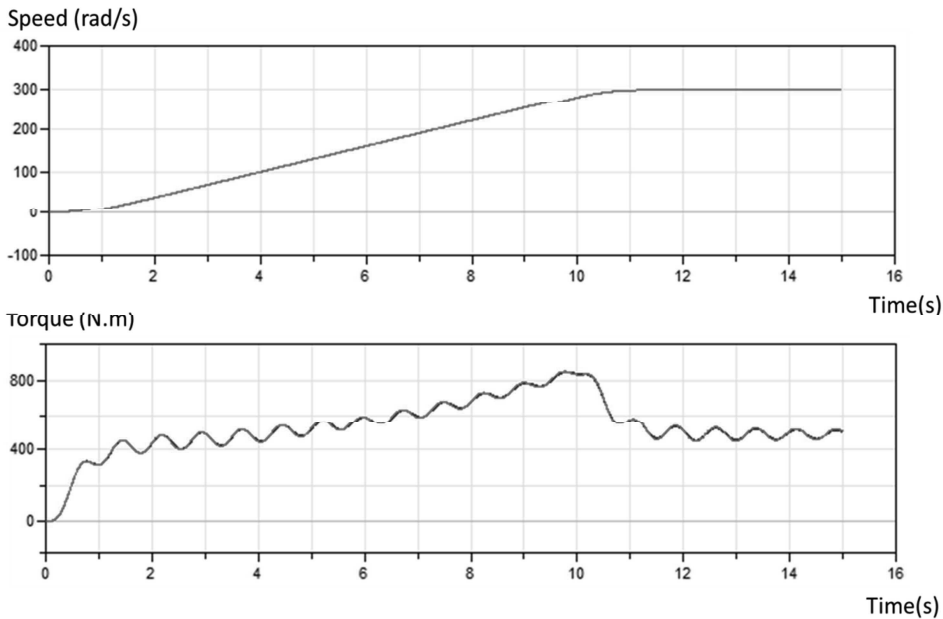


Figure 19 – Torque and speed with inverse and direct simulations

3.2. Reduction approach

The model reduction approach starts with a very detailed model and keeps only the elements that most influence the desired response model. Ersal et al. [19] classify the reduction modeling techniques presented in the literature into frequency-, projection-, optimization-, and energy-based. Only the energy-based methods are studied here because they can work directly on the lumped parameter model without shifting the representation to frequential (transfer function) or state space (matrix) models. The energy-based proper modelling techniques are built on the premise that in a power system, the most important components to model accurately are those characterized by the largest magnitudes of energy (or power) flow. Therefore, these algorithms simplify a given model by eliminating less energetic components, while trying to minimize the effect of the elimination on the overall energy flow. The activity of an energetic element is defined as the time integral of the absolute value of the power flowing through it over a particular time-window for a particular input. In a bond-graph setting, where the flow through an element and the effort across it are denoted as f and e , respectively, the element's activity A_i is defined as:

$$A_i = \int_0^T |f(t)e(t)| dt \tag{6}$$

This metric was defined by Luca in [21]. These indexes are directly present in some programs such as AMESim [7]. They are easily implementable in any environment, as here Dymola / Modelica [22], in the form of sensors as shown in Figure 20.

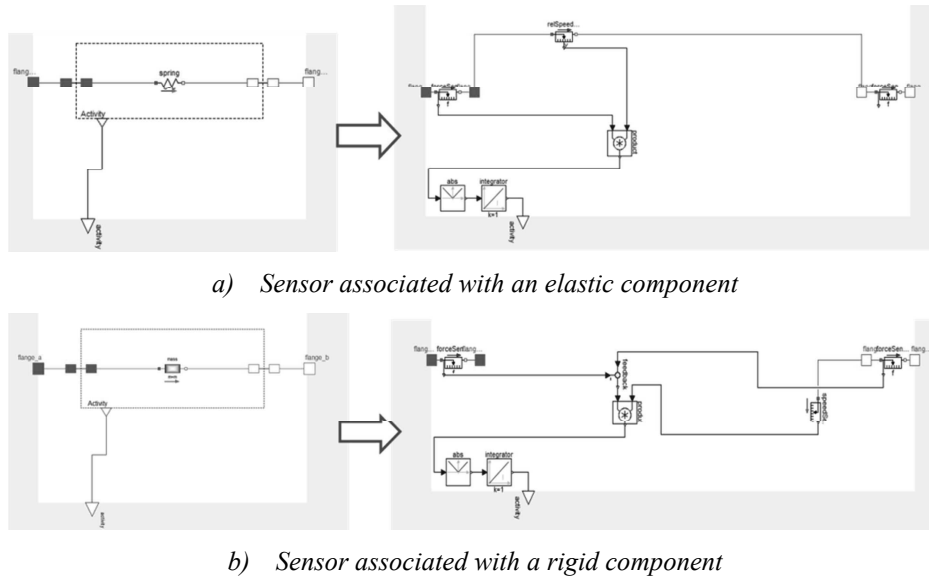
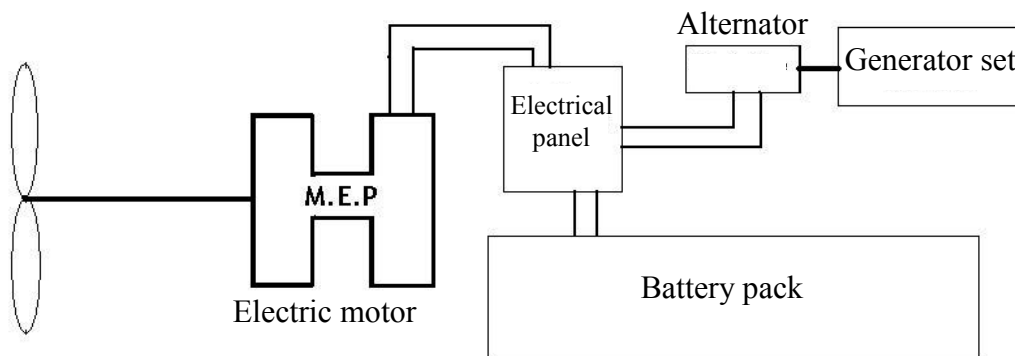
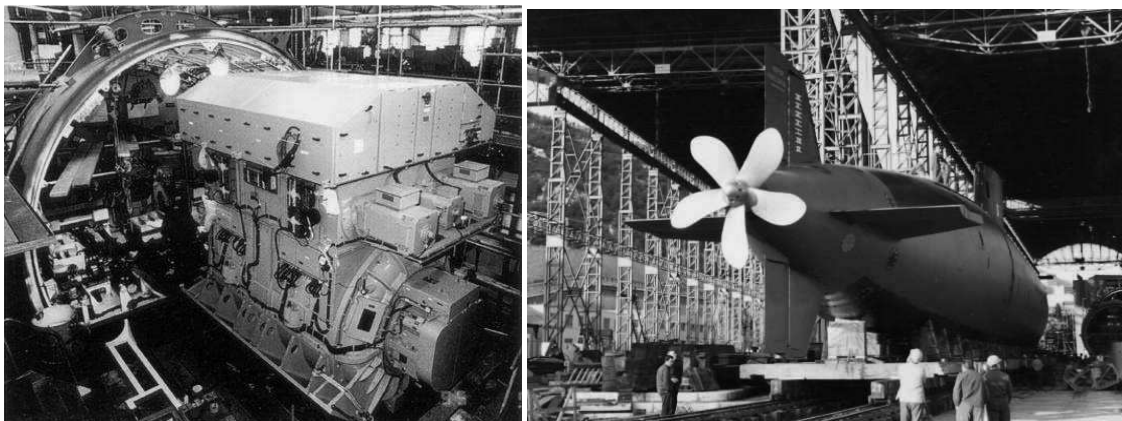
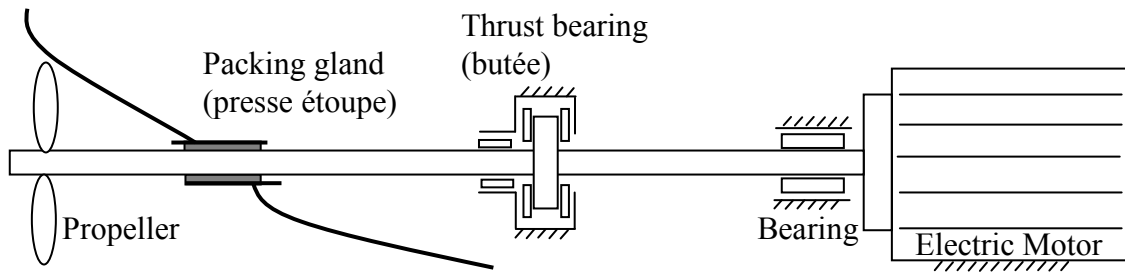


Figure 20 – Activity index sensors

The model reduction will be exemplified here with the modelling of a critical case: the short-circuit torque of a submarine propulsion motor. This calculation corresponds to a sizing scenario for the drive shaft and could be part of the overall design procedure of submarine propulsion. Figure 21 represents the electrical and mechanical diagrams of such a propulsion system.



Electrical components : schematic wiring diagram



Shaft line : mechanical diagram

Figure 21 – Propulsion system (DC propeller motor – SIEMENS)

Figure 22 represents a full lumped model with all electrical and mechanical phenomena where:

- the DC electric motor is modelled by an electromechanical gyrator, an electrical resistance, an electrical inductance, mechanical viscous friction and mechanical inertia;
- the propeller is modelled by inertia and a quadratic torque source ;
- the shaft is modelled by stiffness with low internal damping ;
- the packing gland and the thrust bearing are modelled by dry friction.

The short circuit is modeled by setting the supply voltage to zero after a gradual rise and stabilization. Table 3 gives the evaluation of the element's activities: the third column indicates the value of each activity as a percentage of the overall amount of activities. It may be noted that the motor inertia and shaft stiffness have lower power activities than the motor inertia and the propeller inertia. It therefore seems worthwhile to eliminate them to simplify the model. Figure 24 compares the simulation results for the full model and the reduced model. The difference between the two simulations for the short circuit torque is slight. The reduced model, shown in Figure 23, seems therefore suitable for the sizing of the shaft.

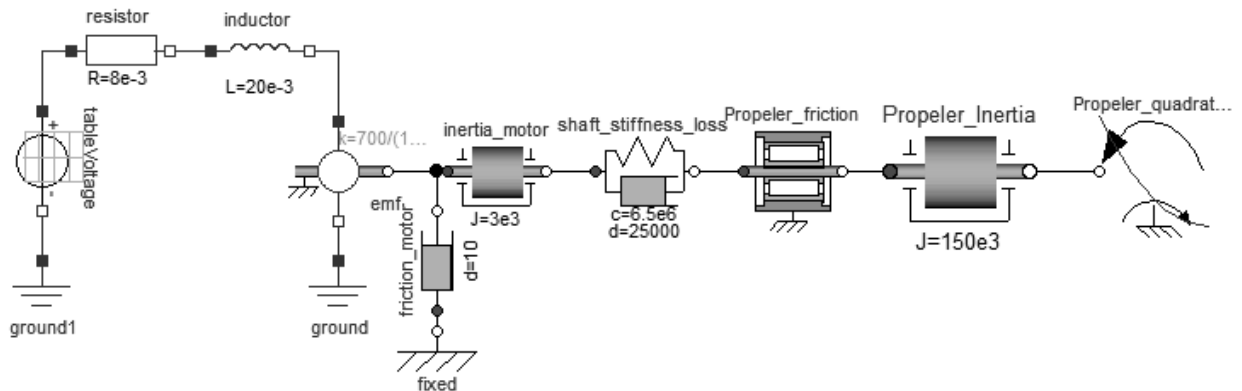


Figure 22 – Full model for the propulsion system

Sensor	Max Value	Percentage
Motor inductor	1.51E+07	33%
Shaft stiffness	6.12E+05	1%
Motor inertia	3.47E+05	1%
Propeller inertia	2.96E+07	65%

Table 3 – Activity indexes

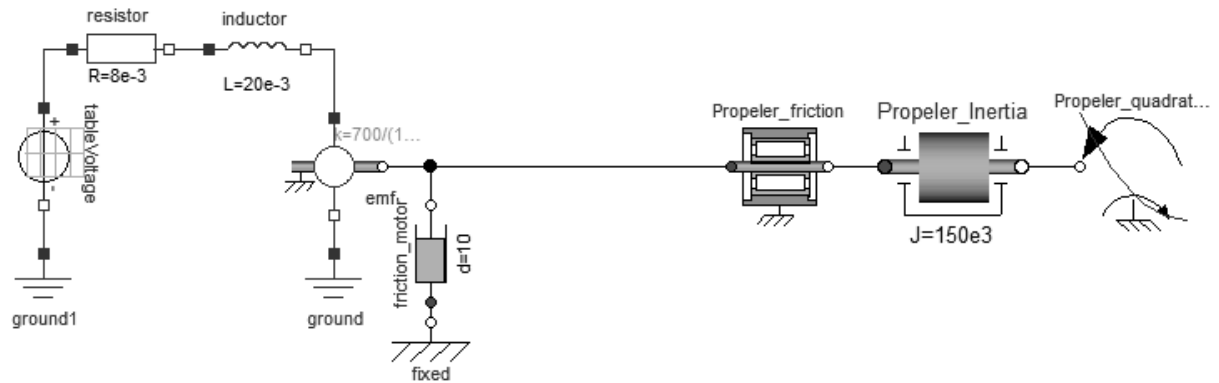


Figure 23 – Reduced model for the propulsion system

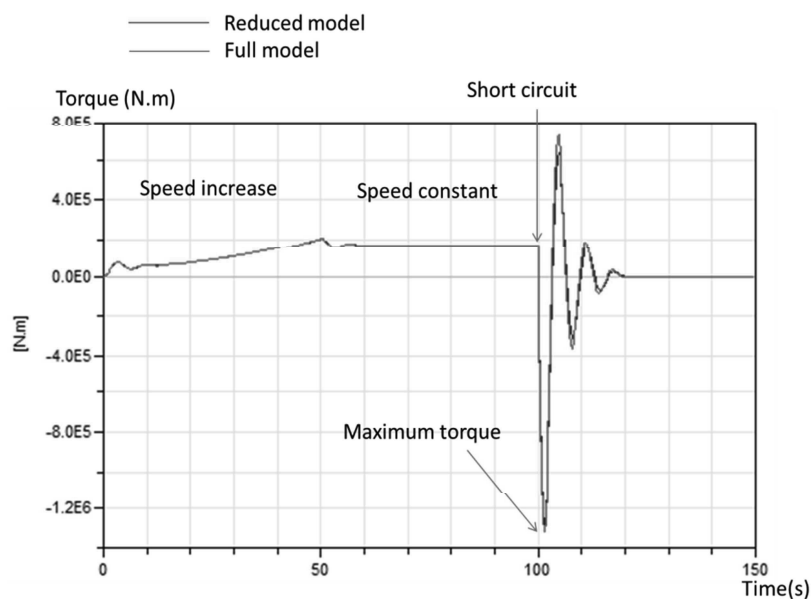


Figure 24 – Transient torque during short circuit for full and reduced model

4. CONCLUSION

The models used during design at system level usually take the form of lumped parameter models. This chapter has shown that, to satisfy the various viewpoints encountered during the design of a mechatronic system, simulation models can take multiple levels of description and different orientations. They need to be simple to minimize the information needed during synthesis, and as exact as possible, in order to reach the main sizing variables. These objectives can be achieved by working on the definition of mission profiles and sizing scenarios and with the use of the right simulation models. Different analysis techniques have been presented and illustrated with examples. Paper 2 shows how inverse simulation presented in this chapter, and scaling laws, presented in the previous chapter, can be used together in order to obtain sizing tools.

5. BIBLIOGRAPHY

- [1] H. Van der Auweraer, J. Anthonis, S. De Bruyne and J. Leuridan, "Virtual engineering at work: the challenges for designing mechatronic products," *Engineering with Computers*, vol. 29, pp. pp. 389-408, 2013.
- [2] P. Hehenberger, F. Poltschak, K. Zeman and W. Amrhein, "Hierarchical design models in the mechatronic product development process of synchronous machines," *Mechatronics*, vol. 20, pp. pp. 864-875, 2010.
- [3] F. Cellier and J. Greifeneder, *Continuous System Modeling*, Springer, Ed., 1991.
- [4] MathWorks, "www.mathworks.com," [Online].
- [5] Scilab, "www.scilab.org," [Online].
- [6] 20-sim, "www.20sim.com," [Online].
- [7] L. Imagine, "www.lmsintl.com," [Online].
- [8] D. C. Karnopp, D. L. Margolis and R. C. Rosenberg, *System Dynamics: Modeling, Simulation, and Control of Mechatronic Systems*, Wiley. com, 2012.
- [9] M. Association. [Online].
- [10] S. E. Mattsson, H. Elmqvist and M. Otter, "Physical system modeling with Modelica," *Control Engineering Practice*, vol. 6, no. 4, pp. 501-510, 1998.
- [11] J. Bals, G. Hofer, A. Pfeiffer and C. Schallert, "Object-oriented inverse modelling of multi-domain aircraft equipment systems with Modelica," in *3rd International Modelica Conference, Linköping, Sweden, November 3-4, 2003*.
- [12] D. J. Murray-Smith, "The inverse simulation approach: a focused review of methods and applications," *Mathematics and Computers in Simulation*, vol. 53, pp. 239-247, 2000.
- [13] J. Liscouet, M. Budinger, J.-C. Maré and S. Orioux, "Modelling approach for the simulation-based preliminary design of power transmissions," *Mechanism and Machine Theory*, vol. 46, no. 3, pp. 276-289, 2011.
- [14] S. E. Mattsson, H. Elmqvist and M. Otter, "Physical system modeling with Modelica," *Control Engineering Practice*, vol. 6, no. 4, pp. 501-510, 1998.
- [15] R. Ngwompo, S. Scavarda and D. Thomasset, "Inversion of Linear Time-invariant SISO Systems Modelled by Bond Graph," *J. Franklin Inst.*, vol. Vol. 333(B), pp. pp. 157-174, 1996.
- [16] C. Maffezzoni, R. Girelli and P. Lluka, "Generating efficient computational procedures from declarative models," *Simulation Practice and Theory* , vol. 4, no. 5, pp. 303-317, 1996.
- [17] A. Fröberg and L. Nielsen, "Efficient Drive Cycle Simulation," *IEEE transactions on vehicular technology*, Vols. Vol. 57, n° 3, pp. pp. 1442-1452, 2008.
- [18] D. Arriola, A. Reysset, M. Budinger, F. Thielecke and J.-C. Maré, "From Airframer Requirements to Detailed Technical Specification of Electromechanical Actuators Aided by Knowledge-Based Methods," in *SAE 2013 AeroTech Congress & Exhibition, Montréal, Quebec, Canada , September 24-26, 2013.*
- [19] T. Ersal, H. K. Fathy, L. S. Louca, D. G. Rideout and J. L. Stein, "A review of proper modeling techniques," in *Proceedings of IMECE2007, November 11-15, 2007, Seattle, Washington, USA.*, 2007.
- [20] H. Group, "www.hamon.com," [Online].
- [21] L. S. Louca and J. L. Stein, "Physical Interpretation of Reduced Bond Graphs.," in *Proceedings*

of 2nd IMACS International Multiconference: Computational Engineering in Systems and Applications (CESA'98), 1998.

- [22] D. S. Dynasim, "www.dynasim.se," [Online].

Paper 2 - Modelling approach for the Simulation-Based Preliminary Design of Power Transmissions

ABSTRACT

The promises of Model Based Design have led to the development of numerous methodologies and software tools, especially for the specific or detailed design stages, from controller design to finite element analysis. However, the Model Based Design of actuation systems lacks methodologies and expressive simulation models that are suited to preliminary design, where key technical decisions are taken considering various design alternatives and few available design details. In order to fill this gap, the present paper illustrates how scaling laws and acausal modelling can be used as a design tool, exploiting inverse simulation capabilities to evaluate technological alternatives quantitatively from limited design detail information. The application of the modelling approach is shown for two major components of mechanical transmission systems: roller bearings and ball and roller screws. The scaling laws presented are validated with manufacturers' data. To conclude, the suitability of the proposed methodology is illustrated with the preliminary sizing of an electromechanical actuator for an aircraft primary flight control surface (aileron).

Keywords: ball-screw, flight control, inverse simulation, model based design, Modelica, modelling, preliminary design, scaling laws.

Referencing: J. Liscouët, M. Budinger, J-Ch. Maré, S. Orioux, *Modelling approach for the simulation-based preliminary design of power transmissions*, Mechanism and Machine Theory, Volume 46, Issue 3, March 2011.



Contents lists available at ScienceDirect

Mechanism and Machine Theory

journal homepage: www.elsevier.com/locate/mechmt

Modelling approach for the simulation-based preliminary design of power transmissions

Jonathan Liscouët, Marc Budinger*, Jean-Charles Maré, Stéphane Orioux

Université de Toulouse, INSA, UPS, Mines Albi, ISAE; ICA (Institut Clément Ader) 135, avenue de Rangueil, F-31077 Toulouse, France

ARTICLE INFO

Article history:

Received 28 August 2009

Received in revised form 25 August 2010

Accepted 16 November 2010

Available online 13 December 2010

Keywords:

Ball screw

Flight control

Inverse simulation

Model-Based Design

Modelica

Modelling

Preliminary design

Scaling laws

ABSTRACT

The promises of Model-Based Design have led to the development of numerous methodologies and software tools, especially for the specific or detailed design stages, from controller design to finite element analysis. However, the Model-Based Design of actuation systems lacks methodologies and expressive simulation models that are suited to preliminary design, where key technical decisions are taken considering various design alternatives and few available design details. In order to fill this gap, the present paper illustrates how scaling laws and acausal modelling can be used as a design tool, exploiting inverse simulation capabilities to evaluate technological alternatives quantitatively from limited design detail information. The application of the modelling approach is shown for two major components of mechanical transmission systems: roller bearings and ball and roller screws. The scaling laws presented are validated with manufacturers' data. To conclude, the suitability of the proposed methodology is illustrated with the preliminary sizing of an electromechanical actuator for an aircraft primary flight control surface (aileron).

© 2010 Elsevier Ltd. All rights reserved.

1. Introduction

The current competitive market environment calls for cheaper, safer and more environmentally friendly systems, along with ever shorter times to market and an increasing demand for quality and advanced functionalities. The preliminary design [1] is a critical phase of a project that engages most of the decisions and development costs. The goal of this phase is to define and technologically embody a concept that complies with all the different engineering disciplines and requirements involved. Later on in the development, it may appear that the solutions identified do not cope with the various and numerous requirements. With rapidly advancing computational technology, simulation-based and virtual prototyping designs offer great potential for reducing cost and improving design quality by supporting early verification and virtual validation of solutions [2,3]. Therefore, in recent decades, a big research effort has been put into developing software tools dedicated to virtual prototyping early in the development process [2–7]. Nevertheless, there is still a lack of simple and expressive (i.e. adequate level of detail) simulation models suited to the needs of preliminary design, where only a few design parameters are available but major technical decisions are to be taken. This paper introduces an original model-based process that automates the sizing task for power transmission systems like actuators. This process provides the designer with a rapid capability to make top-level decisions. For this purpose, the candidate designs must be compared globally, considering the whole set of criteria: power capability, operation domain, service life, reliability and integration (mass and envelope). As an output, the sizing task must allow the designer to specify the parameters that define the power transmission system components. The proposed sizing process is described in detail in Section 2.

Besides the complexity of multi-criteria design, the complexity also stems from the huge number of parameters associated with the above mentioned criteria. Section 3 is dedicated to scaling laws that can reduce the number of parameters to be handled by

* Corresponding author. Tel.: +33 561559960; fax: +33 561559950.

E-mail address: marc.budinger@insa-toulouse.fr (M. Budinger).

Nomenclature	
CAD	Computer Aided Design
FEM	Finite Element Method
RMS	Root Mean Square
SOA	Safe Operating Area
3D	Three-dimensional

the designer. The interest of this choice is illustrated through the general case of rolling bearings, then in the particular case of ball/roller screws.

Section 4 describes the tools supporting the methodology, which are implemented here as a Modelica library.

Section 5 is used to point out the interest of the proposed methodology for the preliminary design of a redundant aileron actuator for a single aisle aircraft. Special attention is paid to the geometrical integration, the mode of operation and the service life.

The last section summarizes the advances made possible by the proposed approach and suggests further developments.

2. Proposed methodology for the preliminary design

As defined by Refs. [10,11] a methodology is a collection of related processes, methods and tools where:

- a process is a logical sequence of tasks performed to achieve a particular objective (“WHATs”);
- a method consists of techniques for performing a task (“HOWs”);
- a tool is an instrument that, when applied to a particular method, can enhance the efficiency of the task (supports the “HOWs”).

The proposed methodology is applied in the framework of Fig. 1 “sizing wave” process that propagates backwards, in the direction opposite to the functional power path. The system components are considered in sequence, from the customer’s power need to the system power source. As shown by the flow diagram of Fig. 1 for a given component, the proposed process is iterative and decomposed into four tasks for each component, which are detailed in the following sections. The process is iterated until the calculated system performance matches the customer’s requirements.

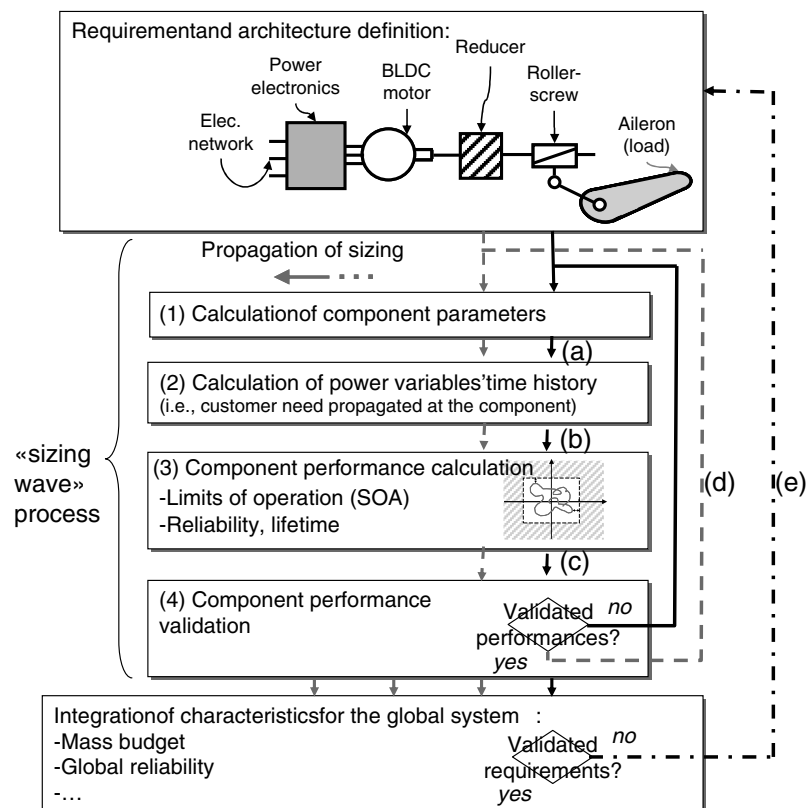


Fig. 1. “Sizing wave” process.

2.1. Task 1: Automatic calculation of the whole vector of component parameters

The proposed "method" is based on reducing the number of component parameters to be handled by the designer. The parameters involved in the sizing process are then automatically calculated with estimation or prediction models [12]. These models should reach a similar level of representativeness and have to reflect the state-of-the-art of technology. An efficient way to ensure this homogeneity is found by developing the models through a uniform approach. The most direct approach is to use databases like some software designers [13] do. This approach has the disadvantage of being cumbersome, or even impossible, to implement in the absence of product ranges, as in aerospace applications. For the same reason, metamodels using response surface methodology [14], interesting for optimization, seem inappropriate here. Some design codes from mechanical design standards may also be used [6]. The latter approach requires a significant level of expertise for each component and is therefore cumbersome to implement and reduces the number of technologies that can be considered, depending on the availability of experts. The use of scaling laws or similarity rules has the advantage of needing only one reference component for the complete evaluation of a range. Such a modelling approach has already been applied for system design or comparison of technologies [15–20].

Estimation models used in system-level design aim to link functional characteristics (input) to secondary characteristics (output). To this end, we propose to define four different types of parameters here:

- *Definition parameters (input)*. To support the designer in pre-specifying or selecting off-the-shelf components, the definition parameters are defined as those given in the product requirement definition and commonly used in manufacturers' datasheets for component selection. For example, the proposed definition parameters for a ball screw are the nominal output force, the pitch, the stroke and the lifetime. Some parameters are defined by requirements (e.g., life time) and architecture choices (e.g. pitch). The others should be defined by iteration during the sizing process (e.g. nominal output force and stroke).
- *Simulation parameters (output)*. From the definition parameters, the scaling laws generate the simulation parameters that are required for the time domain simulation of step 2 (Fig. 1). In the case of a ball screw, the simulation parameters are those affecting the instant power need and the dominant dynamics (e.g. moment of inertia and friction).
- *Integration parameters (output)*. The scaling laws also have to generate the integration parameters that are used to verify that the customer's integration needs are met. The integration parameters are typically associated with mass and geometry (e.g. ball screw's diameter, length and mass per unit length).
- *Operational parameters (output)*. The estimation models also have to generate the operational parameters that define the Safe Operating Area (SOA). The SOA is representative of the limit of operation of the component in terms of its ability to fulfil its mission safely during the whole specified service life (e.g. ball screw's maximum output force, maximum speed and dynamic load).

Input to task 1 is the vector of definition parameters as defined by the designer. The first loop of the sizing wave is run with the initial vector provided by the designer from rough sizing. Output of task 1 is the vector of simulation and integration parameters that is automatically generated by the specifically developed library of component models that integrate the proposed estimation models described in Section 3. Even though this step involves only pure algebraic calculation, the numerical calculations are implemented with the Modelica [21] time domain simulation language, which was selected to meet the specific needs of step 2.

2.2. Task 2: Calculation of power variable time history

The selected "method" consists of the inverse simulation of the full top-level component model that allows backward propagation of power variables. Inverse simulation of power variables is enabled by modelling based on a non-causal language, Modelica [22], which have recently been introduced as industrial "tools". Step 2 requires continuous time dynamic models that are expressed by Differential Algebraic Equations (DAE) and are based on a lumped parameter representation of the component. In the early preliminary design phase, the simulation models have to capture all the relevant states without being too detailed. For example, only the mechanical inertias, electrical resistances, electromotive forces, thermal capacitances and resistances, and the dominant energy losses are relevant for the power sizing and integration of electromechanical transmission components. More detailed phenomena, such as electrical inductance, mechanical compliances, and backlashes (etc.) can be neglected in a first approximation as they usually introduce second-order effects. The Modelica models are simulated here (see Sections 4 and 5) within the Dymola [23] environment. The Modelica choice was motivated by the non-causal and object-oriented capabilities [21] that suit the virtual prototyping of multidisciplinary systems well [3–9]. Compared with a causal approach, where relations between variables are oriented and predefined by procedural statements, non-causal modelling involves only non-oriented relations between variables [21] that are defined by declarative statements. The advantage of a non-causal model is its ability to carry out both the direct and inverse simulations [24,25] which can meet different engineering needs through the mechatronic V design cycle [26]. Corresponding mathematical and numerical aspects are not developed in this article but are described in Ref. [27]. A modal analysis or the verification of a controller is generally supported by a direct simulation. As illustrated in Fig. 2, efficient power sizing avoids modelling the controller when using inverse simulation of the power flows going from the actuated load to the power source through the architecture components [24].

Input of task 2 is the vector of simulation parameters generated during step 1 and the mission profile supplied by the customer. Output of step 2 is the time history of all the component variables (e.g. ball screw's instant screw speed, acceleration or torque) that are automatically calculated using the specifically developed dynamic model library.

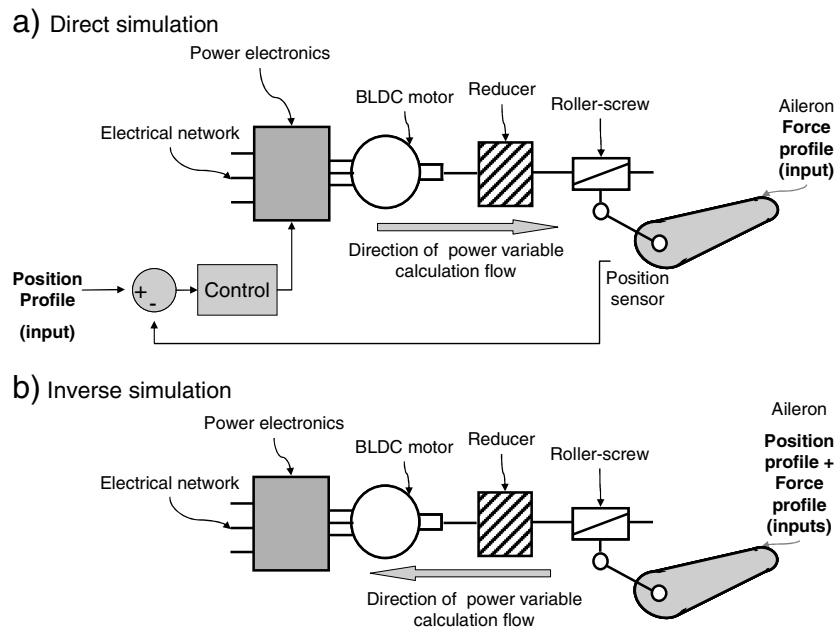


Fig. 2. Inverse vs direct simulation of an actuation system controlled in position.

2.3. Task 3: Performance calculation

The "method" consists of collecting the time domain data and extracting quantities that are representative of the power capability, the operating limits, the service life and the reliability. Safe operation domain analysis and degradation models for lifetime and reliability have been developed and are involved as key "tools" for this task [28]. Correct sizing must ensure that, during a mission, the components' transient and continuous operational boundaries are not exceeded. On the one hand, a mission profile included within the transient operational capabilities of the components prevents rapid degradation (e.g. overheating of electric motor windings). On the other hand, a mission profile included within the continuous operational boundary ensures confidence in the components throughout their operational lifetime by taking slow degradations (e.g. mechanical fatigue and thermal ageing) into account. The continuous operational boundary should include reliability and lifetime aspects. Over time, slow degradations of component properties (e.g. mechanical strength) progressively increase the probability of their being exceeded during a mission and thus increase the probability of failure. In the proposed "method", an adapted formulation of the corresponding reliability has been developed that compares the specified and obtained standard lifetimes to calculate the actual reliability parameters of the component for the specified lifetime. Then the reliability parameters can be tailored efficiently by iterating on the component sizing or lifetime. The methods, models and references associated with this stage are developed further in [28].

The inputs of task 3 are the operational requirements and the time history of the component variables (step 2). The output of task 3 is the effective performance of the actual design in terms of safe operating area (SOA) and reliability for the service life.

2.4. Task 4: Component design validation

The "method" consists of summarising the actual design capabilities and comparing them with the required power needs. The integration parameters are taken directly from step 1 while power capability, operational limits, lifetime and reliability come from step 3. For the time being, the iterative process is based on the designer decision to run another loop modifying the definition parameters with respect to the difference between required and calculated power capabilities. However, it has been observed, in many and various case studies, that convergence is ensured within a few iterations.

2.5. Synthesis and optimization

Once power sizing is achieved for all components, it is possible to synthesize the whole system characteristic, which may take the form of a mass balance, global reliability or overall size. A manual or automatic iteration (optimization) over the entire architecture can be implemented on the parameters of the global architecture. Ref. [29] gives an example of the sizing process automation (link (d) on Fig. 1) and global optimization (link (e) on Fig. 1). The rest of this paper focuses more specifically on the models for the sizing process needed.

3. Preliminary sizing models with scaling laws

Appendix A recalls the notations and geometrical assumptions adopted here for establishing scaling laws.

3.1. Proposal of scaling laws for rolling elements

3.1.1. Proposed model for bearings

Rolling bearings are basic elements present in most mechanical devices. In some applications, like those addressed in this paper (Section 5), the resulting radial and axial forces are very large and cause the rolling bearing to have a major influence on the component geometrical envelope and mass. Therefore, it is interesting to develop a dedicated sizing and simulation model for this basic component and to re-use it later in the roller-screw model. Moreover, the relative simplicity of the rolling bearing makes it a good start for introducing the proposed approach.

In the context of power sizing in preliminary design, bearings are assumed to be ideal rigid pivots. A three-dimensional translational connector is added to this model, in order to simulate withstanding the radial and axial forces transmitted to the bearing and to calculate the equivalent static or dynamic load that is a combination of these forces [33]. Selecting a bearing with an adequate load rating with respect to its mission ensures confident operation throughout its lifetime. Typically, in bearing manufacturers' catalogues (e.g., [30–32]), the primary selection parameter is F_{nom} the nominal equivalent dynamic load. Therefore, the dynamic load is chosen as a definition parameter. The scaling laws, developed in this section, aim to establish the relationships between this definition parameter and the simulation, integration and operational limit parameters.

For mechanical components like bearings, the mechanical stresses in the materials must be kept below elastic, fatigue or contact pressure (Hertz) limits [33]. Taking the stress limit σ_{max} to be the same for a full product range yields

$$\sigma_{max}^* = 1 \Rightarrow F_{nom}^* = l^{*2} \quad (1)$$

where F_{nom} is the nominal load applied to the bearing and l its dimensional parameter.

The integration parameters are the diameters and length of the bearing, which define its geometrical envelope. Assuming geometrical similitude (see Appendix A), all these geometrical dimensions are related to a single scaling ratio l^* . The scaling law or the variation relative to a reference component of bearing mass M is thus expressed by:

$$M^* = l^{*3} = F_{nom}^{*3/2} \quad (2)$$

Since the bearing sizing is based on mechanical stress, the F_{max} maximum load variation is proportional to the nominal load:

$$F_{max}^* = F_{nom}^* \quad (3)$$

The frictional losses increase with the speed, causing the temperature of the bearing to rise. Consequently, the lubricant film becomes thinner and the friction coefficient increases. Beyond a critical temperature, this phenomenon rapidly causes unacceptable wear damage. In other words, the speed limit of the bearings is the image of a maximum admissible temperature increase during steady nominal operation. The heat exchange between the bearing and its environment is mainly convective and, to a first approximation, the convection coefficient is assumed constant. Thus, the variation of the thermal resistance depends on the variation of the external surface area of the bearing. Moreover, the losses in the bearing are proportional to the mechanical power transmitted. Thus:

$$\left. \begin{aligned} Q_{th}^* &= R_{th}^{*-1} = l^{*2} \\ Q_{th}^* &= v^* \cdot F_{nom}^* = \omega^* \cdot l^* \cdot F_{nom}^* \end{aligned} \right\} \Rightarrow \omega_{max}^* = F_{nom}^{*-1/2} \quad (4)$$

where Q_{th} is the thermal power dissipated by the bearing, R_{th} is the thermal resistance equivalent to the convection between the bearing and its environment, v is the tangential velocity of the bearing balls (or rollers), ω is the speed of the bearing and ω_{max} is its maximum admissible speed.

Based on the scaling laws described in this section, it is possible to calculate the three integration parameters (length, diameter and mass) and the two operational limit parameters (maximum admissible speed and load) of the proposed rolling bearing model from the nominal load only and a reference representative of a given technology (e.g. type of materials).

3.1.2. Proposed model for ball and roller screws

Ball and roller screws transform a rotational motion into a translational one or vice-versa. The power is transmitted between the nut and the screw via balls or rollers. The use of rollers instead of balls significantly increases the points of contact. So, while it allows much higher forces to be transmitted, it decreases the power transfer efficiency. Axial pre-loading is commonly used in applications requiring high accuracy and frequent speed reversals. In the context of the preliminary design and for the purpose of simplification, the pre-loading of the ball and roller screw is not taken into account in the following example.

In the context of power sizing for preliminary design, the ball and roller screws are assumed to be rigid but subject to acceleration and frictional losses. Consequently, we propose a simulation model (Fig. 3) made of the screw rotational inertia, an ideal rotational–translational motion transformation, a friction loss depending on the quadrant of operation, the nut translational inertia and, finally, the end-bearing, for which the model is equivalent to that of the rolling bearing described in Section 3.1.1. The sizing of the end-bearing is driven by the equivalent static/dynamic load it has to stand. Therefore, the simulation model of bearings has a 3D force port that interfaces with the radial and axial forces making up this equivalent load.

As shown in Fig. 3, the proposed model involves five simulation parameters: J_s the screw moment of inertia, p the pitch of the screw per unit angle, η_d the direct and η_i the indirect efficiency, and M_n the nut translational inertia. The friction force is calculated [34] from the direct or indirect efficiencies depending on the quadrant of operation (driving or back driving).

Typically, in ball and roller screw manufacturers' catalogues [24,25], the primary definition parameters are pitch and the nominal output force F_{nom} , which ensures confident operation during the component's lifetime. Therefore, the nominal force was chosen to be the definition parameter from which the definition, simulation and operational limit parameters were derived.

As for the bearings, the scaling laws of the ball and roller screws are based on a fixed maximal mechanical stress. The length of the screw depends on the application, i.e. the required stroke, which is a definition parameter. Consequently, this component cannot be scaled fully homothetically like the nut and end-bearing. It is rather interesting to scale its mass M_l and moment of inertia J_l per unit length:

$$\begin{cases} M_l = \int \rho_m \cdot dS \Rightarrow M_l^* = l^{*2} = F_{nom}^* \\ J_l = \int \rho_m \cdot r^2 \cdot dS \Rightarrow J_l^* = l^{*4} = F_{nom}^{*2} \end{cases} \quad (5)$$

The screw mass and inertia are then obtained by multiplying the mass and inertia per unit length by the total length, which is the sum of the stroke plus the nut and end-bearing lengths. The total mass of the ball and roller screw is the sum of its different part masses. Similarly, the overall moment of inertia is the sum of the rotating element moments of inertia. In the same way, the model translational inertia is the sum of the translating element masses.

The efficiency of ball and roller screws mainly depends on rolling frictions. The direct and indirect efficiencies are obtained [31,33] from the friction coefficient, the pitch of the screw, and its diameter, which is deduced from scaling laws.

As for the bearing, ball and roller screws are very sensitive to local deformations. In the same way, the variation of the maximum static force $F_{max,0}$ is proportional to the nominal force (Eq. 3). Another factor limiting the maximum force applied to the screw is the risk of buckling. The maximum force that can be applied to the screw with respect to buckling is obtained by a common calculation of the first mode of deformation (Euler) according to dimensions deduced by scaling laws.

At high rotational velocities, the imperfect balance of the screw causes transversal vibrations that can be damaging. The corresponding maximum rotational velocity is obtained by a common calculation of the first mode of vibration of a full cylindrical shaft mounted on two simple supports. Safety and mounting factors are applied in order to take account of possible inaccuracies in the mounting, as well as different possible mounting configurations. The other screw rotational velocity limit is generally due to the nut mechanism. It is obtained experimentally as the nut maximum admissible translation velocity. The set of scaling laws (Eq. 6) reflects the aforementioned screw speed limits:

$$\begin{cases} \omega_{max,vib}^* = k_m \cdot F_{nom}^{*1/2} \cdot l_s^{*-1} \\ \omega_{max,nut}^* = F_{nom}^{*-1/2} \end{cases} \quad (6)$$

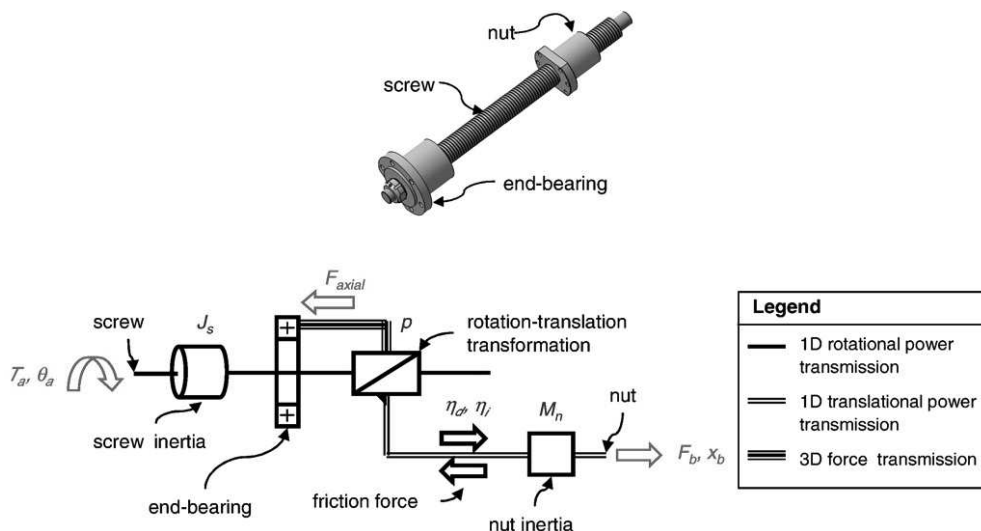


Fig. 3. Main components of ball or roller screws and equivalent model.

where $\omega_{\max,\text{vib}}$ is the screw speed limit due to vibrations, $\omega_{\max,\text{nut}}$ is the screw speed limit due to the maximum admissible nut translational velocity and l_s is the screw length. The resulting lowest speed limit constrains the ball or roller screw operation. The factor k_m is to be applied to the corresponding scaling law to refer to a change of mounting compared to the reference mounting type.

Based on the scaling laws described in this section, it is possible to calculate for the proposed ball and roller screw model: five simulation parameters (screw moment of inertia, screw pitch, direct and indirect efficiencies and nut translational inertia), nine integration parameters (lengths, diameters and masses of the screw, nut and end-bearing) and four operational limit parameters (maximum admissible output forces and screw speeds with respect to vibrations, buckling and nut limit). It is interesting to note that the designer has only to define three definition parameters (screw pitch, nominal output force and stroke) along with a reference representative of a given technology (e.g. recirculating balls and planetary rollers).

3.1.3. Validations of the scaling laws

The scaling laws established above and summarized in Table 1 were compared with the manufacturers' data [30–32] for validation by focusing on the mass. These laws, validated on an industrial product range here, can be used with specific domain components.

Fig. 4(a) to (d) shows the validations in log–log graphs which represent the power laws as straight lines. The scaling laws represented were calculated from a single reference (see Appendix A for the use of references with scaling laws) which was chosen near the geometric mean of the definition parameter range here. These curves show that the manufacturers' products follow the trends given by the established scaling laws. Each comparison is given with an evaluation of the relative range width of the manufacturer's products around the scaling law drawn. Independently of the choice of the reference, the established scaling laws lead to existing or feasible products. It also appears that the manufacturers tend to extend the range of their products by varying some dimensions without keeping homothetic scaling in order to reduce manufacturing and inventory costs. Finally, note the wide range of validity of the established scaling laws, which generally covers three decades of the definition parameter, while the design exploration of an actuator rarely covers more than one decade.

Fig. 4(a) and (b) shows the validity limits of the scaling laws for rolling bearings and end-bearings. The limits occur at either very high or very low values of the definition parameter, where the sizing constraint driving the component dimensions might change. In order to prevent abusive use of the scaling laws, a verification of the definition parameter values with respect to the manufacturer's catalogue ranges has been implemented in the proposed general component model (see Section 4).

4. Tools supporting the methodology

The tools, which support the “HOWs” of the methodology presented in Section 2, take the form of an in-house library of electromechanical component models (Fig. 5) here. The parameter setting interface (upper part of Fig. 5) presents parameters to be set by the user. Minimizing the number of parameters aims at facilitating the manual use, exploration or optimization during the preliminary design phases. These component models can be assembled in any way to form electromechanical power transmission architectures as illustrated in Fig. 6 for the aileron actuator of the Section 5 case study. In this way, the complete flight control actuator model requires a total of seventy-five parameters for electronic, electromechanical, thermal and mechanical components. As shown by the parameter flowchart in Fig. 6, the parameters useful for simulation model (label 3), transient operation domain (label 4), geometrical integration test (label 5), mass budget (label 6) can be provided by sizing models (label 2, scaling law models) from a few definition parameters (label 1) and given reference parameters.

Table 1

Established scaling laws for the rolling bearings and ball and roller screws.

Parameter	Unit	Rolling bearings (incl. end-bearings)	Eq.	Ball and roller screws (nut and screw)	Eq.
<i>Definition parameter(s)</i>		Dynamic load capacity F_{nom} (N)		Nominal output force F_{nom} (N)	
<i>Integration parameters</i>					
Length, diameter, width and depth	m	$l^* = F_{nom}^{*1/2}$	(1)	$l^* = F_{nom}^{*1/2}$ (diameter)	(1)
Mass	kg	$M^* = F_{nom}^{*3/2}$	(2)	$M^* = F_{nom}^{*3/2}$ (nut)	(2)
Mass per unit length	kg/m	–		$M_l^* = F_{nom}^*$ (screw)	(5)
<i>Simulation parameters</i>					
Moment of inertia	kg m ²	–		$J_n^* = F_{nom}^{*5/2}$ (nut)	(5)
Moment of inertia per unit length	kg/m	–		$J_l^* = F_{nom}^{*2}$ (screw)	
<i>Operational limit parameters</i>					
Maximum force	N	$F_{\max}^{*1/2} = F_{nom}^{*1/2}$	(3)	$F_{\max}^* = F_{nom}^*$	(3)
Maximum speed	rd/s	$\omega_{\max}^* = F_{nom}^{*-1/2}$	(4)	$\omega_{\max,\text{vib}}^* = k_m \cdot F_{nom}^{*1/2} \cdot l_s^{*-1}$ $\omega_{\max,\text{nut}}^* = F_{nom}^{*-1/2}$	(6)

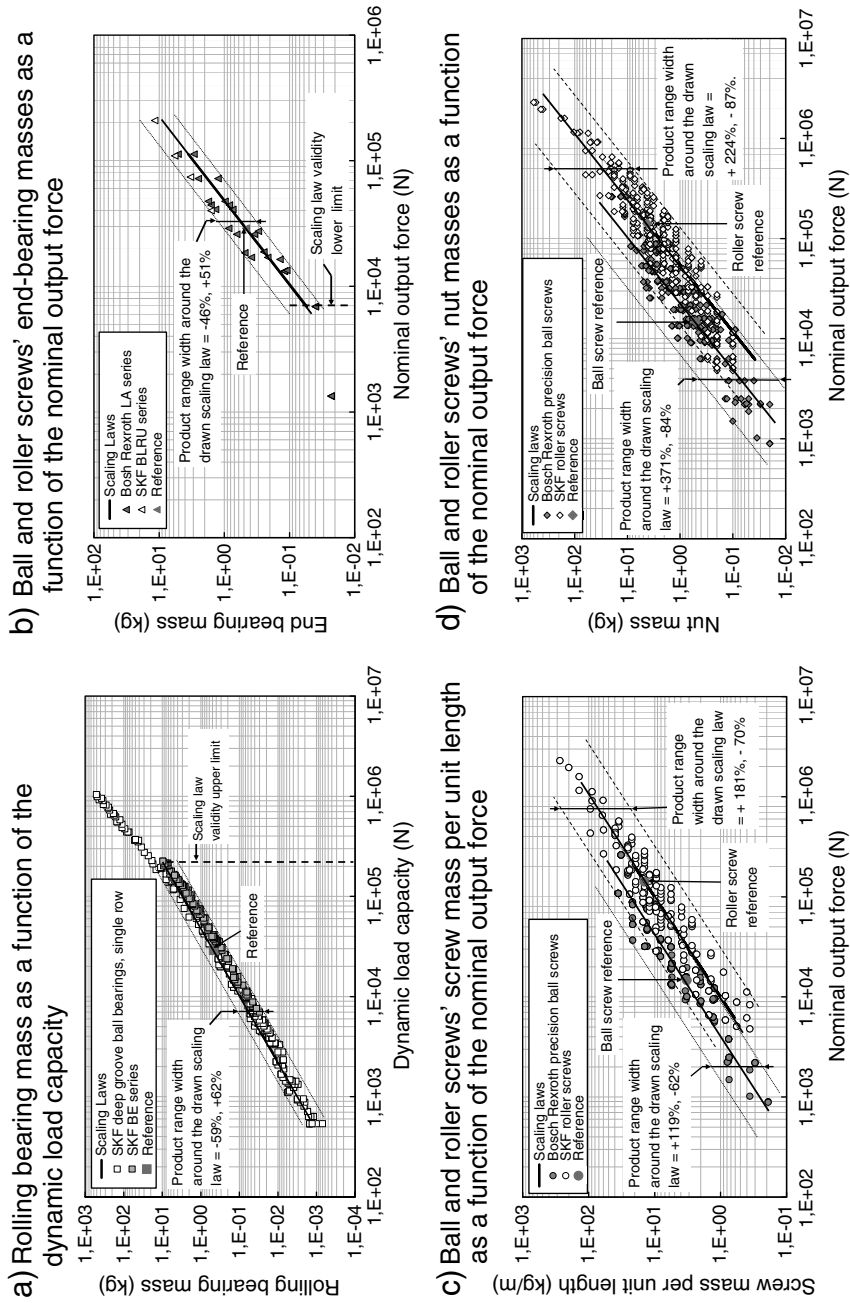


Fig. 4. Scaling laws validation with manufacturers' catalogue ranges.

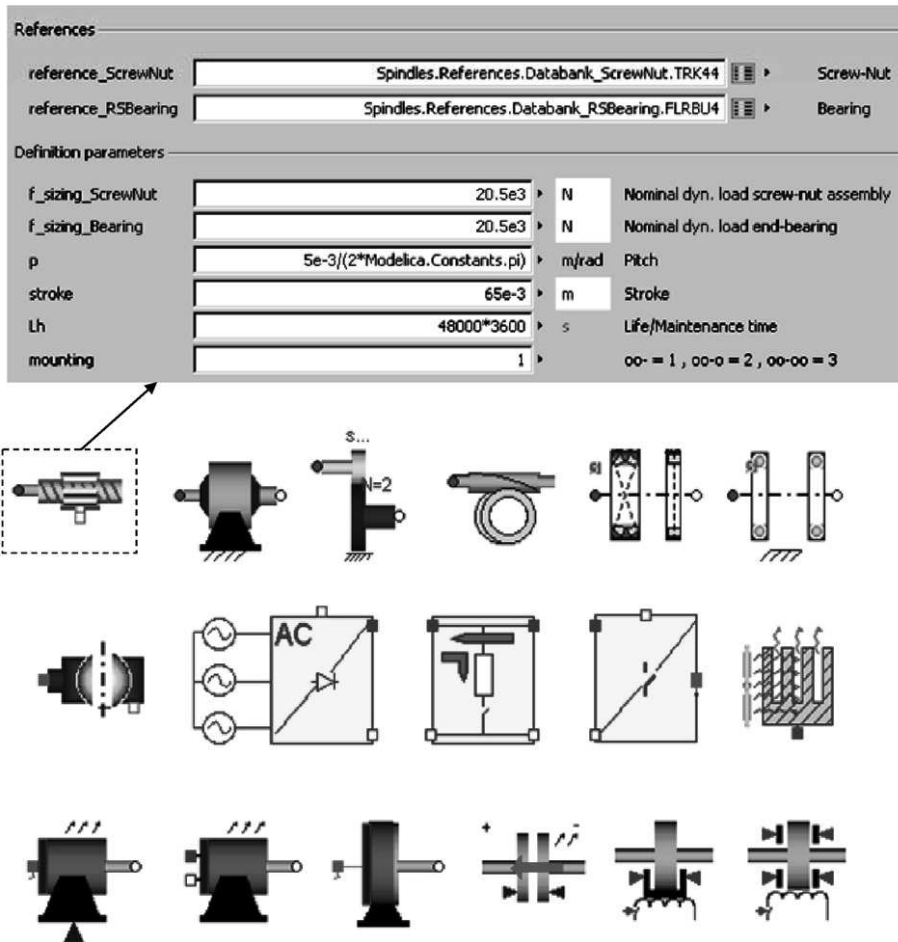


Fig. 5. In-house library of electromechanical component models.

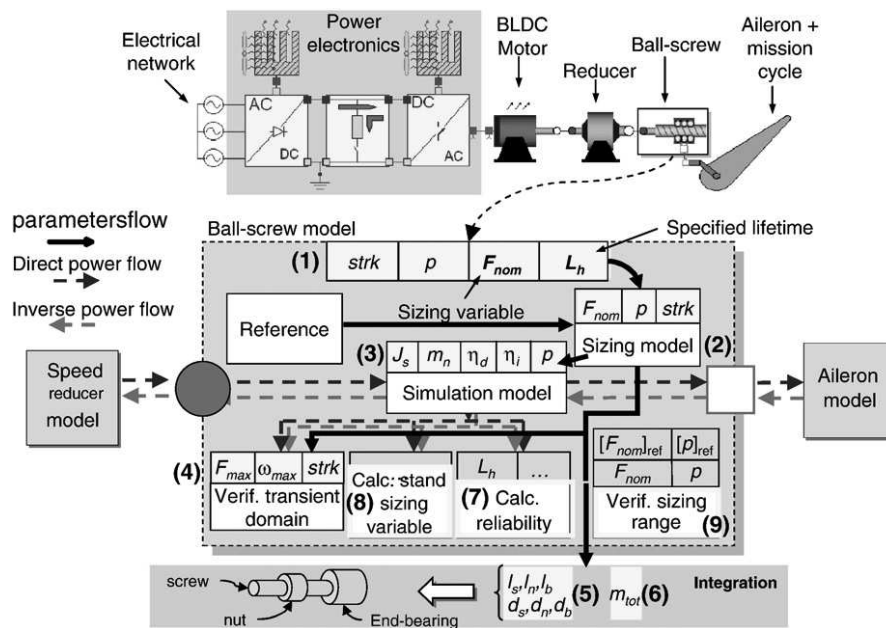


Fig. 6. Proposed model structure for the pre-design (example of the ball screw).

The task 3 in Fig. 1 of the “sizing wave” process is performed for transient and continuous operational boundaries:

- by block (4) of Fig. 6 that computes the margins between the simulated mission profile and the SOA limits.
- by block (8) of Fig. 6 that provides the continuous quantities that are equivalent to the mission profile for a typical reliability of 90%. It helps the user to specify the definition parameters adapted to the mission profile.
- by block (7) of Fig. 6 to size the components for a given reliability.

The task 4 is realized by block (9) of Fig. 6 which enables validating the use of the component in the authorized operation area. This block also verifies that the component remains within an industrial range if the limits of this range are defined in the reference component.

5. Case study: Pre-design of an aileron actuator

Taking advantage of the development of power electronics and permanent magnets, electromechanical actuators show great promise with respect to automatic operating mode, power management, reliability and maintainability, for example. For this reason, it is interesting to study the replacement of current actuators based on a technology that is less promising in these fields (e.g. hydraulic) by electromechanical ones. A good illustration of this trend is the research effort towards the “more electric aircraft” in aeronautics [35]. In this context, the test case presented aims to pre-design an electromechanical actuator driving the ailerons of a single aisle commercial aircraft.

To illustrate the proposed methodology, the study presented focuses on the very first steps of actuator design. In particular, it addresses the electromechanical parts of the power transmission (from the electrical motor to the roller screw), i.e. the power sizing and integration study. Based on the principles described in Section 2, the general methodology is applied as follows. The load model and associated mission profile are supplied by the customer. Then, each component mission profile (e.g. force vs. speed curve for the mechanical components) is computed by inverse simulation, following the entire actuation chain backwards. Thus, every component is sized to match its mission profile. Finally, the integrability of the resulting actuator geometrical envelope within the wing profile is verified and the total mass is computed for analysis.

5.1. Design hypothesis and requirements

For this case study, an electromechanical actuator with the same kinematics as the current hydraulic one (i.e. three pivots, one lever arm and an actuator stroke of 0.04 m, see Fig. 7) is developed. In the current configuration, two actuators are connected to the load in parallel and operate in active-damping mode, where one drives the aileron while the other acts on standby as a damper. When the active actuator fails, it is switched into the damping mode while the other becomes active to take over the mission duty. With the current hydraulic technology, the damping mode is achieved by bypassing the two hydraulic chambers of the actuator cylinder. With an electromechanical solution, the damping mode requires de-clutching the failed actuator and providing damping means. However, for the sake of simplicity the de-clutching and damping functions are not addressed in this study.

The model of the load used for this study is an equivalent aileron moment of inertia of 1 kg m^2 , with a lever arm of 0.045 m. The force generated by the back-up hydraulic actuator is composed of the damping specified by the aircraft manufacturer and the inertia of the hydraulic cylinder. It does not notably impact the power sizing and is therefore neglected. In the same way, the low friction in the pivots of the load kinematics is not taken into account. Finally, the aerodynamic forces are given by the aircraft manufacturer, together with the mission profile as a function of time.

On the one hand, the mechanical components are sized with respect to the maximum force and speed, and also the fatigue cumulated over their specified lifetime. On the other hand, the motor is sized with respect to the maximum force and speed, and

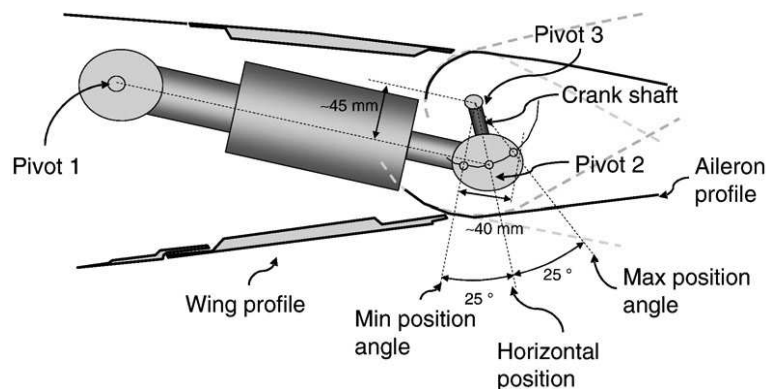


Fig. 7. Kinematics of the hydraulic aileron actuator.

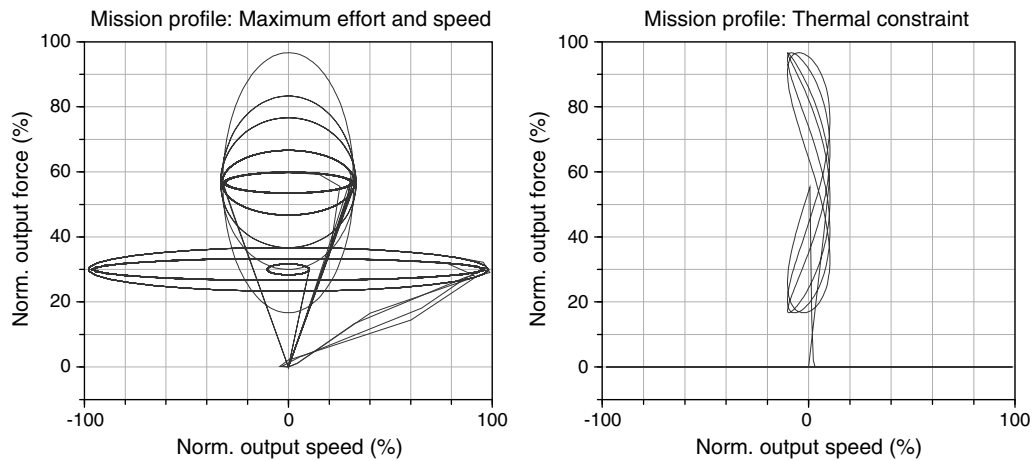


Fig. 8. Mechanical (left) and thermal (right) aileron mission profiles at the actuator output.

also thermal constraints (e.g. temperature and RMS¹ torque). In consequence, we propose to use two mission profiles for the sizing task: one representative of maximum force and speed and the other representative of the thermal loads. Fig. 8 illustrates these two mission profiles propagated at the actuator output (pivot between the actuator and lever arm) in the force-speed power plane.

5.2. Sizing

The sizing methodology described in Section 2 is used to size the components. Links (a), (b) and (c) in Fig. 1 between tasks 1, 2, 3 and 4 are automatically made during the Modelica model simulation. The simulation of a mission profile takes only a few minutes or even less for a relatively long (1000 s) and variable profile. The ability of the component to fulfil its function safely is assessed by verifying the integrity of its SOA during a complete mission cycle (with the same type of force-speed power plane as in Fig. 8 by means of block (4) of Fig. 6) and by calculating its reliability over its entire lifetime for continuous or intermittent duty cycles (block (7) of Fig. 6). Thus, the user can adjust the design iteratively to stay within the component SOA and reach the desired lifetime reliability, while meeting integration requirements. More information about lifetime and reliability models can be found in Ref. [28]. It should be noted that the rated dynamic load criterion is valid only for a component staying within its SOA.

The model structure implemented does not allow direct calculation of the definition parameters corresponding to a specified safe operation. To make this calculation, the corresponding iterative process, link (d) on Fig. 1, has to be carried out by the user. This process is supported by the calculation of the margins between the simulated operation and SOA limits (e.g. maximum nut force and screw speed margins calculated by block (8) of Fig. 6). The user is also supported by the calculation of the rated dynamic load (e.g. rated nut force, block (9) of Fig. 6), which ensures safe operation for the entire component lifetime (typically with a reliability of 90%). This process can be performed automatically as illustrated in Ref. [29].

In order to minimize the size of the electrical motor, the overall reduction ratio of the transmission is set to match the electrical motor maximum speed during the mission cycle. First, the pitch of the roller screw is minimized (5 mm/rev) and thus the mass of the speed reducer is minimized. The speed reducer ratio is adjusted to match the maximum speed (calculated by scaling laws) of the motors in order to minimize the motor output torque and thus its mass. This process corresponds to iterations of link (e) in Fig. 1 and compares several possible solutions. Done by hand here, they can easily be automated as in [29], to minimize mass or integration volume for example.

5.3. Results

The results obtained by following the sizing methodology as described in Section 5.1 are gathered together in Table 2. From these results, it is possible to carry out an efficient mass and integration analysis. Table 2 also includes the component references used by the scaling laws, and off-the-shelf components corresponding to the scaled ones. It is clear that, although the references are often far away from the scaled components (e.g. the nominal torque of the speed reducer reference is more than twenty times that of the scaled one) the scaling laws match existing off-the-shelf products accurately.

The comparison between the scaled and off-the-shelf actuators in Table 2 illustrates the accuracy of the approach developed. It can be seen that the off-the-shelf actuator is heavier than the scaled one. This difference of mass is mainly due to the fact that, when there is no off-the-shelf component exactly matching the scaled one, then the next biggest component is selected. In the same way, the chosen reducer has a maximum reduction ratio lower than the scaled one. In consequence, the electric motor has a greater RMS torque and is heavier. From the dimensions listed in Table 2, the actuator geometry can be represented within the wing profile to verify its integrability as illustrated in Fig. 7. The maximum allowed length of the actuator is given by the distance

¹ The RMS torque is equivalent to the steady state torque that would produce the same motor heating over a given mission cycle.

Table 2
Actuator sizing for a lever arm length of 0.045 m, a component lifetime of 48 000 h and an active/damping configuration (baseline).

	Brushless motor	Speed reducer (epicyclical)	Roller screw (stroke = 0.04 m)	
Reference	MAXON EC-60-167131 RMS torque = 0.83 Nm	REDEX-ANDANTEX SRP1 Nominal torque = 370 Nm Reduction ratio = 7	SKF TRK 44 (roller screw) SKF BLRU 4 (end-bearing) Nominal forces = 86.9 kN	
Diameter	0.06 m	0.17 m	0.086 m	
Length	0.129 m	0.18 m	0.3 m	
Mass	2.45 kg	13.8 kg	11.4 kg	
Scaled	RMS torque ^a = 0.23 Nm	Nominal torque ^a = 17 Nm Reduction ratio = 71	Nominal force ^b = 26 kN Pitch = 7.96 10 ⁻⁴ m/rd	Actuator mass = 3.1 kg
Diameter	0.04 m	0.064 m	0.047 m	
Length	0.09 m	0.078 m	0.142 m	
Mass	0.8 kg	0.8 kg	1.5 kg	
Off-the-shelf	MAXON EC-45-136212, RMS torque = 0.28 Nm	NEUGART PLE 60, Nominal torque = 18 Nm Reduction ratio = 64	SKF TRK 21 (roller screw), Nominal force = 27.85 kN Pitch = 7.96 10 ⁻⁴ m/rd SKF BLRU 2 (end-bearing), Nominal force = 27.9 kN	Actuator mass = 4 kg
Diameter	0.045 m	0.063 m	0.049 m	
Length	0.101 m	0.118 m	0.162 m	
Mass	1.1 kg	1.1 kg	1.8 kg	

^a Sized with respect to the maximum force to be transmitted.

^b Sized with respect to the lifetime (fatigue or thermal constraint).

between the pivots 1 and 2. Mounting all the components in line does not allow the actuator to fit between these two pivots. A possible solution is to mount the brushless motor and the reducer alongside the roller screw, inserting spur gears between the reducer output and the roller-screw input.

In order to take advantage of the proposed methodology, further design explorations were carried out. The first investigation aimed to study the effect of varying the length of the lever arm (increased from 0.045 to 0.065 m), the second aimed to evaluate the influence of the actuator lifetime (reduced from 48 000 to 24 000 flight hours) and the last one assessed the influence of the mode of operation (active/active configuration instead of active/damping configuration).

As shown in Table 3, increasing the lever arm length tends to decrease the actuator mass by 25% as a direct consequence of the sizing of each component. In the baseline, the sizing of the roller screw and the speed reducer is dominated by the maximum force to be transmitted, while the motor is sized with respect to thermal considerations. In consequence, modifying the actuator lifetime, while keeping the same reliability, impacts the motor sizing only and thus limits the mass saving to 6%. On the other hand, dividing the lifetime by two induces a major increase in the operational costs (maintenance, repairs, replacement) of the actuator. Finally, when the two actuators are in an active/active configuration, the individual duty load is divided by two. However, in case of failure, a single actuator must be able to fulfill the mission duty during at least one cycle. Therefore, the maximum force to be transmitted and the thermal constraint in the motor remain identical. Consequently, the sizing is the same for the active/active and active/damping (baseline) configurations.

Finally, besides providing interesting results, this comparative study has shown how the use of the library developed allows fast modelling, and the exploration of different design configurations (active/damping, active/active) and design parameters (lever arm length and lifetime), thus supporting good technical decision-making early in the preliminary design by providing rich insight in an efficient way. This methodology can be extended to more complex multi-domain systems and design criteria. To this end, further component models of electrical power supply (e.g. batteries and ultra-capacitors), modulation (e.g. power electronics), transformation (e.g. electrical motors) as well as mechanical power transmission (e.g. speed reducers) and end-effectors (e.g. rack and pinions and spur gears) have been developed or are under development. In some cases, the high dynamic performance required for the system is a

Table 3
Mass results for different lever arm lengths, component lifetimes and duty ratios.

	Baseline	Lever arm increased by 44 %.	Lifetime divided by 2.	Active/active instead of active/damping configuration.
Duty (%)	100	100	100	50
Lifetime (h)	48 000	48 000	24 000	48 000
Lever arm length (m)	0.045	0.065	0.045	0.045
Roller-screw mass (kg)	1.5 ^a	1.1 ^b	1.5 ^a	1.5 ^a
Speed reducer mass (kg)	0.8 ^a	0.6 ^a	0.8 ^a	0.8 ^a
Electrical motor mass (kg)	0.9 ^b	0.7 ^b	0.7 ^b	0.9 ^b
Total mass (kg)	3.2	2.4	3	3.2
Mass saving (kg)		0.8 (25 %)	0.2 (6%)	0 (0%)

^a Sized with respect to the maximum force to be transmitted.

^b Sized with respect to the lifetime (fatigue or thermal constraint).

critical issue. Therefore, it is planned to extend the component models with a modal analysis capability (e.g. with structural anchorage and transmission compliances) and to take the controller design and its impact on the actuator performance into consideration.

6. Conclusion

The proposed methodology is intended to improve the preliminary design of power transmission systems by providing fast and efficient means for multi-criteria sizing and virtual prototyping. The main advances implied by this methodology are a reduction of the size of the parameters vector to be handled by the designer, generation of a multi-purpose top-level component library and automation of the sizing process. In this aim, a reduced vector of top-level definition parameters has been introduced, from which all other parameters are automatically calculated to feed the simulation models that can support power sizing, service life and reliability studies. Scaling laws have been proposed as the enabling tool for parameter vector reduction. This choice allows all the parameters to be linked to the definition parameters on the basis of physical design constraints. The component models have been developed in an innovative way, not only considering time domain simulation but also addressing reliability, geometrical envelope and mass as a whole. Model implementation has drawn benefit from non-causal modelling and simulation capabilities recently offered by the Modelica language that allows the same models to be used for any step of the proposed process. First, the interest of the proposed methodology has been illustrated by developing and validating the roller screw sizing model. Then, the whole process has been applied to the preliminary sizing of an aileron actuator. The total mass has been rapidly calculated from the automatic sizing process considering power, service and reliability requirements. This case study has shown how the proposed methodology can provide a fast and efficient means of design exploration, being able to deal with power transmission as well as service life or mode of operation. In order to draw even more benefit from this new approach, works are in progress to extend the model library, address environment requirements, include optimisation features and ensure continuity of the model-based systems engineering. In this framework, it is planned to link the present process to requirements and architecting (upper stage) and to 3D CAD and FEM analysis (lower stage).

Acknowledgments

The presented work has been partly funded by the following projects: the French ANR 05-RNTL 028 SIMPA2-C6E2 project (Conception des SYStèmes Electriques Embarqués) and the FP6 European DRESS project (Distributed and Redundant Electromechanical nose gear Steering System).

Appendix A. Scaling law basics

The scaling laws, also called similarity laws, are an efficient way to study the effect of varying representative parameters of a given component. They are used in various domains such as micro-systems, mechanics, hydraulics and fluid mechanics to compare different technologies, to adapt the dimensions of a mock-up in fluid dynamics, to size mechanical, hydraulic or electrical systems, to develop and rationalize product families or to evaluate costs [15,19,20]. In some cases, it is difficult or impossible to identify and write the equations linking the parameters representative of a given overall problem in a simple way. In these particular cases, an alternate solution can be found in by carrying out a dimensional analysis to establish the scaling laws [36,37].

A.1. Notation

This article uses the notation proposed by M. Jufer in [15]. The l^* scaling ratio of a given parameter is calculated as

$$l^* = l/l'$$

where l' is the dimensional parameter taken as the reference and l is the dimensional parameter under study.

For example, the variation of the volume of a shaft (cylinder) in case of an identical variation for all geometrical dimensions is

$$V^* = \frac{V}{V'} = \frac{\pi r^2 l}{\pi r'^2 l'} = r^{*2} l^*$$

where V is the volume of the shaft, l its length and r its radius. The parameters under study are differentiated from the references by a prime symbol.

A.2. Geometrical similitude

Models have been developed with geometrical similitude in this paper. Widely applied, the hypothesis of homothetic scaling for all the geometrical dimensions leads them to be related to all to their reference values by a single scaling ratio. For the cylinder example, this assumption gives:

$$r^* = l^* \Rightarrow V^* = l^{*3}$$

This result remains valid for any other geometry. In the same way, it is possible to calculate the variation of the mass, M , and rotational moment of inertia, J , of the shaft:

$$\begin{cases} M = \int \rho_m dV \Rightarrow M^* = l^{*3} \\ J = \int r^2 dM \Rightarrow J^* = l^{*5} \end{cases}$$

where ρ_m is the mass density of the shaft.

A.3. Reference use

When the characteristics of a reference component are known, it is possible to determine the new characteristics for a given change of parameter. For example:

$$M = M_{ref} \cdot \left(\frac{l}{l_{ref}}\right)^3 \quad \text{and} \quad J = J_{ref} \cdot \left(\frac{l}{l_{ref}}\right)^5$$

References

- [1] INCOSE, Systems engineering handbook, INCOSE Technical Product, 2004.
- [2] L. Han, C.J.J. Paredis, P.K. Khosla, Object-oriented Libraries of Physical Components in Simulation and Design, 2001 Summer Computer Simulation Conference, Orlando, FL, 2001, pp. 1–8.
- [3] G. Ferretti, G. Magnani, P. Rocco, Virtual prototyping of mechatronic systems, Annual Reviews in Control 28 (2004) 193–206.
- [4] H.J. Coelingh, Design Support for Motion Control Systems, University of Twente, Enschede, The Netherlands, 2000, pp. xii–218.
- [5] C.J.J. Paredis, A. Diaz-Calderon, R. Sinha, P.K. Khosla, Composable models for simulation-based design, Engineering with Computers 17 (2001) 112–128.
- [6] F. Roos, Towards a methodology for integrated design of mechatronic servo systems, KTH, Machine Design (2007) viii–203.
- [7] J. van Amerongen, P. Breedveld, Modelling of physical systems for the design and control of mechatronic systems, Annual Reviews in Control 27 (2003) 87–117.
- [8] R. Sinha, C.J.J. Paredis, V.-C. Liang, P.K. Khosla, Modeling and simulation methods for design of engineering systems, Journal of Computing and Information Science in Engineering 1 (2001) 84–91.
- [9] Y.L. Tian, Y.H. Yan, R.M. Parkin, M.R. Jackson, Development of a visualized modeling and simulation environment for multi-domain physical systems, Global Design to Gain a Competitive Edge, Springer, London, 2008, pp. 469–478.
- [10] J.A. Estefan, Survey of Model-Based Systems Engineering (MBSE), INCOSE MBSE Focus Group, May 2007.
- [11] J.N. Martin, Systems Engineering Guidebook: A process for Developing Systems and Products, CRC Press, Inc, Boca Raton, FL, 1996.
- [12] P. Krus, Performance Estimation Using Similarity Models and Design Information Entropy, Workshop on Performance Prediction in System-Level Design, International Design Engineering Technical Conference and Computers and Information in Engineering Conference (IDETC/CIE), Aug. 3 2008.
- [13] ControlEng, ServoSoft software, <http://www.controleng.ca>.
- [14] T. Simpson, J. Peplinski, P. Koch, J. Allen, Metamodels for computer-based engineering design: survey and recommendations, Engineering with Computers 17 (2001) 129–150.
- [15] M. Jufer, Design and Losses—Scaling Law Approach, Nordic Research Symposium Energy Efficient Electric Motors and Drives, Skagen, Denmark, 1996, pp. 21–25.
- [16] G. Ricci, Mass and rated characteristics of planetary gear reduction units, Meccanica 27 (1992) 35–45.
- [17] G. Ricci, Weight and rated characteristics of machines: positive displacement pumps, motors and gear sets, Mechanism and Machine Theory 18 (1983) 1–6.
- [18] K.J. Waldron, Ch. Hubert, Scaling of robotic mechanisms, IEEE International Conference on Robotics & Automation, San Francisco, CA, April 2000.
- [19] B. Multon, H. Ben Ahmed, M. Ruellan, G. Robin, Comparaison du couple massique de diverses architectures de machines tournantes synchrones à aimants, Société de l'Electricité, de l'Electronique et des Technologies de l'Information et de la Communication (SEE), 2006, pp. 85–93.
- [20] G. Pahl, W. Beitz, L. Blessing, J. Feldhusen, K.-H. Grote, K. Wallace, Engineering Design: A Systematic Approach, Springer-Verlag London Limited, London, 2007.
- [21] S.E. Mattsson, H. Elmqvist, M. Otter, Physical system modeling with Modelica, Control Engineering Practice 6 (1998) 501–510.
- [22] Modelica Association, Modelica Modelica Specification version 3.2, <http://www.modelica.org/documents>, march 24, 2010.
- [23] Dassault Systemes-Dynasim AB, Dymola—Dynamic Modeling Laboratory, <http://www.dynasim.se>, 2008.
- [24] J. Bals, G. Hofer, A. Pfeiffer, C. Schallert, Object-Oriented Inverse Modelling of Multi-Domain Aircraft Equipment Systems and Assessment with Modelica, 3rd International Modelica Conference, Linköping, Sweden, 2003, pp. 377–384.
- [25] D.J. Murray-Smith, The inverse simulation approach: a focused review of methods and applications, Mathematics and Computers in Simulation 53 (2000) 239–247.
- [26] VDI 2206: Design methodology for mechatronic systems", Beuth Verlag GmbH, 10772-Berlin, Düsseldorf, Germany, June 2004.
- [27] R. Fotsu Ngwompo, S. Scavarda, D. Thomasser, Inversion of linear time-invariant SISO systems modelled by bond graph, Journal of the Franklin Institute 333 (b) (1996) 157–174, NO 2.
- [28] J. Liscouët, M. Budinger, J.-C. Maré, Design for reliability of electromechanical actuators, Proceedings of the Recent Advances in Aerospace Actuation Systems and Components Conference, May 5–7 2010, INSA de Toulouse, Toulouse, France.
- [29] T. El Halabi, M. Budinger, J.-C. Maré, Optimal geometrical integration of electromechanical actuators, Proceedings of the Recent Advances in Aerospace Actuation Systems and Components Conference, May 5–7 2010, INSA de Toulouse, Toulouse, France.
- [30] SKF, in: SKF (Ed.), Catalogue technique interactif, 2009, <http://www.skf.com>.
- [31] SKF, in: SKF (Ed.), Vis à rouleaux, 2008, <http://www.skfequipements.skf.fr>.
- [32] Bosch Rexroth, in: R. B. Group (Ed.), Precision ball screw assemblies, 2008, <http://www.boschrexroth-us.com>.
- [33] R. Budynas, J.K. Nisbett, Shigley's Mechanical Engineering Design, SI version, McGraw-Hill, New York, 2007.
- [34] J.Ch. Maré, System level modelling of mechanical losses in actuators, Proceedings of the 20th International Conference on Hydraulics and Pneumatics, Prague, Sept 29 - Oct 1, 2008.
- [35] T. Ford, More-electric aircraft, Aircraft Engineering and Aerospace Technology 77 (2005) 02–2005.
- [36] G.I. Barenblatt, Scaling, Cambridge University Press, 2003.
- [37] E.S. Taylor, Dimensional Analysis for Engineers, Oxford University Press, 1974.

Chapter 3 – Evaluation models and sizing for lifetime and reliability

ABSTRACT

This chapter deals with evaluation models, the goal of which is to check the ability of a component to operate in its safe operating area for the required lifetime and reliability. After reviewing the state of the art of the main design drivers that limit the performance and endurance of mechatronic components, this chapter describes the possible models and ways of implementing them in system simulation environments by focusing on lifetime evaluation. The associated paper 3, entitled "An integrated methodology for the preliminary design of highly reliable electromechanical actuators: Search for architecture solutions" and published in the journal Aerospace Science and Technology, describes the reliability aspect with an integrated hybrid (top-down/bottom-up) methodology for generating, selecting and assessing architectures for electromechanical actuators, paying special attention to safety and reliability.

Keywords: safe operating area, lifetime, reliability, degradation phenomena.

TABLE OF CONTENTS

1.	Objectives of evaluation models	69
1.1.	Rapid and gradual degradation phenomena	69
1.2.	Link between evaluation models, estimation and simulation models.....	69
2.	Degradation phenomena.....	71
2.1.	Mechanical power transmission components	71
2.2.	Electrical motors and electrical components	74
2.3.	Power electronics	76
3.	Evaluation models during sizing activities	78
3.1.	Proposed process for sizing for reliability	78
3.2.	From mission profile to rated values	79
3.3.	Lifetime calculation for a selected component.....	81
3.4.	Selection of component for standard reliability	82
3.5.	Effects of reliability	83
4.	Conclusion	87
5.	Bibliography.....	88

NOTATION

Acronyms

EMA	Electro-Mechanical Actuator	RMS	Root Means Square
MTBF	Meant Time Between Failure	SOA	Safe Operating Area
MTTF	Mean Time To Failure		

Nomenclature

a_R	Adaptation factor for lifetime	α	Experimental constant
a_{RC}	Adaptation factor for sizing parameter	β	Experimental constant
b	Failure distribution form factor (Weibull)	φ	Activation energy
E	Experimental constant	λ	Failure rate
f	Failure distribution function	v	Mean speed
k	Boltzmann constant	σ	Applied mechanical stress
$L_{h,10}$	Lifetime		
N_{10}	Number of load cycles for a reliability of 90%		
p	Experimental constant		
Q	Cumulated damage		
q_h	Degradation per time unit		
v	Speed		
V	Voltage		
t	Time		
T	Temperature		
R	Reliability		

Indices

siz	Sized	nom	Nominal
eq	Equivalent	ref	Reference or selected
f	Final	$spec$	Specified
h	Hours	0	Initial
		10	Failure rate of 10%

1. OBJECTIVES OF EVALUATION MODELS

1.1. Rapid and gradual degradation phenomena

The evaluation models determine whether each component will remain within its performance limits and can be expected to have the required lifetime and reliability. The 2 aspects to check are:

- Transient power demands to ensure system performance: the models have to analyze the maximum stress (such as torque or speed) to avoid rapid deterioration. Component degradation can be avoided if the use is kept inside a Safe Operating Area (SOA). This point can be checked by the simulation models of chapter 2 and operating domains deduced from the estimation models of chapter 1.
- Continuous power demands to ensure the endurance of the system: the models have to calculate quantities equivalent to the nominal point of operation and reliability rate in order to avoid critical degradation over time (e.g. fatigue). This point will be treated in greater detail in this chapter.

Not all rapid and gradual degradations may be reached together during a sizing calculation. Nevertheless they must be addressed and validated. To better understand the meaning of “safe operating area” (SOA) of a component, a concept related to rapid degradation phenomenon, Figure 1 shows the example of a brushless electric motor SOA. Here, both the “steady-state operating area” and the “transitory operating area” refer to rapid degradations but address different dynamics. For example, one is linked to the coil insulator maximum temperature for a long working time (low dynamic), while the other can be the maximum demagnetization or saturation torque leading quickly to motor malfunction (high dynamics).

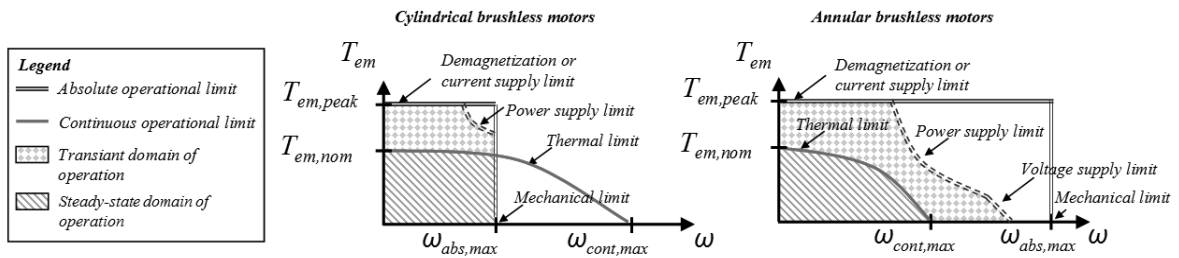
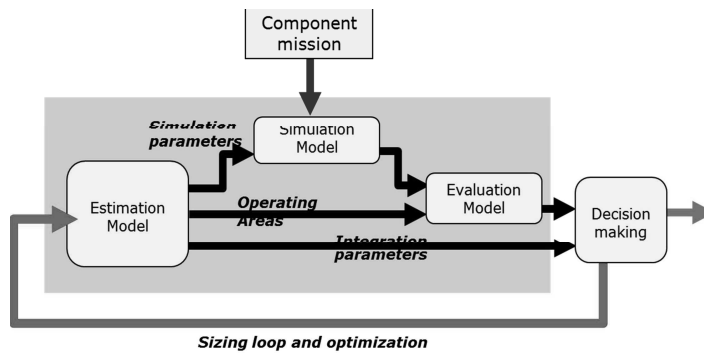


Figure 1 - Brushless electric motor SOA

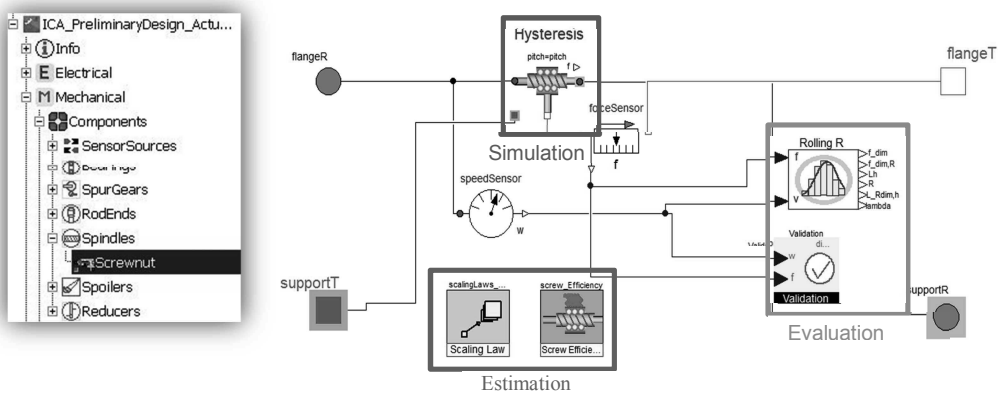
A gradual degradation driver for the motor can be the fatigue of the rolling bearings or insulator ageing, both being fatigue phenomena. The lifetime, which can be expressed in days, hours, or number of revolution, is function of the damage accumulated due to the service conditions, which can depend on force, torque, and temperature, etc. Part 2 is a summary of the main rapid or gradual degradation phenomena to be taken into account in mechatronic design.

1.2. Link between evaluation models, estimation and simulation models

Figure 2a) describes the exchange of information between the estimation models of chapter 1, the simulation models of chapter 2 and the evaluation models of this chapter. This structure of component models is suitable for model-based design of a mechatronics system. Decision-making can be performed either manually or automatically. The example in Figure 2b) is a view of a Modelica implementation of a screw/nut drive model showing the three models mentioned above [1].



a) Component model structure for model-based preliminary design



b) Example of a screw/nut drive model

Figure 2 – Structure of component model for model-based preliminary design

The principle of performance checking to avoid rapid degradation is quite trivial: for a given parameter to be checked, the current value is simply compared with the maximum allowed value. For the screw/nut example, the parameters are the speed and the force, represented as inputs to the validation module of Figure 3. One way to visualize SOA is to plot the ratio $F(t)/F_{max}$ (force) versus the ratio $V(t)/V_{max}$ (speed) and see whether the graph goes beyond the interval $[-1; 1]$ on the x-axis or the y-axis (Figure 3). When the graph exceeds the limits, this means that the component is under sized, and that the sizing values of the component need to be higher, leading to the direct consequences of larger dimensions and mass. Speed V_{max} and force F_{max} values come from estimation models and are re-evaluated when the definition parameters of components change.

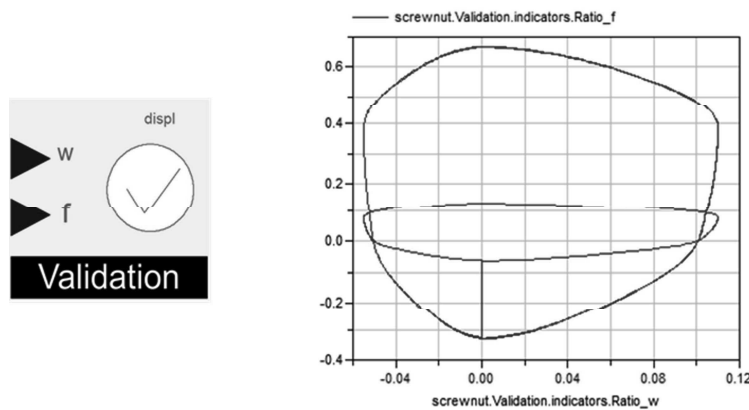


Figure 3 - Validation of SOA for a screw/nut drive

Endurance checking, which enables critical degradation over time to be avoided, goes through the mission profile analysis and calculation of equivalent quantities to the nominal point of operation and reliability rate. In Figure 3 the user has set a desired reliability and lifetime for the component. The calculation module calculates the estimates of lifetime and reliability values for the chosen component and the component definition parameter to select for the desired lifetime and reliability. These calculations are based on the formulas given later in the section 3.

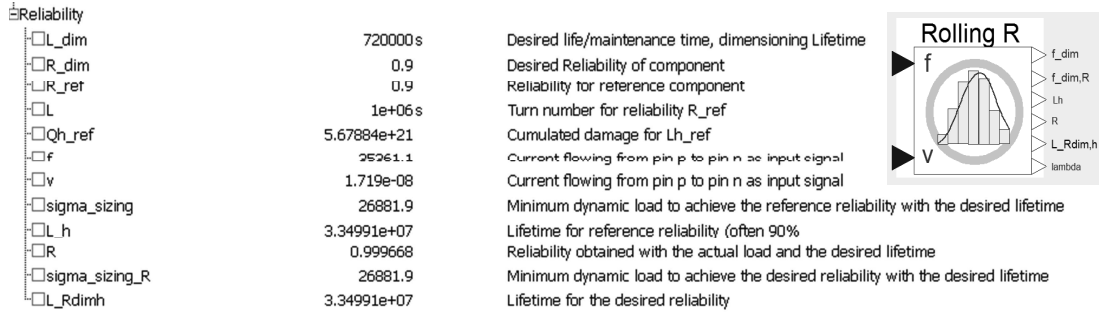


Figure 4 - Example of reliability values for a screw/nut drive [2]

2. DEGRADATION PHENOMENA

For each typical component of actuation systems, we list the causes of rapid and gradual degradation. The plan followed depends mainly on the gradual degradation mechanisms. For these degradation phenomena, only the simplest laws usable at preliminary design level will be given. This section does not describe the detailed design of each component exhaustively but focuses on the selection of a component.

2.1. Mechanical power transmission components

Typical components in mechanical power transmission can be divided into 3 categories according to the type of gradual degradation:

- Rolling mechanisms: bearings, roller/ball-screw and linear ball bearings
- Sliding mechanisms: rod-end, bushing and electromagnetic clutch/brake
- Gears mechanisms: gears, reducers and worm-gear.



a) Rolling mechanisms



c) Sliding mechanisms

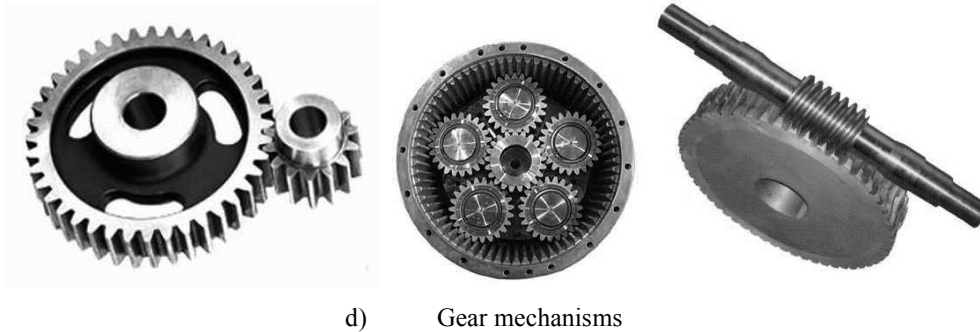


Figure 5 - Mechanical power transmission components

For the last category, the failure mechanism can be complex and involve a mix of various fatigue phenomena. Nevertheless, when normal conditions of functioning (lubrication, sealing, etc.) are assumed, the first fatigue phenomena must be rolling fatigue of bearings, as gears are often designed to have much higher tooth flexural or Hertz stress fatigue limits.

The ISO (15243.2004) system divides mechanical component failure modes into six major categories: **fatigue**, **wear**, corrosion, electrical erosion, **plastic deformation** and **fracture**. During preliminary design, only the first two and the last two are generally studied.

Rapid degradation: maximum speed and force

Drivers of rapid mechanical degradation, unlike drivers of gradual degradation, do not differ if the component is based on a sliding or a rolling working principle. The maximum stress limit is defined by some norms (ISO 281, ISO 3408, ISO 4379, ISO 6336-5, ISO 10300, NF E 22-057-4, NF-E-023-015...) as allowable static load capacity that does not lead to too much plastic deformation or to fracture (for a rolling mechanism, permanent deformation must not exceed 0.01% of the rolling element diameter).

Maximum transitory speed criteria can be linked to part balancing and natural vibration frequency, centrifugal forces, rolling element recirculation principle, or wear damage and the internal temperature limit.

Gradual degradation drivers: rolling fatigue and wear

Under varying stress or repeated deformations, micro-cracks are created in the material of a component, reducing the resistance of this component to stress and plastic deformation. This is referred to as **fatigue**. During a component's lifetime, three stages of failure due to fatigue effects can be identified. They are displayed in a log-log graph in Figure 6, which shows the relationship between the number of cycles and the applied load. During the early life cycle, so-called low cycle failures can be identified which appear within the first 10^4 cycles and are caused by elastic effects. Most of usage of component is above 10^4 cycles, where micro-cracks, as described, reduce the stress resistance. Under a certain stress-level, the component then shows unlimited resistance to stress that is not further reduced by a greater number of cycles. An example of fatigue effects on transmission systems is shown in Figure 7, where fatigue caused the rupture of a tooth of the gear.

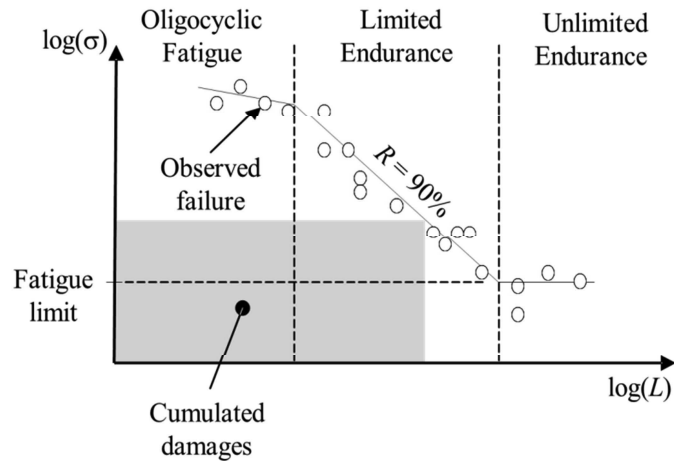


Figure 6 – Applied load σ (force, torque, stress, etc.) vs lifetime L (hours, days, number of cycles, etc.) for mechanical fatigue [3]

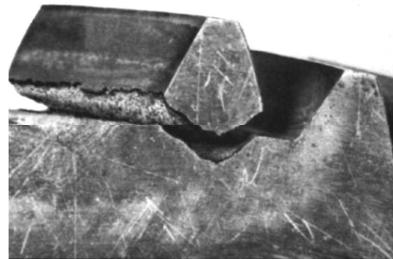


Figure 7 – Breaking of a tooth of a gear due to fatigue induced by the bending stresses caused by the transmission torque [4]

Power transfer between mechanical components always involves to surface contact. In an ideal case, sufficient lubrication should avoid this contact completely, but, in reality, the thin film is not sufficient and friction between surfaces leads to the production of small debris that again increase friction between components because of uneven surfaces. This already occurs before any movement has taken place. At the start of transmission any unevenness of the contact surfaces has to be overcome to allow initial movement which produces very high friction. Even though the surface will be more homogeneous at first, worn surfaces will be subject to increased **wear**. Increased surface degradation will finally lead to de-alignment of surfaces for example, of bearings, or to jamming of gears due to friction forces that are too high. The result is a loss of precision in the transmission system that can in the case of an EMA cause a fatal failure if operation of the power transmission is not directly interrupted. The results of wear on a worm gear mechanism are shown in Figure 8.



Figure 8 – Abrasive wear of a worm gear

Degradation laws: Palmgren Miner and Archard laws

The calculation of fatigue and wear effects are harmonized here. For a mechanical component subject to fatigue this lifetime formula can normally be applied.

$$N_{10} \cdot \sigma^\alpha = Q \tag{1}$$

The concept is based on the Palmgren Miner law [5]. Here N_{10} refers to the standard number of load cycles for bearings (normally 1 million cycles) that can be guaranteed for a standard reliability of 90%, σ^α is the applied stress and Q the resulting sum of cumulated damage. For the same component and the same reliability, the amount of cumulative damage must remain constant and identical whatever the (N_{10}, σ^α) pair leading to degradation of the component. For rolling components, the power coefficient p is a value greater than 1 and indicates that a larger load causes more damage than a load of lower value. For ball bearings, the coefficient α is equal to 3. The cycle number N_{10} has no power coefficient which indicates that the amount of damage is linear and cumulative.

In terms of calculation, it can be important to express the lifetime as a function of the time unit $L_{h,10}$ instead of the number of cycles. With $N_{10}=L_{h,10} \cdot v$ this leads to the calculation of the cumulated damage Q as a function of time:

$$N_{10} \cdot \sigma^\alpha = Q \Leftrightarrow L_{h,10} \cdot \sigma^\alpha \cdot v^1 = Q \tag{2}$$

In a similar way, the influence of wear on the lifetime of a component can be calculated. It was originally defined by the formula of John F. Archard which is a simple model used to describe sliding wear. It is based around the theory of asperity contact and can be a function of speed v .

$$L_{h,10} \cdot \sigma^\alpha \cdot v^{\beta+1} = Q \tag{3}$$

This directly shows, that for fatigue effects the same formula can be used by choosing $\beta=0$ as there is no influence of the speed on the intensity of damage.

2.2. Electrical motors and electrical components

This category consists mainly of components where temperature effects and thermal degradation are the major phenomena leading to failure: electrical motors, cables and wires, capacitors and resistors.



Figure 9 – Example of electrical components: brushless frameless motor, film power capacitor and braking resistor

Rapid degradation: maximum current, voltage and temperature

Motors are composed of mechanical parts (bearings, housing and heat-sink which can be directly machined in the housing) except when they are sold in frameless form. Therefore they inherit all the rapid degradation drivers of the mechanical parts and especially the speed limit. Another speed limit will result from centrifugal forces applied to rotor coils or permanent magnets.

The other main operational limits are due to:

- Current: current and thus torque are limited either by saturation or by magnet demagnetization.

- Temperature: when considering steady-state thermal exchange, the copper losses (which depend on torque and current) and iron losses (which depend on speed) must not exceed the nominal/rated torque or current defined for a given thermal environment.
- Voltage: power electronics limitations can impact motor performance by introducing power limitation or additional speed limitations linked to the voltage limitation.

In Figure 1 the effects of the mechanical, electrical and thermal operational limits for cylindrical brushless motors and annular brushless motors can be seen. The figure also shows that continuous operation limits are much lower than absolute transient operational boundaries.

Gradual degradations: thermal ageing of insulation material

Temperature effects and thermal degradation are the major causes of failure of many electrical components. As described by [6] electrical components fail due to degradation of thermo-insulation which induces arcing, short circuits and leakage currents.

Degradation laws: Arrhenius laws

As the effects of mechanical degradation only apply to the motor and can be calculated in the same way as for mechanical components in section 2.4.3 this section will focus on the thermal effects that are predominately linked to the thermal ageing of the insulation material and overheating of winding. The lifetime of electronic components depends on the class of the insulation materials as illustrated by Table 1 and Figure 10. Thermal ageing of the insulation material is described in [7] [8] as a function of the Arrhenius relation, which gives the speed of chemical reactions induced by temperature.

$$v = A \cdot e^{-\frac{\varphi}{k \cdot T}} \tag{4}$$

Here v is the speed of the reaction, A is an experimental constant, φ is the activation energy required to activate an electron from the material used, $k=0.8617 \cdot 10^{-4}$ eV/K is the Boltzmann constant and T the temperature of operation.

This means that the speed of the reaction, which is the speed of degradation of the component in this case, is increasing exponentially with increasing temperature. Therefore, the total ageing or sum of degradation of a component Q due to temperature is:

$$L_{h,10} \cdot e^{-\frac{\varphi}{k \cdot T}} = Q \tag{5}$$

Some authors, e.g. [6], use a simplified model for thermal degradation :

$$L_{h,10} \cdot e^{\alpha_{th} T} = Q \tag{6}$$

Table 1 - Activation energy and maximum temperature of insulation classes

Insulation class	Max winding temperature (°C) / (K)	α_{th} (K ⁻¹)	
		$L_h = 20\,000$ h	$L_h = 45000$ h
A	105 / 378,15	0,6	0,032
B	130 / 403,15	0,8	0,073
F	155 / 428,15	1,05	0,078
H	180 / 453,15	1,38	0,085
H'	220 / 493,15	1,27	-

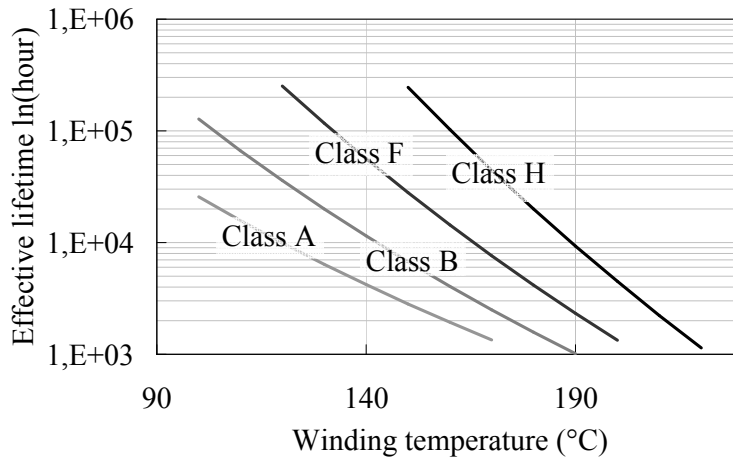


Figure 10 – Winding life time as a function of the temperature of operation for insulation classes A, B, F and H.

For some components small adaptations might be necessary even though their degradation is described mainly by the physical Arrhenius law. For example, when calculating the lifetime and reliability of capacitors or super-capacitors the dependency on the operating voltage V described by [9] or [10] can be taken into account with the equation:

$$L_{h,10} \cdot e^{-\frac{\varphi}{k.T}} \cdot V^p = Q \quad (7)$$

2.3. Power electronics

This category is mainly composed of power semiconductor components subjected to thermo mechanical aging. The Figure illustrates the IGBT modules in an inverter of the TVC actuator for the VEGA launcher.

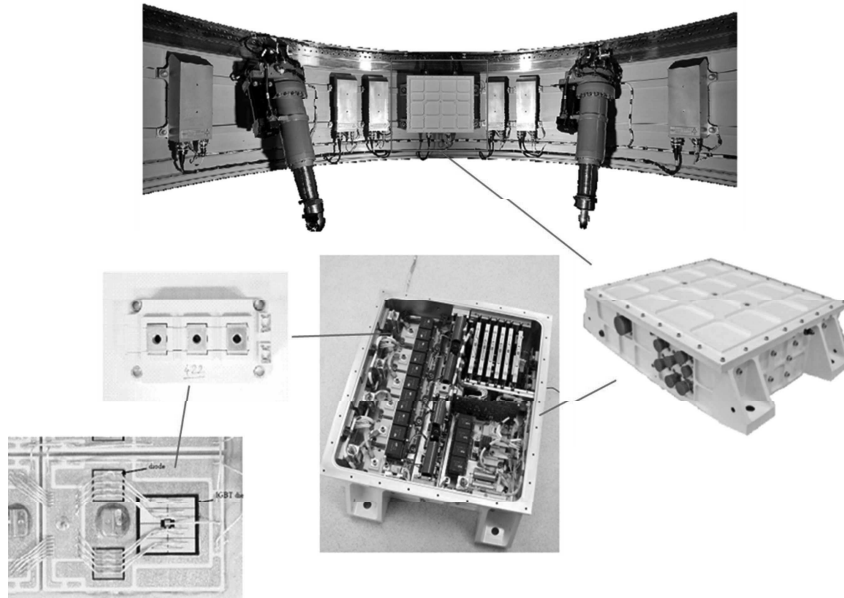


Figure 11 – Twin inverters for TVC EMA actuators of VEGA launcher

Rapid degradation: voltage and temperature

As they consist of different microelectronic components made of different materials as can be seen in Figure 12, various possible failure cases may occur. In terms of Safe Operation Areas (SOA), the IGBT or MOS modules have thermal and electrical limits [11]. Manufacturers provide maximum temperature values for the components. In [11] the chip is specified to fail beyond 125°C in continuous use and 150°C for short period operation. This junction temperature is linked to commutation and conduction losses. Solders melt at temperatures of 180-220°C, which is higher but if the chip heats abnormally, hotspots can be created in the solder, causing earlier failure. Depending on the size and construction of the IGBT or MOS modules, different electrical limits apply, e.g. the voltage throughput.

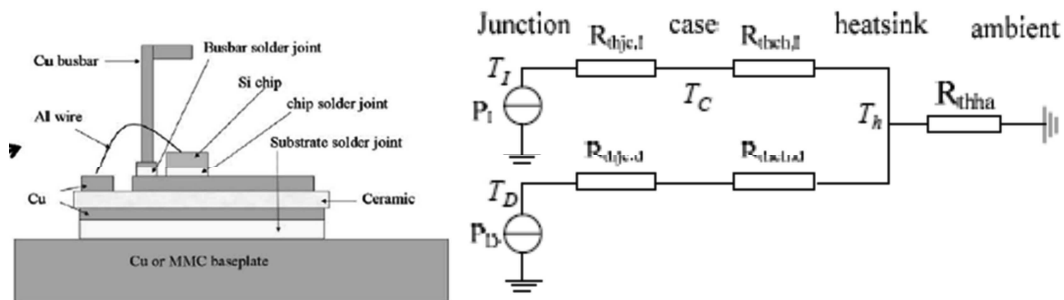


Figure 12 – Thermal model of an IGBT module [12]

Gradual degradation: Thermo-mechanical fatigue

The prediction of the lifetime and reliability of power modules has been discussed in many dissertations and has proved to be a difficult task, due to the complexity of the high temperature micro-electronic module [13]. Typically mechanical failures caused by temperature cycling are more predominant. As a simplification, this thermal-mechanical failure is characterized as cracks or mechanical fatigue that are caused by thermal cycling [14]. As a result, the influence of the change of the temperature between the contact points of different materials, such as junctions, is the major cause of failure for power modules.

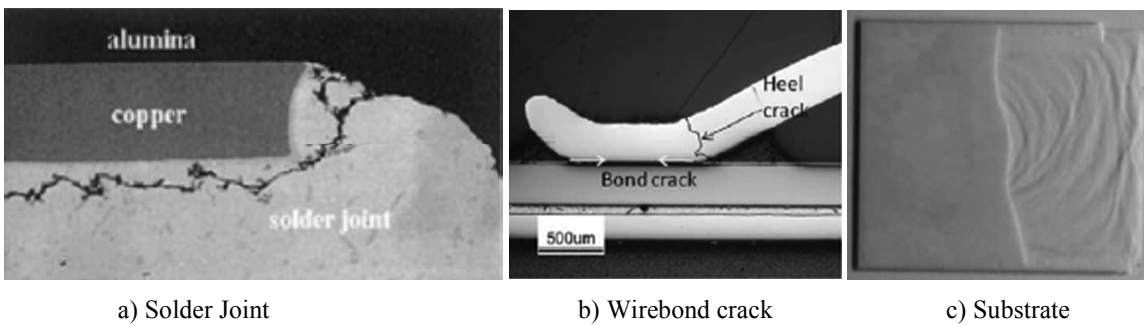


Figure 13 - IGBT module thermo-mechanical failures [15]

Degradation law: Coffin-Manson model

The major causes of IGBT module failure are solder joint fatigue, wire-bond cracks and, less frequently, substrate rupture (Figure 13). As the first two failure principles have the greatest impact and probability, this section focuses on the modelling of solder joint fatigue and wire-bond cracks. The major physical phenomenon, the influence of the change of junction temperature ΔT_j , is described by the modified Coffin-Manson model, a simplified version of which is the equation below. It describes the possible cycles to failure N_f as a function of the change of junction temperature per cycle with an experimental exponential factor α that is constant for a

given application. The factor α depends on the solder material used, the thickness of the solder and other material constraints that influence the shear strength of the material.

$$N_f \cdot \Delta T_j^\alpha = Q \quad (8)$$

Following a calculation procedure [16] proposed by Infineon, a supplier for electronic components and power modules, this equation is valid for the calculation of solder joint fatigue with an experimental factor $2 < \alpha < 4.5$. The failure of IGBT modules due to wire bond cracks that are influenced by the total junction temperature T_j and therefore the Arrhenius relation for the insulation of wires leading to the equation:

$$N_f \cdot \Delta T_j^\alpha \cdot e^{\left(\frac{-Q}{R \cdot T_j}\right)} = Q \quad (9)$$

In the equation below, Q , A and α represent experimental coefficients that depend on the solder and wire materials used and R is the gas constant. For a typical power module solder tin and silver SnAg are used which lead to a factor $Q/R=8690$. Also for solder joint fatigue $\alpha=4.416$ may be applied for the calculation of wire-bond cracks.

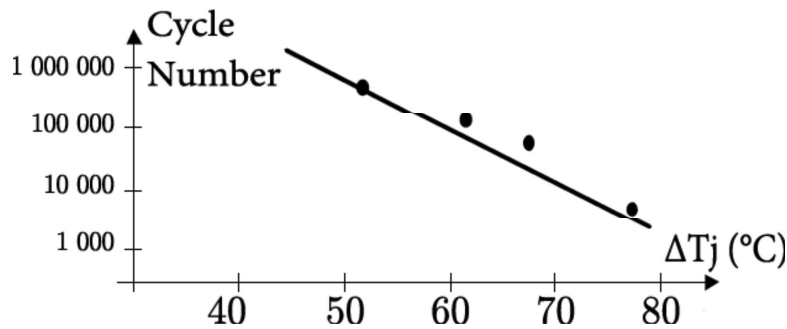


Figure 14 – Thermo-mechanical degradation of IGBTs according to junction temperature

3. EVALUATION MODELS DURING SIZING ACTIVITIES

3.1. Proposed process for sizing for reliability

In this section we will focus only on aspects of design related to gradual degradation. The component selection process to avoid rapid degradation is more obvious and is carried out by comparing the component mission profile to the transitory operating area of the component (Figure 3). The evaluation of a component generally shares the following data:

- A temporal mission profile or operational points representative of main degradation phenomena
- A desired lifetime and a target reliability for the component under consideration

It is then possible to select the component for the most restrictive criterion. If gradual degradation dominates the selection procedure, the design process must generate the definition of the component to be selected. It is also possible to determine the lifetime and reliability of a known component already selected on other criteria. Finally, the process, given in Figure 15, that can be applied for all components follows the following main steps:

1. Definition and simplification of physical laws and interdependencies, see Table 2.
2. Calculation of equivalent effort of mission profile (σ_{eq} , T_{eq} , ΔT_{eq} ...).
3. Calculation of equivalent damage per unit time q_h based on simulation results and calculation of global cumulated damage Q for specified lifetime L_h .
4. Comparison with known reference L_{ref} , N_{ref} , R_{ref} to calculate component failure time L_h , N_h when cumulated maximal damage Q is reached.
5. Sizing of component to reach required lifetime with reference reliability R_{ref} .

6. Calculation of reliability R of component with current mission profile and required lifetime L_{dim} .
7. Sizing towards desired reliability, modification of sizing effort according to the reliability distribution.

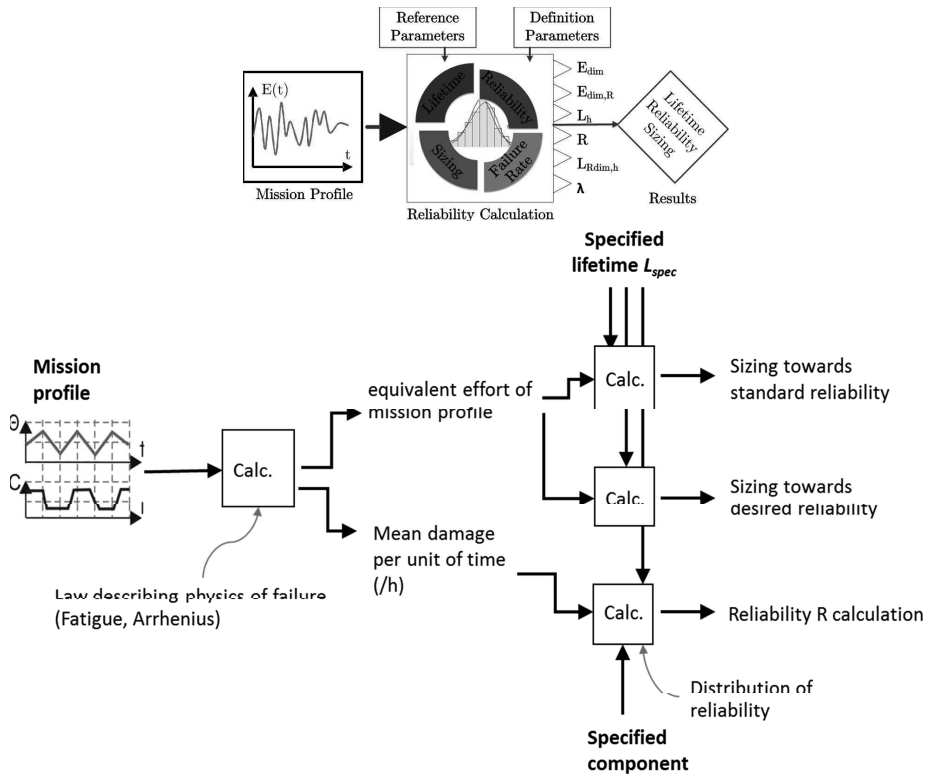


Figure 15 – Proposed methodology for sizing for reliability

Table 2 - Summary of physical degradation calculation for EMA components

Category	Name	Miner-Palmgren	Archard	Arrhenius	Cornell Doublier	Coffin Manson
Mechanical	Bearings	σ^α				
	Reducers & gearboxes	σ^α				
	Wormgears	σ^α	v^β			
Thermal	Electric motors			$e^{-\frac{\varphi}{k.T}}$		
	Braking resistors			$e^{-\frac{\varphi}{k.T}}$		
	Electric wires and inductors			$e^{-\frac{\varphi}{k.T}}$		
	Capacitors			$e^{-\frac{\varphi}{k.T}}$	V^p	
Thermo-mechanical	Power semiconductors			$e^{\left(\frac{-Q}{R.T_j}\right)}$		ΔT_j^α

3.2. From mission profile to rated values

General principle

The components are generally characterized by rated quantities corresponding to a given lifetime or a given number of cycles in a specified environment. However in practice the components are used for different operating point or for variable mission profiles that vary with time. To move from these to equivalent continuous variables, we assume here that the damages is linearly cumulative. Thus, for a degradation law of the following form:

$$N \cdot X^\alpha = Q \quad (10)$$

the degradations of each operating point X_i repeated N_i times accumulate a total damage:

$$Q_T = \sum_i Q_i = \sum_i N_i X_i^\alpha \quad (11)$$

for a total number of cycles: $N_T = \sum_i N_i$.

The equivalent stress X_{eq} is then expressed by :

$$X_{eq} = \left(\frac{\sum_i N_i X_i^\alpha}{\sum_i N_i} \right)^{1/\alpha} \text{ because } Q_T = N_T X_{eq}^\alpha \quad (12)$$

Equivalent effort for mechanical components

For temporal simulation, the sum of cumulated mechanical damage on the mechanical components during a simulation time Q_{sim} can be calculated as below:

$$Q_{sim} = \int_{t_0}^{t_f} |\sigma(t)^\alpha \cdot v(t)^{\beta+1}| dt \quad (13)$$

where t_0 represents the time of the start of the mission cycle, t_f the time of the end of the mission cycle and v the speed of operation.

The equivalent effort σ_{nom} can be calculated as:

$$\sigma_{nom} = \left(\frac{1}{(t_f - t_0) \cdot \bar{v}^{\beta+1}} \cdot \int_{t_0}^{t_f} |\sigma(t)^\alpha \cdot v(t)^{\beta+1}| dt \right)^{\frac{1}{\alpha}} \quad (14)$$

where \bar{v} represents the average of the absolute speed.

Equivalent temperature for electrical components

If the temperature of the insulation is not constant over the mission cycle, the cumulated damage Q_{sim} is based on the integration of the Arrhenius equation:

$$\int_{t_0}^{t_f} \frac{dQ}{dt} \cdot dt = Q_{sim} = \int_{t_0}^{t_f} e^{-\frac{\varphi}{k \cdot T(t)}} dt = \int_{t_0}^{t_f} e^{-\frac{\varphi}{k \cdot T_{eq}}} dt$$

The equivalent temperature T_{eq} can be calculated as:

$$T_{eq} = - \frac{\varphi}{k \cdot \ln \left(\frac{1}{(t_f - t_0)} \cdot \int_{t_0}^{t_f} e^{-\frac{\varphi}{k \cdot T(t)}} dt \right)} \quad (15)$$

because

$$Q_{sim} = \int_{t_0}^{t_f} e^{-\frac{\varphi}{k \cdot T_{eq}}} dt = (t_f - t_0) \cdot e^{-\frac{\varphi}{k \cdot T_{eq}}}$$

Equivalent temperatures of power module junctions

For IGBT modules degradation depends only on the junction temperature change ΔT_j for solder joint fatigue, and depends on ΔT_j and T_j for wire-bond cracks. Therefore, the simulation of the wire-bond crack fatigue will be more difficult as two different parameters influence the function. As an example, the solder joint fatigue will be calculated first.

$$\Delta T_j^\alpha \cdot N = Q = \Delta T_{j,eq}^\alpha \cdot N = \sum_{i=1}^N \Delta T_{j,i}^\alpha \quad (16)$$

Solving this equation for the equivalent temperature change per cycle $\Delta T_{j,eq}$ leads to:

$$\Delta T_{j,eq} = \sqrt[\alpha]{\frac{1}{N} \cdot \sum_{i=1}^N \Delta T_{j,i}^\alpha} \quad (17)$$

This evaluation needs to count the number of cycles, N , and the amplitude of the temperature change in each of the cycles $\Delta T_{j,i}$ through cycle counting algorithms such as the rainflow method [17].

3.3. Lifetime calculation for a selected component

General principle

If a component has already been selected, its effective life N can be calculated from the equivalent stress X_{eq} . The selected component is characterized by a pair of points (X_{ref}, N_{ref}) . N is obtained by assuming that the cumulated damage, as represented **Figure 16**, is equivalent for (X_{ref}, N_{ref}) and (X_{eq}, N) :

$$Q = N_{ref} \cdot X_{ref}^\alpha = N \cdot X_{eq}^\alpha \quad (18)$$

$$N = N_{ref} \cdot \left(\frac{X_{ref}}{X_{eq}} \right)^\alpha$$

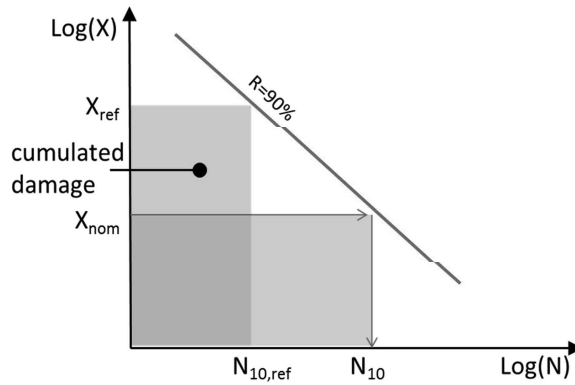


Figure 16 – Lifetime calculation of a given component

Lifetime calculation for mechanical components

The previous expression may be applied directly to the mechanical components. It may also be useful for a simulation that does not represent the whole lifetime to calculate the cumulated damage per unit of time q_h :

$$q_h = \frac{Q_{sim}}{t_f - t_0} = \frac{1}{t_f - t_0} \cdot \int_{t_0}^{t_f} |\sigma(t)^\alpha \cdot v(t)^{\beta+1}| dt \quad (19)$$

For a reference component the corresponding lifetime $L_{h,ref}$ is known as is the corresponding nominal speed and stress to reach this lifetime. These values are normally derived from manufacturers' databases. For bearings, for example, the dynamic load C_r with a reference speed v_{ref} is given for which a nominal lifetime of $N_{ref}=10^6$ revolutions is achieved with a probability of R_{ref} usually of 90%. During simulation, the specific lifetime depending on the mission profile, defined as $L_{h,10}$ can be calculated from this:

$$L_{h,10} = \frac{Q_{ref}}{q_h} = \frac{Q_{ref}}{\frac{1}{t_f - t_0} \cdot \int_{t_0}^{t_f} |\sigma(t)^\alpha \cdot v(t)^{\beta+1}| dt} \quad (20)$$

Equivalent temperature for electrical components

For electrical components, the lifetime $L_{h,10}$ related to the specific mission profile of the application can be derived as a function of reference components and equivalent temperature T_{eq} of the mission profile which was calculated previously :

$$L_{h,10} = L_{h,ref} \cdot e^{\frac{\varphi}{k} \left(\frac{1}{T_{eq}} - \frac{1}{T_{ref}} \right)} \quad \text{because } Q = e^{-\frac{\varphi}{k \cdot T_{ref}}} \cdot L_{h,ref} = e^{-\frac{\varphi}{k \cdot T_{eq}}} \cdot L_{h,10} \quad (21)$$

where T_{ref} and $L_{h,ref}$ are the reference values provided by the manufacturer.

Lifetime calculation of power modules

For power modules, it might be important to identify the number of cycles that are possible before the component fails. This can be calculated directly using the equivalent temperature change:

$$\Delta T_{j,ref}^\alpha \cdot N_{ref} = Q_{ref} = \Delta T_{j,eq}^\alpha \cdot N_{h,10} \quad (22)$$

$$N_{h,10} = N_{ref} \cdot \left(\frac{\Delta T_{j,ref}}{\Delta T_{j,eq}} \right)^\alpha$$

The lifetime of the power modules, or the time until the failure of solder joints here, can be calculated using the damage per unit time from the previous equation as shown below.

$$q_h = \frac{Q_{sim}}{t_{sim}} = \frac{1}{t_{sim}} \cdot \sum_{i=1}^N \Delta T_{j,i}^\alpha \quad (23)$$

Also, it has been assumed here that the total damage that the solder joint can withstand is similar to the total damage until failure of the reference component Q_{ref} depending on its rated condition.

$$L_{h,10} = \frac{Q_{ref}}{q_h} = \frac{Q_{ref} \cdot t_{sim}}{Q_{sim}} = \frac{Q_{ref} \cdot t_{sim}}{\Delta T_{j,eq}^\alpha \cdot N_{sim}} = N_{ref} \cdot \left(\frac{\Delta T_{j,ref}}{\Delta T_{j,eq}} \right)^\alpha \cdot \frac{t_{sim}}{N_{sim}} \quad (24)$$

3.4. Selection of component for standard reliability

General principle

When a desired service life N has to be achieved, an equivalent nominal stress for component sizing $X_{nom,siz}$ needs to be derived. Nominal stresses are generally defined for a given number of cycles, N_{ref} , which gives:

$$Q = N_{ref} \cdot X_{nom,siz}^\alpha = N \cdot X_{eq}^\alpha \quad (25)$$

$$X_{nom,siz} = X_{eq} \cdot \left(\frac{N}{N_{ref}} \right)^{1/\alpha}$$

Selection of a mechanical component

Therefore the mission profile with varying stress and speed has been mapped on a reference point that is described by the equivalent nominal load σ_{eq} and the equivalent nominal speed \bar{v} . This can be expressed more easily if the cumulated damage per unit time q_h has already been calculated. Then, the following relation can be calculated:

$$q_h = \sigma_{siz}^\alpha \cdot \bar{v}^{\beta+1} \quad (26)$$

The equation can then be solved towards the sizing stress σ_{siz} which is similar to the equation introduced earlier:

$$\sigma_{siz} = q_h^{\frac{1}{\alpha}} \cdot \bar{v}^{-\left(\frac{\beta+1}{\alpha}\right)} \quad (27)$$

Electrical components and power modules

For electrical components such as windings of motors and power modules, the lifetime is directly linked to the temperature and not directly to a selection parameter such as a torque or a current. If direct selection of a component is difficult, a target operating temperature can help to select it or to define the associated cooling system. From previous equations, the equivalent dimensioning temperature of operation T_{siz} that achieves the specified desired lifetime $L_{h,spec}$ can be calculated.

$$T_{siz} = - \frac{\varphi}{k \cdot \ln \left(\frac{L_{h,spec}}{L_{h,ref}} e^{-\frac{\varphi}{kT_{eq}}} \right)} \text{ for insulation} \quad (28)$$

$$\Delta T_{j,siz} = \Delta T_{j,eq} \cdot \alpha \sqrt{\frac{N_{h,10}}{N_{dim}}} \text{ for power modules}$$

3.5. Effects of reliability

Reliability basis

The previous calculations were made by considering a general standard reliability provided by manufacturers for the rated conditions of 90% success in completing its mission until the specified lifetime. While the calculation of the lifetime and dimensioning for a desired lifetime of the actuation system is very useful to reach high maintenance intervals needed to reduce operating costs, safety requirements request usually demand a higher reliability than given by the standard reference parameters from manufacturers. The reliability is expressed in terms of the probability of a component or system performing a required function successfully under defined conditions and for a defined period of time. Therefore failure is the contrary event, the termination of the ability of an item to perform a required function. If $F(t)$ is the function of the probability of failure (also called density function), and $f(t)$ is the failure density that occurs in a time interval $[0, t]$, then the Reliability $R(t)$ of a component or a system can be expressed as:

$$R(t) = 1 - F(t) = 1 - \int_0^t f(t) dt \quad (29)$$

At component level, the failure rate λ , which is the probability per unit of time of a failure occurring in a specific interval, is more interesting as it classifies the reliability of a component. The failure rate of a component can be obtained through experiment from the failure density or calculated through the function of failure $F(t)$ or the function of reliability $R(t)$:

$$\lambda(t) = \frac{F(t + \Delta t) - F(t)}{R(t) \cdot \Delta t} = \frac{R(t) - R(t + \Delta t)}{R(t) \cdot \Delta t} \quad (30)$$

The time between two failures of a component is then referred to as the Mean Time To Failure (MTTF) which can also be calculated as:

$$MTTF = \int_0^{+\infty} R(t) dt \quad (31)$$

By adding the Mean Time To Repair (MTTR), the Mean Time Between Failures (MTBF) can be calculated. As the repair time is often neglected or unknown the MTBF is often taken as equal to the MTTF.

$$MTBF = MTTF + MTTR \approx MTTF \quad (32)$$

In this section, the link between reliability parameters and the lifetime is established in a generic way, in order to address different components independently of the failure process (e.g., fatigue and thermal aging). The focus is on the following three reliability parameters: the probability of success R , the failure rate λ , the mean time to failure MTTF.

Electrical components: Exponential failure distribution

Electrical components such as windings and capacitors are subject to random failures during the major part of their service life. A constant failure rate or an exponential failure distribution is then often assumed for simplicity. In Figure 17, the failure density, the number of failures per time, and the failure distribution or failure probability function are shown for an exponential failure distribution.

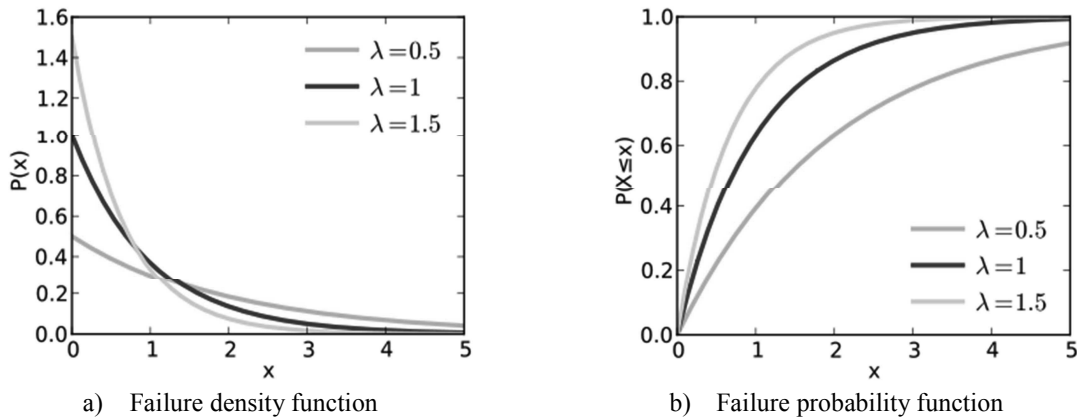


Figure 17 – Exponential Failure distribution for 3 different constant failure rates

This allows a very simple calculation of the components reliability $R(t, \lambda)$, the $MTTF$ and the failure probability $F(t, \lambda)$:

$$R(t, \lambda) = e^{-\lambda t} \quad (33)$$

$$MTTF = \int_0^{+\infty} R(t) dt = \frac{1}{\lambda}$$

$$F(t, \lambda) = 1 - R(t, \lambda) = 1 - e^{-\lambda t}$$

As lifetime is linked to reliability $R = e^{-\lambda L}$, a derated lifetime L_n for a probability of failure of $n\%$ can be evaluated with :

$$L_n = a_n \cdot L_{10} \text{ with } a_n = \frac{\log(R_n)}{\log(R_{10})} \quad (34)$$

Mechanical components: Weibull distribution

When the failure rate λ is not constant, as for mechanical components, multiple options for the description of the reliability functions through a shape factor are available. Besides the exponential distribution, the Normal, Lognormal, Gamma and Weibull distributions are common, the Weibull distribution being the most widely used. The big advantage of the Weibull distribution is that it can be made to fit many distributions by adjusting the shape factors of the function. The shape factor b can therefore imply an increasing hazard rate when $b > 0$ or a decreasing hazard rate when $b < 0$ as well as a constant hazard rate as for the exponential distribution with $b = 0$. The scale parameter μ symbolizes the mean life time of the component $\mu = MTTF$. Differing from an exponential distribution, it cannot be calculated directly, as it is a function of the shape factor. Following this, the hazard rate, the density and the failure distribution function are shown in Figure 18.

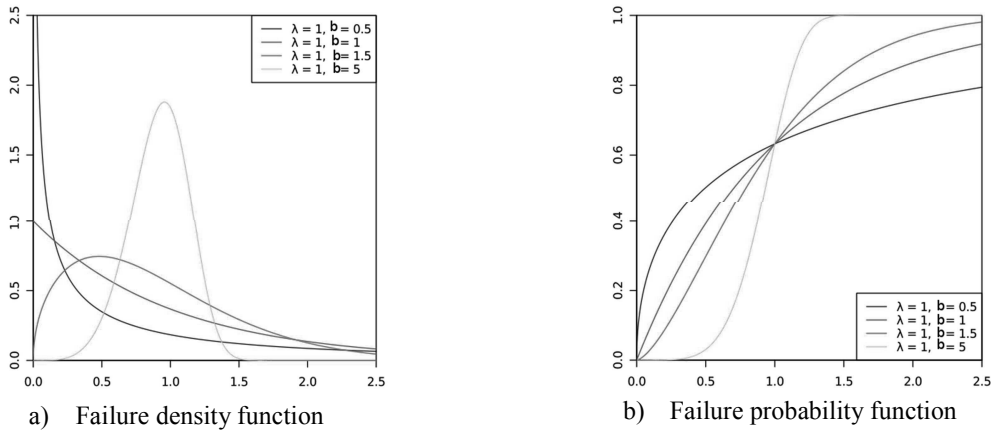


Figure 18 – Weibull Failure distribution with variable failure rate

The failure and reliability values can thus be calculated similarly to the exponential distribution by taking account of b as the shape and μ as the scale parameter. The failure density, the failure probability, the reliability and the variable failure rate can be calculated as:

$$\begin{aligned} \text{failure density: } f(t) &= \frac{b \cdot t^{(b-1)} \cdot e^{-(t/\mu)^b}}{\mu^b} & (35) \\ \text{failure probability: } F(t) &= 1 - e^{-(t/\mu)^b} \\ \text{reliability: } R(t) &= 1 - F(t) = e^{-(t/\mu)^b} \\ \text{failure rate: } \lambda(t) &= \frac{b \cdot t^{(b-1)}}{\mu^b} \end{aligned}$$

From the previous expression, the reliability variation can be expressed as a function of the lifetime variation as:

$$R = R_{ref} \left(\frac{L_{h,spec}}{L_{h,eff}} \right)^b \quad (36)$$

where R is the reliability for the specified lifetime $L_{h,spec}$ and R_{ref} is the standard (reference) reliability corresponding to the effective lifetime $L_{h,eff}$.

Expression (36) also provides a reliability factor a_R that modifies the specified lifetime to match a reliability R_{spec} different from the standard one:

$$L_{h,spec} = a_R L_{h,eff} \quad \text{with } a_R = \left(\frac{\ln(R_{spec})}{\ln(R_{ref})} \right)^{1/b} \quad (37)$$

For the components subject to mechanical fatigue, the previous expression allows us to propose a sizing factor a_{RC} that modifies the sizing parameter (e.g., nominal output torque for the speed reducer) to match a specified reliability as follows:

$$a_{RC} = (a_R)^{-1/p} = \left(\frac{\ln(R_{spec})}{\ln(R_{ref})} \right)^{\frac{1}{bp}} \quad (38)$$

These corrective sizing factors for lifetime and reliability have been computed for $p=3$ and $b=1.5$ in Table 3.

Table 3 - Corrective factors a_R and a_{RC} that modify the specified lifetime or sizing (nominal torque or force) in order to reach a reliability R_{spec} .

R_{spec}	0.9	0.92	0.94	0.96	0.98	0.99
a_R	1	0.86	0.70	0.53	0.33	0.21
a_{RC}	1	1.05	1.13	1.24	1.45	1.68

Relationship of components to systems

Further complications in the determination of reliability are introduced when system reliability is being considered, rather than component reliability. A system consists of several components of which one or more must be working in order for the system to function. Components of a system may be connected in series, as illustrated in Figure 19 which implies that if one component fails, then the entire system fails.



Figure 19 – Reliability block diagram of 2 components in series

In this case, reliability of the entire system is considered, and not necessarily the reliability of an individual component. The system reliability in a series configuration is less than the reliabilities of each component. Thus, series reliability can be expressed in the following relationship:

$$R_{Series} = \prod_{i=1}^n R_{Component,i} \quad (39)$$

and for example of Figure 19:

$$R_{System} = R_{Component1} \times R_{Component2} = 0.90 \times 0.90 = 0.81 \quad (40)$$

When very high system reliabilities are required, the designer or manufacturer must often duplicate components or assemblies, and sometimes even whole sub-systems, to meet the overall system or equipment reliability goals. In systems or equipment such as these, the components are said to be redundant, or in parallel.

Although the reliability of a group of series components decreases as the number of components increases, so the opposite is true for redundant or parallel components. Redundant components can increase the reliability of a system as illustrated by the example of Figure 20:

$$\text{failure probability: } F = (1 - R_1) \times (1 - R_2) = 0.1 \times 0.15 = 0.015 \quad (41)$$

$$\text{reliability: } R = 1 - \text{failure probability} = 1 - 0.015 = 0.985$$

However, this increase in reliability comes at the expense of factors such as weight, space, and manufacturing and maintenance costs.

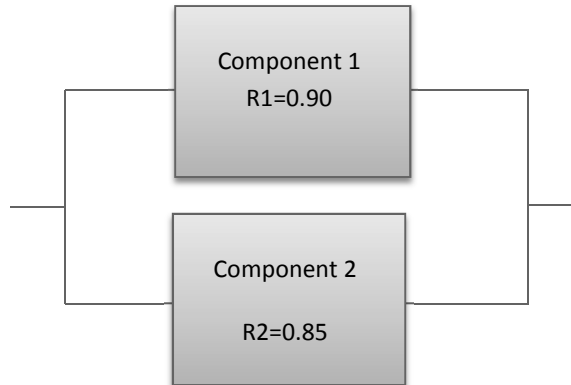


Figure 20 – Example of 2 parallel components

4. CONCLUSION

Some applications, especially in the aeronautical field, require high reliabilities and extended lifetimes. It is therefore essential to address these aspects early in the preliminary design process. With this in mind, this chapter has developed lifetime and reliability calculations that take the sizing and the damage occurring due to operation into account. These calculations have been implemented into an in-house software tool with Modelica language [18]. The proposed approach focuses on systematic failures, which are related to progressive degradation under normal conditions of operation (e.g., fatigue, wear, thermal aging). Other factors of failure appear in manufacturing and operation (e.g., miss-handling, unexpected conditions of operation, external shock). In some fields, e.g. aerospace, the influence of these last factors is minimized by a strict control of the manufacturing and operating conditions. In other fields, this limitation of the proposed approach should be addressed carefully, e.g. by comparing the desired reliability objectives with data based on field experience.

5. BIBLIOGRAPHY

- [1] T. Ros, M. Budinger, A. Reysset and J.-C. Mare, "Modelica Preliminary Design Library for Electromechanical Actuators," in *AST 2013, 4th, International Workshop on Aircraft System Technologies, TUHH, Hamburg, Germany, April 23-24, 2013*.
- [2] D. Morczinek, "Preliminary design for reliability and lifetime prediction of Electromechanical Actuator Systems," Diploma thesis, TUHH/INSA Toulouse, 2012.
- [3] D. Duprat, "Fatigue et mécanique de la rupture des pièces en alliage léger," *Techniques de l'Ingénieur, traité Génie mécanique, 1997*..
- [4] "Neal Consulting Engineers. "Gear Failures: Tooth breakage." from www.tribology.co.uk, 2009., "[Online].
- [5] R. Budynas and J. K. Nisbett, *Shigley's Mechanical Engineering Design*, SI version. New York: McGraw-Hill, 2007..
- [6] J. Gieras and M. Wing., *Permanent Magnet motor Technology - Design and Applications*. M. Decker: 373-379, 1997..
- [7] R. Beeckman, "Nema magnet wire thermal class rating - how to use them and how they are derived".
- [8] E. Brancato, "Estimation of lifetime expectancies of motors," *Electrical Insulation Magazine, IEEE* 8, 3 (may-june 1992), 5 –13..
- [9] S. G. Parler and J. C. Dubilier, *Selecting and Applying Aluminum Electrolytic*, White Paper Cornell Dubilier.
- [10] M. Schwob and G. Peyrache, *Traité de fiabilité*, Masson & Cie, 1969..
- [11] A. Micol, *Approche probabiliste dans la conception des modules de puissance*. PhD thesis, Doctorat de l'Université de Toulouse délivré par l'Université Toulouse III - Paul Sabatier, 2007..
- [12] X. Wen, W. Hu, T. Fan and J. Liu, "Lifetime model research of motor drive systems for electric vehicles.," in *International Conference on Electrical Machines and Systems 2007, Oct. 8-11, Seoul, Korea 2007 (2007)*.
- [13] V. Smet, F. Forest, J.-J. Huselstein, F. Richardeau, Z. Khatir, S. Lefebvre and M. Berkani, "Ageing and Failure Modes of IGBT Modules in High-Temperature Power Cycling," *Industrial Electronics, IEEE Transactions on*, vol. 58, no. 10, pp. pp.4931,4941, 2011.
- [14] A. Christmann, M. Thoben and K. Mainka, "Reliability of power modules in hybrid vehicles (Infineon Technologies AG.)," in *Proceedings PCIM Europe 2009 conference (2009)*.
- [15] H. L. Lu, C. Bailey and C. Yin, "Design for reliability of power electronics modules.," *Microelectronics Reliability* 49 (2009) 1250-1255 (2009)..
- [16] Infineon-Technologies, "Application note, IGBT modules: Definition and use of junction temperature values," 2008.
- [17] SFMM, "Fatigue, Méthode rainflow de comptage des cycles," Groupe de travail 7 de la commission, 1993.
- [18] J. Liscouet, M. Budinger and J.-C. Maré, "Design for reliability of electromechanical actuators," in *Recent Advances in Aerospace Actuation Systems and Components*, Toulouse, 2010.

Paper 3 - An integrated methodology for the preliminary design of highly reliable electromechanical actuators: Search for architecture solutions

ABSTRACT

This paper describes an integrated methodology for finding and assessing architectures of electromechanical actuators with special attention to safety and reliability. The methodology was developed and applied in the framework of the research project DRESS, which aimed to develop and test a highly reliable electromechanical nose gear steering system for a single aisle commercial aircraft. The present paper introduces the integrated methodology proposed for a more systematic design for safety and reliability. Emphasis is placed on the method for finding the most promising candidate architectures that are compliant with the project requirements in general and the safety and reliability requirements in particular. The results obtained by applying the methodology to the DRESS project are presented and discussed.

Keywords: Design for reliability, Electromechanical actuator (EMA), Preliminary design, Conceptual design, Nose gear, Steering.

Referencing: J. Liscouët, J-Ch. Maré, M. Budinger, *An integrated methodology for the preliminary design of highly reliable electromechanical actuators: Search for architecture solutions*, Aerospace Science and Technology, Volume 22, Issue 1, October–November 2012.



Contents lists available at ScienceDirect

Aerospace Science and Technology

www.elsevier.com/locate/aescte



An integrated methodology for the preliminary design of highly reliable electromechanical actuators: Search for architecture solutions

J. Liscouët, J.-C. Maré*, M. Budinger

Université de Toulouse, INSA, UPS, Mines Albi, ISAE, ICA (Institut Clément Ader), 135, avenue de Rangueil, F-31077 Toulouse, France

ARTICLE INFO

Article history:

Received 22 December 2008
Received in revised form 22 May 2011
Accepted 23 May 2011
Available online xxxx

Keywords:

Design for reliability
Electromechanical actuator (EMA)
Preliminary design
Conceptual design
Nose gear
Steering

ABSTRACT

This paper describes an integrated methodology for finding and assessing architectures of electromechanical actuators with special attention to safety and reliability. The methodology was developed and applied in the framework of the research project DRESS, which aimed to develop and test a highly reliable electromechanical nose gear steering system for a single aisle commercial aircraft. The present paper introduces the integrated methodology proposed for a more systematic design for safety and reliability. Emphasis is placed on the method for finding the most promising candidate architectures that are compliant with the project requirements in general and the safety and reliability requirements in particular. The results obtained by applying the methodology to the DRESS project are presented and discussed.

© 2011 Elsevier Masson SAS. All rights reserved.

1. Introduction

The study presented in this paper was conducted in the framework of the European project DRESS (Distributed and Redundant Electromechanical nose gear Steering System) [24,25]. As illustrated in Fig. 1, the project aims to develop and test an electrically powered nose gear steering system [10] with high reliability allowing automatic on-ground guidance. By giving the aircraft a true all-weather (true zero visibility) capability, it will offer significant aircraft operation gains and increase the Air Transport System efficiency. The work reported focuses on the design of the electromechanical actuator (EMA) replacing the current servo hydraulic one scaled to single aisle commercial aircraft (Fig. 1).

To move towards more electric aircraft [15], this challenging project must provide a technology leap, improving safety and reliability to allow automatic guidance with a limited weight impact. Such a critical embedded electromechanical actuation system is very complex to design and to optimize, especially because of its multidisciplinary character [46] and its multiple modes of operation. The design of the power transmission, modulation and transformation must cope with multiple and opposing constraints when considering mass, reliability, safety, shimmy damping and controllability [36,23,37], and operability (towing).

In this paper, an integrated methodology covering the search for and evaluation of high-reliability architectures for the preliminary

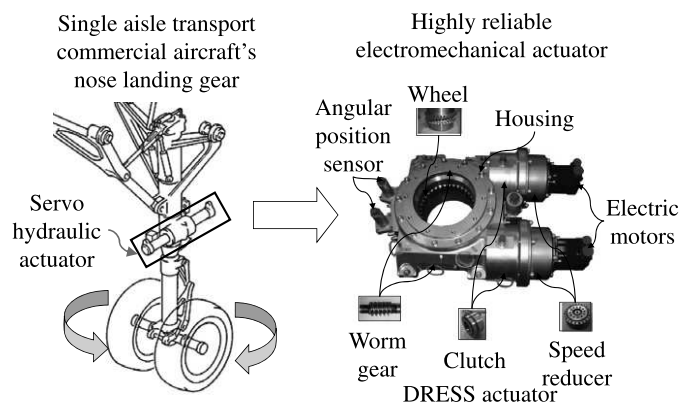


Fig. 1. DRESS – replacing a conventional hydraulic nose gear steering system by a highly reliable EMA.

design of an EMA is introduced. The preliminary (or conceptual) design [45] is a critical phase of a project that engages most of the decisions and development costs. The aim of this methodology is to simplify and speed-up this phase. The focus is on the search for architectures compliant with highly demanding safety and reliability requirements.

In the first part of Section 2, the general principles of the proposed integrated methodology for the search and assessment of EMA architectures are described. In the second part of the section, the approaches finding solutions in the conceptual design are reviewed before presenting the method developed in the DRESS

* Corresponding author.

E-mail address: jean-charles.mare@insa-toulouse.fr (J.-C. Maré).

Nomenclature

CAD	Computer Aided Design	TR	Translational–Rotational
EMA	Electromechanical Actuator	RRR	Rotational–Rotational–Rotational
RR	Rotational–Rotational	RTR	Rotational–Translational–Rotational
RT	Rotational–Translational		

project. In Section 3, the main requirements of the DRESS project are introduced. In Section 4, the method developed in the DRESS project for finding highly reliable EMA architectures is described in more detail together with its results. In Section 5, the reliability of the architectures obtained is quantitatively investigated in order to specify actuator elements in consequence and to assess the severity of the reliability objectives. In Section 6, the process for evaluating the architectures is briefly described and references for further details are provided. In Section 7, the results obtained by applying the integrated methodology to search for and assess highly reliable EMA architectures in the DRESS project are presented. Finally, these results and possible future works are discussed in Section 8.

2. Proposed methodology

2.1. General principle

A design process, such as the V cycle, is inherently highly iterative [50]: It starts with a limited level of detail and a limited number of parameters and criteria to be considered. As the design progresses, the level of detail and number of issues to be taken into account increase. As detailed design information comes late in the process, the designer must proceed in an iterative way. If the selected solution finally fails to meet the requirements regarding the different engineering domains involved, then a large loop back to the first steps of the process might be required. Such a loop has a direct impact on development costs, times and risk.

The purpose of the proposed methodology is to implement more iterative capacities in the early preliminary design phase. In this way, it is possible to take more details and design criteria into account early in the design process. Thus, the size and number of iteration loops are reduced. Consequently, the design process speeds up and is more secure.

In the framework of the DRESS project, the high demand for reliability is a design driver that must be considered early during the generation and selection of architectures [44]. Accordingly, the method described in the next sections specifically addresses this aspect by creating early iterations on the reliability aspect, both qualitatively and quantitatively.

The methodology introduced here deals with the preliminary or conceptual design phase as defined in the generally accepted systematic engineering design process model [45,34,48,35,32,17,22,47], which aims to optimize the search for an optimal design. In this process the conceptual design can be divided into four main highly iterative steps:

1. Specification (requirements).
2. Definition
 - a. Search for principle solutions (concepts).
 - b. Embodiment (solution variants of the chosen concepts).
3. Evaluation (comparison of the chosen concepts).
4. Decision (selection of a concept for the detailed design).

The proposed integrated methodology encompasses the definition and evaluation of highly reliable electromechanical actuators. As previously mentioned, this paper places the emphasis on the

systematic search for principle solutions and their embodiment, which make up the definition phase of the conceptual design.

2.2. Search for architecture solutions: State-of-the-art and proposed method

Solution finding methods aim to find an optimal solution that fulfills all demands in the requirements and can be realized within the time, budget and resource constraints set for the project. As defined in [35], in a systematic approach the first step is to generate a range of solutions from a function structure. A function structure is the compatible combination of sub-functions to give an overall function. In a second step, physical effects are assigned to each of the sub-functions. Solution variants are generated while the function structure is being developed and when physical effects are selected. The solutions generated are then evaluated and compared before selection.

Two main approaches can be distinguished in the development of a new product: (1) Improving or deriving an existing technical solution; (2) Producing a new solution from scratch. In the aeronautics industry, as in many others, starting from a proven existing technical solution (e.g., previous product) is one of the most important means of generating new designs and improving existing ones as it reduces development risk, time and costs. Generating a new solution from scratch offers greater potential for optimization, but also increases the development risk, time and cost. Starting from scratch is generally motivated by a demand for innovation, as is the case in the DRESS project with a demand for a technological breakthrough from hydraulic to electric actuation technology. In both approaches, the search for solutions should start by gathering state-of-the-art information from e.g. technical literature, trade publications, professional fairs and exhibitions, catalogs, patents and analysis of existing products. One of the main interests of this preliminary activity is to avoid the unproductive process of involuntarily re-inventing an already existing technical solution (that might be patent protected). In case of the improvement of or derivation from an existing solution, this information can also be used to identify candidate existing solutions to serve as a basis. In case of the search for an innovative solution this information can feed the search, e.g. with working principles.

The search for an overall solution or individual solution (part of the overall design solution) can be based on conventional, intuitive or discursive methods [35]. Conventional methods include extracting solutions from state-of-the-art information, e.g. by analysis of existing solutions, analysis of natural artifacts (e.g., organisms, structures, processes) or analogies with similar problems. In intuitive methods the designers seek and discover solutions for difficult problems by intuition. Good ideas are developed and modified, until one leads to a solution to the problem. The methods to support intuition for identifying solutions and solving problems range from simple discussions among colleagues to more sophisticated brainstorming methods. The main issue with purely intuition-based methods is that an optimal solution may be simply overlooked. Discursive methods provide a solution in a more systematic step-by-step approach. Note that discursive methods do not exclude intuition, which can be involved in the finding of individual solutions. Discursive methods for deriving new solutions

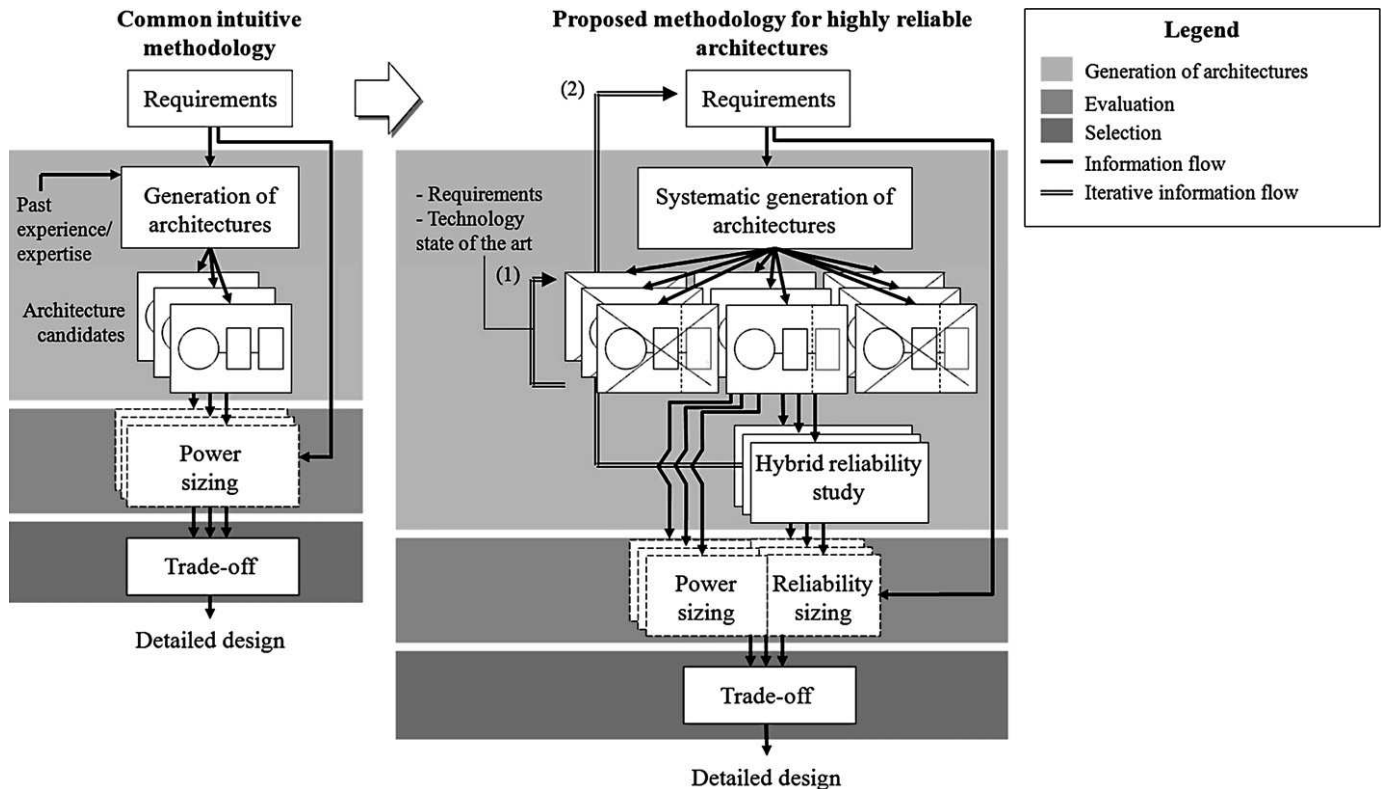


Fig. 2. Common intuitive methodology vs. proposed more systematic methodology for highly reliable EMA architectures.

from existing ones are based on variant design for the specification task (e.g., [16]) and analogical reasoning for the definition task (e.g., [26]). For new solutions from scratch, discursive methods are based on the systematic study of physical processes [40,35], classification schemes [12,35] or first-principle reasoning (e.g., [32, 35,49,6,26]). First principle reasoning is a compositional synthesis process that involves databases of basic knowledge about working principles or components (e.g., design catalogs [42,35]) used as building blocks that are combined together to form solutions.

All the aforementioned methods can be used independently for defining the different parts of the overall solution. In that case, the next step is to combine them to form this overall solution. This task can be conducted intuitively or in a more systematic way. The systematic combination of local solutions is a combinatorial problem, the objective of which is to combine only promising compatible solutions satisfying all the demands of the requirements. In order to manage the solution space (generated solutions) efficiently, i.e. to generate valuable solutions only, this combination should be visually supported e.g. by means of classification schemes also referred to as morphological matrices [51,35]. The advantage of a systematic approach is to encompass the broadest range of solutions and thus to minimize the risk of missing an optimal solution. However, the problem is that more solutions are generally produced than can be seriously considered by the designer. To take advantage of a systematic approach it is therefore essential to limit the number of solutions generated. One can distinguish two main approaches for managing the number of solutions generated: the feasibility and the similarity approaches [33]. In the feasibility approach, design constraints and rules are used to discard (to filter) solutions, e.g. by limiting the number of building blocks in the overall solution or constraining the position of certain blocks. The similarity approach harks back to the concept of classification schemes: Rules of similarity are used to group solutions. The designer can then assess a group by investigating only one or a few of its solutions.

In the DRESS project, the demand for a technological breakthrough from hydraulic to electric technology together with a demand for a highly reliable solution led us to look for a new design from scratch. At the beginning of the DRESS project, a common method based on the intuitive identification and combination of technological solutions was first applied. As shown in Fig. 2, this method starts with the identification of the possible technological solutions. Then, the identified technological solutions are intuitively combined into candidate architectures. Finally, the architectures generated are optimized and evaluated before being compared.

Such common methodology allows proven solutions to be re-used by combining them in an innovative way to obtain new functionalities and by minimizing the development risk. On the other hand, because of the variety of forms (redundancies [20]) and number of solutions for high-reliability architectures, this intuitive approach does not efficiently support the elicitation of the most promising architectures for the given application. In other words, it does not converge to generate a reduced number of valid solutions with confidence in not missing a valuable design. Therefore, a more systematic method has been developed on the basis of first-principle reasoning applied to an in-house expertise based catalog of functions, concepts and proven components for electromechanical actuation applications. In this way, the broadest possible range of solutions is generated to increase the chances of finding an optimal design. The generation of solutions is performed over three distinct levels of abstraction: functional, conceptual and technological (embodiment). The number of solutions is managed by filtering by constraints at each level of abstraction. As a result, the proposed method involves, in compliance with related works in the field of design research (e.g., [38,9,41]), two kinds of steps: divergent (generation) and convergent (filtering). By repeating these two steps over three levels of abstraction, a multiple divergence–convergence solution generation process with an overall convergent trend is obtained as illustrated in Fig. 3. Thus, the

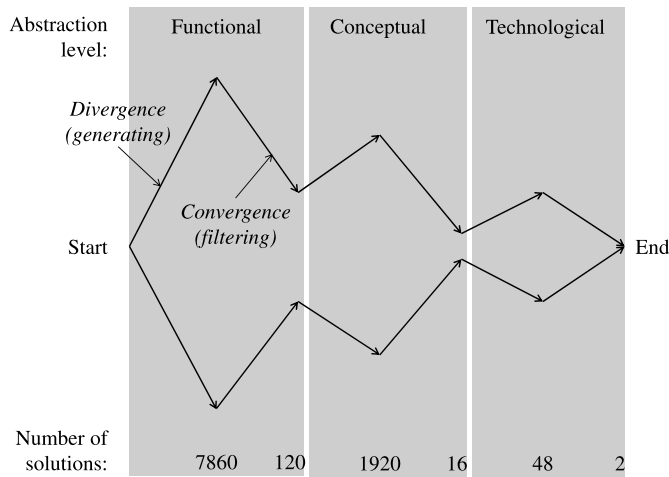


Fig. 3. Multiple convergence–divergence solution generation process of the DRESS project.

proposed method can be qualified as a ‘balanced search’ as defined in [19]. The constraints used for filtering are either domain-neutral (e.g., limited number of basic elements making up the overall design) or domain-based, i.e. imposed by the state-of-the-art of electromechanical technology (e.g., invalidity of a direct-drive solution due to its massive weight impact). Because of the importance of reliability in the DRESS project, special care was taken to establish reliability based constraints (e.g., domain-neutral: fault containment next to the load in the transmission chain, domain-based: no end-effector components with a significant risk of jamming). Finally, as mentioned previously, it is essential to enable visualization of the solution generation to manage the solution space. Therefore, a functional architecture framework for representation of the functional solutions (see Fig. 5) and morphological representations of conceptual and technological solutions (see Fig. 6 and Fig. 7, respectively) have been developed.

The output of this first part of the overall methodology is a reduced number of architectures that are qualitatively compliant and most promising with respect to the requirements.

It is then possible to proceed to a quantitative reliability analysis, in order to allocate reliability targets (failure rates) to the different parts of the EMA. We also propose to take advantage of this analysis here to validate or to support the redefinition of the quantitative reliability requirements very early in the design process. In this way, a second iterative capacity focusing on reliability (Fig. 2) is implemented early in the process.

Finally, as shown in Fig. 2, in addition to the traditional power sizing, the reliability target allocation allows sizing with respect to the reliability of the architecture components for a better evaluation of the different solutions before the trade-off.

3. The nose gear steering system

The work reported here encompasses the design of the electromechanical power transmission from the power electronics to the mechanical interface with the nose gear turning tube (Fig. 1).

The modes of operation and the mission cycle of the nose gear steering system depend on the different aircraft operation phases: towing, taxiing, take-off, flying gear-down, flying gear-up, and landing. For safety purposes, the nose gear steering system also includes a reversionary and an ultimate mode of operation. In case of a single failure, the actuator remains operative by switching to the so-called reversionary mode. In case of a combination of failures, the system becomes passive and leaves the wheel steering free to move. It is assumed that a mission cycle is repeated a given

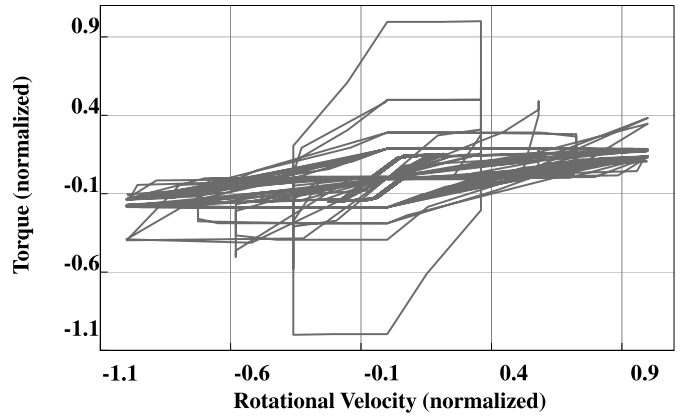


Fig. 4. DRESS mission cycle – torque vs. angular velocity (normalized).

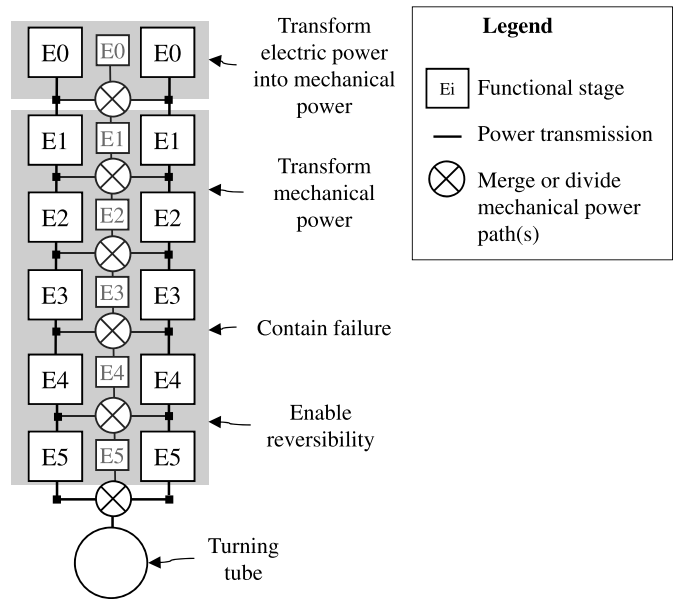


Fig. 5. Actuator functional architecture framework.

number of times per day for the entire life of the aircraft. This allows the required system lifetime to be calculated, e.g. for fatigue and reliability sizing.

In the towing and ultimate operation modes, the steering system is passive: The actuator does not oppose too high a resistant torque against motion of the nose gear, while the aircraft is steered by an operator on the ground. During taxiing, take-off and landing, the steering actuator operates in the closed-loop control position and the steering angle demand is limited according to the aircraft velocity. In the reversionary mode, the actuator might have reduced power (force or speed) capabilities that are sufficient to complete a mission cycle. Fig. 4 illustrates the power need for the steering system in the normalized torque-speed plane.

4. Systematically generating solution concepts

This section illustrates the proposed method for systematically generating solution concepts (architectures) while giving special consideration to mass and safety. The process starts from the results of a requirement and functional analysis of the steering system under study. Once the actuator major sub-functions and requirements driving the design of the electromechanical power transmission have been identified, a functional architecture framework can be developed. As shown in Fig. 5, the proposed functional

architecture framework consists of functional stages taking the form of boxes that are linked together by following the electromechanical power transmission path(s) from the power source to the actuated load. The advantage of this framework is to represent all the solutions at the functional level, while being representative of the physical appearance of the actuator to be developed. All the possible functional architectures are obtained by systematically combining all the identified functions with the help of the architectural framework. The next step consists of embodying this framework at conceptual and then technological level. Because of its systematic aspect, this process generates a large number of solutions. In order to maintain an overview and keep control of this process, it is proposed to filter the solutions generated at the three different levels of detail considered: functional, conceptual and technological, while paying special attention to the safety requirements. This systematic architecture generating and filtering process leads to a limited number of actuator architectures that comply with the system requirements in general and the safety requirements in particular.

A functional analysis of the actuator identifies the actuator functions driving the design of the electromechanical power transmission:

- To transform electric power into mechanical power;
- To distribute and transform mechanical power;
- To allow free castoring during towing;
- To remain operative after a single failure (reversionary mode) and to fail passively (wheel is free to move) after a combination of two failures (ultimate operation mode).

4.1. Functional architecture framework

The previously identified actuator sub-functions and requirements are the foundation of an architectural framework as described in Section 4. Drawing such a framework still requires some high level decisions to be taken. For example, the event of generating a huge number of redundancies (power paths) is not consistent with efficient progress at that point. It is first necessary to define this aspect in greater detail.

For many reasons, such as integration or safety, an actuator can comprise multiple power paths. In order to simplify the development of the functional architecture framework and to cope with the weight constraint, it is first assumed that the number of power paths is limited to two. This balances redundancy needs and weight impact. In order to minimize the number of unique parts and improve maintainability of the system [18], it is subjectively decided to design symmetrically parallel power paths.

In the functional architecture framework, at least one stage must correspond to each actuator sub-function. However, the function “transform mechanical power” can involve more stages as mechanical power can flow in either rotational or translational ways. Transforming a rotational motion into a translational motion would require only two functional stages. Yet it could be interesting to consider a Rotational–Translational–Rotational (RTR) mechanical power transformation, especially because of the high reduction ratio and compactness that this solution might offer (e.g., use of a roller-screw). Therefore, three functional stages correspond to the function “transform mechanical power”.

The resulting functional architecture framework is illustrated in Fig. 5. As shown, the power can flow through single (in gray) or parallel (in black) functional stages (i.e., power paths). To go from a single to a parallel functional stage and vice versa, it is necessary to divide or merge the mechanical power path(s). Thus, each architecture is a unique combination of single and parallel stages, i.e. of black and gray segments alternating through mergers and dividers in Fig. 5.

From a combinatorial calculation, 7860 different possible solutions are found for the given architecture framework:

$$N_f = \overbrace{5!}^{5 \text{ functions (E1-E5) to combine}} \overbrace{2^6}^{\text{Possibilities of redundancy}} = 7860 \quad (1)$$

In order to reduce this number before embodying at conceptual level, it is interesting to study the impact of the safety requirements. The two major undesired failure events that can be caused by the electromechanical part of the actuator are jamming (classified as catastrophic) and loss of torque control (classified as hazardous) at the turning tube. Based on the fail-safe principle, no single failure of the actuator is allowed to lead to these events.

To illustrate the impact of these requirements, it is interesting to start by considering an actuator consisting of a single power path. A failure-inhibiting element has to be mounted downstream of the last component that may fail, in order to ensure that no single failure will lead to the aforementioned undesired events. In case of a single power path, jamming of the landing gear turning tube and loss of torque control are antagonistic failure events. Inhibiting jamming by declutching causes a loss of torque control of the turning tube, and inhibiting a loss of torque control failure by holding position causes jamming of the turning tube. This clearly indicates that at least two independent power paths are necessary. In this way, a single failure occurring in one path can be inhibited by the corresponding element located downstream the failed component, while the remaining healthy path takes over the actuator functions.

To sum up, safety considerations reduce the actuator functional architecture framework to two independent power paths. The power is combined at the turning tube only. These statements completely fix the redundancy and thus reduce the number of different possible solutions from 7860 to 120 (function combinations).

4.2. Conceptual architecture framework

The transition from the functional to the conceptual level of detail consists of deriving each sub-function into physical principles [35]. In consequence, during this transition, the number of solutions is increased.

At conceptual level, the function “transform electric power into mechanical power” can be carried out by either a rotational or a translational electric motor. A comparative preliminary power sizing study led to the selection of a rotational motor on the basis of the mass requirement.

At mechanical transmission level, there are four candidate types of power transformers:

- Rotational–Rotational (RR);
- Rotational–Translational (RT);
- Translational–Rotational (TR);
- Translational–Translational (TT).

They can be associated in three stages, the first stage being driven by a rotational electric motor. This gives eight different possible combinations. The use of a rotational electric motor and the rotational nature of the actuator output (landing gear turning tube) reduce the problem to four possible combinations, which can be resumed in two main concepts, RRR and RTR transmissions. RRR stands for a pure rotational mechanical power transmission, while RTR stands for the use of an intermediate translational transmission (e.g., roller-screw combined with a gear rack).

The function “allow free castoring” ensures the towing capability of the aircraft on the ground. This can be realized in two

Concept solutions		Number of stages	Position in the architecture frame
Translational electric motor	Rotational electric motor	1	E0
TR-RR-RR	RR-RR-RR → RRR	3	E1-E5
TR-RT-TR	RR-RT-TR		
TT-TR-RR	RT-TR-RR → RTR		
TT-TT-TR	RT-TT-TR		
Decutching/re-arming	Reversible transmission	1 or 0	E1-E5
Decutching	Braking	1	E1-E5
Torque summation	Speed summation	1	E6*

* Stage not shown explicitly in the functional architecture frame

Fig. 6. Actuator conceptual architectures.

different ways: making a completely reversible actuator or disconnecting the actuator from the turning tube during towing operations.

Mechanical power flows can be combined in a speed or torque summation scheme. On the one hand, speed summation offers the capacity to drive the turning tube even in case of jamming of one upstream power path; while torque summation would jam the turning tube. On the other hand, torque summation offers the capacity to drive the turning tube even in case of loss of torque control of one upstream power path, while speed summation leads to loss of torque control of the turning tube. Thus, inhibiting a single failure requires braking and decutching elements in the speed summation and torque summation configurations respectively. At technological level, speed summation can be realized with a planetary gear train directly mounted on the turning tube. Because of the number of rotating elements in such a component, it is not acceptable in terms of risk of jamming. Additionally, this component would have a mass greater than the specified mass. Therefore, only torque summation is considered with the corresponding decutching elements. Additionally, the decutching element can be used to ensure the function “allow free castoring” if it can be decutching and re-armed during operation. The resulting conceptual architectures are illustrated synthetically in a morphological fashion in Fig. 6.

Before discarding translational motors and speed summation with respect to technological constraints, there were 1920 different possible solution concepts:

$$N_{c1} = \underbrace{5!}_{\text{Function combination}} \underbrace{8}_{\text{Linear or rotary motors, mechanical transmission}} \underbrace{2}_{\text{Speed or effort summation, decutching or braking}} = 1920 \quad (2)$$

The aforementioned decisions, obtained by systematic reasoning and their impacts on the other actuator functions reduced this number to 16:

$$N_{c2} = \underbrace{4}_{\text{RLR or RRR transmission}} \underbrace{4}_{\text{Positioning of the clutching}} = 16 \quad (3)$$

4.3. Technological architectures

Usually, rotational electric motors used in EMAs are DC, synchronous (brushless) or induction motors, with cylindrical shape and internal rotor.

The induction motor consists of a simple assembly, and is robust and cheap. However, it has a low torque density compared with the DC and synchronous permanent magnet motors. For this reason, its use is generally limited to industrial applications.

The DC motor is easy to control and minimizes the cost of the associated controller. Also, it delivers a smooth torque. However,

this advantage is balanced by the presence of brushes, which have to be protected from harsh environments and are subject to wear.

The high performance synchronous permanent magnet (brushless) motor [8] has high efficiency and power density. It requires a rather more complex and expensive controller than a DC motor to offer the same torque smoothness. The absence of brushes significantly reduces the maintenance needs and inhibits critical behavior in a harsh environment. Its mass and reliability advantages make this motor the current standard for aeronautical applications.

In the DRESS project, the partner responsible for motor manufacturing provided a high performance permanent magnet synchronous motor with physically and magnetically decoupled phases, which has a higher torque to mass ratio and very interesting features for high-reliability operation [27].

Rotational-rotational mechanical power transmission can be obtained by combining cycloidal reducers, harmonic drives, planetary trains, worm gears, spur gears, etc. For integration purposes, worm gears and spur gears offer interesting means of interfacing with the turning tube. Cycloidal and harmonic reducers have a higher power density than planetary trains but are dedicated to rather high transmission ratio ranges while planetary trains are more relevant for lower transmission ratios. Therefore, it is interesting to consider planetary trains for small transmission ratios and cycloidal or harmonic reducers for high transmission ones.

The roller-screw technology was identified as the most suitable solution for carrying out RTR mechanical power transformations interfacing with the turning tube, especially for integration purposes and because of its high load capacity and transmission ratio.

Disconnecting the complete actuator from the turning tube during towing operations or from one power path in case of failure can be done by an electromechanical clutch. This clutch can be mounted only upstream of the component interfacing with the turning tube. Therefore this interfacing component is located in a single path from a safety point of view, and has to be jamming resistant. The failure behavior of roller-screws and worm gears is well known and not subject to jamming in normal operating conditions. In the same way, spur gears are simple components that can be adequately oversized to ensure resistance to jamming.

An ultimate solution against jamming could be to develop an in-house decutching system that would be installed in parallel to the interface between the actuator and the turning tube. Basically, it would isolate the failed power path by pushing its interfacing element (e.g., rack, pinion, worm screw) out of the turning tube gear. On the one hand, such a device would raise re-arming issues to ensure its necessary testability against dormant failure and would have a significant impact on the system’s mass, maintainability and reliability. On the other hand, it is not proved that it will be sufficient to ensure the jamming resistance of the actuator. Therefore, it is not considered further here. Fig. 7 summarizes the resulting power transmission candidates at the technological level in a morphological fashion.

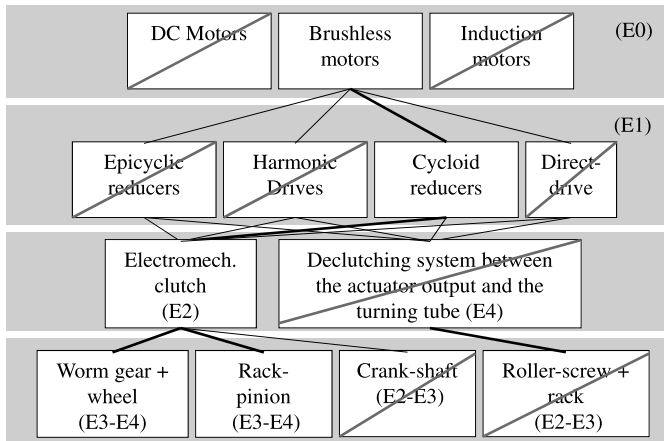


Fig. 7. Actuator technological architectures.

Before filtering on technological level, there were 48 different technological solutions:

$$N_{t1} = \underbrace{3}_{\text{Motor types}} \underbrace{4}_{\text{Speed reducer types}} \underbrace{4}_{\text{RRR or RTR transmissions}} = 48 \quad (4)$$

Filtering with respect to technological constraints (imposed by partnerships and technology state of the art) allowed a reduction of the number of different possible solutions from 48 to 2 (Fig. 7). Such a limited number of candidate architectures is acceptable for preliminary reliability analysis, pre-sizing and comparison studies.

5. Reliability analysis

The objectives of the present reliability analysis are:

- To allocate reliability targets (failure rates) to the different parts of the EMA;
- To validate or support the redefinition of the quantitative reliability requirements if necessary;
- To enable sizing for reliability [30].

The evaluation of the candidate architectures regarding reliability is based on general fault trees for the three failure events that can be caused by the electromechanical power transmission part of the actuator:

- Jamming of the nose landing gear;
- Loss of torque control;
- Reversionary mode.

The reversionary mode refers to the fail operative condition, where one power path fails and is disconnected while the remaining healthy power path carries the actuator functions alone for a limited duration.

In a common reliability analysis based on fault trees, the failure probabilities of the different components and their effects are propagated through the trees up to the desired upper level effect (e.g., to system level) to obtain the occurrence rates of the failure events studied [20,43]. First, this traditional bottom-up methodology is used here to check the validity of the candidate architectures with respect to the reliability objectives. Second, a hybrid (top-down/bottom-up) methodology, described below, is proposed to define reliability targets for the different parts of the EMA and thus to reach the system reliability objectives. In order to support the design for reliability, this methodology focuses on assessing the failure rates for two main groups of components. The first group

consists of components located in the single power path (downstream of the clutches). Because of their safety criticality, their design impacts the overall system reliability strongly. The second group of interest consists of the system parts located upstream of the power electronics (including command, logic, etc.). They form the non-power transmission part of the system and are called system upper part here for practical reasons. Assessing the reliability of the system upper part supports a consistent design for reliability at the overall steering system level.

5.1. Reliability calculation assumptions

In order to reduce the problem complexity, the different architecture components are assumed to have failure rates invariant with time for both the electric and mechanical components [20, 11]. Their failure probabilities can therefore be described with the exponential distribution function.

Reliability calculation requires failure rate data for all the components involved in the candidate architectures. Most of the values used in this study are adapted from published summaries [39].

Reliability calculation also requires the operating times of the system parts to be taken into account. If a system is not working continuously during a mission it is less exposed to failure and thus can reach a higher reliability level over its lifetime. It is assumed that the safety critical components and the clutches are always exposed to failure except during in-flight phases, where they are not operating. The system upper parts are assumed to be exposed during taxiing, take-off, landing and gear-down phases. Thus, for a typical mission, the operating times of the critical components and system upper part correspond to 35% and 30% of a flight hour respectively.

5.2. Hybrid methodology for assessing reliability targets

The proposed methodology for assessing component reliability targets is based on a common bottom-up fault tree approach modified with a top-down propagation of top-level failure rate objectives. The usual process has component failure probabilities as inputs and the occurrence probabilities of the top-level events under study as outputs. Here, this process is modified in order to take the occurrence probabilities of the studied top-level events as inputs and to output the relationships between the reliabilities required for the safety critical components and the system upper-part. In this respect, the common fault tree calculations are mathematically adapted to include the top-level events and the safety critical component probabilities of failure as inputs and the corresponding required maximum probability of system upper-part failure as output. The detailed calculations are described in [29] (in French). In this way, varying the critical component probabilities of failure provides, for the given reliability objectives, the numerical relationships between the maximum acceptable probabilities of failure of the system upper-part and the safety critical components.

The relationships obtained, as illustrated in Fig. 8, support the trade-off between critical components and the system upper-part reliability requirements. In this way, the proposed methodology efficiently supports a consistent design for reliability from component level to system level.

5.3. Probability of jamming

The jamming of the turning tube being classified as catastrophic implies a failure rate of 10^{-9} per flight hour as required by the aviation authorities [28]. This failure is inhibited in case of jamming of a component located upstream the electromechanical clutch. This implies a properly operating clutch. The jamming of any component located downstream of the electromechanical clutch (including clutch output shafts) would make the turning tube jam.

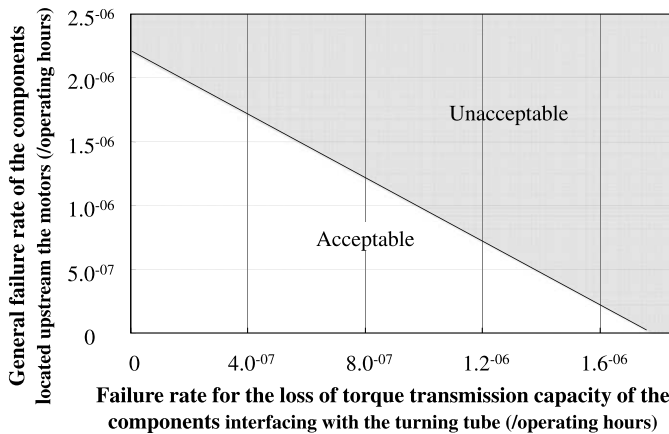


Fig. 8. Maximum acceptable system upper part failure rates versus critical component loss of torque transmission capacity failure rates.

Therefore, these critical components must be designed with special consideration to jamming resistance.

The other focus of this study is the target reliability of the system upper part. The jamming of a component located in the system upper part must be combined with a clutch blocked in the engaged position to really cause the jamming of the landing gear leg turning tube. Due to the very low probability of this event, power electronics reliability is not restricted by the jamming reliability target. Thus, from the jamming reliability target of 10^{-9} per flight hour; it is possible to assess a target jamming failure rate of 2×10^{-9} per operating hour and per path for the critical components.

5.4. Probability of loss of torque control

The loss of torque control is classified as hazardous, implying a failure rate specified by the aviation authorities of 10^{-7} per flight hour [28]. However, in order to move towards an automatic on ground guidance, a failure rate of 10^{-9} per flight hour is targeted. The control of the torque is lost if the two power paths simultaneously either declutch to prevent failure propagation or loose torque control at any point of their architecture.

In order to assess the reliabilities of the critical components and system upper part, it is interesting to draw the relationship for an overall system failure rate for a loss of torque control of 10^{-9} per flight hour obtained following the methodology described in Section 5. Fig. 8 illustrates the relationship obtained in terms of maximum acceptable system upper-part failure rates versus critical component failure rates.

As shown, in case of ideal failure behavior (no failure) of the system part, the maximum acceptable failure rate for the loss of torque control of a safety critical component is about 10^{-4} per flight hour and per path. On the other hand, in case of ideal failure behavior (no failure) of the critical components, the parts upstream of the power electronics have a maximum acceptable general failure rate of about 10^{-4} per operating hour and per path. Note that reliability levels of 10^{-4} per operating hour are not design constraining.

5.5. Probability of reversionary mode

The reversionary mode characterizes the case of an active actuator failure, i.e. a power path has been disconnected to inhibit a failure occurring in one of its elements and the remaining healthy path has taken over the actuator functions. Being in reversionary mode dramatically reduces the reliability of the actuator with respect to the loss of torque control. Indeed, in this case, a general

failure of the system parts upstream of the power electronics or a loss of torque control of the critical components automatically leads to declutching of the remaining power path, i.e. it leads to a total loss of torque control.

Calculation shows that the target probability for switching to the reversionary mode can significantly constrain the reliabilities of the critical components and system upper part. Additionally, it shows that it is not possible to reach a failure rate lower than about 5×10^{-6} per flight hour for this event. Based on this revision of the reliability target, the maximum acceptable loss of torque control of the critical components and the maximum acceptable general failure rates becomes about 10^{-6} per flight hour and per path.

5.6. Conclusions of the reliability analysis

The reliability analysis permits a jamming failure rate of 2×10^{-9} per operating hour for the safety critical components independently of the actuator architecture. It supports the assessment of the maximum acceptable general and loss-of-torque failure rates for the critical components and system upper part. As a result, these failure rates are calculated as 10^{-6} per operating hour. Finally, the methodology presented has pointed out the excessive severity of the first reliability target for the occurrence of the reversionary mode and has provided a more realistic assessment with an order of magnitude of 5×10^{-6} per flight hour.

Based on these results, it is possible to take measures to reach the overall reliability target for the actuator. It should be noted that high reliability of a component can be ensured by adequate sizing (e.g., derating) and design (e.g., internal redundancy) for reliability, scheduled maintenance or monitoring [20,11].

In other words, the proposed methodology results provide a way of obtaining a consistent design for reliability from component to system level.

6. Architecture assessment

The evaluation of the candidate architectures identified for comparison (e.g., in terms of power, mass, integration) is outside the scope of the present article. However, this activity is a major part of the proposed overall methodology described in Section 2. More information about the achievements related to this activity is available in [30,2,5,1,13,21,31], where the authors propose a methodology and a software tool for the computer aided design of electromechanical actuators. Within the framework of preliminary design, the focus is on the selection and sizing of various components used in the actuator architectures. The design criteria addressed are the mass, environmental integration (installation) [2,5,1,13,21,31] and operational reliability [35] for given force and speed profiles. The library of components developed for the simulation takes advantage of the non-causal and object oriented characteristics of the Modelica language [14]. Thus, the library models can carry out an inverse simulation of the energy flows going from the mechanical load to the power source. Additionally, the number of parameters to be entered by the user is minimized by the use of scaling laws [4], which return all the parameters that are necessary for the simulation. To support the design process efficiently, the scaling laws developed are representative of the physical constraints driving the sizing of the different types of components considered [31]. The proposed methodology and software tool are illustrated with the sizing and comparison of actuator architectures for aircraft landing gear steering [30,5,1] and extraction/retraction systems [13], and flight control systems [5,21,31]. These examples also demonstrate how the library developed allows fast modeling, which is useful for an exploration of different design configurations and parameters. In this way, the capacity for taking technical

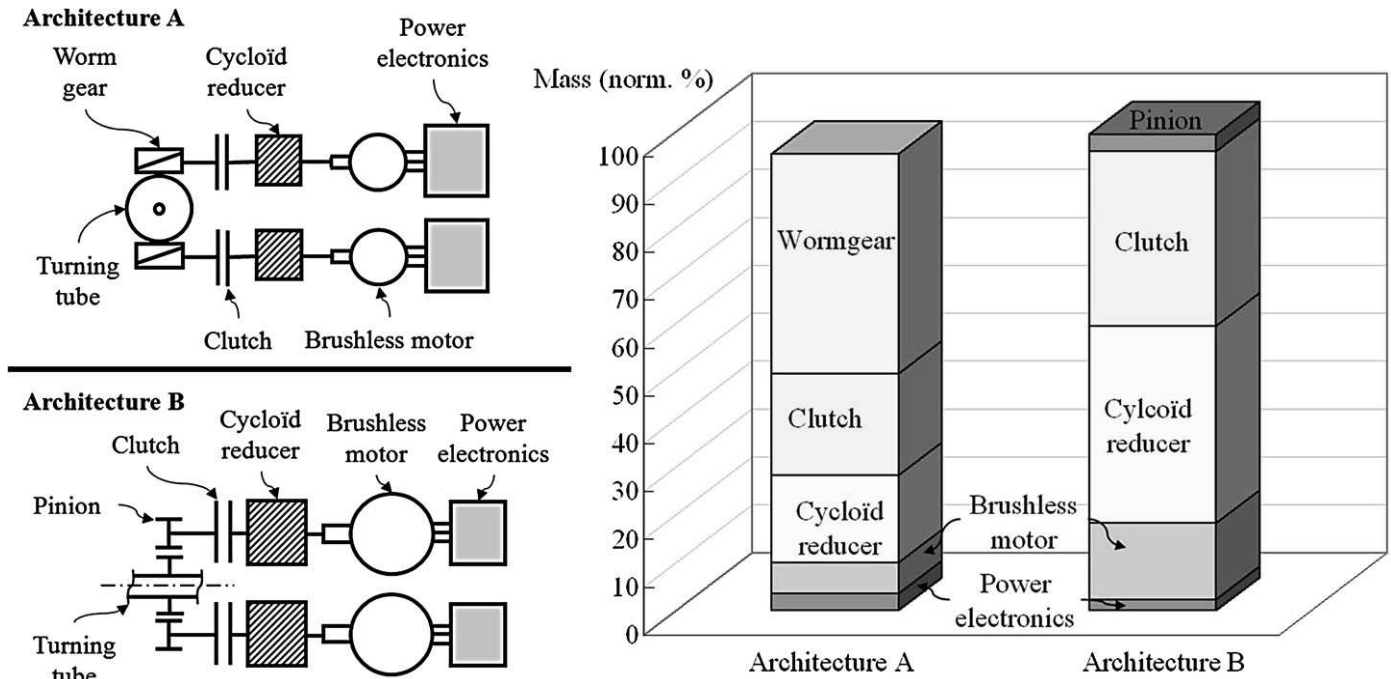


Fig. 9. Schematics (left) and mass comparison (right) of the candidate architectures.

decisions early in the preliminary design is improved by providing rich insight into the design in an efficient way.

Finally, within the overall methodology described in Section 2, the aforementioned evaluation approach provides additional iteration capacities, in particular with respect to the power, mass, environmental integration and reliability aspects.

7. Results

The comparison study of the candidate architectures identified in Section 4 is conducted on the basis of the approach introduced in the previous section.

The nose gear steering system operates for limited times compared with the other airborne systems. Thus its energy consumption does not have a significant impact on the overall aircraft performance. On the other hand, its weight can be significant and thus impact the overall aircraft performance. Therefore, the comparison study conducted focused on the mass criteria. The results are shown in Fig. 9, right.

During the study, it appeared that the mass consideration for the application in question (with rather low dynamics) favored architectures with a high overall transmission ratio. As a result, both candidate solutions reached nearly the same total mass (Fig. 9).

As for the mass information, the proposed evaluation approach provides the dimensions of the different architecture components. In this way, it is possible to proceed to an integration study, which leads to comparable total volumes (not detailed here) for both candidate architectures and underlies their integrability on the landing gear leg.

It should be noted that the mass analysis conducted does not include the actuator housing mass. And yet this part of the actuator appears as a key contributor to the total mass. This point should be therefore addressed in further work to enlarge the proposed methodology and the scope of the associated software tool.

In the framework of the DRESS project, the candidate architecture based on the worm-gear design has been selected for the detailed design. Among the different motivations for this choice is the interest for studying an original solution, while the other ar-

chitecture, based on a spur gear, was already being considered in an independent research project [7].

8. Conclusion

The methodology presented has opened up the discussion and the applied design approach, which were originally only driven by intuition and experience. The very demanding requirements, including severe operational aspects (e.g., free mode for towing, free mode in ultimate response to failure), did not allow an efficient application of a common intuitive methodology in the search for solutions. Instead, a more systematic methodology has been developed and applied. While covering a broad range of solutions, it generates and evaluates a reduced number of the most promising architectures that are compliant with the project requirements in general and the safety reliability requirements in particular.

Starting from a countless number of possible solutions, two most promising architectures were identified by paying a particular attention to the safety and reliability aspects. Moreover, besides interesting results, the preliminary evaluation activity provided a limited framework for the specific design of these solutions, significantly reducing the remaining development time and effort. Hence the proposed methodology has proved to be a significant step towards designing electromechanical actuators for safety and reliability.

In order to take advantage of this methodology, work is in hand to extend it to a more multidisciplinary design including thermal and hydraulic aspects. In this way, it will support efficient and fast trade-offs between different actuator technologies. Work is also in progress to implement optimization capability in order to address more design parameters and criteria [13]. For a more robust design, it is planned to study the uncertainty of the models used in the evaluation activity, along with the associated impact on the results. Finally, towards an even more integrated design approach, work for more continuity between the proposed methodology for preliminary design and the following detailed design phase is ongoing (e.g., in terms of CAD modeling [3]).

References

- [1] Marc Budinger, Jonathan Liscouët, Stéphane Orioux, Jean-Charles Maré, Automated preliminary sizing of electromechanical actuator architectures, in: ELECTRIMACS 2008 Conference, Québec, 2008.
- [2] Marc Budinger, Jonathan Liscouët, Y. Cong, Jean-Charles Maré, Simulation based design of electromechanical actuators with Modelica, in: ASME IDETC/CIEC, San Diego, 2009.
- [3] Marc Budinger, Amine Fraj, Toufic Antoine El-Halabi, Jean-Charles Maré, Coupling CAD and system simulation framework for the preliminary design of electromechanical actuators, in: IDMME Virtual Concept, Bordeaux, 2010.
- [4] Marc Budinger, Jonathan Liscouët, Fabien Hospital, Jean-Charles Maré, Estimation models for the preliminary design of electro-mechanical actuators, Proceedings of the IMechE, Part G: Journal of Aerospace Engineering, doi: 10.1177/0954410011408941, in press.
- [5] Marc Budinger, et al., Preliminary design of electromechanical actuators with Modelica, in: The 7th Modelica Conference, Como, 2009, pp. 168–177.
- [6] A. Chakrabarti, M.X. Tang, Generating conceptual solutions on FuncSION: Evolution of a functional synthesizer, in: The 4th AID International Conference on Artificial Intelligence in Design, Stanford, 1996, pp. 603–622.
- [7] Pierre-Yves Chevalier, Sébastien Grac, Pierre-Yves Liégeois, More electrical landing gear actuation system, in: R3ASC'10 Recent Advances in Aerospace Actuation Systems and Components Conference 2010, Toulouse, 2010, pp. 9–16.
- [8] J. Cros, P. Viarouge, Synthesis of high performance PM motors with concentrated windings, IEEE Transactions on Energy Conversion 17 (2) (2002) 248–303.
- [9] N. Cross, Engineering Design Methods: Strategies for Product Design, 4th ed., John Wiley & Sons, Chichester, 2008.
- [10] Norman S. Currey, Aircraft Landing Gear Design: Principles and Practices, American Institute of Aeronautics and Astronautics (AIAA), Washington, DC, USA, 1988.
- [11] B.S. Dhillon, Mechanical Reliability: Theory, Models and Applications, AIAA Education Series, Washington, 1988.
- [12] D. Dreiholz, Classification schemes for the search of solutions, Konstruktion 27 (1975) 233–240 (in German).
- [13] Toufic El-Halabi, Marc Budinger, Jean-Charles Maré, Optimal geometrical integration of electromechanical actuators, in: R3ASC'10 Recent Advances in Aerospace Actuation Systems and Components 2010, Toulouse, 2010.
- [14] Hilding Elmqvist, Sven Erik Mattsson, Martin Otter, Modelica: The new object-oriented modeling language, in: The 12th ESM European Simulation Multiconference, Manchester, 1998, pp. 127–131.
- [15] Terry Ford, More-electric aircraft, Conference reports, 2005.
- [16] J.E. Fowler, Variant design for mechanical artifacts: A state-of-the-art survey, Engineering with Computers 12 (1) (1996) 1–15.
- [17] M.J. French, Conceptual Design for Engineers, 3rd ed., Springer-Verlag, London, 1999.
- [18] D. Frey, J. Palladino, J. Sullivan, M. Atherton, Part count and design of robust systems, Systems Engineering 10 (2007) 203–221.
- [19] Gerd Fricke, Successful individual approaches in engineering design, Research in Engineering Design 8 (3) (1996) 151–165.
- [20] Herbert Hecht, System Reliability & Failure Prevention, Artech House, Boston, 2004.
- [21] Fabien Hospital, Marc Budinger, Jonathan Liscouët, Jean-Charles Maré, Model based methodologies for the assessment of more electric flight control actuators, in: The 13th AIAA/ATIO Aviation Technology, Integration and Operation Conference, Fort Worth, 2010.
- [22] Vladimir Hubka, Wolfgang Ernst Eder, Design Science: Introduction to Needs, Scope and Organization of Engineering Design Knowledge, Springer, 1996.
- [23] T.-H. Huynh, Gaetan Pouly, Jean-Philippe Lauffenburger, Michel Basset, Active shimmy damping using direct adaptive fuzzy control, in: IFAC World Congress Korea, 2008.
- [24] Georges Iordanidis, Stéphane Dellac, DRESS: Distributed and redundant electromechanical nose wheel steering system, in: SAE AeroTech Congress and Exhibition, Seattle, 2009.
- [25] Georges Iordanidis, et al., An overview of modelling and simulation activities for an all-electric nose wheel electric system, in: R3ASC'10 Recent Advances in Aerospace Actuation Systems and Components 2010, Toulouse, 2010, pp. 137–144.
- [26] G. Issa, S. Shen, M.S. Chew, Using analogical reasoning for mechanism design, IEEE Expert 9 (3) (1994) 60–69.
- [27] S. Ivanov, F. Labrique, P. Sente, Control under normal and fault operation of a PM synchronous motor with physically and magnetically decoupled phases, Electrical Engineering 1 (2009).
- [28] Joint Aviation Authorities (JAA), Joint Aviation Requirements, Part 25, Large Aeroplanes, 1989.
- [29] Jonathan Liscouët, Preliminary design of electromechanical actuators: A hybrid, direct/inverse approach, Doctoral degree, Université de Toulouse, Toulouse, 2010 (in French).
- [30] Jonathan Liscouët, Marc Budinger, Jean-Charles Maré, Design for reliability of electromechanical actuators, in: R3ASC'10 Recent Advances in Aerospace Actuation Systems and Components 2010, Toulouse, 2010, pp. 174–182.
- [31] Jonathan Liscouët, Marc Budinger, Jean-Charles Maré, Stéphane Orioux, Modelling approach for the simulation-based preliminary design of power transmissions, Mechanism and Machine Theory 46 (3) (2011) 276–289.
- [32] Y.-C. Liu, A. Chakrabarti, T. Blich, Towards an 'ideal' approach for concept generation, Design Studies 24 (4) (2003) 341–355.
- [33] Y.-C. Liu, A. Chakrabarti, S.J. Lu, Design heuristics for pruning the number of mechanism solutions in computer-based conceptual design, in: The 2nd ICCAE International Conference on Computer and Automation Engineering, vol. 3, Singapore, 2010, p. 235.
- [34] Damien Motte, Robert Björnemo, Bernard Yannou, On the interaction between the engineering design and the development process models – Part I: Elaborations on the generally accepted process models, in: Research into Design – Supporting Sustainable Product Development, 2011, pp. 87–95.
- [35] G. Pahl, W. Beitz, J. Feldhusen, K.H. Grote, Engineering Design: A Systematic Approach, 3rd ed., Springer, London, 2007.
- [36] Gaetan Pouly, T.-H. Huynh, Jean-Philippe Lauffenburger, Michel Basset, Indirect fuzzy adaptive control for active shimmy damping, in: IFAC World Congress Korea, 2008.
- [37] Gaetan Pouly, Jean-Philippe Lauffenburger, Michel Basset, Reduced order H^∞ control design of a nose landing gear steering system, in: R3ASC'10 Recent Advances in Aerospace Actuation Systems and Components Conference 2010, Toulouse, 2010, pp. 97–104.
- [38] Stuart Pugh, Total Design: Integrated Methods for Successful Product Engineering, Pearson Addison-Wesley, Harlow, 1991.
- [39] Reliability Information Analysis Center (RIAC), RIAC Automated Databook, 2006.
- [40] Wolf Georg Rodenacker, Methodical Design, 4th ed., Springer, Berlin, 1991 (in German).
- [41] N.F.M. Roozenburg, J. Eekels, Product Design: Fundamentals and Methods, John Wiley & Sons, Chichester, 1995.
- [42] K. Roth, Designing with Design Catalogues, vols. I–III, 3rd ed., Springer, Berlin, 1996–2000 (in German).
- [43] SAE Committee S-18, ARP 4761: Guidelines and Methods for Conducting the Safety Assessment Process on Civil Airborne System and Equipment, 1996.
- [44] SAE Systems Integration Requirements Task Group AS-1C, ARP 4754: Certification Considerations for Highly-Integrated or Complex Aircraft Systems, 1996.
- [45] Technical Board International Council on Systems Engineering (INCOSSE), Systems Engineering Handbook, 2004.
- [46] T. Tomiyama, V. D'Amelio, J. Urbanic, W. ElMaraghy, Complexity of multidisciplinary design, Annals of the CIRP 56 (1) (2007) 185–188.
- [47] David G. Ullman, The Mechanical Design Process, McGraw-Hill Higher Education, New York, 2003.
- [48] Karl T. Ulrich, Steven D. Eppinger, Product Design and Development, 4th ed., McGraw-Hill, New York, 2008.
- [49] Y. Umeda, T. Tomiyama, Functional reasoning in design, IEEE Expert 12 (2) (1997).
- [50] Verein Deutscher Ingenieure (VDI), VDI 2206: Design methodology for mechatronic system, 2004.
- [51] Fritz Zwicky, Discovering, Inventing, Researching in the Morphological World, Droemer, Knauer, Munich, 1966–1971 (in German).

Chapter 4 – Metamodels for model-based-design of mechatronic systems

ABSTRACT

This chapter illustrates how metamodeling techniques can be applied to models used in preliminary design of mechatronic systems. After a review of the state of the art in the different families of metamodels, standard regression techniques are applied to obtain estimation models from catalogue data and to represent transient simulations. Emphasis is placed on the possibility of using dimensional analysis and transformations to extend the scope of these expressions and these methods. The publication that follows this chapter, entitled "Scaling-law-based metamodels for the sizing of mechatronic systems" and published in the journal Mechatronics, illustrates how these approaches can be adapted to the generalization and synthesis of scaling laws from finite element simulations.

Keywords: metamodel, surrogate model, response surface, dimensional analysis, transformation, Design of Experiments.

TABLE OF CONTENTS

1.	Introduction	91
1.1.	Generalities about metamodels.....	91
1.2.	Metamodels and model based design of electromechanical actuators	92
2.	State of the art	92
2.1.	Graphical syntheses and classifications of methods.....	92
2.2.	Response surface families	95
2.3.	DoE and validation	98
2.4.	Transformations.....	101
3.	Estimation models from statistical data	102
3.1.	Example of gear boxes.....	103
3.2.	Example of heat sink	105
4.	Metamodeling of simulation and evaluation models	108
4.1.	Transient thermal response of a brushless motor.....	108
4.2.	RMS current into the DC-link capacitor of an inverter.....	110
4.3.	Effect of stiffness an inertia on closed loop stability.....	111
5.	Conclusion.....	114
6.	Bibliography.....	115

NOTATION

Acronyms

DAE	Differential-Algebraic Equations	PWM	Pulse Width Modulation
DACE	Design and Analysis of Computer Experiments	RBF	Radial Based Function
DC	Direct Current	RSM	Response Surface Model
DoE	Design of Experiments	RMS	Root Mean Square
EMA	Electro-Mechanical Actuator	R ²	Normal regression parameter
LHC	Latin Hyper Cube	SSE	Sum of Squared Error
LVDT	Linear Variable Differential Transformer	SSTOT	Total Sum of Squares
MSE	Mean Squared Error	TVC	Thrust Vector Control
ODE	Ordinary Differential Equations		

Nomenclature

x	Input parameters	θ	Vector of parameters or temperature rise
y	Output response	ε	Error
R_{th}	Thermal resistance	λ	Box-Cox transformation coefficient or Lagrange multiplier coefficient
C_{th}	Thermal capacitance		
W, H, L	Geometrical dimensions		
U	Voltage		
I	Current		
m	Modulation index		
$\cos(\varphi)$	Power factor		
f	Frequency		

1. INTRODUCTION

1.1. Generalities about metamodels

A metamodel [1] is a simplified or approximate descriptive model of another model. Metamodel are also called surrogate model [2] or response surface approximations [3]. This approach is also known as behavioural modelling or black-box modelling. When only a single design variable is involved, the process is known as curve fitting.

A surrogate model is an engineering method used when an outcome of interest cannot be easily calculated with a cheap explicit mathematical relationship. Different cases may be encountered:

- The knowledge is in the form as statistical database and no mathematical models are available;
- The design problem requires physical experiments;
- The design model is solved through a costly numerical simulation which can take many minutes or hours to complete;
- The design model is light but implicit and needs to be inverted to access the quantity of interest.

The surrogate model can be used during design and optimization tasks to evaluate design objective and constraint functions as functions of design variables. An important distinction can be made between two different applications of surrogate models:

- Design optimization: the aim is to find the optimal parameter vector. Optimization process and metamodel building are linked in order to update the experiment/simulation at a new promising location found by a search;
- Design space approximation: the aim is to represent the global behaviour of the system. Optimization can still occur as a post processing step but with no update procedure.

Here, we focus on the second case which can be approached in two ways [4]:

- One level: the first approach generates one metamodel for the target answer expressed directly with the parameters of the models. In the case of an electromechanical system, this can result in a metamodel that expresses the global mass of the actuator as a function of design parameters;
- Multi-levels: The second approach builds several simple metamodels and assembles them to form the objective function. In the case of an electromechanical system, several explicit weight estimation metamodels of components can be summed to obtain the total weight.

Figure 1 shows the difference between the first approach and the second approach. The second multi-level approach, which leads to simple (and reusable) approximations representing complex responses, will be privileged here.

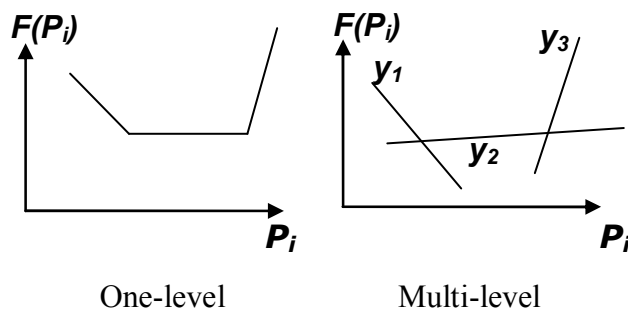


Figure 1 – Building one- and multi-level metamodels

The section 2 will present the state of the art for these methods by focusing on a phenomenological description.

1.2. Metamodels and model based design of electromechanical actuators

In the preliminary steps of system design, different types of models are needed in order to obtain complete sizing for an actuation system: Figure 2a) of Chapter 3 illustrates the component model structure composed of simulation, estimation and evaluation models.

The **estimation models** (Chapter 1) take a reduced set of independent parameters (e.g. max load, stroke) and estimate all the dependent parameters/component characteristics: simulations (e.g. inertia, efficiency), integration (e.g. mass, dimensions) and validation of safe operating area (e.g. max speed, degradation parameters).

The objective of **simulation models** (Chapter 2) is to calculate all the variables of power, energy (force, speed, temperature, etc.) useful for the selection of components. The transient simulation of an EMA is becoming mandatory because, unlike in hydraulic actuators, some strong coupling exists between the transient power demand, the thermal behaviour of motors, the inertial loads and the fatigue of mechanical components.

The last model is the **evaluation model** (Chapter 3), intended to check the ability of a component to operate in its safe operating area for the required lifetime and reliability.

Metamodels can be used to represent or construct these models:

- For **estimation models**: scaling laws are an easy way to develop estimation models [5] but, when these laws are not suitable, metamodels can be used. Characteristics of components from datasheets can thus be fitted to speed up the design exploration (analysis of different scenarios, optimization). Section 3 will illustrate this point with examples of reducers and heatsinks. The characteristics of the components can also be obtained from finite element simulations or dedicated design codes. However, these simulations are time consuming or can be implicit and require iterations of solvers. They do not lend themselves to the preliminary design of EMA. Paper 4 shows how a new form of scaling-laws-based metamodels can be used in order to express their results in a very compact way;
- For **simulation and evaluation models**: the goal is to replace long transient simulations (in the case of a procedure optimization) by algebraic expressions. Section 4 illustrates the building of metamodels with thermal, electrical or control-loop simulations.

2. STATE OF THE ART

2.1. Graphical syntheses and classifications of methods

Metamodels are relatively simple mathematical relationships between input parameters and output response:

$$y = f(\underline{x}, \underline{\theta}) \quad (1)$$

where:

- x is a vector of x_i input parameters or variables which can be design parameters (useful for the optimization problem) and environmental parameters (with probability distribution, for reliability/uncertainty study);
- y is the output response;
- θ is a vector of parameters associated with the family of functions to construct the surface.

The building of these functions is often based on limited data coming from physical experiments or numerical simulations. The planning for experimentation is called Design of Experiments (DoE). Figure 2 illustrates the difficulties encountered in the development of such models:

- The input parameters or output variable may present uncertainties. In the case of physical experiments the error distribution is often modelled by a normal distribution of zero mean and uniform variance;
- The model chosen to perform the modelling does not match the phenomenon. The error introduced has a non-uniform distribution.

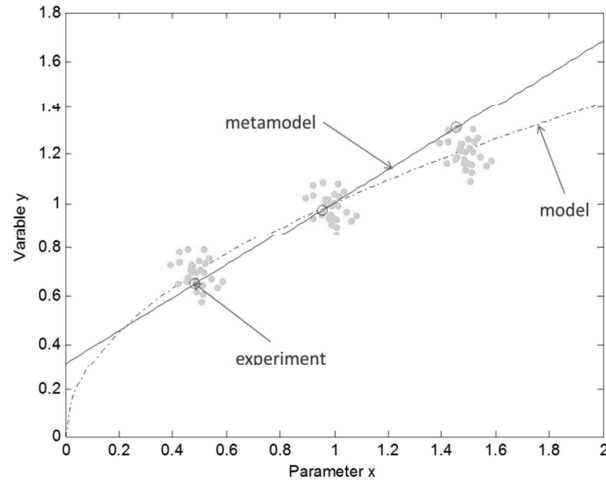


Figure 2 – Error sources

In the case of physical experiments, the main source of error derives from the uncertainty on y . Assuming that errors on x are zero and that the model chosen to represent the phenomenon is correct, Figure 3 illustrates that the choice of experiments greatly influences the quality of the metamodel. In design and analysis of physical experiments, random variation is accounted for by spreading the sample points out in the design space and by taking multiple data points (replicates).

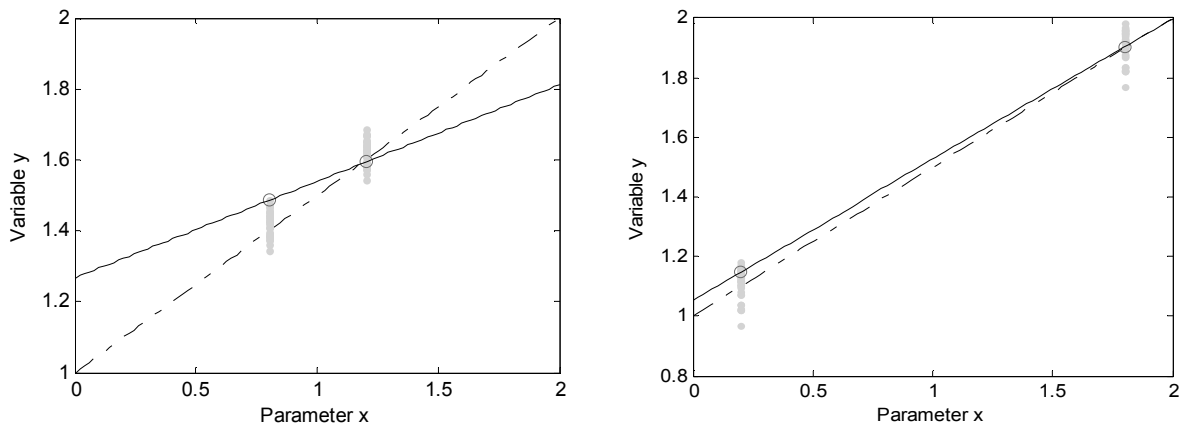


Figure 3 – Measurement errors

In the case of computer experiments, the simulations are deterministic and the main source of error is the model chosen to represent the phenomenon. Sample points should be chosen to fill the design space in order to better assess the distribution of the error and refine the choice of model as illustrated Figure 4.

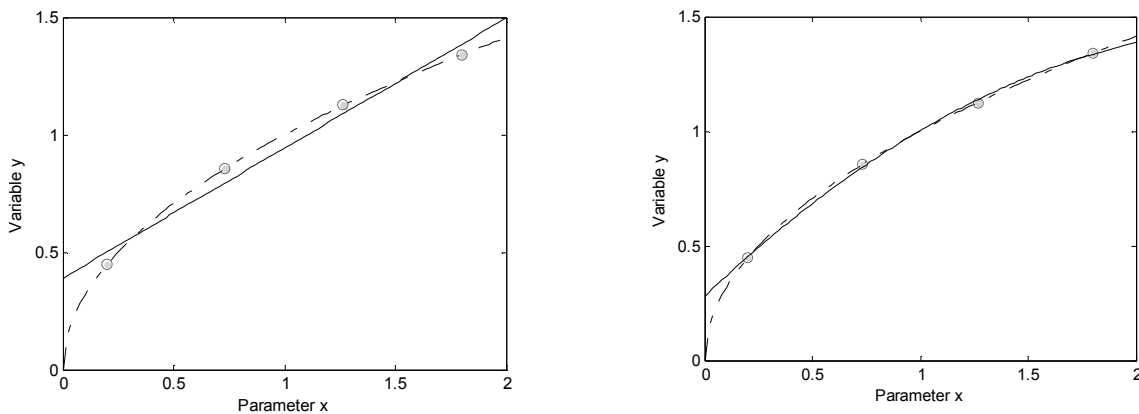


Figure 4 – Model errors

These graphics (Figure 3 and Figure 4) highlight the importance of the DoE definitions and how the form of the model form is selected. Simpson at al. [1] add another criterion to the two just mentioned so as to classify the different approximation techniques. This last criterion is the type of algorithm used to choose the vector θ of equation (1). Figure 5 shows different metamodeling approaches and classifies them according to these three criteria.

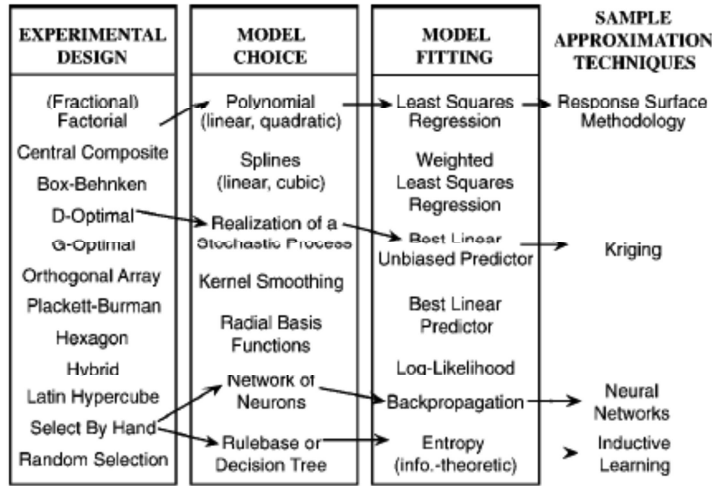


Figure 5 – Classification of Approximation techniques (Source : [1])

A metamodel is obtained through several stages [1] as shown in Figure 6:

1. Implementation of the detailed design model on which DoE will be performed;
2. Selection of design parameters and response variables;
3. Reduction of design parameter numbers if necessary: dimensional analysis [6] and/or screening techniques [3] can be used for this step;
4. Generation of a DoE suited to a complete regression;
5. Choice of the form of the regression function and selection of transformations to apply to data;
6. Construction of the metamodel [3] [2];
7. Check on the quality of the regression;
8. Implementation and use of the metamodel.

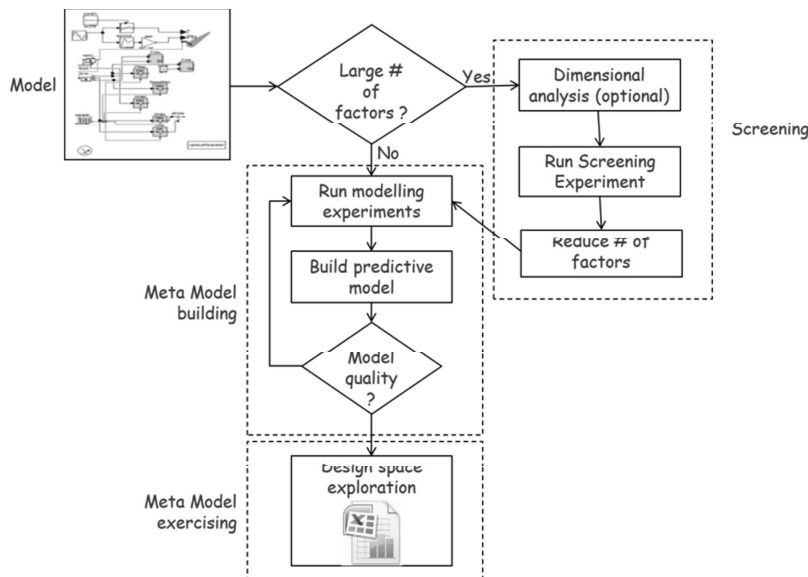


Figure 6 – Metamodelling process

As mentioned previously, we can differentiate between (i) traditional Design of Experiments (DoE) and response surface (RS) modelling where errors come mainly from variability of experiments (Modeling for physical experiments) and (ii) Design and Analysis of Computer Experiments (DACE) where errors come mainly from the choice of model. As illustrated in Figure 7, the DoE, fitting algorithm and validation are not the same.

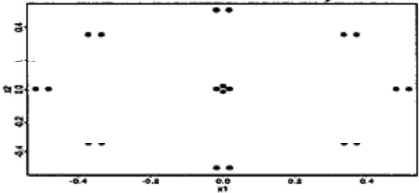
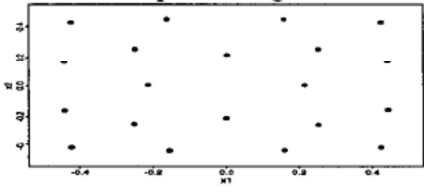
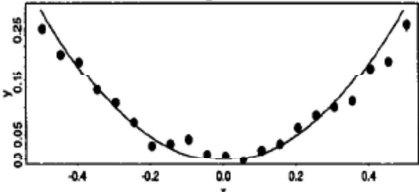
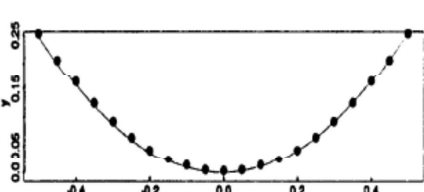
	DOE/RS Modeling for Physical Experiments	DACE/Kriging Models for Computer Experiments
Experimental Design Input settings at which to obtain output	Account for Variability 	Space Filling 
Models Inexpensive model to estimate output at untried input	Least Squares Fit 	Maximum Likelihood Estimate 
Validation Determine fit accuracy	t-tests, F-statistics R2, R2adj; Residual plots (see, e.g., Ref. 33)	Cross-validation Mean Squared Error (see, e.g., Ref. 25)

Figure 7 – Models for physical experiments vs computer experiments (Source: [7])

2.2. Response surface families

There are a number of families of models that approximate a response surface. A primary criterion of choice relates to the flexibility or the ability to follow a surface with peaks and valleys. We illustrate the different families using an example of a damped sine function of one parameter, x , here:

$$f(x) = e^{-\frac{x^2}{10}} \sin(x) \tag{2}$$

The observation range of the parameter x enables a curve with a more or less regular behaviour to be obtained as shown in Figure 8.

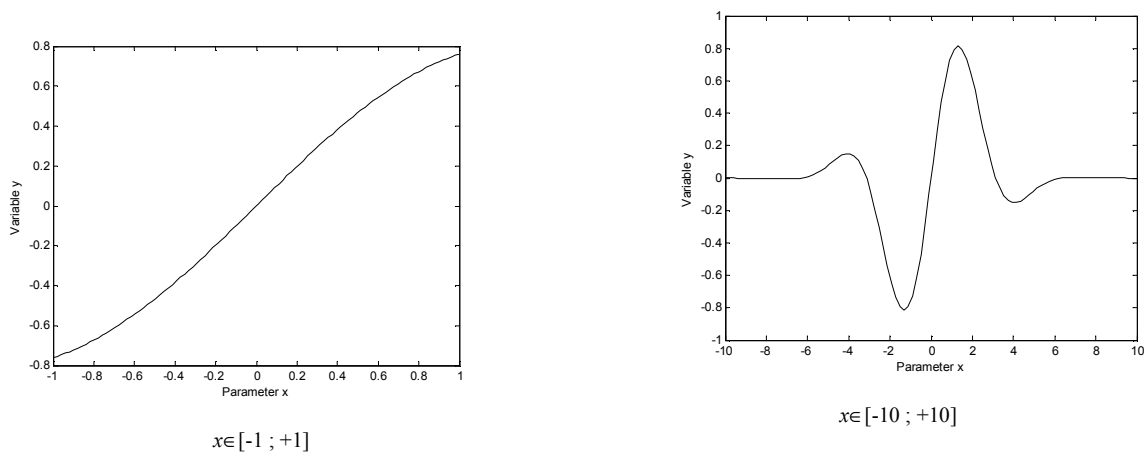


Figure 8 – Function to be approximated

The response surfaces generally have few discontinuities. This property means that approximations can be obtained in different ways.

Non-parametric regressions weigh the simulation results to obtain a smooth surface. They include: K-nearest-neighbour, which averages the values of the K responses at the experimental points closest to x ; Kernel regression, which averages neighboring values with a weighted average expressed by a kernel function. Non-parametric regression requires larger sample sizes than regression based on parametric models.

Parametric regressions are based on models requiring the estimation of a finite number of parameters that express the effects of basis functions on the response surface. With **polynomial interpolation or regression** [3], the basis functions are $\{1, x, x^2, \dots, x^p\}$. The idea is to obtain a surface that is differentiable and continuous. For a polynomial development of order 2 ($p = 2$), the expression is:

$$y = f(\underline{x}, \underline{\theta}) = \theta_0 + \sum_{i=1}^k \theta_i x_i + \sum_{i=1}^k \sum_{j=1}^k \theta_{ij} x_i x_j \quad \text{with } \underline{x} = \begin{pmatrix} x_1 \\ \dots \\ x_{k_x} \end{pmatrix} \quad (3)$$

which, for the n experiments, can be written with a matrix representation:

$$\underline{Y} = \underline{X} \cdot \underline{\theta} + \underline{\varepsilon}$$

with $\underline{Y} = \begin{pmatrix} y^{(1)} \\ \dots \\ y^{(n)} \end{pmatrix}_{n \times 1}$, $\underline{X} = \begin{pmatrix} 1 & x_1^{(1)} & \dots & x_{k_x}^{2(1)} \\ \dots & \dots & \dots & \dots \\ 1 & x_1^{(n)} & \dots & x_{k_x}^{2(n)} \end{pmatrix}_{n \times k_\theta}$, $\underline{\theta} = \begin{pmatrix} \theta_0 \\ \dots \\ \theta_{k_\theta} \end{pmatrix}_{k_\theta \times 1}$, $\underline{\varepsilon} = \begin{pmatrix} \varepsilon^{(1)} \\ \dots \\ \varepsilon^{(n)} \end{pmatrix}_{n \times 1}$ (4)

where :

- k_x is the number of design parameters;
- n is the number of experiments of the DoE;
- p is the order of the polynomial function;
- k_θ is the size of vector θ .

If $n=k_\theta$, the matrix X is square and the interpolation is possible:

$$\underline{\theta} = \underline{X}^{-1} \underline{Y} \quad (5)$$

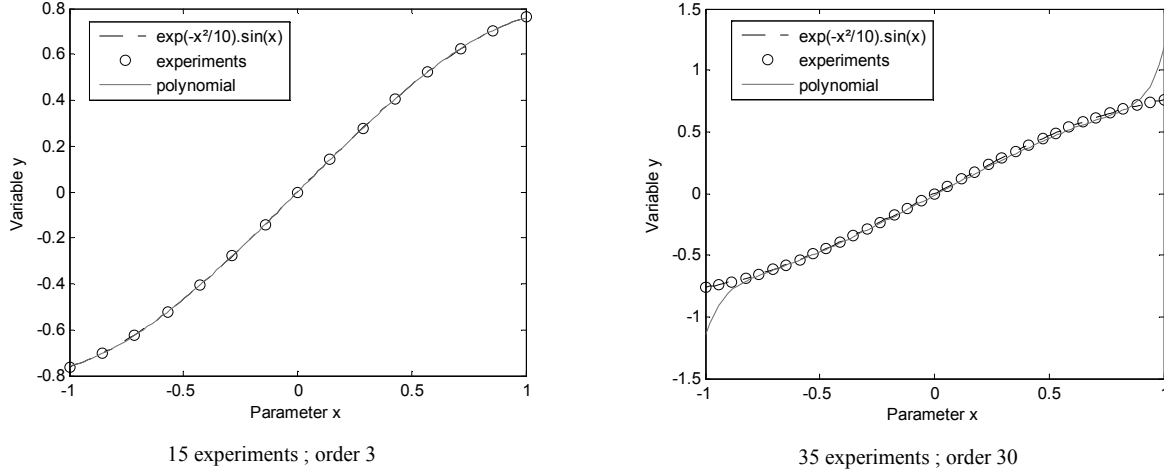
In the most common case, where k_θ is lower than n , interpolation is impossible. The objective of regression is to find an approximation showing an error of zero mean and a minimum standard deviation. The errors are expressed by:

$$\underline{\varepsilon} = \underline{Y} - \underline{X} \cdot \underline{\theta} \quad (6)$$

The standard deviation is a function of the sum of the quadratic error $\underline{\varepsilon}' \underline{\varepsilon}$ and is minimum for:

$$\underline{\theta} = (\underline{X}' \underline{X})^{-1} \underline{X}' \underline{Y} \quad (7)$$

As illustrated by Figure 9, a polynomial of order 3 approximate the range $x \in [-1 ; +1]$ well. Larger values of Taylor expansion terms will usually yield a more accurate approximation. However, the greater the number of terms, the more flexible the model becomes. The response may be corrupted as illustrated Figure 9 with a polynomial of order 30. To enable interpolation without the use of a high-order polynomial, Multivariate Adaptive Regression Splines [8] use linear or cubic spline functions with a partitioning of the data into disjoint regions, each of which can be treated independently.


Figure 9 – Polynomial approximation

Other metamodel families assume that samples taken close together are likely to have highly correlated response values, whereas samples taken far apart are not. **Radial basis functions**, which are radially-symmetric functions, and **Kriging methods** [9] [10] are thus underpinned by the idea that the sample response values exhibit spatial correlation. RBF and Kriging methods have been found useful for modelling general surfaces that have many peaks and valleys and when exact interpolation of samples is desired. A common choice for the basis functions of RBF are the Gaussian functions:

$$y = f(\underline{x}, \underline{\theta}) = \mu + \sum_{i=1}^n \theta_i e^{-\|\underline{x} - \underline{x}^{(i)}\|^2 / \sigma^2} = \mu + \sum_{i=1}^n \theta_i \prod_{j=1}^{k_x} e^{-|x_j - x_j^{(i)}|^2 / \sigma_j^2} \quad (8)$$

Kriging functions have a similar form:

$$y = f(x, \theta) = \mu + \sum_{i=1}^n \theta_i \prod_{j=1}^{k_x} e^{-|x_j - x_j^{(i)}|^{p_j} / \sigma_j^2} \quad (9)$$

with:

- μ the mean value of experiments; this mean value is a common choice but can be replaced by a polynomial approximation;
- p_j a smoothness parameter which is between 1 and 2 for kriging and frozen at 2 for RBF;
- σ_j is a parameter called correlation parameter or kernel width/radius.

Kriging has more parameters (p_j and σ_j) and is therefore more flexible but more complex to implement.

The interpolation process with these functions is:

- Calculate the expected mean value of the output variable

$$\underline{\mu} = \text{mean}(\underline{Y}) \quad (10)$$

- Evaluate the correlation matrix \underline{R} and the function parameters $\underline{\theta}$

$$\underline{Y} = \underline{I}\underline{\mu} + \underline{R}\underline{\theta}$$

$$\text{with } \underline{R} = \begin{pmatrix} r_{1,1} & \dots & r_{1,n} \\ \dots & \dots & \dots \\ r_{n,1} & \dots & r_{n,n} \end{pmatrix}_{n \times n} \quad \text{where } r_{i,j} = \prod_{k=1..k_x} e^{-|x_k^{(i)} - x_k^{(j)}|^2 / \sigma^2} \quad (11)$$

$$\text{and } \underline{\theta} = \underline{R}^{-1}(\underline{Y} - \underline{I}\underline{\mu})$$

- Predict the response values at the selected point x^*

$$y(\underline{x}^*) = \underline{\mu} + \underline{r}\underline{\theta} \text{ with } \underline{r} = \begin{pmatrix} r_1 \\ \dots \\ r_n \end{pmatrix}_{n \times 1} \text{ where } r_i = \prod_{k=1..k_x} e^{-|x_k^* - x_k^{(i)}|^2 / \sigma^2} \quad (12)$$

Figure 10 compares a polynomial and an RBF function: they are comparable for a smooth surface, but the RBF function shows more flexibility in following complex surfaces.

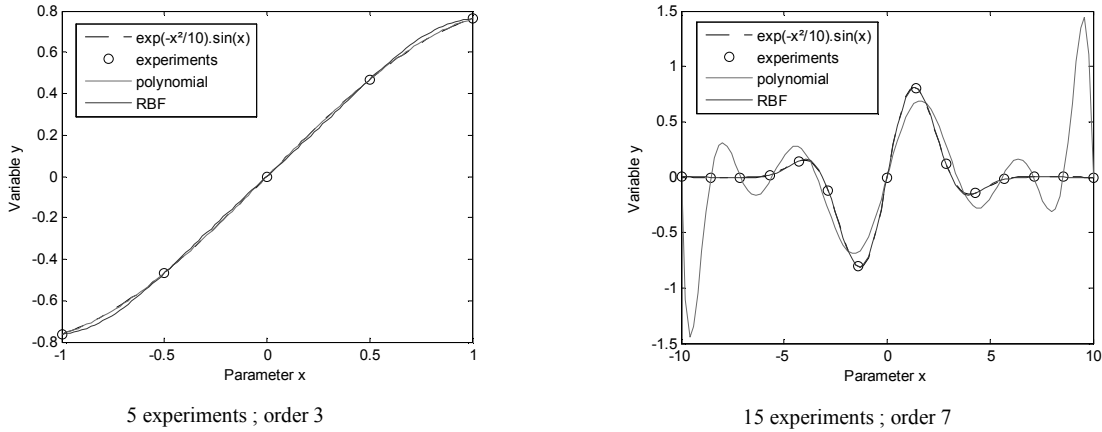


Figure 10 – RBF and polynomial comparison

The prediction quality of RBF or kriging functions depends greatly on the estimation of parameters p_j and σ_j . Figure 11 illustrates the effect of parameter σ for RBF functions. This radius sets the scale at which the basis function is significantly non-zero and corresponds to a size of the spheres of influence of the points with known function values. The unknown parameters p_j and σ_j are generally chosen to maximize a likelihood function. Much research effort has been directed at devising suitable training strategies. Another key benefit from the estimation of these parameters is that it provides an estimated error of predictions [2].

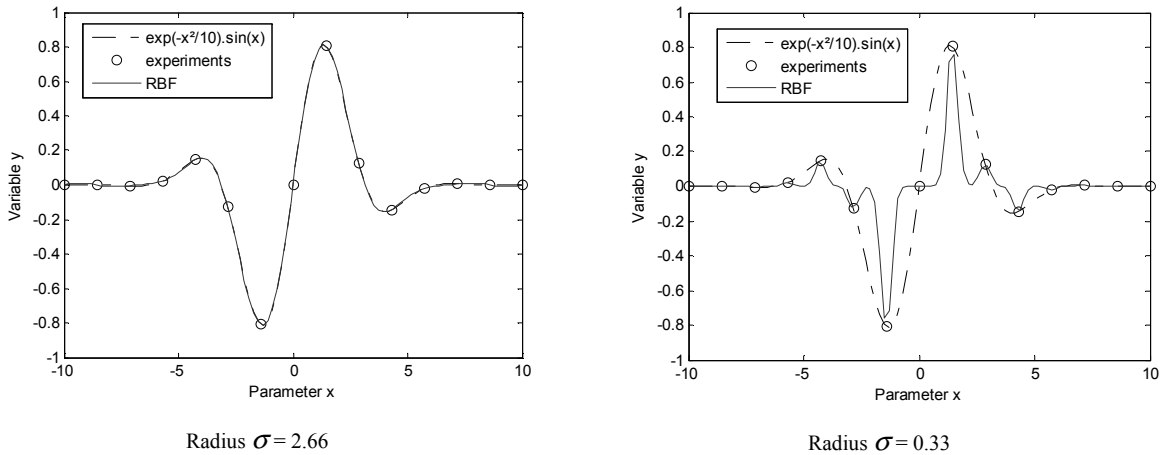


Figure 11 – Effect of radius parameter

2.3. DoE and validation

The quality of a metamodel depends not only on the model chosen but also on the DoE. Design parameters x_i are characterized by areas of variation that may be of different magnitudes. DoE techniques normalize these domains between -1 and 1 (or between 0 and 1) for all parameters. This normalization facilitates the comparison of the effects of various design parameters and the planning of the DoE. Figure 12 shows the different DoE graphically in the case of 2 or 3 design parameters. The choice of the DoE

depends on the objective (screening, building a response surface) and the choice of the model (quadratic, RBF, kriging). A more detailed description of DoE can be found in [2] [3].

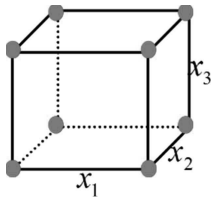
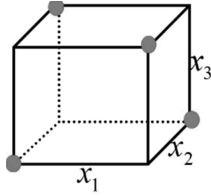
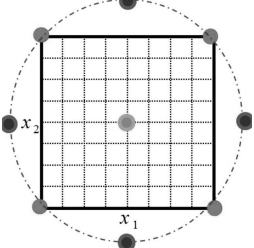
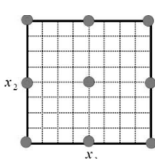
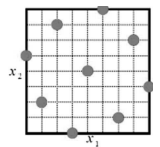
$y = b_0 + \sum b_i X_i + \sum b_{ij} X_i X_j + \sum b_{ii} X_i^2 + \dots + \varepsilon$ <div style="display: flex; justify-content: space-around; margin-top: 10px;"> <div style="text-align: center;">↑ Mean value</div> <div style="text-align: center;">↑ Main effect</div> <div style="text-align: center;">↑ Interaction</div> <div style="text-align: center;">↑ Higher orders</div> <div style="text-align: center;">↑ Error</div> </div>						
DoE name	Graphical representation	Numerical representation				
<p>2 level Full Factorial Design</p> <p><i>For screening step: suitable for main and interaction effects.</i></p> <p>All levels are present an equal number of times. Require 2^k experiments where k is the number of parameters.</p>		$\begin{bmatrix} x_1 & x_2 & x_3 \\ -1 & -1 & -1 \\ -1 & -1 & +1 \\ -1 & +1 & -1 \\ -1 & +1 & +1 \\ +1 & -1 & -1 \\ +1 & -1 & +1 \\ +1 & +1 & -1 \\ +1 & +1 & +1 \end{bmatrix}$				
<p>Fractional Factorial Design</p> <p><i>For screening step: suitable for main and interaction effects.</i></p> <p>Not all combinations of levels are experimented because they are not required for the estimation of coefficients. Useful for studies with a large number of parameters.</p>		$\begin{bmatrix} x_1 & x_2 & x_3 \\ -1 & -1 & +1 \\ -1 & 1 & -1 \\ -1 & -1 & -1 \\ -1 & 1 & 1 \end{bmatrix}$				
<p>Central Composite Design</p> <p><i>For building step: well suited to quadratic models.</i></p> <p>Experiments are added to model quadratic terms. The new samples are placed in the middle to assess the curvature of the surface and at the periphery to reduce the effects of uncertainties.</p>		$\begin{bmatrix} x_1 & x_2 \\ -1 & -1 \\ -1 & +1 \\ +1 & -1 \\ +1 & +1 \\ -1,41 & 0 \\ +1,41 & 0 \\ 0 & -1,41 \\ 0 & +1,41 \\ 0 & 0 \end{bmatrix}$				
<p>Full factorial (X levels) and Latin Hyper Cube</p> <p><i>For building step: suitable for model of order higher than 2 or for RBF and kriging functions.</i></p> <p>Samples are placed to fill the design space uniformly. LHC DoE allows a large number of levels to be evaluated for each parameter while minimizing the number of experiments.</p>	<p>Full factorial (3 levels)</p>  <p>Latin HyperCube</p> 	<table border="0"> <tr> <td>Full Factorial</td> <td>Latin HyperCube</td> </tr> <tr> <td> $\begin{bmatrix} x_1 & x_2 \\ -1 & -1 \\ -1 & 0 \\ -1 & +1 \\ 0 & -1 \\ 0 & 0 \\ 0 & +1 \\ +1 & -1 \\ +1 & 0 \\ +1 & +1 \end{bmatrix}$ </td> <td> $\begin{bmatrix} x_1 & x_2 \\ +0.40 & -0.33 \\ -0.03 & +0.74 \\ +0.16 & +0.21 \\ +0.87 & +0.97 \\ -0.37 & -0.06 \\ +0.57 & -0.89 \\ -0.72 & +0.45 \\ -0.85 & -0.40 \\ -0.15 & +0.66 \end{bmatrix}$ </td> </tr> </table>	Full Factorial	Latin HyperCube	$\begin{bmatrix} x_1 & x_2 \\ -1 & -1 \\ -1 & 0 \\ -1 & +1 \\ 0 & -1 \\ 0 & 0 \\ 0 & +1 \\ +1 & -1 \\ +1 & 0 \\ +1 & +1 \end{bmatrix}$	$\begin{bmatrix} x_1 & x_2 \\ +0.40 & -0.33 \\ -0.03 & +0.74 \\ +0.16 & +0.21 \\ +0.87 & +0.97 \\ -0.37 & -0.06 \\ +0.57 & -0.89 \\ -0.72 & +0.45 \\ -0.85 & -0.40 \\ -0.15 & +0.66 \end{bmatrix}$
Full Factorial	Latin HyperCube					
$\begin{bmatrix} x_1 & x_2 \\ -1 & -1 \\ -1 & 0 \\ -1 & +1 \\ 0 & -1 \\ 0 & 0 \\ 0 & +1 \\ +1 & -1 \\ +1 & 0 \\ +1 & +1 \end{bmatrix}$	$\begin{bmatrix} x_1 & x_2 \\ +0.40 & -0.33 \\ -0.03 & +0.74 \\ +0.16 & +0.21 \\ +0.87 & +0.97 \\ -0.37 & -0.06 \\ +0.57 & -0.89 \\ -0.72 & +0.45 \\ -0.85 & -0.40 \\ -0.15 & +0.66 \end{bmatrix}$					

Figure 12 – DoE synthesis

To assess the quality of a Response Surface Model, various error measures and regression parameters can be examined:

- The Sum of Squared Errors (SSE) can be calculated as:

$$SSE = \sum_{i=1}^n \left(y^{(i)} - y_{est}^{(i)} \right)^2 \quad (13)$$

where y_{est} is the output value predicted by the metamodel.

- The Mean Squared Error (MSE) measures the average of the squares of the errors :

$$MSE = \frac{SSE}{n - p + 1} \quad (14)$$

- The Total Sum of Squares (SSTOT) is the sum, over all experiments, of the differences between each experiment and the overall mean:

$$SSTOT = \sum_{i=1}^n \left(y^{(i)} - \bar{y} \right)^2 \quad (15)$$

where the mean output value for all experiments is:

$$\bar{y} = \frac{\sum_{i=1}^n y^{(i)}}{n} \quad (16)$$

SSTOT only takes information from the experiments not from the metamodel.

- The normal regression parameter R^2 can be calculated with the above error measures as:

$$R^2 = 1 - \frac{SSE}{SSTOT} \quad (17)$$

A value close to 1 indicates a good quality of the model.

RBF and Kriging functions have exact interpolation of the given sample response values, which prevent to direct use of these criteria. Cross validation techniques are thus used to evaluate the quality. To compute the cross-validation error, the surrogate model training data is split (randomly) into q roughly equal subsets. Each of these subsets is removed in turn from the complete training data and the model is fitted to the remaining data. At each stage the removed subset is predicted using the model that has been fitted to the remaining data. The cross-validation error is then calculated as:

$$\mathcal{E}_{cv} = \frac{\sum_{i=1}^n \left(y^{(i)} - y_{est}^{(i)} \right)^2}{n} \quad (18)$$

The cross-validation error can also be used for surrogate model parameter estimation and model selection.

Graphical tools can also be used to help judge the quality of a model:

- The scatter plot which represents model-predicted values versus simulated values. Ideally the samples should follow the straight line $y=x$. Figure 13 gives two examples of scatter. To improve the results of regression models, the order can be increased or data transformation can be used. If areas with errors are not in the area to be explored during the design, it may be decided to keep the model while limiting its validity range.
- The residual plot, Figure 14, which represents the difference between model-predicted values and simulated values. A uniform scatter of points with small mean square error indicates that the regression model fits the data well. A visible pattern in this diagram can be explained by an unsuitable choice of regression model.

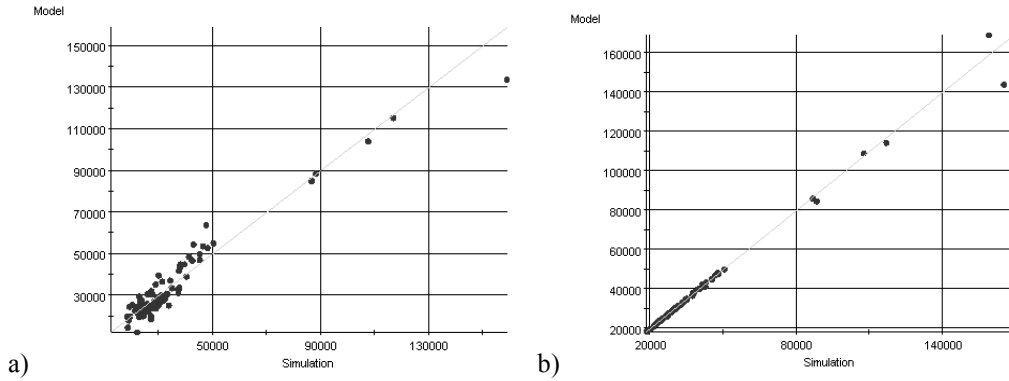


Figure 13 – Scatter plots

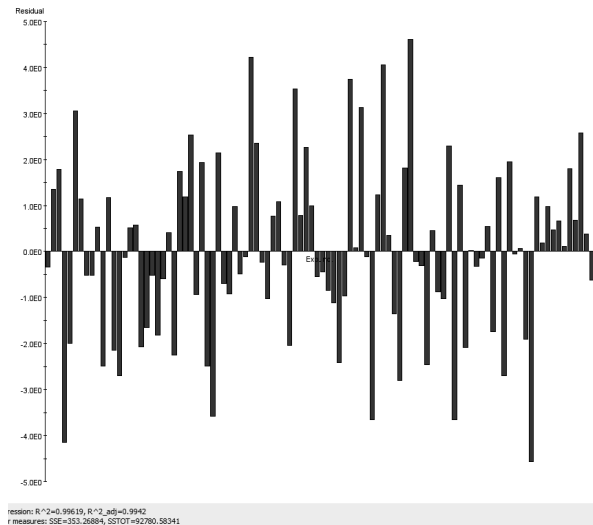


Figure 14 – Residual plots

2.4. Transformations

In the case of metamodels established on numerical simulations, the errors mainly depend on the choice of model. Some transformations of the data handled can be used to improve the quality of predictions. In particular, for the prediction at points involving extrapolation (i.e. outside the initial study domain), the surface will often be more accurate if it contains some well-chosen “structural component”.

These transformations can be applied:

- to all the data, input parameters x and output y , with dimensional analysis. Papers [11] [12] and [6] illustrate this approach. Coupled with sensitivity analysis, the grouping of parameters in order to obtain dimensionless numbers significantly reduces the number of parameters to be handled. A physical basis is also given to the regression.
- to the outputs with power or logarithmic transformations. Box and Cox [13] give a detailed description of the type of processing and the analysis that can be made. In simplified terms, if the regression is performed on y^λ and not on y there, the analysis of the error in the estimation allows the most appropriate power λ to be chosen.

For statistical analysis of data from catalogues, errors can be modelled by a noise with zero mean and variance proportional to the output amplitude. The linear regressions are, however, usually based on the assumption that the error is uniform. To ensure that this last assumption is met, the following transformation can be performed on the equation (4):

$$\hat{Y} = \hat{X} \cdot \theta + \hat{\varepsilon} \quad (19)$$

$$\text{with } \hat{\underline{Y}} = \begin{pmatrix} y^{(1)} / y^{(1)} = 1 \\ \dots \\ y^{(n)} / y^{(n)} = 1 \end{pmatrix}_{n \times 1}, \underline{X} = \begin{pmatrix} 1 / y^{(1)} & x_1^{(1)} / y^{(1)} & \dots & x_{k_x}^{2(1)} / y^{(1)} \\ \dots & \dots & \dots & \dots \\ 1 / y^{(n)} & x_1^{(n)} / y^{(n)} & \dots & x_{k_x}^{2(n)} / y^{(n)} \end{pmatrix}_{n \times k_\theta},$$

$$\underline{\mathcal{E}} = \begin{pmatrix} \mathcal{E}^{(1)} / y^{(1)} \\ \dots \\ \mathcal{E}^{(n)} / y^{(1)} \end{pmatrix}_{n \times 1}$$

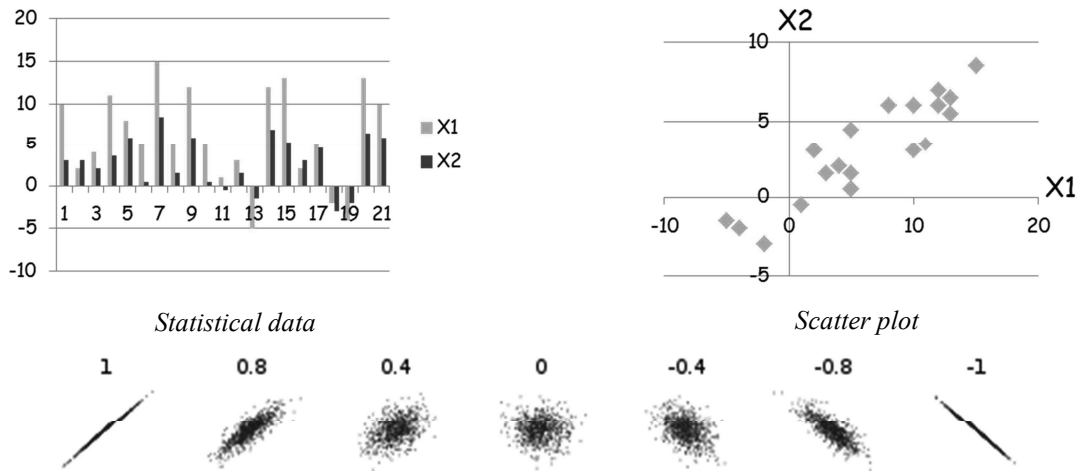
3. ESTIMATION MODELS FROM STATISTICAL DATA

The objective of this section is to show how it is possible to implement estimation models from statistical data typically coming from manufacturer’s catalogues or previous studies. This statistical approach is particularly useful when scaling laws are impossible to establish or generate inappropriate models. With statistical data, DoE is impossible and the sample points cannot be chosen. To determine the most important parameters to keep as design parameters, two tools (Figure 15) are used here:

- a graphical tool: the scatter plot, which displays data as a collection of points, each having the position on the horizontal axis determined by the value of one variable and the position on the vertical axis determined by the value of the other variable. This kind of plot is also called a scatter chart, scatter diagram or scatter graph. One of the most powerful aspects of a scatter plot, however, is its ability to show non-linear relationships between variables. Furthermore, if the data is represented by a model that is a mixture of simple relationships, these relationships will be visually evident as superimposed patterns;
- a numerical tool: the Pearson product-moment correlation coefficient which is a measure of the linear dependence between two variables X and Y, giving a value between +1 and -1. It is widely used as a measure of the strength of linear dependence between two variables. The correlation coefficient r_{xy} is defined by the relation:

$$r_{xy} = \frac{\sum_{i=1}^n (x^{(i)} - \bar{x})(y^{(i)} - \bar{y})}{\sqrt{\sum_{i=1}^n (x^{(i)} - \bar{x})^2 \sum_{i=1}^n (y^{(i)} - \bar{y})^2}} \quad (20)$$

with \bar{x} and \bar{y} mean values of $x^{(i)}$ and $y^{(i)}$ samples.



Scatter plot and correlation coefficients

Figure 15 – Scatter plot and correlation

The two tools can suggest various kinds of correlations between variables:

- positive: rising scatter plot, correlation coefficient close to 1;
- negative: falling scatter plot, correlation coefficient close to -1;
- uncorrelated: no distinct pattern in the scatter plot, correlation coefficient close to 0.

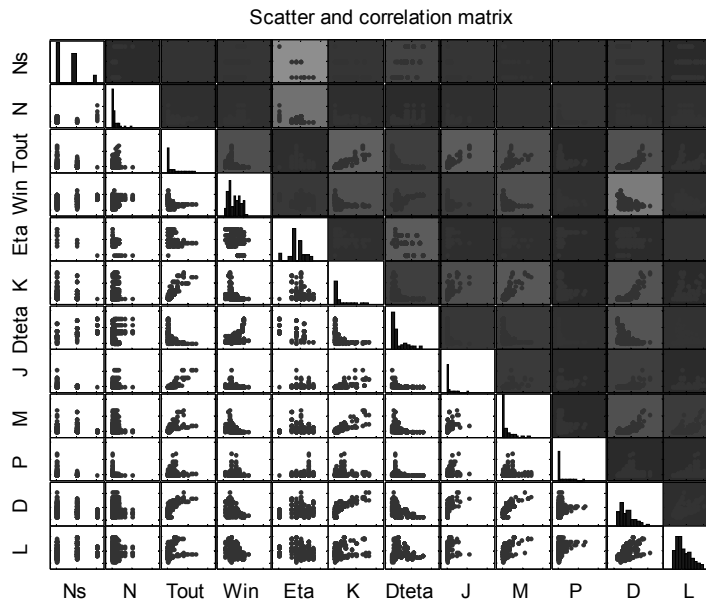
3.1. Example of gear boxes

A database of speed reducers including over 720 references of manufacturers such as Neugart, Redex Andatex, Harmonic drive, and Sumitomo will be analysed here. The first objective is to determine the most important parameters for estimating the mass or inertia of a reducer. Correlation analysis between the different characteristics of reducers can take the form of a matrix summarizing this set of values graphically. This matrix is symmetrical and can also be used also to superimpose scatter plots.

Figure 16 shows the correlation analysis performed in Excel or Matlab. It can be concluded from this example that the output torque has the most significant effect on the mass. The stiffness is strongly correlated with the mass but is not an independent parameter and therefore cannot be used here. The reduction ratio is weakly correlated to the mass.

	number stage	ratio	torque output	rate input	efficiency	torsional stiffness	backlash	inertia input	mass	Power	Diameter	Length
	(-)	(-)	(Nm)	(tr/min)	(%)	(Nm/arcmin)	(arcmin)	(kg cm ²)	(kg)	(W)	(mm)	(mm)
	Ns	N	Tout	Win	Eta	K	Dteta	J	M	P	D	L
Ns	1											
N	0,35450125	1										
Tout	-0,2040004	0,00070407	1									
Win	0,53051261	0,04077852	-0,43671583	1								
Eta	-0,73417898	-0,60873002	0,08845588	-0,27292672	1							
K	-0,2260475	0,0700009	0,01667002	-0,12728106	0,06251145	1						
Dteta	0,68030539	0,18242422	-0,32047954	0,63989789	-0,50521074	-0,33298718	1					
J	-0,23878505	0,05752925	0,88568582	-0,3018039	0,08214942	0,77594224	-0,25692035	1				
M	-0,10381446	-0,00020668	0,80074081	-0,44297658	0,07308041	0,85329096	-0,28896769	0,58756642	1			
P	-0,20318226	-0,2440105	0,29081522	-0,12748389	0,35783086	0,21901128	-0,16789681	0,3479299	0,29526058	1		
D	-0,26393542	0,04308085	0,79819097	-0,65233631	0,15663879	0,82023445	-0,46578206	0,6402751	0,79158006	0,24569978	1	
L	0,29395175	-0,09875818	0,35025998	-0,13999483	0,00015464	0,28026656	-0,02363722	0,17644432	0,59226977	0,35562667	0,42859163	1

This matrix was obtained using Excel Data / Data Analysis / Correlation Analysis and colored by Home / Style / Conditional Formatting / gradation.



This matrix was obtained using `plotmatrix` and `corrcoef` Matlab functions

Figure 16 – Scatter plot and correlation matrix of the speed reducers statistical data

The analysis of the range of Sumitomo cyclo drives (1 stage) in Figure 17 confirms this trend: the main parameter influencing the mass or inertia is the output torque. Regression of the data according to this parameter gives:

- For the mass, a good approximation with a simple linear relationship. The regression coefficient R^2 is 0.97. There is thus a relation of the form $M=k.T$ confirming the scaling law $M^*=T^*$.
- For the inertia, the relationship is not purely linear. A second order regression gives good results with a regression coefficient R^2 of 0.99. However, a Box-Cox analysis [13], Figure 18, shows that the data are suitable for a transformation y^λ with lambda equal to 0.6. The regression of order 1 is thus of the form $J=k.T^{1/0.6}=kT^{1.67}$. Once again a result similar to the scaling law, $J^*=T^{*5/3}=T^{*1.67}$, has been found.

For other technologies, such as epicyclic gears or harmonic drives, the reduction ratio has an influence that remains lower than the torque, but is not negligible. A combination of a power law for the torque and a polynomial regression for the reduction ratio can then be used.

	ratio	torque output	torsional stiffness	inertia input	mass	Diameter	Length
	(-)	(Nm)	(Nm/arcmin)	(kg cm ²)	(kg)	(mm)	(mm)
	N	Tout	K	J	M	D	L
N	1						
Tout	0,05166641	1					
K	0,1246428	0,9927334	1				
J	-0,01326534	0,97044096	0,96071272	1			
M	0,05140194	0,99933564	0,99281595	0,96849584	1		
D	0,08802438	0,97717008	0,97205652	0,90188716	0,9792652	1	
L	0,09920762	0,96210266	0,95688965	0,87412428	0,9634068	0,99709268	1

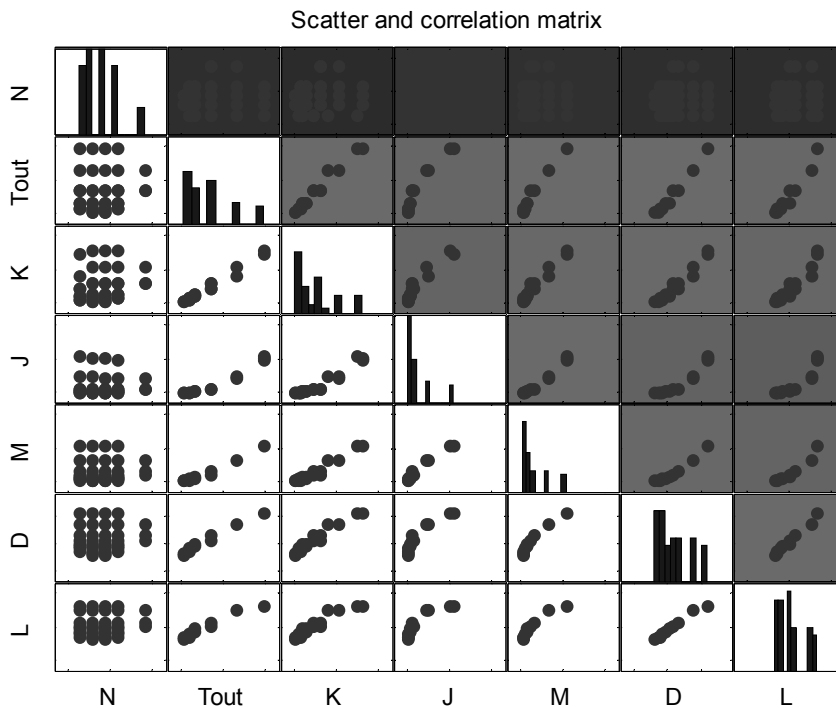


Figure 17 – Scatter plot and correlation of Sumitomo cyclo reducers

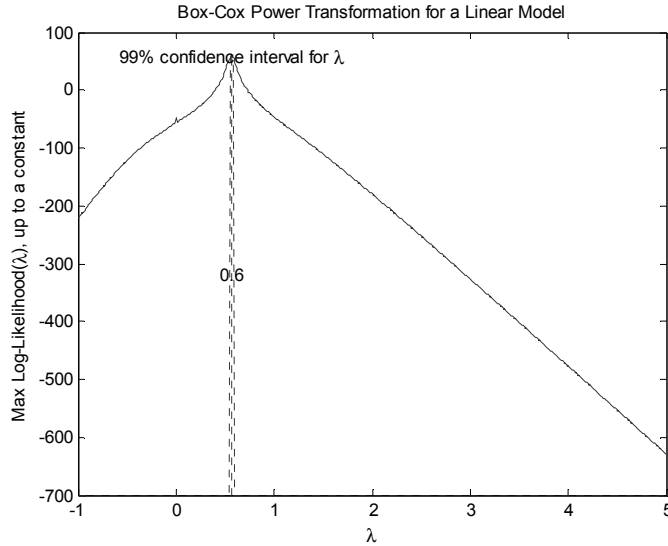


Figure 18 – Box-Cox analysis of inertia data

3.2. Example of heat sink

The previous example showed that power-law based transformations give a more compact expression. A multiple inputs expression, taking the form of a product of power laws, can be linearized by a logarithmic transformation:

$$y = a_0 \prod_i x_i^{a_i} \Rightarrow \log(y) = \log(a_0) + \sum_j a_j \log(x_j) \quad (21)$$

A set of p data can be expressed by the following matrix expression:

$$\begin{pmatrix} \log(y_1) \\ \dots \\ \log(y_p) \end{pmatrix} = \begin{pmatrix} 1 & \log(x_{11}) & \dots \\ \dots & \dots & \dots \\ 1 & \log(x_{p1}) & \dots \end{pmatrix} \begin{pmatrix} \beta_0 \\ \dots \\ \beta_p \end{pmatrix} + \begin{pmatrix} \varepsilon_1 \\ \dots \\ \varepsilon_p \end{pmatrix} \longrightarrow Y = X \cdot \tilde{\beta} + \tilde{\varepsilon} \quad (22)$$

, with $\beta_0 = \log(a_0)$ and $\beta_i = a_i$ for $i \neq 0$.

This form can assess, for example the thermal resistance $R_{th,n}$ of a heat sink according to its dimensions W, H, L, W_f, D_f, H_s (Figure 19). A correlation analysis of statistical data from a database of heat sinks (84 references of AAVID Thermalloy extruded heatsinks), show that the outer lengths W, H and L are related to the quantity sought $R_{th,n}$ and also to secondary lengths W_f, D_f and H_s . Only the outer lengths are thus kept as input parameters:

$$R_{th,n} = kW^a H^b L^c \quad (23)$$

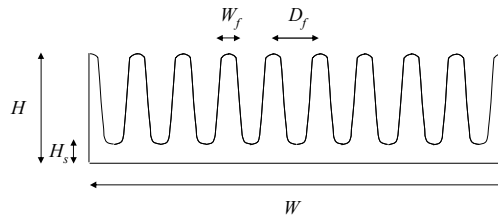


Figure 19 – Heat sink section (Length L)

The coefficients obtained from regression do not necessarily have physical foundations. Reference [14] describes how to add constraints taking the dimensional analysis into account. If all the factors influencing

the secondary parameter are represented by the choice of primary parameters x_i , the dimensions of $\prod x_i^{a_i}$ should be the same as those of y . These constraints resulting from the dimensional analysis can be expressed in a matrix form:

$$R \cdot \tilde{\beta} = b \text{ or } C(\beta) = R \cdot \tilde{\beta} - b = 0 \quad (24)$$

where R expresses the units of x_i and b the units of y .

With one constraint, the optimum is, as shown in Figure 20, where the objective is tangent to the constraint. The normals obtained by the gradients of the functions are therefore collinear:

$$\overrightarrow{\text{grad}}(L) - \lambda_L \overrightarrow{\text{grad}}(C) = \vec{0} \quad (25)$$

with λ_L the Lagrange multiplier.

With n constraints, n Lagrange multipliers are added:

$$\overrightarrow{\text{grad}}(L) - \sum_k \lambda_k \overrightarrow{\text{grad}}(C_k) = \vec{0} \quad (26)$$

A minimum is obtained for:

$$\begin{pmatrix} \tilde{\beta} \\ \tilde{\lambda} \end{pmatrix} = \begin{pmatrix} X^t X & R^t \\ R & 0 \end{pmatrix}^{-1} \begin{pmatrix} 2X^t Y \\ b \end{pmatrix} \quad (27)$$

where $\tilde{\beta}$ is the vector of exponents that minimizes the quadratic error and verifies the constraints coming from dimensional analysis.

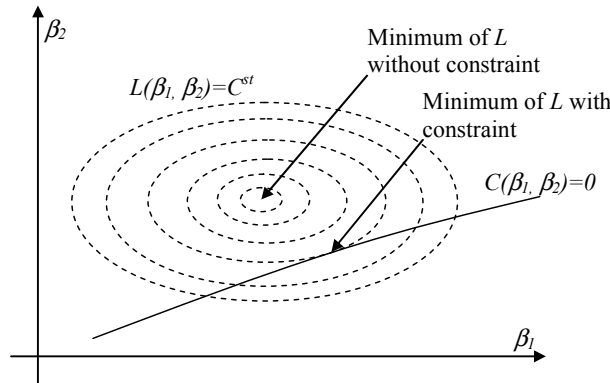


Figure 20 – Minimization with or without constraints

In the heatsink context, physical characteristics involved in natural convection, such as fluid compressibility β , density ρ , viscosity μ , thermal conductivity of air λ and gravity acceleration g have to be taken into account. The units for quantities of primary and secondary parameters, expressed by the matrix R and the vector b , are defined in Figure 21. For more details on this method of regression and associated Matlab algorithms, the reader is invited to refer to reference [14].

Unité	W	H	L	W_f	D_f	H_s	β	ρ	g	μ	λ
m	1	1	1	1	1	1	0	-3	1	-1	1
kg	0	0	0	0	0	0	0	1	0	1	1
s	0	0	0	0	0	0	0	0	-2	-1	-3
K	0	0	0	0	0	0	-1	0	0	0	-1

Unité	$R_{th,n}$
m	-2
kg	-1
s	3
K	1

R
Figure 21 – Constraints matrix

The resulting regression has the following form:

$$R_{th,n} = a_0 \cdot W^{-1} H^{-0,5} L^{-0,75} \rho^{-0,75} g^{-0,33} \mu^{0,75} \lambda^{-1} \tag{28}$$

which gives with scaling law notation:

$$R_{th,n}^* = W^{*-1} H^{*-0,5} L^{*-0,75} \tag{29}$$

Figure 22 compares the results obtained by this scaling law, on the abscissa, to data catalogue values, on the ordinate for all different catalogue dimensions (W , H and L). A perfect estimation would give a straight line. Note that the scaling law obtained by regression on the AAVID catalogue data remains valid for another range of heatsinks from the manufacturer Arcel. A polynomial regression without transformation gives results of much lower quality which are not transferable to another technology.

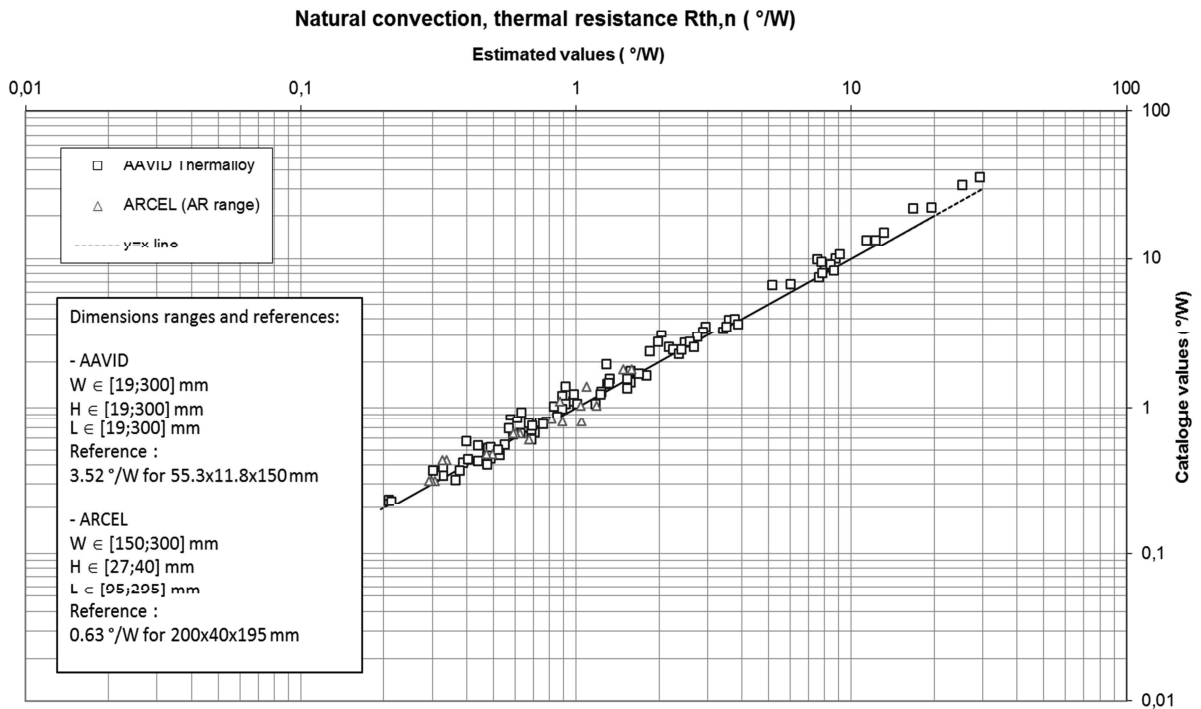


Figure 22 – Estimated vs catalogue’ thermal resistances

4. METAMODELING OF SIMULATION AND EVALUATION MODELS

As part of the preliminary design of actuators, transient simulations of the mission profile or critical scenarios are often used to obtain some useful sizing parameters. Lumped parameter models (simulation models) can be completed by additional calculations (evaluation models) as for rolling mean fatigue or thermal ageing. Using these DAE (differential algebraic equation) or ODE (ordinary differential equation) simulations during optimization phases can be extremely costly in computer time. In this context, it may be important to distinguish between a simulation model, a reduced model and a metamodel (Figure 23):

- A **simulation model** is an abstract description of a component or a system combining several components. A simulation model admits inputs, outputs, design parameters and response parameters. In a simulation model, the relationships between design parameters and response parameters are implicit because they are calculated during the simulation.
- A **reduced model** has the same implicit characteristics as a simulation model but is characterized by a reduction in the number of states or parameters represented in order to accelerate the simulation.
- A **metamodel** is an abstract description of a model for a specific application which corresponds to an explicit function between a specific response variable and several design parameters. A metamodel represents the link between the design parameters and response parameters by an algebraic equation that is very fast to evaluate.

This section will illustrate how metamodels can be applied to these simulation and evaluation models to provide an approximation of the desired quantities while using much less computer time.

Three examples will illustrate the usefulness of metamodels during preliminary design. The first deals with the transient temperature rise of an electric motor subjected to a torque step. The second shows how to evaluate an RMS current with an algebraic equation instead of using a transient simulation at PWM constant time. The last illustrates how it is possible to take the imperfections of a mechanical component into account in the closed-loop performance of an actuator.

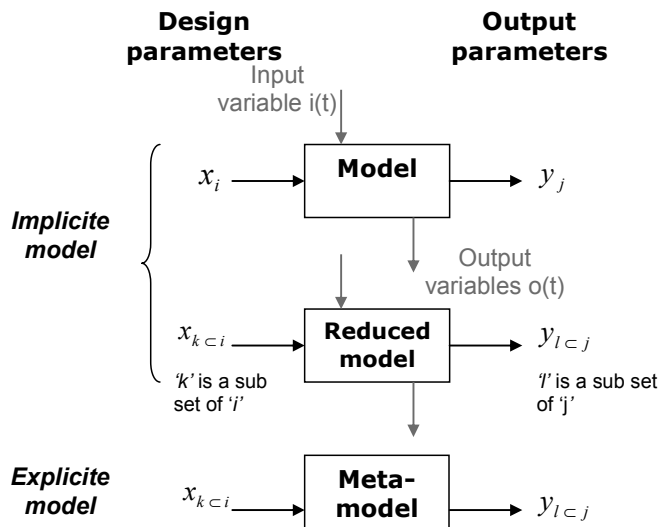


Figure 23 – Reduced vs metamodels

4.1. Transient thermal response of a brushless motor

The selection of a motor may require the assessment of the maximum winding temperature during a constraining scenario with a high torque. Paper 5 used this kind of calculation for a spoiler actuator which must be able to maintain full extension at full effort on the control surface during a given time. For this transient simulation, the thermal model of a motor, given in Figure 24, has to distinguish the temperature of the winding from the temperature of the yoke by using a two thermal body model.

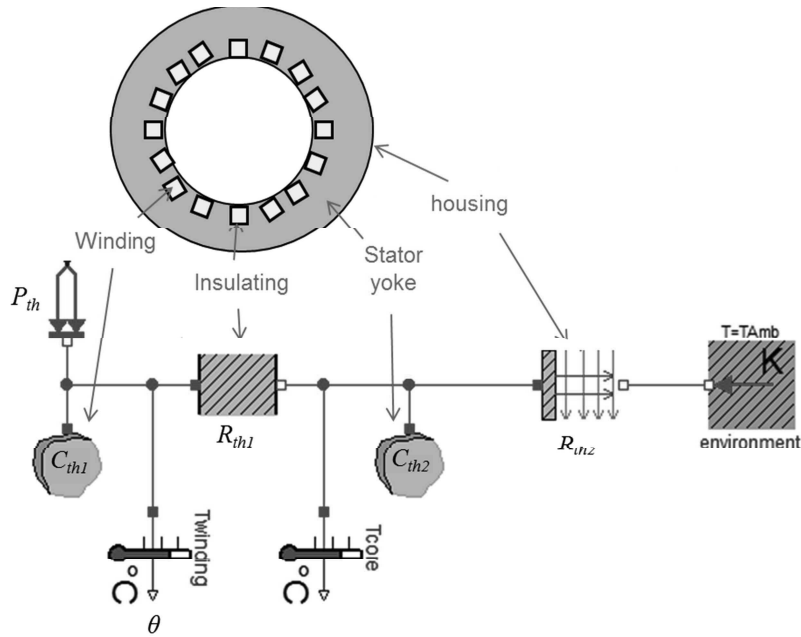


Figure 24 - Thermal model of the motor

The relationship needed to define the temperature increase is characterized by 6 parameters:

- The heat capacity of the winding C_{th1} ;
- The heat capacity of the yoke C_{th2} ;
- The thermal resistance between the winding and the yoke R_{th1} ;
- The thermal resistance between the yoke and the ambient air R_{th2} ;
- The thermal losses P_{th} ;
- The temperature increase θ of the winding after a given time t .

The desired function could be derived from the direct solution of differential equations of the lumped parameters model shown in Figure 24. The thermal impedance $Z_{th}(p) = \theta(p)/P_{th}(p)$ is given by the following Laplace transfer function :

$$Z_{th}(p) = (R_{th1} + R_{th2}) \frac{\left(1 + \frac{R_{th1} \cdot R_{th2}}{R_{th1} + R_{th2}} C_{th2} p\right)}{1 + ((R_{th1} + R_{th2}) C_{th1} + R_{th2} C_{th2}) p + R_{th1} C_{th1} R_{th2} C_{th2} p^2} = R_{th_eq} \frac{1 + T_0 p}{(1 + T_1 p)(1 + T_2 p)} \quad (30)$$

This gives the following step response:

$$\theta(t) = R_{th_eq} P_{th} \left((1 - e^{-t/T_1}) \cdot \frac{T_1 - T_0}{T_1 - T_2} + (1 - e^{-t/T_2}) \cdot \frac{T_0 - T_2}{T_1 - T_2} \right) \quad (31)$$

However, the aim here is to illustrate how a designer can obtain algebraic expressions from any numerical models. Metamodels thus enable him to focus more on sequencing the calculations than on solving them. For this example, the main factors are identified by dimensional analysis [11] [12], which reduces the number of parameters to be studied without any loss of information. The Buckingham theorem [11] [12] can be used to reduce this number to 4 dimensionless parameters:

$$\pi_4 = f(\pi_1, \pi_2, \pi_3) \quad \text{with} \quad \pi_1 = \frac{R_{th1}}{R_{th2}}, \quad \pi_2 = \frac{C_{th1}}{C_{th2}}, \quad \pi_3 = \frac{t}{R_{th1} C_{th1}} \quad \text{and} \quad \pi_4 = \frac{\theta}{R_{th1} P_{th}}$$

With a Latin Hypercube DOE of 100 experiments, a third order polynomial development provides a coefficient of regression R better than 0.99 for this function. This type of expression can be obtained even if the thermal resistances are non-linear as in the case of convection or radiation or if the thermal model is

more complex and involves more elements (after a possible sensitivity analysis step). However the results obtained when the function is evaluated outside the range studied are to be handled with caution: the errors obtained can be coarse as shown in Figure 25.

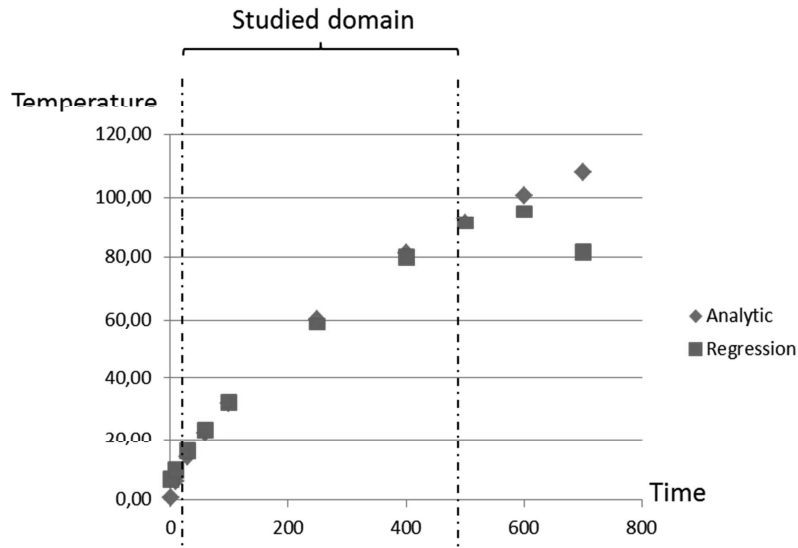


Figure 25 – Error outside studied domains

4.2. RMS current into the DC-link capacitor of an inverter

The inverter is classically realized with a 3-phases IGBT module that generates the motor AC voltage according to the PWM modulation control signal. The DC bus link capacitor provides a low impedance path for the ripple currents associated with PWM frequency switching. The RMS-current in the DC-link capacitors is the main source of loss. Industrial data sheets give an equivalent serial resistance (R_s) which enable these losses to be calculated. This alternating current takes the form represented in Figure 26 and requires PWM time scale simulations. Obtaining an RMS average of this current analytically is not as simple as in the case of a chopper converter. Renken [15] develops this calculation for the case of PWM modulation with sine/triangle intersection. We show here how it is possible to find the same result directly from simulation analysis using metamodeling techniques.

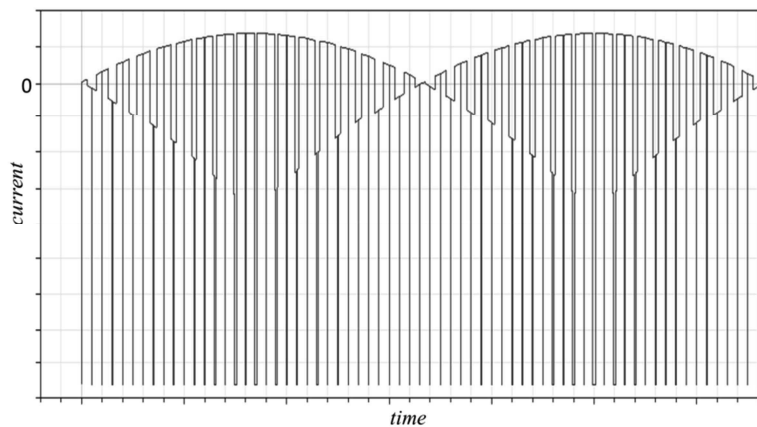


Figure 26 – Alternating current flowing into DC link capacitor

Initially, the RMS current is assumed to be a function of all the characteristic parameters of the study: U_{DC} the DC bus voltage, m the modulation index, $\cos(\varphi)$ the power factor of the load, f the switching frequency of the inverter, f_{mod} the modulation frequency, and I_{ACm} the current amplitude absorbed by the load. Thus:

$$I_{C\ RMS} = f(U_{DC}, m, \cos(\varphi), f, f_{mod}, I_{ACm}) \quad (32)$$

As a first step, the influence of each of these parameters is investigated with a 2-levels screening DoE ($2^8 = 64$ experiments). Correlation or Sobol [16] analyses of the results lead to the conclusion that only

I_{ACm} , m and $\cos(\varphi)$ have an influence on the RMS current. I_{ACm} is the major contributor and is strongly linearly correlated with $I_{C\ RMS}$. Using these results and dimensional analysis, the problem (32) can therefore be rewritten as:

$$\frac{I_{C\ RMS}}{I_{ACm}} = f(m, \cos(\varphi)) \quad (33)$$

where each coefficient I_{RMS}/I_{ACm} , m and $\cos(\varphi)$ is a dimensionless number.

The metamodel can now be built using a more complete DoE, here an LHC with 64 experiments. A 4th order polynomial regression is performed from these data. A Box-Cox analysis [13] is then carried out to determine whether a transformation improves the standard deviation of the error.

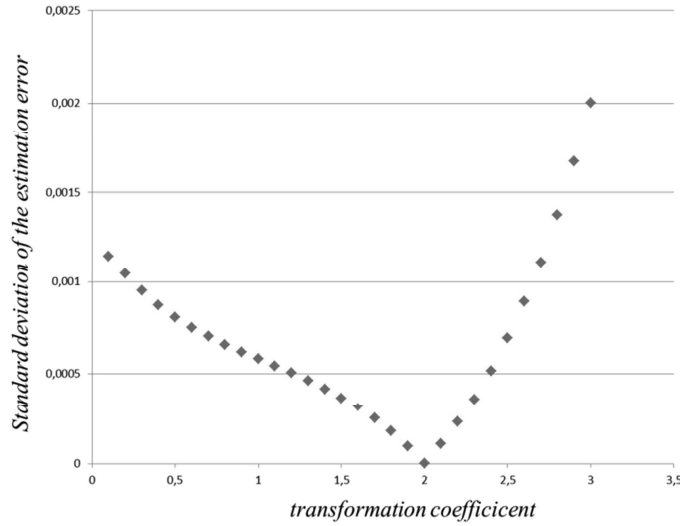


Figure 27 – Box-Cox analysis of the transformation coefficient

The figure clearly shows that the regression is suitable for a power 2 transformation. The regression is finally conducted with $(I_{C\ RMS} / I_{max})^2$ data. The following expression is finally obtained (the coefficients with very low values are neglected):

$$\begin{aligned} \frac{I_{C\ RMS}}{I_{max}} &= \sqrt{0.14m + 0.55m \cdot \cos(\varphi)^2 - 0.56m^2 \cdot \cos(\varphi)^2} \\ &= \sqrt{0.14m + (0.55m - 0.56m^2) \cos(\varphi)^2} \end{aligned} \quad (34)$$

where $m \in [0, 1]$ and $\cos(\varphi) \in [0, 1]$

This expression is identical to the equation obtained analytically in [15]:

$$\frac{I_{C\ RMS}}{I_{max}} = \sqrt{\frac{\sqrt{3}}{4\pi} m + \left(\frac{\sqrt{3}}{\pi} m - \frac{9}{16} m^2 \right) \cos(\varphi)^2} \quad (35)$$

Other numerical studies verify that this expression remains valid for PWM modulation with addition of harmonic 3 (in this case $m \in [0, 2/\sqrt{3}]$). The same metamodeling methodology can be applied to obtain the expression of the RMS current for other types of modulation.

4.3. Effect of stiffness an inertia on closed loop stability

The power sizing does not usually take account of the internal stiffness of an electromechanical actuator. This stiffness may have a destabilizing effect during the synthesis of control loops however. It may therefore be useful, during the preliminary design, to have rules for proper designs taking these stability aspects into account. The objective here is use metamodeling techniques to obtain an algebraic equation that is simple to handle and enables the design to be constrained so as to have an actuator that is naturally suitable for the required closed-loop performance.

Figure 28 shows a typical position cascade control scheme composed of 3 control loops [17]. The bandwidths characteristics typically encountered are: between 500Hz and 1000Hz for the current loop

which is not dependent on the load, tens of Hz for the speed loop, and a few Hz to ten Hz for the position loop [18]. The mechanical mode resonance frequencies are generally below 50Hz or 30Hz. It is therefore possible to neglect the current loop, which does not occur in the area where mechanical effects have an influence. As the study here only concerns the stability and sets aside the precision aspect, the corrector of the speed loop is taken to be purely proportional. If the motor is assumed to be equivalent to an inertia, the mechanical transmission to a stiffness and the load to an inertia, the dynamics of the actuator can be modelled as in Figure 29 with in a) a perfectly rigid actuator and in b) an actuator having elasticity in the mechanical transmission part. Dissipation effects on stability are not represented but the choice of the structure of the speed loop, Figure 29, is used to represent a stabilizing action equivalent to a viscous friction.

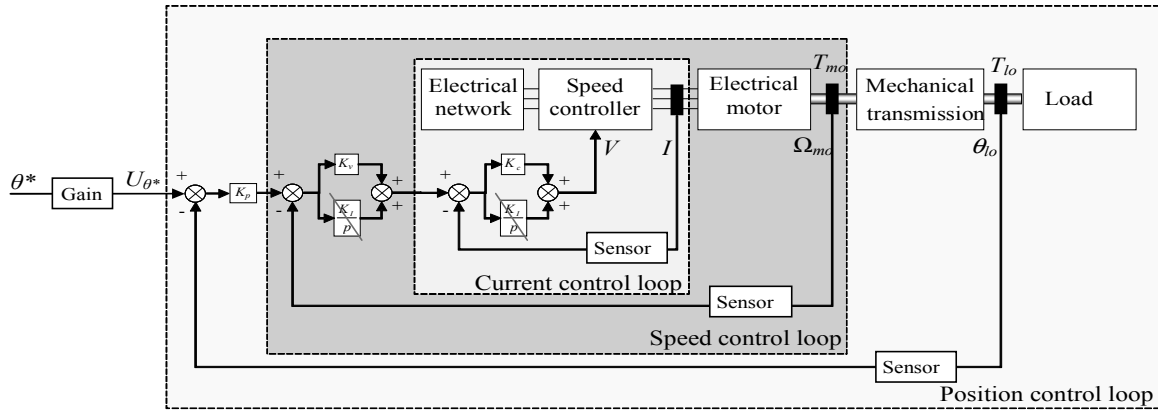


Figure 28 - Classical cascade control of EMA actuators

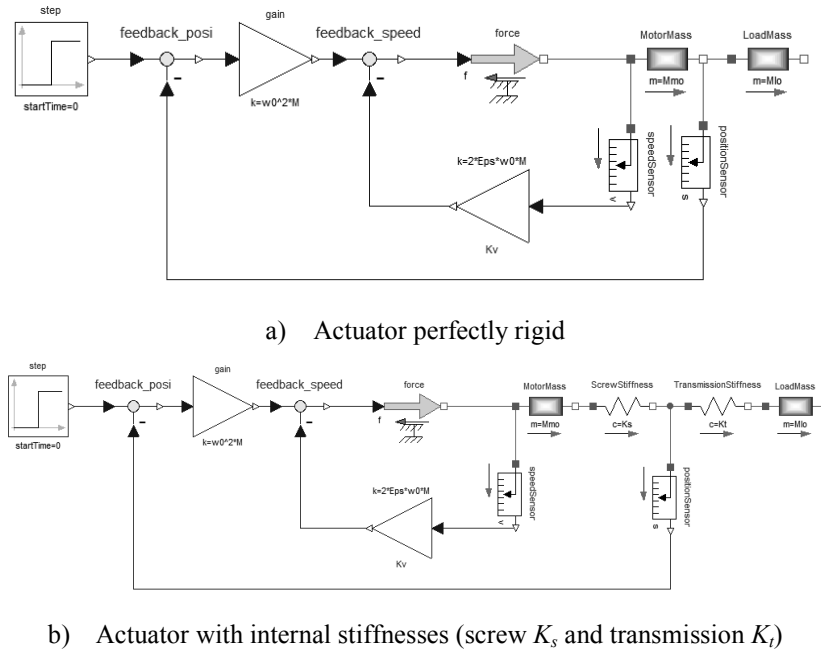


Figure 29 – Models adopted for a) controller synthesis and b) stability analysis

If the actuator is assumed to be infinitely rigid, as in Figure 29a, and therefore to be a purely inertial load, the correctors are easy to calculate to obtain a bandwidth ω_b and a damping coefficient ξ (usually set to $1/\sqrt{2}$). These performance levels are generally imposed by the actuator specifications. In these conditions; the parameters K_p and K_v are expressed by:

$$K_p = \omega_0^2 M \text{ and } K_v = 2\xi\omega_0 M \quad (36)$$

where $M = M_{lo} + M_{mo}$ is the global inertia, i.e. the sum of the load inertia M_{lo} and the motor equivalent inertia M_{mo} .

These coefficients give the following closed loop transfer function:

$$T_{CL} = \frac{1}{1 + 2\xi \frac{p}{\omega_0} + \frac{p^2}{\omega_0^2}} \quad (37)$$

For these values of corrector parameters, taking account of the internal stiffnesses can destabilize the control loop. These internal stiffnesses are thus of the screw / nut system K_S and thus of the rod ends K_T . The position is usually measured by a linear LVDT sensor placed between these two stiffnesses. To highlight the variables that may influence the stability, it is interesting to analyse the transfer function linking the actuation force F and the motor speed \dot{X}_{mo} :

$$T_F = \frac{\dot{X}_{mo}}{F} = \frac{1}{Mp} \cdot \frac{1 + \frac{p^2}{\omega_A^2}}{1 + \frac{p^2}{\omega_R^2}} \quad (38)$$

where:

- $\omega_A = \sqrt{\frac{K_{eq}}{M_{lo}}}$ is the antiresonance angular frequency;
- $K_{eq} = \frac{K_S K_T}{K_S + K_T}$ is the equivalent stiffness;
- $\omega_R = \omega_A \sqrt{1 + k_J}$ is the resonance angular frequency;
- $k_J = \frac{M_{lo}}{M_{mo}}$ is the inertia ratio between load and motor.

We see that the pure inertial behaviour is modified by resonance pole and antiresonance zero which are linked together by the inertia ratio. The following interesting dimensionless numbers appear:

- $k_\omega = \frac{\omega_A}{\omega_0}$, the ratio of the antiresonance frequency and the required bandwidth which generally takes a value between 2 and more of 10 ;
- $k_J = \frac{M_{lo}}{M_{mo}}$, the inertia ratio close to 1 for highly dynamic applications such as TVC but can take low values of 1/100 for less dynamic flight control applications;
- $k_K = \frac{K_S}{K_T}$, the ratio of the stiffness of the screw and of the structure. This ratio has values of more than 10 for prestressed roller screws but may decrease significantly in the presence of backlash.

A state space representation of the model Figure 29b can be used to obtain the damping parameters of the different modes. To assess the risk of instability with these dimensionless parameters, the value of inertia ratio k_J leading to instability of the control loop (set with parameters of equations (36)) is evaluated according to the parameters k_ω and k_K . Figure 30 shows the evolution of k_J for this instability limit. It may be noted that for a flight control application, such as an aileron characterized by values of k_ω and k_K of about 10, there is considerable latitude in the choice of the equivalent inertia of the motor and thus the gear ratios. Applications with higher bandwidth, however, can be constrained by this design criterion. A first-

order regression of these results gives better results after a logarithmic transformation and leads to the following very simple expression:

$$k_{J\text{lim}} = 0.6k_{\omega}^{-2}k_K^{-0.78} \quad (39)$$

for the analysis range of $k_K \in [1-10]$ and $k_{\omega} \in [2-10]$.

Negative values of the two power coefficients suggest that a Box-Cox transformation y^{λ} can be applied. The application of a λ coefficient -1 minimizes the error of regression of a third-order polynomial development:

$$k_{J\text{lim}}^{-1} = -1 + k_{\omega}^2 + k_{\omega}^2 k_K$$

thus

$$k_{J\text{lim}} = \frac{1}{k_{\omega}^2(k_K + 1) - 1} \quad (40)$$

This expression can be easily used in a design procedure to constrain the motor inertia, stiffness of the screw-nut system or reduction ratio. The same modeling approach could be adapted to other types of control loop types [19].

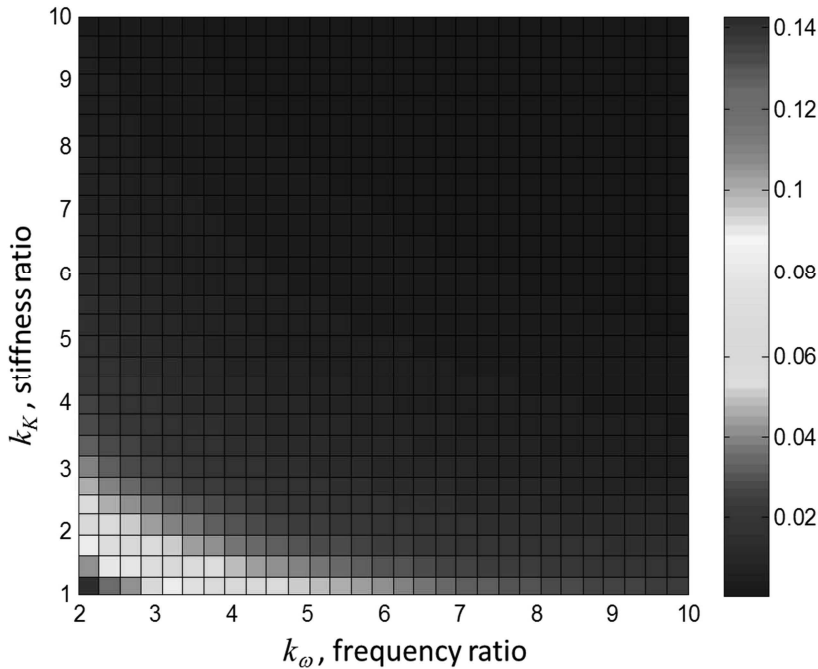


Figure 30 – Evolution of the inertia ratio k_J leading to instability

5. CONCLUSION

We have shown here that metamodeling techniques are very useful to reduce computation time and allow the design and optimization of mechatronics systems. The decomposition of the complete design problem into simpler subproblems means we can settle for standard regression techniques. Their assembly in a design code will enable all design constraints to be taken into account. Chapter 5 will illustrate this aspect. As part of the design of physical systems, conventional linear regression can rely on other concepts in order to extend its scope. Dimensional analysis can reduce the number of parameters to be taken into account and provide more robust expressions that are more general. The transformations allow the use of forms of functions such as power laws to express the characteristics of a component based on its dimensions. Paper 4 shows how these approaches can be combined to extend the use of scaling laws in order to extract compact estimation models from finite element simulations.

6. BIBLIOGRAPHY

- [1] T. Simpson, J. Peplinski, P. Koch and J. Allen, "Metamodels for Computer-Based Engineering Design: Survey and Recommendations," *Engineering with Computers*, vol. 17, pp. 129-150, 2001..
- [2] A. Forrester, A. Sóbester and A. J. Keane, *Engineering design via surrogate modelling: a practical guide*, J. Wiley, 2008.
- [3] H. M. Raymond, D. C. Montgomery and M. A.-C. Christine, *Response surface methodology : process and product optimization using designed experiments*, 4 ed., John Wiley & Sons, 2006.
- [4] E. Stinstra, *The Meta-Model Approach for Simulation-Based Design Optimization*, PHD thesis, Tilburg University ed., 2006.
- [5] M. Budinger, J. Liscouët, F. Hospital and J.-C. Maré, "Estimation models for the preliminary design of electromechanical actuators," *Proceedings of the Institution of Mechanical Engineers, Part G: Journal of Aerospace Engineering*, vol. 226, no. 3, pp. 243-259, 2012.
- [6] D. Lacey and C. Steele, "The Use of Dimensional Analysis to Augment Design of Experiments for Optimization and Robustification," *Journal of Engineering Design*, Vols. Vol. 17, No. 1, p. pp. 55–73, 2006.
- [7] T. Simpson, A. Booker, D. Ghosh, A. Giunta, P. Koch and R.-J. Yang, "Approximation Methods in Multidisciplinary Analysis and Optimization:A Panel Discussion," in *9th AIAA/ISSMO Symposium on Multidisciplinary Analysis & Optimization*, Atlanta, 2002.
- [8] J. Friedman, "Multivariate Adaptive Regression Splines," *Ann. Statist.* , vol. Volume 19, no. Number 1, pp. 1-67, 1991.
- [9] M. Stein, *Interpolation of Spatial Data: Some Theory for Kriging*, Springer (New York), 1999.
- [10] J. Kleijnen, "Kriging metamodeling in simulation: A review," *European Journal of Operational Research*, Vols. Vol. 192, No. 3, pp. pp. 707-716, 2009.
- [11] G. Vignaux and J. Scott, "Simplifying regression models using dimensional analysis," *Austral. & New Zealand J. Statist.*, vol. 41, pp. pp 31-41, 1999.
- [12] C. Gogu, R. Haftka, S. Bapanapalli and B. Sankar, "Dimensionality Reduction Approach for Response Surface Approximations: Application to Thermal Design," *AIAA Journal*, vol. 47, no. 7, pp. 1700-1708, 2009.
- [13] G. E. P. Box and D. R. Cox, "An Analysis of Transformations," *Journal of the Royal Statistical Society. Series B (Methodological)*, vol. 26, no. 2, pp. 211-252, 1964.
- [14] P. Mendez and F. Ordóñez, "Scaling laws from statistical data and dimensional analysis," *Journal of Applied Mechanics*, Vols. Volume 72, Issue 5, pp. pp 648-658, 2005.
- [15] F. Renken, "Analytic Calculation of the DC-Link Capacitor Current for Pulsed Three-Phase Inverters," in *EPE 2005, Dresden.*, 2005.
- [16] I. Sobol, "Sensitivity estimates for non-linear mathematical models," *Math Modeling Comput Exp*, vol. 4, p. pp. 407–414, 1993.
- [17] G. Grellet, *Actionneurs électriques: Principes, modèles, commandes*, Eyrolles, 1989.
- [18] G. Ellis, *Control System Design Guide*, 2004 ed., Elsevier.
- [19] F. Roos, H. Johansson and J. Wikander, "Optimal selection of motor and gearhead in

mechatronic applications," *Mechatronics*, vol. 16, no. 1, pp. 63-72, 2006.

Paper 4 - Scaling-law-based metamodels for the sizing of mechatronic systems

ABSTRACT

This paper presents a new metamodel form and associated construction procedure adapted to the sizing tasks of mechatronics systems. This method of meta-modeling uses scaling laws to extract compact forms of design models from local numerical simulations (FEM). Compared to traditional metamodels (polynomial response surfaces, kriging radial basis function) the scaling-law-based metamodels have the advantage of a light, compact form and good predictive accuracy over a wide range of the design variables (several orders of magnitude). The general regression process is first explained and then illustrated on different examples: a purely numerical test function, a limited angle electromagnetic actuator and a flexible mechanical hinge.

Keywords: metamodels, surrogate modelling, scaling laws, Buckingham theorem, components sizing, preliminary/conceptual design.

Referencing: M. Budinger, J-Ch. Passieux, Ch. Gogu, A. Fraj, *Scaling-law-based metamodels for the sizing of mechatronic systems*, Mechatronics, Available online 19 December 2013.



Contents lists available at ScienceDirect

Mechatronics

journal homepage: www.elsevier.com/locate/mechatronics

Scaling-law-based metamodels for the sizing of mechatronic systems

Marc Budinger^{*}, Jean-Charles Passieux, Christian Gogu, Amine Fraj

Université de Toulouse, INSA/UPS, Institut Clément Ader, Toulouse 31077, France

ARTICLE INFO

Article history:

Received 23 March 2013
5 September 2013
Accepted 30 November 2013
Available online xxx

Keywords:

Metamodels
Surrogate modeling
Scaling laws
Buckingham theorem
Components sizing
Preliminary/conceptual design

ABSTRACT

This paper presents a new metamodel form and associated construction procedure adapted to the sizing tasks of mechatronics systems. This method of meta-modeling uses scaling laws to extract compact forms of design models from local numerical simulations (FEM). Compared to traditional metamodels (polynomial response surfaces, kriging, radial basis function) the scaling-law-based metamodels have the advantage of a light, compact form and good predictive accuracy over a wide range of the design variables (several orders of magnitude). The general regression process is first explained and then illustrated on different examples: a purely numerical test function, a limited angle electromagnetic actuator and a flexible mechanical hinge.

© 2013 Elsevier Ltd. All rights reserved.

1. Introduction

A mechatronic system [1,2] expands the capabilities of conventional mechanical systems through the integration of different technological areas (Fig. 1) around:

- A power transmission part, which is a combination of components from mechanical, electrical, power electronics or fluid power technologies.
- An information processing part, which is a combination of electronics, instrumentation, automatic, signal processing, and information technologies.

The Refs. [3,4] highlight that the design of such multi-domain systems require different modeling layers as represented Fig. 2:

- A mechatronic layer, to take into account the functional and physical coupling between components. This level of modeling is usually done using 0D-1D models [3] also called lumped parameter models represented by algebraic equations, ordinary differential equations (ODE) or differential algebraic equations (DAE) [5].
- A specific domain layer, to describe the performance limits and parameters necessary in the previous layer, based on a geometric representation. The specific domain phenomena are generally represented through partial differential equations

(PDE). This level of modeling can be achieved, for simplified geometries using analytical models or, for complex 2D and 3D geometries, using numerical approximations like finite element method (FEM) for instance.

The design of the power part with a system integrator's point of view should allow to optimally size and specify the components of multiple technologies [6] interacting together. This system level design, distinct of component design, needs to represent in the mechatronic layer the key informations of the specific domain layer with dedicated models [7–9]. The latter enables the designer to take multiple design constraints into account easily. They are referred to as “estimation models” in this paper. They directly and explicitly link a few primary characteristics, such as overall dimensions of components, to the secondary characteristics needed for the sizing [9] and optimization [10]. The capacities required of these estimation models are: to present a form that is simple to handle and to implement in different calculation tools, to lend themselves to easy analytical manipulations, and to be reusable in an area slightly different from the one where they were initially employed. To satisfy these constraints, simplified analytical models are often used [11,12]. Among them, scaling laws have proved effective to represent a physical phenomenon over wide ranges of variation [13,8]. However, these models are valid under certain conditions, among which one can mention geometry and material similarities, and uniqueness of the driving physical phenomenon. For the system designer the models should be as predictive as possible. Detailed finite element models, able to precisely predict the physical phenomena are still too time-consuming in

^{*} Corresponding author. Tel.: +33 561559960; fax: +33 561559950.
E-mail address: marc.budinger@insa-toulouse.fr (M. Budinger).

Nomenclature

CAD	computer aided design	LHC	latin hypercube
FEM	finite element method	SLAWMM	scaling-law-based metamodels
3D	three-dimensional	std	standard deviation of a variable
LAT	limited angle torque	mean	mean value of a variable
DoE	design of experiments		

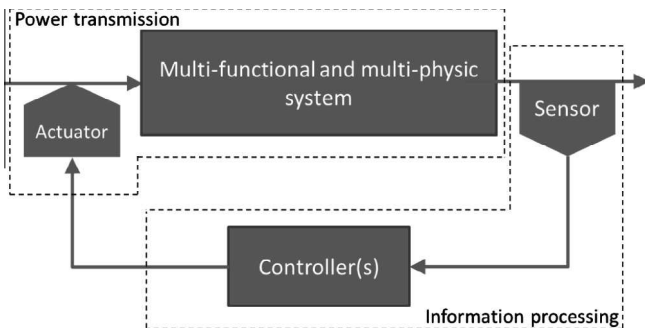


Fig. 1. Mechatronic system (based on Ref. [3]).

such a context. Despite a recent thrust of work on model order reduction [14,15], the computational cost of finite element models remains prohibitive in the preliminary design phase. The use of metamodeling techniques [16–18] is thus interesting for this purpose. In this paper, we propose an enhanced power law type model based on metamodels to represent the models of the specific domain layer (Fig. 2) into the mechatronic layer.

The second section of this paper will show the interest of scaling laws to establish the estimation models needed by the system designer. In the third section, a metamodeling method based on scaling laws will be proposed to extract simple, global expressions of estimation models from local numerical simulations (FEM). The regression process is first illustrated with a mathematical function and then with two examples of mechatronic components from different domains: a limited-angle electromagnetic actuator and a flexible mechanical hinge. Noise effects and comparisons with classical metamodeling techniques are illustrated through these examples.

2. Estimation models with scaling laws

2.1. Scaling laws and Buckingham theorem

Scaling laws based on dimensional analysis, also called similarity laws or allometric models, have been very successfully used

throughout the past decades for solving scientific and engineering problems and for presenting results in a compact form. In the design of mechatronic systems scaling laws [8,13], allow estimation models to be obtained from a single reference component by using three main modeling assumptions:

- (a) Material similarity: all material and physical properties are assumed to be identical to those of the component as the reference.
- (b) Geometric similarity: the ratio of all the lengths of the component under consideration to all the lengths of the reference component is constant.
- (c) Uniqueness of design driver: only one main dominant physical phenomenon drives the evolution of the secondary characteristic y .

The mathematical form of scaling laws is a power law:

$$y = kL^a \tag{1}$$

With y the secondary characteristic to be estimated, L the main dimension of the component, and k and a constants. For simplicity of notation, in this article, k means a constant coefficient which may have different numerical values in the different equations.

This form and the conditions for obtaining Eq. (1) are demonstrated here using the Buckingham theorem [19–21]. An estimation model seeks to identify a relationship between $2 + n + m$ parameters:

$$f\left(y, \underbrace{L, d_1, d_2, \dots, d_n}_{1+n}, \underbrace{p_1, \dots, p_m}_m\right) = 0 \tag{2}$$

with:

- 1 parameter corresponding to the secondary characteristic y to be estimated;
- $1 + n$ parameters characterizing the geometrical dimensions L and d_i ;
- m parameters characterizing physical and material properties p_i .

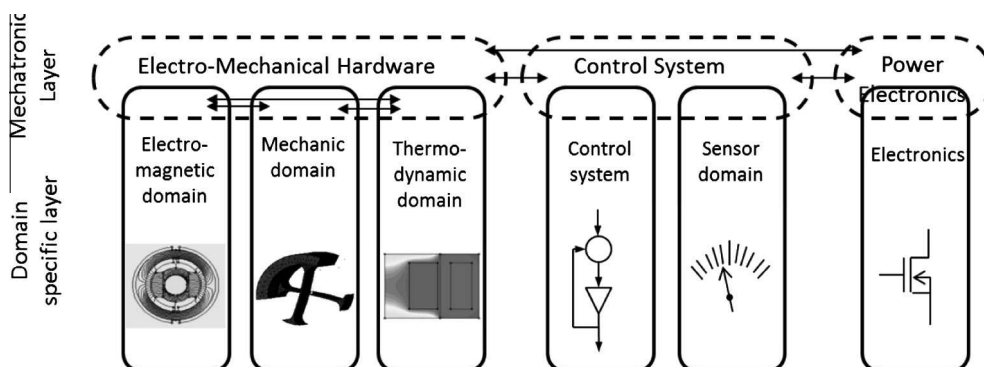


Fig. 2. Hierarchical design models (based on Ref. [4]).

Depending on the number of physical units u (e.g. m, kg, s, etc.) involved in the problem, this relationship can be rewritten using dimensionless parameters π_i :

$$f' \left(\underbrace{\pi_y, \pi_1, \pi_2, \dots, \pi_n}_n, \underbrace{\pi_{p1}, \dots, \pi_{pm'}}_{m'} \right) = 0 \quad (3)$$

where

$$\pi_y = yL^{a_y} \prod p_i^{a_i} \quad (4)$$

$$\pi_i = \frac{d_i}{L} \quad (5)$$

$$\pi_{pi} = L^{a_{pi}} \prod p_j^{a_j} \quad (6)$$

The number m' , usually smaller than m , depends on the number of physical units u as expressed by the Buckingham theorem:

$$m' = 1 + m - u \quad (7)$$

If only one main simple physical phenomenon drives the evolution of the secondary characteristic y , the number m' is often equal to zero. If m' is not equal to zero, the remaining dimensionless numbers can generally be expressed through ratios of material properties with similar units. These m' dimensionless number thus do not depend on L . With this condition and the first two assumptions a. and b., the π_i and π_{pi} dimensionless numbers are constant and it follows that:

$$\pi_y = yL^{a_y} \prod p_i^{a_i} = \text{constant} \quad (8)$$

which gives relation (1) if we assume the material or physical properties p_i to be constant during the sizing.

2.2. Examples of scaling laws

To illustrate the construction and use of such laws, two examples will be given here. These examples address conventional components of mechatronic systems: brushless motors and bearings. We assume here that the main design criterion for the motor is the winding temperature. The dominant thermal phenomenon will be assumed to be convective. The bearings are for their part designed to withstand a maximum mechanical stress.

For the brushless motors, Eqs. 2, 3, and 1 become the following:

- For thermal aspects: the current density J can be linked to the dimensions through

$$f \left(\underbrace{J, L, d_1, d_2, \dots, d_n}_{1+n}, \underbrace{\rho, \theta, h}_m \right) = 0 \quad (9)$$

which, according to the Buckingham theorem, leads to

$$f' \left(\frac{\rho J^2 L}{h\theta}, \underbrace{\frac{d_1}{L}, \frac{d_2}{L}, \dots, \frac{d_n}{L}}_n \right) = 0 \text{ where } m' = 0 \quad (10)$$

and

$$J = kL^{-0.5} \quad (11)$$

- For magnetic aspects: the torque T can be linked to dimensions and current density through

$$f \left(\underbrace{T, L, d_1, d_2, \dots, d_n}_{1+n}, \underbrace{J, B_r}_m \right) = 0 \quad (12)$$

which, according to the Buckingham theorem, leads to

$$f' \left(\frac{T}{JB_r L^4}, \underbrace{\frac{d_1}{L}, \frac{d_2}{L}, \dots, \frac{d_n}{L}}_n \right) = 0 \text{ where } m' = 0 \quad (13)$$

and

$$T = kJL^4 \quad (14)$$

with: J the current density, L the length of the motor, d_i other geometrical dimensions, ρ the resistivity of the copper, θ the maximal temperature rise for the winding insulation, h the convection coefficient, B_r the remanent induction of the permanent magnet, and T the electromagnetic torque.

Combining these two aspects provides an estimate of torque depending on motor size:

$$T = kL^{3.5} \quad (15)$$

The assumptions a. and b. allow the motor weight to be estimated:

$$M = kL^3 = kT^{3/3.5} \quad (16)$$

With the same approach, the weight of the bearing can be estimated from their load-bearing capacity C :

$$C = kL^2 \text{ and } M = kL^3 = kC^{3/2} \quad (17)$$

More details and examples of the development of such laws for mechanical and electromechanical components are given in [8]. Figs. 3 and 4 compare these relationships to data from industrial catalogues, and show that scaling laws can provide good fits for the quantities of interest of such components.

2.3. Interests and limitations of scaling laws

Scaling laws have assets that make them attractive for the design of mechatronic systems [22,23,9]. Their simple form makes them easy to manipulate and customize as they require only one reference to determine the multiplier coefficient k , the power coefficient a being determined by the physical phenomena. They have a monotonous progression valid over a wide range of sizes (several orders of magnitude) which avoids the risk of possible mathematical aberrations of metamodels used outside their construction bounds.

However they have some limitations. Although the similarity of the materials can be easily verified for a given technology, the geometric similarity is not necessarily verified or sought. For motors (Fig. 3), this point mainly explains the estimation errors of scaling laws in Fig. 3. Manufacturers have a tendency to use the same motor diameter (i.e. the same iron sheet) for different lengths and torques. Obtaining a scaling law also requires a dominant physical phenomenon. For example, in the case of the electric

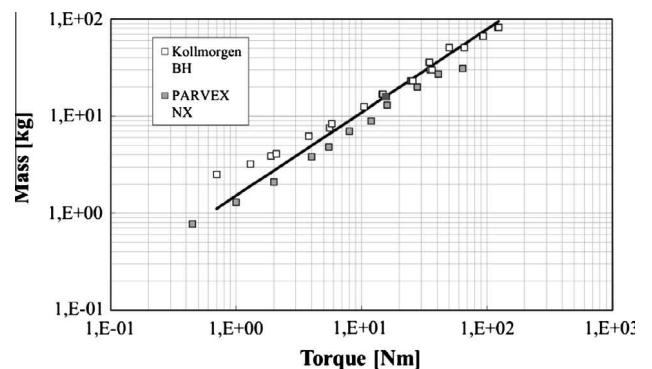


Fig. 3. Brushless motor masses according to the nominal torque.

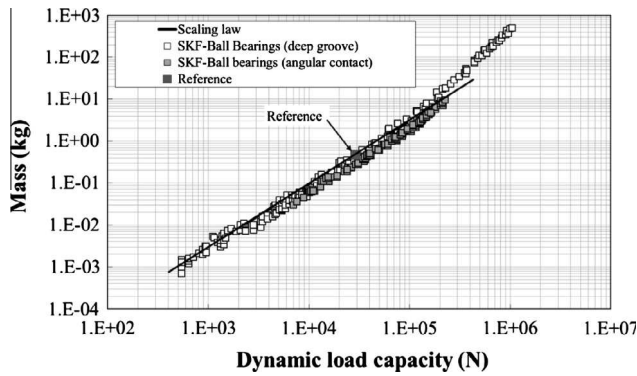


Fig. 4. Bearing masses according to the load capacity.

motor, if the conductive heat transfer phenomenon cannot be neglected, relations (9) and (10) should take the form:

$$f\left(\underbrace{J, L, d_1, d_2, \dots, d_n}_{1+n}, \underbrace{\rho, \theta, h, \lambda_1, \lambda_2, \dots}_m\right) = 0 \quad (18)$$

which gives

$$f'\left(\frac{\rho J^2 L}{h\theta}, \frac{d_1}{L}, \frac{d_2}{L}, \dots, \frac{d_n}{L^n}, \frac{\lambda_1}{hL}, \frac{\lambda_2}{hL}, \dots, m'\right) = 0 \quad (19)$$

with λ_i the thermal conductivities of the various materials of the motor.

In this case, either a global scaling law would have been impossible to establish or its domain of validity would have been smaller.

3. Scaling laws based on regression

The objective of this section is to show how it is possible to increase the use and validity of scaling laws through appropriate regression techniques as proposed by our method.

3.1. Form of models

To maintain the physical meaning and benefits of scaling laws, the regression model will be based on the power form (1). However, to eliminate assumptions b. (geometric similarity) and c. (uniqueness of design driver), estimation models of the following, more general form will be sought:

$$y = f(L, \pi_1, \pi_2, \dots) = k(\pi_1, \pi_2, \dots) L^{a(\pi_1, \pi_2, \dots)} \quad \text{with } \pi_i = \frac{d_i}{L} \quad (20)$$

where

- y is the parameter to be estimated.
- L is the main dimension of the system.
- d_i are the secondary dimensions of the system.
- π_i are the dimensionless numbers representative of form factors of the system.

With geometrical similarity, the form factors are constant ($\pi_i = C^{st}$) and the form (20) simplifies into the classic scaling law form (1). The desired form of model (20) lends itself to direct regression less easily than polynomial response surfaces [24], radial basis functions [16,25], or kriging [26,27] directly on the parameter y . The objective of the coming sections is to give an approach to determine the shapes of functions $k(\pi_1, \pi_2, \dots)$ and $a(\pi_1, \pi_2, \dots)$ representative of multiplier and power coefficients.

3.2. Regression process

Fig. 3 describes the overall meta-modeling process proposed to carry out regressions of form (20). The three main steps of the process are described below and the details of each step are described in the following subsections.

- **Step 1 – data generation:** the objective is first to generate the combinations of variables L and π_i to be simulated. With deterministic computer experiments, these sample points should be chosen to fill the design space. Once the DoE is defined, a call is then made to the finite element codes, or any other sizing code, to obtain the desired data y . The data y are then projected according to form (20) by calculating the coefficients k and a for each configuration π_i of form factor parameters.
- **Step 2 – study of the general shape of the function:** the evolution of each coefficient k and a is then analysed to determine the overall shape to be imposed on function (20) through the choice of the forms of functions $k(\pi_1, \pi_2, \dots)$ and $a(\pi_1, \pi_2, \dots)$. These forms of functions cannot be initially assumed and depend on each problem.
- **Step 3 – building of the metamodel:** based on the function forms selected in the previous step, a regression process is applied to simulation data. A comparison of the results predicted using Eq. (20) with the initial data y can then validate the quality of these regressions.

Even though the model form of Eq. (20) cannot be expressed by linear combination of basis functions, some of its characteristics are interesting and will be used for the proposed meta-modeling process. The following subsections describe the choices made here for each of these steps according to these characteristics.

3.2.1. Step 1 – Data generation

The range of variation for the parameter L is potentially very large and is potentially much smaller for the shape parameters π_i . The proposed process will use a DoE (design of experiments) which is logarithmically distributed on n_L levels for the parameter L and linearly distributed on n_π levels for the p parameters π_i . This simple DoE enables the design space to be filled. This DoE (step 1.1), mainly similar to a full factorial design, requires at least three levels for each parameter in order to calculate (steps 1.3) and analyse (steps 2.1 and 2.2) coefficients k and a .

According to this DOE, calls are then made (step 1.2) to the finite element codes, or any other sizing code, to obtain the desired data y . The final number of data y is $n_L \cdot n_\pi^p$. The conventional regression techniques use these simulation data directly. Here in order to adapt the data to form (20) and as a power law can be represented linearly in logarithmic-scale graphs, the projection of the data y onto the coefficients a and k (step 1.3 of Fig. 5) is done in a logarithmic plane plotting the y according to L data for each combinations of the form factors π_i . Fig. 6 represents the graphs where, for each combination of coefficients π_i , the evolution of y according to L follows a power law and is therefore described by a straight line in a logarithmic plane. The algorithm computes the slopes a of the segments between two consecutive values of L and returns the mean average slope $mean(a)$ for each combinations of π_i . The multiplier coefficient k is calculated for each curve by minimizing the least square error for the average slope. In order to check that the data are well fitted by power laws, a quality criterion is also calculated. This criterion expressed by the relation $std(a)/mean(a)$ is usually very close to zero and shows that the problem is well expressed by using a scaling law for a given configuration of form factors. After this step, the $n_L \cdot n_\pi^p$ values y are transformed into n_π^p values vectors for all coefficients a and k .

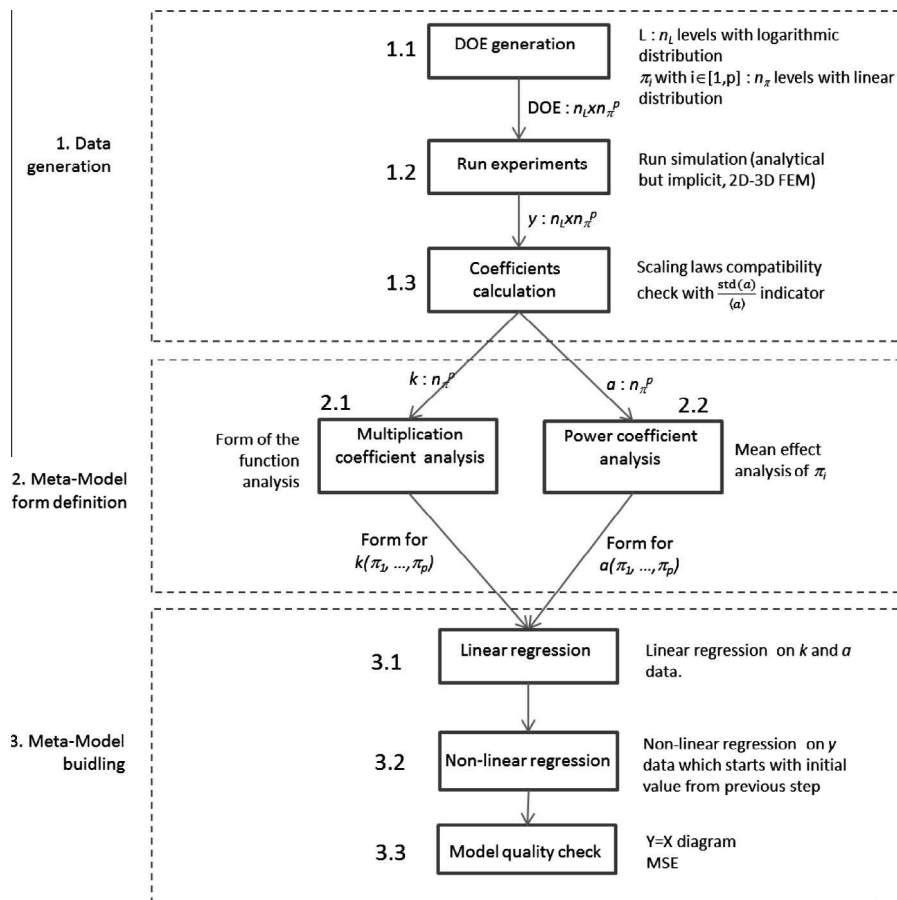


Fig. 5. Meta-modeling process.

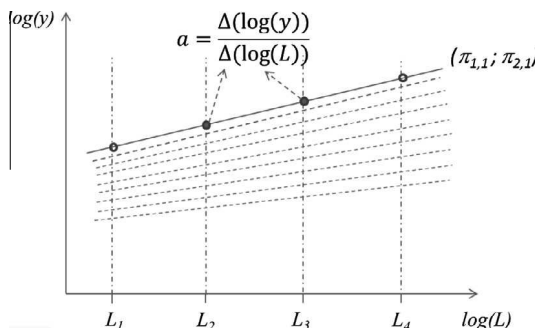


Fig. 6. Power law coefficients calculation.

3.2.2. Step 2 – Metamodel form definition

The objective of this step is to determine the form that can be given to functions $a(\pi_1, \pi_2, \dots)$ and $k(\pi_1, \pi_2, \dots)$.

The power coefficient $a(\pi_1, \pi_2, \dots)$ of scaling laws is constant if the physical phenomenon that drives the design of the system does not depend on the form factors π_i . If the physical phenomenon switches from one to another (e.g. convection to conduction for thermal transfer), the power coefficient is a function that changes between 2 extreme values. If the switch between the two physical phenomena is progressive (often the case for components of mechatronics systems) then the surface $a(\pi_1, \pi_2, \dots)$ will be characterized by a small number of peaks and valleys and can potentially be well approximated by a polynomial function. It remains to determine the exact form of the polynomial function. Since all

the parameters π_i do not usually affect the power coefficient it is useful to conduct a sensitivity analysis at this point. Step 2.2 thus corresponds to a sensitivity analysis, which is conducted here by performing a linear regression after normalization between -1 and $+1$ of parameters π_i . The analysis of the regression coefficients leads to the quantification of the average influence of each parameter. Only relevant parameters will be considered in the final expression of $a(\pi_1, \pi_2, \dots)$. Note that any other technique of sensitivity analysis could be used here (e.g. ANOVA [28] or Sobol's indices [29]).

The multiplication coefficient $k(\pi_1, \pi_2, \dots)$ of scaling laws can often take the form of products of functions, some of which may also be expressed in the form of power laws. Step 2.1 (Fig. 5) analyses these options by using a logarithmic plane again as the functions that can be decomposed into products are represented by parallel curves in logarithmic-scale graphs (Fig. 7a). The power laws are represented by straight lines (Fig. 7b). If:

$$k(\pi_1, \pi_2, \dots) = f(\pi_1)g(\pi_2, \dots) \text{ or } \log(k(\pi_1, \pi_2, \dots)) = \log(f(\pi_1)) + \log(g(\pi_2, \dots)) \quad (21)$$

the evolution of values of $k(\pi_1, \pi_2, \dots)$, a function of π_1 for different $\pi_{i \neq 1}$ configurations, can give 3 possibilities: factorizable (Fig. 7a), factorizable with a power law (Fig. 7b), or non-factorizable (Fig. 7c). This type of analysis can be carried out for each variable π_i and quantified by indicators describing:

- The possibility of factorizing $k(\pi_1, \pi_2, \dots)$ by a function of π_i . To assess this possibility we introduce the indicator defined by $(\max(E) - \min(E)) / (\max(\log(k)) - \min(\log(k)))$, where E quantifies

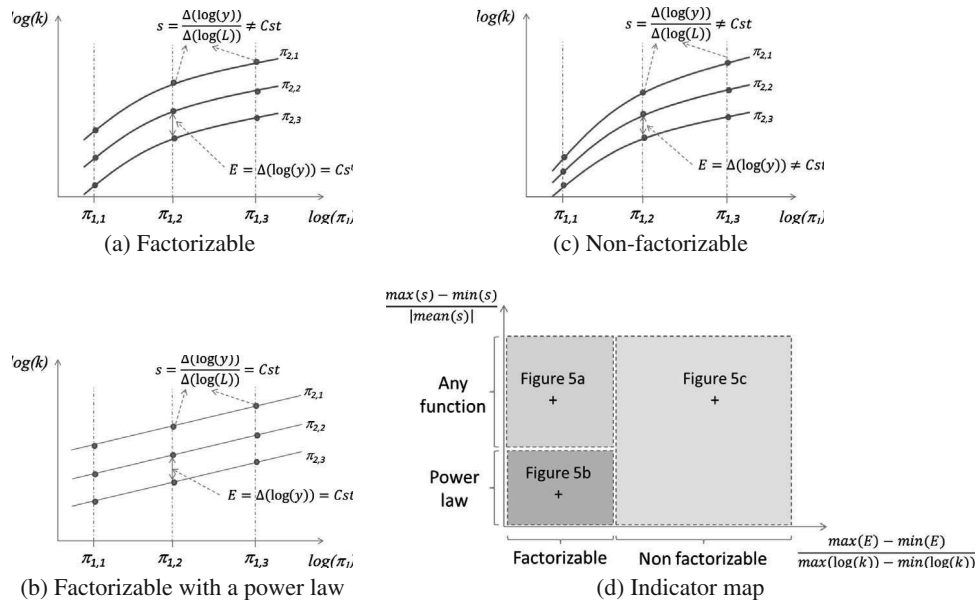


Fig. 7. Multiplication coefficient form analysis.

the difference between two curves for different values of π_i . If the difference between two curves is constant, this indicator is equal to zero and points out the possibility of factorization.

- The opportunity of expressing this function by a power law. To assess this, we introduce the indicator $(\max(s) - \min(s)) / |\text{mean}(s)|$, where s quantifies the slope of a curve. If the slope is constant, the indicator is equal to zero and indicates a power law.

These criteria can be condensed graphically on a plane, as illustrated in Fig. 7d, to quickly assess the form that the function $k(\pi_1, \pi_2, \dots)$ should have.

3.2.3. Step 3 – Metamodel building

The last step aims to build the metamodels from data generated in step 1 and according to the forms of functions defined in step 2. This process of regression is done in two sub-steps:

- The first uses the data a and k (outputs of step 1.3, Fig. 5): a least squares polynomial regression, using the most influential parameters, is directly performed on the data a to obtain an approximation for $a(\pi_1, \pi_2, \dots)$. Depending on the decomposition of $k(\pi_1, \pi_2, \dots)$ derived from the indicators of step 2.1 (Fig. 7d), the regression is performed on each of the factorizable functions. Power laws are processed first by linear regression in logarithmic planes. Functions that cannot be expressed by power laws are approximated by polynomial functions using least squares regression.
- The second uses y data directly (outputs of step 1.2, Fig. 5): this nonlinear regression is initialized with results of the first regression and minimizes relative errors thanks to the lsqnonlin function of Matlab.

Finally a comparison of the two regression functions with respect to the initial data y can validate the quality of these regressions.

3.3. Example with a test function

A purely numerical example will help to illustrate and detail the various steps of the process described in Section 3.2. This test function, which uses the form of Eq. (20), is:

$$y = \pi_1^{-1} (4 + 5\pi_2\pi_3)\pi_4^3 L^{2+0.1\pi_2} \tag{22}$$

A numerical uniformly distributed noise can be added to y data in order to test the robustness of the process to the possible computer noise of design codes or to variations due to neglected phenomena. For the first numerical application, this noise is set to +/-1% of y data. The different stages of regression, shown from Figs. 8–11, are:

- Step 1.1, the generation of a design of experiments: L with 4 levels between 1 and 10^4 and each parameter π_i with 3 levels between respectively .5 and 2, 1 and 10, 2 and 7, 1 and 10. The number of simulations and data y is $4.3^4 = 324$.
- Step 1.3, the y data projection: The straight lines (cf. Fig. 8) imply the power law nature of the relationship. For the example of Fig. 8, the slope a is equal to 3. The deviation from a power law is expressed by a quality indicator, $\text{std}(a)/\text{mean}(a)$ as explained in 3.2.1, which has the value of 0.24% and also

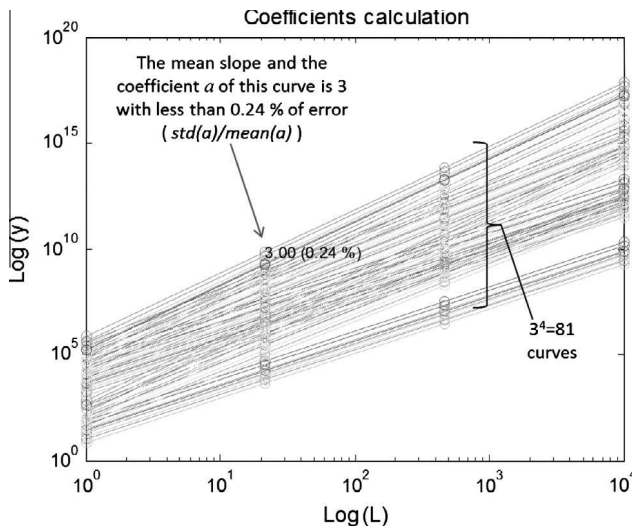


Fig. 8. Power law coefficients calculation for the test function.

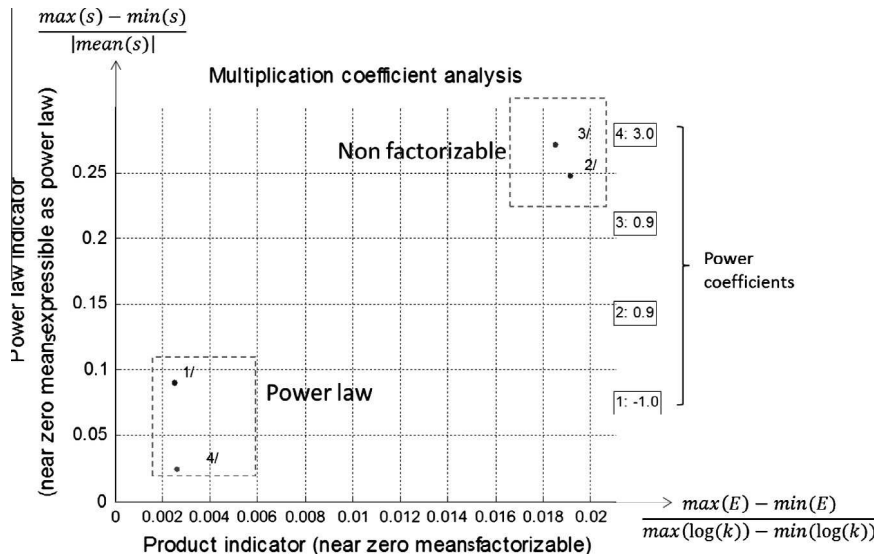


Fig. 9. Form analysis of multiplication coefficient k for the test function.

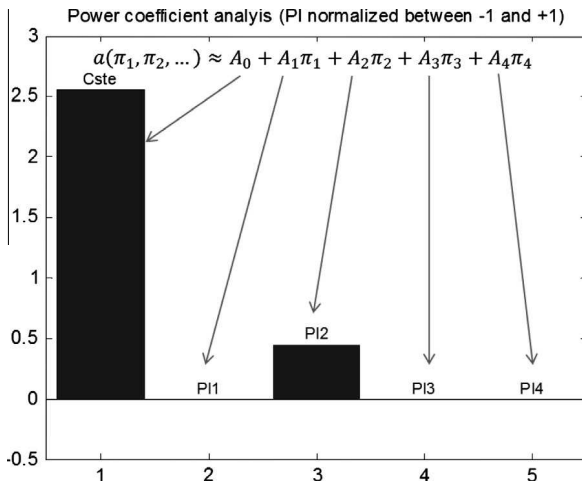


Fig. 10. Sensitivity analysis for the power coefficient a of the test function.

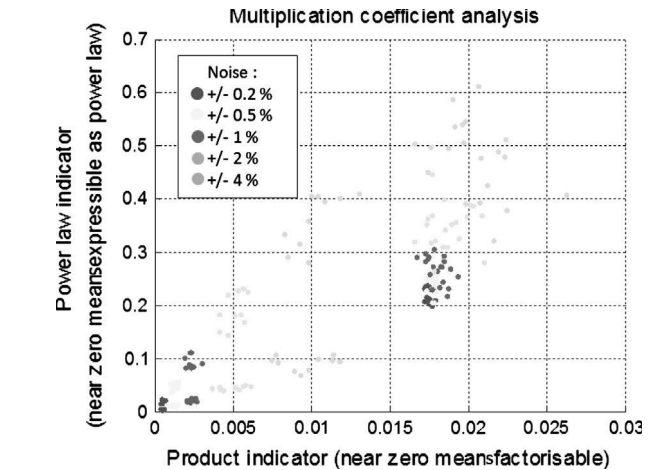
appears in Fig. 8. Without the parameter L the remaining design of experiments now has $3^4 = 81$ values for each parameter a and k .

- Step 2, a study of the general shape of the function: Fig. 9 shows the analysis (step 2.1) of the possible form for the function $k(\pi_1, \pi_2, \dots)$. From indicators presented in Fig. 7 and Section 3.2.2, it follows that the parameters π_1 and π_4 are suitable for factorization using power laws. Fig. 10 illustrates the sensitivity analysis (step 2.2) to determine parameters influencing the evolution of the a coefficient. Only the parameter π_2 has to be kept here. We thus select an equation with the following form:

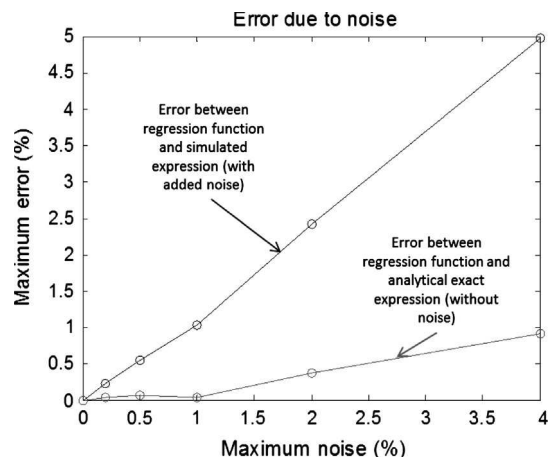
$$y = k(\pi_1, \pi_2, \dots) L^{a(\pi_1, \pi_2, \dots)} = k'(\pi_2, \pi_3) \pi_1^{a_1} \pi_4^{a_4} L^{a(\pi_2)} \quad (23)$$

with $k'(\pi_2, \pi_3)$ and $a(\pi_2)$ second order polynomial functions.

- Step 3, the construction of the metamodel based on functions forms selected in the previous step: functions $k'(\pi_2, \pi_3)$ and $a(\pi_2)$ will be approximated by polynomial function. The first regression allows functions $k(\pi_1, \pi_2, \dots)$ and $a(\pi_1, \pi_2, \dots)$ to be obtained independently by a log plane study (for the power law) or linear regression (for the other function). This first regression (step 3.1) gives:



(a) Effect of noise on step 2.1



(b) Effect of noise on step 3

Fig. 11. Noise effect on indicator map and final regression quality.

$$y = (4.84 - 0.14\pi_2 - 0.37\pi_3 + 5.01\pi_2\pi_3 + 0.01\pi_2^2 + 0.03\pi_2^2)\pi_1^{-0.99}\pi_4^3 L^{(2+0.10\pi_2)} \quad (24)$$

The second non-linear regression (step 3.2) working directly on y and π_i data enables us to find:

$$y = (3.988 + 0.002\pi_2 + 0.002\pi_3 + 5.001\pi_2\pi_3)\pi_1^{-1}\pi_4^3L^{(2+0.10\pi_2)} \quad (25)$$

For the 2 regressions, the mean square error minimizes the relative and not the absolute errors. The regression quality check shows that less than 1% of error is achieved with Eq. (25). Without noise, exact relationship is found directly with the first and second regression.

Even though numerical simulations are deterministic, errors may exist due to simplifications of the mathematical model or systematic errors of the numerical scheme. To quantify the effect of errors on the proposed process more precisely, we assume here that the error is similar to white noise of amplitude proportional to the quantity of interest y . The calculation process was repeated for different values of maximum noise: 0.2%, 0.5%, 1%, 2% and 4%. Fig. 9 shows the results of step 2.1 and 3.3 for these different levels. Fig. 11a) was plotted with 10 runs for each noise level. Fig. 11b) quantifies the maximum error found between the expression and the simulation results (with noise) or the pure analytical formula (without noise). From these results we can conclude that:

- Step 3 (regression), with its two regression sub-steps, is quite robust to noise and even decreases the influence of noises.
- Step 2.1 (determination of the shape of the coefficient k) is more sensitive to noise but allows the form of the function to be distinguished for noise levels less than $\pm 2\%$. The FEM simulations should therefore have a meshing quality sufficient to allow for this step.

3.4. Comparison with other analysis and regression methods

Ref. [16] gives a classification of the different approximation techniques according to 3 criteria: the type of doe, the choice of model and the model fitting approach. Here, the proposed meta-modeling approach is based on:

- A full factorial DoE with logarithmic distribution of levels distribution for the main dimension L parameter.

- A model choice based on scaling laws and power laws.
- A fitting approach using mainly linear and non-linear least square regression based on a projection of the data on scaling law coefficients.

Classic regression procedures generally start with a screening step mainly focusing on selection of the input parameters. The process assumes that this selection has been performed thanks to a previous sensitivity analysis or the designer's knowledge. Preliminary analysis, here, is devoted to determining the exact form of the model. Indicators and a graphical synthesis, similar to the Morris method [30], have been proposed for this purpose.

Compared to the classical meta-modeling approaches (polynomial, kriging, radial basis functions, etc.) the advantage of the method proposed here lies mainly in its physical justification, demonstrated here by using the Buckingham theorem. A recent review about dimensional analysis and pi-theorem illustrated by an example of application to the modeling of a Flexible Manufacturing System can be found in [21]. Some other authors [31–33] have also used this theorem with the main objective of reducing the number of parameters to be handled by polynomial regressions. Other authors [34] have used dimensional analysis to determine constraints on power law regressions. Their approach, like other approaches solely based on dimensional analysis, however requires handling of all the parameters representing the dimensions and physical properties. Moreover, the scaling laws employed are pure power laws without the possibility of using other functions to express multipliers or power coefficients.

The approach proposed here does not directly use dimensional analysis but the particular form of the functions representing the physical characteristics of a component subjected to a change in size in the case of particular similarities. Previous studies [35,20] on similarity have also worked on the development of models valid in the case of non-similarities (called distorted models) but have not been applied to numerical simulations within a general framework. The possibility of keeping constant the ratios of some of the dimensions reduces the complexity of representation of the detailed design models. A compact model is then obtained with only the relevant design parameters for the design of mechatronic

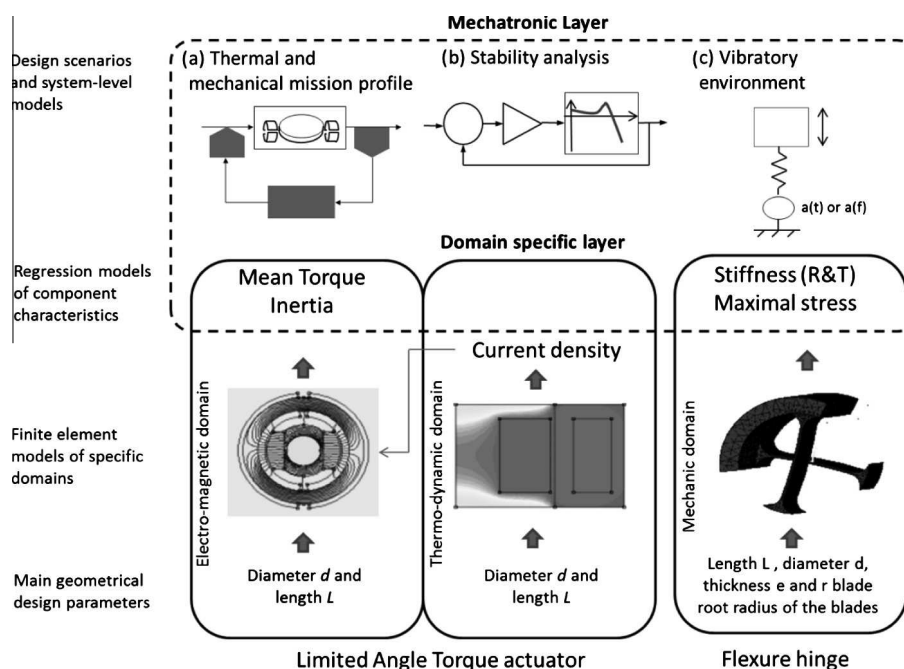
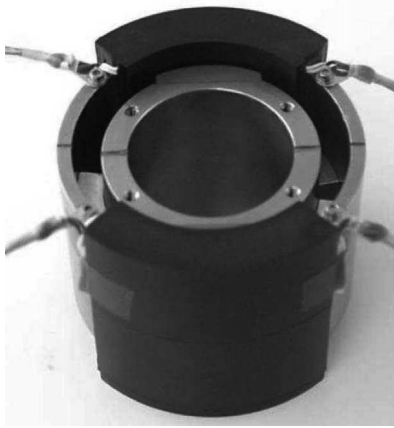
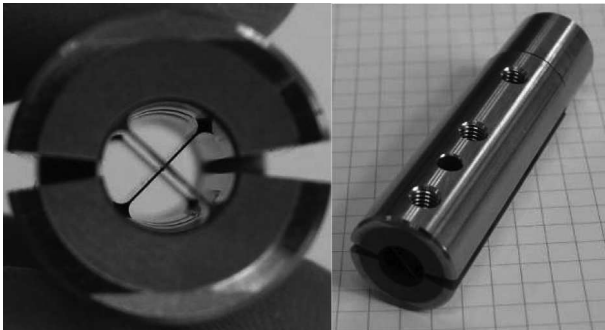


Fig. 12. Estimation models: interface between mechatronic and domain specific layers.



(a) Limited Angle Torque (LAT) actuator (source : [37]): thermal and electromagnetic domains



(b) Flexural hinge (source [38]): mechanical domain

Fig. 13. Mechatronic component from different domains.

layer without having to handle all the parameters of the detailed design.

4. Case studies

The objective here is to illustrate the proposed regression process on mechatronic components from different domains. The main focus is placed on the illustration of the regression process and not to on the complete design study of a system. Ref. [10] presents a methodology for the optimal preliminary design of electro-mechanical actuators using a model-based approach with different types of models (estimation, simulation, evaluation and meta-model).

The components considered are:

- An electromagnetic limited angle actuator [36], as shown in Fig. 13a from [37], which illustrates the thermal and electromagnetic domains.
- A flexural hinge composed of thin blades, as shown in Fig. 13b from [38], which illustrates the structural and mechanical domains.

The regression process could be applied to other types of motor, such as a brushless motor or a voice coil actuator [39], other flexural hinge [39,38] or any other physical mechatronic components. These 2 components associated with a mirror, a position sensor and control electronic could be used to build up a scanning mechanism [40]. The overall design of such mechatronic systems requires consideration of the various constraints that have a direct impact on the size of the components. These design constraints may come from different types of specifications:

- Performance specifications, particularly in terms of motion range, accuracy or bandwidth: the motion is linked to the rotational stiffness of the hinge and to the torque capability of the LAT actuator; the accuracy and the bandwidth are linked with resonance modes, which depend on the inertia and stiffness of components.
- Endurance specifications, particularly in terms of life time and resistance to extreme stresses: the flexural link should be used at stress levels consistent with these specifications.

These two points are influenced by the environmental mechanical stress (vibration, acceleration) or thermal stress (a function of the type of heat transfer and the ambient temperature). Embedded applications add constraints of integration (size, volume or mass). All these constraints can be represented (Fig. 12) by design scenarios such as:

- (a) Thermal and mechanical mission profiles: these mission profiles are representative of the movement of the mirror during scanning. These time simulations can be used to calculate the average electromagnetic torque developed by the LAT. One can note that there exists a coupling of this torque with the rotational stiffness of flexural hinges.
- (b) Stability analysis: the transfer function of the overall multi-physic system can be used to estimate the closed loop performance especially in terms of bandwidth and stability margins. The indicators will be significantly influenced by the rotational resonance modes.
- (c) Vibratory environment: transient or frequential profiles for acceleration at the support can be used to represent the aggressive vibratory environment. The transverse or longitudinal modes of resonance are all influenced by the transverse or longitudinal stiffness of the flexible pivots and the mass of components.

To manage all these constraints and iterate quickly between mechatronic and domain specific layers during preliminary sizing, it may be interesting to have estimation models expressing, for example:

- For the LAT actuator, torque or inertia depending on the dimensions.
- For the flexure hinge, stiffness (in translation or in rotation), maximal stress depending on the dimensions.

The following paragraphs show how these models can be obtained using the regression process presented in this article. The results of scaling-law-based metamodels are compared to polynomial approximations [24] or Radial Basis Functions (RBF) [41] and kriging [27].

4.1. Limited angle actuator study

The objective here was to illustrate how it is possible to link the continuous torque T to the main dimensions, the length, L , and the diameter, d , of the actuator. All radial dimensions were geometrically similar to d . With such a choice, one has two design parameters influencing significantly the torque and inertia of the actuator, two main characteristics for the system level design, without representing all dimensional parameters used during the component level design. The desired equation thus took the following form:

$$T = f(L, \pi_1) = k(\pi_1)L^{\alpha(\pi_1)} \text{ with } \pi_1 = \frac{d}{L} \quad (26)$$

The design code, to which the regressions were applied, was set up using two 2D finite element simulations (Fig. 14) with FEMM soft-

ware [42]. A first thermal simulation found the permissible current density J for static continuous operation. The thermal environment was modeled by convective heat transfer between the periphery of the actuator and the environment. A second electromagnetic simulation used the previously calculated current density in order to obtain the continuous torque.

Several cases illustrate the regression method:

- The winding was moulded with or without a potting resin that ensured better conductive thermal transfer. This point addressed the effect of assumption c. (Section 3.1). An equivalent thermal conductivity of copper and resin or air was deduced from a homogenization of the winding [43,44].
- Two DoE for different ranges were used to test the robustness and validity of the regressions obtained outside their original design. The two DoE had 4 levels for L and 6 levels for π_1 which led to 24 experiments. The difference between the DoE came from their range: for L , [20;60] mm for the first DoE and [10;100] mm for the second, and for π_1 , [0.5;2.5] for the first DoE and [0.1;5] for the second.

Fig. 15 illustrates the step 2.1 of the process for the cases of winding with or without potting. In the case of winding with potting, the power coefficient varies between 3.42 and 3.49. Without potting, this coefficient varies between 3.23 and 3.48. The 2 cases have a power coefficient varying between 3.5 (demonstrated in Section 3.2), characteristic of purely convective thermal transfer, and 3, characteristic of a purely conductive thermal transfer. A coil without potting is naturally more influenced by the conductive effect. For both cases, it was interesting not to consider parameter $\alpha(\pi_1)$ as a constant.

Next, the proposed approach was applied to a winding with potting. The form of the scaling-law-based metamodel (SLAWMM) was:

$$T = k(\pi_1)L^{\alpha(\pi_1)} = c_1\pi_1^{c_2}L^{c_3+c_4\pi_1+c_5\pi_1^2} \quad (27)$$

It was compared to three other approximations depending on the two design variables L and d : a 3rd order polynomial response surface (RSM) [24], a Gaussian Radial Basis Function (RBF) [41] and a kriging approximation [26]. The polynomial functions were built with the same DoE as the scaling-law-based metamodels. The RBF and kriging approximations were built with a specific DoE: a latin hypercube (LHC) with the same range and number of experiments as the scaling-law-based metamodels, in this case 24. The polynomial regression, RBF and kriging functions were obtained with L and d parameters and not with L and π_1 which would not have been such a good choice. The least square regression for polynomial functions has minimized the relative error and not the absolute error in order to avoid gross errors on small actuators. The Gaussian width factor of RBF was chosen by minimizing a cross validation error

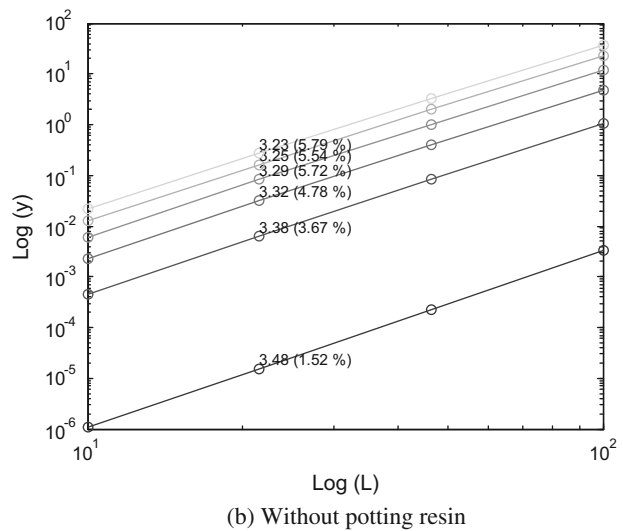
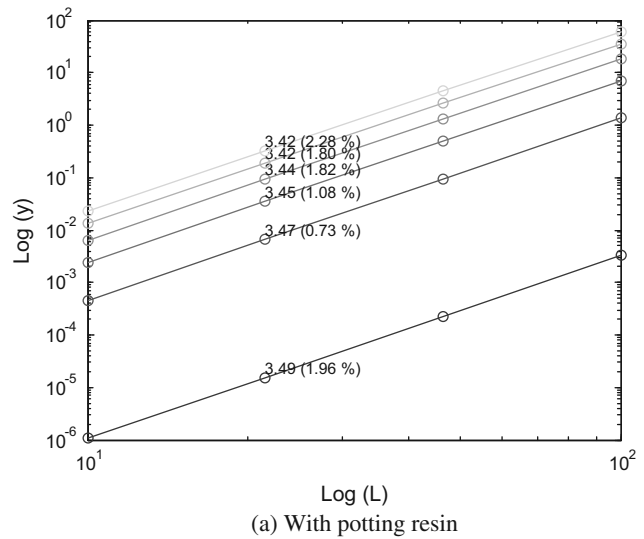


Fig. 15. Effect of conductive thermal transfer on the power coefficient.

[41]. The kriging approximation used a quadratic regression model and a Gaussian correlation function.

Fig. 16 illustrates step 3.3, the model quality check, of the regression process. These validations were performed by comparing the 48 simulated results, 24 for the SLAWMM DoE and 24 for the LHC DoE, with the estimated results using each metamodel. Each approximation was thus tested with 24 configurations of the initial DoE that served for their construction and 24 other con-

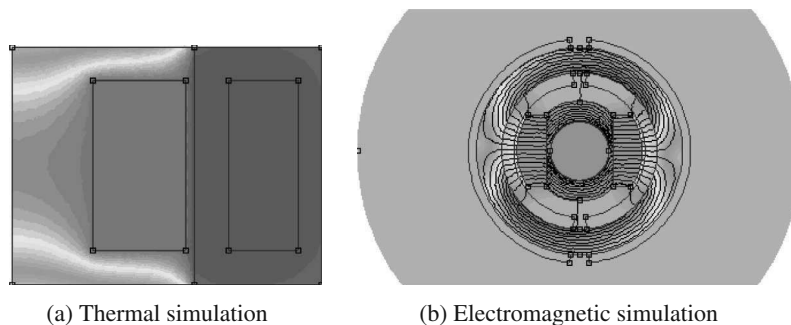


Fig. 14. 2D finite element simulations of the LAT actuator.

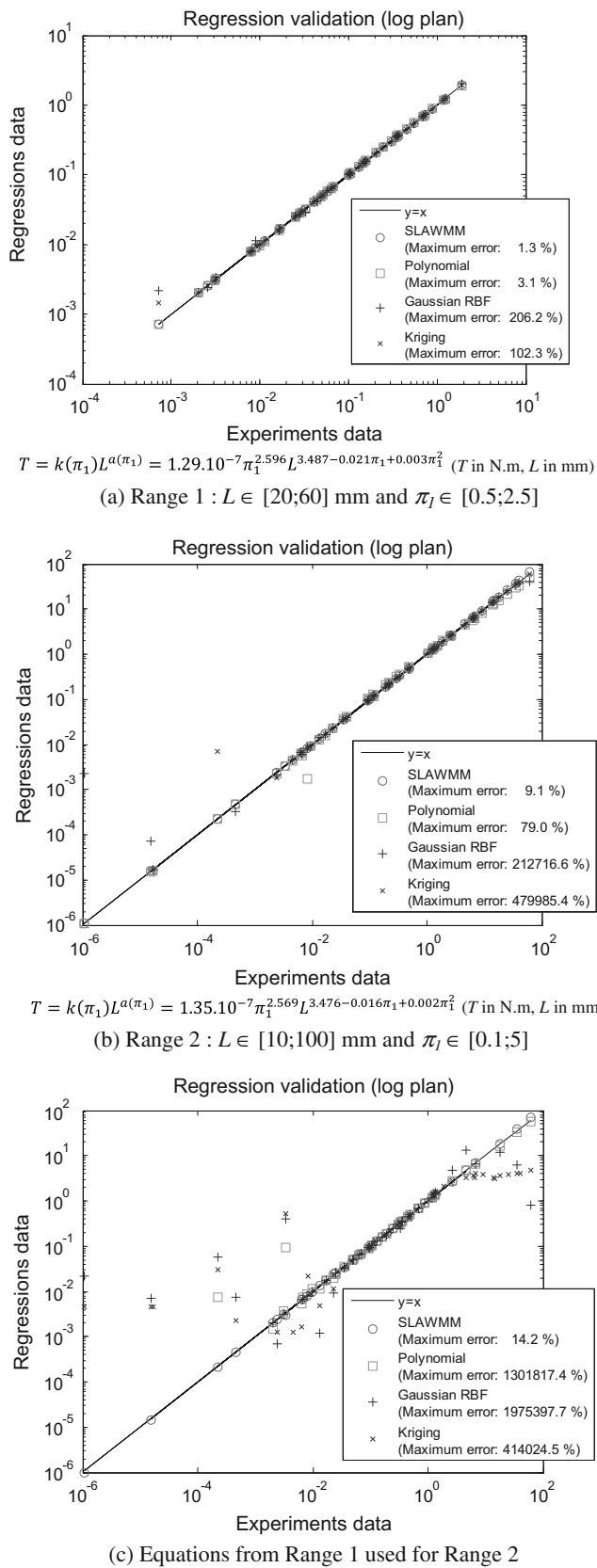


Fig. 16. Quality check of the regressions for different range of study.

figurations within the same range. Note that the DoE using range 2 was much wider than when using range 1, leading to four additional orders of magnitude of variations on the output quantity

that was being approximated. In all cases (range 1 and range 2), the scaling-law-based metamodells (SLAWMM) showed good prediction qualities: less than 2% and 10% of maximum error for the range 1 (Fig. 16a) and range 2 (Fig. 16b) regression. The expressions obtained for Eq. (18) differ slightly between the 2 ranges (see figure captions). Polynomial approximations, on the other hand, even with twice number of coefficients to be determined, showed a larger maximum error: 3% (Fig. 16a) and 79% (Fig. 16b) for range 1 and 2 respectively. For range 2, the maximum error was 18.5% at the points of the DoE used for polynomial response surface construction but increases to 79% with the 24 configurations of the DoE that did not serve for its construction (predictive capability). Radial basis functions and kriging led to even worse results. These two metamodells had difficulty in coping with the very wide range of variation of the output quantity, which led, in particular to large errors for very small values.

When the predictive capability of metamodells was assessed by testing them at points well outside their construction bounds, regression-based scaling laws remained valid (less than 15% error in Fig. 16c). Gaussian RBF and kriging functions, with their high flexibility enabling a multiple peaks surface response to be represented, were at a disadvantage in this case of fairly monotonous surfaces: they could give very poor results at points involving large extrapolation. All three classic regression techniques (RSM, RBF and kriging) gave very poor results, even negative torque for small actuators, when they were used well outside the points that served for their construction (equations of range 1 used into range 2 as illustrated in Fig. 16c).

Power law forms are thus interesting as “structural components” for the specific metamodells of sizing problems where geometrical dimensions can have a wide range of variation. This robustness property can be important when conducting explorative design studies in areas not originally planned. As the regression form has a physical basis, some coefficients can be fixed after a first complete study. For example, the c_3 coefficient of Eq. (27) can be fixed at 3.5 (see section 3.2) and future FEM simulations with different configurations have to find just 4 coefficients (c_1, c_2, c_4 and c_5) with a reduced size DOE.

4.2. Flexural hinge study

The objective here was to illustrate how it is possible to link the rotational stiffness, K_r , to the main dimensions: L the length, d the diameter, e the thickness, and r the blade root radius (Fig. 17a) of a flexural hinge composed of 2 thin blades of titanium alloy. The desired equation thus took the following form:

$$K_r = f(d, \pi_1, \pi_2, \pi_3) = k(\pi_1, \pi_2, \pi_3) d^{\alpha(\pi_1, \pi_2, \pi_3)} \text{ with } \pi_1 = \frac{r}{d}, \pi_2 = \frac{e}{d} \text{ and } \pi_3 = \frac{L}{d} \quad (28)$$

The design code, to which the regressions were applied, is set up using a 3D finite element simulation (Fig. 17b) with ANSYS software [45]. This static analysis gave the angular deflection for a given torque on the hinge, which, by ratio, gave the rotational stiffness. The meta-modeling process was applied to this data K_r , but could also have been applied to other quantities of interest for the design, such as the stress-to-deflection ratio or the radial stiffness. This regression problem involves more parameters than the previous application example and allows us to illustrate the interest of the multiplication coefficient form analysis (step 2.1 of the process given in Fig. 5).

The DoE used had 4 levels for L and 3 levels for each π_i parameters. The range studied was: $d \in [5;50]$ mm, $\pi_1 \in [0.05;0.015]$, $\pi_2 \in [0.01;0.04]$ and $\pi_3 \in [0.5;2]$. As illustrated by the result of step 2.1 (Fig. 18), the power coefficient a was

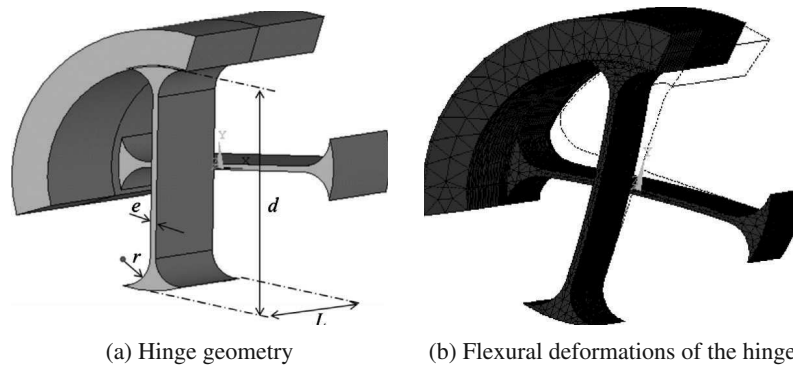


Fig. 17. Geometry of the flexible hinge (2 blades).

constant and equal to 3 for any π_i parameters configurations. Thus, only one physical phenomenon drove the evolution of the rotational stiffness: the elasticity of the material. Fig. 19, the result of step 2.1, shows that the influence of π_2 and π_3 parameters can be modeled by power laws expressions. The form of the π_1 function cannot be a power law and was modeled here by a polynomial response surface here. The form of the scaling-law-based metamodel was be thus:

$$K_r = (c_0 + c_1\pi_1 + c_2\pi_1^2)\pi_2^3\pi_3^4d^3 \quad (29)$$

The regressions results were (with K_r in N m/rad and d in m):

$$K_r = (1.93 \cdot 10^{10} + 3.10 \cdot 10^{10}\pi_1 + 2.30 \cdot 10^{11}\pi_1^2)\pi_2^{2.96}\pi_3^{1.05}d^3 \quad (30)$$

for the first one, where regression was carried out with a and k data (see step 3 Section 3.2.3).

$$K_r = (1.93 \cdot 10^{10} + 3.10 \cdot 10^2\pi_1 + 2.30 \cdot 10^{11}\pi_1^2)\pi_2^3\pi_3^4d^3 \quad (31)$$

for the second one, carried out on the y data with a least squares fit (see step 3 Section 3.2.3).

For the last regression, powers of π_2 and π_3 parameters were set to 3 and 1 respectively. Eq. (31) presents a simple form that can be handled and implemented in different calculation tools. As shown in Fig. 20, the relative error is controlled for a wide range of results with a maximum error of less than 15%. These results are com-

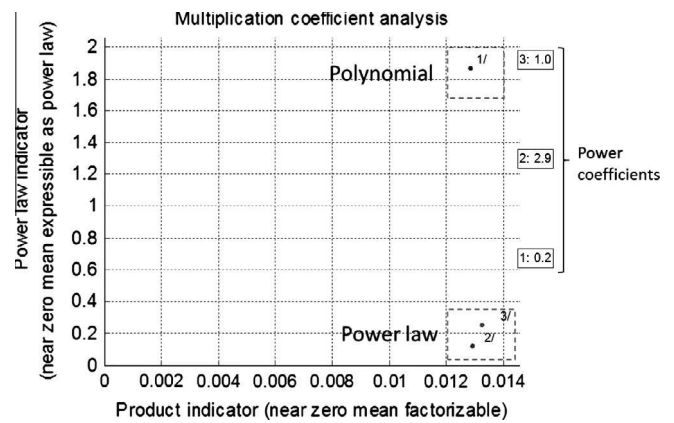


Fig. 19. Multiplication coefficient form analysis.

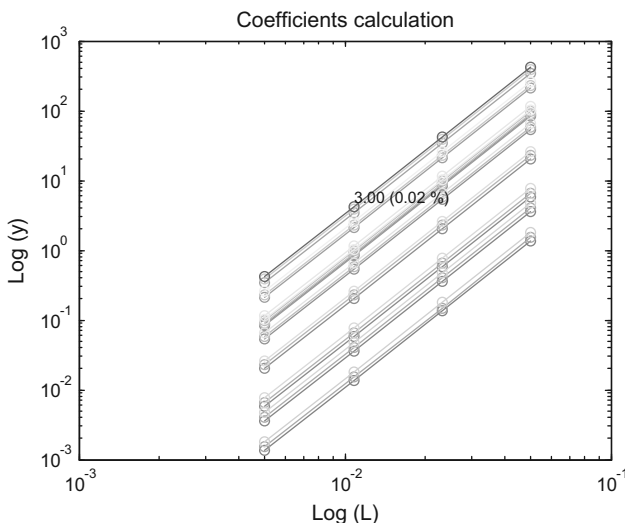


Fig. 18. Scaling laws with geometrical similarity.

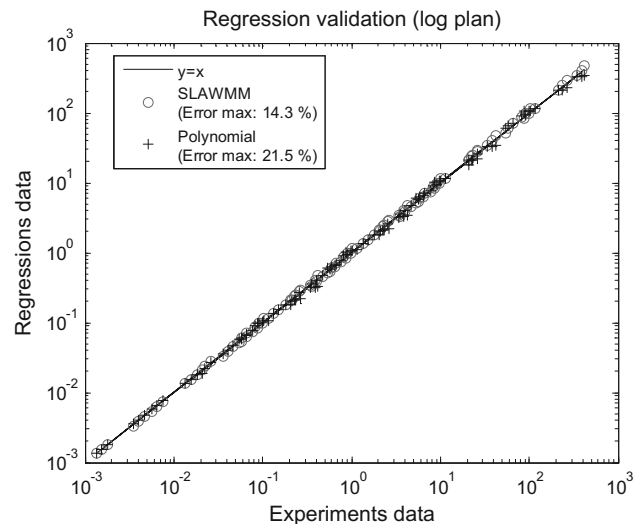


Fig. 20. Quality check of the regressions.

pared to a 3rd order polynomial function here, which was the metamodel that performed the least poorly of the three alternatives (polynomial response surface, radial basis function, kriging) in the previous application example. The expression of the polynomial response surface required the determination of a large number of parameters: 26 parameters compared to 5 for the proposed form, and showed a maximum error of 21%. The scaling-law-based metamodel allows light and compact models to be

obtained, which can be easily integrated into other design algorithms.

5. Conclusion

The design of mechatronic systems requires estimation models to make the link between the design details of each component and the overall design of the system. The article has shown that scaling laws possess interesting properties for performing this role during the sizing tasks. A demonstration of the criteria for obtaining these scaling laws with the Buckingham theorem highlighted the assumptions required for this work. Two of these assumptions, geometric similarity and the uniqueness of the design criteria, limit the generality of their use. A method was proposed to overcome these limitations and generalize the form of scaling laws. The process of regression adapted to this form was described and validated on various examples. The regressions obtained were compared to classical metamodelling and showed the interest of the physical basis of scaling-law-based metamodelling for preliminary sizing of mechatronic components: their shape is easy to handle while remaining valid over a wide range of sizes, even for prediction or extrapolation purposes. The proposed form of regression can be applied to various fields encountered in mechatronic systems and is illustrated here by simulations on thermal, electromagnetic and mechanical examples.

References

- [1] VDI-Richtlinien. Design methodology for mechatronic systems. VDI, Düsseldorf.
- [2] Auslander DM. What is mechatronics? *IEEE/ASME Trans Mechatron* 1996;1(1):5–9.
- [3] Van der Auweraer H, Anthonis J, De Bruyne S, Leuridan J. Virtual engineering at work: the challenges for designing mechatronic products. *Eng Comput* 2013;29:389–408.
- [4] Hehenberger P, Poltschak F, Zeman K, Amrhein W. Hierarchical design models in the mechatronic product development process of synchronous machines. *Mechatronics* 2010;20:864–75.
- [5] Cellier F, Greifeneder J. Continuous system modeling. Springer, Ed.; 1991.
- [6] Roos F, Johansson H, Wikander J. Optimal selection of motor and gearhead in mechatronic applications. *Mechatronics* 2006;16(1):63–72.
- [7] Raymer DP. Aircraft design: a conceptual approach, 4th ed.. AIAA Education Series; 2006.
- [8] Budinger M, Liscouët J, Hospital F, Maré J-C. Estimation models for the preliminary design of electromechanical actuators. *Proc Inst Mech Eng, Part G: J Aerosp Eng* 2012;226(3):243–59.
- [9] Liscouët J, Budinger M, Maré J-C, Orieux S. Modelling approach for the simulation-based preliminary design of power transmissions. *Mech Mach Theor* 2011;46(3):276–89.
- [10] Budinger M, Reysset R, El Halabi T, Vasiliu C, Mare JC. Optimal preliminary design of electromechanical actuators. In: *Proc IMechE Part G: J Aerosp Eng*. To be published.
- [11] Gomis-Bellmunt O, Campanile F, Galceran-Arellano S, Montesinos-Miracle D, Rull-Duran J. Hydraulic actuator modeling for optimization of mechatronic and adaptronic systems. *Mechatronics* 2008;18(10):634–40.
- [12] Gomis-Bellmunt O, Galceran-Arellano S, Sudrià-Andreu A, Montesinos-Miracle D, Campanile LF. Linear electromagnetic actuator modeling for optimization of mechatronic and adaptronic systems. *Mechatronics* 2007;17(23):153–63.
- [13] Pahl G, Beitz W. Engineering design: a systematic approach. Springer, Ed.; 2007.
- [14] Bialecki R, Kassab A, Fic A. Proper orthogonal decomposition and modal analysis for acceleration of transient FEM thermal analysis. *Int J Numer Methods Eng* 2005;62:774–97.
- [15] Ryckelynck D, Chinesta F, Cueto E, Ammar A. On the a priori model reduction: overview and recent developments. *Arch Comput Methods Eng* 2006;13(1):91–128.
- [16] Simpson T, Peplinski J, Koch P, Allen J. Metamodels for computer-based engineering design: survey and recommendations. *Eng Comput* 2001;17:129–50.
- [17] Chung S-U et al. Design and experimental validation of doubly salient permanent magnet linear synchronous motor for precision position control. *Mechatronics* 2013.
- [18] Chinesta F et al. PGD-based computational vademecum for efficient design, optimization and control. *Arch Comput Methods Eng* 2013;20(1):31–59.
- [19] Taylor ES. Dimensional analysis for engineers. Oxford University Press; 1974.
- [20] Murphy G. Similitude in engineering. New York: The Ronald press company; 1950.
- [21] Miragliotta G. The power of dimensional analysis in production systems design. *Int J Prod Econ* 2011;131:175–82.
- [22] Pfenning M, Thielecke F, Carl UB. Recent advances towards an integrated and optimized design of high-lift actuation systems. *SAE Int J Aerosp* 2010;3(1):55–64. <http://dx.doi.org/10.4271/2009-01-3217>, 2010.
- [23] Petersheim MD, Brennan SN. Scaling of hybrid-electric vehicle power train components for hardware-in-the-loop simulation. *Mechatronics* 2009;19:1078–90.
- [24] Raymond HM, Montgomery DC, Christine MA-C. Response surface methodology: process and product optimization using designed experiments. 4th ed. John Wiley & Sons; 2006.
- [25] Jin R, Chen W, Simpson TW. Comparative studies of metamodelling techniques under multiple modelling criteria. *Struct Multidisc Optim* 2001;23:1–13.
- [26] Stein M. Interpolation of spatial data: some theory for Kriging. New York: Springer; 1999.
- [27] Kleijnen J. Kriging metamodeling in simulation: a review. *Eur J Operat Res* 2009;192(3):707–16.
- [28] Damon R, Harvey W. Experimental design, ANOVA, and regression. New York: Harper & Row; 1987.
- [29] Sobol I. Sensitivity estimates for non-linear mathematical models. *Math Model Comput Exp* 1993;4:407–14.
- [30] Morris MD. Factorial sampling plans for preliminary computational experiments. *Technometrics* 1991;33(2):161–74.
- [31] Gogu C, Haftka RT, Bapanapalli SK, Sankar BV. Dimensionality reduction approach for response surface approximations: application to thermal design. *AIAA J* 2009;47(7):1700–8.
- [32] Vignaux GA, Scott JL. Simplifying regression models using dimensional analysis. *Austral & New Zealand J Statist* 1999;41:31–41.
- [33] Lacey D, Steele C. The use of dimensional analysis to augment design of experiments for optimization and robustification. *J Eng Des* 2006;17(1):55–73.
- [34] Mendez P, Ordóñez F. Scaling laws from statistical data and dimensional analysis. *J Appl Mech* 2005;72(5):648–58.
- [35] Young DF. Basic principles and concepts of model analysis. *Exp Mech* 1971;11(4):325–36.
- [36] Tsai C, Lin S, Huang H, Cheng Y. Design and control of a brushless DC limited-angle torque motor with its application to fuel control of small-scale gas turbine engines. *Mechatronics* 2009;19:29–41.
- [37] Bencheikh N, Le Letty R, Claeysen F, Magnac G, Migliorero G. Limited angle torque actuator for fine angular positioning. In: *Proc 12th Int Conf New Actuat. Actuatur 2010. Germany: Bremen, 14–16 June, 2010*; 2010.
- [38] Santos I, Ortiz de Zárate I, Migliorero G. High accuracy flexural hinge development. In: *Proc 11th Eur Space Mech Tribol Symp. ESMATS 2005, 21–23 September 2005. Switzerland: Lucerne*; 2005.
- [39] Zhou Q, Ben-Tzvi P, Fan D, Goldenberg AA. Design of fast steering mirror systems for precision laser beams steering. In: *Robot Sens Environ, 2008. ROSE 2008. International Workshop on, October; 2008*. p. 144–9.
- [40] Vinals J, et al. MTG scan mechanism predevelopment: design & performance. In: *14th Eur Space Mech Tribol Symp. ESMATS 2011, Constance, Germany, 28–30 September 2011*; 2011.
- [41] Forrester A, Söbester A, Keane AJ. Engineering design via surrogate modelling: a practical guide. J. Wiley; 2008.
- [42] Meeker D. Finite element method magnetics software. www.femm.info.
- [43] Idoughi L, Mininger X, Bouillault F, Bernard L, Hoang E. Thermal model with winding homogenization and FIT discretization for stator slot. *IEEE Trans Magn* 2011;47(12):4822–6.
- [44] Perrins WT, McKenzie DR, McPhedran RC. Transport properties of regular arrays of cylinders. *Proc R Soc Lond* 1979;A 369:207–25.
- [45] ANSYS. www.ansys.com.

Chapter 5 – Design graphs for sizing procedures and optimization problems definition

ABSTRACT

This last chapter focuses on the proper combination of the previous models to develop sizing and optimization procedures. The state of the art on tools and methods available for design and optimization is reviewed. A first category of methods and tools, known as Multi-Disciplinary Optimization (MDO), uses Design of Experiments, Metamodels and Optimization algorithms on numerical models. A second category uses constraint networks and graphs theory to represent the constraints and the links between algebraic models. The chapter exemplifies how to use these methods together with graphical tools. These design graphs can be used pedagogically to introduce students to the design. They can also be implemented by algorithms to help the designer in cases of more complex devices. The associated paper, entitled "Optimal preliminary design of electromechanical actuators" and published in the Aerospace Science and Technology journal, show how to implement the different types of models (estimation, simulation and evaluation models) and to combine them into a process dedicated for design and optimization.

Keywords: sizing procedure, optimization problem, graph theory, matching problem.

TABLE OF CONTENTS

1.	From models to optimal preliminary design of mechatronic systems	119
1.1.	Design models and possible association	119
1.2.	Sizing procedure vs optimization.....	119
2.	State of the art	120
2.1.	Design Frameworks	120
2.2.	Sizing procedure representations.....	123
3.	Sizing procedure definition and design graph	127
3.1.	Objectives	127
3.2.	Input and outputs of an optimization problem	127
3.3.	Ordering methodology and process	128
3.4.	“Design Graph”: Sizing procedure synthesis through graphical manipulations	129
3.5.	“Graph Size”: Sizing procedure synthesis through algorithmic manipulations.....	131
3.6.	Typical problems	133
4.	Conclusion.....	140
5.	Bibliography.....	141

NOTATION

Acronyms

BFS	Breadth First Search	N ² D	N square diagram
DFS	Depth First Search	SCC	Strong Connected Component
DSM	Design Structure Matrix	SIL	Software In the Loop
EMA	Electro Mechanical Actuator	0D/1D	Lumped parameter model
HIL	Hardware In the Loop	2D/3D	Distributed parameter model
H&K	Hopcroft & Karp		
KBE	Knowledge Based Engineering		
MDO	Multi Disciplinary Optimization		

1. FROM MODELS TO OPTIMAL PRELIMINARY DESIGN OF MECHATRONIC SYSTEMS

This chapter is dedicated to the generation of sizing procedures used during the preliminary optimal sizing of physical parts of mechatronic systems. The inputs are the objectives and design constraints coming from the specifications document or the chosen architecture. As output, specifications for components (rod end, roller or ball screw, gear reducer, brushless motor ...) are generated in order to obtain an assembled actuation system that fully meets the requirements. The objective is not to design the components in detail, but to specify each of them as well as possible, taking all design scenarios into account.

1.1. Design models and possible association

The previous chapters have presented the different types of models required for the analysis and synthesis of a mechatronic system. These models establish links and constraints between the specifications of the overall system and the component characteristics to be selected. The models (chapters 1-4) can be implemented in different types of environment and decision making can be achieved by different optimization methods. Figure 1 illustrates three different options.

The first one implements all the models in a computer algebra environment (Matlab, Excel). The design and optimization performed in the same environment. This solution does not address time transient phenomena problems. However, it has the advantage of being very suitable for taking multiple design criteria into account and providing fast optimization. Examples of such implementation are presented in [1] [2] and [3].

The second one implements all the models in a simulation environment for algebraic differential equations (e.g. Modelica) and the optimization is performed by external MDO software [4]. This solution allows fine simulation models with time transients to be managed. Examples of such implementation are given in [5] and [6]. However, one main drawback is the optimization times, which can become very long. In addition, some design scenarios may not be represented by system simulation models.

The third one is a mix of the first two first solutions and can be achieved with a compact representation of time-consuming temporal simulations or FEM simulation using meta-modeling techniques [7]. This solution makes it easy to manage multiple design criteria and to obtain a reasonable optimization time. This is the solution that will be developed in this chapter.

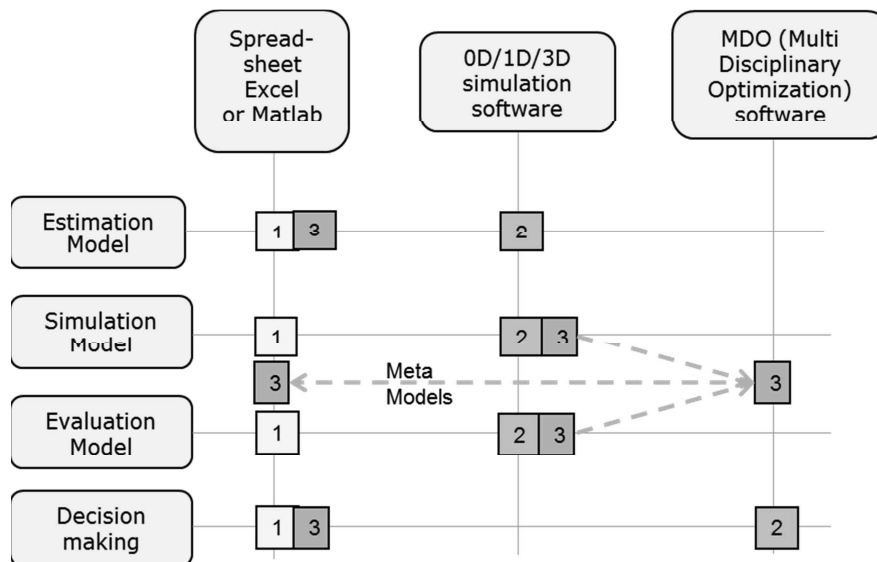


Figure 1 - Models implementations and associations

1.2. Sizing procedure vs optimization

Generally the engineering models enable the designer to determine the opposite relationship to those desired during sizing, i.e. calculate the performance of the system (which is required by the specification) from the characteristics of components (which are sought during sizing). In the third case of Figure 1, all representative models of the design can be reduced to a set of algebraic equations that can be manipulated in order to solve this inverse problem. There are essentially two types of solutions to the problem:

- selection or sizing procedures, a judicious succession of calculations and tests, which determine the main characteristics of components to select.
- optimization algorithms that minimize the difference between desired and achieved performance by changing the main characteristics of components.

In this chapter, we seek to make joint use of these two approaches (procedures and optimization). Part 2 of this chapter will present the state of the art in tools implementing these two solutions or their associations and the different ways of representing a design procedure. Part 3 will then show the typical problems encountered in the implementation of a design procedure. We will focus on their resolution using simple graphical means or using algorithms from graph theory. The different approaches and issues will finally be illustrated with simple examples.

2. STATE OF THE ART

2.1. Design Frameworks

Once the physical system is defined, the various components and the control scheme can be integrated virtually thanks powerful, complete and connectable engineering platforms : 0D-1D simulation, co-simulation with multi-body simulation, rapid prototyping, HIL, SIL, reduced models from finite elements, etc. More details about virtual prototyping are available in reference [8]. Here, we focus on the software tools usable during the physical system conceptual synthesis phase.

Industrial sizing tools

During synthesis steps, the designer of mechatronic systems may use, industrial component design or selection tools. A first category takes the form of sizing tools based on engineering standards. Figure 2 illustrates the example of MIT Calc [9] which proposes a set of Excel sheets devoted to the design of mechanical components such as reducers, couplings, and so on. These tools are more usable by specialists of specific domains than by designers of mechatronic systems as the coded calculations are more oriented towards analysis and validation and require the definition of a large number of technological and dimensional parameters.

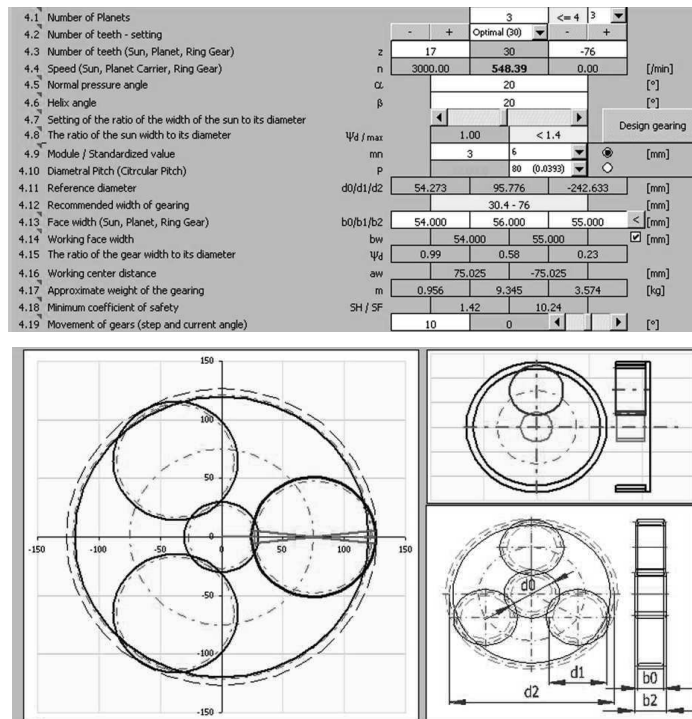


Figure 2 - Geometrical and strength design and validation of epicyclic gearing with MIT Calc [9]

A second category includes selection procedures proposed by some manufacturers of components. Figure 4 illustrates the sequence of calculations and tests proposed by Harmonic Drive to select a gearhead in their ranges [10]. These procedures need catalogue' data, the access to which needs to be automated for an optimization process. Although these sizing procedures highlight the key design drivers of the components,

they may have to be adapted or modified to reflect specificities of the overall system and to better integrate the overall design process.

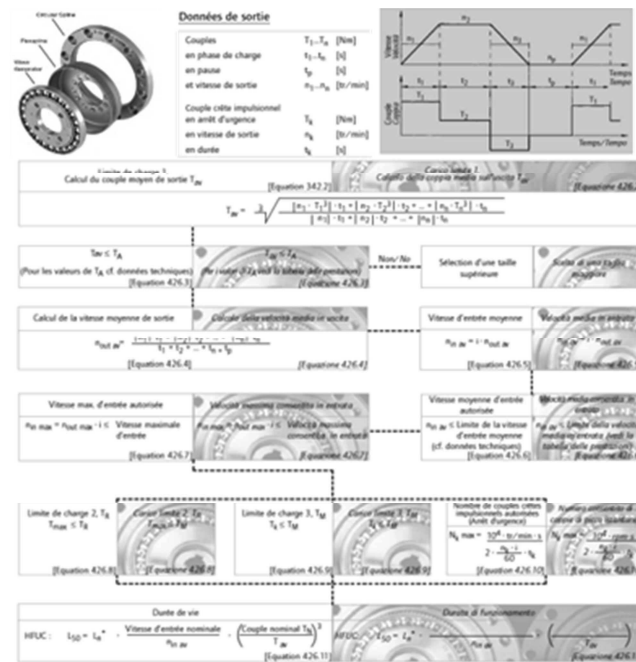


Figure 3 – Example of a gearhead selection procedure (Harmonic Drive)

A final category takes the form of selection tools for mechatronic assemblies intended for the industrial field such as reducers, motors and inverters. Often offered by solution providers [11], some tools, such as Servosoft [12], shown in Figure 4, are independent. They are characterized by a large database, load and mission profile definition, sizing variable calculation and selection of components with filters on given criteria. Architectures are modifiable according to a given, reduced set of topologies. The optimization capabilities are weak and selection criteria or modelling capabilities are devoted to industrial applications, so cannot always match specific applications.

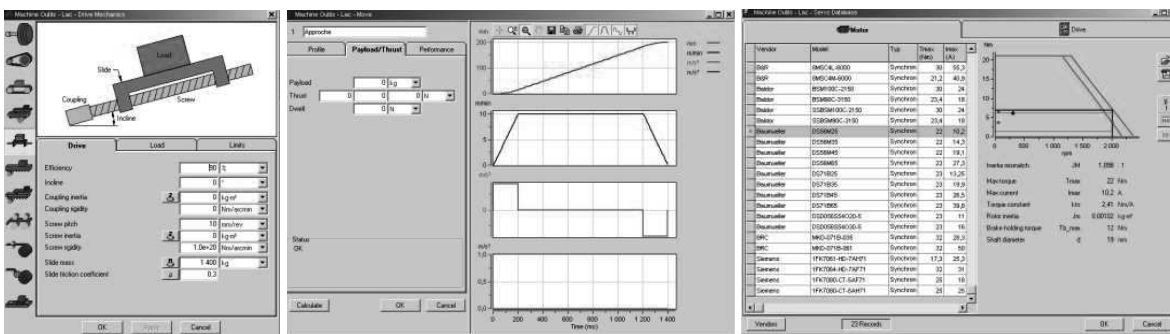


Figure 4 – Sizing of servo systems (Servosoft) [12]

Although these tools are interesting by their technological content, they are too rigid or incomplete to satisfy the design objectives set.

Multidisciplinary Design Optimization (MDO) frameworks

Another category of tools comes from Multi-disciplinary Design Optimization (MDO) [4]. MDO is a field of engineering that uses statistical and optimization methods to solve design problems incorporating all relevant disciplines represented by 2D/3D FEM analyses, 0D/1D simulations and algebraic calculations simultaneously. Each specific computation is considered as a black box which can be called directly, analysed with design of experiments (DoE), and represented with surrogate or meta-models. All calculations can be linked together and used for design exploration, sensitivity, optimization and robustness analyses.

iSight [13], Optimus [14], modeFRONTIER [15] are examples of such frameworks. Figure 5 gives an overview of the Optimus environment.

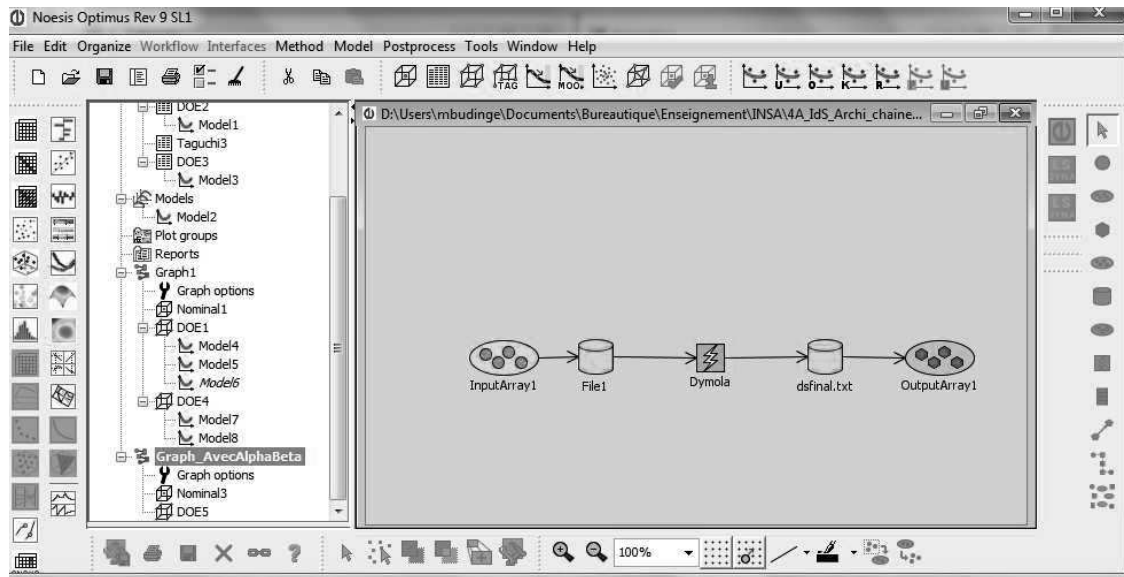


Figure 5 – Optimus MDO framework

These optimization and statistical enabling tools allow the steps of the design process to be linked in a freely chosen sequence. They do not, however, provide help in choosing how the connections in the calculations are structured, or which parameters are to be taken into account as design parameters, constraints or objectives.

Knowledge Based Engineering (KBE) and component based frameworks

Knowledge Based Engineering (KBE) is a discipline combining knowledge-based approaches and computer aided design. The KBE software packages are dedicated to centralizing all the know-how and expertise for the design of a specific product. Scientific concepts and methodologies used in these environments are:

- Knowledge bases and computer-aided design: the knowledge of the components is capitalized with unoriented algebraic equations (declarative approach) [16]. These components can be easily assembled to describe different architectures.
- Constraint networks, graph theory and optimization: the set of equations initially defined in declarative form is oriented in order to obtain a calculation procedure usable by an optimization algorithm.

The adaptation or analysis of the equations may be supported by symbolic computations, interval calculations or artificial intelligence. These KBE tools can be:

- linked to a CAD software as in Genus Designer [16] which captures the configuration rules and performs process automation for Solidworks ;
- dedicated to a specific domain as in Enventive [17] for the conceptual design of planar mechanisms (optimization, tolerance, sensitivity analysis) ;
- developed over several domains, as in the case for FST institute software (TUHH university) which, from the same basis, supports the preliminary design of lift mechanisms [18], hydraulic networks [19] and EMA of aircraft. Figure 6 illustrates the general process and gives an example of a graphical user interface.
- General, such as TKSolver [20], Ascend [21], Cades [22], Design sheet [23], Design 43 [24] or PaceLab suite [25]. Figure 7 illustrates the graphical user interface of TKSolver, a declarative language that enables a set of algebraic equations to be used with different inputs depending on the design objectives.

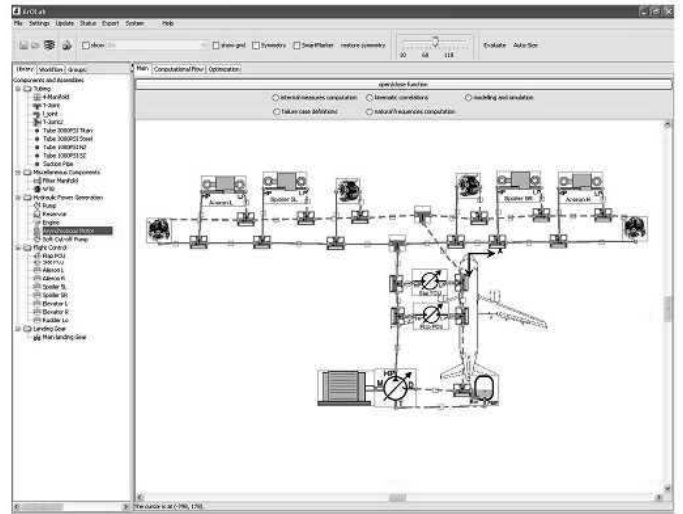
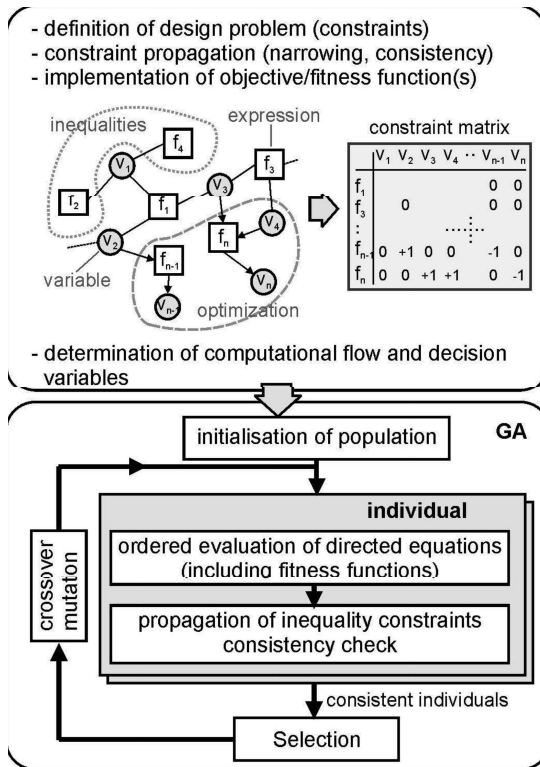


Figure 6 – New computer-aided methods for preliminary architecting and sizing of lift and hydraulic systems [18] [19]

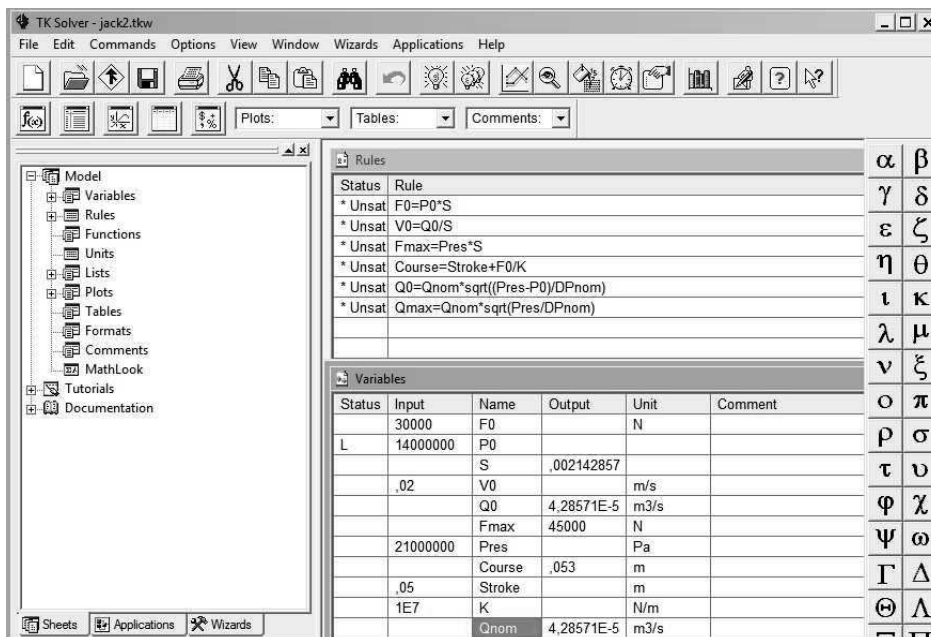


Figure 7 – Declarative TK Solver framework

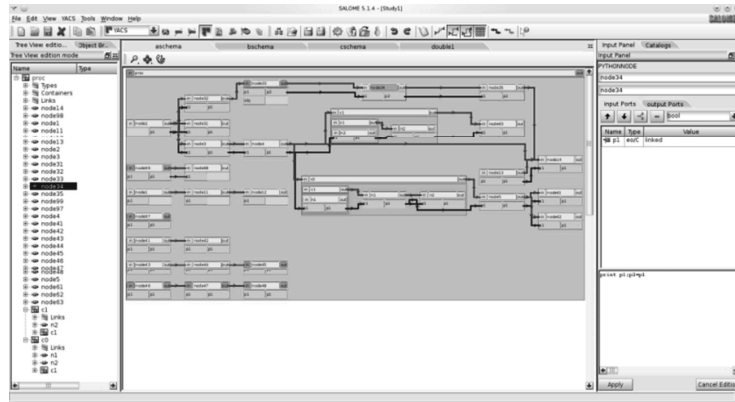
These tools can provide an interesting and important help for the designer especially when the system becomes complex with multiple technologies. Paired with MDO tools, they might represent the future of the design of mechatronic systems.

2.2. Sizing procedure representations

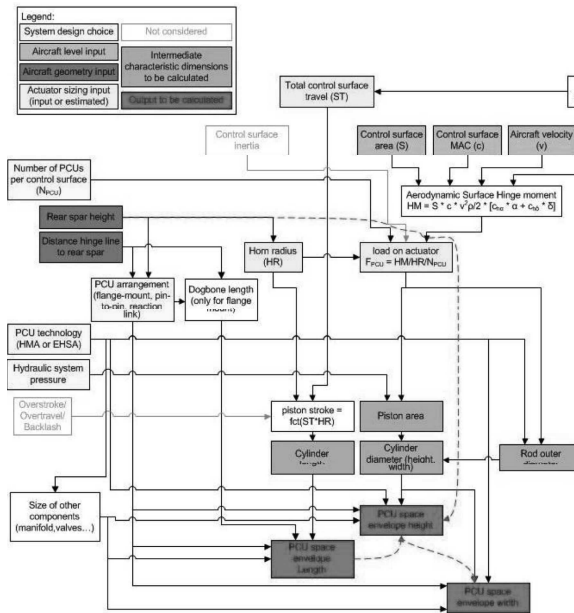
The sizing procedure can be considered as a major part of the whole preliminary sizing process. When the problem is complex, with numerous interactions between components of various fields (mechanical, electrical, etc.), methods for the representation and analysis of such interactions become valuable. We will focus here, on the representation methods.

Causal diagram

The causal diagram is a graphical tool representing the causal relationships between variables. It is, in fact an oriented graph representing a calculation scheme. Figure 2 gives examples of causal diagrams used in the Salome platform for the Pre- and Post-Processing of numerical simulations [26] or for a space envelope estimation performed by [27].



a) Yacs editor of Salome platform [26]



b) Space envelope estimation for aerospace application [27]

Figure 8 – Causal diagram examples

With a causal diagram, the couplings between the different entities can be difficult to visualize. A major problem is that of algebraic loops, which is well known in industrial processes where Excel spread-sheets bring together component sizing procedures that must not present circular reference errors (i.e. loops) such as $y=f(x)$ and $x=g(y)$. Several solutions are possible: reject the possibility of such loopbacks in the construction of the causal diagram [28], solve all the coupled equations (this analytical solution is not always possible even with a symbolic maths package) analytically, solve these equations using a numerical solver. For the latter, two implementations are possible. In the first, the numerical solver used is internal to the calculation procedure and its computer support. This sizing procedure is difficult to export to other optimization or calculation tools, however. For the second implementation, the code generated, which corresponds to the sizing procedure, postpones the task of numerical solver to the optimization algorithm. It is then necessary to add design parameters and additional constraints in the optimization problem to manage these algebraic loops.

N² diagrams

The N²D formalisms were introduced in the 1970s by the system engineer Robert J. Lano [29]. N is the number of entities considered. This diagram is a causal diagram where the graphical entities (blocks) and interactions (arrows) are dictated by an organization convention as shown in Figure 9. The inputs of the blocks are represented by vertical arrows while the outputs must be horizontal arrows. This display provides a quick visual summary of the organization of the system studied. In particular, the couplings and algebraic loops between blocks are easily identifiable, for example, Figure 9, when a block "2" provides an input to block "3" and block "3" provides an input to block "2".

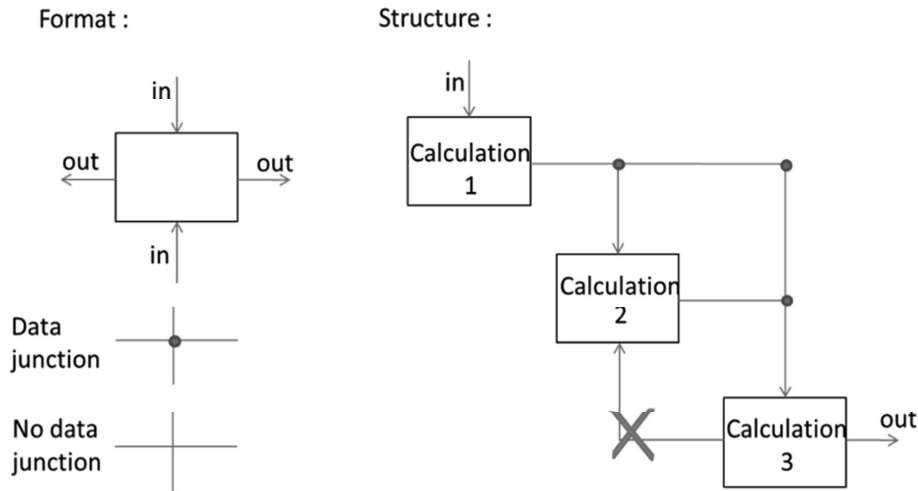


Figure 9 – N² diagram principle

DSM matrixes

A Design Structure Matrix or Dependency Structure Matrix (DSM) is the adjacency matrix of an N²D. The DSM, as its name implies, is a matrix representing links or information exchanges which can be used at various levels: working group, system level, component level [30]. It draws dependency between entities, parameters, etc. In the example of Figure 10, a cross located at row 'i' and column 'j' means parameter/task 'i' depends on parameter/task 'j'. This highlights links between the front and rear piston sizes, meaning that if two different teams are working on those two tasks they will share information. This will be called strong connected components later. In this representation, a perfect sequence is represented by a lower triangular matrix, while an upper box that is non-empty represents a feedback loop.

	1	2	3	4	5	6	7	8	9	10	11	12	13
1 CUSTOMER REQUMENTS	(X)												
2 SYSTEM LEVEL PARAM'S	X	(X)											
3 WHEEL TORQUE		X	(X)										
4 PISTON - FRONT SIZE		X	X	(X)	X								
6 PISTON - REAR SIZE		X	X	X	(X)								
6 PEDAL MECH. ADVANT.	X	X		X	X	(X)			X	X			
7 LINING COEFF. - REAR		X		X	X	X	(X)		X	X			
8 LINING COEFF. - FRT.		X		X	X	X	X	(X)	X	X			
9 BOOSTER REACT. RATIO		X	X	X	X	X	X	X	(X)	X			
10 ROTOR DIAMETER	X	X	X	X	X	X	X	X	X	(X)			
11 BOOSTER - MAX STROKE									X		(X)		
12 CALIPER COMPLIANCE		X		X		X			X			(X)	
13 ABS MODULATOR DISPL.												X	(X)

Figure 10 – DSM applied to automotive brake system design [31]

Graphs and dependency matrixes

Finally, a sizing procedure is quite similar to a constraint network [32][34] where sizing parameters represent variables and equalities/inequalities represent constraints. Therefore, all the tools applied to the representation of constraint networks and so graph theory, can be applied. Thus, various algorithms applying to graph theory can be integrated into a global calculation ordering method.

In the following sub-parts, different graphical representations will be used. Some of them represent how equations match parameters, in which case both equations (square node) and non-determined parameters (circular node) are represented in a non-oriented graph. Let us take the equation (declarative equation, not imperative assignment) of Figure 11a, to show this representation. Matching is generally represented in what is called a bi-partite graph, Figure 11b, with all the equation nodes on one side and on all all the non-determined parameter nodes on the other side. A matching parameter/equation is then represented by a double-column. Once equations are oriented (one parameter is matched to the equation, i.e. is calculated by the equation), Figure 11c, a simplified graph can be drawn with no more equation nodes.

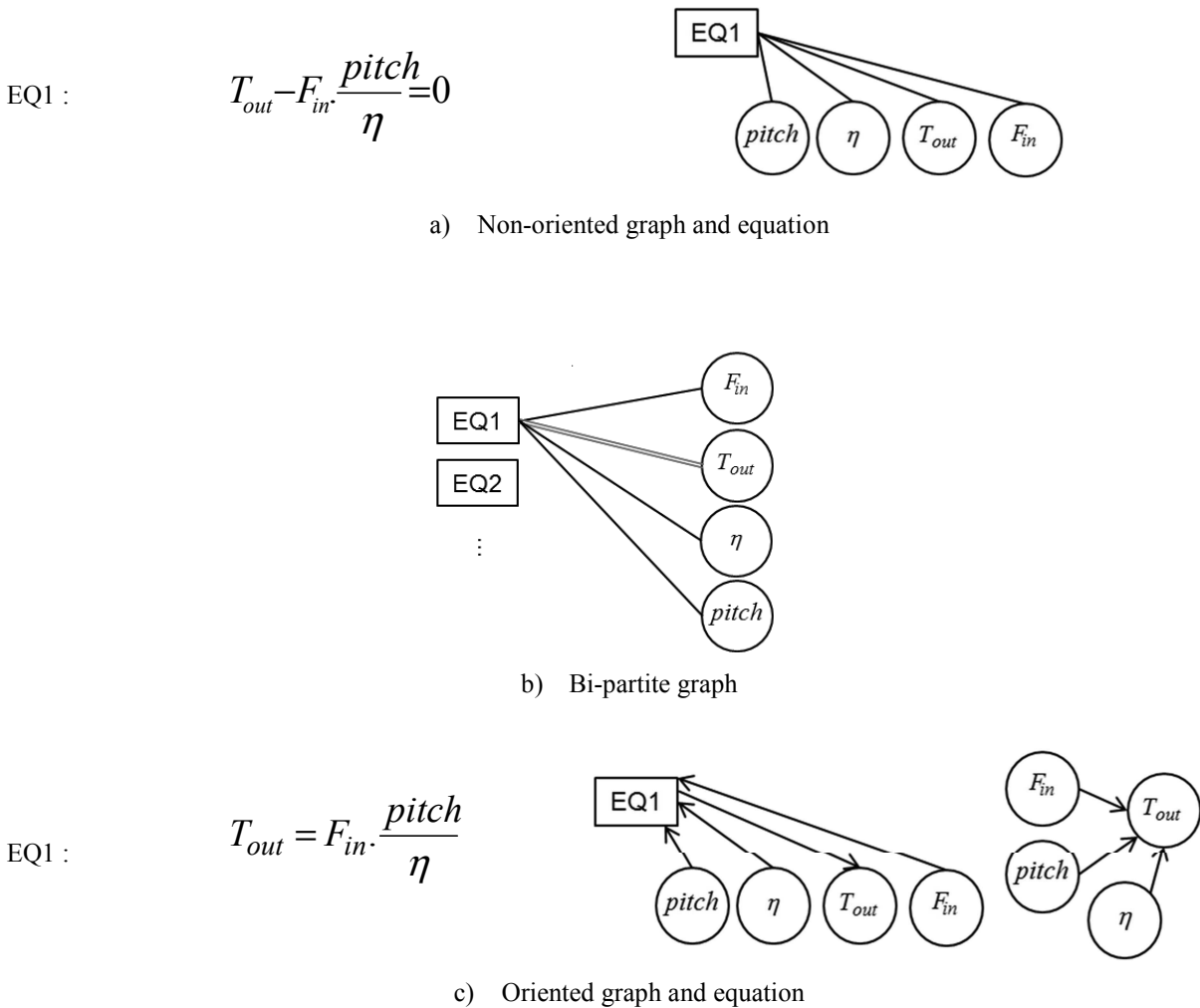


Figure 11 – Graph representations of equation

A set of equations can be represented by a graph or also by a dependency matrix. To understand this concept, let us take a simple mathematical example which is represented by a non-oriented graph as in Figure 12a. In this example, , where ‘y’ is a known parameter and thus is not represented. Once treated, the simple problem presented below will look like Figure 12b where the sizing sequence is once again represented by a lower triangular matrix.

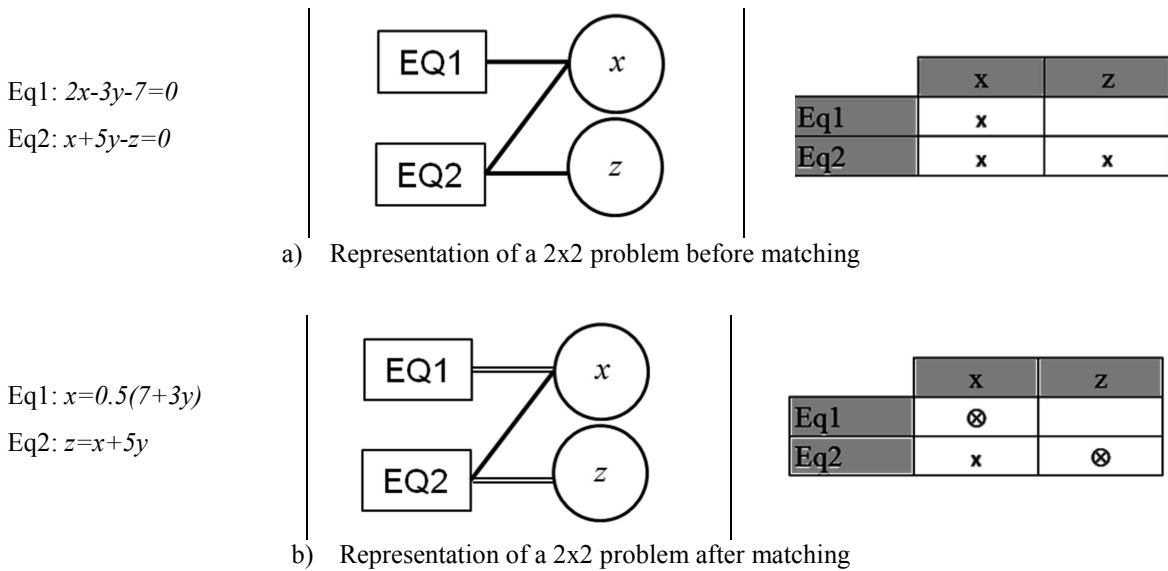


Figure 12 – Matching of a 2x2 problem

3. SIZING PROCEDURE DEFINITION AND DESIGN GRAPH

3.1. Objectives

The set of models presented in the previous chapters (simulation, evaluation and estimation models) can be expressed by algebraic equations or represented with algebraic equations using meta-models. KDE tools can store and use these models according to needs. This section will show how to represent a set of design calculations and how to order flows of information into a sizing procedure. In order to have a well posed sizing procedure that is easy to use in any computing environment, the procedure must be explicit without an internal numerical solver. Section 3.2 presents the typical inputs and outputs of such procedure used in an optimization problem. Section 3.3 describes the proposed methodology and process. Section 3.4 illustrates how to set up a sizing procedure manually using graphical tools. Section 3.5 illustrates a computer implementation using algorithms from graph theory. Section 3.6 identifies the typical possible main problems that may arise on elementary examples.

3.2. Input and outputs of an optimization problem

An optimization problem can be formulated mathematically as follows:

$$\begin{aligned} &\text{Minimize objective function} && f(x) \\ &\text{Subject to equality and inequality constraints} && h(x) = 0, g(x) < 0 \\ &\text{By action on the parameters vector in the range} && x_{low} < x < x_{up} \end{aligned}$$

where:

- the goal is the objective function f ;
- design alternatives are expressed by a set of values assigned to the design variables x within a design domain;
- constraints (h & g) limit the number of alternatives to those satisfying physical principles and design specifications, that is to say feasible design.

The functions (f , g , h) can be explicit or implicit, algebraic or performed by subroutines that solve systems of differential equations iteratively. The goal of this section is to define such functions within a sizing procedure. The calculation steps of the sizing procedure should be time efficient and so only algebraic explicit functions without iteration loops are to be implemented. The number of design parameters x and constraints g and h should also be minimized to reduce the design search space and thus the optimization time.

The optimization problem can be defined only when the sizing procedure is known. To represent it, an influence diagram [33] can be used. For aerospace actuations systems:

- the main design parameters can be internal reduction ratios (roller screw pitch and reducer ratio), integration parameters (anchorage to airframe and transmission to load points), shape of the displacement curve, oversizing coefficient, etc.;
- the main objective is often the total mass obtained by the sum of the masses of all the components estimated through scaling laws;
- the constraints are used to represent some design drivers that cannot be addressed in a direct way by the sizing procedure. Oversizing coefficients to take care of these constraints during optimization.

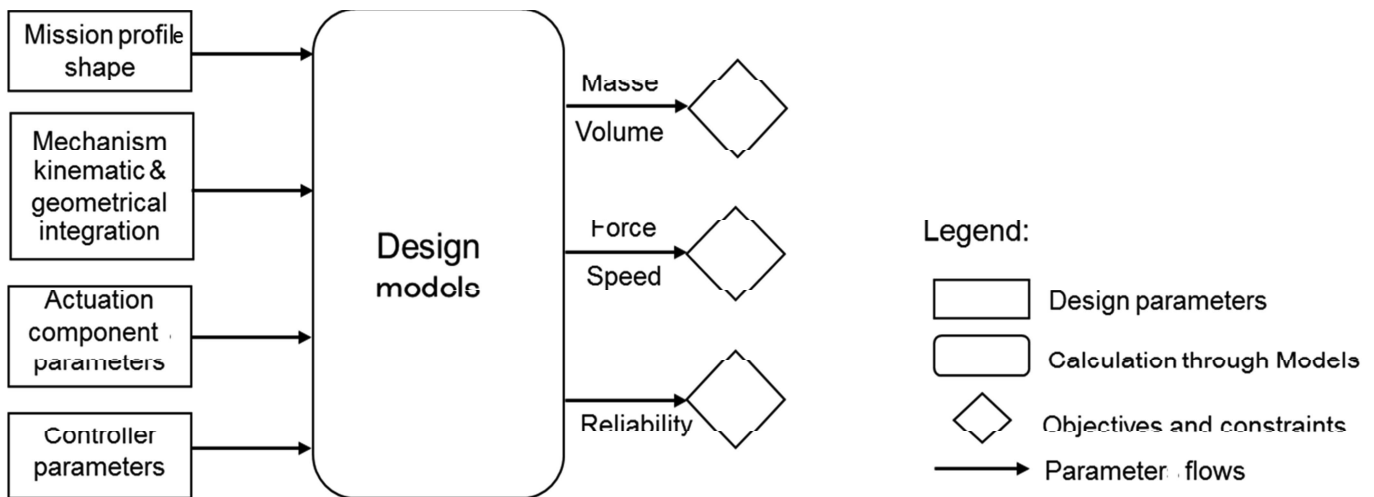


Figure 13 – Influence diagram for optimal design of aerospace actuation systems

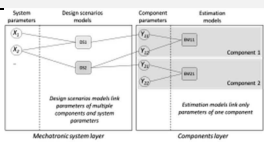
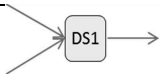
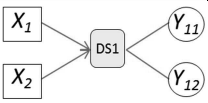
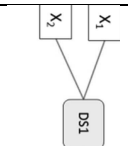
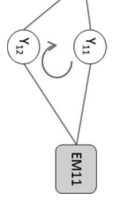
3.3. Ordering methodology and process

The equation ordering methodology is organized in 3 main steps summed up in Table 1: problem definition with equations/inequations and parameters, orientations of these equations (matching problem), treatment of algebraic loops. The implementation of the methods of the process is detailed in the following two sub-sections. This global method helps to reveal additional design parameters and to structure the sizing procedure which can be used by an optimization algorithm.

This process of triangularization may be applied to any type of knowledge represented by a set of algebraic equations and parameters. However, in the case of a mechatronic system, it is possible to distinguish two levels of knowledge:

- a component layer that represents the knowledge of specific domains for each component. This knowledge is represented by parameters (definition, integration, simulation, evaluation) and equations (estimation models of Chapter 1, metamodels of Paper 4) linking these parameters and only those of one component. Each set of equations and parameters is independent component by component and can be thus stored and reused in the form of library.
- a system layer that represents the system-level interactions between components and specifications for any sizing scenario. This layer is made up of all parameters from the specifications and all representative equations for simulation or evaluation models (Chapters 3 and 4). These equations can link characteristics of multiple components from the component layer freely.

Table 1 - Synthesis of the proposed methodology

	Process (« WHATs »)		Methods (« HOWs »)	Tools (implement the «HOWs »)	
				DesignGraph tools (section 3.4)	GraphSize tool (section 3.5)
1	Problem definition	1.1	Gather all the equations/inequalities describing the problem.		Component knowledge in component layer. Design scenario and requirement parameters in mechatronic layer.
2	Orientate the problem	2.1	Match equations/parameters		Hopcroft and Karp algorithm [34]
		2.2	Identify and highlight over-constrained and under-constrained singularities		Dulmage-Mendelsohn decomposition [35]
		2.3	Errors are fixed by the designer manually modifying parameters status (to determined/input) or moving inequalities to constraint while introducing safety factors.		
3	Break problem calculation loops.	3.1	Identify and highlight algebraic loops or strongly connected components (SCC)		Tarjan algorithm [36]
		3.2	Identify and highlight the minimum set of parameters to be fixed in each SCC to suppress calculation loop errors.		Heuristic algorithm [37]
		3.3	Loops are displaced to upper layer manually by the designer.		

3.4. “Design Graph”: Sizing procedure synthesis through graphical manipulations

For design problems characterized by a reduced set of equations, a skilled designer will be able to order design constraints of his area of knowledge quickly and intuitively. It is, however, also possible to represent and order these equations graphically. This graphical representation, called "Design Graph" here, can be used with advantage as a teaching tool with students or as an analysis tool for an engineer in the case of new design scenarios or new technology.

The problem definition, Task 1 of Table 1, is realized with a bipartite graph for each design layer (mechatronic system layer and components layer) as represented in Figure 14 where :

- the parameters are set at mechatronic system layer level from requirements specifications (performance, constraints) and at component layer level by listing the components of the architecture and their main characteristics.
- equations are then introduced to link the different parameters: at mechatronic system layer level with equations representing design scenarios, at component layer level with estimation models.

At this point the relationships between the parameters and equations are represented as non-oriented edges. It is not necessary to express the equations in detail.

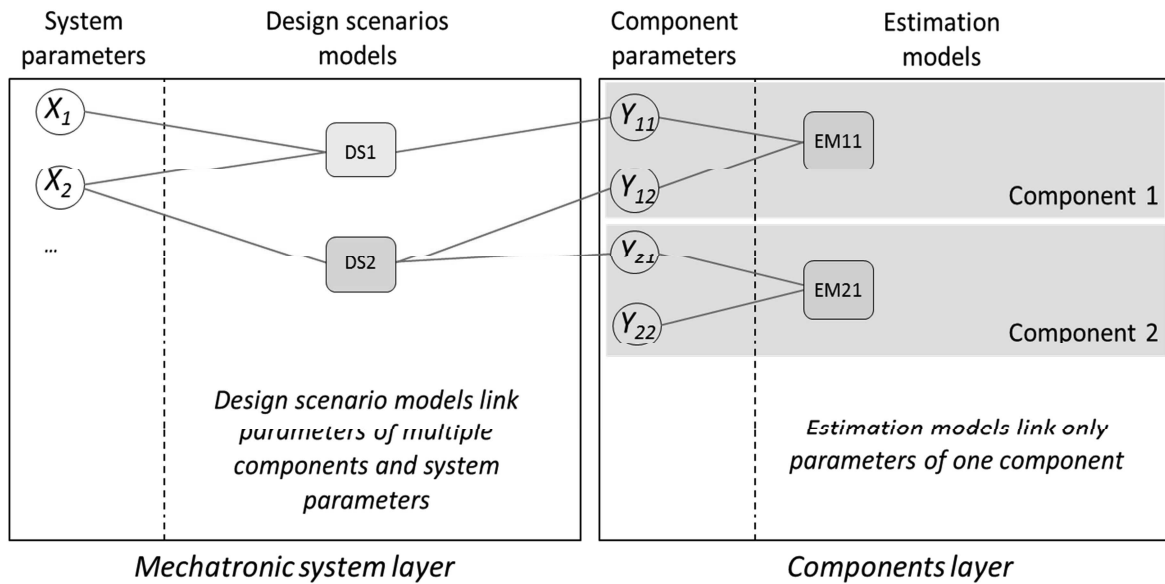


Figure 14 – Component layer and Mechatronic system layer

The orientation of the equations is the next step and corresponds to Task 2 of Table 1. The parameters set by the specifications are selected as inputs for the sizing procedure. Some parameters in the specification may take the form of outputs if the wording of the requirement defines them as an objective to be minimized or maximized or as a maximum or minimum limit constraint to be respected. Figure 15a summarizes the graphical notation that can be taken to represent these parameters in a form approaching an influence diagram (Figure 13) in order to prepare the implementation of the optimization problem.

As an equation can generate only one output, the edges have to be oriented to have only one output per calculation node (Figure 15b). If a given equation remains undetermined for several parameters (Figure 15c), some design assumptions have to be made by stating some parameters as known. These new design parameters can be included in the optimization problem and their optimal value can be determined via the optimization algorithm. A preferred choice for these new design parameters would be parameters participating in a large number of equations (such as reduction ratio) and values defined within a known range (min, max). These assumptions balance the number of equations available and the number of parameters to be determined by the calculation procedure. Example 1 of the section 3.6 illustrates this case of an under-constrained problem.

If several equations of design scenarios have the same output, Figure 15d, the problem may be over-constrained. Two solutions can be applied: adding a safety factor and managing one of the equations as a constraint in the optimization problem, or giving the assignment to the most restrictive equation when direct comparison is possible. Example 1 of the section 3.6 illustrates this case of an over-constrained problem.

The treatment of possible algebraic loops is the last step and corresponds to Task 3 of Table 1. We typically find an algebraic loop when the selection of a component involves the use of characteristics of this same component. This case is represented graphically by a loop involving a design scenario equation and an estimation model equation as shown in Figure 15e. Adding a new design parameter, such as an oversizing coefficient, and a constraint to be checked by the optimization algorithm makes the sizing procedure explicit. Example 3 of the section 3.6 illustrates this case.

At the end of this graphical treatment, the final sequence of equations can be represented as a triangular N^2 diagram or a dependency matrix in order to check that the sequence of equations is explicit.

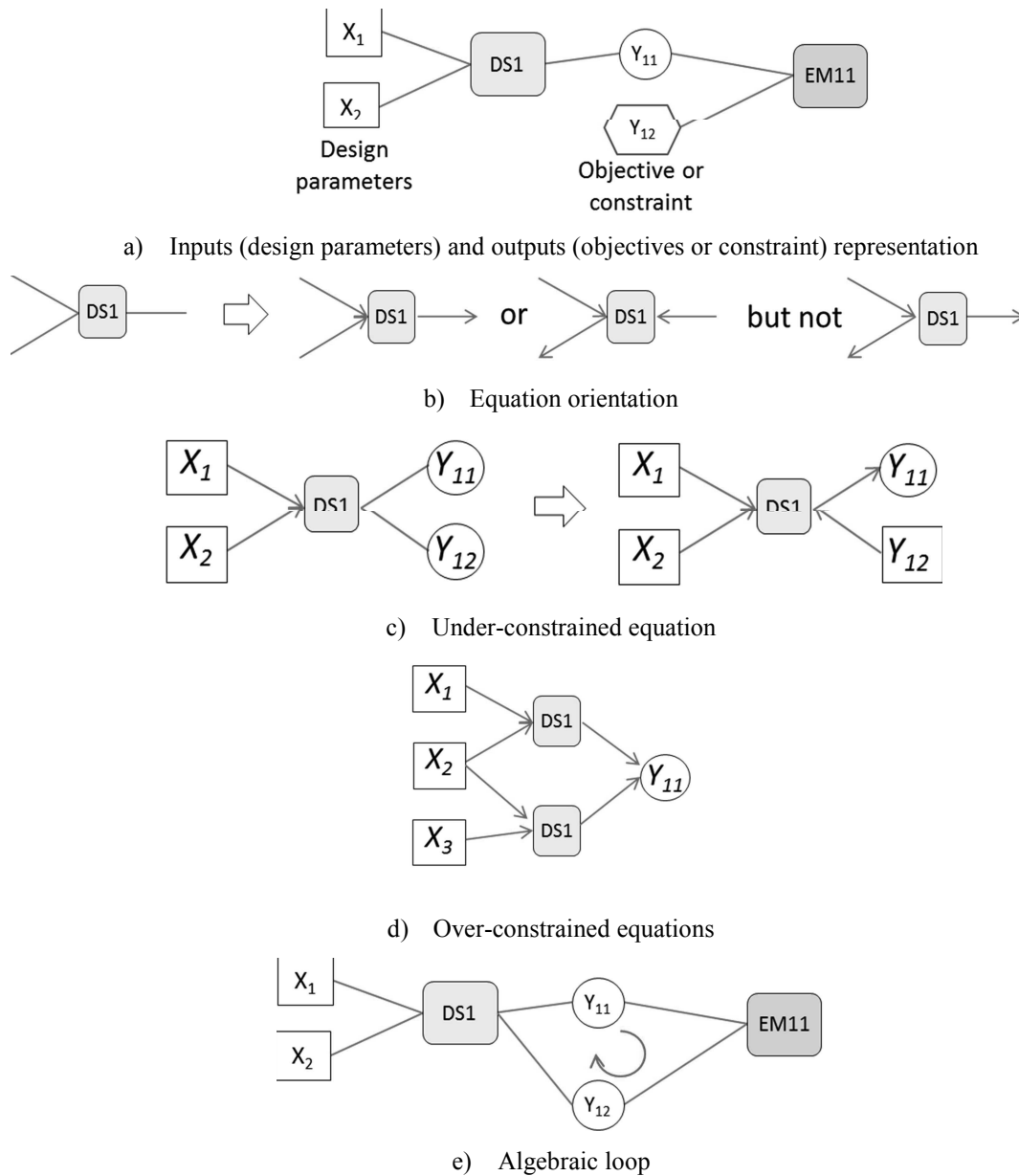


Figure 15 – Graphical orientation of equations

3.5. “Graph Size”: Sizing procedure synthesis through algorithmic manipulations

In the case of a design of a multi-domain product characterized by a large set of equations, it can be difficult for an engineer to pose and order the equations properly in order to establish a design procedure. A computer tool, that can help him in this work, then becomes of interest. Here, we present a Matlab implementation of such software that we have called "Graph Size."

For the problem definition, Task 1 of Table 1, "Graph Size" represents the equations and parameters in the two layers, the component layer and the mechatronic system layer, defined in the previous two paragraphs. This decomposition facilitates the reuse of models through component libraries (Component layer) or sizing scenario libraries (Mechatronic system layer). The relations, called rules, may take the form of equations or inequalities. The tool automatically lists the parameters from the equations. These rules can be declared in an equation section, and will then be analysed to be ordered, or in a constraint section, and will then be used as constraints in the optimization algorithm.

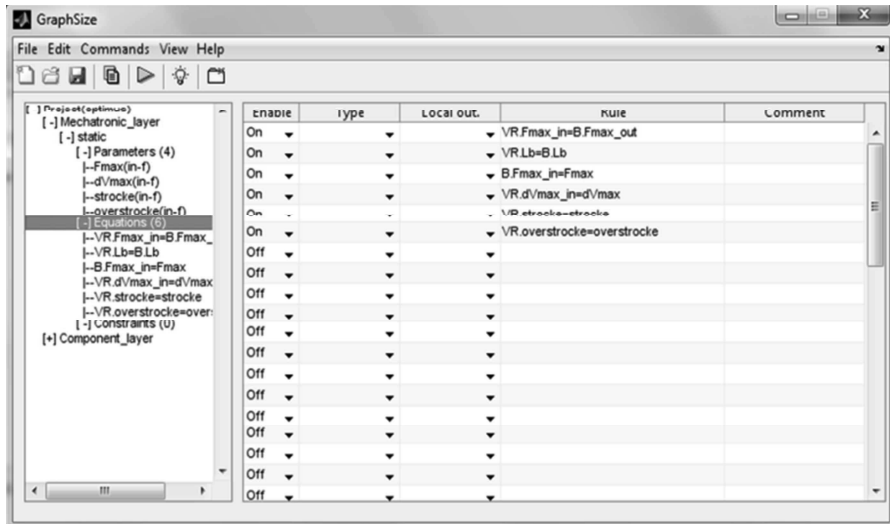


Figure 16 – Graph Size and the 2 layers (components & system)

The problem is thus defined by a given number of non-oriented equations/inequalities. Most of the time, optimal values are obtained for a solution around the constraint. As an example, for a motor where the design driver is the coil maximum temperature, we may check that $T_{coil} \leq T_{max}$, leading to an over-sizing. But if in addition to that inequality, the motor mass is minimized final, the final result will tend to an equality $T_{coil} = T_{max}$. Therefore, at first, inequalities in the equations section will be considered as equalities and only if the problem is over-constrained, will some adaptation be made by adding an over-sizing parameter and moving superfluous inequalities to the constraints section.

So, having a problem of ‘n’ equations that are functions of ‘m’ unknown parameters, it will first be interesting to assign one output parameter to each equation in order to orient the problem. The orientation of the equations corresponds to Task 2 of Table 1. This means that the equations will be transformed as follows: $f_i(x_1, x_2, \dots, x_m) = 0 \rightarrow x_2 = f_i'(x_1, x_3, \dots, x_m)$. To ensure that the assignment number is as high as possible, an augmenting path method will be applied. This method is based on the matching Hopcroft & Karp algorithm [34]. Before applying the H&K algorithm, a heuristic method is applied to match equations (rows) and parameters (columns). It consists of matching each equation to the first free column encountered that is linked to the row, repeating the principle from first to last row. Then, if the matching is lower than the maximum possible assignment (minimum matrix dimension), H&K is applied to an assigned matrix (like the one presented in Figure 12). The algorithm presented in [34] consists of two steps (a breadth first search or BFS and a depth first search or DFS), repeated till the assignment does not increase. It must be applied to a graph that is not disjoint (i.e. all the nodes are reachable by performing a DFS or BFS with a single starting node):

- i. Generate the graph by applying a breadth first search (BFS) starting from all currently free row nodes (equations) and stopping when a first free column node (parameter) is encountered. During this step, while descending the graph tree, a parameter node is linked to its matching equation node, while an equation is linked to the remaining parameters. During the breadth first search, dependency matrix crosses are replaced by level orders so as to identify the path orientation and simplify the following step.
- ii. Starting from a free column node, a depth first search (DFS) is applied crossing decreasing indices of the dependency matrix. Then, when an augmenting path is encountered, matching along the path is modified and the algorithm returns to step i).

The next step will identify parts of the problem presenting under-constrained (more unknown parameters than equations) or over-constrained singularities [35]. Of course, if $n \neq m$, the problem is singular, but we will see that $n = m$ does not necessarily mean the problem is not singular. This step may help the designer to fix parameters as inputs and modify inequality equations into constraints.

When the equation orientation has been done, and some dependency matrices, as shown in Figure 12 can be drafted, feedback loops and strongly connected components or SCC (represented by bold squares in the figure) will be extracted thanks to a Tarjan algorithm [38][36]. And here comes the last step (task 3 of

Table 1) of the method. For each SCC, a heuristic algorithm fixes the minimal number of internal parameters to determine all the other parameters encountered in the SCC [40][37]. Normally, these particular parameters are used as inputs to the numerical iteration loops, and then all other parameters are obtained and the inputs values are calculated again until the error between fixed and obtained value falls below an acceptable value. In our case, the SCC input parameters will be extracted at input level and defined with a range, then the value calculated within SCC will be compared to the input through an additional constraint. These problem solving choices were driven by the desire to use an independent solver generating a standard code which can be imported into as many calculation/optimization environments as possible.

3.6. Typical problems

Global concepts were presented in the previous parts and the idea is now to present a few examples to highlight the interest of such methods. The examples discussed here are deliberately simple to facilitate the demonstration but they treat each of the typical issues encountered in the implementation of sizing procedure.

Under-constrained singularity: hydraulic jack

The aim is to implement the selection procedure for a hydraulic servo-actuator (jack and servovalve) to ensure a nominal effort F_0 and a nominal speed V_0 for a useful stroke dx . The anchorage structure has a stiffness K and does not tolerate efforts higher than F_{max} . The maximum flow rate Q_{max} required by the actuator should be minimized to reduce the mass of the hydraulic supply system.

The physical equations for such a system are given in Table 2 and can be represented using a Design Graph as shown in Figure 17.

Table 2 – Hydraulic jack equations

Eq1: $F_{max} \geq S \cdot P_{net}$	F_{max} : stall load
	S : piston section
	P_{net} : network pressure
	C : total stroke
Eq2: $C = dx + K \cdot F_0$	dx : desired stroke
	K : structure stiffness
	F_0 : maximal load
Eq3: $F_0 = S \cdot P_0$	P_0 : maximal pressure
Eq4: $V_0 = Q_0 / S$	V_0 : maximal speed
	Q_0 : maximal flow
Eq5: $Q_0 = Q_{nom} \sqrt{\frac{P_{net} - P_0}{dP_{nom}}}$	Q_{nom} : nominal valve flow
	dP_{nom} : nominal valve pressure drop
Eq6:	
$Q_{max} = Q_{nom} \sqrt{\frac{P_{net}}{dP_{nom}}}$	Q_{max} : no load flow

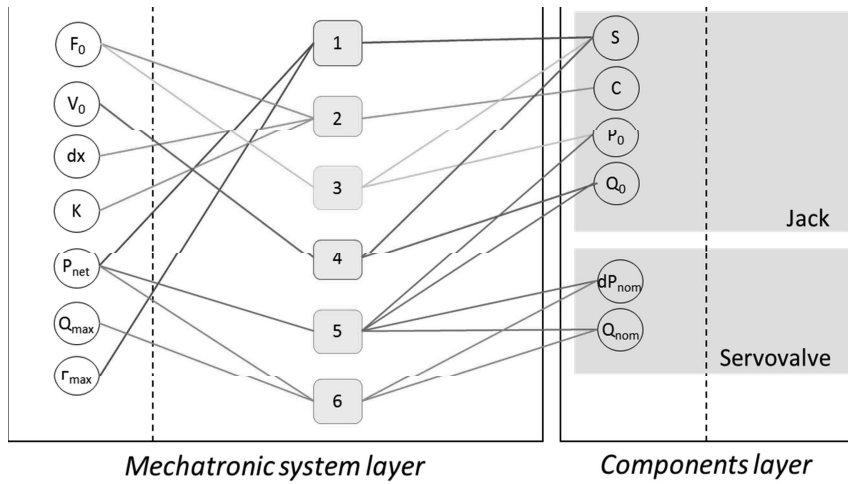
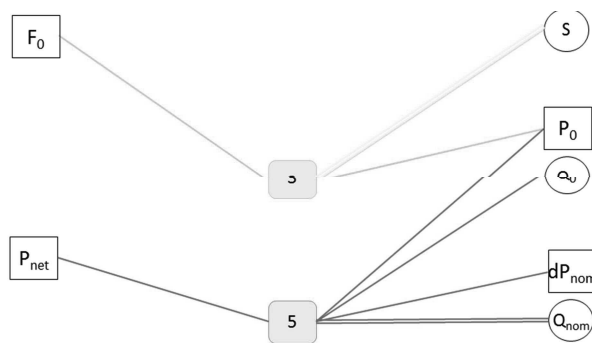


Figure 17 – Servo-actuator design graph (non-oriented)

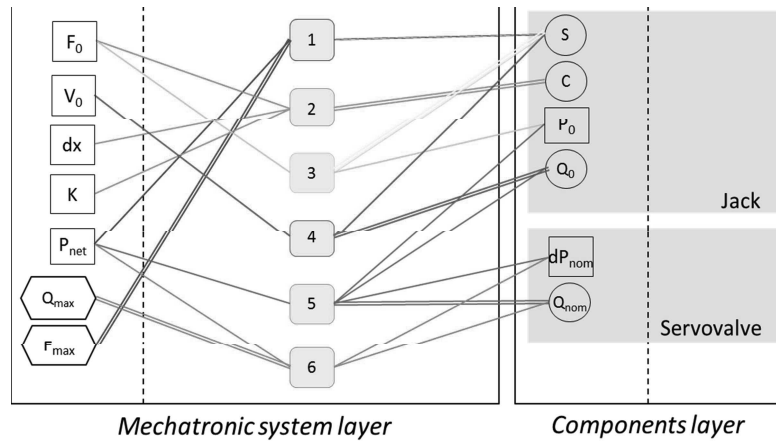
Among the listed parameters, some will be determined as input by the customer's specification document: F_0 , V_0 , dx , P_{net} and K ; while others are objectives: Q_{max} (which must be minimized) or constraints: F_{max} (limited by structure maximum allowable load). But even if some parameters are defined as outputs they are still undetermined and therefore the problem is reduced to 6 equations and 8 parameters.

	HC					SC							
$Q_{max}=Q_{nom}*(P_{net}/dP_{nom})^{0.5}$	x				x	x	o						
$Q_0=Q_{nom}*((P_{net}-P_0)/dP_{nom})^{0.5}$	x					x	x	o	x				
$F_0=S*P_0$			x				x	o					
$F_{max}=S*P_{net}$	x							x	o				
$V_0=Q_0/S$				x				x	o				
$C=dx+K*F_0$		x	x	x					o				
	P_{net}	dx	K	F_0	V_0	Q_{max}	dP_{nom}	Q_{nom}	P_0	S	F_{max}	Q_0	C

Figure 18 – Dependency matrix for the hydraulic jack



a) Under-constraint equations



b) Oriented equations

Figure 19 – Servo-actuator design graph (oriented)

Within the HC set, we find parameters Q_{max} , dP_{nom} , Q_{nom} , P_0 , S , F_{max} and Q_0 . As mentioned before Q_{max} and F_{max} may be outputs, and it seems strange to fix piston section S , so this leaves: P_0 , Q_0 , dP_{nom} and Q_{nom} . The design graph can also highlight the sub-constraints: calculation nodes 3 and 5 (Figure 19a) need 2 parameters to be assumed known to allow the sequencing of computations. As dP_{nom} may be given by valve technology, it may be taken as input and P_0 is easy to limit to a range equal to $[0, P_{net}]$, so it will be taken as a second input (variable).

Therefore, helping the designer choose parameters to fix in order to solve an under-constrained singularity will lead to the result of Figure 20.

$C = dx + K * F_0$																								
				x	x	x													0					
$F_0 = S * P_0$	x																			0				
$F_{max} = S * P_{net}$		x																		x	0			
$V_0 = Q_0 / S$																				x		0		
$Q_0 = Q_{nom} * ((P_{net} - P_0) / dP_{nom})^{0.5}$		x	x																			x	0	
$Q_{max} = Q_{nom} * (P_{net} / dP_{nom})^{0.5}$			x																				x	0
	P_0	P_{net}	dx	K	F_0	V_0	dP_{nom}	C	S	F_{max}	Q_0	Q_{nom}	Q_{max}											

Figure 20 – Perfectly matched hydraulic jack problem

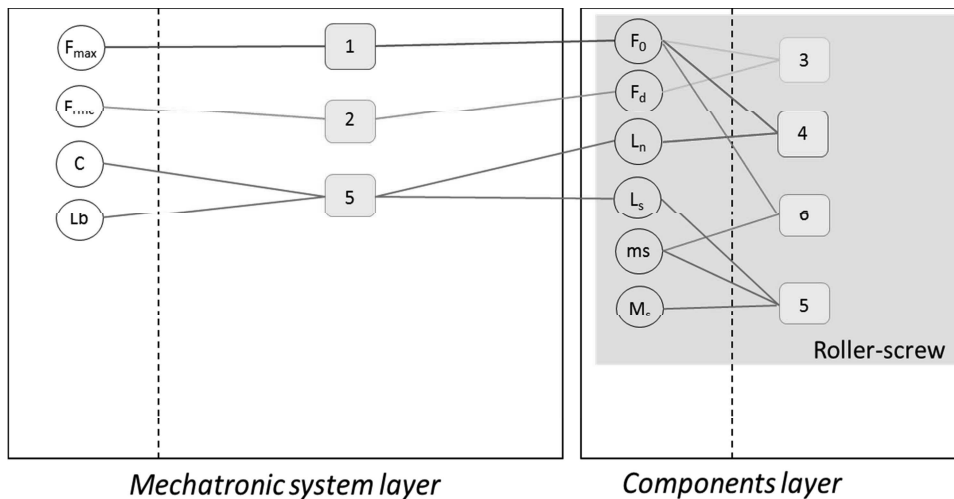
An optimization problem with P_0 as design parameter, Q_{max} as objective and F_{max} as constraint is thus obtained. The optimization enables a classical hydraulic design rule to be found: the pressure P_0 must be equal to $2/3$ of P_{net} in order to minimize Q_{max} .

Over-constrained singularity: roller-screw

Here we consider an over-constrained problem that is quite simple but which presents the way to solve this kind of singularity. The objective is to select a roller screw subject to two constraints: a static load and a dynamic load. Let us consider the equations of Table 3 from some scaling laws (3, 4, 6) as explained in Chapter 2.

Table 3 – Roller-screw equations (initial set)

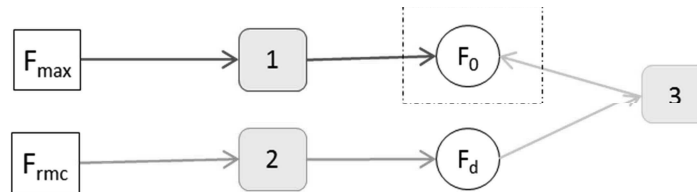
<i>Eq1:</i> $F_0 \geq F_{max}$	F_0 : roller-screw static load
<i>Eq2:</i> $F_d \geq F_{rmc}$	F_{max} : maximum applied load
<i>Eq3:</i> $F_d = F_{dref} (F_0 / F_{0ref})^{0.9}$	F_d : roller-screw dynamic load
<i>Eq4:</i> $L_n = L_{nref} (F_0 / F_{0ref})^{0.5}$	F_{rmc} : rolling fatigue applied load
<i>Eq5:</i> $L_s = C + L_n + L_b$	F_{dref} : roller-screw dynamic load (reference component)
<i>Eq6:</i> $m_s = m_{sref} (F_0 / F_{0ref})$	F_{0ref} : roller-screw static load (reference component)
<i>Eq7:</i> $M_s = m_s L_s$	L_n : roller-screw nut length
	L_{nref} : roller-screw nut length (reference component)
	L_s : screw length
	C : actuator stroke
	L_b : thrust bearing width
	m_s : screw linear mass
	m_{sref} : screw linear mass (reference component)
	M_s : screw total mass



Mechatronic system layer

Components layer

a) Full non-oriented graph



b) Over-constrained part

Figure 21 – Roller-screw design graph

As reference component data are available for sizing just like F_{max} and F_{rmc} specifications, and as the thrust bearing will be considered to be sized first, then the problem is in fact expressed in 7 equations with 6 undetermined parameters.

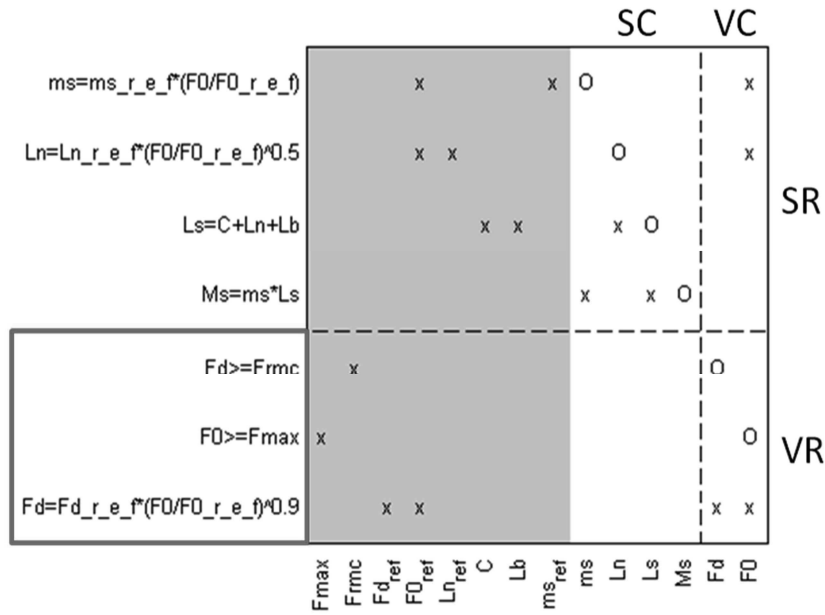


Figure 22 – Dependency matrix for the rollers-screw with Av sub-matrix

The matrix obtained clearly points out that one of the last 3 equations must be removed to obtain a non-singular problem. To do this, one of the inequalities must be moved to constraints ($F_d \geq F_{rnc}$ for example). Yet, without modifying the other equation (considered as: $F_0 = F_{max}$), if fatigue is the sizing criterion, the constraint will never be met. That is why a degree of freedom ‘ k_c ’ must be introduced to the equation: $k_c * F_0 = F_{max}$, with k_c a variable input within the range $[1; Inf]$ here. Then the final result is the one presented in the figure below, where k_c represents an over-sizing coefficient to validate dynamic sizing. The new problem is then given in Table 4.

Table 4 – Roller-screw equations (new set)

Eq1: $F_0 = k_c * F_{max}$	F_0 : roller-screw static load
Eq2: $F_d = F_{dref} * (F_0 / F_{0ref})^{0.9}$	F_{max} : maximum applied load
Eq3: $L_n = L_{nref} * (F_0 / F_{0ref})^{0.5}$	F_{dref} : roller-screw dynamic load (reference component)
Eq4: $L_s = C + L_n + L_b$	F_{0ref} : roller-screw static load (reference component)
Eq5: $m_s = m_{sref} * (F_0 / F_{0ref})$	L_n : roller-screw nut length
Eq6: $M_s = m_s * L_s$	L_{nref} : roller-screw nut length (reference component)
Cst1: $F_d \geq F_{rnc}$	L_s : screw length
	C : actuator stroke
	L_b : thrust bearing width
	m_s : screw linear mass
	m_{sref} : screw linear mass (reference component)
	M_s : screw total mass
	F_d : rollers-screw dynamic load
	F_{rnc} : rolling fatigue applied load

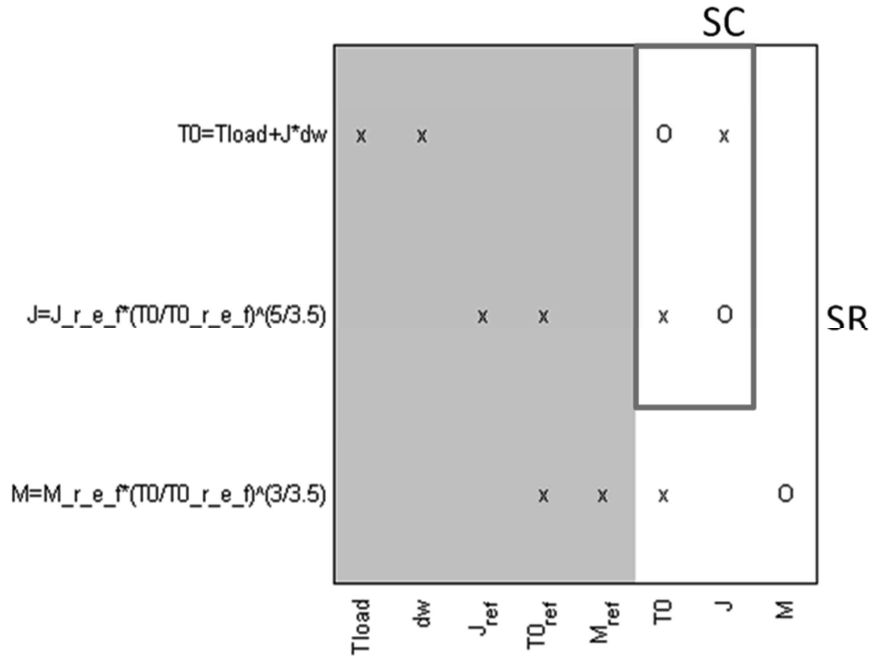


Figure 24 – Brushless electric motor sizing procedure highlighting SCC

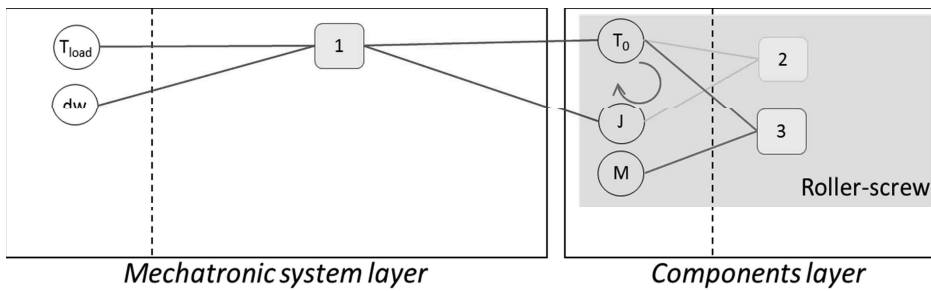


Figure 25 – Brushless motor design graph

In Figure 24, an SCC appears since the computations of T_0 and J computation are linked. Design graph also highlights this algebraic loop. To break the loop, and as the SCC set size is 2, we may only fix one of the parameters as input (variable), say J . Then, the validation formula has to be moved to a constraint: $J - J_{ref} \cdot (T_0 / T_{0ref})^{5/3.5} = 0$.

Since equality is a very hard constraint to validate, we may accept a relative error: $(J - J_{calculated}) / J_{calculated} \leq 0.01$, with $J_{calculated} = J_{ref} \cdot (T_0 / T_{0ref})^{5/3.5}$. The new problem is then given in Table 6.

Table 6 – Brushless electric motor equations (new set)

$Eq1: T_0 = T_{load} + J \cdot dw$	T_0 : motor maximum torque
$Eq2: J_{calculated} = J_{ref} \cdot (T_0 / T_{0ref})^{5/3.5}$	T_{load} : torque demanded
$Eq3: M = M_{ref} \cdot (T_0 / T_{0ref})^{3/3.5}$	J : motor inertia
<u>Cst1:</u>	dw : acceleration demand
$(J - J_{calculated}) / J_{calculated} \leq 0.01$	J_{ref} : motor inertia (reference component)
	T_{0ref} : motor maximum torque (reference component)
	M : motor mass
	M_{ref} : motor mass (reference component)

An other way is to introduce an oversizing coefficient within Eq1 and reuse the initial equation as a constraint: Eq1 : $T_0 = k_m T_{load}$ and Cst1 : $T_0 > T_{load} + J.dw$.

These new sizing procedures have no algebraic loops, thanks to the introduction of a new design parameter and a new constraint for the optimization problem.

4. CONCLUSION

In this chapter, we have shown that ordering the calculation steps of a whole, highly constrained sizing procedure is not always an easy task. We proposed graphical representations or algorithms that can be applied to highlight the different problems the designer has to face (singularity, calculation loop) and may help him solve these problems by proposing alternatives. Finally the problem is formulated to be implemented easily in all solvers/optimization tools. So the goal is actually to help the designer define a standard structured problem. This is especially useful for mechatronic design because of the highly constrained sizing and the interaction among fields. The paper 5 illustrates optimal preliminary design with the example of a spoiler electromechanical actuator. The proposed approach, based on meta-models obtained using the surfaces response methods and scaling laws models, is used to explore the influence of anchorage points and transmission ratio on the different design constraints and the overall mass of the actuator.

5. BIBLIOGRAPHY

- [1] M. Budinger, T. E. Halabi et J.-C. Maré, «Optimal preliminary design of electromechanical actuation systems,» chez « *More electrical* » *aircraft technologies, Symposium SPEC*, Lyon, France, 2011.
- [2] F. Messine, B. Nogarede et J.-L. Lagouanelle, «Optimal design of electromechanical actuators: a new method based on global optimization,» *Magnetics, IEEE Transactions on*, vol. 34, n° 11, pp. 299-308, jan 1998.
- [3] F. Roos, «Towards a methodology for integrated design of mechatronic servo systems,» 2007.
- [4] J. Sobieszcanski-Sobieski et R. Haftka, «Multidisciplinary aerospace design optimization: survey of recent developments,» *Structural optimization*, vol. 14, pp. 1-23, 1997.
- [5] T. El-Halabi, M. Budinger et J.-C. Maré, «Optimal geometrical integration of electromechanical actuators,» chez *Recent Advances in Aerospace Actuation Systems and Components*, Toulouse, France, 2010.
- [6] M. Rottach, C. Gerada, T. Hamiti et P. W. Wheeler, «Fault-tolerant electrical machine design within a Rotorcraft Actuation Drive System optimisation,» chez *Power Electronics, Machines and Drives (PEMD 2012), 6th IET International Conference on*, 2012.
- [7] T. Simpson, J. Peplinski, P. Koch et J. Allen, «“Metamodels for Computer-Based Engineering Design: Survey and Recommendations,» *Engineering with Computers*, vol. 17, pp. 129-150, 2001..
- [8] H. Van der Auweraer, J. Anthonis, S. De Bruyne et J. Leuridan, «Virtual engineering at work: the challenges for designing mechatronic products,» *Engineering with Computers*, vol. 29, pp. pp. 389-408, 2013.
- [9] MIT Calc, [En ligne]. Available: www.mitcalc.com.
- [10] Harmonic Drive, «General catalog,» [En ligne]. Available: www.harmonicdrive.net/support/catalogs/.
- [11] Kollmorgen, [En ligne]. Available: www.kollmorgen.com/en-us/service-and-support/technical/motioneering/.
- [12] ControlEng, [En ligne]. Available: www.controleng.ca/servosoft/.
- [13] Dassault system, [En ligne]. Available: www.3ds.com/products-services/simulia/portfolio/isight-simulia-execution-engine/.
- [14] Noesis, [En ligne]. Available: www.noesisolutions.com/Noesis/.
- [15] ESTECO, [En ligne]. Available: www.esteco.com/modelfrontier/.
- [16] L. Allain, Capitalisation et traitement des modèles pour la conception en génie électrique, PhD thesis, INP Grenoble, 2003.
- [17] GenusSoftware, [En ligne]. Available: www.genussoftware.com/GenusDesigner.htm.
- [18] Enventive, [En ligne]. Available: www.enventive.com.
- [19] M. Pfennig, U. Carl et F. Thielecke, «Recent Advances Towards an Integrated and Optimized Design of High Lift Actuation Systems,» chez *SAE Int. J. Aerosp. 3(1):55-64, 2010, doi:10.4271/2009-01-3217*.
- [20] C. Dunker, F. Thielecke et T. Homann, «New Computer-Aided Methods for Preliminary Architecting and Sizing of Aircraft Hydraulic Systems,» chez *Deutscher Luft- und Raumfahrtkongress, Bremen 27. - 29. Sept. 2011*.

- [21] Universal technical systems, [En ligne]. Available: www.uts.com.
- [22] Ascend, [En ligne]. Available: ascend4.org.
- [23] Vesta System, [En ligne]. Available: vesta-system.cades-solutions.com.
- [24] S. Reddy, K. Fertig et D. Smith, «Constraint management methodology for conceptual design tradeoff studies,» chez *Proceedings of the ASME design engineering technical conference, 1996.*
- [25] R. Alber et S. Rudolph, «"43" - A Generic Approach for Engineering Design Grammars,» chez *AAAI Technical Report SS-03-02.*
- [26] PACE, [En ligne]. Available: www.pace.de.
- [27] Salome, [En ligne]. Available: www.salome-platform.org/about/yacs.
- [28] S. Liscouet-Hanke et K. Huynh, «A Methodology for Systems Integration in Aircraft Conceptual Design – Estimation of Required Space,» chez *SAE Technical Paper 2013-01-2235, 2013, doi:10.4271/2013-01-2235.*
- [29] B. Delinchant, F. Wurtz, D. Magot et L. Gerbaud, «A Component-Based Framework for the Composition of Simulation Software Modeling Electrical Systems,» *SIMULATION*, vol. Vol. 80, n° 1 Issue 8, 2004.
- [30] NASA, Techniques of Functional Analysis, NASA Systems Engineering Handbook, 1995.
- [31] T. Browning, «Applying the design structure matrix to system decomposition and integration problems: a review and new directions,» *IEEE transactions on engineering management*, vol. 48, no.3, pp. 292-306, 2001.
- [32] T. Black, C. Fine et E. Sachs, «A method for systems design using precedence relationships: an application to automotive brake systems,» Massachusetts Institute of Technology, 1990..
- [33] E. Gelle et B. Faltings, «Solving mixed and conditional constraint satisfaction problems,» *Kluwer academic publishers*, no. 8, pp. 107-141, 2003..
- [34] D. Serrano, Constraint management in conceptual design, PhD thesis, Massachusetts Institute of Technology, 1987.
- [35] R. J. Malak, L. Tucker et C. Paredis, «Compositional modelling of fluid power systems using predictive tradeoff models,» *International of fluid power*, vol. 10 number 2, pp. 45-56, 2009..
- [36] I. Duff et T. Wiberg, «Remarks on implementations of $O(n^2)$ assignment algorithms,» *ACM transactions on mathematical software*, vol. 14, no. 3, pp. 267-287, 1988..
- [37] A. Pothen et C. Fan, «Computing the block triangular form of a sparse matrix,» *ACM transactions on mathematical software*, vol. 16, no. 4, pp. 303-324, 1990..
- [38] J. Helary, Algorithmique des graphes, Rennes university publication, 2004.
- [39] S. Reddy, K. Fertig et D. Smith, «Constraint management methodology for conceptual design tradeoff studies,» *Proceedings of the ASME design engineering technical conference, 1996.*
- [40] M. J. Buckley, K. W. Fertig et D. E. Smith, «Design Sheet: An Environment for Facilitating Flexible Trade Studies During Conceptual Design,» chez *Aerospace Design Conference*, Irvine, California, 1992.
- [41] M. Budinger, J. Liscouet, J. Mare et others, «Estimation models for the preliminary design of electromechanical actuators,» *Proceedings of the Institution of Mechanical Engineers, Part G: Journal of Aerospace Engineering*, vol. 226, n° 13, pp. 243-259, 2012.

Paper 5 - Optimal preliminary design of electromechanical actuators

ABSTRACT

This paper presents a methodology for the optimal preliminary design of electro-mechanical actuators. The main design drivers, design parameters and degrees of freedom that can be used for preliminary design and optimization of EMA are described. The different types of models used for model based design (estimation, simulation, evaluation and meta-model), and their associations are presented. The process preferred for its effectiveness in terms of flexibility and computational time is then described and illustrated with the example of a spoiler electromechanical actuator. The proposed approach, based on meta-models obtained using the surfaces response methods and scaling laws models, is used to explore the influence of anchorage points and transmission ratio on the different design constraints and the overall mass of the actuator.

Keywords: design exploration, electromechanical actuator, flight control, inverse problem, inverse simulation, Modelica, Meta-Models, Response Surface Methodology, scaling laws, spoiler.

Referencing: Budinger, M., Reysset, A., El Halabi, T., Vasiliu, C. & Maré J.-C., *Optimal preliminary design of electromechanical actuators*, Proceedings of the Institution of Mechanical Engineers, Part G: Journal of Aerospace Engineering, 2013.

Optimal preliminary design of electromechanical actuators

Marc Budinger¹, Aurélien Reysset¹, Toufic El Halabi¹, Catalin Vasiliu² and Jean-Charles Maré¹

Proc IMechE Part G:
J Aerospace Engineering
0(0) 1–19
© IMechE 2013
Reprints and permissions:
sagepub.co.uk/journalsPermissions.nav
DOI: 10.1177/0954410013497171
uk.sagepub.com/jaero



Abstract

This paper presents a methodology for the optimal preliminary design of electro-mechanical actuators. The main design drivers, design parameters and degrees of freedom that can be used for preliminary design and optimization of electro mechanical actuator are described. The different types of models used for model-based design (estimation, simulation, evaluation and meta-model), and their associations are presented. The process preferred for its effectiveness in terms of flexibility, and computational time is then described and illustrated with the example of a spoiler electromechanical actuator. The proposed approach, based on meta-models obtained using the surfaces response methods and scaling laws models, is used to explore the influence of anchorage points and transmission ratio on the different design constraints and the overall mass of the actuator.

Keywords

Design exploration, electromechanical actuator, flight control, inverse problem, inverse simulation, Modelica, meta-models, response surface methodology, scaling laws, spoiler

Date received: 11 January 2013; accepted: 19 June 2013

Context

The current technical developments in aviation aim at making aircraft more competitive, greener and safer. The more electric aircraft (MEA) offers interesting perspectives in terms of performance, maintenance, integration, reconfiguration, ease of operation and management of power.^{1,2} Using electricity as the prime source of energy for non-propulsive embedded power systems is considered by aircraft makers as one of the most promising means to achieve the abovementioned goals. Actuation for landing gears and flight controls is particularly concerned as it is one of the main energy consumers. This explains why, during recent years, a great effort has been put into the development of Power-by-Wire (PbW) actuators at research level (e.g. POA, MOET, DRESS and ACTUATION 2015 European projects). This recently enabled PbW actuators to be introduced in the new generation of commercial aircraft,^{3,4} in replacement of conventional servo-hydraulic ones (e.g. Boeing B787 electro mechanical actuator (EMA) brake or spoiler, Airbus A380 EHA and EBHA). On their side, space launchers are following the same trend for thrust vector control (TVC) as illustrated by the European VEGA project⁵ and NASA projects.⁶ However, these technological step changes induce new challenges, especially for the preliminary design process for actuation systems

and components which cannot simply duplicate former practices.

Section “Model-based design for electromechanical actuation systems” sums up the main requirements, design drivers and design choices for EMA design. This section also describes the different types of models needed. The different possible associations for those models are then presented, and the most efficient and flexible process will be described in details. Section “Spoiler actuator case study” illustrates the different steps, models and tools for the presented methodology with the case study of a spoiler EMA.

Model-based design for electromechanical actuation systems

Figure 1 shows the V-cycle design⁷ of a mechatronic system such as an EMA (architecture is described in section “Case study and actuator architecture

¹INSA/UPS, Institut Clément Ader, Université de Toulouse, Toulouse 31077, France

²Polytechnic University of Bucharest, Bucharest 060032, Romania

Corresponding author:

Marc Budinger, INSA/UPS, Institut Clément Ader, Université de Toulouse, Toulouse 31077, France.

Email: marc.budinger@insa-toulouse.fr

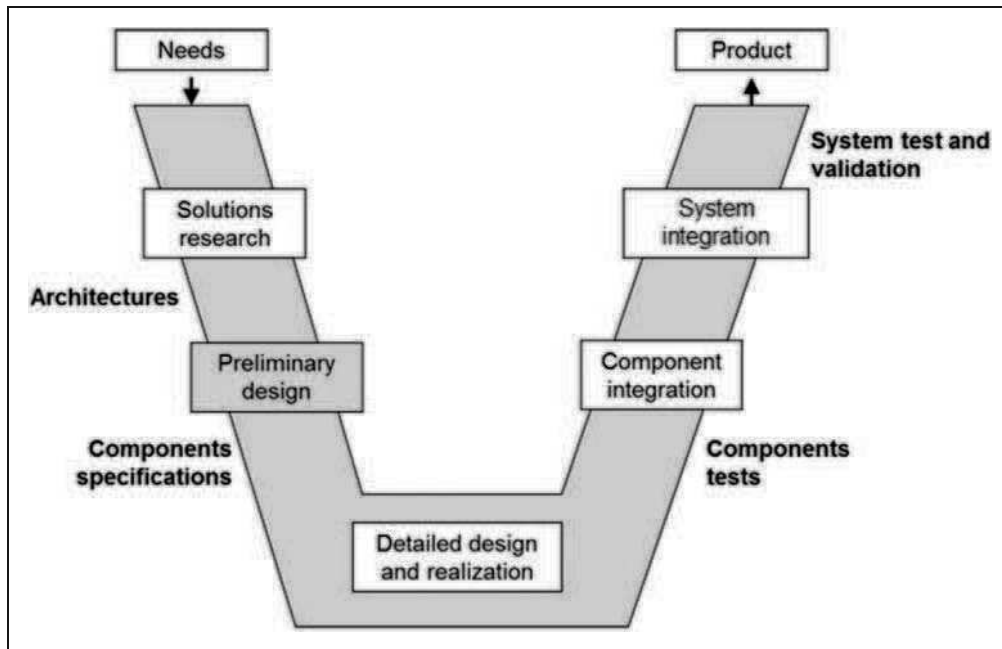


Figure 1. V-cycle design for a mechatronic system.

presentation”). The described methodology is dedicated to the descending branch of the V-cycle corresponding to preliminary optimal sizing and device parts features synthesis. The inputs are the objectives and design constraints coming from the specifications document or the chosen architecture. As output components (rod end, roller or ball screw, gear reducer, brushless motor, etc.) specifications are generated in order to obtain an assembled actuation system which fully meets upper requirements.

Requirements and key design drivers of actuation systems

As contributors to the safety of embedded critical functions, aerospace actuators are subjected to numerous specific design requirements. These requirements are translated into design constraints which the designer must meet by discerning choices. Based on recent examples Refs.^{5–8,42,43,47} Table 1 summarizes these design constraints, design degrees of freedom and their possible interactions. One can notice that the designer choices are numerous; their impact coupled and they should address multiple domains. The study and comparison of different possible architectures must thus be supported by efficient design methodologies.

Models needs for electromechanical preliminary design

To accelerate the design process, a general trend is to extend the role of modelling in design and specification.^{7,16} At preliminary steps of system design, different types of models are needed in order to get a

complete sizing: simulation, estimation and evaluation models.

The objective of **simulation models** is to calculate all the variables of power, energy (force, speed, temperature, etc.) useful for the components selection. The transient simulation of an EMA is becoming mandatory because, unlike hydraulic actuators, some strong coupling exists between the transient power demand, the thermal behavior of motors, the inertia loads and the fatigue of mechanical components. These simulations are usually based on lumped parameters models,^{12,46} also called 0D-1D models, run either in direct or inverse mode^{13,17} in environments such as Matlab/Simulink, Dymola,¹⁸ AMESim,⁹ etc. Ref.¹³ describes the use of inverse simulation with Modelica for actuators sizing. Yet, to run this kind of models, which only suits for analysis and not for validation, component parameters may be known, that is why some other types are needed.

Estimation models allow to estimate from a reduced set of independent parameters (e.g. max load, stroke) all the dependent parameters/component characteristics: simulations (e.g. inertia, efficiency, etc.), integration (e.g. mass, dimensions) and validation of safe operating area (e.g. max speed, degradation parameters, etc.). This is a way to replace component data-sheets when they are not available (often the case for aerospace application) or to speed up the design exploration (analysis of different scenarios, optimization, etc.). Ref.¹⁰ describes some estimation models based on scaling laws for the main components of an electromechanical actuator.

The last model is the **evaluation model** whose goal is to check the ability of a component to operate in its safe operating area for the required lifetime and

Table 1. Main design drivers and designer choices during EMA design.

Requirements	Description	Designer choices and/or degree of freedom						
		Architecture	Technologies	Component specifications	Displacement curve control parameters	Kinematic and transmission ratios	Design models and tools	Reliability allocation
Functions	Main functions	⊗						
	Specific mode of operation ⁹	⊗						
Performances	Transient high forces			⊗				
	Dynamic. Precision ⁵ and accuracy ¹⁰	⊗	⊗	⊗		⊗		
Environment	Thermal ¹¹	⊗	⊗	⊗				
	Vibration ^{12,13}		⊗	⊗				⊗
Cost	No Recurrent Cost			⊗				
	Recurrent Cost		⊗				⊗	
Safety	Fail safe (winding short circuit, jamming, shock) ^{6,12}	⊗	⊗	⊗				
	Life time/MTBF/failure rate ^{1,14,45}							⊗
Integration	Mass	⊗	⊗	⊗		⊗		
	Geometrical envelope ^{15,44}	⊗	⊗	⊗			⊗	

reliability. Ref.¹¹ describes the possible models and ways of implementing them in system simulation environments. Figure 2 describes the information exchanges between those different models and defines the structure suitable for model-based design of mechatronic systems. Decision making can be performed either manually as in Ref.¹³ or automatically as described in the following paragraph.

Models implementation and possible associations

These defined models can be implemented in different types of environments. Decision making can be achieved by different optimization methods. Figure 3 illustrates three different options:

1. All the models are implemented in a computer algebra environment (Matlab, Excel). The design and optimization are done in the same environment. This solution does not address time transient phenomena problematic. However, it has the advantage suit well taking into account multiple design criteria and exhibit fast optimization. Examples of such implementation were presented in Refs.;^{14,15,19}
2. All the models are implemented in a simulation environment for algebraic differential equations (e.g. Modelica) and the optimization is done by external MDO software.²⁰ This solution allows managing fine simulation models with time transients. Yet, one main drawback is the optimization times which can become very long. Examples of such implementations are given in Refs.;^{21,22}
3. A mix of the first two solutions can be achieved with a compact representation of time-consuming temporal simulations using meta-modeling techniques.²³ This solution allows to easily manage multiple design criteria and to obtain reasonable optimization time. However, special care should be addressed to the accuracy of meta-models.

This last solution will be developed in the paper. The use of meta-optimization is common for studies with finite elements methods in various fields.²⁴ But here, the meta-models applied to 3D multi-body and 0D/1D simulations and the estimation models based on scaling laws are used to speed up the optimization of the actuator.

Proposed methodology for optimal design of EMAs

As defined by Refs.,^{25,26} a methodology is a collection of related process, methods and tools where:

1. A process is a logical sequence of tasks performed to achieve a particular objective (“WHATs”);
2. A method consists of techniques for performing a task (“HOWs”);

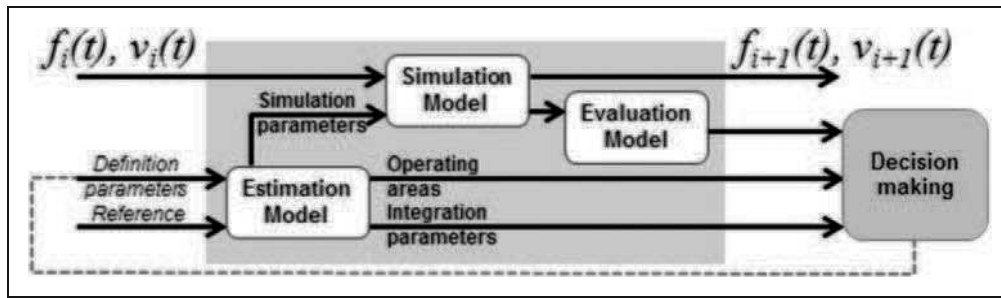


Figure 2. Component models structure for model-based preliminary design.

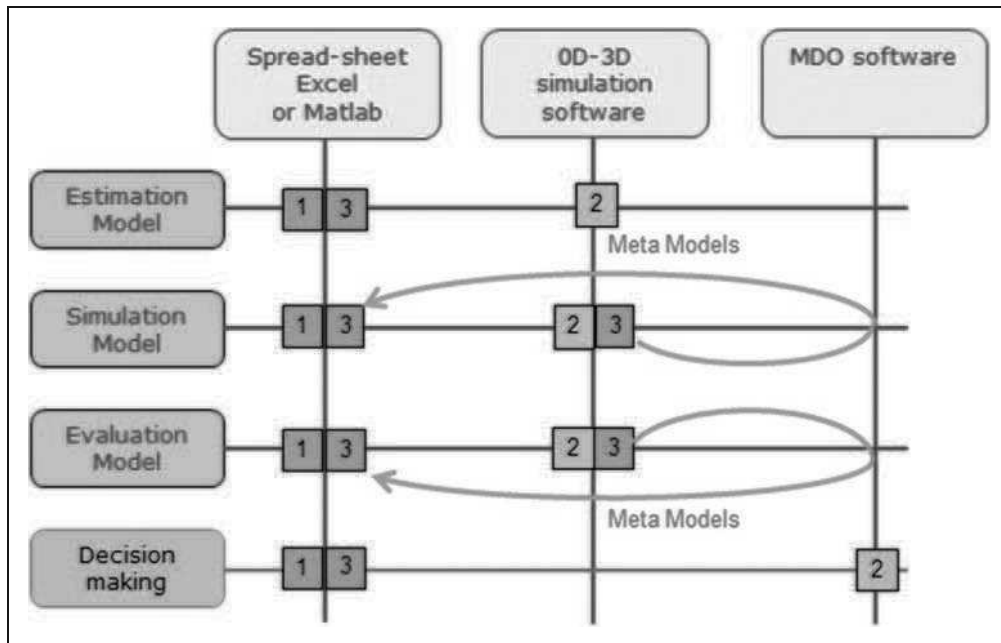


Figure 3. Model implementations and associations.

3. A tool is an instrument that, when applied to a particular method, can enhance the efficiency of the task (supports the “HOWs”).

Table 2 presents those three aspects. The main functional requirements and design degrees of freedom are given as inputs for this process. The actuator architecture and combination of power transmission components are also defined to meet the application functional requirements.

Spoiler actuator case study

Case study and actuator architecture presentation

It is proposed in this section to illustrate the design methodology using the case of a linear EMA. This actuator is actuating a spoiler/airbrake with typical specifications for a business jet. The so-called spoiler is only performing airbrake functions. Thereby possible primary flight control functions of commercial aircrafts are not taken here into consideration: control

surfaces are thus controlled symmetrically with a given displacement curve.

Main functional requirement. The main functional requirement for the actuator is to move the mechanical load to three predetermined positions (0° , 20° and 50°) against mainly the aerodynamic forces. The retracted position (0°) has to be held without energy consumption. Anchorage points on the structure and the control surface are not imposed by the aircraft maker and therefore, can be a degree of freedom for the design process.

The severe failure rate requirements at aircraft level are achieved with resort to multiple control surfaces. Thus, the requested failure rate of one actuator is compatible with a simplex architecture. However, minimizing mass is an objective. The architecture should also be safe regarding different critical cases:

- no dissymmetric deflection during a power loss: the actuator should thus fail-freeze;

Table 2. Synthesis of the proposed methodology.

	Process ("Whats")	Section	Methods ("Hows")	Tools (supports the "hows")
1	Sizing scenarios definition (section Task 1: Sizing scenarios definition)	1.1	Determine components design drivers.	Checklist by fields (mechanical, electrical, thermal, etc.) or components.
		1.2	Determine sizing scenarios to verify the design drivers and the actuator functions.	- Verification matrix
2	Determination of the active design drivers (section Task 2: Initial sizing and active design drivers)	2.1	Perform initial power sizing (not optimized) using a "sizing wave" procedure and complementary simulations.	In-house Modelica library: - Inverse simulation (Modelica). - Estimation models (scaling laws).
3	Sizing procedure setting-up and optimization problem definition (section Task 3: Sizing procedure and optimization problem definition)	3.1	Determining the calculation steps order for the sizing procedure.	- N ² diagram.
		3.2	Define the optimization problem.	- Influence diagram.
4	Creation of meta-models (section Task 4: Meta-models synthesis)	4.1	Non explicit calculations from step 3 may be replaced by meta-models.	- RSM models.
5	Design optimization (section Task 5: Optimization and design exploration)	5.1	Identify important parameters with quick exploration and reduce design space.	- Excel table.
		5.2	Optimize in the reduced space.	- Excel solver
6	Validate "optimal" solution (section Task 6: Validation)	6.1	Repeat sizing performed during step 2 to the result obtained in step 5.	In-house Modelica library: - Backward simulation (Modelica). - Estimation models (scaling laws).

- no degradation of the surface control during gust: in order to avoid mechanical damage, a load limitation must be performed by folding down the control surface;
- no degradation of the actuator or the surface control due to a jamming of the control surface during the actuator motion.

Actuator architecture. The physical architecture of the actuator is based on the Moog linear actuator presented in Ref.²⁷ This architecture should be also close to the EMA actuator actuating several spoilers of the commercial aircraft Boeing 787.²⁸ Figure 4 presents a picture of the Boeing 787 actuator prototype and describes an association of component meeting the requirements of section "Main functional requirement" where:

- The selected technologies, brushless motor, gear reducer and screw meet the main function with a minimum mass compared to a direct drive solution. The main drawback of both screw and reducer is the jamming failure mode. This failure mode is however not an issue for the fail-freeze specification. Even if

the 787 spoiler actuator uses a ball screw, a roller screw will be used instead during the sizing and optimization of this specific application.

- A one-stage spur-gear reducer with intermediary wheel allows at the same time to adapt the brushless motor speed and the parallel axes distance (distance between motor and roller screw axes).
- A power-off brake can hold the spoiler without consuming any energy (normal mode or power failure).

To meet the functions described in the previous paragraph, a control architecture with a force feedback sensor can be used. Figure 5 gives the principle of this last one. Main loops for typical control architecture are: current, speed and position loops. Load control can also be implemented like in the examples of aerospace actuators described in Refs.^{5,29} to limit external perturbations (high frequency vibration, gust load, etc.). In this case the load control is realized through a force feedback to torque control of the motor. The activation of the load control also leads to decrease of the authority of the main position loop to allow the drop of the surface in presence of excessive air loads.

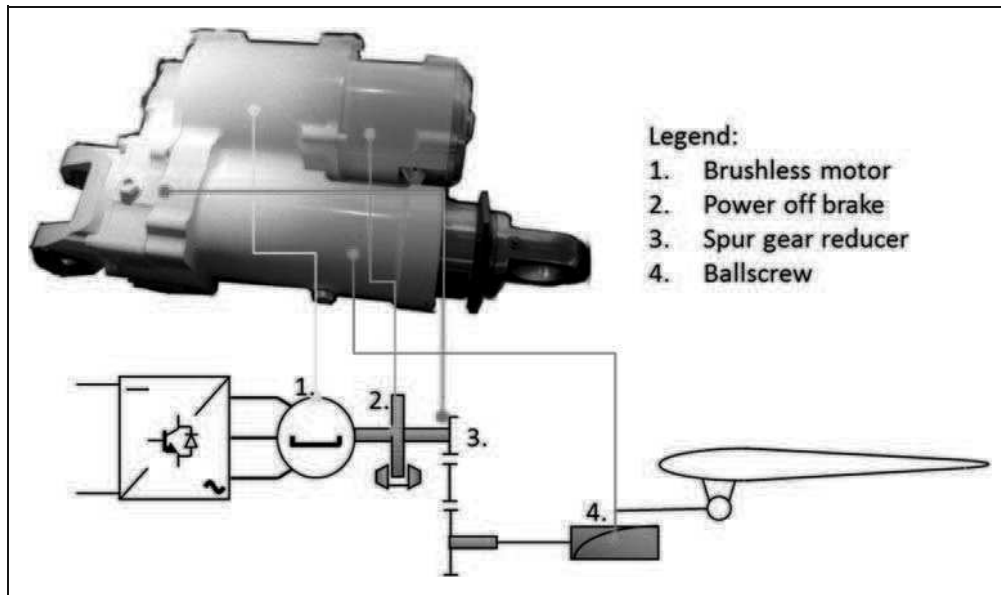


Figure 4. Physical architecture.

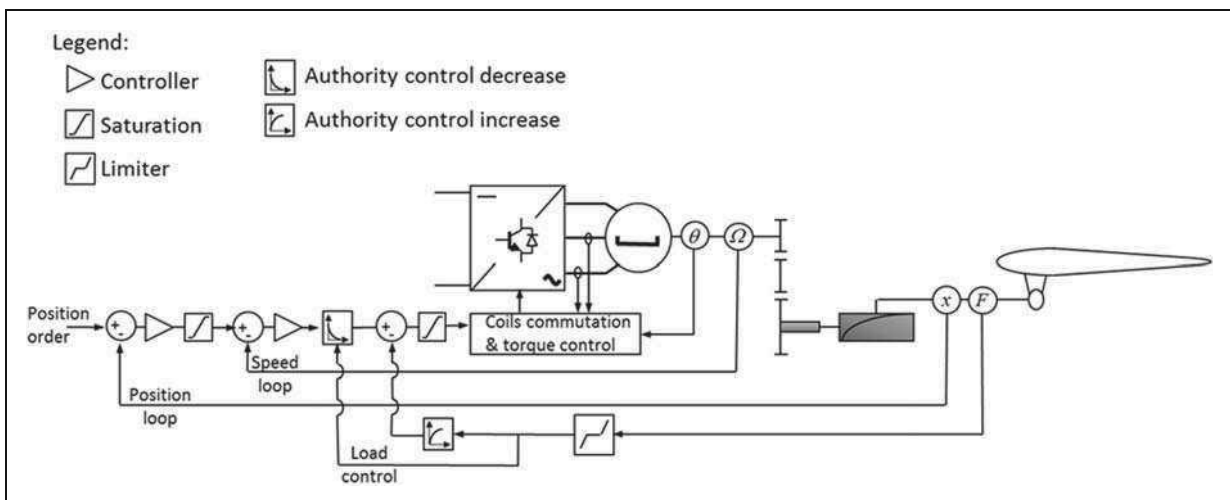


Figure 5. Control architecture.

Task 1: Sizing scenarios definition

Definition of design drivers and induced design drivers. The objective of task 1 is to represent by a set of scenarios the degradation phenomena and functions of the actuator. Those scenarios form the basis for the calculations to be carried out during the design.

The degradations of the components can be of two different types, depending on the phenomena dynamics:





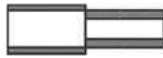


- What is called rapid degradation (e.g. permanent deformation, fracture, maximum insulator temperature, etc.) on transient power demand. They must be avoided to ensure maximum performance of the actuator.

- What is called gradual degradation (e.g. mechanical fatigue, insulator ageing, etc.). They must be such as to ensure endurance and reliable operation of the actuator throughout its life.

Additionally, the components present some imperfections which increase stresses on themselves (e.g. inertia) or on other components (e.g. friction, copper losses, etc.) and can create new critical cases (e.g. high stress induced by jamming of inertial loads). Those imperfections are called here induced design drivers.

Design drivers determination. The determination of the components design drivers can be assisted by checklists for the different technologies or components. Table 3 is a possible representation of those lists.

Table 3. Main design drivers of EMA components.

Technology	Design drivers	Component	Key design drivers selected for the application
Mechanical components	<p><u>Due to force transmission:</u></p> <ul style="list-style-type: none"> • Maximum stress (rapid) • Fatigue/wear (gradual)²² <p><u>Due to vibratory environment:</u></p> <ul style="list-style-type: none"> • Stress at resonance frequency (gradual)¹³ <p><u>Induced design drivers:</u></p> <ul style="list-style-type: none"> • Mechanical losses and friction which increase force/torque especially at low speed^{30,46} 	Rod end	- Maximum stress (rapid)
			
		Roller Screw	- Maximum stress (rapid) - Fatigue stress (gradual) - Vibratory stress (gradual) - Mechanical losses and friction (induced)
			
		Thrust bearing	- Maximum stress (rapid) - Fatigue stress (gradual) - Mechanical losses and friction (induced)
			
Pinions	- Maximum stress (rapid and gradual) - Mechanical losses and friction (induced)		
			
Housing	- Maximum stress for force transmission (rapid and gradual) - Vibratory stress (gradual) - Machining constraints		
			
Electrical components	<p><u>Current stress:</u></p> <ul style="list-style-type: none"> • Saturation of ferromagnetic materials (rapid) • Demagnetization of permanent magnet (rapid) <p><u>Thermal stress:</u></p> <ul style="list-style-type: none"> • Insulating ageing¹⁷ (gradual) <p><u>Induced design drivers:</u></p> <ul style="list-style-type: none"> • Rotor inertia which increases electromagnetic torque for high dynamic application¹⁷ or when jamming or brutal stop³¹ • Rotor inertia : bandwidth effect³² • Copper and iron losses: effect on sizing of heat sink and housing 	Brushless motor	- Maximal torque due to teeth saturation (rapid) - Mean torque and maximal temperature due to thermal stress (gradual) - Maximal speed (rapid) - Rotor inertia (induced)
			
		Power-off brake	- Maximal torque (rapid)
			

Some references are quoted to allow further study or justify the importance of listed items. Ref.¹⁰ also recalls those points.

Sizing scenarios and corresponding mission profiles. They should permit to validate the fact that the solution meets all the functions and associated performance of section “Main functional requirement” and is not submitted to inappropriate damages listed in section “Design drivers determination”. In the case of EMAs,

those scenarios are mainly characterized by finite time dependent mission profiles.

For the present case study, the following examples of scenarios can be defined:

- To take into account the mechanical stresses a mission profile representative of the maximum speed. For maximum load and fatigue phenomena: a succession of extension/retraction for different speeds of the aircraft;

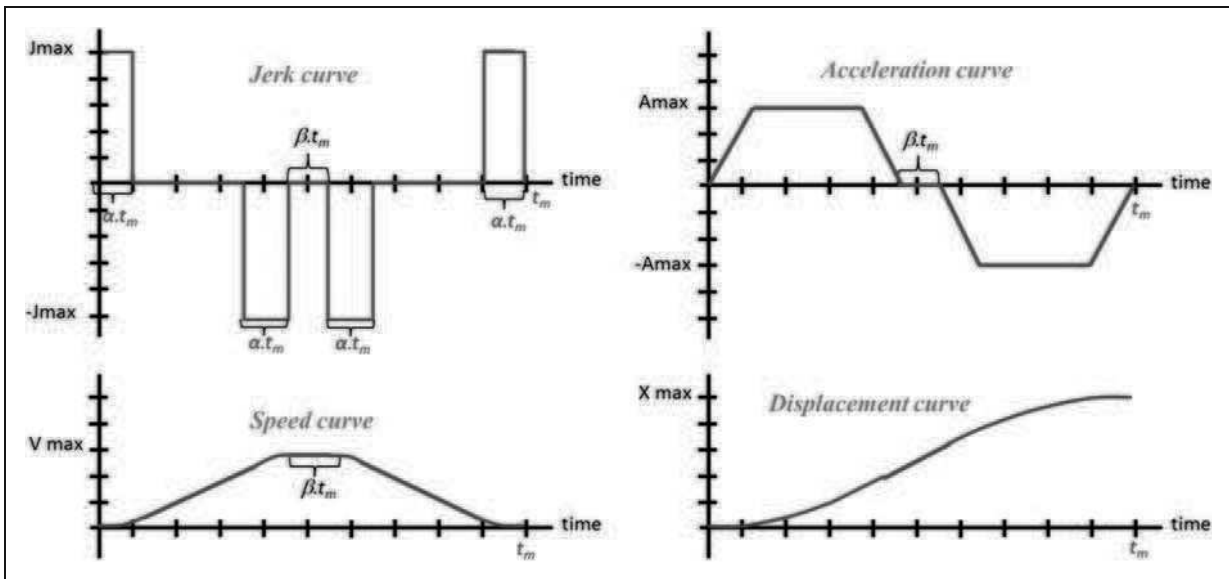


Figure 6. S curve displacement for mechanical profile.

- To represent the thermal stresses: holding of the control surface opened at 50° and submitted to full load for 3 min within an ambient temperature of 30°C ;
- To take into account the effect of the motor inertia: a jamming of the control surface occurring at full speed;
- To ensure adequate dynamics during load limitation: an active retraction of the spoiler under the effect of a gust;
- To take into account the vibratory environment: a lateral sinusoidal acceleration of 10 g between 5 and 2000 Hz³³ (validation of screw and housing resonant frequencies and induced stresses).

Scenario a) to d) can be described by transient simulations of 0D-1D models. Figure 6 describes spoiler angle time evolution for the a) mechanical mission profile. Ref.³⁴ explains how to take into account scenario e) during the preliminary design phase using analytical models. Table 4 is a verification and validation matrix to check that all design features or drivers are covered by those five scenarios.

Task 2: Initial sizing and active design drivers

In the considered case study, the initial sizing aims at the identification of the active design criteria and helps simplifying the models used for the selection of the actuator components. This first design is made for a given set of anchorage and transmission points that will be modified during the optimization phase coming later on. But, even for this first design, different types of simulation models are used.

Sizing wave. An in-house Modelica library for the preliminary design of EMAs, shown in Figure 7, has been

developed to implement all the components models presented in section “Actuator architecture” according to the structure of Figure 2. Object-orientated and class inheritance properties of Modelica language facilitate the implementation of such a structure. The models are thus structured in a way that they can combine inverse simulation together with parameters estimation (using scaling laws). Components from the created Modelica library can be combined to represent various EMAs’ architectures. The studied architecture has been sized up with a few number of simulations by following the “sizing wave” process described in Ref.¹³ where inverse simulation means to size successively each component propagating power from the load to the power source. This step is usually called power sizing and components selection, with respect to previously defined scenarios a) and b).

From this initial power sizing, it is interesting to note that:

- The motor inertia does not impact the maximum electromagnetic torque because the load is mainly aerodynamic and can be considered as a nonlinear stiffness depending on airspeed and surface steering;
- The friction models of mechanical components have to be taken into account for the motor sizing;
- Thermal aspect is really important for motor selection;
- The requested lifetime and reliability are not critical for this case study and can be neglected.

Critical cases. For selected components, the needed parameters to simulate scenarios c) and d) can be calculated using the scaling laws. The type of simulation used for c) and d) scenarios is direct simulation.

Table 4. Verification matrix.

Checking points		Scenarios				
Type	Description	a) Mechanical profile	b) Thermal profile	c) Jamming at full speed	d) Gust and load limitation	e) Vibratory environment
Functions	Displace and hold the spoiler in position	⊗	⊗			
	No degradation due to jamming			⊗		
	Gust load limitation				⊗	
Design drivers	Maximum stress for mechanical components	⊗				
	Maximum speed for mechanical components	⊗				
	Fatigue mechanical components	⊗				
	Induced effects of efficiency and friction	⊗	⊗		⊗	
	Stress due to vibrations					⊗
	Maximal torque for motor and power off brake	⊗				
	Maximum speed for motor	⊗		⊗		
	Maximum temperature for brushless motor		⊗			
	Induced effect of inertia			⊗	⊗	

Components can be oversized to meet the requirements issued from all those scenarios.

For the considered case study:

- According to the reduction ratio, the mechanical components may be oversized in order to bear the stress induced by the jamming of the spoiler running at full speed.
- The maximum motor torque must allow a retraction fast enough to limit extreme load occurring during a gust.

For scenario e), the length of the actuator is relatively short; that is why the vibratory environment has no significant impact on the housing induced stress. Therefore, the main design driver will be the minimal machining thickness constraint.

Initial sizing overview. Table 5 gives an overview of the masses, estimated thanks to scaling laws, for the various components of the EMA and the related criteria leading to their selection, criteria which should be considered during optimization (task 3).

The process leading to those results is the following:

- Choose first the anchorage points on structure farthest of the hinge axis to facilitate actuator integration;
- Select average values for all other parameters (defined in section “Optimisation problem definition”).

- If motor thermal constraint is not validated, increase motor size (i.e. thermal over-sizing coefficient).
- If jamming induced stress constraint is not validated, increase mechanical safety coefficient.

Task 3: Sizing procedure and optimization problem definition

Objectives. The objective of this step is to define the sizing problem as an optimization problem which can be formulated mathematically as follows:

Minimize objective function: $f(x)$

Subject to equality and inequality constraints:

$h(x) = 0, g(x) < 0$

By action on the parameters vector in the range:

$x_{low} < x < x_{upp}$

where

- The goal, here the global mass, is the objective function f ;
- Design alternatives are expressed by a set of values assigned to the design variables x within a design domain;
- Constraints (h and g) limit the number of alternatives to those satisfying physical principles and design specifications, that is to say feasible design.

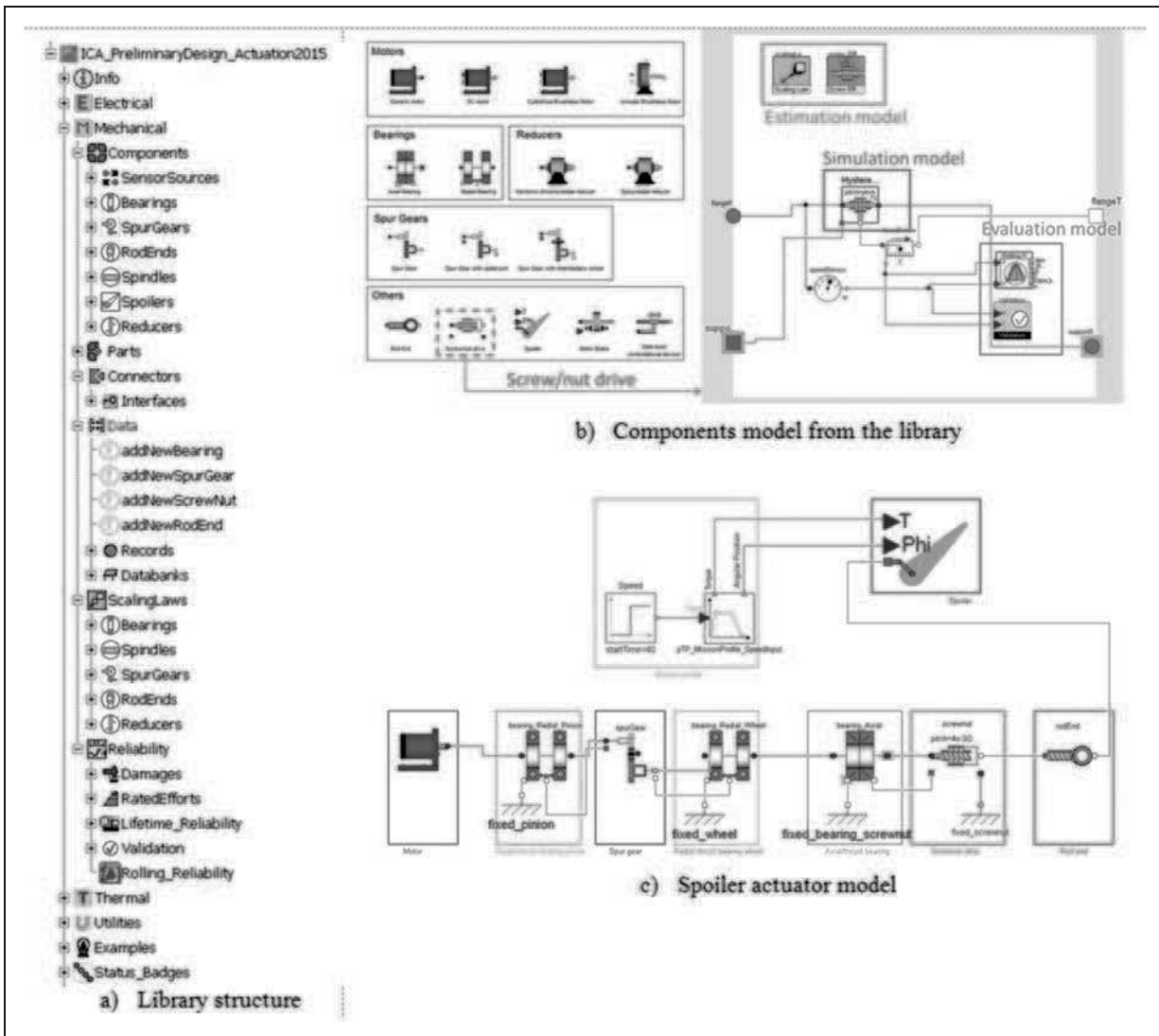


Figure 7. In-house Modelica library for the preliminary design of EMAs.

Table 5. Initial sizing.

Component	Active design drivers	Mass (kg)
Rod end	<ul style="list-style-type: none"> • Maximum stress (rapid) 	0.47
Roller Screw	<ul style="list-style-type: none"> • Maximum stress (rapid) • Mechanical losses and friction (induced) 	0.64
Thrust bearing	<ul style="list-style-type: none"> • Maximum stress (rapid) • Mechanical losses and friction (induced) 	0.94
Pinions	<ul style="list-style-type: none"> • Maximum stress (rapid and gradual) • Mechanical losses and friction (induced) 	0.65
Housing	<ul style="list-style-type: none"> • Maximum stress for force transmission (rapid) 	1.41
Brushless motor with housing	<ul style="list-style-type: none"> • Maximal torque due to magnetic saturation at teeth (rapid) • Mean torque and maximal temperature due to thermal stress (gradual) • Maximal speed (rapid) • Rotor inertia (induced) 	4.18
Power-off brake	<ul style="list-style-type: none"> • Maximal torque (rapid) • Global mass 	0.65 8.94

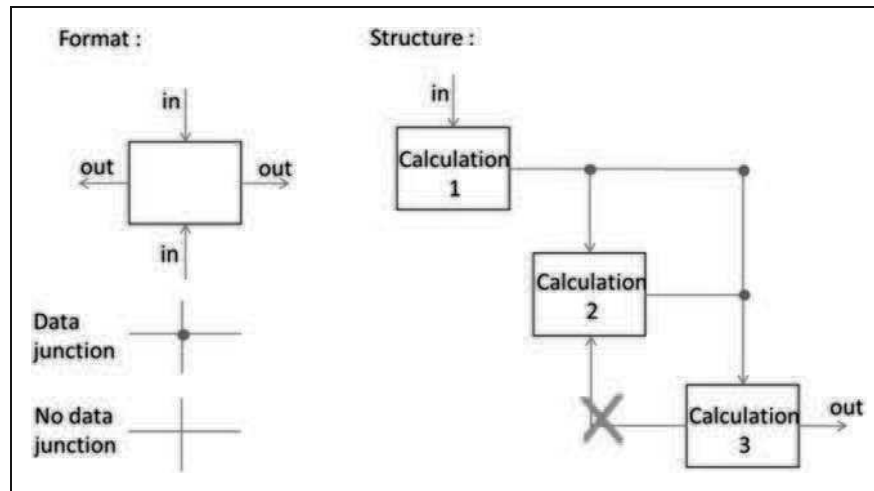


Figure 8. N^2 diagram principle.

The functions (f , g , h) can be explicit or implicit, algebraic or realized by subroutines that solve iteratively systems of differential equations. The goal of this task is to define those functions within a sizing procedure. The calculation steps of the sizing procedure should be time efficient, and to do so, only algebraic explicit functions without iteration loops are to be implemented. The number of design parameters x and constraints g and h should also be minimized to reduce design search space and thus, optimization time.

Sizing procedure definition. The sizing procedure is the sequence of calculation steps to be carried out for defining the actuator components. As mentioned before, step 2 allows to determine the minimum number of design criteria to consider in order to have a correct but lighter optimization problem. This procedure can be represented as an algorithm or flowchart. The Design-Structure-Matrix (DSM)³⁵ or N^2 diagrams³⁶ can also represent this sequence. All those representations are useful for the assessment of the models needed and exchanged quantities and for the visualization of the sequencing quality. Figure 8 recalls the principle of representation by N^2 diagrams. The objective is here to avoid any information feedback/loop thanks to a good choice of calculations order or by introducing additional constraints and design parameters being managed by the optimization algorithm. In the case of DSM matrix representation, the objective is to obtain a triangular matrix.

Figure 9 represents the sizing procedure for the EMA of the spoiler for the present case study. As an example, the bearing is sized before the roller screw in order to get the values necessary to define the length of the screw. Constraints have been added in order to make the design matrix triangular: calculations of the resonant frequency of transversal vibrations of the screw, of motor temperature and of maximum load during jamming. The corresponding

oversizing coefficients are added to the first set of design parameters and are driven by the optimization solver. Some models, as the multi-body and thermal models, require long time dependent simulations: their behavior will be translated into explicit mathematic functions thanks to meta-modeling techniques (Section “Task 4: Meta-models synthesis”).

Optimisation problem definition. The optimization problem can be defined only when the sizing procedure is known. To represent it, an influence diagram,³⁷ Figure 10, can be used. Here:

- The main design parameters are internal reduction ratios (roller screw pitch p and reducer ratio N), integration parameters (anchorage to airframe x_a , y_a and transmission to load x_t , y_t points), shape of the displacement curve (α , β displacement curve parameters as described in Figure 6), oversizing coefficient (jamming coefficient k_{jam} , brushless motor thermal coefficient k_{therm} and screw vibration coefficient k_{vib});
- The main objective is the total mass obtained by the sum of the masses of all the components estimated thanks to scaling laws;
- The constraints are used to represent some design drivers which cannot be addressed in a direct way by the sizing procedure. Oversizing coefficients enable to take care of these constraints during optimization.

Task 4: Meta-models synthesis

Process. To facilitate and accelerate the design exploration during optimization, it is more suitable to use models with only static parameters and without time dependent variables. The meta-modeling techniques²³ enable to extract a response surface from a set of simulation results. The calculated meta-models have

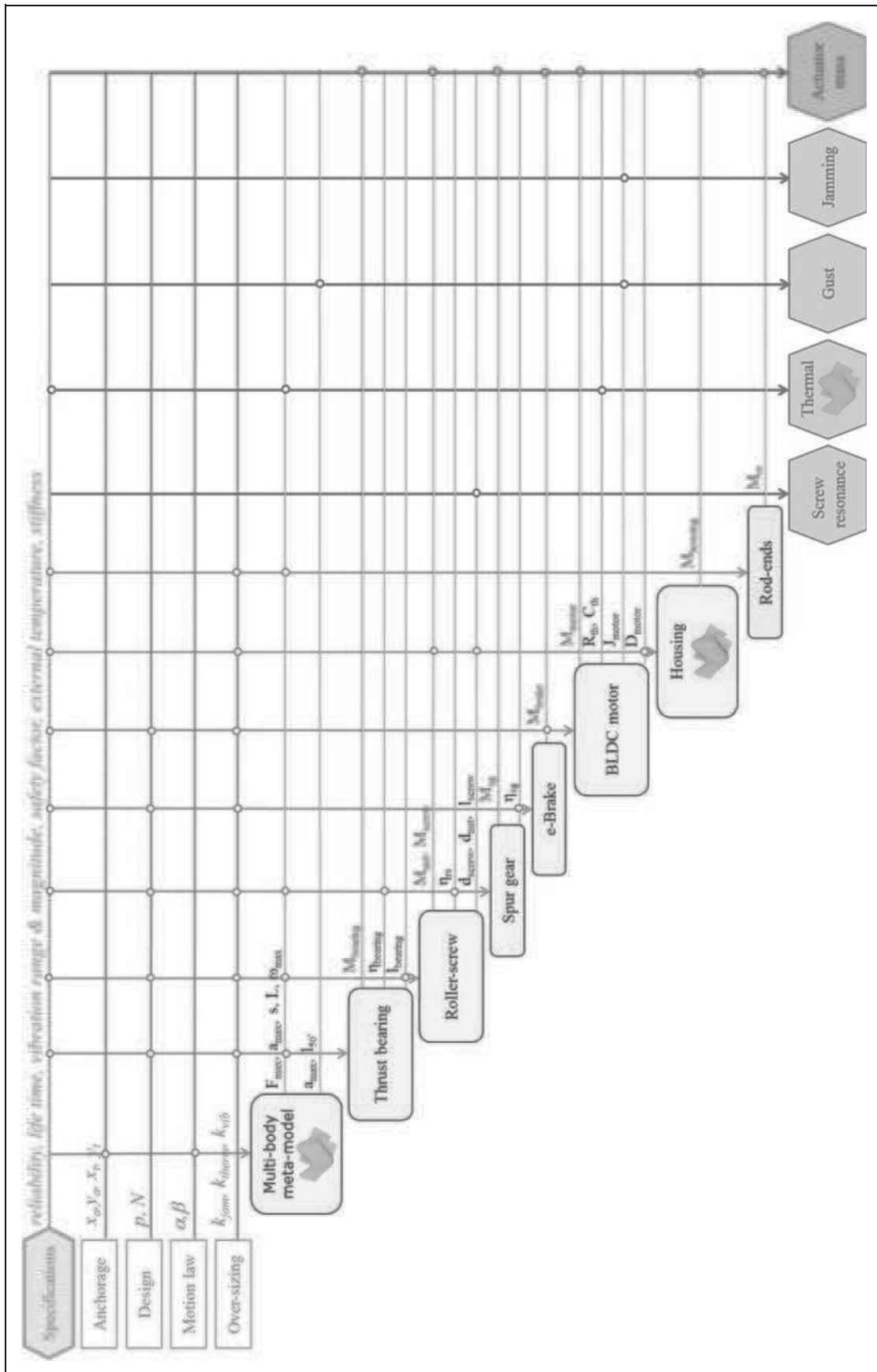


Figure 9. N² diagram of the sizing procedure.

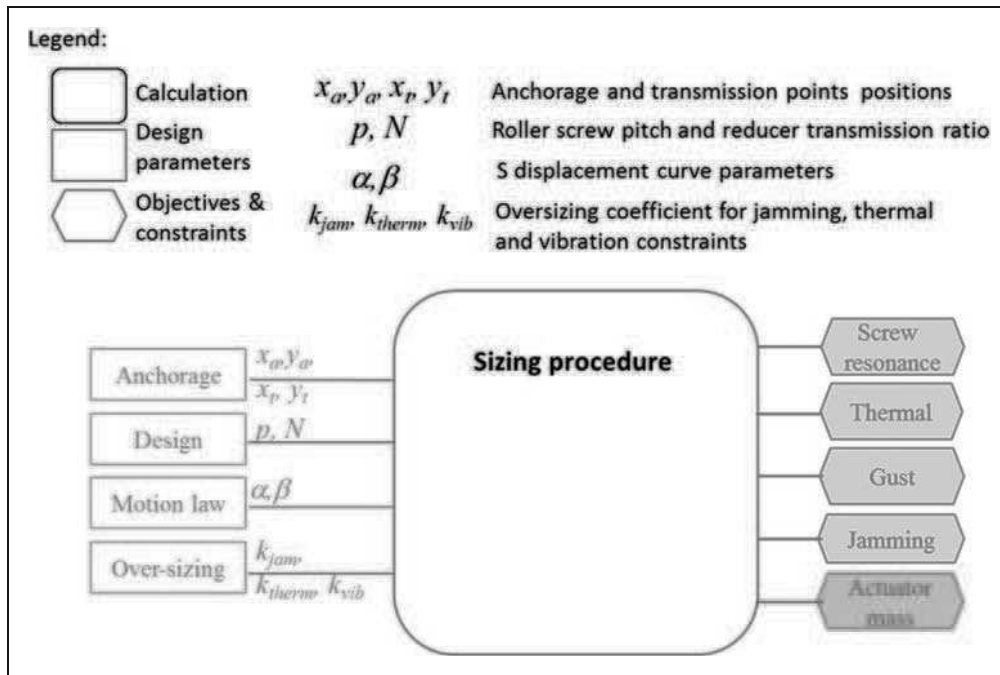


Figure 10. Influence diagram of the optimization problem.

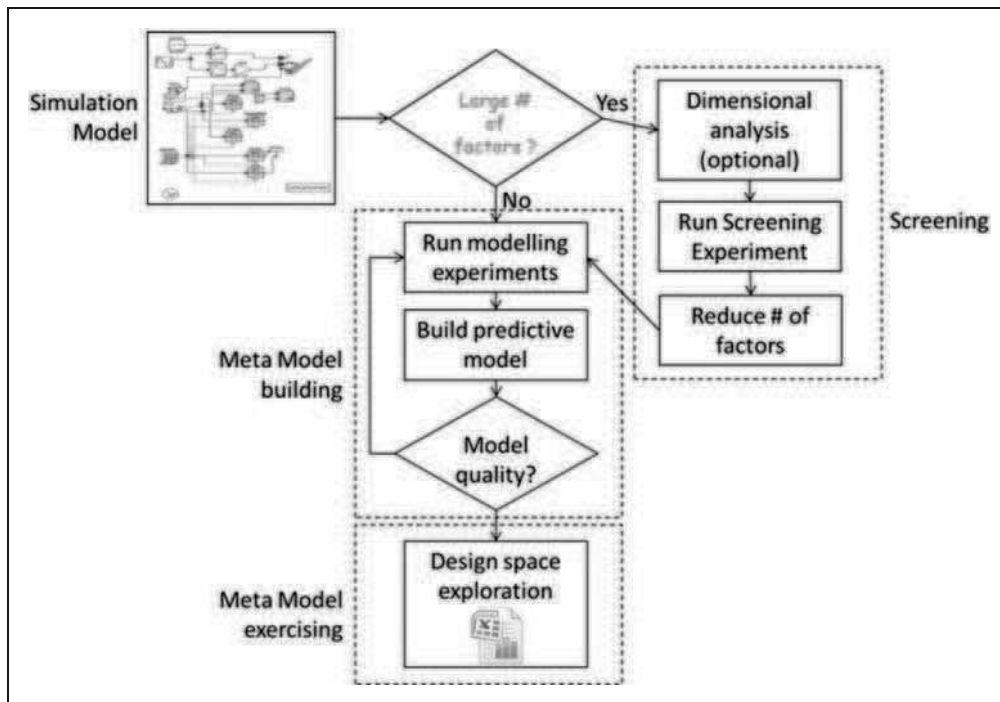


Figure 11. Meta model synthesis process.

here a polynomial form to facilitate their easy implementation into a calculation sheets (e.g. in the MS Excels environment) (Task 5, section “Task 5: Optimization and design exploration”). The generation of a meta-model follows the process shown Figure 11 and is performed here with the Optimus software.³⁸

Multi-body meta-model. The meta-models representing multi-body simulation link the effect of actuator geometric integration (anchorage x_a, y_a and transmission x_t, y_t points parameters, Figure 12) and the displacement curve form (α, β displacement curve parameters) to useful sizing criteria as stroke, maximum speed, maximum load, RMS and RMC load.

The identification of the main factors is done through screening. This screening step allows to conclude that for this application case, parameters α and β have only an influence on the maximum speed.

The meta-model building is realized here with a Latin Hypercube DOE of 1000 experiments. It is important to note that the model quality depends on the mathematical function used to represent the behavior³⁹ for example, assuming $1/F_{max}$ has a polynomial form better suits than expressing directly F_{max} as a polynomial function. With a second-order development, the meta-model provides a regression coefficient R better than 0.999 for all calculated values.

Thermal meta-model. The meta-model described here will be used to get the maximal temperature of the motor winding during scenario b) (cf. section ‘‘Sizing scenarios and corresponding mission profiles’’). For this example,

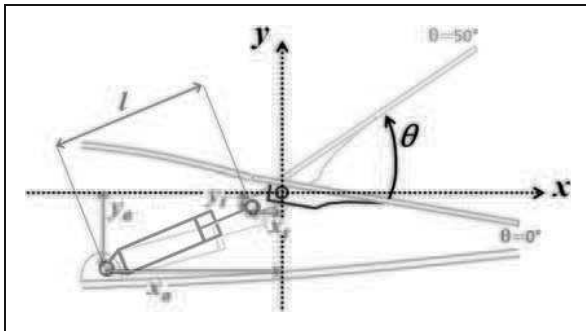


Figure 12. Anchorage and transmission points.

the main factors' identification is done by dimensional analysis^{40,41} which will reduce the number of parameters to be studied without any loss of information. The thermal model of a motor given in Figure 13, distinguish the temperature of the winding from the temperature of the yoke by using a two thermal bodies model.

The relationship to define is characterized by six parameters:

- The heat capacity of the winding C_{th1} ;
- The heat capacity of the yoke C_{th2} ;
- The thermal resistance between the winding and the yoke R_{th1} ;
- The thermal resistance between the yoke and the ambient air R_{th2} ;
- The thermal losses P_{th} ;
- The temperature increase θ of the winding after a given time t .

Buckingham theorem^{41,41} can be used to reduce this number to 4 dimensionless parameters:

$$\pi_4 = f(\pi_1, \pi_2, \pi_3) \text{ with } \pi_1 = \frac{R_{th1}}{R_{th2}}, \pi_2 = \frac{C_{th1}}{C_{th2}},$$

$$\pi_3 = \frac{t}{R_{th1} C_{th1}} \text{ and } \pi_4 = \frac{\theta}{R_{th1} P_{th}}$$

With a Latin Hypercube DOE of 100 experiments, a third-order development provides a coefficient of regression R better than 0.99 for this function. The desired function could also be derived from the direct solution of differential equations of the lumped

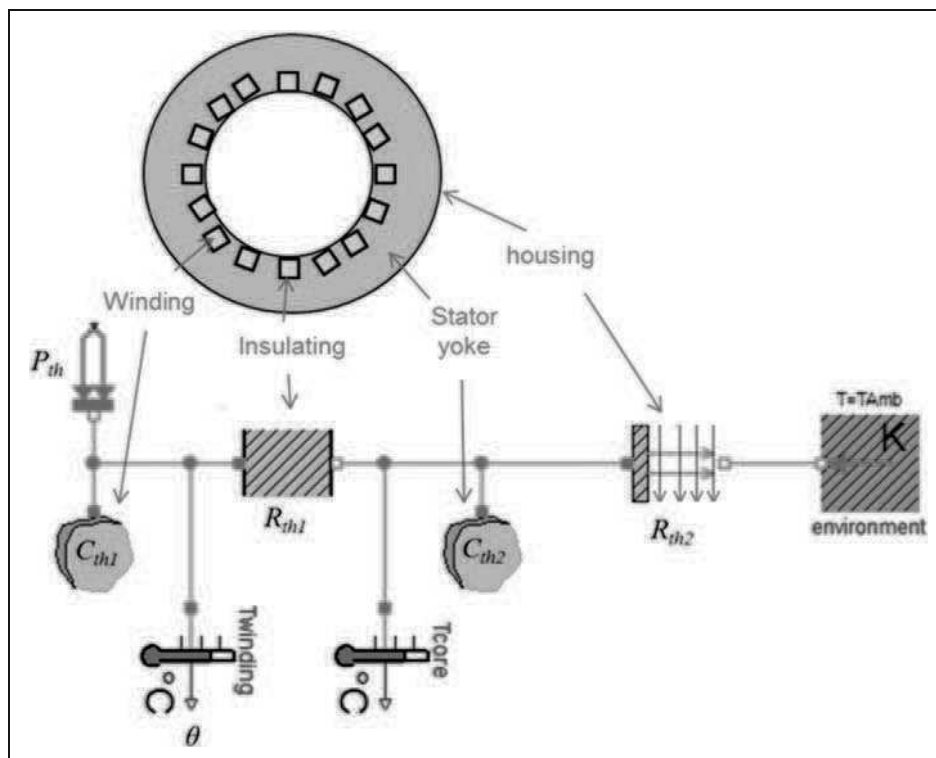
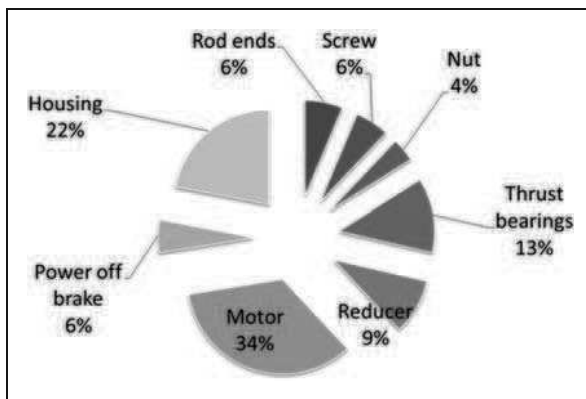


Figure 13. Thermal model of the motor.

Table 6. Optimum configurations.

Parameters	Range	Initial sizing	Optimal sizing (discrete screw pitch)			
Pitch p [mm]	[2;5]	5	2	3	4	5
Reducer ratio N [-]	[1;5]	3.00	2.44	4.40	5.00	4.99
Transmission x_t [mm]	[-50;0]	-25.0	-33.4	-33.7	-37.0	-50.0
Transmission x_t [mm]	[-80; -30]	-55.0	-80.0	-80.0	-80.0	-80.0
Anchorage x_a [mm]	[-400; -300]	-400.0	-400.0	-400.0	-396.3	-400.0
Anchorage x_a [mm]	[-150;50]	-150.0	-149.8	-149.7	-148.0	-150.0
S curve coefficient β [-]	[0.05;04]	0.25	0.4	0.4	0.4	0.4
Jamming oversizing k_{jam} [-]	[1;4]	1.02	1.47	1.48	1.43	1.44
Thermal oversizing k_{ther} [-]	[1;4]	1.10	1.18	1.21	1.20	1.19
Vibration oversizing k_{vib} [-]	[1;4]	1	1	1	1	1
Total mass [kg]		8.94	6.42	6.01	5.99	5.92

**Figure 14.** Mass distribution of an optimal sizing (pitch of 5 mm/rev).

parameters model shown in Figure 13. The aim here is to show that the designer can however get an algebraic expression from any numerical models. The meta-models thus allow him to focus more on the sequencing of calculations than on the solving of each calculation.

Task 5: Optimization and design exploration

The optimization process has been implemented using spreadsheet in the MS Excel environment taking benefit of the work done at previous steps: structuring the problem (task 3) and synthesizing meta-models (task 4). The design procedure is thus explicit and easily adaptable to any solvers or exploration functions (e.g. data tables, scenarios). Table 6 summarizes the optimal results obtained after 20 min of computation on a standard PC (Intel core i5 processor) with nonlinear GRG solver and Multi-Start option. The optimization has been carried out for different integer values screw pitches in millimeters to take into account manufacturing constraints and to evaluate the effect of this important parameter. Figure 14 gives the mass distribution for the optimal solution obtained using a 5 mm/rev screw pitch.

It is important to remark that the proposed process generates a gain of 33% on the mass in comparison with the initial sizing of section “**Task 2: Initial sizing and active design drivers**”. The initial sizing has been done choosing an anchorage point on the structure which facilitates the geometrical integration and taking average values for lever arm. At this point, a major part of the actuator mass was devoted to the brushless motor (almost 50%) due to a low global reduction ratio.

The parameters obtained for the optimal solutions highlight that:

- As inertial torque due to the motor inertia has limited impact on the maximal electromagnetic torque, the S curve parameter, β (constant speed ratio), has been maximized in order to minimize motor maximal speed. The conclusion can change if accelerations are higher and/or load features are different as for TVC actuators.³⁰
- The lever arm has been maximized to minimize load and component masses. The conclusion can be different if the actuator is longer, as for a landing gear extension/retraction actuator, where the housing mass, representing the major part of actuator mass, increases significantly with its length in order to resist to transverse vibratory stress.³⁴
- The global reduction ratio is limited here by the jamming requirement. This ratio can be different if the expected lifetime is greater (as for an aileron actuator) or for a different type of aircraft.

The different pitch values can be compared through design explorations around the optimal points. The graphs given in Figure 15 illustrate the evolution of the overall mass and main design constraints according to the two most influent parameters, i.e. the location the transmission point (parameters x_t and y_t). The other design parameters are set to the optimal values of Table 6. Each constraint is represented with dotted lines and defines a feasible solution search area with upper and lower

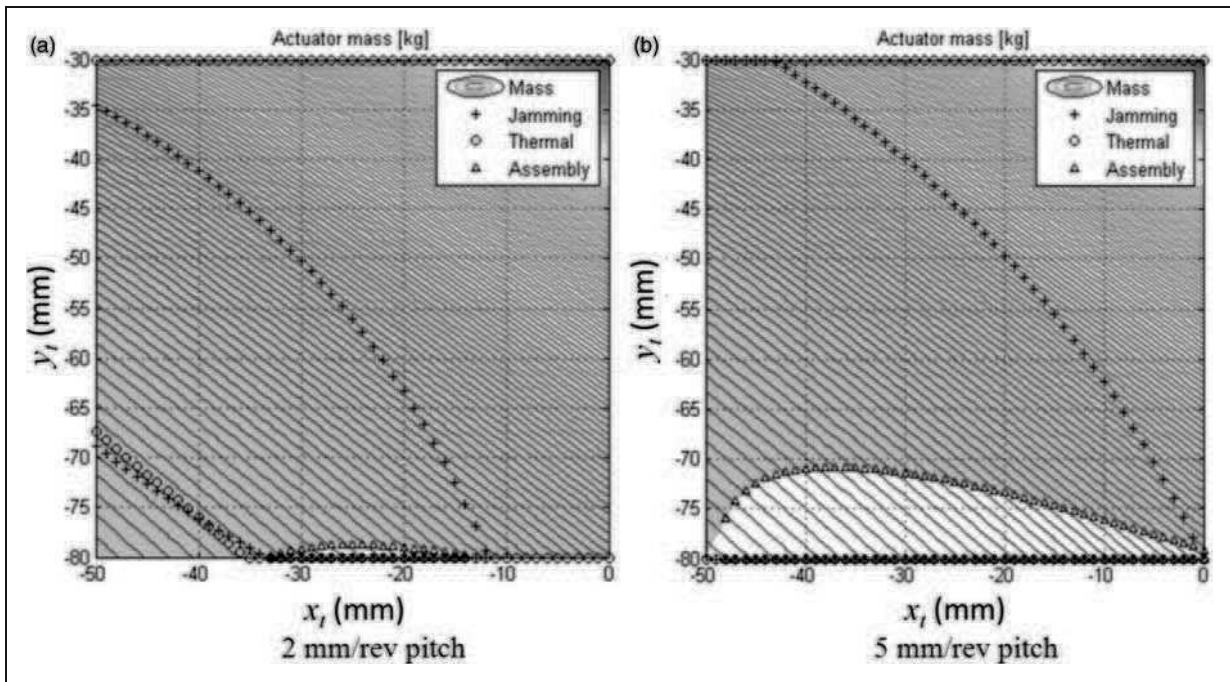


Figure 15. Mass and constraints exploration.

Table 7. Scaling laws and on the shell components comparison.

Component definition	Scaling laws estimation for optimal configuration	Nearby industrial components
Rod-end	58 kN (0.34 kg)	SKF-SAKB22F 58.5 kN (0.46 kg)
Plain bearing	58 kN (0.04 kg)	SKF-GE17C 56 kN (0.05 kg)
Screw	5 mm/tr-18 mm-58 kN (0.34 kg)	SKF-BRC21 × 5 (0.47 kg)
Nut	Ø38 mm. 54 mm (0.24 kg)	Ø45 mm. 64 mm (0.40 kg)
Thrust bearing	58 kN (0.76 kg)	SKF-5308E 65.5 kN (1.15 kg)
Reducer	16/40/80 module 1 (0.02 kg/0.10 kg/0.41 kg)	QTC-MSGAI-20/35/100 (0.02 kg/0.09 kg/0.68 kg)
Motor (frameless)	6.6 Nm (linear) (1.76 kg)	KOLLMORGEN-RBE021 14 6.4 Nm (2.18 kg)
Motor (housing)	(0.24 kg)	
Brake	4.5 N.m (0.33 kg)	OGURA-TMB-0.6 (6 Nm) (0.32 kg)
Housing d1/e1/d2/e2	38/2/87/2 mm (1.33 kg)	38/2/87/2 mm (1.33 kg)
Total mass	≈ 6.0 kg	≈ 7.1 kg

bounds. For a 2 mm pitch, Figure 15(a), the feasible design field is clearly limited by all these constraints. Therefore, the designer has a poor design flexibility. While for a 5 mm pitch, Figure 15(b), the feasible search space is much bigger. The designer can thus choose a slightly different solution without adding significant weight to the actuator, while increasing robustness with regard to the assembly and jamming constraints.

Task 6: Validation

For validation, it is particularly important to check that for the optimal parameters:

- The response surface approximation, established during task 4 (section “Task 4: Meta-models

synthesis”), is sufficiently accurate. Otherwise, it is necessary to construct the response surface again, refining mathematical formula around the point of interest;

- The simplification assumptions established during task 2 (section “Task 2 : Initial sizing and active design drivers”), remain effective. If a design driver defined as inactive during the initial design becomes dominant for the optimal configuration, this new constraint must be integrated and the optimization launched again.

In the case study considered here, time domain simulations validate the results obtained within spreadsheets. It may also be interesting to validate the estimation models results (extrapolation of selected industrial components features) comparing

them to real industrial components extracted from manufacturer datasheets. Table 7 compares optimal results for a 5 mm/rev screw pitch using scaling (column 1) to real industrial components (column 2). The mass deviation gives an idea of the mass penalty which may be due to components standardization and discretization of a product range. Yet, the scaling laws, in the case of a specific design as typically encountered till now in aerospace domain, allow specifying or estimating new components features.

Solution using standard components does not differ a lot from obtained “optimal” configuration, with a difference lower than 20% on the overall mass. This difference is mainly due to weak manufacturer product choices when considering thrust bearing and roller-screw components.

It may be noted that the overall methodology is well suited to collaborative work and development of multi-domain systems:

- The rationalization of the sizing scenarios determination in step 1 is well suited to group meetings;
- The distribution of work is intrinsic to the methodology. The system engineer can define the sizing procedure (step 2) and achieve the final optimization in excel (step 5). Experts of different technical areas (kinematics and mechanical power transmission, thermal of electrical motors, etc.) can establish meta-models;
- Thanks to distinction between simulation models and estimation models (scaling laws), the management of supplier’s data is facilitated. The updating of scaling laws references enables to take into account technical developments or to compare some technologies;
- Meta-modeling takes into account multiple design criteria within multiple domains;
- Verification/validation are done through steps 1 and 6.

Conclusion

A technology shift towards more electric solutions is emerging in aerospace actuation. New technology brings new challenges, especially for the preliminary design process of actuation systems and components that cannot simply duplicate former practices. In this way, it is no longer meaningful to proceed to static sizing by typical operating points as was possible for hydraulic actuators that do not induce strong couplings in design. Instead, it is necessary to take into account transient mission profiles covering all possible sizing drivers (e.g. maximum speed and torque, fatigue, thermal behaviour, vibrations and shocks) and addressing various design criteria (e.g. geometrical envelope, weight and reliability). For this purpose, appropriate models and methodologies should be

developed to support an efficient optimal preliminary design. In this paper, a structure for component model has been presented in order to transform the system simulation tools into design tools. This model structure is based on three different types of models: estimation, simulation and evaluation models. This paper also mainly describes a six-step design methodology to define the sizing scenarios to consider and gradually transform the corresponding transient simulations into design models combining judiciously scaling laws and response surface approximation into selection procedures established using N2 diagram. This decomposition facilitates the optimization model, the exploration of the design space, taking into account multiple design constraints. This methodology fits well in a collaborative engineering work for the decomposition of tasks and studies; verification/validation process, the rapid updating of technological references; and the optimization and knowledge management process. This methodology has been illustrated with a study case of an EMA dedicated to spoiler actuation which is realistic and representative of the number of functions, the multiple points of views for design and the different technological domains to take into account in order to achieve preliminary design of an EMA. This case study has illustrated the interest of the methodology and has enabled to describe all the tasks. This methodology is applicable to other configurations (TVC, landing gear actuator, etc.), other technologies (hydraulic, power electronics, control) and even other technical systems.

Funding

The work presented was partly funded by the European ACTUATION 2015 project (Modular Electro Mechanical Actuators for ACARE 2020 aircraft and helicopters).

References

1. Rosero JA, Ortega JA, Aldabas E and Romeral L. Moving towards a more electric aircraft. *Aerospace and Electronic Systems Magazine, IEEE*, 2007; 22 (3): 3,9.
2. Weimer JA. The role of electric machines and drives in the more electric aircraft. In: *Electric machines and drives conference*, Madison, Wisconsin, 2003. IEMDC’03. IEEE International, vol. 1, June 2003, pp.11–15.
3. van den Bossche D. A380 primary flight control actuation system. In: *International conference on recent advances in aerospace actuation systems and components*, Toulouse, France, Jun 2001, pp.1–4.
4. Todeschi M. Airbus – EMAs for flight actuation systems – perspectives. In: *International conference on recent advances in aerospace actuation systems and components*, Toulouse, France, May 2010, pp.1–8.
5. Dée G, Vanthuyne T and Alexandre P. An electrical thrust vector control system with dynamic force feedback. In: *International conference on recent advances in aerospace actuation systems and components*, Toulouse, France, June 2010, pp.75–79.

6. Cowan JR and Weir RA.. Design and test of electro-mechanical actuators for thrust vector control. *The 27th aerospace mechanisms symposium*. 1992, pp.349–366.
7. VDI, *Design methodology for mechatronic systems*. Düsseldorf.
8. Chevalier P-Y, Grac S and Liegois P-Y. More electrical landing gear actuation systems. In: *Recent advances in aerospace actuation systems and components*, Toulouse, France, May 2010.
9. Auweraer H, Anthonis J, Bruyne S, et al. Virtual engineering at work: the challenges for designing mechatronic products. *Eng Comput* 2013; 29: 389–408.
10. Budinger M, Liscouët J, Hospital F, et al. Estimation models for the preliminary design of electromechanical actuators. *Proc IMechE, Part G: J Aerospace Engineering* 2012; 226: 243–259.
11. Liscouët J, Budinger M and Maré J-C. Design for reliability of electromechanical actuators. In: *Recent advances in aerospace actuation systems and components*, Toulouse, France, May 2010.
12. Cellier F and Greifeneder J. *Continuous system modeling*. New York: Springer, 1991.
13. Liscouët J, Budinger M, Maré J-C, et al. Modelling approach for the simulation-based preliminary design of power transmissions. *Mech Mach Theory* 2011; 46: 276–289.
14. Budinger M, Halabi TE Maré J-C. Optimal preliminary design of electromechanical actuation systems. In: *More electrical aircraft technologies, symposium SPEC*, Lyon, France, November 2011.
15. Messine F, Nogarede B and Lagouanelle J-L. Optimal design of electromechanical actuators: a new method based on global optimization. *Magn IEEE Trans* 1998; 34: 299–308.
16. INCOSE, *Systems engineering handbook*. I.T. Product, 2004.
17. Murray-Smith DJ. The inverse simulation approach: a focused review of methods and applications. *Math Comput Simul* 2000; 53: 239–247.
18. Mattsson SE, Elmquist H and Otter M. Physical system modeling with Modelica. *Control Eng Pract* 1998; 6: 501–510.
19. Roos F. Towards a methodology for integrated design of mechatronic servo systems. PhD Thesis, Royal Institute of Technology, Stockholm, Sweden, 2007.
20. Sobieszcanski-Sobieski J and Haftka RT. Multidisciplinary aerospace design optimization: survey of recent developments. *Struct Optim* 1997; 14: 1–23.
21. Rottach M, Gerada C, Hamiti T, et al. Fault-tolerant electrical machine design within a rotorcraft actuation drive system optimisation. In: *6th IET international conference on power electronics, machines and drives (PEMD 2012)*, March 2012, pp.1–6.
22. El-Halabi T, Budinger M and Maré J-C. Optimal geometrical integration of electromechanical actuators. In: *Recent advances in aerospace actuation systems and components*, Toulouse, France, May 2010.
23. Simpson T, Peplinski J, Koch P, et al. Metamodels for computer-based engineering design: survey and recommendations. *Eng Comput* 2001; 17: 129–150.
24. Keane AJ and Nair PB. *Computational approaches for aerospace design: the pursuit of excellence*. New York, USA: John Wiley & Sons, 2005.
25. Estefan JA. Survey of model-based systems engineering (MBSE). INCOSE Technical report, May 2007.
26. Martin JN. *Systems engineering guidebook: a process for developing systems and products*. Boca Raton, FL: CRC Press, 1996.
27. Davis M A. High performance electromechanical servoactuation using brushless DC motors. Technical bulletin 150, MOOG, Technical report, 1984.
28. Flight control systems. In: *Moog-navy league: sea, air and space. Special Edition*, Available at: www.moog.com/literature/Space_Defense/Naval/Navy_League_Newsletter.pdf (accessed January 2013).
29. Schaefer WS, Inderhees LJ and Moynes JF. Flight control actuation system for the B-2 advanced technology bomber. *SAE Tran* 1991; 100: 284–295.
30. Grand S. Electromechanical actuators design for thrust vector control. In: *Recent advances in aerospace actuation systems and components*, Toulouse, France, November 2004.
31. Hagen J, Moore L, Estes J, et al. The X-38 V-201 flap actuator mechanism. In: *Proceedings of the 37th aerospace mechanisms symposium*, Johnson Space Center, May 2004.
32. Schinstock DE and Scott DA. Controller design for EMA in TVC incorporating force feedback. NASA/MSFC, Technical report, 1998.
33. DO 160 E, *Environmental Conditions and Test Procedures For Airborne Equipment, standard for environmental test of avionics hardware*, EUROCAE ED-14E, March 2005.
34. Hospital F, Budinger M, Reysset A, et al. Preliminary design of linear actuator housings for aerospace vibratory environment. Paper submitted to *Aircraft Eng Aerosp Technol*, Emerald.
35. Browning TR. Applying the design structure matrix to system decomposition and integration problems: a review and new directions. *IEEE Trans Eng Manage* 2001; 48: 292–306.
36. NASA (Ed.) *Techniques of functional analysis, NASA systems engineering handbook*. 1995. Washington DC, USA: NASA.
37. Malak RJ, Tucker L and Paredis CJJ. Compositional modelling of fluid power systems using predictive trade-off models. *Int J Fluid Power* 2009; 10: 45–56.
38. Poles S, Vassileva M and Sasaki D. Multiobjective optimization software. In: Branke J, et al. (Eds) *Multiobjective optimization*, vol. 5252. Berlin: Springer, 2008, pp.329–348.
39. Montgomery DC and Runger GC. *Applied statistics and probability for engineers*. 4th ed. New York, USA: John Wiley & Sons, 2006.
40. Vignaux VA and Scott JL. Theory & methods: simplifying regression models using dimensional analysis. *Aust N Z J Stat* 1999; 41: 31–41.
41. Gogu C, Haftka RT, Bapanapalli SK, et al. Dimensionality reduction approach for response surface approximations: application to thermal design. *AIAA J* 2009; 47: 1700–1708.
42. Fuerst D and Neuheuser T. Development, prototype production and testing of an electromechanical actuator for a swashplateless primary and individual helicopter

- blade control system. In: *1st international workshop on aircraft system technologies*, Hamburg, Germany, March 2007, pp.7–19.
43. Kopala DJ and Doel C. High performance electromechanical actuation for primary flight surfaces (EPAD program results). In: *Recent advances in aerospace actuation systems and components*, Toulouse, France, June 2001.
44. Budinger M, Fraj A, Halabi TE, et al. Coupling CAD and system simulation framework for the preliminary design of electromechanical actuators. In: *IDMME virtual concept*, Bordeaux, France, October 2010.
45. Liscouet J, Mare J-C and Budinger M. An integrated methodology for the preliminary design of highly reliable electromechanical actuators: search for architecture solutions. *Aerosp Sci Technol* 2011; 22(1): 9–18.
46. Maré J-C. Friction modelling and simulation at system level – a practical view for the designer. In: *Proceedings of the Institution of Mechanical Engineers, Part I, Journal of Systems and Control Engineering*, 2012 (Paper accepted).
47. Collins A. EABSYS: electrically actuated braking system. In: *Electrical machines and systems for the more electric aircraft (Ref. No. 1999/180)*, IEE Colloquium, 1999, pp.4/1–4/5.

Appendix

Notation

Pseudonyms

DOE	Design of Experiments
EBHA	Electrical Back-up Hydraulic Actuator
EHA	Electro-Hydrostatic Actuator
EMA	Electro Mechanical Actuator
MDO	Multi-Disciplinary Optimization
MEA	More Electric Aircraft
MTBF	Mean Time between Failures
PbW	Power-by-Wire
RSM	Response Surface Method
RMC	Root Mean Cube
RMS	Root Mean Square
TVC	Thrust Vector Control

Variables and constraints

A_{max}	Maximal acceleration of mechanical profile
C_{th}	Thermal capacitance
d_{comp}	Diameter of component (with <i>comp</i> the name of component)
$f(x)$	Objective function
F_{max}	Maximal force
g	gravity acceleration
$g(x)$	Constraint function (inequality)
$h(x)$	Constraint function (equality)
J	Inertia
J_{max}	Maximal Jerk of mechanical profile
k_{jam}	Oversizing coefficient for jamming constraints
k_{therm}	Oversizing coefficient for thermal constraints
k_{vib}	Oversizing coefficient for vibration constraints
L	Length of actuator
l_{comp}	Length of component (with <i>comp</i> the name of component)
M_{comp}	Mass of component (with <i>comp</i> the name of component)
N	Reducer transmission ratio
p	Roller screw pitch
R_{th}	Thermal resistance
s	Stroke
t_m	Motion time of mechanical profile
V_{max}	Maximal speed of mechanical profile
x	Design variables
x_a, y_a	Anchorage point coordinates
X_{max}	Displacement of mechanical profile
x_t, y_t	Transmission point coordinates
α	Constant Jerk ratio of mechanical profile
β	Constant speed ratio of mechanical profile
θ	Temperature increase
η_{comp}	Efficiency of component (with <i>comp</i> the name of component)
π_i	dimensionless parameters

Postface and perspectives

As presented in the preface of this document, my research work undertaken in recent years has been developed on different areas: technologies, models and methods. These different aspects will be summarized here and the prospects, which I consider for each axe, will be given.

1. TECHNOLOGIES

1.1. Collaborative work on electromechanical actuators

The aerospace environment of Toulouse generated for our team contracts and projects about electromechanical actuators for flight control and landing gear systems. Our work is mainly devoted to the design and the modeling of these systems as a whole. The realization of prototypes with demanding aerospace standards was most often done by industrial partners of these collaborative projects. Our contribution in these projects was focused on architectures, methods and models of existing actuator technologies. The system level design of such technologies, exhibiting multi-domain aspects (mechanical, electrical machines, power electronics, etc.) with coupled constraints of the embedded environment and strong objectives of integration, includes very interesting challenges.

1.2. Towards innovative mechatronic components and systems

If the primary functions and core technologies of electromechanical actuators, such as electric machines with permanent magnets and mechanical power transformation with roller screws are intensely studied and optimized at the industrial level, it may be interesting to study secondary functions or new functions of actuators with innovative technologies of electromechanical conversions. The proposed work as perspective track would be to study the use of resonant piezoelectric actuators, an area where I have experience through my PhD thesis work [1], for the realization of these functions.

A first axis concerns mechatronic components for EMA. The EMA have advantages compared to hydraulic actuator such as easier maintenance and better energy management. However, they have some disadvantages such as higher mass. Moreover, in order to fulfill some particular operational modes (e.g. the function of free castoring for the nose landing gear steering actuator) or to meet fail safe requirements (e.g. the free fall function for the extension/retraction actuator of landing gear), they require the addition of bulky components such as clutches, electromagnetic brakes or complex electromechanical systems. Piezoelectric technology seems to be an interesting track to follow to meet those functions of clutch, brake or disconnection devices. Indeed piezoelectric materials are characterized by a density of force 10 to 100 times higher than the electromagnetic solutions [2] and thus allow to imagine solutions close to the mechanical load. The stroke generated by piezoelectric ceramics are however very small and have to be amplified by a mechanical resonance to avoid sensitive mechanisms to variations in temperature and wear. The first research works of the state of the art on the subject modulate the contact force and the apparent coefficient of friction by vibrations and action on the normal force [3] [4]. I'm starting this topic with some research projects of INSA students. The first goal is to compare different operating configurations as illustrated in Figure 1. It would be then interesting to develop the most interesting concept within the Research Axis Assemblies, a transverse axis of the ICA laboratory. For relatively small effort, as a few hundreds of N, this type of device can be applied for pin-puller mechanisms which are used to release pre-stressed structures in space applications. It is therefore possible to consider funding as R&T projects of CNES on the subject before working on the higher effort ranges, several tens of kN, typical of aircraft actuators.

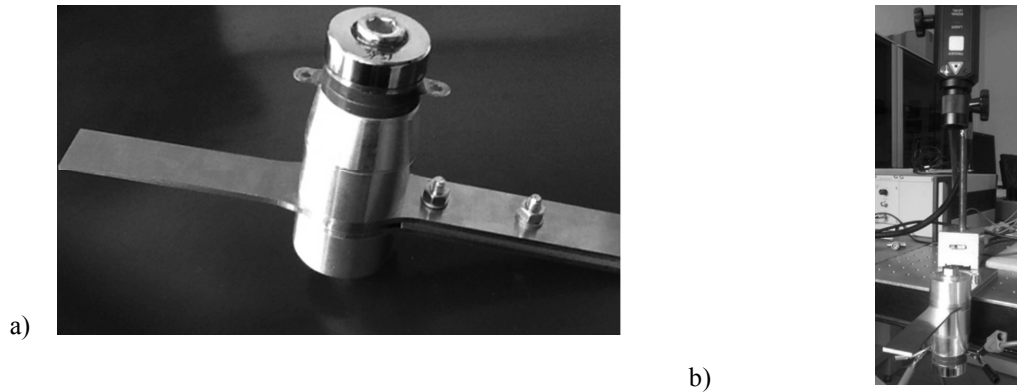


Figure 1 – First prototype for piezoelectric disconnection device

A second axis relates to embedded systems serving different functions than the flight controls as the de-ice systems on the leading edge of wings or engine inlets. Classical solutions use warm air which is bled from engines and is ducted into a cavity beneath the surface to be anti-iced and heats the surface up to a few degrees above 0 °C, preventing ice from forming. A bleed less aircraft needs to fulfill this function by electrical means such as heated resistive elements embedded in the leading edges of wings and tail surfaces. This solution, however, requests high electric power and has a significant impact on the mass of the electrical network. Other solutions using pneumatic or electromechanical actuators have been developed and present good performance while being more energy efficient but are still bulky. The resonant piezoelectric actuators thus seem also to be advantageous to fulfill to this function in a more compact way. Early American work [5] shows that it is possible to break the ice instantly using resonant piezo actuators (Figure 2). However levels of stress in ceramics are high and can lead to their destruction. A multi-partner collaboration begins with ISAE / ENSICA, for control and measurement, Carleton University (Canada), for ice-phobic materials, and Airbus for realistic specifications. The objectives are: the study of different resonance modes and corresponding stress level for a leading edge, choice of the most appropriate excitations, design of the actuators and study of surface coating to reduce the shear strength of the ice. These early studies begin with a collaborative funding of Toulouse (TTIL) that will fund several interships and a test bench. European fundings allowing collaboration with Canada are also possible depending on results.

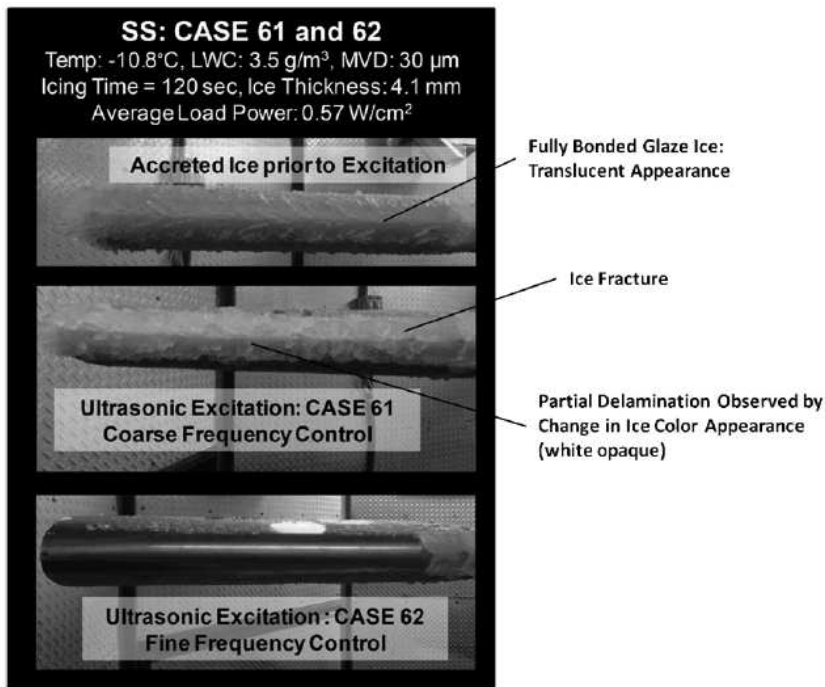


Figure 2 – Rotor blade ultrasonic deicing [5]

2. MODELS

2.1. Models for design at system level

Any engineering or scientific activity is supported by models which must be adapted to the considered study. The design of mechatronic systems requires specific models that formed the first chapters of this document. The mechatronic devices are usually represented by models of system simulation. If these models are useful in the synthesis of control, they are not sufficient for the design of the physical part. It has been shown that it was necessary to add to these models, useful for analysis, other types of models to make design. These models were called here, estimation models and evaluation models. They provide access to the required technological knowledge of components without requiring the design of each component in detail.

2.2. Towards a knowledge transfer from specific domain to system level domain

The regression algorithm presented in the paper 4, aims to provide estimation models usable at system level from knowledge of specific domains. A perspective work area will be on the improvement and the use of this regression process. The potential application areas are many, but the first works will concern the thermal field. The Electromechanical actuators, as all more electrical systems, are indeed highly constrained by their temperature. For the simulation of the thermal behaviour, a wide range of tools, such as finite elements or finite volumes, is available. However, all these tools require a defined geometry. Consequently, they are used in the bottom of the V-cycle or in the ascending phase using reduction techniques models, but are totally unsuitable for the descending phase (i.e. preliminary design). The objective of this work would be the generation of analytical laws of thermal models for geometries and boundary conditions misrepresented by the available semi-empirical laws. This work starts in collaboration with I. Hazyuk, new researcher in the team, and F. Sanchez, research engineer funded through Syrena and Actuation 2015 projects. First works have tested the algorithm SLAWMM to configurations found in the literature [6] and have shown the interest of such models to compare cooling architectures (Figure 3). The following of this theme goes through a funding application to a doctoral thesis from MEGEP school and a deposit of ANR project in 2014 in response to the call FRAE "Modelling and simulation of thermal models." This latter project was set up in collaboration with the company Epsilon specialized in thermal simulation.

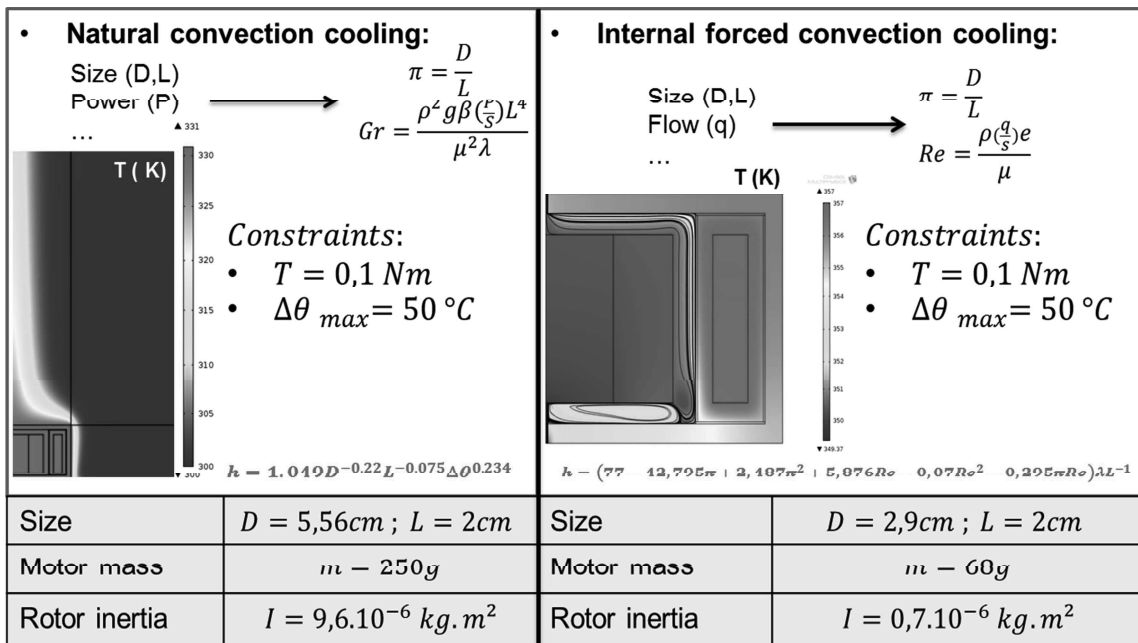


Figure 3 – Cooling architectures comparison for a LAT actuator

3. METHODS

3.1. Formalization of the design problem at system level

To design EMA actuators, different combinations of models have been tested. The combined use of the three types of model (estimation, simulation and evaluation) in a Modelica environment is interesting for the design requiring the evaluation of transitory profiles mission. The main interest of this kind of implementation is for initial sizing. Direct interaction with the designer and the simulation tool provides insight into the design problem. These simulations also allow the main design criteria for the application to be determined. However, the optimization of the device by direct appeal of this type of simulation is time consuming. It is more efficient to represent transient simulations required by meta- models. The set of algebraic equations representing the design problem can then be formalized by design graph or by algorithms from the graph theory.

3.2. Towards a computer aided sizing of mechatronic systems

The combined use of different types of models to realize design tools was applied to no propulsion systems (actuators, mutualized power electronics). A new collaboration with the laboratory Laplace (X. Roboam) on this design tools thematic is being prepared via a grant application for a Phd funding (Cifre Airbus). It aims to extend these approaches to multi-domain propulsion systems (thermodynamics, mechanics, electrotechnics, power electronics). In this context a first study contract with D. Leray, researcher of the ICA laboratory, and J. Thauvin, research engineer, prepares this thesis on reducer aspect.

If the graphs design helped to formalize some industrial problems or are used by our students, the algorithmic scheduling of equations is quite new for our team and start via the thesis of A. Reysset. A perspective work therefore regards the extension of this research axis to provide algorithms and tools needed to sizing at system level with: a multi-view approach by taking into account various design scenarios, the compact representation of models (using metamodels or reduced models), the capitalization of knowledge in the form of libraries, the scheduling of equations according to the need of the considered design problem (optimization, robustness study, etc..). The computer implementation of such an environment starts, but will certainly require additional national or european projects.

4. BIBLIOGRAPHY

- [1] M. Budinger, Contribution à la conception et à la modélisation d'actionneurs piézoélectriques cylindriques à deux degrés de liberté de type rotation et translation, Thèse INP Toulouse, 2003.
- [2] B. Nogarede, "Moteurs piézoélectriques," *Techniques de l'ingénieurs*, vol. D3765, 1996.
- [3] K.-T. Chang, "Development of Ultrasonic Clutch Module with Piezoelectric Vibrators," *International Journal of Applied Science and Engineering*, vol. 4, no. 2, pp. 205-213, 2006.
- [4] G. L., Etude du phénomène de lubrification active électroactive à l'aide d'actionneurs piézoélectriques, thèse INP Toulouse, 2006.
- [5] A. Overmeyer, J. Palacios and E. Smith, "Actuator Bonding Optimization and System Control of a Rotor Blade Ultrasonic Deicing System," in *53rd AIAA/ASME/ASCE/AHS/ASC Structures, Structural Dynamics and Materials conference*, Honolulu, Hawai, 2012.
- [6] M. Budinger, I. Hazyuk, F. Sanchez and J.-C. Maré, "Scaling-law-based metamodels for the sizing of actuation systems," in *Recent Advances in Aerospace Actuation Systems and Components*, Toulouse, 2014.

Annexe 1 – Curriculum Vitae, version détaillée (Française)

1. CURRICULUM VITAE

1.1. Situation administrative et professionnelle

Date et lieu de naissance : 24 mai 1975 à Mt St Martin (54)
Situation de famille : Marié, 2 enfants
Situation professionnelle : Maître de conférences au département de génie mécanique de l'INSA de Toulouse.

Adresse personnelle : 17, rue Saint Hyacinthe
31500 Toulouse
Tel. : (0033) 05 62 16 39 36
(0033) 06 66 70 00 11
marc_budinger@yahoo.com

Adresse professionnelle : INSA Toulouse, Institut Clément Ader
135 Avenue de Rangueil
31004 Toulouse, France
Tel. : (0033) 05 61 55 99 60
marc.budinger@insa-toulouse.fr

1.2. Formation

2000-2003 : **Thèse** au Laboratoire d'Electrotechnique et d'Electronique Industrielle (UMR CNRS-ENSEEIH Toulouse). Doctorat en Génie Electrique obtenu le 26 mai 2003.
Qualifié en 60ème (mécanique) et 63ème section (électrotechnique et électronique).

1995-2000 : Elève de l'**ENS de Cachan** après admission sur concours 1ere année.
DEA Génie Electrique ENSEEIHT-UPS Toulouse (Mention : Très Bien, 1^{er}).
Agrégation de Physique Appliquée (Classement : 1^{er}).
Maîtrise EEA Orsay-ENS Cachan (Mention : Très Bien).
Licence Ingénierie Electrique Orsay-ENS Cachan (Mention : Bien).

1993-1995 : Classes préparatoires Math Sup, Spé Technologiques T.

1.3. Activités d'enseignement

INSA - Toulouse, 2006-

Cours, TD et TP en ingénierie système (actionneurs électriques, simulation globale et locale, automatique) et en génie mécanique (automatique, simulation système, vibrations). Pour plus de détails voir la section description des enseignements à INSA Toulouse.

Lycée A. Bourdelle - Montauban, 2005-2006

Cours, TD et TP d'Electronique en BTS Systèmes Electronique 2ère année (10 h/semaine)

Cours, TD et TP en première Génie Mécanique (3 h/semaine)

Lycée Champollion - Figeac, 2004-2005

Cours, TD et TP d'Electronique en BTS Systèmes Electronique 1ère année (10 h/semaine)

Cours et TD d'Electrotechnique en BTS productique 1ère année (2 h/semaine)

Ecole Nationale Supérieure d'Ingénieurs en Constructions Aéronautiques (ENSICA) - Toulouse, 2002-2006

TP du module CSF (Contrôle de Structures Flexibles) du master recherche SAID (simulation d'une aile active et obtention d'un modèle pour la commande à l'aide d'ANSYS).

2010-

Cours et TD sur la conception préliminaire d'actionneurs aéronautique

Ecole Supérieure d'Ingénieurs de Poitiers (ESIP) – Poitiers, 2005-2007

Cours et TD sur les actionneurs et transducteurs piézoélectriques (structures, modélisation et commande) en dernière année AGE (Automatique et Génie Electrique).

Ecole Nationale Supérieure d'Arts et Métiers (ENSAM) - Bordeaux, 2000 et 2003-2004

TD-TP d'Electronique, d'Electrotechnique et d'Electronique de puissance.

Ecole Nationale Supérieure d'Electrotechnique, d'Electronique, d'Informatique et d'Hydraulique de Toulouse (ENSEEIHT) - Toulouse, 2000-2003

Micro Projet d'électronique de puissance (étude et réalisation d'un onduleur)

TER (Travaux d'Etude et de Recherche) sur les moteurs piézo-électriques (simulation éléments finis et réalisation d'un petit moteur ultrasonore)

Projet Long CEM (simulation et mesures CEM en électronique de puissance)

CESI (Centre d'Etudes Supérieures Industrielles) Aquitaine - Bordeaux, 2000-2004

Cours, TD et TP dans le module de remise à niveau en physique de la formation ingénieur.

1.4. Responsabilité administratives, examens et concours

INSA Toulouse – 2007-2011

Responsable de la 4ème année Génie des Systèmes Industriels (GSI).

Concours TIPE - Paris, juillet 2003- 2005

Examineur aux oraux en section PT, TSI et PSI.

Agrégation de Physique Appliquée - Paris, 2006-2009

Membre du jury. Rédaction de 2 sujets d'écrit.

1.5. Expériences professionnelles

JEUMONT Industrie (groupe FRAMATOME) – Jeumont (59)- Septembre 1998 à Juin 1999

Poste de scientifique du contingent DGA au bureau d'étude des activités électromécaniques. Participation au dimensionnement d'un moteur électrique de sous-marin (moteur synchrone à aimants permanents de 3 MW à grand nombre de phases).

Laboratoire d'Electrotechnique et de Machines Electriques - EPFL (Suisse) – Juin et juillet 1997

Dimensionnement d'actionneurs et de moteurs linéaires à aimants permanents.

LESiR (Laboratoire d'Electrotechnique, de Signal et de Robotique ENS Cachan) - Mai 1997

Alimentation d'un moteur linéaire à réluctance variable.

JEUMONT Industrie (groupe FRAMATOME) – Jeumont (59)- Juin et Juillet 1996

Stage ouvrier sur la plate-forme d'essais de moteurs électriques (mesures électriques et thermiques).

2. ENSEIGNEMENT

Intitulé Code apogée	Type et niveau d'enseignement	Description de l'enseignement
Introduction à l'Ingénierie Système I2IC IS11	CM-TD-PJ 2IC 30 h /an Responsable d'UF	Ce module est une introduction à l'ingénierie des systèmes sur les aspects analyse fonctionnelle, mise en place d'un cahier des charges, modélisation et conception système pluri technique (meca/élec/hydro/commande). Un sujet d'étude au choix des étudiants (direction assistée, motorisation d'ascenseur, commande de vol) permet d'illustrer et d'appliquer ces notions. <i>Apport personnel : Création de l'UF</i>
Systèmes dynamiques I3IC SD11	TD 3IC spring semester 20 h /an	Ce module concerne les outils mathématiques et les concepts nécessaires à la modélisation de systèmes dynamiques : transformée de Laplace, fonction de transfert, diagramme de Bode, espace d'état. <i>Apport personnel : Mise en place une série de TD adaptés aux spring semester, étudiant américains en échange (développement mathématique moins abstrait).</i>
Modélisation multiphysique I4IS MP11	CM-TD 4GM-IS 4AE-IS 35 h /an Responsable d'UF	Ce module pose les bases de la modélisation de systèmes mécatroniques à paramètres localisés : approches réseaux en elec/meca/thermique/hydro, bond graph, solvers ODE/ADE, modélisation causal/acausal. Outils : Modelica, Simulink, AMESim <i>Apport personnel : Création de l'UF sur l'aspect énergie en collaboration avec J-Ch Maré</i>
Chaînes d'énergie et d'instrumentation I4IS EI11	CM-TD-PJ 4GM-IS 4AE-IS 35 h /an	Ce module traite de la conception de transmissions de puissance multi domaine en meca/hydro/elec sous les aspects analyse, synthèse et dimensionnement. En plus des CM-TD, un PJ aux choix permet aux étudiants d'illustrer et d'appliquer les connaissances acquises. <i>Apport personnel : Création du module en collaboration avec J-Ch Maré</i>
Asservissement I4GM SY11	TD 4GM-IM 15 h /an	Ce module concerne la commande des systèmes bouclés : précision/stabilité, synthèse de correcteurs, retour d'état.
Simulation numérique I4IS MT22	CM-TD 4GM-IS 25 h /an	Ce module traite de la simulation numérique appliquée à l'électromagnétisme, la mécanique des fluides et la mécanique des structures. Les aspects locaux (FEM, CFD) et globaux (Simulation multicorps, système 0D/1D) et leur liens sont abordés et illustrés à travers deux exemples concrets (régulateur de pression de common rail, miroir piloté). <i>Apport personnel : Création du module sur les aspects électromagnétisme, simulation système, et mis en place des projets fils rouge.</i>

Conception d'architectures I4IS CA11	CM-TD-PJ 4GM-IS 4AE-IS 20 h /an Responsable d'UF	Sur la partie PJ mécatronique de cet UF, les étudiants sont amenés à concevoir un système mécatronique depuis la mise en place d'un cahier des charges avec un client réel (industriel), la proposition d'architectures, le dimensionnement et la simulation d'un prototype virtuel. Exemples de sujets : actionneur de pilotage de tuyère de fusée, actionneur de frein d'avion. <i>Apport personnel : Création du module en collaboration avec J-Ch Maré</i>
PTP Energies 5ème année	PJ et TP simulation 20 h /an	Les étudiants sont amenés par une série de TP à modéliser un véhicule hybride léger sous Modelica et à proposer une commande simple permettant d'optimiser la consommation. Certains d'entre eux peuvent participer à la mise en place d'un véhicule électrique léger et de son banc de roulage au travers de PJ. <i>Apport personnel : Création du module d'enseignement et mise en place des PJ</i>

3. RECHERCHE

3.1. Résumé des travaux de recherche

Actuellement (Institut Clément Ader ICA, INSA Toulouse, 2006-)

Sujet : Conception préliminaire des systèmes mécatroniques et des actionneurs électromécaniques.

Mots clés : Modélisation, Simulation, Actionneurs électromécaniques, Conception préliminaire.

Dans le cadre du Post-Doc (IMS ex IXL, Université Bordeaux I, 2003-2004)

Sujet : Etude de la fiabilité des microsystèmes (MEMS).

Responsable : Claude Pellet (équipe Capteur et Microsystèmes)

Mots clés : Microsystèmes, MEMS, claquage électrique, micro actionneur thermique, couplage thermo-mécanique, transformateur piézoélectrique, technologie hybride

Dans le cadre du DEA et de la thèse (LAPLACE ex LEEI, Toulouse, 2000-2003)

Sujet : Actionneurs piézo-électriques à deux degrés de liberté (translation et rotation)

Directeur de thèse : Bertrand Nogarede (Responsable de l'équipe Machines et Mécanismes Electroactifs du LEEI)

Mots clés : Actionneurs piézoélectriques, matériaux électro-actifs, mécanique vibratoire, modélisation analytique et éléments finis, électronique d'alimentation et de commande.

3.2. Encadrement de chercheurs

Encadrement de thèses

Jonathan Liscouet (2007-2010)

« Conception préliminaire des actionneurs électromécaniques- Approche hybride, directe/inverse », thèse soutenue le 4 janvier 2010.

Ecole doctorale MEGEP, encadrement à 50% avec J-Ch Maré.

Thèse financée sur les projets européen DRESS (Distributed and Redondant Electrical nose gear Steering System, 2007-2009) et ANR SIMPA2-C6E2 (Conception des SYStèmes Electriques Embarqués, 2007-2009).

4 revues, 6 conférences, INCOSE FOUNDATION and STEVENS INSTITUTE OF TECHNOLOGY Doctoral Award 2009.

Toufic El Halabi (2008-2012)

« Méthodologies pour la conception optimale des systèmes d'actionnement électromécaniques », thèse soutenue le 22 mars 2012.

Ecole doctorale MEGEP, encadrement à 50% avec J-Ch Maré.

Thèse financée sur le projet FUI pôle de compétitivité ASTECH CISACS (Concept Innovant de Système d'Actionnement de Commandes de vol secondaires et de Servitudes, 2008-2012)

1 revue, 3 conférences avec actes, 2 conférences sans actes.

Fabien Hospital (2009-2012)

« Conception préliminaire des actionneurs électromécaniques basée sur les modèles : lois d'estimations et règles de conception pour la transmission de puissance mécanique », thèse soutenue le 22 octobre 2012.

Ecole doctorale MEGEP, encadrement à 50% avec J-Ch Maré.

Thèse financée sur une bourse AMN.

3 revues, 1 conférence.

Amine Fraj (2010-2014)

Cette thèse traite des de la conception préliminaire d'actionneurs électromécaniques et hydrauliques sur les aspects incertitudes, liens avec la 3D.

Ecole doctorale MEGEP, encadrement à 50% avec J-Ch Maré.

Thèse financée sur le projet de coopération aerospace-valley SYRENA (SYstème de REGulation Nouvelle Architecture, 2010-2013).

1 revue, 3 conférences.

Xavier Giraud (2011-2014)

Cette thèse traite de la conception préliminaire et l'optimisation de réseaux électriques d'avion sur les aspects synthèses des logiques, allocation des charges, modèles d'estimations.

Ecole doctorale AA, co-encadrement ICA (M. Sartor, M. Budinger), Laplace (X. Roboam, H. Piquet).

Financée sur une bourse Cifre Airbus.

1 revue, 2 conférences.

Aurélien Reyssset (2012-2015)

Cette thèse traite d'outils d'aide à la conception d'EMA et de la standardisation des composants électromécaniques.

Ecole doctorale MEGEP, encadrement à 50% avec J-Ch Maré.

Financée sur le projet européen ACTUATION 2015 (2012-2015).

3 revues, 2 conférences.

Masters recherche ou projets de fin d'étude (ERASMUS) :

Toufic El Halabi (2008, master recherche MEGEP) : Mise en place d'une librairie Modelica de dimensionnement à l'aide de simulations inverses.

Daniel Ortega (2009, projet de fin d'étude ERASMUS, Espagne) : Dimensionnement préliminaire en électronique de puissance.

Amine Fraj (2010, projet de fin d'étude ENIS, Tunisie) : Lien Modelica/Catia et conception préliminaire/CAO.

Hiba Elouni (2011, projet de fin d'étude ENIS, Tunisie) : Obtention de méta-modèles à base de lois d'échelles.

Robert Vallmajo Ribas (2011, projet de fin d'étude ERASMUS, Espagne) : Conception préliminaire de carter en environnement vibratoire sévère.

David Morczinek (2012, projet de fin d'étude TUHH, Allemagne) : Durée de vie et fiabilité des composants mécatroniques.

3.3. Participation à des contrats industriels

Contrat SAGEM – ENSICA (2005)

Etude de faisabilité d'un système générateur de vibrations pour tripode optique.

Projet ANR SIMPA2-C6E2 (Conception des SYStèmes Electriques Embarqués, 2007-2009)

Outils, modèles et méthodologies d'aide à la conception d'actionneurs électromécaniques.

Projet FUI pôle de compétitivité ASTECH CISACS (Concept Innovant de Système d'Actionnement de Commandes de vol secondaires et de Servitudes, 2008-2012)

Optimisation de la conception de systèmes d'actionnement de trains d'atterrissage (Messier Bugatti), dimensionnement préliminaire d'un actionneur EMA de spoiler pour avion d'affaires (SAGEM SD, Dassault aéronautique).

Projet de coopération aerospace-valley SYRENA (SYstème de REgulation Nouvelle Architecture, 2010-2013)

Conception préliminaire d'actionneurs hydrauliques et électromécaniques pour la régulation d'entrée d'air de turbines d'hélicoptères.

Projet Européen FP7 ACTUATION 2015 (Modular Electro Mechanical Actuators for ACARE 2020 aircraft and helicopters, 2012-2015)

Outils d'aide à la conception d'actionneurs EMA et analyse de l'effet de la standardisation des composants.

3.4. Mobilité

Congé pour Recherches et Conversions Thématiques (CRCT) d'un semestre avec mobilité, de février à juillet 2013, à l'université TUHH d'Hambourg et plus particulièrement à l'institut FST (systèmes aéronautiques).

Annexe 2 – Curriculum Vitae, short version (English)

PERSONAL INFORMATION

Name: Marc BUDINGER

Position: Associate professor, Department of Mechanical Engineering at INSA Toulouse

Adress:

Home :	University :
17, rue Saint Hyacinthe	INSA Toulouse, , Institut Clément Ader
31500 Toulouse	135 Avenue de Ranguail
(33) 05 62 16 39 36	31004 Toulouse, France
(33) 06 66 70 00 11	(33) 05 61 55 99 60
marc_budinger@yahoo.com	marc.budinger@insa-toulouse.fr

RESEARCH

My current research topic concerns the model based design of electromechanical actuators and actuation systems. I am currently investigating the conjoint use of estimation/prediction models, 0D/1D simulation models, reliability models and metamodels for design and optimization.

My previous research activities have included the design of an electrical submarine propulsion motor (military service), piezoelectric actuators (Phd) and MEMS (post doc).

EDUCATION

2000-2003	Phd on Piezoelectric ultrasonic actuators <i>ENSEEIH, Toulouse</i>
1999-2000	Master of science in Electrical Engineering <i>ENSEEIH, Toulouse</i>
1995-1998	Applied Physics Aggregation (french teaching diploma) <i>ENS Cachan, Orsay University, Paris</i>

PUBLICATIONS

2 patents, 10 journal papers, 35 conference papers.

TEACHING/ADMINISTRATION EXPERIENCE

- 2006- Associate Professor – *INSA Toulouse, Mechanical Engineering Department*
Courses (lectures, tutorials and labs) in systems engineering (control, system dynamics and power systems design), electrical engineering (electrical actuators, electromagnetic FEM simulation) and mechanical engineering (vibrations).
Responsible of the fourth year for the specialty systems engineering.
- 2004-2006 Applied physics teacher for High Level Technician – *Academy of Toulouse*
Aggregation of Applied Physics : recruitment jury member

OTHER WORK EXPERIENCES

- 2003-2004 Post-Doc researcher - *CNRS, IXL, University of Bordeaux*
MEMS, electrical breakdown, thermal micro actuator, thermo-mechanical coupling, piezoelectric transformers, hybrid technology.
- 1998-1999 Military Service, design engineer - *JEUMONT Industrie (FRAMATOME)*
Electric motor submarine (permanent magnet brushless motor of 3 MW).

Annexe 3 – Publications

Articles dans des revues internationales avec comité de lecture (classées IWK)

1. V. Budinger-Pommier, M. Budinger, *Sizing optimization of piezoelectric smart structures with meta-modeling techniques for dynamic applications*, International Journal of Applied Electromagnetics and Mechanics, accepté le 16 décembre 2013.
2. F. Hospital, M. Budinger, A. Reysset, J-Ch. Maré, *Preliminary design of aerospace linear actuator housings*, Aircraft Engineering and Aerospace Technology (Emerald), accepté le 8 décembre 2013.
3. M. Budinger, J-Ch. Passieux, Ch. Gogu, A. Fraj, *Scaling-law-based metamodels for the sizing of mechatronic system*, Mechatronics (Elsevier), accepté le 30 novembre 2013, doi: 10.1016/j.mechatronics.2013.11.012.
4. X.Giraud, M.Sartor, X.Roboam, B.Sareni, H.Piquet, M.Budinger, S.Vial, *Load allocation problem for optimal design of aircraft electrical power*, International Journal of Applied Electromagnetics and Mechanics, Volume 43, Number 1-2, pp. 37-49, 2013.
5. M. Budinger, A. Reysset, T. El Halabi, C. Vasiliu, J-Ch. Maré, *Optimal preliminary design of electromechanical actuators*, Proceedings of the Institution of Mechanical Engineers, Part G: Journal of Aerospace Engineering, Accepté 19-7-2013.
6. M. Budinger, J. Liscouet, F. Hospital, J-Ch Maré., *Estimation models for the preliminary design of electromechanical actuators*, Proceedings of the Institution of Mechanical Engineers, in Proceedings of the Institution of Mechanical Engineers, Part G: Journal of Aerospace Engineering Volume 226 Issue 3, March 2012, , 0954410011408941.
7. J. Liscouet, J-Ch. Mare, M. Budinger, *An integrated methodology for the preliminary design of highly reliable electromechanical actuators: Search for architecture solutions*, Aerospace Science and Technology, Volume 22, Issue 1, October–November 2012, Pages 9–18.
8. J. Liscouet, M. Budinger, J-Ch. Mare, S. Orioux, *Modelling approach for the simulation-based preliminary design of power transmissions*, Mechanism and Machine Theory, Vol. 46, n° 3, 276-289, Mars 2011.
9. M. Budinger, J-F. Rouchon, B. Nogarede, *A Mason type analysis of cylindrical ultrasonics micromotors*, The European Physical Journal Applied Physics, n° 25, 57-65, 2004.
10. M. Budinger, J-F. Rouchon, B. Nogarede, *Analytical modeling for the design of a piezoelectric rotating-mode motor*, IEEE/ASME Transactions on Mechatronics, Vol. 9, n°1, mars 2004.

Articles dans des revues internationales ou nationales avec comité de lecture (non classées IWK)

1. M. Budinger, D. Gilibert, J-F. Rouchon, B. Nogarede, *Modélisation par méthode variationnelle d'un actionneur piézoélectrique à rotation de mode. Approche analytique et numérique*, Revue internationale de génie électrique, Vol. 7/1-2, 2004, pp. 223-251.
2. M. Budinger, C. Henaux, J-F. Rouchon, B. Nogarede, *Development of an artificial hand with piezoelectric actuators*, ELECTROMOTION, Vol. 9, number 2, p 87, April - June 2002.
3. M. Budinger, J-F. Rouchon, C. Henaux, B. Nogarede, *Un exemple de motorisation piézo-électrique et de son alimentation associée pour applications « embarquées »*, REE, février 2002.

Chapitres d'ouvrage ou d'encyclopédie

1. M. Budinger, F. Hospital, J. Liscouet, B. Multon, A. Reysset, J-Ch Maré, *Chaînes de transmission de puissance mécatroniques - Modèles d'estimation*, Techniques de l'Ingénieur, Référence BM8026, 10 avr. 2013.
2. M. Budinger, J. Liscouet, F. Hospital, B. Multon, *Chaînes de transmission de puissance mécatroniques - Mise en place des modèles d'estimation pour la conception préliminaire*, Techniques de l'Ingénieur, Référence BM8025, 10 oct. 2011.

Brevets

3. M. Budinger, J-F. Rouchon, B. Nogarede, *Moteur électroactif monophasé*, déposant : CNRS-INPT, FR2844114 (2004-03-05), WO2004021555 (2004-03-11).
4. M. Budinger, J-F. Rouchon, B. Nogarede, *Moteur piézoélectrique permettant au moins deux degrés de liberté, en rotation et en déplacement linéaire*, déposant : CNRS-INPT, FR2854284 (2004-10-29), WO2004098039 (2004-11-11).

Conférences

1. M. Budinger and L. Brault , ACTUATION 2015, *Model based design of electromechanical actuators, Conference : Design of complex dynamic systems*, Modelica and FMI standards, 17 septembre 2013, Toulouse. Invited lecture.
2. D. Arriola, A. Reysset, M. Budinger, F. Thielecke, J-Ch. Maré, *From Airframer Requirements to Detailed Technical Specification of Electromechanical Actuators Aided by Knowledge-Based Methods*, SAE 2013 AeroTech Congress & Exhibition, Montréal, Quebec, Canada , September 24-26, 2013.
3. Th. Ros T., M. Budinger, A. Reysset, J-Ch Mare, *Modelica Preliminary Design Library for Electromechanical Actuators*, AST 2013, 4th International Workshop on Aircraft System Technologies, TUHH, Hamburg, Germany, April 23-24, 2013
4. X. Giraud, H. Piquet, M. Budinger, X. Roboam, M. Sartor and S. Vial. *Knowledge-based system for aircraft electrical power system reconfiguration*. Proceedings of 2nd International Conference on Electrical Systems for Aircraft Railway And Ship Propulsion 2012 (ESARS 2012) - Bologna 2012
5. X. Giraud, M. Sartor, X. Roboam, B. Sareni, H. Piquet, M. Budinger and S. Vial. *Comparative study of stochastic optimization methods to solve load allocation problem for aircraft electrical power system design*. Proceedings of XII-th International Workshop on Optimization and Inverse Problems in Electromagnetism (OIPE 2012) - Ghent 2012
6. A. Fraj , M. Budinger , T. El Halabi , J-Ch. Maré, G-C. Negoita, *Modelling approaches for the simulation-based preliminary design and optimization of electromechanical and hydraulic actuation systems*, 8th AIAA Multidisciplinary Design Optimization Specialist Conference, 23-26 April 2012, Honolulu, Hawaii, USA.
7. M. Budinger , T. El Halabi , J-Ch. Maré , *Optimal preliminary design of electromechanical actuation systems*, « More electrical » aircraft technologies, Symposium SPEC, November 8 & 9, 2011, Lyon.
8. J. Liscouët, M. Budinger, J-Ch. Maré, *Scaling laws for the simulation based preliminary design of electro-mechanical actuators*, AST 2011, Hamburg, Germany, march 31-april 1, 2011.
9. T. El Halabi, M. Budinger, J-Ch. Maré, *Optimal geometrical integration of electromechanical actuators* , OPTIMUS User Meeting 2010, Antwerp, 22 and 23 November 2010.
10. A. Fraj, T. El Halabi, M. Budinger, J-Ch. Maré, *Coupling CAD and system simulation framework for the preliminary design of electromechanical actuators*, Proceedings of IDMMME - Virtual Concept 2010, Bordeaux, France, October 20 – 22, 2010.
11. F. Hospital, M. Budinger, J. Liscouet, J-Ch Maré, *Model Based Methodologies for the Assessment of More Electric Flight Control Actuators*, Proceedings of the 13th AIAA/ISSMO Multidisciplinary

- Analysis Optimization Conference, American Institute of Aeronautics and Astronautics, Fortworth, 13-15 Septembre, 2010.
12. T. El Halabi, M. Budinger, Maré J-Ch, *Optimal geometrical integration of electromechanical actuators*, Proceedings of the 4th international conference on Recent Advances in Aerospace Actuation Systems and Components, June 24-26, 2010
 13. J. Liscouet, M. Budinger, J-Ch. Maré, *Design for reliability of electromechanical actuators*, Proceedings of the 4th international conference on Recent Advances in Aerospace Actuation Systems and Components, June 24-26, 2010
 14. L. Allain, M. Budinger, J. Liscouet, Y. Lefevre, J. Fontchastagner, A. Abdenour, *Preliminary Design of Electromechanical Actuators with Modelica*, Modelica 2009, Proceedings 7th Modelica Conference, Como, Italy, Sep. 20-22, 2009.
 15. Budinger M., Liscouët J., Cong. Y., Mare J-Ch., *Simulation Based Design of Electromechanical Actuators with Modelica*, IDETC 09, San Diego, 30 aout, 2 septembre 2009.
 16. J-Ch Maré, M. Budinger, *Comparative analysis of energy losses in servo-hydraulic, electro-hydrostatic and electro-mechanical actuators*, The 11th Scandinavian International Conference on Fluid Power, SICFP'09, June 2-4, 2009, Linköping, Sweden.
 17. J. Liscouet, S. Orieux, M. Budinger, J-Ch. Maré, *Electromechanical nose gear steering actuator – study of high reliability architectures*, Conference SAE A- Landing Gear Systems – The 21st century, Toulouse, 8-10 april 2008.
 18. M. Budinger, S. Orieux, J. Liscouet, J-C Maré, *Automated preliminary sizing of electromechanical actuator architectures*, ELECTRIMACS 2008, Québec, 8-11 june 2008.
 19. P. Ginet, C. Lucat, F. Ménil, M. Budinger, H. Debéda, *New screen-printed MEMS : study of a metallic thermal microactuator*, SMART SYSTEMS INTEGRATION 2007, Paris, March 27-28, 2007
 20. P. Ginet, C. Lucat, M. Budinger, F. Ménil, *New Screen-printed Thermal Microactuator*, Nano/Micro Engineered and Molecular Systems, 2007. NEMS '07. Jan. 2007, Bangkok, Thailand
 21. M. Budinger, H. Débéda, C. Lucat, C. Pellet, *Transformateur piézoélectrique : piste de l'intégration hybride*, 3ème journées micro robotique, décembre 2004, EPFL, Lausanne.
 22. D. Veyrié, M. Budinger, C. Pellet, F. Pressecq, J.L. Roux, A. Tetelin, *Modeling of water vapor permeation inside bcb-sealed packages for microsystems*, DTIP 2005.
 23. V. Pommier, M. Budinger, Ph.Lever, J. Richelot, J. Bordeneuve, *FEM design of a piezoelectric active control structure. Application to an aircraft wing model*, ISMA 2004, 20-22 septembre 2004, Louvain, Belgique.
 24. M. Budinger, C. Pellet, *Claquage électrostatique et protection en surtension des MEMS*, 2èmes Journées du RTP Fiabilité, 15 et 16 mars 2004, Carry le Rouet.
 25. M. Budinger, S. Muratet, J-Y Fourniols, C. Pellet, *Modélisation analytique de micro actionneurs thermiques*, 2èmes Journées du RTP Fiabilité, 15 et 16 mars 2004, Carry le Rouet.
 26. C. Henaux, M. Budinger, B. Nogarede, *Supply for piezoelectrics actuators : a survey on exiting and optimised supplies*, EPE 2003, septembre 2003, Toulouse.
 27. M. Budinger, F. Giraud, J-F Rouchon, B. Lemaire-Semail, B. Nogarede, *Feeding and control electronic of a piezoelectric actuator*, ACTUATOR'2002, juin 2002, Bremen, Allemagne
 28. M. Budinger, J-F. Rouchon, B. Nogarede, *Analytical stator study of cylindrical ultrasonic motors*, ACTUATOR'2002, juin 2002, Bremen, Allemagne
 29. M. Budinger, J-F. Rouchon, B. Nogarede, *Modélisation, en vue du dimensionnement, du moteur piézo-électrique à rotation de mode*, MAGELEC'2001, 13-14 décembre 2001, Toulouse, France.
 30. M. Budinger, *Modélisation du moteur piézo-électrique à rotation de mode*, JCGE'01, 13-14 novembre 2001, Nancy, France.

31. M. Budinger, C. Henaux, J-F. Rouchon, B. Nogarede, *Un exemple de motorisation piézo-électrique et de son alimentation associée pour applications « embarquées »*, EF'2001, 14-15 novembre 2001, Nancy, France.
32. M. Budinger, C. Henaux, J-F. Rouchon and B. Nogarede, *Developement of an artificial hand with piezoelectric actuators*, ELECTROMOTION'01, June 19-20, 2001, Bologna, Italy.

Publications pédagogiques

1. M. Budinger, D. Leray, Y. Debleser, *Eoliennes et vitesse variable*, Revue 3EI, n°20, mars 2000
2. M. Budinger, B. Nogarede, *Un actionneur d'avenir pour la grande diffusion: le moteur piezo-électrique à ondes progressives*, Revue 3EI, n°21, juin 2000
3. M. Budinger, J-F Rouchon,, B. Nogarede, *Simulation et réalisation d'un moteur piézo-électrique*, CETSIS'2001, 29-30 octobre 2001, Clermont-Ferrand, France.
4. V. Pommier, M. Budinger, G. Pérusot, *Les énergies renouvelables : étude et optimisation du fonctionnement d'un système photovoltaïque*, CETSIS'2003, novembre 2003, Toulouse, France.
5. M. Budinger, *Initiez-vous aux moteurs piézoélectriques pour moins de 1 €*, Revue 3EI, n° 37, juin 2004
6. V. Pommier, M. Budinger, B. Mouton, S. Leleu, *Contrôle actif de vibrations*, CETSIS'2005, octobre 2005, Nancy, France et revue J3EA.
7. V.Pommier, M. Budinger, S. Leleu, B. Mouton, *Contrôle actif de vibrations*, Journal sur l'enseignement des sciences et technologies de l'information et des systèmes, Vol. 5, Hors série n°2, 2006
8. J-Ch. Maré, M. Budinger, *Experiences in project-based System Engineering education at INSA Toulouse*, Insight, March 15, 2008.
9. F. David, A. Brel, M. Budinger, *Construire un mini radeau à moteur innovant avec des objets de récupération*, Revue 3EI, n°56, mars 2009